ORGANOIDS AS MODEL SYSTEMS FOR HUMAN DEVELOPMENT, DISEASE AND CLINICAL APPLICATIONS

EDITED BY: Eumorphia Remboutsika and Thimios Mitsiadis
PUBLISHED IN: Frontiers in Cell and Developmental Biology,
Frontiers in Physiology and Frontiers in Genetics

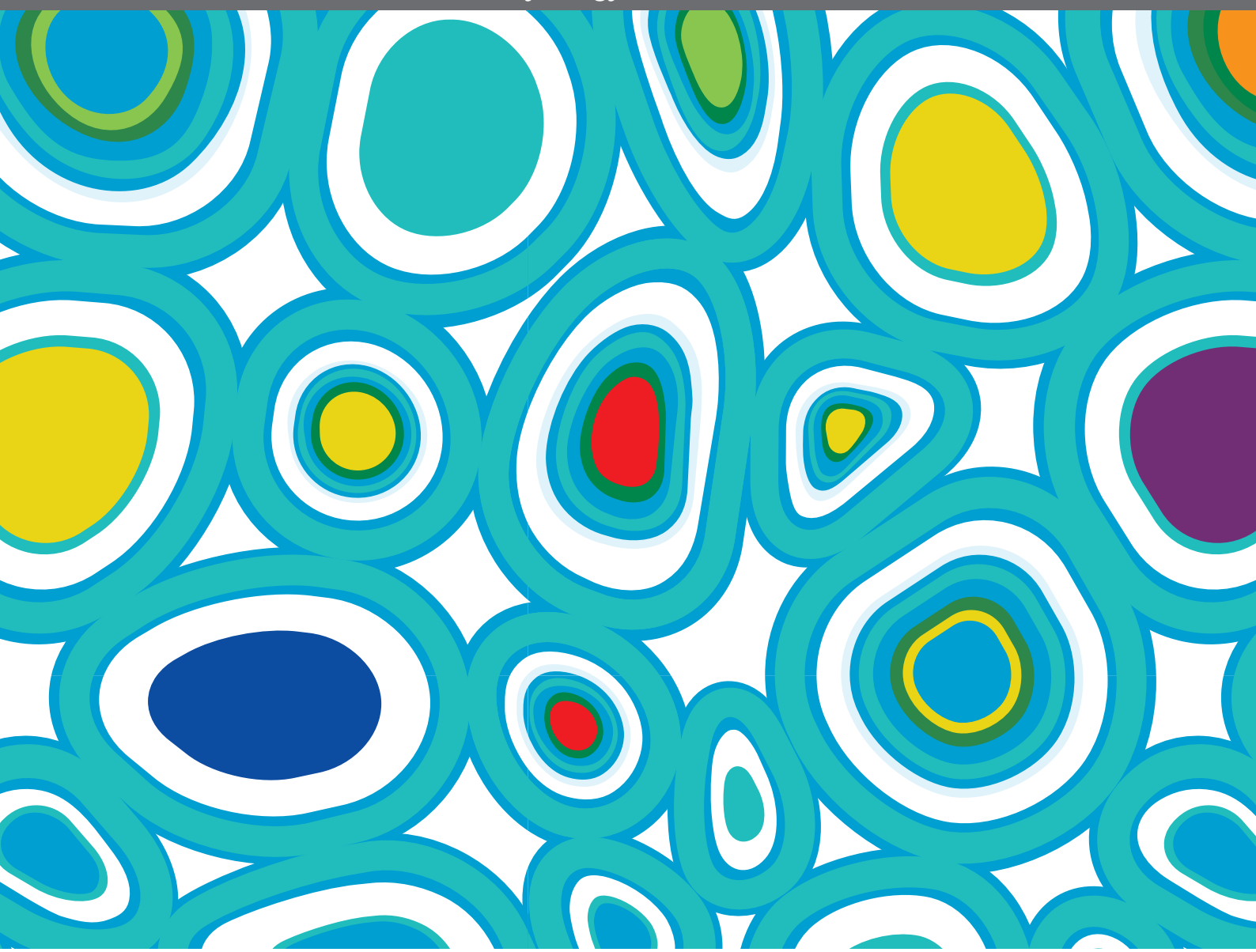

frontiers Research Topics

frontiers

ISSN 1664-8714
ISBN 978-2-88971-660-9
DOI 10.3389/978-2-88971-660-9

About Frontiers

Frontiers is more than just an open-access publisher of scholarly articles: it is a pioneering approach to the world of academia, radically improving the way scholarly research is managed. The grand vision of Frontiers is a world where all people have an equal opportunity to seek, share and generate knowledge. Frontiers provides immediate and permanent online open access to all its publications, but this alone is not enough to realize our grand goals.

Frontiers Journal Series

The Frontiers Journal Series is a multi-tier and interdisciplinary set of open-access, online journals, promising a paradigm shift from the current review, selection and dissemination processes in academic publishing. All Frontiers journals are driven by researchers for researchers; therefore, they constitute a service to the scholarly community. At the same time, the Frontiers Journal Series operates on a revolutionary invention, the tiered publishing system, initially addressing specific communities of scholars, and gradually climbing up to broader public understanding, thus serving the interests of the lay society, too.

Dedication to Quality

Each Frontiers article is a landmark of the highest quality, thanks to genuinely collaborative interactions between authors and review editors, who include some of the world's best academicians. Research must be certified by peers before entering a stream of knowledge that may eventually reach the public - and shape society; therefore, Frontiers only applies the most rigorous and unbiased reviews.
Frontiers revolutionizes research publishing by freely delivering the most outstanding research, evaluated with no bias from both the academic and social point of view. By applying the most advanced information technologies, Frontiers is catapulting scholarly publishing into a new generation.

What are Frontiers Research Topics?

Frontiers Research Topics are very popular trademarks of the Frontiers Journals Series: they are collections of at least ten articles, all centered on a particular subject. With their unique mix of varied contributions from Original Research to Review Articles, Frontiers Research Topics unify the most influential researchers, the latest key findings and historical advances in a hot research area! Find out more on how to host your own Frontiers Research Topic or contribute to one as an author by contacting the Frontiers Editorial Office: frontiersin.org/about/contact

ORGANOIDS AS MODEL SYSTEMS FOR HUMAN DEVELOPMENT, DISEASE AND CLINICAL APPLICATIONS

Topic Editors:
Eumorphia Remboutsika, National and Kapodistrian University of Athens, Greece
Thimios Mitsiadis, University of Zurich, Switzerland

Citation: Remboutsika, E., Mitsiadis, T., eds. (2021). Organoids as Model Systems for Human Development, Disease and Clinical Applications.
Lausanne: Frontiers Media SA. doi: 10.3389/978-2-88971-660-9

Table of Contents

frontiers in Cell and Developmental Biology

ORIGINAL RESEARCH
published: 05 March 2019
doi: 10.3389/fcell.2019.00025

Generation of Vestibular Tissue-Like Organoids From Human Pluripotent Stem Cells Using the Rotary Cell Culture System

Cristiana Mattei[1,2], *Rebecca Lim*[3], *Hannah Drury*[3], *Babak Nasr*[1,4,5], *Zihui Li*[2], *Melissa A. Tadros*[3], *Giovanna M. D'Abaco*[2], *Kathryn S. Stok*[2], *Bryony A. Nayagam*[6] *and Mirella Dottori*[1,2,7]*

[1] Centre for Neural Engineering, Melbourne School of Engineering, The University of Melbourne, Melbourne, VIC, Australia, [2] Department of Biomedical Engineering, Melbourne School of Engineering, The University of Melbourne, Melbourne, VIC, Australia, [3] School of Biomedical Sciences and Pharmacy, Faculty of Health and Medicine, University of Newcastle, Newcastle, NSW, Australia, [4] Department of Electrical and Electronic Engineering, Melbourne School of Engineering, The University of Melbourne, Melbourne, VIC, Australia, [5] ARC Centre of Excellence for Integrative Brain Function, The University of Melbourne, Melbourne, VIC, Australia, [6] Departments of Audiology and Speech Pathology and Department of Medical Bionics, The University of Melbourne, Melbourne, VIC, Australia, [7] Illawarra Health and Medical Research Institute, University of Wollongong, Wollongong, NSW, Australia

Hair cells are specialized mechanosensitive cells responsible for mediating balance and hearing within the inner ear. In mammals, hair cells are limited in number and do not regenerate. Human pluripotent stem cells (hPSCs) provide a valuable source for deriving human hair cells to study their development and design therapies to treat and/or prevent their degeneration. In this study we used a dynamic 3D Rotary Cell Culture System (RCCS) for deriving inner ear organoids from hPSCs. We show RCCS-derived organoids recapitulate stages of inner ear development and give rise to an enriched population of hair cells displaying vestibular-like morphological and physiological phenotypes, which resemble developing human fetal inner ear hair cells as well as the presence of accessory otoconia-like structures. These results show that hPSC-derived organoids can generate complex inner ear structural features and be a resource to study inner ear development.

Keywords: vestibular hair cells, human pluripotent stem cells, organoids, human fetal tissue, inner ear

OPEN ACCESS

Edited by:
Thimios Mitsiadis,
University of Zurich, Switzerland

Reviewed by:
Nikolaos Dimitrakakis,
Wyss Institute for Biologically Inspired Engineering at Harvard Medical School, United States
Adrian Rodriguez-Contreras,
City College of New York (CUNY), United States
Alexandros Efthimis Tsouknidas,
University of Western Macedonia, Greece

***Correspondence:**
Mirella Dottori
mdottori@uow.edu.au

Specialty section:
This article was submitted to Stem Cell Research, a section of the journal Frontiers in Cell and Developmental Biology

Received: *29 November 2018*
Accepted: *12 February 2019*
Published: *05 March 2019*

Citation:
Mattei C, Lim R, Drury H, Nasr B, Li Z, Tadros MA, D'Abaco GM, Stok KS, Nayagam BA and Dottori M (2019) Generation of Vestibular Tissue-Like Organoids From Human Pluripotent Stem Cells Using the Rotary Cell Culture System. Front. Cell Dev. Biol. 7:25. doi: 10.3389/fcell.2019.00025

INTRODUCTION

Each human inner ear contains ∼90,000 sensory hair cells that convert sound and motion from mechanical energy to electrical signals within the mammalian cochlea (hearing) and balance (vestibular) organs, respectively. Inner ear hair cells are exquisitely sensitive, and this feature also renders hair cells prone to damage, disease, and vulnerable to aging. Once damaged, human inner ear hair cells do not regenerate and their destruction can ultimately lead to loss of hearing and/or balance.

Inner ear hair cells of the auditory and vestibular systems are structurally similar: all have hair bundles or stereocilia that emanate from their apical surface. The mode of activation is also similar: sound waves or head movement causes deflection of these stereocilia resulting in a cascade of ion fluxes and signaling molecules that excites hair cells. However, there is a diversity of hair cell types

within the inner ear, each with distinct roles. This suggests there are different signaling molecules, transcription factors, and pathways of differentiation that drive cells to become one of four types; vestibular (type I or type II) hair cells or cochlear (inner or outer) hair cells.

Over the last decade, stem cell biology has advanced significantly, such that human pluripotent stem cells (hPSCs) can be generated from any individual. One of the greatest benefits of this technology is that it provides an opportunity to study human tissue at a cellular level, particularly cell types that would otherwise be inaccessible and/or difficult to access in human. Deriving human inner ear hair cell-like cells from pluripotent stem cells has proved surprisingly challenging to date and has only been published by a select few (Ronaghi et al., 2014; Ohnishi et al., 2015; Koehler et al., 2017) and only one describing generation of human inner ear organoids and vestibular hair cells used spinner flasks/orbital shakers (Koehler et al., 2017). All studies are limited by their comparisons to rodent anatomy and physiology.

We have recently developed a three-dimensional organoid cell culture model using rotary cell culture (RCCS) (Mattei et al., 2018). The new model produces large numbers of dorsal hindbrain progenitors, a region from which we know the inner ear sensory hair cells and neurons are derived. Here we describe an alternative method based on the utilization of the RCCS for generating inner ear organoids consisting of an enriched population of inner ear hair cell-like cells, which display key functional properties of human inner ear hair cell phenotypes along with appropriate anatomical features. We show that microgravity-derived organoids consist of cells which are both ATOH1 and myosin VIIa immunoreactive and show kinocilia-like projections surrounded by stereocilia. Importantly, organoid-derived cells are physiologically similar to developing human fetal vestibular hair cells, exhibiting comparable voltage-activated conductance, and exhibit the presence of inner ear-like accessory structures. These findings are significant for establishing a human inner ear *in vitro* model to study development of the vestibular system and also pursue therapies to treat inner ear degeneration.

MATERIALS AND METHODS

Culture and Differentiation of hPSCs

This project is approved by University of Melbourne Human Ethics committee (#1545384 and 1545394). Human ES cell lines, H3 (kindly provided by E. Stanley and A. Elefanty, Murdoch Institute Children Research, Australia) and H9 (WA09, WiCell), and human iPS cell line 007 (Hernández et al., 2016), were maintained as bulk culture in feeder-free conditions on vitronectin (StemCell Technologies) coated dish (Corning) using Tesr-E8 basal medium (StemCell Technologies). For induction, aggregates of 1,000 hPS cells were plated in U-bottom ultra-low attachment 96-multiwell plates (Corning) in Tesr-E8 basal medium to form embryoid bodies. After 24 h, embryoid bodies were transferred into the RCCS (Synthecon) in N2B27 medium containing 1:1 mix of neurobasal (NB) medium with DMEM/F12 medium, 1% insulin/transferrin/selenium, 1% N2 supplement, 1% retinol-free B27 supplement, 1% glutamax, 1% penicillin streptomycin (Life Technologies), 0.3% glucose (Sigma Aldrich), supplemented with inhibitors SB431542 (10 μM, Tocris) and LDN 193189 (100 nM, KareBay Biochem). Medium change was performed on day 3 of induction, replaced with N2B27 medium supplemented with FGF (20 ng/ml, Peprotech) on day 7 and changed on day 10. On day 14 medium change was performed and organoids were cultured with NB medium containing 1% insulin/transferrin/selenium, 1% N2 supplement, 1% retinol-free B27 supplement, 1% glutamax, 1% penicillin streptomycin, supplemented with FGF and EGF (20 ng/ml, Peprotech) up to day 28 and with supplement-free NB medium up to day 56. On day 56 medium change was performed and replaced with supplement-free NB medium and 1:4 DMEM/F12 containing 1% N2 supplement, 1% glutamax and 0.6% glucose. At every medium change the DMEM/F12 concentration was gradually increased by 25%. From day 14 to day 133 medium change was performed every third day. The RCCS was placed in an incubator at 5% CO_2 and 37°C and speed rate was gradually increased overtime to ensure a continuous falling motion of organoids. Bright field images of organoids were obtained using a ZEISS Observer z1 with ZEN imaging software.

RCCS Set Up Procedure

At day 1, 300 embryoid bodies were transferred into each RCCS 10 ml-vessel through the sterile valves on the top of the vessel, using a 10 ml syringe as instructed in the manufacturer's operation manual. The RCCS was placed in an incubator at 5% CO_2 and 37°C. At day 1, the speed rate was 18 RPM as indicated by the tachometer's display on the RCCS power supplier. By day 28 speed rate was increased by 5–6 RPM and up to 30 RPM by day 98 till day 133. Speed rate was gradually increased over time depending on organoid size, to ensure a continuous falling motion of organoids through the medium during vessel rotation and therefore facilitate their exposure to nutrients, as instructed by the manufacturer.

Immunohistochemistry

Organoids were collected and fixed with 4% paraformaldehyde for 1 h on ice. Fixed samples were incubated overnight at 4°C with 20% sucrose to cryoprotect. Samples were embedded with O.C.T. compound (VWR Chemicals) and sectioned using a cryostat to obtain 12–14 μm sections. For immunostaining, cryosections were permeabilized using 0.2% Triton-X100 solution and incubated with primary and secondary antibodies in 10% Fetal Calf Serum (Millipore)/phosphate buffered saline DPBS (Life Technologies) blocking solution. The following primary antibodies were used: anti-Tub alpha 4a (mouse, 1:250, Sigma-Aldrich, T6793), anti-Myo7a (rabbit, 1:100, Proteus, 256790), anti-Ctbp2 (mouse, 1:400, BD Transduction Lab, 612044), anti-Pax2 (rabbit, 1:200, BioLegend, 901001), anti-Atoh1 (rabbit, 1:500, Proteintech, 212151AP), anti-PAX7 (mouse, 1:20, DSHB), anti-Pax6 (mouse, 1:80, DSHB), anti-Sox2 (mouse, 1:50, R&D, MAB2018) and anti-TubβIII (mouse, 1:500, Merch, MAB1637). FActin was stained using fluorescein (FITC) phalloidin (1:80, Thermo Fisher Scientific, F432). Alexa Fluor 488 and 568 conjugated anti-mouse IgG and Alexa Fluor 488

and 568 conjugated anti-rabbit IgG were used as secondary antibodies at a final concentration of 1:1000 (Life Technologies). Nuclei were visualized using DAPI counterstain (1 μg/ml final concentration, Sigma-Aldrich). Samples were mounted onto glass slides using moviol mountant followed by image capture using a Nikon A1R confocal microscope or ZEISS AxioObserver z1 fluorescence microscope.

AM1-44 Labeling

Organoids were incubated with AM1-44 dye solution (10 μM, Biotium, 70038) in NB media for 30 seconds at room temperature. Under these conditions, the dye has been demonstrated to enter hair cells via mechanotransduction channels (Gale et al., 2001; Meyers et al., 2003; Herget et al., 2013). After incubation the sample was immediately fixed with 4% paraformaldehyde for 1 h on ice and incubated overnight at 4°C with 20% sucrose, embedded with O.C.T. compound and sectioned using a cryostat to obtain 12–14 μm sections. Nuclei were visualized using DAPI counterstain. Samples were mounted onto glass slides using moviol mountant followed by image capture using a ZEISS Observer z1 fluorescence microscope.

Helium Ion Microscopy

Samples were washed using DPBS and fixed with 2.5% paraformaldehyde/2.5% glutaraldehyde for 1 hour on ice. This was followed by sequential dehydration with ethanol (30, 50, 75, 85, 95, and 100%: 15 min washing). Fixed samples were then dried by means of a critical point drier (Balzers CPD 030, BAL-TEC) with performing 8 exchange cycles of CO_2. All additional fill, heating, and venting steps were performed at medium speed as well. After drying, the samples were carefully removed and adhered to double-sided copper tapes on aluminum stubs. Samples were imaged via the Helium Ion Microscope (HIM) (Carl Zeiss, Orion Nanofab) operating at an accelerating voltage of 30 and a beam current of ∼0.5 pA. No further metallic coating was performed since the HIM is armed with a very low voltage electron gun (flood gun) to compensate positive surface charge accumulation on the insulating biological samples. Under these experimental conditions, no obvious beam damage or change in morphology was observed on the samples surface. During imaging the electron beam energy and the X and Y deflectors were adjusted correspondingly to ensure that the best possible image could be obtained.

Kinocilia Length Measurement

To compare the length of longer stereocilia and kinocilia in RCCS-derived organoid and human fetal vestibular tissue, respectively, ImageJ software was used to estimate the measurements from images taken using HIM (Carl Zeiss, Orion Nanofab) by manually drawing straight lines along the cilia. Estimating the length of curved cilia was performed by drawing two straight lines which intersect at the inflection point of the cilium. An example is provided in **Supplementary Figure 3**. HIM pictures of the samples were taken at same magnification and inclination. The cilia length was documented in μm and the raw data of $n = 6$ measurements from $n = 1$ organoid and $n = 1$ fetal tissue are shown in **Supplementary Figure 3**. Cilia length data in **Figure 2** are shown as mean ± SD. For comparison of cilia length, statistical analysis was performed using GraphPad Prism 7 software. Data passed the Normality Test with Shapiro-Wilk method and alpha = 0.05, showing a normal distribution. Statistical analysis to compare the means of the cilia lengths from the organoid and fetal tissue was performed using the *T*-Test with Holm-Sidak method and alpha = 0.05.

Micro-Computed Tomography

Samples were washed with distilled water (Life Technologies) and placed on parafilm suspended in a CT scan tube and scanned with microCT (μCT50, Scanco Medical AG, Bruttisellen, Switzerland) at an energy of 55 kVp, an intensity of 72 μA, 0.5 mm Al filter, and an integration time of 1,500 ms, with a voxel resolution of 0.8 μm. Parafilm was also used to secure the samples from above and avoid dehydration. Contours were drawn to isolate samples from tube and parafilm. Data were filtered using a 3D constrained Gaussian filter with finite filter support (1 voxel) and filter width ($\sigma = 1.2$). A threshold was applied at 27% of the maximum grayscale value to separate the calcium components from the organoid and background. A second threshold from 10 to 26.9% was applied to separate the organoid from the background. In order to remove insignificant particles, morphometric component labeling was used to find all calcium components larger than 200 voxels (∼100 μm^3), and a histogram of the number of components and size of these components was produced. From this the mean component volume, as well as the largest and smallest components in a measurement were found. Additionally, the combined volume of all components in a measurement was calculated. The high resolution enabled capture of very small components, however, the organoid mass was too large to capture in its entirety at the same resolution; i.e., the data becomes too large to use. For this reason, measurements of some samples were made in two stacks. As organoids have a very low x-ray attenuation and are therefore difficult to segment, to avoid artifact detection, components smaller than 200 voxels were eliminated. This counteracted the issue, but in turn could also eliminate viable components of interest.

Electrophysiology

To perform recordings of inner ear organoids, vesicle-like structures were dissected, opened and flatted on a glass coverslip with the outer side facing up. A net was used to hold the organoid vesicle in place on the coverslip. The organoid vesicles are transferred to a recording chamber containing oxygenated Liebovitz's L15 cell culture medium (containing in mM; 1.26 $CaCl_2$, 0.98 $MgCl_2$, 0.81 $MgSO_4$, 5.33 KCl, 0.44 KH_2PO_4, 137.93 NaCl, 1.34 Na_2HPO_4, 5 Na-pyruvate; Life Technologies, Australia; pH 7.45, 305 mOsM) and perfused at a rate of 2 bath volumes/min. Whole cell patch clamp recordings were done using borosilicate glass microelectrodes (3–5 MOhm; King Precision Glass Inc., CA, USA) filled with potassium gluconate internal recording solution containing (in mM); 42 KCl, 98 K.gluconate, 4 HEPES, 0.5 EGTA, 1 $MgCl_2$, 5 Na.ATP. All experiments were done at room temperature (22°C). Recording from developing human fetal hair cells has been approved by The University of Newcastle Human Ethics Committee and was

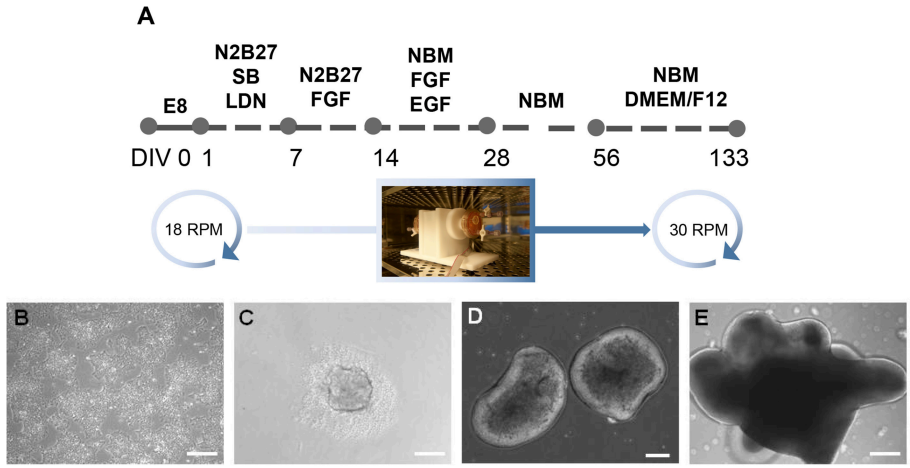

FIGURE 1 | Generation of inner ear organoids using the RCCS. **(A)** Schematic overview of RCCS protocol where an initial and final speed rotation of 18 and 30 RPM (rotations per minute) respectively, was applied. Photo of RCC set up in the tissue culture incubator was taken by Stefano Frausin (University of Melbourne). **(B)** HPSCs maintained as bulk culture at 0 DIV. **(C)** HPSCs-derived aggregate at DIV 1. HPSCs-derived organoids at **(D)** 14 and **(E)** 56 DIV. Scale bars, **(B,D,E)** 200 μm, **(C)** 100 μm.

done as previously described (Lim et al., 2014). Briefly, inner ears were isolated from the products of conception aged 12–14 weeks gestation in an ice-cold modified glycerol artificial cerebrospinal fluid (ACSF) containing (in mM) 250 glycerol, 26 $NaHCO_3$, 11 glucose, 2.5 KCl, 1.2 NaH_2PO_4, 1.2 $MgCl_2$, and 2.5 $CaCl_2$ bubbled with 5 % CO_2/95% O_2. The vestibular triad comprising the anterior and horizontal cristae ampullares and utricle were dissected and placed in the recording chamber. Recordings were made in Liebovitz'a L15 cell culture media, as described above for organoid vesicles. Cells were visualized using infrared differential interference contrast (IR-DIC) optics. Recordings were obtained using an Axopatch 200B amplifier running Axograph X software and sampled at 20 kHz and filtered at 2–10 kHz. Voltage protocols were used to characterize cell type. Instantaneous tail currents (at $t = 0$, when switched to −30 mV from membrane potential range −120 to +20 mV) were measured and used to plot activation and deactivation curves. These were fitted using the Boltzmann equation (Lim et al., 2011) to calculate G_{max}, the maximum conductance; $V_{½}$, potential at half-activation; and S, voltage required for an *e*-fold change in conductance. No correction was made for liquid junction potential (∼–4 mV) and no leak subtraction was used. The Shapiro-Wilk test for normality (SPSS) showed the majority of electrophysiological data were normally distributed. Consequently, data were analyzed using independent sample *t*-tests. G_{Max} data for Na^+ channels were not normally distributed and were analyzed using Mann U Whitney test. Data are described as mean values ± SD. "*n*" refers to the number of recorded cells.

Representative Data and Reproducibility

Derivation of organoids was replicated 7 times in independent experiments from 2 hES cell lines, H3 and H9, and 1 hPS cell line, 007-5, with a total of 38 organoids assessed for ATOH1 expression. Efficiency of our protocol was assessed through a semi-quantitative analysis of ATOH1 expression in hPSC-derived organoids at different timepoints (from 7 DIV to 133 DIV) as number of ATOH1+ clusters where each cluster counts >8–10 cells. Immunofluorescence images for hair cell markers, MYO7A and CTBP2, are representative of at least $n = 3$ organoids derived from $n > 3$ independent experiments.

RESULTS

Generation of Neural Organoids From hPSCs Using Microgravity

Our former study described a dynamic three dimensional (3D) RCCS to support derivation of neural organoids from hPSCs (Mattei et al., 2018). The RCCS was initially utilized at the National Aeronautics and Space Administration (NASA) to culture 3D cellular aggregates under microgravity in order to investigate the biological effects of such conditions on human tissues (Wolf and Schwarz, 1991). The RCCS offers advantages over other static organoid culture systems because it sustains long-term cultures by providing a continuous fluid flow that enables efficient transfer of oxygen and nutrients together with exchange of waste (Carpenedo et al., 2007). We previously reported that hPSC-derived neural organoids generated in the RCCS were biased to midbrain-hindbrain fate, as shown by upregulated expression of *ENGRAILED1*, *HOXA2,* and *GBX2* during neural induction (Mattei et al., 2018). Furthermore, as early as 14 days (14 DIV) within the RCCS, organoids develop as irregular shapes that later form numerous vesicular protrusions with a bright appearance surrounding an inner dense core (**Figure 1**). The described vesicular morphology, combined with previous observations reported by Hashino et al. (Liu et al., 2016; Koehler et al., 2017) and the dorsal specification of our hindbrain-committed organoids suggested by expression of PAX7 (**Supplementary Figure 1A**) encouraged us to further

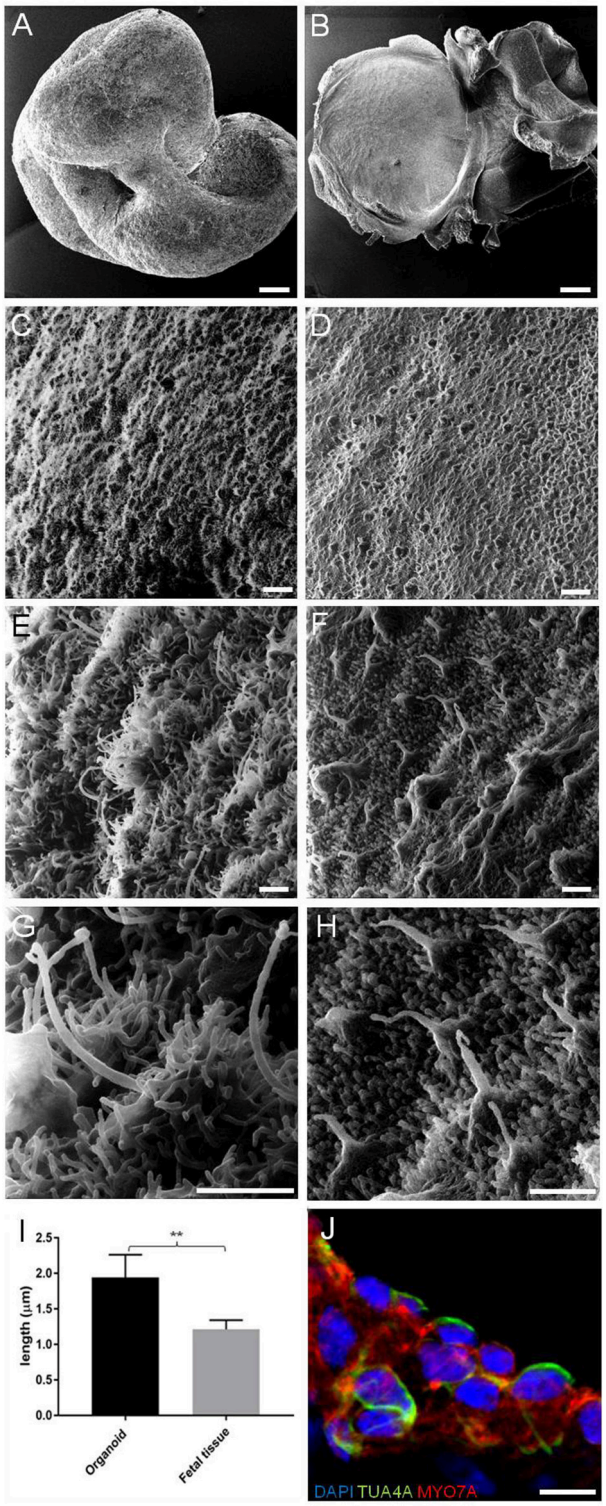

FIGURE 2 | HIM images of RCCS-derived organoids and human fetal utricle tissue. **(A)** Low magnification imaging of whole hESCs-derived organoid at 56 DIV. **(B)** Human fetal utricle at 10 weeks (∼day 70) of gestation. **(C,D)** Ciliated epithelium in organoid **(C)** and in macula of fetal utricle **(D)**. **(E–H)** High magnification images showing longer cilia on organoid's surface **(E,G)**

(Continued)

FIGURE 2 | resembling kinocilia in fetal utricle **(F,H)**. **(I)** Comparison of the mean (± SD) length of longer cilia in organoid and kinocilia in fetal tissue ($n = 6$ measurements each from one organoid and one fetal tissue) (**$p < 0.001$). *T*-Test was used to assess significance. **(J)** Hair cells in organoid expressing TUBA4A and MYO7A. Scale bars, **(A,B)** 100 μm, **(C,D)** 5 μm, **(E,F,G,H)** 1 μm, **(J)** 10 μm.

investigate the presence of dorsal hindbrain-derived structures such the inner ear tissue.

Organoids Are Enriched With Hair Cell-Like Cells on Their Outer Surface

We first investigated the ultrastructural morphology of our inner ear organoids at 56 days *in vitro* (DIV) using helium ion microscope (HIM; **Figure 2**). The HIM analyses revealed that the surface of the organoid consisted of a dense layer of ciliated cells (**Figure 2C**) protruding homogeneous bundles with occasional single longer cilia (**Figures 2E,G**). The surface morphology of the organoids closely resembled aspects of the human fetal vestibular apparatus aged 10 weeks gestation (∼70 days; **Figures 2B,D,F,H**), which corresponds to when vestibular hair cells express hair cell specific marker, myosin VIIa. However, cochlear hair cells don't express myosin VIIa until week 12 of gestation in human (Locher et al., 2013; Lim and Brichta, 2016). At high magnification, we observed single elongated cilia on surface of the organoid, similar in morphology to the kinocilia of human fetal utricular hair cells (**Figures 2G,H,I**). The kinocilium-like phenotype found within organoids was further supported by expression of alpha-acetylated tubulin (TUBA4A) in single, hair-like protrusions on the apical surface of the hair cells (**Figure 2L**; Lim and Brichta, 2016; Koehler et al., 2017).

Taken together, these data suggest hPSC-derived organoids are comprised of large populations of ciliated cells, consistent with the developing human inner ear.

Development of Inner Ear Accessory Structures Within Organoids

We also used HIM to assess morphological changes in organoids cultured for longer periods. High magnification imaging revealed that the surface of mature organoids at 98 DIV consist of some crystalline-like structures partially embedded in a loose filamentous matrix which resemble developing otoconial membrane and otoliths (**Figure 3A**). To further examine whether the structures were crystalline in their molecular structure, we employed micro-computed tomography (CT) of whole inner ear organoids at 70, 84, and 98 DIV time points. At all three timepoints, scans revealed mineral components within the organoids which increased in number (**Figure 3B**) and volume (**Figure 3C**) with time in culture. Mineral components were primarily located on the surface of the organoid surface, with a smaller number located internally (**Figures 3D,E**) (**Supplementary Table 2**). The three-dimensional reconstruction of imaged structures revealed irregular and crystalline-like shapes (**Figures 3D',E'**) that may resemble the typical barrel-shaped morphology of human otoconia (Sánchez-Fernández and Rivera-Pomar, 1984).

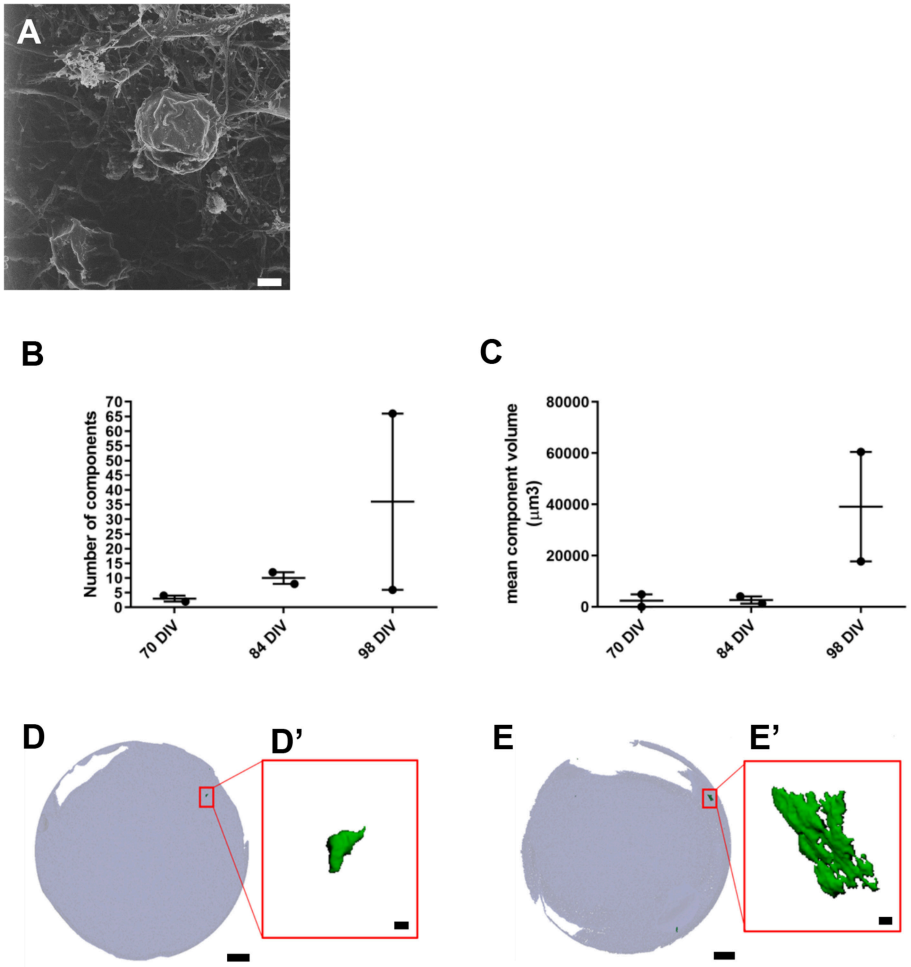

FIGURE 3 | Presence of inner ear crystalline structures in RCCS-derived organoids. **(A)** HIM image of organoid at 98 DIV shows the presence of a filamentous membrane covering the surface of organoid (arrow and otoconia-like structures (arrowhead). **(B–E)** Micro-computed tomography of organoids reveals the presence of mineral components suggestive of otoconia. Total component volume **(B)** and mean component volume **(C)** of organoids at 70, 84, and 98 DIV ($n = 2$ at each timepoint). Data shown as mean with range and individual values plotted. Representative micro-CT images of whole organoid scan at 70 DIV **(D)** and 98 DIV **(E)** and magnified three-dimensional reconstructions **(D',E')** of one mineral component. Scale bars, **(A)** 2 µm, **(D,E)** 200 µm, **(D',E')** 10 µm.

Overall these data provide novel evidence of inner ear vestibular-like phenotype of the hPSC-derived organoids with the presence of calcium carbonate otoconia, which are a distinguishing feature of vestibular system. Significantly, the presence of otoconia-like structures within the hPSC-derived organoids also demonstrates their capacity to form complex, multilayered structures analogous to human inner ear tissue.

RCCS-Derived Organoids Express Hair Cell Specific Markers Consistent With Inner Ear Development

Immunostaining analyses were performed on RCCS-derived organoids to examine expression of hair cell markers that are found in the developing human inner ear. High expression of myosin VIIa (MYO7A), a hair-cell specific marker, was observed within the organoid's cystic-like protrusions at 56 DIV (**Figures 4A,B**). Images of sectioned organoids at 35 DIV show an enriched population of cells positive for MYO7A and the hair cell ribbon synapse specific marker, CTBP2 (MYO7A+/CTBP2+) on the outer surface (**Figure 4C**). The expression of these hair cell markers on the surface of the organoid is consistent with results from HIM analyses. Interestingly, CTBP2 expression was predominantly localized to the nucleus (**Figure 4C'**). At a high magnification we observed several MYO7A+ cells showing a typical hair cell-like shape (**Figure 4E**) comparable with MYO7A+ hair cells in the human fetal vestibular system (**Figures 4D,D'**).

Immunostaining analyses of PAX2 and ATOH1 were also performed at earlier stages of organoid formation, which are key factors involved in otic placode formation and inner ear hair cell specification, respectively. Immunostaining of 7 DIV organoids show expression of PAX2 and ATOH1 particularly in the outer cellular layers (**Figures 4F,G**). ATOH1 expression

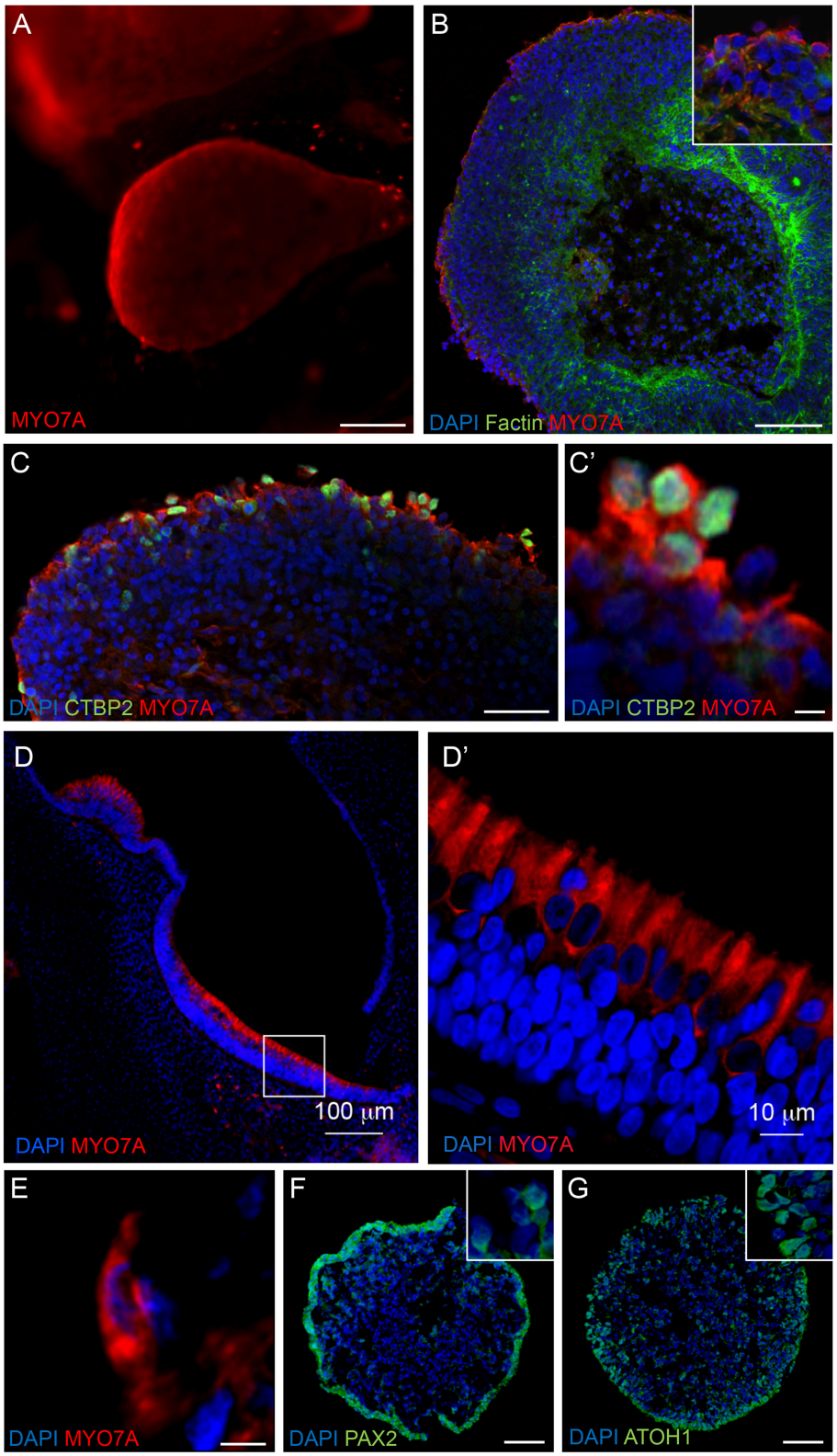

FIGURE 4 | Expression of hair cell and otic placode markers in RCCS-derived organoids. **(A)** HESC-derived organoids show MYO7A+ protrusions on surface at 56 DIV. **(B,C)** cells in the outer epithelium of vesicles expressing MYO7A and f-ACTIN **(B)** as well as CTBP2 **(C,C')** at 35 DIV. **(D–E)** Human fetal saccule at 11 WG

(Continued)

FIGURE 4 | consists of hair cells expressing MYO7A **(D)** which defines the typical cylindrical shape of type II hair cells **(D')** and similarly detected within organoid at 35 DIV **(E)**. **(F,G)** Expression of PAX2 **(F)** and ATOH1 **(G)** in occasional otic-pit-like clusters of cells in the outer epithelium of hiPSC-derived organoid at 7 DIV. Scale bars, **(A)** 200 μm, **(B,D)** 100 μm, **(C,F,G)** 50 μm, **(D')** 10 μm, **(C',E)** 5 μm.

persists long-term as it was also detected in organoids cultured up to 133 DIV (**Supplementary Table 1**).

Cells expressing PAX6, a neural progenitor marker, were also found within the organoids at 21 DIV (**Supplementary Figure 1B**), however, these cells were mainly localized within the internal regions of the organoids and separate to the PAX2+ pool (**Figure 4F**). Cells positive for SOX2 expression, a marker of supporting cells that surround inner ear hair cells and also in type II vestibular hair cells (Oesterle et al., 2008), were also observed in the organoids at 35 DIV (**Supplementary Figure 1C**). Consistent with expression of neural markers within younger organoids, high levels of βIII Tubulin expression was observed within the organoids at 49 DIV (**Supplementary Figure 1D**), which appeared to penetrate into the outer MYO7A+ sensory epithelial layer (**Supplementary Figure 1D'**).

Taken together, RCCS-derived organoids show expression of inner ear progenitor, hair cell, and neuronal markers at different time points of differentiation, suggesting that the growing organoids recapitulate aspects of inner ear development.

Functional Assessments of Organoid-Derived Hair Cells and Comparison to Human Fetal-Derived Vestibular Hair Cells

Patch clamp analyses were conducted to assess functional properties of organoid-derived hair cell-like cells in comparison with human fetal hair cells. We recorded from a total of 27 cells from organoids arising from three independent hPSC lines (H9, H3, and 007). In some organoids, infra-red differential interference contrast optics showed the presence of neuroepithelial-like rosettes (**Figure 5A**, left), which contained hair cell-like cells. Human fetal vestibular hair cells are shown in **Figure 5A** (right). We are not able to definitively determine vestibular hair cell type by morphology in human vestibular neuroepithelium at any stage of development examined (10–16 WG). However, using a voltage-activated protocol (**Figure 5B**, inset) we are able to determine whether a hair cell has type I, or type II vestibular hair cell characteristics, or non-hair cell characteristics. Of the 27 recorded cells from organoids, 15 had whole cell conductances consistent with those from mammalian type II vestibular hair cells. Our analysis focused on these 15 organoid cells with type II vestibular hair cell like characteristics. In our recordings from organoid cells (aged between 10 and 17 weeks in culture) there was no evidence of any cells possessing the type I hair cell specific $G_{K,L}$ conductance (●). Neither the organoid cell aged 17 weeks in culture or vestibular hair cell aged 14 weeks gestation showed type I hair cell characteristics (**Figure 5B**). Using the protocol with hyperpolarizing prepulse (−120 mV) and a ladder of voltages from −120 to +20 mV (inset), we observe in both organoid cells and developing human hair cells, fast outward currents that are consistent with K^+ currents. Of the 15 organoid cells, 20% had outward K^+ currents that inactivated by 10% from peak maximum amplitude to steady state amplitude at +20 mV (**Figure 5B**, left). Tail currents (*) also showed the presence of an A-like current (outlined inset), in a subset of organoid cells with otherwise type II hair cell characteristics. Using the type II hair cell voltage-activation protocol (**Figure 5C**, inset), a series of depolarizing steps from −120 to +20 mV shows outward currents, consistent with K^+ currents in both organoid cells and developing human vestibular hair cells. There is variation in the maximum peak current amplitude at +20 mV between organoid cells and developing human hair cells. Analysis of tail currents after stepping from a test voltage (−120 to +20 mV) to −30 mV in organoid cells and developing hair cells showed significant differences in G_{MAX} between organoid cells (2.25 ± 0.28 nS, $n = 6$) and hair cells (5.55 ± 0.08 nS, $n = 10$, $p < 0.05$) (**Figure 5D**; **Supplementary Table 3**). Normalized fits of the conductance—voltage data also showed that organoid cells had more depolarized $V_{½}$ compared to developing human vestibular hair cells (organoid cells: 2.60 ± 0.62 mV, $n = 6$ vs. human hair cells:−19.58 ± 0.38 mV, $n = 10$, $p < 0.05$) but similar slopes (organoid cells: 7.10 ± 0.47 nS.mV, $n = 6$, human hair cells: 6.24 ± 0.35 nS.mV, $n = 10$, $p > 0.05$). A total of 9 (of 15) organoid cells showed the presence of fast activating, fast inactivating inward currents that are consistent with Na^+ currents (**Figure 5E**, left) that are also present in developing rodent (Wooltorton et al., 2007) and human vestibular hair cells (**Figure 5E**, right; Lim et al., 2014). The conductance of presumptive Na^+ channels in organoid cells was higher than those in human vestibular hair cells but were not statistically significantly different (G_{MAX} = 10.93 ± 0.45 nS, $n = 9$ vs. 5.82 ± 0.17, $n = 10$, respectively, U = 33, $p = 0.327$). Normalized fits of the presumptive Na^+ conductance—voltage plots showed organoid cells were significantly more depolarized $V_{½}$ than human hair cells (organoid cells: −18.45 ± 0.64 mV, $n = 9$, human hair cells −36.5 ± 0.62 mV, $n = 10$, $p < 0.05$) but similar slopes (organoid cells; 5.36 ± 0.60 nS.mV, $n = 9$ vs. human hair cells 5.32 ± 0.54 nS.mV, $n = 10$, $p > 0.05$) (**Figure 5F**; **Supplementary Table 3**). These electrophysiological results show voltage-activated currents between human derived hPSCs organoids and human fetal vestibular hair cells are similar.

Active mechanotransduction channels may be detected by examining cellular uptake of styryl dye AM1-44 (Gale et al., 2001; Meyers et al., 2003; Herget et al., 2013). Brief application of AM1-44 to organoids (84 DIV) showed fluorescence was present in distinct and discrete cellular regions at the organoids' surface (**Supplementary Figure 2**). These results suggest active mechanotransduction channels may be present in organoids, however this needs to be validated with additional studies such as recording currents elicited from controlled mechanical stimulation.

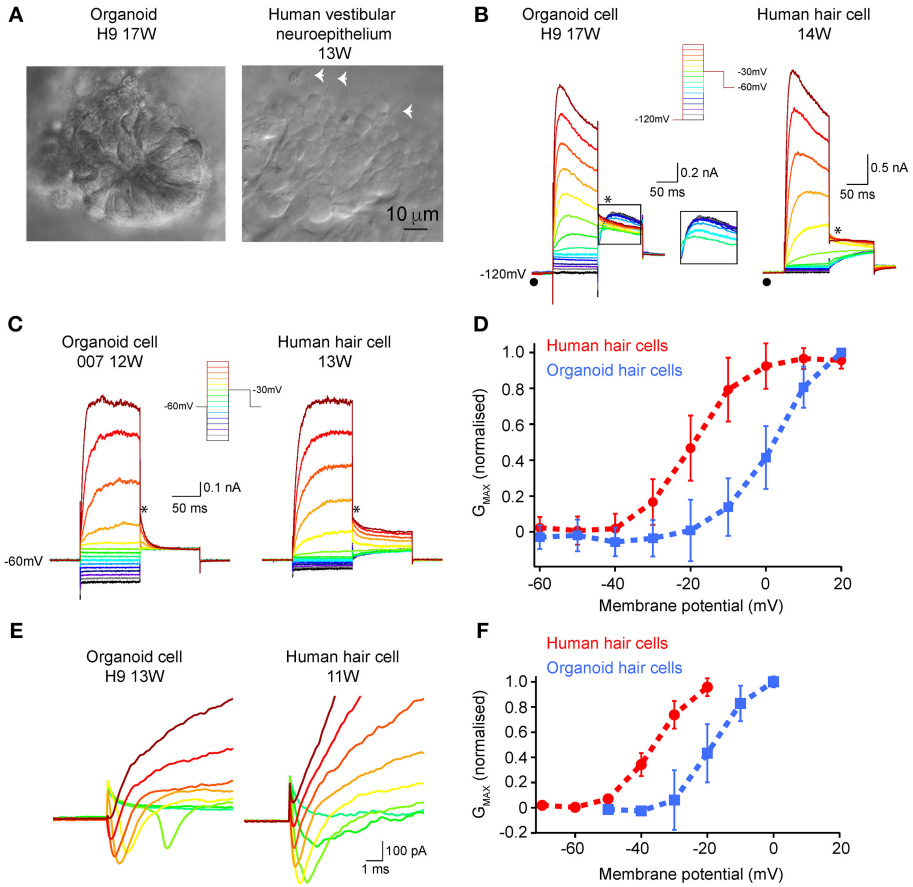

FIGURE 5 | Electrophysiological characterization of hair-cell like organoid cells and human fetal vestibular hair cells. **(A)** Infra-red differential interference contrast optics images of organoids and human vestibular epithelium aged 17 weeks in culture and 13 weeks gestation, respectively. The white arrowheads in right panel show hair bundles. **(B)** Using a hyperpolarizing pre-pulse to −120 mV (inset), organoid cells (left) and human vestibular hair cells (right) show fast activating outward currents, presumably K^+ currents which vary in amplitude. The pre-pulse to −120 mV (λ) does not elicit the type I hair cell specific $G_{K,I}$ current in any organoid or human fetal hair cells. In some organoid cells there is evidence for an "A-like" current when analyzing tail currents (*), that is not observed in developing human hair cells. **(C)** Using a type-II hair cell voltage protocol (inset), organoid cells, and human hair cells have similar characteristics, with outward currents that are inactivating. Tail currents were measured (*) and used to calculate Gmax, $V_{1/2}$, and slope. **(D)** Normalized conductance– voltage plots of tail currents recorded in organoid cells ($n = 6$ cells; blue line) and human fetal hair cells ($n = 10$ cells; red line) show differences in $V_{1/2}$. Data are mean ± SD **(E)** Inward presumptive Na^+ currents in organoid (left) and human vestibular hair cells (right) aged 11 weeks and 13 weeks respectively. **(F)** Normalized conductance—voltage plots of inward Na^+ currents show more depolarized $V_{1/2}$ in organoid cells ($n = 9$ cells; blue line) compared to human fetal hair cells ($n = 10$ cells; red line), while slopes are similar. Data are mean ± SD.

DISCUSSION

Investigators worldwide recognize the value of hPSCs and more recently, the dynamic 3D culture systems, as unique means for *in vitro* modeling. While overcoming technical limitations is an ongoing challenge, important findings for developmental studies and *in vitro* disease modeling have been achieved for several tissues of interest, including neural tissue (Kadoshima et al., 2013; Lancaster et al., 2013; Mariani et al., 2015; Muguruma et al., 2015; Qian et al., 2016; Birey et al., 2017; Kuwahara et al., 2017). This includes generation of inner ear organoids from mouse and human PSC first reported by Hashino and colleagues (Liu et al., 2016; Koehler et al., 2017). These studies used an ATOH-1 reporter cell line to monitor hair cell development in mouse and subsequently in human PSC derived-organoids alongside immunohistochemical and electrophysiological analyses. Here, we demonstrate that inner ear organoids can also be generated from hPSC using RCCS, however with some significant advancements. Using HIM, micro-computed tomography, and electrophysiology we show unique structural, functional, and phenotypic properties of immature vestibular hair cells and associated otoconia that closely resemble the human fetal vestibular system. To the best of our knowledge, this is the first study to directly compare structural and functional properties of hPSC-derived inner ear organoids with human fetal vestibular tissue. Significantly, we also describe the formation of otoconia, thereby demonstrating a more structurally complete model of inner ear development.

The formation and maturation of RCCS hPSC-derived organoids mimic distinct stages of human inner ear development with a similar temporal profile. The human inner ear first arises from a patch of otic placode progenitors surrounding

the rhombomere 5 of dorsal hindbrain (Bruska et al., 2009). Similarly, a layer of cells expressing PAX2, an otic placode marker, were identified on the surface of organoids during the first week of neural induction. By 3 weeks in culture, vesicle protrusions were forming from the organoid, which may mimic the otic-like vesicles observed in human fetal inner ear (Koehler et al., 2017). Expression of ATOH1 is crucial for all stages of inner ear development, thereby being a major marker for tracking hair cell induction and maturation (Bermingham et al., 1999; Shailam et al., 1999). Using immunofluorescence analyses, ATOH1 expression was observed within the hPSC-derived organoids at several time points in culture ranging from 7 to 133 DIV. During neural induction stages, ATOH1 shows a similar spatial expression to PAX2, which may be associated with induction of otic placode like-progenitors. Of note, ATOH1 expression is detected in at least 58% of organoids, demonstrating the efficiency and robustness of the RCCS protocol for deriving hindbrain-like organoids that supports inner ear specification. Maturation of hPSC-derived hair cells within the organoid vesicles followed an inside-out radial differentiation pattern, whereby MYO7A+ cells were mainly found on the outer edge of vesicles and βIII tubulin-expressing neurons within the vesicle/organoid center. This pattern is contrary to *in vivo* inner ear development and may be caused by the physical forces of fluid flow imposed on the organoids generated by a rotating system, which may affect tissue polarization as previously described (Chen et al., 2000; Helmke and Davies, 2002; Helmke, 2005; Mammoto and Ingber, 2010). The neuronal-epithelial regions found in the organoids is consistent with inner ear development whereby the vestibular nerve begins to innervate the undifferentiated sensory epithelium by 7 WG (Lim and Brichta, 2016). The neuronal component may arise from the PAX6+ pool detected within the younger organoids, further supporting a model of inner ear neurogenesis.

HIM showed a dense layer of ciliated hair-like cells spanning across the surface of the organoid at 56 DIV. The images clearly showed the presence of kinocilia, a unique feature of vestibular hair cells on the organoid surface that closely resembled the morphology of human fetal vestibular tissue at ∼70 days gestation. It should be noted that during development, auditory hair cells also express a long stereocilia, resembling a kinocilium, however these are lost during development beginning at 24 weeks gestation (Igarashi, 1980; Lavigne-Rebillard and Pujol, 1986) and are not found in mature adult human cochlea. The maturation of hair cell-like cells was shown by functional MET channels and voltage-activated currents. While stereocilia have been described in electron microscopy studies of inner ear, few have described vestibular hair cell development of tip links where MET channels are localized. However, tip links and therefore presumably MET channels, are present by 14 WG in cochlea hair cells (Igarashi, 1980; Rhys Evans et al., 1985), which is consistent with AM1-44 results from organoids.

Electrophysiological analyses from organoid-derived cells shows these cells are electrically active and express a number of different ion channels. Organoid cells showed the presence of voltage-gated Na^+ and K^+ channels in hair cells. Typically, voltage activated K^+ conductances in organoid like cells resemble those recorded from human fetal type II hair cells (Lim et al., 2014). The conductance of K^+ channels in fetal hair cells was greater than organoid cells suggesting a higher proportion of functional K^+ channels in fetal hair cells at the ages examined. Interestingly, however there was also a subset of organoid cells that also have a fast activating and fast inactivating outward K^+ current that are consistent with "A-like" currents that are not observed in fetal human hair cells. A-like currents however, have been recorded from isolated adult human vestibular hair cells (Oghalai et al., 1998). Like human fetal hair cells (Lim et al., 2014) and developing rat hair cells (Wooltorton et al., 2007), there were also a subset of organoid cells that expressed Na^+ conductances. However, the kinetics of Na^+ channel activation was more depolarized in organoid cells than human fetal or developing rodent vestibular hair cells. These electrophysiological results from organoid cells supported anatomical findings which showed immunofluorescent labeling of hair cell specific markers and MET channel results. Importantly, comparing the results from organoid cells to human fetal vestibular hair cells shows organoids derived from RCCS are functional and express a heterogeneity of hair cell types.

Following maturation of hair cell-like cells, using micro-computed tomography, we were able to detect increasing amounts of mineral deposits within the growing organoids that are consistent with formation of inner ear otoconia which are detected in human fetal tissue as early as 7 WG with the otoconial membrane being fully mature by 22 WG (Lim and Brichta, 2016). Loss and dislodgement of otoconia have been associated with benign paroxysmal positional vertigo, age-related dizziness, and in response to trauma, particularly blast induced trauma (Ross et al., 1976; Lim, 1984; Thalmann et al., 2001; Jang et al., 2006; Zalewski, 2015). The capacity of the RCC hPSC-derived organoids to promote the development of otoconia may serve as a pioneering approach to model vestibular pathologies that involve otoconia.

Generation of organoids showing an inner-ear phenotype was performed under microgravity conditions, despite the organoids being fated toward a cortical phenotype using dual SMAD inhibitors. We and others have previously showed that microgravity may influence stem cell differentiation and signaling (Chiang et al., 2012; Lei et al., 2014; Mattei et al., 2018). It is not well understood how microgravity may influence cell fate and differentiation, however activation of Wnt signaling has been suggested to be involved (Lei et al., 2014) which is required for hindbrain development. Given the efficiency of ATOH1 expression, our findings suggest that RCCS may be a highly suitable platform for deriving cells of hindbrain lineages, such as the inner ear. Further studies are needed to determine how microgravity may enable stem cell/progenitor differentiation toward a hindbrain phenotype, which also provides insight into understanding inner ear development.

In summary, these data demonstrate efficient generation of organoids from hPSC using microgravity, which recapitulate some key structural and developmental components of human inner ear development, including the formation of functional vestibular-like hair cells, neurons, and otoconia. These findings support the RCCS system to be a valuable platform for further advancing complex *in vitro* models of the human vestibular system.

DATA AVAILABILITY

All datasets generated for this study are included in the manuscript and/ or the supplementary files.

ETHICS STATEMENT

This study was carried out in accordance with the recommendations of Australian National Health and Medical Research guidelines with written informed consent from all subjects. All subjects gave written informed consent in accordance with the Declaration of Helsinki. The protocol was approved by University of Melbourne Human Ethics committee (#1545384 and 1545394) for use of human pluripotent stem cell lines and recordings from developing human fetal hair cells has been approved by The University of Newcastle Human Ethics Committee (#H-693-0608 and H-569-0503).

AUTHOR CONTRIBUTIONS

CM: conception and design, collection and assembly of data, data analysis and interpretation, manuscript writing, final approval of manuscript. RL, GD, KS, and BAN: conception and design, financial support, provision of study material, collection, and assembly of data, data analysis and interpretation, manuscript writing, final approval of manuscript. HD and ZL: collection and assembly of data, data analysis and interpretation, final approval of manuscript. BN: provision of study material, collection and assembly of data, data analysis and interpretation, final approval of manuscript. MT: administrative support, provision of study material, data analysis and interpretation, final approval of manuscript. MD: conception and design, financial support, administrative support, provision of study material, collection and assembly of data, data analysis and interpretation, manuscript writing, final approval of manuscript.

FUNDING

This study was supported by the University of Melbourne and Melbourne International Research Scholarship (CM), Australian Research Council Future Fellowship (MD; FT130100514), Garnett Passe and Rodney William Memorial Foundation Research Scholarship (BAN), ARC Stem Cells Australia and NHMRC Project Grant (RL; APP1048232). The helium ion microscopy and confocal microscopy were performed at the Materials Characterization and Fabrication Platform (MCFP) at the University of Melbourne.

ACKNOWLEDGMENTS

We acknowledge Dr Tomoko Hyakumura for her technical assistance embedding and cutting the human vestibular material.

SUPPLEMENTARY MATERIAL

The Supplementary Material for this article can be found online at: https://www.frontiersin.org/articles/10.3389/fcell.2019.00025/full#supplementary-material

Supplementary Figure 1 | Expression profile of RCCS-derived organoids**. (A–C)** HESC-derived organoids show expression of dorsal hindbrain marker PAX7 **(A)** and neural marker PAX6 **(B)** at 21 DIV as well as supporting hair cell marker SOX2 **(C)** at 35 DIV, where white dash line delineates organoid boundary. **(D)** TUBβIII neural mass in hESC-derived organoid at 49 DIV with some processes spreading up to the outer surface and **(D')** infiltrating a MYO7A+ sensory epithelium. Scale bars, **(A,C)** 20 μm, **(B,D)** 50 μm, **(C,D')** 10 μm.

Supplementary Figure 2 | Mechanotransduction of RCCS-derived organoids. HESC-derived organoid at 84 DIV is capable of uptake AM1-44 dye. Scale bar, 10 μm.

Supplementary Figure 3 | Kinocilia length measurements. An example of procedure used for estimating kinocilium length in **(A)** organoid and **(B)** fetal tissue. Straight lines were drawn along the cilia (dash lines in red) to estimate the length. **(C)** Raw data of $n = 6$ kinocilium measurements each for an organoid and fetal tissue as plotted in **Figure 2I**. Scale bar, 1 μm.

Supplementary Table 1 | Expression efficiency of ATOH1 in inner ear organoids. ATOH1 expression in organoids derived from hPSC lines (H3 hESC, H9 hESC and 007–5 iPSC lines) in n=7 biological replicate experiments from 7 to 133 DIV. 58% of organoids showed ATOH1 expression.

Supplementary Table 2 | Volume of components in each measurement by micro-computed tomography. The table shows the total number of components, as well as the mean, smallest and largest component volumes in each measurement, and the combined total volume of all components in a measurement. The two measurements (scans) of any single sample have not been pooled.

Supplementary Table 3 | G_{Max}, $V_{½}$, and slope values of IV relationship of K^+ and Na^+ currents in organoid and human hair cells. Unless otherwise specified, all statistical analyses were independent sample *t*-tests. $^*p < 0.05$, + Mann U Whitney statistical analysis.

REFERENCES

Bermingham, N. A., Hassan, B. A., Price, S. D., Vollrath, M. A., Ben-Arie, N., Eatock, R. A., et al. (1999). Math1: an essential gene for the generation of inner ear hair cells. *Science* 284, 1837–1841. doi: 10.1126/science.284.5421.1837

Birey, F., Andersen, J., Makinson, C. D., Islam, S., Wei, W., Huber, N., et al. (2017). Assembly of functionally integrated human forebrain spheroids. *Nature* 545, 54–59. doi: 10.1038/nature22330

Bruska, M., Ulatowska-Blaszyk, K., Weglowski, M., Wozniak, W., and Piotrowski, A. (2009). Differentiation of the facio-vestibulocochlear ganglionic complex in human embryos of developmental stages 13–15. *Folia Morphol.* 68, 167–173. Available online at: http://citeseerx.ist.psu.edu/viewdoc/download?doi=10.1.1.1014.1356&rep=rep1&type=pdf

Carpenedo, R. L., Sargent, C. Y., and McDevitt, T. C. (2007). Rotary suspension culture enhances the efficiency, yield, and homogeneity of embryoid body differentiation. *Stem Cells* 25, 2224–2234. doi: 10.1634/stemcells.2006-0523

Chen, N. X., Ryder, K. D., Pavalko, F. M., Turner, C. H., Burr, D. B., Qiu, J., et al. (2000). Ca(2+) regulates fluid shear-induced cytoskeletal reorganization and gene expression in osteoblasts. *Am. J. Physiology. Cell Physiol.* 278, C989–C997. doi: 10.1152/ajpcell.2000.278.5.C989

Chiang, M.C., Lin, H., Cheng, Y.C., Yen, C.H., Huang, R.N., and Lin, K.H. (2012). Beta-adrenoceptor pathway enhances mitochondrial function in human neural stem cells via rotary cell culture system. *J. Neurosci. Methods* 207, 130–136. doi: 10.1016/j.jneumeth.2012.04.005

Gale, J. E., Marcotti, W., Kennedy, H. J., Kros, C. J., and Richardson, G. P. (2001). FM1-43 dye behaves as a permeant blocker of the

hair-cell mechanotransducer channel. *J. Neurosci.* 21, 7013–7025. doi: 10.1523/JNEUROSCI.21-18-07013.2001

Helmke, B. P. (2005). Molecular control of cytoskeletal mechanics by hemodynamic forces. *Physiology* 20, 43–53. doi: 10.1152/physiol.00040.2004

Helmke, B. P., and Davies, P. F. (2002). The cytoskeleton under external fluid mechanical forces: hemodynamic forces acting on the endothelium. *Ann. Biomed. Eng.* 30, 284–296. doi: 10.1114/1.1467926

Herget, M., Scheibinger, M., Guo, Z., Jan, T. A., Adams, C. M., Cheng, A. G., et al. (2013). A simple method for purification of vestibular hair cells and non-sensory cells, and application for proteomic analysis. *PLoS ONE* 8:e66026. doi: 10.1371/journal.pone.0066026

Hernández, D., Millard, R., Sivakumaran, P., Wong, R. C., Crombie, D. E., Hewitt, A. W., et al. (2016). Electrical stimulation promotes cardiac differentiation of human induced pluripotent stem cells. *Stem Cells Int.* 2016:1718041. doi: 10.1155/2016/1718041

Igarashi, Y. (1980). Cochlea of the human fetus: a scanning electron microscope study. *Arch. Histol. Jpn.* 43, 195–209. doi: 10.1679/aohc1950.43.195

Jang, Y. S., Hwang, C. H., Shin, J. Y., Bae, W. Y., and Kim, L. S. (2006). Age-related changes on the morphology of the otoconia. *Laryngoscope* 116, 996–1001. doi: 10.1097/01.mlg.0000217238.84401.03

Kadoshima, T., Sakaguchi, H., Nakano, T., Soen, M., Ando, S., Eiraku, M., et al. (2013). Self-organization of axial polarity, inside-out layer pattern, and species-specific progenitor dynamics in human ES cell-derived neocortex. *Proc. Natl. Acad. Sci. U.S.A.* 110, 20284–20289. doi: 10.1073/pnas.1315710110

Koehler, K. R., Nie, J., Longworth-Mills, E., Liu, X. P., Lee, J., Holt, J. R., et al. (2017). Generation of inner ear organoids containing functional hair cells from human pluripotent stem cells. *Nat. Biotechnol.* 35, 583–589. doi: 10.1038/nbt.3840

Kuwahara, A., Nakano, T., and Eiraku, M. (2017). Generation of a three-dimensional retinal tissue from self-organizing human ESC culture. *Methods Mol. Biol.* 1597, 17–29. doi: 10.1007/978-1-4939-6949-4_2

Lancaster, M. A., Renner, M., Martin, C. A., Wenzel, D., Bicknell, L. S., Hurles, M. E., et al. (2013). Cerebral organoids model human brain development and microcephaly. *Nature* 501, 373–379. doi: 10.1038/nature12517

Lavigne-Rebillard, M., and Pujol, R. (1986). Development of the auditory hair cell surface in human fetuses. a scanning electron microscopy study. *Anat. Embryol.* 174, 369–377. doi: 10.1007/BF00698787

Lei, X., Deng, Z., Zhang, H., Zhao, H., Zhou, J., Liu, S., et al. (2014). Rotary suspension culture enhances mesendoderm differentiation of embryonic stem cells through modulation of Wnt/beta-catenin pathway. *Stem Cell Rev.* 10, 526–538. doi: 10.1007/s12015-014-9511-6

Lim, D. J. (1984). Otoconia in health and disease. a review. *Ann. Otol. Rhinol. Laryngol. Suppl.* 112, 17–24. doi: 10.1177/00034894840930S404

Lim, R., and Brichta, A. M. (2016). Anatomical and physiological development of the human inner ear. *Hear. Res.* 338, 9–21. doi: 10.1016/j.heares.2016.02.004

Lim, R., Drury, H. R., Camp, A. J., Tadros, M. A., Callister, R. J., and Brichta, A. M. (2014). Preliminary characterization of voltage-activated whole-cell currents in developing human vestibular hair cells and calyx afferent terminals. *J. Assoc. Res. Otolaryngol.* 15, 755–766. doi: 10.1007/s10162-014-0471-y

Lim, R., Kindig, A. E., Donne, S. W., Callister, R. J., and Brichta, A. M. (2011). Potassium accumulation between type I hair cells and calyx terminals in mouse crista. *Exp. Brain Res.* 210, 607–621. doi: 10.1007/s00221-011-2592-4

Liu, X. P., Koehler, K. R., Mikosz, A. M., Hashino, E., and Holt, J. R. (2016). Functional development of mechanosensitive hair cells in stem cell-derived organoids parallels native vestibular hair cells. *Nat. Commun.* 7:11508. doi: 10.1038/ncomms11508

Locher, H., Frijns, J. H., van Iperen, L., de Groot, J. C., Huisman, M. A., and Chuva de Sousa Lopes, S. M. (2013). Neurosensory development and cell fate determination in the human cochlea. *Neural Dev.* 8:20. doi: 10.1186/1749-8104-8-20

Mammoto, T., and Ingber, D. E. (2010). Mechanical control of tissue and organ development. *Development* 137, 1407–1420. doi: 10.1242/dev.024166

Mariani, J., Coppola, G., Zhang, P., Abyzov, A., Provini, L., Tomasini, L., et al. (2015). FOXG1-Dependent dysregulation of GABA/glutamate neuron differentiation in autism spectrum disorders. *Cell* 162, 375–390. doi: 10.1016/j.cell.2015.06.034

Mattei, C., Alshawaf, A., D'Abaco, G., Nayagam, B., and Dottori, M. (2018). Generation of neural organoids from human embryonic stem cells using the rotary cell culture system: effects of microgravity on neural progenitor cell fate. *Stem Cells Dev.* 27, 848–857. doi: 10.1089/scd.2018.0012

Meyers, J. R., MacDonald, R. B., Duggan, A., Lenzi, D., Standaert, D. G., Corwin, J. T., et al. (2003). Lighting up the senses: FM1-43 loading of sensory cells through nonselective ion channels. *J. Neurosci.* 23, 4054–4065. doi: 10.1523/JNEUROSCI.23-10-04054.2003

Muguruma, K., Nishiyama, A., Kawakami, H., Hashimoto, K., and Sasai, Y. (2015). Self-organization of polarized cerebellar tissue in 3D culture of human pluripotent stem cells. *Cell Rep.* 10, 537–550. doi: 10.1016/j.celrep.2014.12.051

Oesterle, E. C., Campbell, S., Taylor, R. R., Forge, A., and Hume, C. R. (2008). Sox2 and JAGGED1 expression in normal and drug-damaged adult mouse inner ear. *J. Assoc. Res. Otolaryngol.* 9, 65–89. doi: 10.1007/s10162-007-0106-7

Oghalai, J. S., Holt, J. R., Nakagawa, T., Jung, T. M., Coker, N. J., Jenkins, H. A., et al. (1998). Ionic currents and electromotility in inner ear hair cells from humans. *J. Neurophysiol.* 79, 2235–2239. doi: 10.1152/jn.1998.79.4.2235

Ohnishi, H., Skerleva, D., Kitajiri, S., Sakamoto, T., Yamamoto, N., Ito, J., et al. (2015). Limited hair cell induction from human induced pluripotent stem cells using a simple stepwise method. *Neurosci. Lett.* 599, 49–54. doi: 10.1016/j.neulet.2015.05.032

Qian, X., Nguyen, H. N., Song, M. M., Hadiono, C., Ogden, S. C., Hammack, C., et al. (2016). Brain-region-specific organoids using mini-bioreactors for modeling ZIKV exposure. *Cell* 165, 1238–1254. doi: 10.1016/j.cell.2016.04.032

Rhys Evans, P. H., Comis, S. D., Osborne, M. P., Pickles, J. O., and Jeffries, D. J. (1985). Cross-links between stereocilia in the human organ of Corti. *J. Laryngol. Otol.* 99, 11–19. doi: 10.1017/S0022215100096237

Ronaghi, M., Nasr, M., Ealy, M., Durruthy-Durruthy, R., Waldhaus, J., Diaz, G. H., et al. (2014). Inner ear hair cell-like cells from human embryonic stem cells. *Stem Cells Dev.* 23, 1275–1284. doi: 10.1089/scd.2014.0033

Ross, M. D., Peacor, D., Johnsson, L. G., and Allard, L. F. (1976). Observations on normal and degenerating human otoconia. *Ann. Otol. Rhinol. Laryngol.* 85, 310–326. doi: 10.1177/000348947608500302

Sánchez-Fernández, J. M., and Rivera-Pomar, J. M. (1984). A scanning electron microscopy study on human otoconia genesis. *Acta Otolaryngol.* 97, 479–488. doi: 10.3109/00016488409132925

Shailam, R., Lanford, P. J., Dolinsky, C. M., Norton, C. R., Gridley, T., and Kelley, M. W. (1999). Expression of proneural and neurogenic genes in the embryonic mammalian vestibular system. *J. Neurocytol.* 28, 809–819. doi: 10.1023/A:1007009803095

Thalmann, R., Ignatova, E., Kachar, B., Ornitz, D. M., and Thalmann, I. (2001). Development and maintenance of otoconia: biochemical considerations. *Ann. N. Y. Acad. Sci.* 942, 162–178. doi: 10.1111/j.1749-6632.2001.tb03743.x

Wolf, D. A., and Schwarz, R. P. (1991). Analysis of gravity-induced particle motion and fluid perfusion flow in the NASA-designed rotating zero-head-space tissue culture vessel. *NASA Technical Paper,* p. 3143.

Wooltorton, J. R., Gaboyard, S., Hurley, K. M., Price, S. D., Garcia, J. L., Zhong, M., et al. (2007). Developmental changes in two voltage-dependent sodium currents in utricular hair cells. *J. Neurophysiol.* 97, 1684–1704. doi: 10.1152/jn.00649.2006

Zalewski, C. K. (2015). Aging of the human vestibular system. *Semin. Hear.* 36, 175–196. doi: 10.1055/s-0035-1555120

Conflict of Interest Statement: The authors declare that the research was conducted in the absence of any commercial or financial relationships that could be construed as a potential conflict of interest.

frontiers in Physiology

ORIGINAL RESEARCH
published: 11 April 2019
doi: 10.3389/fphys.2019.00422

Self-Assembly of an Organized Cementum-Periodontal Ligament-Like Complex Using Scaffold-Free Tissue Engineering

*Avik Basu[1], Kristi Rothermund[1], Meer N. Ahmed[1] and Fatima N. Syed-Picard[1,2,3]**

[1]Department of Oral Biology and Center for Craniofacial Regeneration, School of Dental Medicine, University of Pittsburgh, Pittsburgh, PA, United States, [2]Department of Bioengineering, Swanson School of Engineering, University of Pittsburgh, Pittsburgh, PA, United States, [3]McGowan Institute for Regenerative Medicine, Pittsburgh, PA, United States

OPEN ACCESS

Edited by:
Thimios Mitsiadis, University of Zurich, Switzerland

Reviewed by:
Monica Mattioli-Belmonte, Polytechnical University of Marche, Italy
Giovanna Orsini, Polytechnical University of Marche, Italy

***Correspondence:**
Fatima N. Syed-Picard
syedpicard@pitt.edu

Specialty section:
This article was submitted to Craniofacial Biology and Dental Research, a section of the journal Frontiers in Physiology

Received: *08 January 2019*
Accepted: *27 March 2019*
Published: *11 April 2019*

Citation:
Basu A, Rothermund K, Ahmed MN and Syed-Picard FN (2019) Self-Assembly of an Organized Cementum-Periodontal Ligament-Like Complex Using Scaffold-Free Tissue Engineering. Front. Physiol. 10:422. doi: 10.3389/fphys.2019.00422

A major challenge in regenerating periodontal tissues is emulating its complex structure containing both mineralized and soft tissues. In this study, scaffold-free tissue constructs engineered using periodontal ligament cells (PDLCs), which contain a population of adult stem/progenitor cells, self-assembled into an organized multi-tissue structure comprising a mineralized cementum-like core enclosed within a periodontal ligament (PDL)-like tissue. Scaffold-free engineered constructs were formed by culturing human PDLCs to form a cell sheet on six-well dishes containing two minutien pins placed 7 mm apart. The cell sheet was contracted by the cells to roll into the pins forming a cylindrical construct anchored on either end by the pins. These tissues were approximately 1 mm in diameter and 7 mm long and contained only the cells and their endogenous matrix. These scaffold-free engineered constructs exhibited two structurally distinct tissues, one in the center of the construct and another on the periphery. The center tissue was mineralized and expressed alkaline phosphatase and bone sialoprotein, similar to cementum. The peripheral tissue was not calcified and expressed periodontal ligament-associated protein-1 and periostin, which is characteristic of the periodontal ligament. This tissue organization was seen after *in vitro* culture and maintained *in vivo* following subcutaneous implantation in immunocompromised mice. These data demonstrate that scaffold-free tissue engineering facilitates PDLCs to self-assemble into an organized cementum-PDL-like complex. These engineered tissues could be used as implantable grafts to regenerate damaged periodontal tissues or as model systems to study PDLC biology and mechanisms driving organized tissue assembly within the periodontium.

Keywords: periodontal ligament stem cells, periodontium, tissue engineering, self-assembly, organoid, periodontal regeneration

INTRODUCTION

The periodontium is composed of multiple specialized tissues surrounding the tooth root that function to support the tooth and anchor it to the jaw. The root surface is lined by mineralized cementum, which is tethered to the alveolar bone by the periodontal ligament (PDL), and all of these structures are covered by the gingiva. It is estimated that 38.5% of adults in the United States have moderate-to-severe periodontitis (Eke et al., 2012), a disease that results in the breakdown of the cementum, PDL, and alveolar bone and leads to tooth loss. Developing a successful and predictable therapy to repair these structures is therefore of great importance. Rebuilding a complex structure like the periodontium comprising both soft and hard tissues is a major challenge in regenerative medicine. The achievement of this goal will require several concurrent processes including the recruitment and differentiation of cells to form multiple tissues in a spatially organized manner (Bartold et al., 2016). A better understanding of the biology of the cells involved in these processes and the molecular signals driving cell differentiation and tissue patterning within the periodontium would lead to the development of enhanced therapies to treat periodontitis.

A population of stem/progenitor cells has been identified in the periodontal ligament that are clonogenic and multipotent with the ability to differentiate into cementoblasts, PDL fibroblasts, and osteoblasts (Seo et al., 2004). A significant amount of research is directed toward developing new cell-based therapies to treat periodontitis using these periodontal ligament cells (PDLCs). However, creating these types of therapies involves stimulating PDLCs to regenerate the multiple periodontal tissues in an anatomically correct manner and preventing disorganized or spontaneous tissue formation that could lead to anomalies such as ankyloses. To address this challenge, many researchers are designing complex scaffolds with graded properties to direct the formation of organized periodontal tissues (Sowmya et al., 2017; Varoni et al., 2018; Wu et al., 2018). During development, cells drive the synthesis and assembly of organized multi-tissue structures using their endogenous extracellular matrix (ECM) for structure. The optimal approach of generating an effective therapy involves understanding and emulating these developmental processes.

Scaffold-free tissue engineering is a method of tissue regeneration where cells generate and organize their endogenous ECM to form a three-dimensional (3D) structure. Unlike traditional tissue engineering methods, scaffold-free tissue engineering bypasses the use of an exogenous scaffold material to form a 3D tissue. Because of this, scaffold-free tissue engineering methods follow similar pathways of tissue assembly seen naturally during development. A number of scaffold-free tissue engineered constructs have been shown to be able to self-assemble into organized multi-tissue or organ constructs (Muraglia et al., 2003; Bosnakovski et al., 2004; Syed-Picard et al., 2009, 2013, 2014; Smietana et al., 2010; Eiraku et al., 2011; Lee et al., 2017; Ovsianikov et al., 2018). Previously, we have shown that scaffold-free tissues formed from bone marrow stromal cells organize into a bone-like structure covered with an outer periosteum, and scaffold-free dental pulp cell constructs organize into a dentin-pulp complex (Syed-Picard et al., 2009, 2013, 2014; Smietana et al., 2010). In this study, we found that similar 3D, scaffold-free constructs generated from PDLCs self-assemble into a spatially organized PDL-cementum-like complex. We have characterized cell differentiation and tissue assembly within these engineered tissues after *in vitro* culture and *in vivo* implantation. The development of an engineered tissue that organizes into multiple structures of the periodontium could be used as a graft tissue to replace structures damaged by periodontitis and would also provide a powerful model system to study PDLC biology and periodontal tissue assembly yielding important mechanistic information that will enhance future cellular therapies to treat periodontitis.

MATERIALS AND METHODS

Periodontal Ligament Cell Isolation

Healthy human third molars were obtained from the University of Pittsburgh School of Dental Medicine following routine extraction. The collection of human third molars for these studies was not considered human subject research because the teeth were discarded tissues and were completely de-identified prior to being transferred to the investigators of this study. Therefore, patient consent was not required to use this tissue. Teeth were collected from both male and female patients within the age range of 12–22 years. The teeth were cleaned in a solution of phosphate buffered saline containing penicillin-streptomycin (P/S; Gibco), and the PDL was dissected from the root surface of the teeth. The PDL tissue was minced with a scalpel and digested in an enzyme solution containing 3 mg/ml collagenase (MP Biochemical) and 4 mg/ml of dispase (Worthington Biochemical) at 37°C for 30–60 min. The digest was then passed through a 70-μm cell strainer to obtain a single cell solution. Cells were plated at an initial density of 10–20,000 cells/cm^2 in growth medium (GM) containing Dulbecco's Modified Eagle Medium (DMEM; Gibco), 20% fetal bovine serum (FBS; Atlanta Biologicals), and 1X P/S. Cells were expanded and cryogenically frozen for future experiments. Cells were used for experiments between passages 2 and 4. Cells isolated from different patients were kept separate, not pooled. All *in vitro* experiments were repeated using cells from at least three different patients to ensure reproducibility.

Formation of Scaffold-Free Engineered Tissues

Scaffold-free constructs were formed using similar methods as previously described (Syed-Picard et al., 2009, 2013). Construct dishes were prepared by filling wells of six-well plates with 3 ml of polydimethylsiloxane (PDMS; Dow Corning), and the PDMS was allowed to cure to form a solid layer at the bottom of the wells. The PDMS was coated with 3 μg/cm^2 laminin (Gibco) to facilitate PDLC adhesion, and the dishes were exposed to UV light for approximately 90 min. PDLCs were

plated onto these construct dishes at an initial density of 200,000 cells/well in GM supplemented with 5 mg/ml ascorbic acid (Sigma), 10^{-8} M dexamethasone (dex; Sigma), 5 mM β-glycerophosphate (βGP; MP Biochemical), and 5 ng/ml fibroblast growth factor 2 (FGF2; Peprotech). Once the cells became confluent, 2 minutien pins (Fine Science Tools) were positioned in the center of the dish approximately 7 mm apart, and the culture medium was switched to now containing DMEM with 5% FBS, 5 mg/ml ascorbic acid, 10^{-8} M dex, 5 mM βGP, 5 ng/ml FGF2, and 2 ng/ml transforming growth factor β1 (TGFβ1; Peprotech). Cells formed tissue sheets that naturally detached from the substrate and contracted toward the pins to form a cylindrical scaffold-free tissue, anchored on either end by the pins. Constructs were cultured for an additional 7 or 14 days after formation of *in vitro* analyses or constructs were implanted subcutaneously in mice after 7 days in culture. Dexamethasone, ascorbic acid, and βGP are medium supplements known to induce osteogenic differentiation. FGF2 and TGFβ1 were also added to our culture medium in order to fully emulate the culture conditions used to previously form these types of scaffold-free engineered tissues from dental pulp cells and bone marrow stromal cells (Syed-Picard et al., 2009, 2013). This facilitated the ability to make direct comparisons across engineered tissues formed from cells originating from different tissues.

To ensure the biological and technical reproducibility of the results presented in this study, we have engineered scaffold-free PDLC constructs using cells isolated from a total of five different patients. In total, for these studies, we have generated 80 (n = 80) scaffold-free PDLC constructs.

Animal Implantation

All animal procedures were approved by the University of Pittsburgh Institute of Animal Care and Use Committee. Balb/c immunocompromised mice, 8–10 weeks in age, were anesthetized through the inhalation of isoflurane gas, and the surgical field was cleaned with betadine and ethanol. Approximately 1 cm incisions were made through the skin on the backs of the mice, and a subcutaneous pocket was created through blunt dissection. One scaffold-free PDLC construct was placed into each pocket, and four samples were placed into each animal. A total of 16 scaffold-free PDLC constructs were implanted into animals for this study; we performed experiments using four animals, implanting four samples/animal.

Histology and Immunofluorescent Staining

Following *in vitro* culture or *in vivo* implantations, samples were fixed in a solution of 4% paraformaldehyde overnight. Subsequent to fixation, some samples were decalcified in a solution of 0.4 M ethylenediaminetetraacetic acid (EDTA) for 1–2 h. Samples were embedded in paraffin, and 5 μm longitudinal sections were prepared. Sections were stained for hematoxylin and eosin (H&E) to characterize cell and tissue morphology and structure, and un-decalcified sections were also stained for Alizarin Red to detect mineralization. Immunostaining was performed to detect bone sialoprotein (BSP; Millipore); periostin (Novus); periodontal ligament-associated protein 1 (PLAP-1), also known as asporin (Invitrogen); or alkaline phosphatase (ALP; Abcam). Fluorescently tagged secondary antibodies, Alexa Fluor 546 goat anti-mouse and Alexa Fluor 488 goat anti-rabbit (Invitrogen), were used to detect the signal. Negative controls to our immunostaining were performed in parallel by omitting the primary antibody. DAPI (4′,6-diamidino-2-phenylindole, dihydrochloride) staining was performed to detect nuclei, and slides were mounted with Immu-mount aqueous mounting medium (Thermo Scientific). Brightfield images were acquired using a Nikon Eclipse TE200-E inverted microscope, and fluorescent images were taken using a Nikon Eclipse Ti inverted microscope.

Micro-Computed Tomography (μCT)

μCT scans of the engineered tissues were acquired both after *in vitro* culture and following *in vivo* implantation to detect and localize mineral deposition. The tissues were fixed in 4% paraformaldehyde overnight. The samples were then dried overnight in air. μCT scans were taken using a Scanco μCT 50 system (Scanco Medical AG, Bruttisellen, Switzerland). The scans were performed in air with the following parameters: 45 kVp energy, 10 μm voxel size, 200 μA intensity, 0.36° rotation step (180° angular range), 800 ms exposure, and 1 average frame per view. The Scanco μCT software (HP, Open VMS/DECwindows Motif 1.6) was used for 3D reconstruction and viewing of images. A threshold of 550–1,000 units (gray scale) was set to visualize mineral and 180–550 units (gray scale) to visual soft tissue.

RESULTS

Characterization of Scaffold-Free PDLC Constructs Following *in vitro* Culture

Figure 1 shows a timeline of scaffold-free PDLC construct formation. Scaffold-free 3D-engineered tissues were formed by plating PDLCs onto construct dishes. Four to five days after cell plating, the cells became confluent. The cells formed a tissue sheet that started delaminating from the substrate and rolling toward two pins in the center of the dish at 8–9 days after plating. Ten to eleven days following cell plating, the cell sheet completed rolling up to form solid, cylindrical, scaffold-free construct anchored on either end by the minutien pins. Constructs were cultured for 7 or 14 days following 3D tissue formation.

H&E staining shows that the scaffold-free PDLC constructs are solid and cellular (**Figures 2A,B**). Higher magnification images show that the constructs have two distinct structures (**Figures 2A′,B′**). In the center region of the constructs, the density of cells appears higher, and the cells are more round in shape. On the periphery of the constructs, there is a clear separate structure where the cells are more elongated in shape along the longitudinal axis of the construct. The engineered tissues became highly mineralized as seen by positive alizarin red staining (**Figures 2C,D**). The mineral was localized to

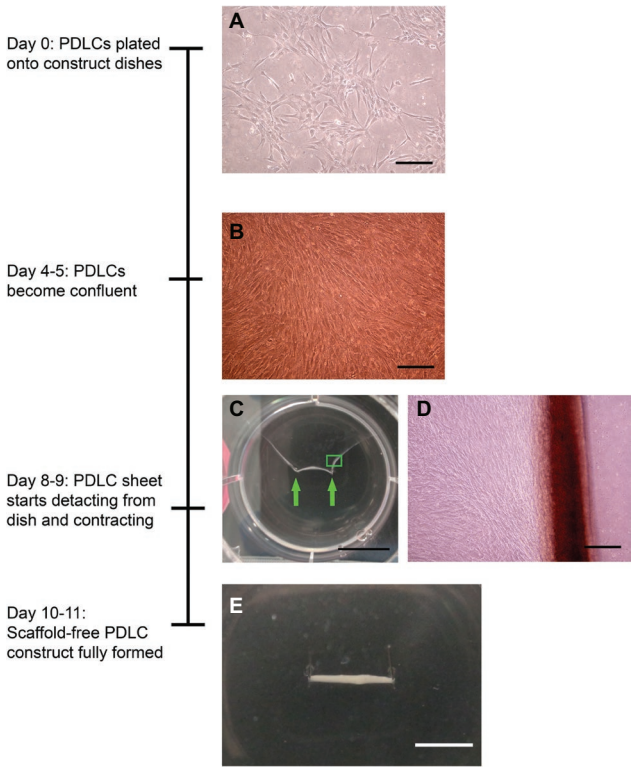

FIGURE 1 | Time line of scaffold-free PDLC construct formation. **(A)** Micrograph of PDLCs after attaching to construct dishes. **(B)** Micrograph of PDLCs reaching confluence on construct dishes approximately 4–5 days following cell plating. **(C)** Image of PDLC sheet contracting from sides of well of six-well plates toward two pins placed in the center of dish; green arrows are pointing to pins. **(D)** Higher magnification micrograph of green boxed area is shown in **(C)**. **(E)** Image of final, cylindrical scaffold-free PDLC construct anchored to the dish on either end by pins. Scale bars: **(A,B,D)** = 200 μm, **(C)**: 10 mm, and **(E)**: 5 mm.

the center of the constructs, and the periphery of the constructs, the region corresponding to the elongated cell phenotype seen in H&E, completely lacks mineral (**Figures 2C′,D′**). These data are further validated by 3D μCT reconstructions of the engineered tissues showing a mineralized structure enclosed within a soft tissue (**Figures 2E,F**). These data show that scaffold-free tissue engineering facilitates PDLCs to self-assemble into two distinct structures one in the core of the construct and a second on the periphery. These structures are morphologically different, and furthermore, the tissue at the center of the construct becomes mineralized, whereas the peripheral tissue does not.

Immunostaining was performed to further characterize PDLC differentiation and tissue assembly within the scaffold-free construct. At 7 days in culture following construct formation, periodontal ligament-associated protein 1 (PLAP-1) and periostin, markers of PDL, were strongly expressed on the periphery of the construct and also found in the center (**Figures 3A,C**). At 14 days, PLAP-1 and periostin expression were more specifically localized to only the peripheral structure of the engineered tissues (**Figures 3F,H**). This indicates that the peripheral PDLCs are exhibiting a periodontal ligament fibroblast phenotype. Since the localization of PLAP-1 and periostin expression becomes more specific to the periphery of the engineered tissue between 7 and 14 days, perhaps this additional time in culture facilitates tissue organization or maturation. Following both 7 and 14 days in culture, the expression of alkaline phosphatase (ALP) and bone sialoprotein (BSP), molecules characteristic of bone and cementum, was localized to the center of the construct (**Figures 3B,D,G,I**). This indicates that the PDLCs at the center of the engineered tissues are differentiating toward an osteo/cementoblast phenotype. Double labeling of BSP and periostin shows the distinct expression patterns of these two proteins within the engineered tissues (**Figures 3E,J**). These data demonstrate that when cultured as a 3D scaffold-free construct, PDLCs self-assemble such that the cells in the center of the construct differentiate into osteo/cementoblast-like cells and deposit a mineralized tissue and the peripheral PDLCs differentiate into PDL fibroblast-like cells producing a tissue resembling the periodontal ligament.

Characterization of Scaffold-Free PDLC Constructs Following *in vivo* Implantation

Following 7 days of *in vitro* culture, scaffold-free PDLC constructs were implanted subcutaneously in immunocompromised mice to assess the effect of the *in vivo* environment on the engineered tissues. While implanted, the scaffold-free engineered tissues remodeled from the cylindrical shape seen *in vitro* to more of a spherical shape. Following a 4-week implantation, H&E staining showed that the PDLC constructs maintained the tissue morphology seen after *in vitro* culture with a dense, cellular core tissue and a morphologically distinct peripheral tissue comprising elongated cells and matrix (**Figures 4A,A′**). Furthermore, the center tissue within the explants was mineralized as seen by positive alizarin red staining (**Figures 4B,B′**), and the peripheral tissue remained uncalcified. μCT verified that the explants comprised a mineralized core localized within a soft tissue (**Figure 4C**).

Immunostaining of the explants showed that PLAP-1 (**Figures 5A,A′**) and periostin (**Figures 5C,C′**) were strongly expressed only on the periphery of the construct. ALP (**Figures 5B,B′**) and BSP (**Figures 5D,D′**) expressions were localized in the center of the constructs, in a similar region of the mineral deposition. After *in vivo* implantation, only a low level of ALP expression is seen. ALP is an early marker of osteo/cementogenic cell differentiation involved at early stages of mineral deposition. It is therefore not surprising that strong ALP expression is not seen after *in vivo* implantation; since at this point, the engineered tissues may be developing into a more mature phenotype. Double labeling of periostin and BSP shows that there is no overlap in signal further supporting the formation of two distinct tissues (**Figures 5E,E′**). This indicates that after *in vivo* implantation the PDLC-engineered tissues were able to maintain the tissue organization assembled during *in vitro* culture with an osteo/cementogenic center enclosed within a PDL-like tissue.

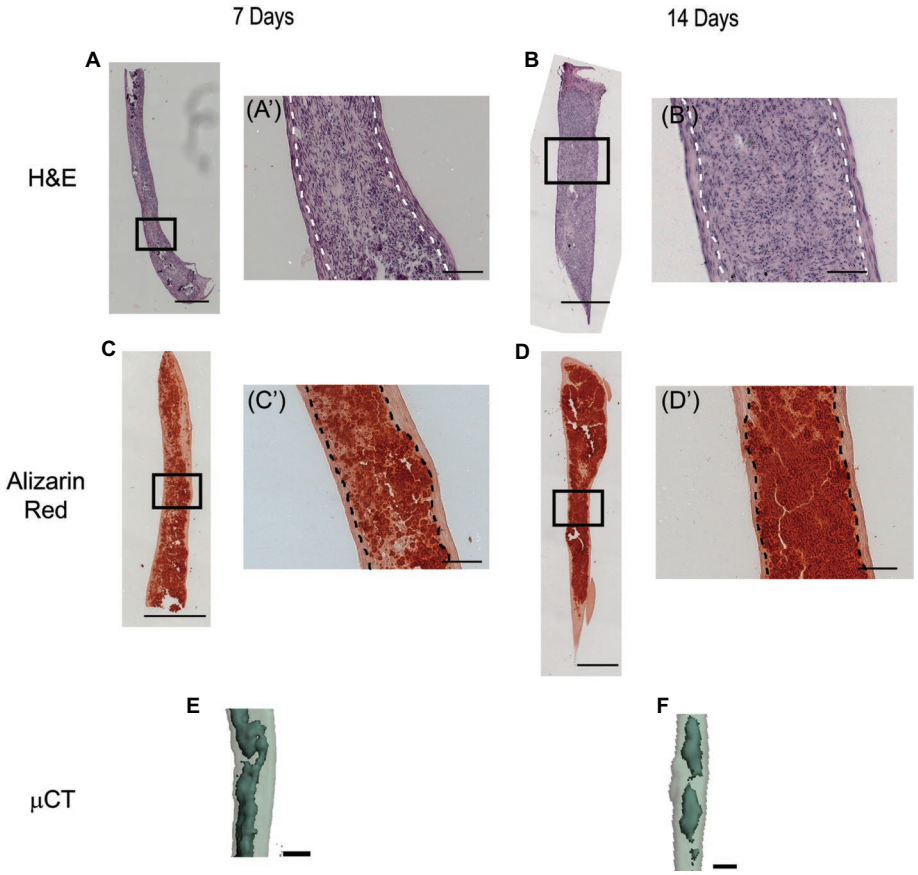

FIGURE 2 | H&E, alizarin red staining, and μCT analysis of scaffold-free PDLC constructs following *in vitro* culture. **(A)** Image of H&E staining of full, longitudinal histological section of scaffold-free construct following 7 days in culture shows that the construct is solid and highly cellular. **(A′)** Higher magnification image of boxed region shown in **(A)** shows that the scaffold-free constructs formed two different tissue structures, a center dense tissue with round cells and a peripheral structure containing cells and matrix elongated along the longitudinal axis of the construct; the white dotted line delineates the two structures. Similar histological features are seen in scaffold-free constructs following 14 days in culture. **(B)** H&E staining of full histological section of scaffold-free construct after 14 days in culture. **(B′)** Higher magnification of boxed region shown in **(B)**; the white dotted line separates the peripheral and the core structures. **(C)** Image of alizarin red staining of full-length, longitudinal histological section of engineered tissue after 7 days in culture shows positive staining for calcium (red) indicative of mineral deposition along the length of the samples. **(C′)** Higher magnification image of boxed region in **(C)** shows that positive alizarin red staining is localized to the center of the construct and a band of uncalcified tissue is on the periphery; the dashed black line separates the mineralized tissue center from the unmineralized peripheral tissue. A similar localization of mineralized tissue is seen after 14 days of culture. **(D)** Alizarin red staining of full histological section of engineered tissues after 14 days in culture. **(D′)** Higher magnification image of boxed region in **(D)**; dashed black line separates peripheral uncalcified tissue from the center mineralized tissue. **(E)** Three-dimensional rendering of μCT scan of segment of engineered tissue after 7 days in culture shows mineralized tissue (dark, solid gray) localized within soft tissue (light, translucent gray). A similar 3D rendering is seen after 14 days in culture. **(F)** Three-dimensional rendering of μCT scan of segment of engineered tissue after 14 days in culture shows mineralized tissue (dark, solid gray) enclosed within a soft tissue (light, translucent gray). Scale bars: **(A–D)** = 500 μm; **(A′–D′,E,F)** = 100 μm.

DISCUSSION

An effective therapy to regenerate the periodontium will require directing cells to rebuild the various periodontal tissues in an organized manner. Understanding the cellular mechanisms facilitating periodontal tissue patterning is therefore critical. In this study, unique 3D scaffold-free constructs were formed from PDLCs that facilitated the cells to self-assemble to form an osteo/cementogenic core with a periodontal ligament-like periphery, similar to what is seen naturally on the surface of a tooth root. The formation of these organized structures is seen after *in vitro* culture and is maintained after *in vivo* implantation. These engineered constructs could be used as functional grafts to rebuild periodontal defects or used as a controllable model system to study periodontal ligament cell fate decisions and the complex tissue assembly involved in rebuilding the periodontium.

Cell sheet engineering is another form of scaffold-free tissue engineering that has been explored as a method to regenerate the periodontium (Hasegawa et al., 2005; Iwata et al., 2009; Zhou et al., 2012; Chen et al., 2016). The 3D scaffold-free constructs that we have formed and characterized in this present work differ from the cell sheets that have been previously reported in multiple significant ways. Cell sheets are formed

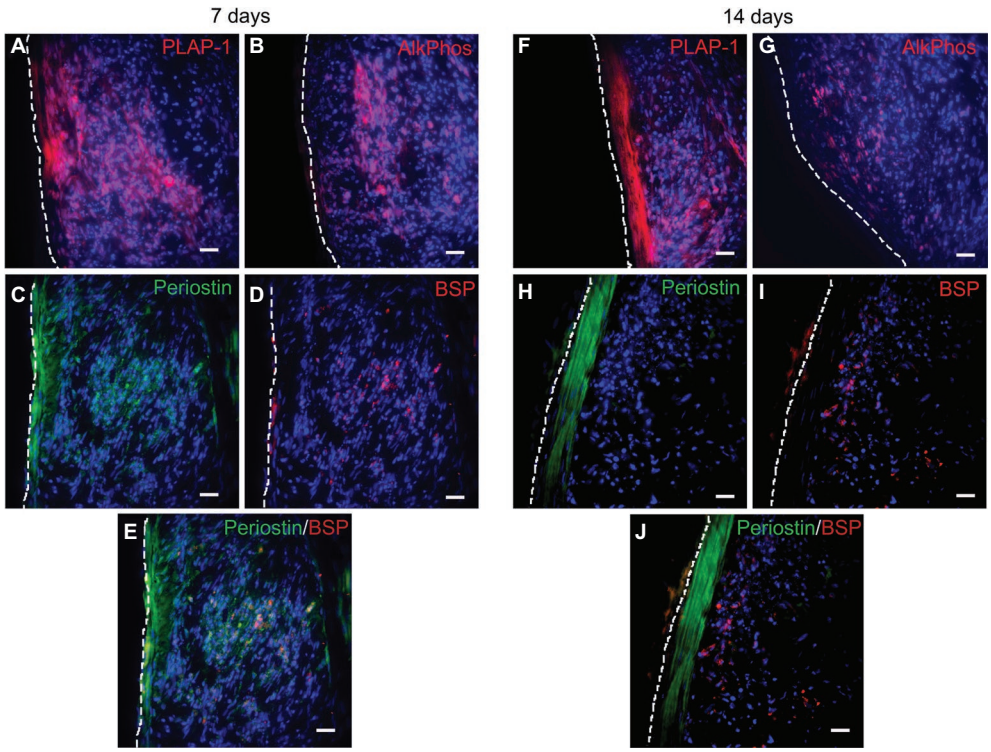

FIGURE 3 | Immunofluorescent staining of scaffold-free PDLC constructs after *in vitro* culture. **(A)** PLAP-1 (red) is found expressed strongly at the periphery of the PDLC and also in the center after 7 days in culture. **(B)** ALP (red) is found expressed in the center of the scaffold-free tissue after 7 days in culture. **(C)** Periostin (green) is strongly expressed on the periphery and also found in the center of scaffold-free construct following 7 days of culture. **(D)** BSP (red) expression is found localized mainly in the center of the engineered tissue following 7 days of culture. **(E)** Merged image of **(C)** and **(D)** showing the separate localized expression of periostin (green) and BSP (red). **(F)** PLAP-1 (red) expression is found strongly associated to the periphery of the construct at 14 days in culture. **(G)** ALP (red) expression can be seen localized to the center of the engineered tissue at 14 days in culture. **(H)** Following 14 days in culture, periostin (green) is only expressed on the peripheral tissue of the scaffold-free construct. **(I)** BSP (red) expression is localized to the center of the scaffold-free construct following 14 days in culture. **(J)** Merged image of **(H)** and **(I)** showing localized expression of periostin (green) and BSP (red). In all images, DAPI was used to stain cell nuclei (blue), and white dashed line denotes the edge of the engineered tissue. Scale bars in all images = 100 μm.

by culturing cells to confluence and allowing the cells to produce their endogenous extracellular matrix to form a layer of tissue that can be separated from the substrate. In our system, the cells first form cell sheets and then are further cultured so that the cell sheet contracts and rolls up into a robust 3D cylindrical tissue. The shape and dimensionality of our constructs therefore are very different what is seen in cell sheets. Furthermore, our scaffold-free system facilitated cells within the same engineered tissue to self-assemble to form both osteo/cementogenic and PDL-like tissues, a feature that has not yet been seen in cell sheets. The previously reported research on the use of scaffold-free cell sheets, however, has established the safety and feasibility of utilizing cellular, scaffold-free engineered tissues for regenerating periodontal tissues. Researchers have found that PDLC sheets aid in periodontal regeneration in both small and large animal defect models (Hasegawa et al., 2005; Iwata et al., 2009; Zhou et al., 2012). Furthermore, studies have been performed to assess the use of autologous PDLC sheets for periodontal regeneration in humans (Chen et al., 2016). This research validates the safety and feasibility of translating scaffold-free cellular tissue engineering therapies into humans.

In this study, scaffold-free PDLC constructs were shown to organize into two morphologically distinct tissues, an outer fibrous PDL-like structure and an inner mineralized tissue. The formation of a PDL-like structure on the periphery of the engineered tissues was determined in part by the positive expression of PLAP-1 and periostin. PLAP-1, also known as asporin, is a member of the small leucine-rich proteoglycan (SLRP) family and is preferentially expressed in the periodontal ligament. PLAP-1 has been shown to prevent osteo/cementogenic differentiation of PDLCs and the mineralization of PDL tissue by inhibiting the Smad signaling pathway (Yamada et al., 2001, 2007; Ueda et al., 2016). Periostin is an extracellular matrix protein found in a number of tissues, including the PDL, periosteum, cardiac valves, alveolar wall, and cancer-associated stroma, and has multiple functions including involvement in extracellular matrix assembly and in cell adhesion (Horiuchi et al., 1999; Kii and Ito, 2017). Within the PDL, periostin has been shown to have a role in tissue remodeling in response to mechanical loading, and periostin-deficient mice develop an early onset periodontal disease phenotype (Rios et al., 2005, 2008). This factor is therefore critical for proper PDL homeostasis. It could be argued that since periostin is also expressed naturally

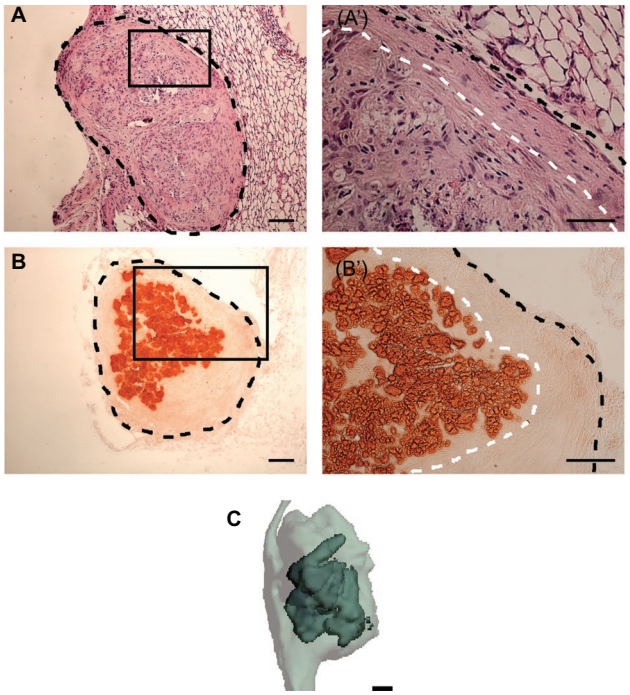

FIGURE 4 | H&E, alizarin red staining, and μCT analysis of scaffold-free PDLC constructs following *in vivo* implantation. **(A)** H&E staining of histological section of engineered tissue explant following 4-week subcutaneous implantations. Black, dashed line outlines explant. **(A′)** Higher magnification image of boxed region in **(A)** shows the formation of two morphologically distinct tissues on the explant, a core tissue and a separate tissue on the periphery; black, dashed line outlines the sample and white, dashed line separates the inner and outer tissue structures. **(B)** Alizarin red staining of full explant following 4-week implantation. Black, dashed line outlines full explant. **(B′)** Higher magnification image of boxed region in **(B)** shows that the core of the explant is stained positively for alizarin red while the periphery does not. Black, dashed line outlines the explant and the white, dashed line delineates the mineralized core tissue from the peripheral unmineralized tissue. **(C)** Three-dimensional rendering of μCT scan of explant shows mineralized tissue (dark, solid gray) localized within soft tissue (light, translucent gray). Scale bars: **(A,B′,C)** = 100 μm, **(A′)** = 50 μm.

in the periosteum, the peripheral tissues on the scaffold-free PDL constructs could be reminiscent of a periosteal structure rather than a PDL-like tissue; however, the peripheral tissue on these engineered tissues is structurally dissimilar to a periosteum. In our previous studies, we have reported the formation of a periosteum-like structure on scaffold-free tissues engineered using bone marrow stromal cells (Syed-Picard et al., 2009, 2014). In these studies, the engineered periosteum, in addition to exhibiting biochemical characteristics of a periosteum, also displayed morphological features of a natural periosteum comprising both the fibrous and cambium layers of a true periosteum. These types of structural landmarks characteristic of a periosteum were not seen in the scaffold-free PDL constructs reported here. Therefore, in this current study, the localized expression of periostin and PLAP-1 on the periphery of the scaffold-free PDL constructs in addition to the morphology and uncalcified nature of the peripheral tissue is indicative of PDL tissue formation.

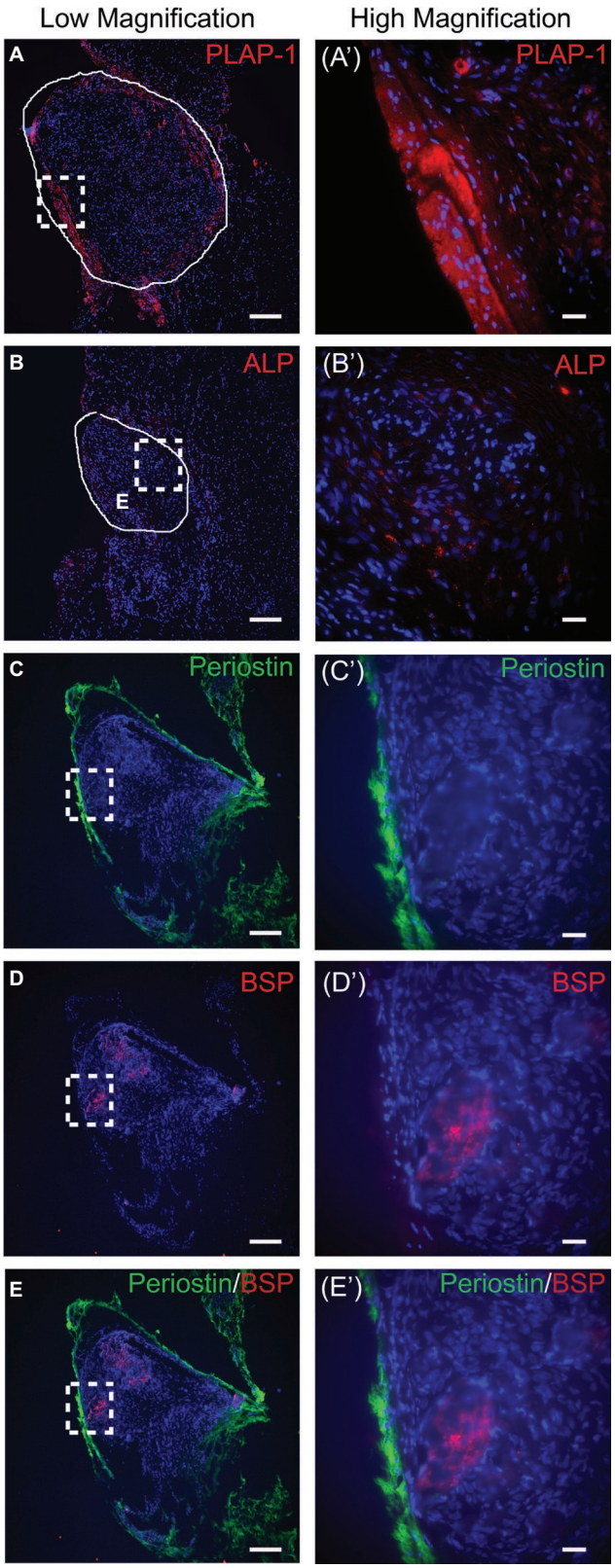

FIGURE 5 | Immunofluorescent staining of scaffold-free PDLC constructs after 4-week *in vivo* implantation. **(A)** PLAP-1 (red) is expressed strongly on

(Continued)

FIGURE 5 | the periphery of the scaffold-free constructs; solid white line outlines engineered tissue. **(A′)** Higher magnification image of dashed boxed region shown in **(A)**. **(B)** Faint ALP (red) expression can be seen localized in the center of the scaffold-free constructs after implantation; solid white line outlines construct. **(B′)** Higher magnification image of dashed boxed region shown in **(B)**. **(C)** Periostin (green) is expressed on the periphery tissue of scaffold-free construct following implantation. **(C′)** Higher magnification image of boxed region in **(C)**. **(D)** BSP (red) is expressed in the center tissue of scaffold-free construct following implantation. **(D′)** Higher magnification image of boxed region in **(D)**. **(E)** Merged image of **(C)** and **(D)** further validates that periostin (green) is expressed on periphery tissue and BSP (red) is expressed in the center tissue of engineered construct. **(E′)** Higher magnification of boxed region shown in **(E)**. In all images, DAPI was used to stain cell nuclei (blue). Scale bars: **(A**–**E)** = 100 μm; **(A′**–**E′)** = 50 μm.

Natural periodontal ligament has a characteristic morphology consisting of cells and ECM fibers oriented perpendicular to the surface of the cementum and the alveolar bone. These morphological features are a result of the mechanical forces placed on the PDL *in situ* during tooth development, eruption, and function (Nanci and Ten Cate, 2013). Unlike true PDL, the PDL-like tissue in our engineered constructs appears to be aligned parallel to the osteo/cementogenic core tissue. We speculate that this result is because the engineered constructs are being generated and cultured without the mechanical stimuli present in the natural tooth socket. Potentially, subjecting our engineered constructs to the mechanical environment of natural PDL could stimulate the cells and ECM in the PDL-like tissue to rearrange to more closely emulate what is seen in natural PDL. These engineered constructs could be a useful model system to study the effect of mechanical loading on PDL cells and ECM.

Scaffold-free tissue engineering of PDLC resulted in the formation of an osteo/cementogenic tissue localized in the center of the construct. Cementum is biochemically very similar to bone and dentin; therefore, from compositional perspective, it is very difficult to distinguish these tissues. The extracellular matrices of all of these mineralized tissues comprise predominately type I collagen, and these tissues all contain similar enzymes and non-collagenous extracellular matrix proteins, including ALP and BSP, which are involved in mineralization processes (Nanci and Ten Cate, 2013). In this study, we characterized the tissue located at the center of our construct based on its mineralized nature and the positive expression of ALP and BSP; however, these characteristics alone are not sufficient to truly define the tissue at the core of construct as cementum instead of bone. Due to the compositional similarities between bone and cementum, some have argued that cementoblasts are simply positional osteoblasts, and cementum is a specialized type of bone located on the surface of the tooth between the dentin and the PDL (Foster, 2012). Based on this type of positional identity, the mineralized tissue localized at the core of the scaffold-free engineered tissues formed in this study can be characterized as cementum-like since it is located within a PDL-like tissue.

Here, we have established a scaffold-free engineered tissue that could be used as a controllable model system to study the assembly of periodontal tissues and have provided the foundational characterization of these engineered constructs. However, tissue-engineered model systems do not fully emulate native structures since they are not generated in a setting that fully encompasses the complex milieu of chemical and mechanical signals provided in an *in situ* environment. In our current study, we implanted our engineered PDLC constructs subcutaneously in mice. In future studies, it would of interest to evaluate these scaffold-free constructs after implantation either into the tooth socket or in the periodontal space between dentin and alveolar bone. In addition, in this study, the PDLC constructs were formed in static culture, and it is established that mechanical stimuli are critical for periodontal tissue organization and morphology. It is, therefore, critical to further assess these engineered tissues following mechanical stimulation to assess if these engineered tissues respond to external forces in a similar manner to native tissues.

We have formed scaffold-free engineered tissues using PDLCs that self-assembled into an organized PDL-cementum-like complex. These engineered tissues have feasible regenerative potential for treating periodontal disease, and furthermore, these engineered constructs could be used as unique and powerful model system to study the mechanisms driving PDLCs to properly assemble a cementum-PDL complex.

ETHICS STATEMENT

All animal procedures were approved by the University of Pittsburgh Institute of Animal Care and Use Committee.

AUTHOR CONTRIBUTIONS

AB was involved in study design, performed experiments, and collected and analyzed data. KR and MA performed experiments and collected data. FS-P was involved in study design, data analysis and interpretation, and manuscript preparation.

FUNDING

The acquisition of microcomputed tomography data was supported by the National Institutes of Health S10 OD021533 grant to the University of Pittsburgh, Center for Craniofacial Regeneration. This research was funded by the National Institute of Dental & Craniofacial Research of the National Institutes of Health under Award Number R00 DE025088 to FS-P.

ACKNOWLEDGMENTS

The authors would like to thank Dr. Kostas Verdelis, Rong Chong, and Lyudmila Lukashova for help with μCT analysis.

REFERENCES

Bartold, P. M., Gronthos, S., Ivanovski, S., Fisher, A., and Hutmacher, D. W. (2016). Tissue engineered periodontal products. *J. Periodontal Res.* 51, 1–15. doi: 10.1111/jre.12275

Bosnakovski, D., Mizuno, M., Kim, G., Ishiguro, T., Okumura, M., Iwanaga, T., et al. (2004). Chondrogenic differentiation of bovine bone marrow mesenchymal stem cells in pellet cultural system. *Exp. Hematol.* 32, 502–509. doi: 10.1016/j.exphem.2004.02.009

Chen, F. M., Gao, L. N., Tian, B. M., Zhang, X. Y., Zhang, Y. J., Dong, G. Y., et al. (2016). Treatment of periodontal intrabony defects using autologous periodontal ligament stem cells: a randomized clinical trial. *Stem Cell Res. Ther.* 7, 33–44. doi: 10.1186/s13287-016-0288-1

Eiraku, M., Takata, N., Ishibashi, H., Kawada, M., Sakakura, E., Okuda, S., et al. (2011). Self-organizing optic-cup morphogenesis in three-dimensional culture. *Nature* 472, 51–56. doi: 10.1038/nature09941

Eke, P. I., Dye, B. A., Wei, L., Thornton-Evans, G. O., Genco, R. J., and CDC Periodontal Disease Surveillance Workgroup: James Beck, Gordon Douglass, Roy Page (2012). Prevalence of periodontitis in adults in the United States: 2009 and 2010. *J. Dent. Res.* 91, 914–920. doi: 10.1177/0022034512457373

Foster, B. L. (2012). Methods for studying tooth root cementum by light microscopy. *Int. J. Oral Sci.* 4, 119–128. doi: 10.1038/ijos.2012.57

Hasegawa, M., Yamato, M., Kikuchi, A., Okano, T., and Ishikawa, I. (2005). Human periodontal ligament cell sheets can regenerate periodontal ligament tissue in an athymic rat model. *Tissue Eng.* 11, 469–478. doi: 10.1089/ten.2005.11.469

Horiuchi, K., Amizuka, N., Takeshita, S., Takamatsu, H., Katsuura, M., Ozawa, H., et al. (1999). Identification and characterization of a novel protein, periostin, with restricted expression to periosteum and periodontal ligament and increased expression by transforming growth factor beta. *J. Bone Miner. Res.* 14, 1239–1249. doi: 10.1359/jbmr.1999.14.7.1239

Iwata, T., Yamato, M., Tsuchioka, H., Takagi, R., Mukobata, S., Washio, K., et al. (2009). Periodontal regeneration with multi-layered periodontal ligament-derived cell sheets in a canine model. *Biomaterials* 30, 2716–2723. doi: 10.1016/j.biomaterials.2009.01.032

Kii, I., and Ito, H. (2017). Periostin and its interacting proteins in the construction of extracellular architectures. *Cell. Mol. Life Sci.* 74, 4269–4277. doi: 10.1007/s00018-017-2644-4

Lee, J. K., Link, J. M., Hu, J. C. Y., and Athanasiou, K. A. (2017). The self-assembling process and applications in tissue engineering. *Cold Spring Harb. Perspect. Med.* 7:a025668. doi: 10.1101/cshperspect.a025668

Muraglia, A., Corsi, A., Riminucci, M., Mastrogiacomo, M., Cancedda, R., Bianco, P., et al. (2003). Formation of a chondro-osseous rudiment in micromass cultures of human bone-marrow stromal cells. *J. Cell Sci.* 116, 2949–2955. doi: 10.1242/jcs.00527

Nanci, A., and Ten Cate, A. R. (2013). *Ten Cate's oral histology: Development, structure, and function*. St. Louis, Mo: Elsevier. p. 11, 211, 222.

Ovsianikov, A., Khademhosseini, A., and Mironov, V. (2018). The synergy of scaffold-based and scaffold-free tissue engineering strategies. *Trends Biotechnol.* 36, 348–357. doi: 10.1016/j.tibtech.2018.01.005

Rios, H., Koushik, S. V., Wang, H., Wang, J., Zhou, H. M., Lindsley, A., et al. (2005). Periostin null mice exhibit dwarfism, incisor enamel defects, and an early-onset periodontal disease-like phenotype. *Mol. Cell. Biol.* 25, 11131–11144. doi: 10.1128/MCB.25.24.11131-11144.2005

Rios, H. F., Ma, D., Xie, Y., Giannobile, W. V., Bonewald, L. F., Conway, S. J., et al. (2008). Periostin is essential for the integrity and function of the periodontal ligament during occlusal loading in mice. *J. Periodontol.* 79, 1480–1490. doi: 10.1902/jop.2008.070624

Seo, B. M., Miura, M., and Gronthos, S. (2004). Investigation of multipotent postnatal stem cells from human periodontal ligament. *Lancet* 364, 149–155. doi: 10.1016/S0140-6736(04)16627-0

Smietana, M. J., Syed-Picard, F. N., Ma, J. J., Kostrominova, T., Arruda, E. M., and Larkin, L. M. (2010). The effect of implantation on scaffoldless three-dimensional engineered bone constructs (vol 45, pg 512, 2009). *In Vitro Cell. Dev. Biol. Anim.* 46:82. doi: 10.1007/s11626-009-9251-0

Sowmya, S., Mony, U., Jayachandran, P., Reshma, S., Kumar, R. A., Arzate, H., et al. (2017). Tri-layered nanocomposite hydrogel scaffold for the concurrent regeneration of cementum, periodontal ligament, and alveolar bone. *Adv. Healthc. Mater.* 6:1601251. doi: 10.1002/adhm.201601251

Syed-Picard, F. N., Jayaraman, T., Lam, R. S. K., Beniash, E., and Sfeir, C. (2013). Osteoinductivity of calcium phosphate mediated by connexin 43. *Biomaterials* 34, 3763–3774. doi: 10.1016/j.biomaterials.2013.01.095

Syed-Picard, F. N., Larkin, L. M., Shaw, C. M., and Arruda, E. M. (2009). Three-dimensional engineered bone from bone marrow stromal cells and their autogenous extracellular matrix. *Tissue Eng. A* 15, 187–195. doi: 10.1089/ten.tea.2007.0140

Syed-Picard, F. N., Ray, H. L., Kumta, P. N., and Sfeir, C. (2014). Scaffoldless tissue-engineered dental pulp cell constructs for endodontic therapy. *J. Dent. Res.* 93, 250–255. doi: 10.1177/0022034513517901

Syed-Picard, F. N., Shah, G. A., Costello, B. J., and Sfeir, C. (2014). Regeneration of periosteum by human bone marrow stromal cell sheets. *J. Oral Maxillofac. Surg.* 72, 1078–1083. doi: 10.1016/j.joms.2014.02.005

Ueda, M., Goto, T., Kuroishi, K. N., Gunjigake, K. K., Ikeda, E., Kataoka, S., et al. (2016). Asporin in compressed periodontal ligament cells inhibits bone formation. *Arch. Oral Biol.* 62, 86–92. doi: 10.1016/j.archoralbio.2015.11.010

Varoni, E. M., Vijayakumar, S., Canciani, E., Cochis, A., De Nardo, L., Lodi, G., et al. (2018). Chitosan-based trilayer scaffold for multitissue periodontal regeneration. *J. Dent. Res.* 97, 303–311. doi: 10.1177/0022034517736255

Wu, M., Wang, J., Zhang, Y., Liu, H., and Dong, F. (2018). Mineralization induction of gingival fibroblasts and construction of a sandwich tissue-engineered complex for repairing periodontal defects. *Med. Sci. Monit.* 24, 1112–1123. doi: 10.12659/MSM.908791

Yamada, S., Murakami, S., Matoba, R., Ozawa, Y., Yokokoji, T., Nakahira, Y., et al. (2001). Expression profile of active genes in human periodontal ligament and isolation of PLAP-1, a novel SLRP family gene. *Gene* 275, 279–286. doi: 10.1016/S0378-1119(01)00683-7

Yamada, S., Tomoeda, M., Ozawa, Y., Yoneda, S., Terashima, Y., Ikezawa, K., et al. (2007). PLAP-1/asporin, a novel negative regulator of periodontal ligament mineralization. *J. Biol. Chem.* 282, 23070–23080. doi: 10.1074/jbc.M611181200

Zhou, Y. F., Li, Y. S., Mao, L., and Peng, H. (2012). Periodontal healing by periodontal ligament cell sheets in a teeth replantation model. *Arch. Oral Biol.* 57, 169–176. doi: 10.1016/j.archoralbio.2011.08.008

Conflict of Interest Statement: The authors declare that the research was conducted in the absence of any commercial or financial relationships that could be construed as a potential conflict of interest.

frontiers in Physiology

MINI REVIEW
published: 26 June 2019
doi: 10.3389/fphys.2019.00814

New Advances in the Study of Bone Tumors: A Lesson From the 3D Environment

Margherita Cortini[1], *Nicola Baldini*[1,2†] *and Sofia Avnet*[1*†]

[1] Orthopaedic Pathophysiology and Regenerative Medicine Unit, IRCCS Istituto Ortopedico Rizzoli, Bologna, Italy,
[2] Department of Biomedical and Neuromotor Sciences, University of Bologna, Bologna, Italy

Bone primary tumors, such as osteosarcoma, are highly aggressive pediatric tumors that in 30% of the cases develop lung metastasis and are characterized by poor prognosis. Bone is also the third most common metastatic site in patients with advanced cancer and once tumor cells become homed to the skeleton, the disease is usually considered incurable, and treatment is only palliative. Bone sarcoma and bone metastasis share the same tissue microenvironment and niches. 3D cultures represent a new promising approach for the study of interactions between tumor cells and other cellular or acellular components of the tumor microenvironment (i.e., fibroblasts, mesenchymal stem cells, bone ECM). Indeed, 3D models can mimic physiological interactions that are crucial to modulate response to soluble paracrine factors, tumor drug resistance and aggressiveness and, in all, these innovative models might be able of bypassing the use of animal-based preclinical cancer models. To date, both static and dynamic 3D cell culture models have been shown to be particularly suited for screening of anticancer agents and might provide accurate information, translating *in vitro* cell cultures into precision medicine. In this mini-review, we will summarize the current state-of-the-art in the field of bone tumors, both primary and metastatic, illustrating the different methods and techniques employed to realize 3D cell culture systems and new results achieved in a field that paves the way toward personalized medicine.

Keywords: 3D culture, sarcoma, bone metastasis, tumor niche, microenvironment

OPEN ACCESS

Edited by:
Thimios Mitsiadis,
University of Zurich, Switzerland

Reviewed by:
Nikolaos Dimitrakakis,
Wyss Institute for Biologically Inspired Engineering and Harvard Medical School, United States
Carole Aimé,
UMR8640 Processus d'Activation Sélectif par Transfert d'Energie Uni-électronique ou Radiatif (PASTEUR), France
Eumorphia Remboutsika,
National and Kapodistrian University of Athens, Greece

***Correspondence:**
Sofia Avnet
sofia.avnet@ior.it

†These authors have contributed equally to this work

Specialty section:
This article was submitted to Craniofacial Biology and Dental Research, a section of the journal Frontiers in Physiology

Received: *08 April 2019*
Accepted: *11 June 2019*
Published: *26 June 2019*

Citation:
Cortini M, Baldini N and Avnet S (2019) New Advances in the Study of Bone Tumors: A Lesson From the 3D Environment. Front. Physiol. 10:814. doi: 10.3389/fphys.2019.00814

INTRODUCTION

Cancer is a complex disease that thrives in a heterogeneous and adaptive tumor microenvironment (Park et al., 2014). Bone sarcomas and bone metastasis (BM) share the same environment and the niche, where tumor cells can seed and proliferate. Osteosarcoma (OS), chondrosarcoma (CS), and ewing sarcoma (ES) are the most common malignant primary bone tumors, accounting for 70% of all such malignancies. Despite the advent of chemotherapy has widely improved patient survival, sarcomas are still considered deadly and, in a high percentage of cases, incurable diseases (Lewis, 2009). Similarly, BM form when carcinoma cells have homed to the skeleton and, at this stage, the disease is usually considered incurable, treatment with current modalities is only palliative and often associated to uncomfortable side effects (Fornetti et al., 2018).

Bone sarcomas are a disease of mesenchymal origin; they originate in the bone, where the mesenchymal stem cells (MSC) are both ontogenic progenitor tumor cells (Mohseny et al., 2009; Lye et al., 2016) and stromal cells that participates to tumor development (Xiao et al., 2013; Cortini et al., 2017). In the bone, the tumor-supporting stroma is formed by osteoblasts (the bone forming cells deriving from MSC), osteoclasts (the bone resorbing cells), endothelial and immune cells,

and MSC. Osteoclasts adhere to bone surface and the spectrum of factors involved in their activation may depend on tumor type. As an example, osteoclasts can be metabolically fueled directly by tumor cells (Lemma et al., 2016, 2017) or also stimulated by tumor-induced osteoblasts (Sousa and Clezardin, 2018). In OS, the presence of osteoclasts in the tumor microenvironment may foster the osteoblastic behavior of tumor cells and increase their aggressiveness (Costa-Rodrigues et al., 2011) and is considered a bad prognostic factor (Salerno et al., 2008). Similarly, in BM, the pathogenic process forms when the delicate balance between bone deposition and resorption is disrupted (Alfranca et al., 2015).

Given the complexity and heterogeneity of bone tumors, the therapeutic strategies aimed at their eradication has exhibited a consistent slow-down to respect to many other carcinomas. Clearly, a better understanding of bone cancer oncogenesis is warranted to overcome drug resistance and improve low survival rate. A number of obstacles impede the study of bone cancers with the current means. These include the physical difficulty of manipulating bone as a tissue, the rarity of the tumors for sarcoma, the difficulties of obtaining tumor tissue fragments from human patients for BM, and the limited number of models that effectively mimic human disease. For all these reasons, the need for new cell models for bone cancers is becoming crucial.

In this review, we focused on the cellular models that are currently available for the study of BM or sarcomas. Such models have long been restricted to the two dimensions (2D) of dishes – an obvious obstacle to investigating structure and organization in cultured cells. However, a variety of 3D cell culture methods have recently emerged and are changing the way that multicellular systems are modeled.

ADVANCES IN 2D SYSTEMS

For decades, monolayer cultures have been the leading light in wet biology; Harrison (1907) developed the first cell culture from a nerve fiber in 1907 and demonstrated that tissue specimens could live out of the body for as long as a 4 weeks time. Since then, 2D monolayers have been worldwide extended and the culture technique substantially improved. Nowadays, monolayer cultures have been upgraded for the study of single or multiple populations. Co-seeding, transwell membranes and conditioned culture medium are examples of how cells can be easily handled. Cancer cells can be treated with conditioned medium of other cells that play a consistent role in tumor growth (i.e., fibroblasts or MSC) (Sasser et al., 2007; Iser et al., 2016). Transwell allows the culturing of two cell types seeded in separate compartments (**Figure 1**; Chiovaro et al., 2015; Avnet et al., 2017). Lastly, co-seeding two different cell population in the same compartment is also possible, but discrimination of the studied effect on one of the two populations requires the physical separation of the cells that is expensive and not always possible (Molloy et al., 2009).

Despite this, differences in cell morphology, migration, polarization, interaction with the ECM but also cell metabolism and regional genotypic and phenotypic changes (Dhiman et al., 2005; Chitcholtan et al., 2013; Russell et al., 2017), or chemoresistance (Colella et al., 2018) are often far from being confirmed in 3D models. Altogether, these difference are surely due to the lack of spatial relationships and adequate culture conditions. Among the others, one example is that cells respond differently to hard substrates like lab plastic than they do on softer ones that resemble the ECM (Engler et al., 2006).

THE UPGRADE TO THE *IN VITRO* THIRD DIMENSION

Three dimensional architecture is one of the main issues at the basis of tissue and organ formation; this level of complexity starts during embryonic development and further enhances with cell-to-cell contacts that pose the basis to intracellular functions (Fitzgerald et al., 2015). Furthermore, cells are surrounded by an ECM that crucially determines cell differentiation, proliferation, and homeostasis (Kinney et al., 2014). An ideal 3D culture model should thus properly mimic not only oncogenesis, and maintenance of tumor cell growth, but also imitate the interactions between cells intermingled within the ECM. To date, with this aim, several technologies have been developed and explored: static 3D cultures include the seeding of cells in spheroid-like structure without the extracellular matrix, and the seeding of cells in matrices or scaffolds, made of natural or synthetic biomaterials (**Figure 1**); dynamic 3D cultures include either spheroids or scaffolds cultured in bioreactors, and the seeding of cells in microfluidic perfused devices (**Figure 1**).

Spheroids

One of the pioneer studies that has opened the field to 3D cultures is the work by Sutherland et al. (1971); they were among the first to observe that lung cells grown in suspension would form spheroids that develop with an outer zone containing proliferating cells, a poorly nourished and oxygenated intermediate zone containing few cells in mitosis, and a central zone of necrosis, a typical feature of physiological tumor masses. Forced-floating spheroids are the simplest method to generate spheroids: cells are prevented to attach to the well bottom, resulting in floating aggregates and cell-cell contacts. The hanging-drop method is the most widely used and is a static technology (Kelm et al., 2003). Adversely, rotating cell culture bioreactor, spinner flasks or stirred-tank cultures (Santo et al., 2016) force homogenous spheroid formation by continuous agitation (Breslin and O'Driscoll, 2013). Also in this case, spheroids can be formed by a single cell type or can mimic interactions between multiple cells, such as tumor and stromal cells (Ishiguro et al., 2017). These culture systems are highly reproducible and have low production costs; already in 1971 it was clear that spheroids had the potential to be used for drug screening or to test radiation therapies (Sutherland et al., 1971). Despite the advantages, not all cell lines form spheroids and some form only unpredictable cell aggregates.

Matrices and Scaffolds

As for spheroids, cells seeded into matrices or on scaffolds can be cultured either in static or dynamic cultures using rotating cell culture bioreactors.

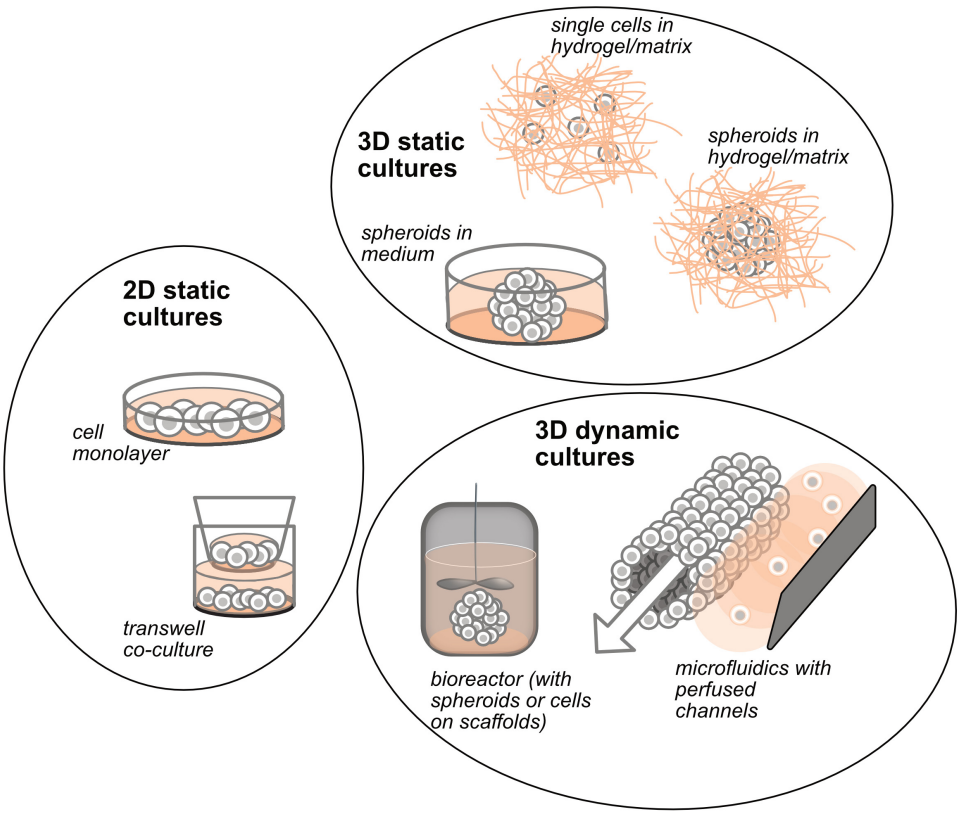

FIGURE 1 | Schematic representation of the different and most used 2D and 3D *in vitro* culture systems.

A hydrogel-based matrix is a network of physically or chemically cross-linked polymer molecules of hydrophilic nature that allows to retain large amounts of water (Ahmed, 2015) and provide a 3D biomimetic environment supporting cell proliferation and differentiation (Peck and Wang, 2013). The major advantage of hydrogels is their customization according to the specific features of the ECM. As an example, hydrogels can be designed to shrink or swell based on the environmental stimuli that they receive (Ahmed, 2015), and can be easily enriched with specific cell adhesion ligands to mimic soft tissues. Hydrogels are of synthetic or natural origin (Li and Kumacheva, 2018), and are mainly based on matrigel, collagen or fibrin. Matrigel derives from a mouse sarcoma and has the most heterogeneous composition. The chief components are structural proteins such as laminin, nidogen, collagen, and heparan sulfate proteoglycans. Matrigel polymerization depends on temperature. Collagen-based hydrogels rely also on pH and plays a crucial role in cancer progression and is the most common protein of mammalian ECM. However, the pH-dependency makes collagen-based hydrogels unsuitable for the study of the effects of tumor acidosis, a feature that is crucial for the development of bone cancer (Cortini et al., 2017; Avnet et al., 2019), or of cancer-induced bone pain (Yoneda et al., 2015; Di Pompo et al., 2017).

Traditionally described as tools made of polymeric biomaterials, 3D scaffolds have the advantage to provide recapitulation of the ECM by providing, like hydrogels, attachment sites and interstitial space for the cells that can grow and proliferate, forming 3D structures (Breslin and O'Driscoll, 2013). Scaffold stiffness can be tuned to influence cell adhesion, proliferation and activation (Keogh et al., 2010). Materials used for scaffold fabrication must be biocompatible and must induce molecular biorecognition from cells (Carletti et al., 2011). ECM-mimicking biomaterials are made of collagen, hyaluronan, matrigel, elastin, laminin-rich-extracellular matrix, and also alginate, chitosan, silk and are considered as the most biocompatible. Synthetic biomaterials include polyethylen glycol, hyaluronic acid-PEG, polyvinyl alcohol, polycaprolactone, or two-phase systems such as polyethylene glycol-dextran. A number of biomaterials, such as ceramics, can fall in the natural or synthetic category (Thakuri et al., 2018).

Microfluidic Devices

Recent advancements in tissue engineering have led to the development of living multicellular microculture systems, which are maintained in controllable microenvironments and function with organ level complexity [for an extensive review see Huh et al. (2011)]. The applications of these "on-chip" technologies are becoming increasingly popular for cancer studies (Sontheimer-Phelps et al., 2019). Continuous perfusion of media through the microfluidic network is the major innovation in these systems

(Chung et al., 2017) since it mimics blood flow and enables exchange of nutrients, oxygen and metabolites with the blood tissue that are crucial for modeling living cancer tissues. Invading cells detaching from a solid tumor are exposed to the novel microenvironment of the circulatory system. Depending on the size of the vessel, the blood flow velocity can reach 0.03–40 cm/s, with arterial hemodynamic shear-force of 4.0–30.0 dyn/cm^2 and venous shear-force of 0.5–4.0 dyn/cm^2 (McCarty et al., 2016). Therefore, tumor cells must promptly adapt from static growth to fluid shear stress (Mitchell and King, 2013; Phillips et al., 2014), a condition that is far from being taken into account on static cultures. Until few years ago, microplates supported only 2D environments (Wu et al., 2010). More recently, the third dimension has been introduced to support 3D aggregates (Toh et al., 2007; van Duinen et al., 2015; Lanz et al., 2017). Finally, microfluidics has allowed the design and the development of self-organized organ-like cell aggregates that originate from multipotent stem cells, the organoids, and has opened a whole new level of biomimicry to be achieved (Yu et al., 2019). Representative examples are the blood brain barriers, the 3D neuronal networks, the kidney, liver or the intact gut epithelium or, when mentioning cancer tissues, glioma, breast cancer or sarcoma models (Sontheimer-Phelps et al., 2019).

This technology has the power to add multiple cell lines in the same chip. As an example, it is possible to mimic the tumor-endothelial cells interaction that is fundamental for the metastasization process, including angiogenesis, intravasation and cancer cell colonization (Zervantonakis et al., 2012). Likewise, microfluidics have been thoroughly studied to better recapitulate the cancer cell-immune cell interactions, with the ultimate aim of increasing knowledge on cancer immunotherapies (Boussommier-Calleja et al., 2016).

Finally, formation of 3D spheroids by using hanging drops have been combined to microfluidic platforms for drug testing or chemoresponses assays (Marimuthu et al., 2018). The next big challenge is the full validation of these models and subsequently the implementation in drug development pipelines of the pharmaceutical industry and ultimately in personalized medicine applications.

STUDYING THE PATHOGENESIS OF TUMOUR NICHE IN 3D *IN VITRO* SYSTEMS OF BONE CANCERS

Many papers have discussed the importance of switching from 2D to 3D cultures in a number of tumor cell lines (Praharaj et al., 2018), including bone sarcoma (De Luca et al., 2018). Novel models have now been acquainted also for bone cancers, and for tumor-related bone microenvironment (**Table 1**), and that include 3D tumor-resembling structure endothelial or fibroblastic cells in order to develop antiangiogenic therapies and to better understand vasculature expansion (Lee et al., 2006; Reddy et al., 2008; de Nigris et al., 2013). 3D OS cells have been combined with 2D endothelial HUVEC cells to form a well-organized network, including tubule-like structures that infiltrated the tumor spheroids, like new vessels *in vivo*. In this model, HUVEC proliferation and expression of angiogenesis-associated genes was possible induced by VEGF secretion from quiescent OS cells, embedded in matrix at the center of the spheroid, and stressed by the hypoxic core (Chaddad et al., 2017). The vasculature also seemed to direct the reactivation of dormant disseminated tumor cells. Targeting the vascular niches in such early steps of BM delays or even prevents the metastatic relapse (Kusumbe, 2016). Likewise, a functional tri-culture has been developed for studying metastatic breast cancer that has spread to the bone. This includes a stable vascular networks within a 3D native bone matrix cultured on a microfluidic chip; this niche-on-a-chip is characterized by controlled flow velocities, shear stresses, and oxygen gradients. Interestingly, MSC, which have undergone phenotypical transition toward perivascular cell lineages, support the formation of capillary-like structures lining the vascular lumen (Marturano-Kruik et al., 2018). MSC are associated with the tumor microenviroment since they are recruited by tumor cells from the bloodstream and are a considerable component of the general host response to tissue damage caused by cancer cells (Cortini et al., 2016; Avnet et al., 2017; Cortini et al., 2017). In another breast cancer metastatic model, MSC stimulate tumor extravasation and activation of the cancer cell receptor CXCR2 and the bone-secreted chemokine CXCL5 (Bersini et al., 2014). Chemokines and interleukins are also responsible for chemo-attraction of immune cells that, once recruited to the niche, become part of the tumor bulk and play a fundamental role in the tumor TME. Microfluidic platforms retain also the possibility to monitor immune cell migration and analyze their contribution to the formation of the metastatic niche through spatial compartmentalization (Gopalakrishnan et al., 2015; Boussommier-Calleja et al., 2016).

Microfluidics have been also used to successfully recreate the complex bone marrow TME (Torisawa et al., 2014). The microchip device included two different compartments: one for the specific growth of osteoblasts and one for medium change. Because osteoblastic tissues require long-term cultures, this design was proven successful as it allowed the formation of a thick mineralized osteoblastic tissue *in vitro* in a 1 month time period (Hao et al., 2018). The bone niche can be also recreated by using bone scaffolds (Marturano-Kruik et al., 2016). In ES, for example, cell growth rate is far slower *in vivo* than that observed *in vitro*, thereby more likely reproducing reliable growth conditions (Fong et al., 2013) and mimicking critical signaling cascades, such as the IGF-1R/PI3K7mTOR signaling pathway (Lamhamedi-Cherradi et al., 2014).

ASSAYING CHEMORESISTANCE IN 3D *IN VITRO* SYSTEMS OF BONE CANCERS

Arai et al. (2013) found that spheroid cells displayed more chemoresistance to doxorubicin corresponding to higher IC50 values than conventional monolayer cells (Baek et al., 2016a) in more than 11 OS cell lines. Similarly, Baek et al. (2016b) confirmed that OS cells were more chemoresistant in 3D compared to 2D culture. Similar results were obtained also with cisplatin. Likewise, the use of MG-63 spheroids effectively

TABLE 1 | 3D models for bone cancers.

3D model	Tumor setting	Relevance	References
3D collagen gel system containing osteoblast-like cells	Metastasis from endometrial, prostate and breast cancer	Prostate cancer cells produced morphological evidence of blastic reaction and evidence of local invasion	Sourla et al., 1996
3D hybrid hydrogel system composed of collagen and alginate	Invasive breast cancer Osteosarcoma	Human mammary fibroblast cells facilitated migration of breast cancer cells out of spheroids and into the surrounding matrix	Thakuri et al., 2018
3D spheroids in combination with 2D endothelial cells		Formation of tubule-like structures that mimic vessel sprouting and angiogenesis	Chaddad et al., 2017
Microfluidic niche-on-a-chip	Metastatic breast cancer	Formation of a self-assmebled vasculature network supported by MSC	Marturano-Kruik et al., 2018
Triculture system in microfluidics	Metastatic breast cancer	Extravasation and micrometastasis generation of breast cancer cells within a bone-like microenvironment	Bersini et al., 2014
Microfluidics bone-marrow-on-a-chip	Hematological diseases	Analysis of drug responses and toxicity	Torisawa et al., 2014
Microfluidics bone-on-a-chip	Metastatic breast cancer	Interaction between cancer cells and bone matrix that lead to tumor colonization	Hao et al., 2018
Bioreactors	Ewing sarcoma	Recreation of the bone niche that mimics native tumor properties	Marturano-Kruik et al., 2016
Bone scaffold	Ewing sarcoma	Analysis of cell cytotoxicity to respect to 2D	Fong et al., 2013
Spheroids	Osteosarcoma	Analysis of chemoresistance	Arai et al., 2013
Spheroids	Osteosarcoma	Analysis of cell cytotoxicity to doxorubicin	Baek et al., 2016a
Spheroids	Osteosarcoma	Analysis of cell cytotoxicity to cisplatin	Baek et al., 2016b
Spheroids	Osteosarcoma	Analysis of cell chemoresistance to oxidovanadium(IV)	Leon et al., 2016
Spheroids	Chondrosarcoma	Analysis of cell chemoresistance to doxorubicin and mafosfamide	Monderer et al., 2013
Spheroids	Chondrosarcoma	Analysis of cell cytotoxicity to respect to salinomycin	Perut et al., 2018
Microfluidics co-culture of tumor and MSC	Ewing sarcoma	Resistance of tumor cells to IGF-1R inhibitors due to the presence of MSC	Santoro et al., 2017

predicted the cytotoxicity of oxidovanadium(IV) *in vivo* models (Leon et al., 2016). 3D CS cultures are resistant to doxorubicin and mafosfamide, when compared to standard monolayer cultures (Monderer et al., 2013). However, the use of 3D spheroids allowed to reveal that treatment with the ionophore salinomycin, previously uncharacterized for its effects on CS, significantly enhanced the cytotoxic effect to doxorubicin in 3D structures (Perut et al., 2018).

Finally, drug sensitivity of tumor cells might be strongly affected by microenvironmental factors that include the presence of MSC (Avnet et al., 2017; Senthebane et al., 2017), also when co-cultured with cancer cells in 3D structures. As an example, the 3D assembly of ES cells with MSC elicits ligand-mediated activation of the insulin-like growth factor-1 receptor (IGF-1R), thereby mediating resistance to IGF-1R inhibitors (Santoro et al., 2017).

FROM PRECLINICAL MODELS TO CLINICAL VALIDATION

The main aim of expanding the knowledge on culture systems is to be able to translate the molecular features of the 3D cell cultures of individual patients using them as a platform for drug screening and to identify biomarkers and new drug targets (Breslin and O'Driscoll, 2013). Findings using 3D models that more accurately reflect human sarcoma biology are likely to translate into improved clinical outcomes (Gao et al., 2017). As an example moving in this direction, Pauli and colleagues have made a great effort in describing a precision-medicine platform that integrates whole-exome sequencing with a living biobank that enables high-throughput drug screens on patient-derived tumor organoids. To date, 56 tumor-derived organoid cultures and 19 patient-derived xenograft models have been established from the 769 patients enrolled in an Institutional Review Board–approved clinical trial (Pauli et al., 2017). These types of approach have the potential not only to select the appropriate therapeutic option, but also to improve the knowledge on the molecular cues that lay at the basis of tumor development.

CONCLUSION

Three dimensional models offer early promise in establishing robust preclinical platforms for the identification of crucial molecular pathways and for the assessment of clinical efficacy of novel drugs to inhibit cancer development and progression. Despite the perfect model currently does not exist and 3D approaches are characterized by weaknesses, these greatly expand the spectrum of cancer subtypes that might be considered for new drug screening and for the development of personalized medicine. In the field of bone cancers, rare and deadly diseases, this is of paramount importance to improve the clinical outcomes.

AUTHOR CONTRIBUTIONS

All authors listed have made a substantial, direct and intellectual contribution to the work, and approved it for publication.

FUNDING

This study was funded by the Italian Association for Cancer Research (AIRC IG# 21403 to NB) and by the financial support for Scientific Research "5xMille 2016 Ministry of Health" (to NB).

REFERENCES

Ahmed, E. M. (2015). Hydrogel: preparation, characterization, and applications: a review. *J. Adv. Res.* 6, 105–121. doi: 10.1016/j.jare.2013.07.006

Alfranca, A., Martinez-Cruzado, L., Tornin, J., Abarrategi, A., Amaral, T., de Alava, E., et al. (2015). Bone microenvironment signals in osteosarcoma development. *Cell Mol. Life Sci.* 72, 3097–3113. doi: 10.1007/s00018-015-1918-y

Arai, K., Sakamoto, R., Kubota, D., and Kondo, T. (2013). Proteomic approach toward molecular backgrounds of drug resistance of osteosarcoma cells in spheroid culture system. *Proteomics* 13, 2351–2360. doi: 10.1002/pmic.201300053

Avnet, S., Di Pompo, G., Chano, T., Errani, C., Ibrahim-Hashim, A., Gillies, R. J., et al. (2017). Cancer-associated mesenchymal stroma fosters the stemness of osteosarcoma cells in response to intratumoral acidosis via NF-kappaB activation. *Int. J. Cancer* 140, 1331–1345. doi: 10.1002/ijc.30540

Avnet, S., Di Pompo, G., Lemma, S., and Baldini, N. (2019). Cause and effect of microenvironmental acidosis on bone metastases. *Cancer Metastasis Rev.* doi: 10.1007/s10555-019-09790-9. [Epub ahead of print].

Baek, N., Seo, O. W., Kim, M., Hulme, J., and An, S. S. (2016a). Monitoring the effects of doxorubicin on 3D-spheroid tumor cells in real-time. *Onco. Targets Ther.* 9, 7207–7218. doi: 10.2147/OTT.S112566

Baek, N., Seo, O. W., Lee, J., Hulme, J., and An, S. S. (2016b). Real-time monitoring of cisplatin cytotoxicity on three-dimensional spheroid tumor cells. *Drug Des. Devel. Ther.* 10, 2155–2165. doi: 10.2147/DDDT.S108004

Bersini, S., Jeon, J. S., Dubini, G., Arrigoni, C., Chung, S., Charest, J. L., et al. (2014). A microfluidic 3D in vitro model for specificity of breast cancer metastasis to bone. *Biomaterials* 35, 2454–2461. doi: 10.1016/j.biomaterials.2013.11.050

Boussommier-Calleja, A., Li, R., Chen, M. B., Wong, S. C., and Kamm, R. D. (2016). Microfluidics: a new tool for modeling cancer-immune interactions. *Trends Cancer* 2, 6–19. doi: 10.1016/j.trecan.2015.12.003

Breslin, S., and O'Driscoll, L. (2013). Three-dimensional cell culture: the missing link in drug discovery. *Drug Discov. Today* 18, 240–249. doi: 10.1016/j.drudis.2012.10.003

Carletti, E., Motta, A., and Migliaresi, C. (2011). Scaffolds for tissue engineering and 3D cell culture. *Methods Mol. Biol.* 695, 17–39. doi: 10.1007/978-1-60761-984-0_2

Chaddad, H., Kuchler-Bopp, S., Fuhrmann, G., Gegout, H., Ubeaud-Sequier, G., Schwinte, P., et al. (2017). Combining 2D angiogenesis and 3D osteosarcoma microtissues to improve vascularization. *Exp. Cell Res.* 360, 138–145. doi: 10.1016/j.yexcr.2017.08.035

Chiovaro, F., Martina, E., Bottos, A., Scherberich, A., Hynes, N. E., and Chiquet-Ehrismann, R. (2015). Transcriptional regulation of tenascin-W by TGF-beta signaling in the bone metastatic niche of breast cancer cells. *Int. J. Cancer* 137, 1842–1854. doi: 10.1002/ijc.29565

Chitcholtan, K., Asselin, E., Parent, S., Sykes, P. H., and Evans, J. J. (2013). Differences in growth properties of endometrial cancer in three dimensional (3D) culture and 2D cell monolayer. *Exp. Cell Res.* 319, 75–87. doi: 10.1016/j.yexcr.2012.09.012

Chung, M., Ahn, J., Son, K., Kim, S., and Jeon, N. L. (2017). . Biomimetic Model of Tumor Microenvironment on Microfluidic Platform. *Adv. Healthc. Mater.* 6:1700196. doi: 10.1002/adhm.201700196

Colella, G., Fazioli, F., Gallo, M., De Chiara, A., Apice, G., Ruosi, C., et al. (2018). Sarcoma spheroids and organoids-promising tools in the era of personalized medicine. *Int. J. Mol. Sci.* 19:615. doi: 10.3390/ijms19020615

Cortini, M., Avnet, S., and Baldini, N. (2017). Mesenchymal stroma: role in osteosarcoma progression. *Cancer Lett.* 405, 90–99. doi: 10.1016/j.canlet.2017.07.024

Cortini, M., Massa, A., Avnet, S., Bonuccelli, G., and Baldini, N. (2016). Tumor-activated mesenchymal stromal cells promote osteosarcoma stemness and migratory potential via IL-6 secretion. *PLoS One* 11:e0166500. doi: 10.1371/journal.pone.0166500

Costa-Rodrigues, J., Fernandes, A., and Fernandes, M. H. (2011). Reciprocal osteoblastic and osteoclastic modulation in co-cultured MG63 osteosarcoma cells and human osteoclast precursors. *J. Cell Biochem.* 112, 3704–3713. doi: 10.1002/jcb.23295

De Luca, A., Raimondi, L., Salamanna, F., Carina, V., Costa, V., Bellavia, D., et al. (2018). Relevance of 3d culture systems to study osteosarcoma environment. *J. Exp. Clin. Cancer Res.* 37:2. doi: 10.1186/s13046-017-0663-5

de Nigris, F., Mancini, F. P., Schiano, C., Infante, T., Zullo, A., Minucci, P. B., et al. (2013). Osteosarcoma cells induce endothelial cell proliferation during neo-angiogenesis. *J. Cell Physiol.* 228, 846–852. doi: 10.1002/jcp.24234

Dhiman, H. K., Ray, A. R., and Panda, A. K. (2005). Three-dimensional chitosan scaffold-based MCF-7 cell culture for the determination of the cytotoxicity of tamoxifen. *Biomaterials* 26, 979–986. doi: 10.1016/j.biomaterials.2004.04.012

Di Pompo, G., Lemma, S., Canti, L., Rucci, N., Ponzetti, M., Errani, C., et al. (2017). Intratumoral acidosis fosters cancer-induced bone pain through the activation of the mesenchymal tumor-associated stroma in bone metastasis from breast carcinoma. *Oncotarget* 8, 54478–54496. doi: 10.18632/oncotarget.17091

Engler, A. J., Sen, S., Sweeney, H. L., and Discher, D. E. (2006). Matrix elasticity directs stem cell lineage specification. *Cell* 126, 677–689. doi: 10.1016/j.cell.2006.06.044

Fitzgerald, K. A., Malhotra, M., Curtin, C. M., O'Brien, F. J., and O'Driscoll, C. M. (2015). Life in 3D is never flat: 3D models to optimise drug delivery. *J. Control Release* 215, 39–54. doi: 10.1016/j.jconrel.2015.07.020

Fong, E. L., Lamhamedi-Cherradi, S. E., Burdett, E., Ramamoorthy, V., Lazar, A. J., Kasper, F. K., et al. (2013). Modeling ewing sarcoma tumors in vitro with 3D scaffolds. *Proc. Natl. Acad Sci. U.S.A.* 110, 6500–6505. doi: 10.1073/pnas.1221403110

Fornetti, J., Welm, A. L., and Stewart, S. A. (2018). Understanding the bone in cancer metastasis. *J. Bone Miner. Res.* 33, 2099–2113. doi: 10.1002/jbmr.3618

Gao, S., Shen, J., Hornicek, F., and Duan, Z. (2017). Three-dimensional (3D) culture in sarcoma research and the clinical significance. *Biofabrication* 9:032003. doi: 10.1088/1758-5090/aa7fdb

Gopalakrishnan, N., Hannam, R., Casoni, G. P., Barriet, D., Ribe, J. M., Haug, M., et al. (2015). Infection and immunity on a chip: a compartmentalised microfluidic platform to monitor immune cell behaviour in real time. *Lab Chip* 15, 1481–1487. doi: 10.1039/c4lc01438c

Hao, S., Ha, L., Cheng, G., Wan, Y., Xia, Y., Sosnoski, D. M., et al. (2018). A spontaneous 3D bone-on-a-chip for bone metastasis study of breast cancer cells. *Small* 14:e1702787. doi: 10.1002/smll.201702787

Harrison, R. G. (1907). Observations of the living developing nerve fiber. *Anat. Rec.* 1, 116–128.

Huh, D., Hamilton, G. A., and Ingber, D. E. (2011). From 3D cell culture to organs-on-chips. *Trends Cell Biol.* 21, 745–754. doi: 10.1016/j.tcb.2011.09.005

Iser, I. C., Ceschini, S. M., Onzi, G. R., Bertoni, A. P., Lenz, G., and Wink, M. R. (2016). Conditioned medium from adipose-derived stem cells (ADSCs) promotes epithelial-to-mesenchymal-like transition (EMT-Like) in glioma cells In vitro. *Mol. Neurobiol.* 53, 7184–7199. doi: 10.1007/s12035-015-9585-4

Ishiguro, T., Ohata, H., Sato, A., Yamawaki, K., Enomoto, T., and Okamoto, K. (2017). Tumor-derived spheroids: relevance to cancer stem cells and clinical applications. *Cancer Sci.* 108, 283–289. doi: 10.1111/cas.13155

Kelm, J. M., Timmins, N. E., Brown, C. J., Fussenegger, M., and Nielsen, L. K. (2003). Method for generation of homogeneous multicellular tumor spheroids applicable to a wide variety of cell types. *Biotechnol. Bioeng.* 83, 173–180. doi: 10.1002/bit.10655

Keogh, M. B., O'Brien, F. J., and Daly, J. S. (2010). Substrate stiffness and contractile behaviour modulate the functional maturation of osteoblasts on a collagen-GAG scaffold. *Acta Biomater.* 6, 4305–4313. doi: 10.1016/j.actbio.2010.06.001

Kinney, M. A., Hookway, T. A., Wang, Y., and McDevitt, T. C. (2014). Engineering three-dimensional stem cell morphogenesis for the development of tissue models and scalable regenerative therapeutics. *Ann. Biomed. Eng.* 42, 352–367. doi: 10.1007/s10439-013-0953-9

Kusumbe, A. P. (2016). Vascular niches for disseminated tumour cells in bone. *J. Bone Oncol.* 5, 112–116. doi: 10.1016/j.jbo.2016.04.003

Lamhamedi-Cherradi, S. E., Santoro, M., Ramammoorthy, V., Menegaz, B. A., Bartholomeusz, G., Iles, L. R., et al. (2014). 3D tissue-engineered model of Ewing's sarcoma. *Adv. Drug Deliv. Rev.* 7, 155–171. doi: 10.1016/j.addr.2014.07.012

Lanz, H. L., Saleh, A., Kramer, B., Cairns, J., Ng, C. P., Yu, J., et al. (2017). Therapy response testing of breast cancer in a 3D high-throughput perfused microfluidic platform. *BMC Cancer* 17:709. doi: 10.1186/s12885-017-3709-3

Lee, T. H., Bolontrade, M. F., Worth, L. L., Guan, H., Ellis, L. M., and Kleinerman, E. S. (2006). Production of VEGF165 by Ewing's sarcoma cells induces vasculogenesis and the incorporation of CD34+ stem cells into the expanding tumor vasculature. *Int. J. Cancer* 119, 839–846. doi: 10.1002/ijc.21916

Lemma, S., Di Pompo, G., Porporato, P. E., Sboarina, M., Russell, S., Gillies, R. J., et al. (2017). MDA-MB-231 breast cancer cells fuel osteoclast metabolism and activity: a new rationale for the pathogenesis of osteolytic bone metastases. *Biochim. Biophys. Acta Mol. Basis Dis.* 1863, 3254–3264. doi: 10.1016/j.bbadis.2017.08.030

Lemma, S., Sboarina, M., Porporato, P. E., Zini, N., Sonveaux, P., Di Pompo, G., et al. (2016). Energy metabolism in osteoclast formation and activity. *Int. J. Biochem. Cell Biol.* 79, 168–180. doi: 10.1016/j.biocel.2016.08.034

Leon, I. E., Cadavid-Vargas, J. F., Resasco, A., Maschi, F., Ayala, M. A., Carbone, C., et al. (2016). In vitro and in vivo antitumor effects of the VO-chrysin complex on a new three-dimensional osteosarcoma spheroids model and a xenograft tumor in mice. *J. Biol. Inorg. Chem.* 21, 1009–1020. doi: 10.1007/s00775-016-1397-0

Lewis, V. O. (2009). What's new in musculoskeletal oncology. *J. Bone Joint Surg. Am.* 91, 1546–1556. doi: 10.2106/JBJS.I.00375

Li, Y., and Kumacheva, E. (2018). Hydrogel microenvironments for cancer spheroid growth and drug screening. *Sci. Adv.* 4:eaas8998. doi: 10.1126/sciadv.aas8998

Lye, K. L., Nordin, N., Vidyadaran, S., and Thilakavathy, K. (2016). Mesenchymal stem cells: from stem cells to sarcomas. *Cell Biol. Int.* 40, 610–618. doi: 10.1002/cbin.10603

Marimuthu, M., Rousset, N., St-Georges-Robillard, A., Lateef, M. A., Ferland, M., Mes-Masson, A. M., et al. (2018). Multi-size spheroid formation using microfluidic funnels. *Lab Chip* 18, 304–314. doi: 10.1039/c7lc00970d

Marturano-Kruik, A., Nava, M. M., Yeager, K., Chramiec, A., Hao, L., Robinson, S., et al. (2018). Human bone perivascular niche-on-a-chip for studying metastatic colonization. *Proc. Natl. Acad Sci. U.S.A.* 115, 1256–1261. doi: 10.1073/pnas.1714282115

Marturano-Kruik, A., Villasante, A., and Vunjak-Novakovic, G. (2016). Bioengineered models of solid human tumors for cancer research. *Methods Mol. Biol.* 1502, 203–211. doi: 10.1007/7651_2016_353

McCarty, O. J., Ku, D., Sugimoto, M., King, M. R., Cosemans, J. M., Neeves, K. B., et al. (2016). Dimensional analysis and scaling relevant to flow models of thrombus formation: communication from the SSC of the ISTH. *J. Thromb. Haemost.* 14, 619–622. doi: 10.1111/jth.13241

Mitchell, M. J., and King, M. R. (2013). Computational and experimental models of cancer cell response to fluid shear stress. *Front. Oncol.* 3:44. doi: 10.3389/fonc.2013.00044

Mohseny, A. B., Szuhai, K., Romeo, S., Buddingh, E. P., Briaire-de Bruijn, I., de Jong, D., et al. (2009). Osteosarcoma originates from mesenchymal stem cells in consequence of aneuploidization and genomic loss of Cdkn2. *J. Pathol.* 219, 294–305. doi: 10.1002/path.2603

Molloy, A. P., Martin, F. T., Dwyer, R. M., Griffin, T. P., Murphy, M., Barry, F. P., et al. (2009). Mesenchymal stem cell secretion of chemokines during differentiation into osteoblasts, and their potential role in mediating interactions with breast cancer cells. *Int. J. Cancer* 124, 326–332. doi: 10.1002/ijc.23939

Monderer, D., Luseau, A., Bellec, A., David, E., Ponsolle, S., Saiagh, S., et al. (2013). New chondrosarcoma cell lines and mouse models to study the link between chondrogenesis and chemoresistance. *Lab Invest.* 93, 1100–1114. doi: 10.1038/labinvest.2013.101

Park, T. S., Donnenberg, V. S., Donnenberg, A. D., Zambidis, E. T., and Zimmerlin, L. (2014). Dynamic interactions between cancer stem cells and their stromal partners. *Curr. Pathobiol. Rep.* 2, 41–52. doi: 10.1007/s40139-013-0036-5

Pauli, C., Hopkins, B. D., Prandi, D., Shaw, R., Fedrizzi, T., Sboner, A., et al. (2017). Personalized in vitro and in vivo cancer models to guide precision medicine. *Cancer Discov.* 7, 462–477. doi: 10.1158/2159-8290.CD-16-1154

Peck, Y., and Wang, D. A. (2013). Three-dimensionally engineered biomimetic tissue models for in vitro drug evaluation: delivery, efficacy and toxicity. *Expert Opin. Drug Deliv.* 10, 369–383. doi: 10.1517/17425247.2013.751096

Perut, F., Sbrana, F. V., Avnet, S., De Milito, A., and Baldini, N. (2018). Spheroid-based 3D cell cultures identify salinomycin as a promising drug for the treatment of chondrosarcoma. *J. Orthop. Res.* 36, 2305–2312. doi: 10.1002/jor.23880

Phillips, K. G., Kuhn, P., and McCarty, O. J. (2014). Physical biology in cancer. 2. The physical biology of circulating tumor cells. *Am. J. Physiol. Cell. Physiol.* 306, C80–C88. doi: 10.1152/ajpcell.00294.2013

Praharaj, P. P., Bhutia, S. K., Nagrath, S., Bitting, R. L., and Deep, G. (2018). Circulating tumor cell-derived organoids: current challenges and promises in medical research and precision medicine. *Biochim. Biophys. Acta Rev. Cancer* 1869, 117–127. doi: 10.1016/j.bbcan.2017.12.005

Reddy, K., Zhou, Z., Jia, S. F., Lee, T. H., Morales-Arias, J., Cao, Y., et al. (2008). Stromal cell-derived factor-1 stimulates vasculogenesis and enhances Ewing's sarcoma tumor growth in the absence of vascular endothelial growth factor. *Int. J. Cancer* 123, 831–837. doi: 10.1002/ijc.23582

Russell, S., Wojtkowiak, J., Neilson, A., and Gillies, R. J. (2017). Metabolic profiling of healthy and cancerous tissues in 2D and 3D. *Sci. Rep.* 7:15285. doi: 10.1038/s41598-017-15325-5

Salerno, M., Avnet, S., Alberghini, M., Giunti, A., and Baldini, N. (2008). Histogenetic characterization of giant cell tumor of bone. *Clin. Orthop. Relat. Res.* 466, 2081–2091. doi: 10.1007/s11999-008-0327-z

Santo, V. E., Estrada, M. F., Rebelo, S. P., Abreu, S., Silva, I., Pinto, C., et al. (2016). Adaptable stirred-tank culture strategies for large scale production of multicellular spheroid-based tumor cell models. *J. Biotechnol.* 221, 118–129. doi: 10.1016/j.jbiotec.2016.01.031

Santoro, M., Menegaz, B. A., Lamhamedi-Cherradi, S. E., Molina, E. R., Wu, D., Priebe, W., et al. (2017). Modeling Stroma-Induced Drug Resistance in a Tissue-Engineered Tumor Model of Ewing Sarcoma. *Tissue Eng. Part A* 23, 80–89. doi: 10.1089/ten.TEA.2016.0369

Sasser, A. K., Sullivan, N. J., Studebaker, A. W., Hendey, L. F., Axel, A. E., and Hall, B. M. (2007). Interleukin-6 is a potent growth factor for ER-alpha-positive human breast cancer. *FASEB J.* 21, 3763–3770. doi: 10.1096/fj.07-8832com

Senthebane, D. A., Rowe, A., Thomford, N. E., Shipanga, H., Munro, D., Mazeedi, M., et al. (2017). The role of tumor microenvironment in chemoresistance: to survive, keep your enemies closer. *Int. J. Mol. Sci.* 18:1580. doi: 10.3390/ijms18071586

Sontheimer-Phelps, A., Hassell, B. A., and Ingber, D. E. (2019). Modelling cancer in microfluidic human organs-on-chips. *Nat. Rev. Cancer* 19, 65–81. doi: 10.1038/s41568-018-0104-6

Sourla, A., Doillon, C., and Koutsilieris, M. (1996). Three-dimensional type I collagen gel system containing MG-63 osteoblasts-like cells as a model for studying local bone reaction caused by metastatic cancer cells. *Anticancer Res.* 16, 2773–2780.

Sousa, S., and Clezardin, P. (2018). Bone-targeted therapies in cancer-induced bone disease. *Calcif. Tissue Int.* 102, 227–250. doi: 10.1007/s00223-017-0353-5

Sutherland, R. M., McCredie, J. A., and Inch, W. R. (1971). Growth of multicell spheroids in tissue culture as a model of nodular carcinomas. *J. Natl. Cancer Inst.* 46, 113–120.

Thakuri, P. S., Liu, C., Luker, G. D., and Tavana, H. (2018). Biomaterials-based approaches to tumor spheroid and organoid modeling. *Adv. Healthc. Mater* 7:e1700980. doi: 10.1002/adhm.201700980

Toh, Y. C., Zhang, C., Zhang, J., Khong, Y. M., Chang, S., Samper, V. D., et al. (2007). A novel 3D mammalian cell perfusion-culture system in microfluidic channels. *Lab Chip* 7, 302–309. doi: 10.1039/b614872g

Torisawa, Y. S., Spina, C. S., Mammoto, T., Mammoto, A., Weaver, J. C., Tat, T., et al. (2014). Bone marrow-on-a-chip replicates hematopoietic niche physiology in vitro. *Nat. Methods* 11, 663–669. doi: 10.1038/nmeth.2938

van Duinen, V., Trietsch, S. J., Joore, J., Vulto, P., and Hankemeier, T. (2015). Microfluidic 3D cell culture: from tools to tissue models. *Curr. Opin. Biotechnol.* 35, 118–126. doi: 10.1016/j.copbio.2015.05.002

Wu, M. H., Huang, S. B., and Lee, G. B. (2010). Microfluidic cell culture systems for drug research. *Lab Chip* 10, 939–956. doi: 10.1039/b921695b

Xiao, W., Mohseny, A. B., Hogendoorn, P. C., and Cleton-Jansen, A. M. (2013). Mesenchymal stem cell transformation and sarcoma genesis. *Clin. Sarcoma. Res.* 3:10. doi: 10.1186/2045-3329-3-10

Yoneda, T., Hiasa, M., Nagata, Y., Okui, T., and White, F. (2015). Contribution of acidic extracellular microenvironment of cancer-colonized bone to bone pain. *Biochim. Biophys. Acta* 1848(10 Pt B), 2677–2684. doi: 10.1016/j.bbamem.2015.02.004

Yu, F., Hunziker, W., and Choudhury, D. (2019). Engineering microfluidic organoid-on-a-chip platforms. *Micromachines* 10:165. doi: 10.3390/mi10030165

Zervantonakis, I. K., Hughes-Alford, S. K., Charest, J. L., Condeelis, J. S., Gertler, F. B., and Kamm, R. D. (2012). Three-dimensional microfluidic model for tumor cell intravasation and endothelial barrier function. *Proc. Natl. Acad. Sci. U.S.A.* 109, 13515–13520. doi: 10.1073/pnas.1210182109

Conflict of Interest Statement: The authors declare that the research was conducted in the absence of any commercial or financial relationships that could be construed as a potential conflict of interest.

frontiers in Genetics

MINI REVIEW
published: 19 September 2019
doi: 10.3389/fgene.2019.00873

Mathematical Models of Organoid Cultures

Sandra Montes-Olivas[1], Lucia Marucci[1,2,3†] and Martin Homer[1†]*

[1] Department of Engineering Mathematics, University of Bristol, Bristol, United Kingdom, [2] School of Cellular and Molecular Medicine, University of Bristol, Bristol, United Kingdom, [3] Bristol Centre for Synthetic Biology, University of Bristol, Bristol, United Kingdom

Organoids are engineered three-dimensional tissue cultures derived from stem cells and capable of self-renewal and self-organization into a variety of progenitors and differentiated cell types. An organoid resembles the cellular structure of an organ and retains some of its functionality, while still being amenable to *in vitro* experimental study. Compared with two-dimensional cultures, the three-dimensional structure of organoids provides a more realistic environment and structural organization of *in vivo* organs. Similarly, organoids are better suited to reproduce signaling pathway dynamics *in vitro*, due to a more realistic physiological environment. As such, organoids are a valuable tool to explore the dynamics of organogenesis and offer routes to personalized preclinical trials of cancer progression, invasion, and drug response. Complementary to experiments, mathematical and computational models are valuable instruments in the description of spatiotemporal dynamics of organoids. Simulations of mathematical models allow the study of multiscale dynamics of organoids, at both the intracellular and intercellular levels. Mathematical models also enable us to understand the underlying mechanisms responsible for phenotypic variation and the response to external stimulation in a cost- and time-effective manner. Many recent studies have developed laboratory protocols to grow organoids resembling different organs such as the intestine, brain, liver, pancreas, and mammary glands. However, the development of mathematical models specific to organoids remains comparatively underdeveloped. Here, we review the mathematical and computational approaches proposed so far to describe and predict organoid dynamics, reporting the simulation frameworks used and the models' strengths and limitations.

Keywords: organoids, mathematical modeling, agent-based models, 3D tissue, differential equations, computational modeling

OPEN ACCESS

Edited by:
Thimios Mitsiadis,
University of Zurich, Switzerland

Reviewed by:
Nenad Filipovic,
University of Kragujevac, Serbia
Eumorphia Remboutsika,
National and Kapodistrian University of Athens, Greece
Claudio Cantù,
Linköping University, Sweden

***Correspondence:**
Martin Homer
martin.homer@bristol.ac.uk

†These authors share last authorship

Specialty section:
This article was submitted to Stem Cell Research, a section of the journal Frontiers in Genetics

Received: *10 May 2019*
Accepted: *20 August 2019*
Published: *19 September 2019*

Citation:
Montes-Olivas S, Marucci L and Homer M (2019) Mathematical Models of Organoid Cultures. Front. Genet. 10:873. doi: 10.3389/fgene.2019.00873

BACKGROUND

Biological models can recapitulate functions at the molecular, cellular, and tissue levels. Nowadays, there are several biological models which are used to emulate different aspects of human body functions (Shamir and Ewald, 2014). However, some of these models still have drawbacks that prevent them from being faithful representations. For instance, animal models can predict toxicological and pharmaceutical reactions but are limited by the differences between animal and human structural physiology; furthermore, *in vivo* systems are complex to analyze, due to interactions and feedback across cell types, regulation levels, and internal and external environments (Hartung, 2008; Shanks et al., 2009). Traditional two-dimensional (2D) cell cultures are appealing

for their simplicity and efficiency but are also limited by their setting and lack accurate representation of the interactions between the cellular and extracellular environments (Duval et al., 2017). Similarly, three-dimensional (3D) cell aggregates formed by terminally differentiated cells lack the capacity of self-organization, self-renewal, and differentiation into specific cell types (Yin et al., 2016).

Organoid technology has emerged as a tool to bridge the gap between cellular- and tissue/organ-level biological models, giving a more realistic representation of the *in vivo* tissue spatial organization and of the interactions between the cellular and extracellular environments, while retaining certain physiological functions (Lancaster and Knoblich, 2014). An organoid is a multicellular 3D tissue construct derived from stem cells and grown *in vitro*. Organoids can better recreate the natural development and the maintenance of tissue, thanks to the intrinsic ability of stem cells to form complex structures and differentiate into organ-specific cells when provided with specific exogenous factors.

Nevertheless, complex biological systems require a system-level understanding as they integrate many mechanisms across scales. Typically, they involve intracellular protein interactions, signaling pathways, and genetic networks, along with intercellular biomechanical interactions among cells, also dependent on the culture environment. Mathematical and computational *in silico* models are valuable tools to study the interconnections and dynamics arising from these mechanisms (Kriete and Eils, 2014); they can be used to predict system behaviors when perturbations to wild-type conditions occur, in conditions not easy to implement experimentally, and can provide guidance in the design of new experiments (Szallasi et al., 2010). From a mathematical modeling perspective, an organoid is a complex biological system, with the benefit over the experimental counterparts of well-defined initial conditions and quantifiable mechanical properties and interactions with the culturing environment. Computational models can help to predict the system behavior as a function of quantifiable parameters, with the final aim of obtaining robust and reproducible biological models to perform clinical studies (Dahl-Jensen and Grapin-botton, 2017). To date, computational descriptions of organoids remain underdeveloped as compared with the advances realized in the development of experimental protocols.

The aim of this review is to survey recent advances in the area of mathematical and computational organoid modeling and to highlight the importance of engaging biologists with the development and analysis of these models, in order to gain a quantitative description and prediction of organoid dynamics and physiology.

MATERIALS AND METHODS

A literature review was performed using PubMed and Web of Science with the following keywords: organoid, developmental organoid, gastruloid, computational model, mathematical model, computational modelling, and mathematical modelling. All papers published at any time were included. The search retrieved 21 results. Of these, we considered only original studies in which a mathematical or computational model was developed to aid in the understanding of fundamental mechanisms presented in organoids, their functionality, or their morphology. The review excludes studies where organoids were used only as biological models or where mathematical or computational models were employed to simulate or confirm a hypothesis not directly related to specific organoid characteristics. Therefore, a total of 10 original papers were included (see **Table 1**—which (I) summarizes key features of the models considered and (II) provides references and links to source codes of useful agent-based frameworks—and **Figure 1**, which illustrates pictorially the different model classes).

MATHEMATICAL MODELS OF ORGANOIDS

Intestinal Organoids

The intestinal epithelium undergoes continuous self-renewal: proliferation and consequent differentiation of adult stem cells enable maintenance of intestinal homeostasis and functions (Uma, 2010). Due to this self-renewal, the intestinal epithelium is also susceptible to rapid production and dispersion of tumor cells, and colorectal cancer is one of the most common cancers worldwide (Granados-Romero et al., 2017). Intestinal organoids are a valuable tool to study intestinal tissue dynamics and support the discovery of new oncologic treatments for intestinal cancer (Wallach and Bayrer, 2017). In 2009, Clevers' group published the first protocol to produce intestinal organoids (Sato et al., 2009). Since then, the experimental techniques for intestinal organoids have been further refined (Nakamura and Sato, 2018).

To date, most mathematical models of organoids have focused on intestinal organoids. In 2012, Buske and colleagues developed the first intestinal organoid computational model (Buske et al., 2012), building on a previous formalism they developed for the intestinal crypt (Buske et al., 2011). Their 3D individual-cell-based computational model can simulate intestinal organoid organization and formation according to experimental data of cell turnover and spatial distribution. The model was developed using the computational framework Computational Geometry Algorithms Library (CGAL) (Fabri et al., 2000), defining a basement membrane network formed by a triangulated network of stiff polymers, representing the cells as spheres in contact with this network. Cells were modeled as elastic objects that adhere and interact with the simulated basal membrane network through the network of mesh points. The basal membrane network connects with each cell and repels them in order to prevent penetration due to cell movement and organoid growth. Additionally, stem cell maintenance and differentiation were simulated by accounting for the number of neighboring cells active in Wnt and Notch signaling (**Figure 1A**). For example, undifferentiated cells differentiate into Paneth (terminally differentiated) cells if there are not enough Paneth cell neighbors to supplement Wnt. Additionally, if there are neither enough goblet (secretory differentiated) cells to supply Notch nor enough Paneth cells, then stem cells will differentiate into goblet cells until enough

TABLE 1 | An overview of (I) articles that present computational models of organoid systems and (II) access information of software frameworks mentioned for agent-based models.

I. Overview of *in silico* organoid models

Model type	Basis of the model	Author/ references	Simulated cell types	Software	Space	Model outcome	Figure ref.
Agent-based model	Intestinal organoid	Buske et al., 2012	Undifferentiated, Paneth, enterocyte, goblet cells	CGAL	3D	Provides an analysis of the biomechanical impact alongside with Wnt and Notch signaling dynamics in the spatiotemporal organization of intestinal organoids	**Figure 1A**
		Langlands et al., 2016	Stem cells and Paneth cells	CHASTE	2D	Presents a biomechanical analysis of the Paneth cells' role in the production of crypt fission	**Figure 1B**
		Almet el al., 2018	Hard and soft cells	CHASTE	2D	Analyzes the biomechanical properties of hard cells and soft cells and the required population proportions to produce crypt fission	**Figure 1B**
		Thalheim et al., 2018	Stem, Paneth, goblet, and enterocyte cells	CGAL	3D	Explores the growth pattern of intestinal organoids produced by Wnt and Notch signaling dynamics and attempts to simulate a cyst-like growth pattern	**Figure 1A**
	Optic-cup organoid	Okuda et al., 2018a	Embryonic stem cells (ESCs)	Custom C++ software	3D	Describes the effect that individual-cell mechanical forces have in the formation of the optic cup by performing *in vitro* and *in silico* experimentation	**Figure 1C**
Equation-based model	Intestinal organoid	Yan et al., 2018	Stem, committed progenitor, terminally differentiated and dead cells	MATLAB	3D	Investigates the growth patterns and spatial distributions of cell populations in the presence of exogenous substances such as Wnt, BMP, and HGF	**Figure 1D**
	Cerebral organoid	McMurtrey, 2016	Metabolic active brain cells	MATLAB	3D	Examines diverse diffusion models to test and predict growth patterns of cerebral organoids	**Figure 1E**
		Berger et al., 2018	Human neuroepithelial stem cells (NESCs)	COMSOL Multiphysics 4.3	3D	Introduces a computational model of oxygen transport and consumption in midbrain-specific organoids	**Figure 1F**
	Gastruloids	Etoc et al., 2016	Human ESCs (hESCs)	MATLAB	2D	Presents a model based on the dynamics of BMP4, pSMAD1, NOGGIN, and receptor re-localization to determine the micropatterns produced in gastruloids	**Figure 1G**
		Tewary et al., 2017	Human pluripotent stem cells (hPSCs)	MATLAB	2D	Develops a reaction-diffusion model of BMP4 and NOGGIN dynamics and complements it with a positional information system to study the fate patterning of gastruloids	**Figure 1H**

II. Agent-based software frameworks

Framework	Author/reference	Access
CGAL	Fabri et al., 2000	https://www.cgal.org/
CellSys	Hoehme and Drasdo, 2010	http://msysbio.com/software/cellsys
CHASTE	Mirams et al., 2013; Pitt-Francis et al., 2009	http://www.cs.ox.ac.uk/chaste
CompuCell3D	Swat et al., 2012	http://www.compucell3d.org
MecaGen	Delile et al., 2014	https://github.com/juliendelile/MECAGEN
EmbryoMaker	Marin-Riera et al., 2016	http://www.biocenter.helsinki.fi/salazar/software.html
PhysiCell	Ghaffarizadeh et al., 2018	http://PhysiCell.MathCancer.org
PhisiBoSS	Letort et al., 2018	https://github.com/sysbio-curie/PhysiBoSS
ya||a	Germann et al., 2019	https://github.com/germannp/yalla

neighbors exist to supply Notch. The parameters used in this model, related to the Wnt– differentiation threshold, migration force, and friction coefficient between basement membrane and cells, were employed to fit spatial label index data, which provided cell turnover of the different cell types, spatial distribution, and cell ratios (Buske et al., 2011). They performed simulations in different scenarios to test the impact of biomechanics and Wnt– and Notch– signaling on the stabilization of the stem cell niche population, which provided information regarding cell organization due to intrinsic and extrinsic regulations.

Recently, Thalheim et al. modified this model to investigate the growth pattern of intestinal organoids based on the interdependences between Wnt and Notch signaling in stem cell lineage specification (Thalheim et al., 2018). They introduced an

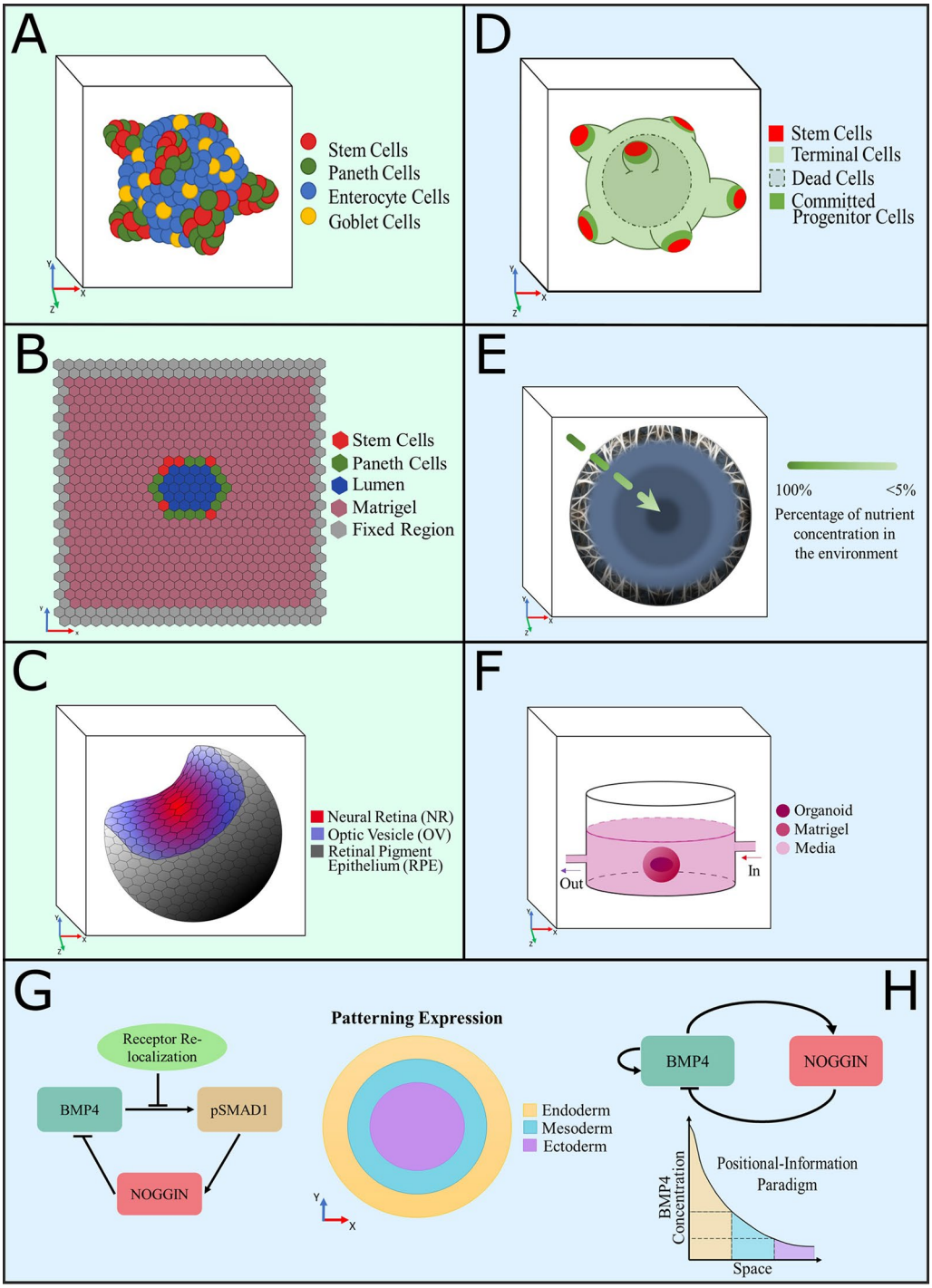

FIGURE 1 | Graphical representation of computational models developed to understand the intrinsic dynamics of organoid cultures. **(A–C)** Agent-based models, **(D–H)** equation-based models, color coded as per description in each panel. **(A)** A 3D model of intestinal organoids developed to investigate the distribution of cell populations and growth patterns provoked by Wnt and Notch signaling dynamics (Buske et al., 2012; Thalheim et al., 2018). **(B)** A 2D model of the cross section of a confluent intestinal epithelial layer, designed to study the biomechanical interactions between cells to produce crypt fission (Langlands et al., 2016; Almet et al., 2018). **(C)** Representation of a simulated optic-cup organoid (Okuda et al., 2018a). **(D)** Computational model of colon organoids created to study the effect of exogenous substances in the growth pattern and spatial distributions, to compare them with cancer phenotypes (Yan et al., 2018). **(E)** Diffusion model of a spheroid that simulates the consumption of nutrients in cerebral organoids to predict growth patterns (McMurtrey, 2016). **(F)** Model of oxygen consumption by a midbrain organoid grown in a millifluidic chamber to compare it with the oxygen consumption that occurred in the common well (Berger et al., 2018). **(G, H)** Equation-based reaction-diffusion models of gene networks used to simulate and predict fate patterning expression in gastruloids. The patterning expression and positional information paradigm plots show the signaling expressions of each primary germ layer observed experimentally (Etoc et al., 2016; Tewary et al., 2017).

apical network into the model to define the interaction among cells and to stabilize the cell organization by maintaining cell neighborhoods. Likewise, they attempted to simulate a cyst-like growth pattern that results from exogenous Wnt-3 treatment. However, their model cannot mimic the flattening of cells that is observed experimentally as it does not account for changes in cell shape due to increasing pressure. Nevertheless, this model predicts fluctuations in the stem cell niche and organoid growth patterns produced by changes in the molecular regulation of Wnt and Notch signaling pathways. Their simulation results suggest that Paneth cells and Wnt activity control the growth pattern of intestinal organoids by regulating the pluripotency of intestinal stem cells.

Langlands et al. (2016) developed a 2D model based on the intestinal crypt model created by Dunn et al. (2012). This model was created in the Cancer, Heart and Soft Tissue Environment (CHASTE) agent-based modeling framework (Pitt-Francis et al., 2009; Mirams et al., 2013), and its principal aim was to explore the role of Paneth cells during crypt fission (**Figure 1B**). The parameters implemented in this model were based on previous experimental data reported by Pin et al. (2015), which suggest that Paneth cells have a greater Young modulus, and new experimental data (i.e. adhesion assays), which indicate that Paneth cells have a greater adhesion ratio to the basement membrane in comparison with stem cells. Note that the mechanical stiffness of a cell is related to its Young modulus: a stiffer cell with a large Young modulus value can be represented as a hard material, while a softer cell would have a smaller Young modulus. Thus, the model only considers two cell types: Lgr5+ stem cells (stem cells, thus undifferentiated) and Paneth cells, the latter defined to be stiffer than the Lgr5+ cells. Different proliferation properties of the two cell populations were not modeled. The model was recently extended by Almet et al. (2018) to further explore the biomechanical properties involved in intestinal organoid crypt fission. Instead of defining Paneth and stem cells, they distinguished between soft cells (i.e. cells with lower Young modulus) and hard cells (i.e. cells with greater Young modulus) to allow a broader set of implementations of the model for other types of organoids. They introduced the ability to modify the adhesiveness of hard cells to the basement membrane and examined the effect of different stiffness ratio and cell population proportion values. These models allowed hypotheses about the link between cell biomechanical properties and crypt domain generation in intestinal organoids to be addressed, which could not have been possible with experimentation alone. One of the main limitations of these models is the lack of description of other cell types involved in the generation of intestinal organoids (e.g. goblet and enterocyte cells) and the effect of signaling pathways (e.g. Wnt and Notch pathways) in cellular differentiation. Nevertheless, the Almet et al. formalism can represent the impact of specific biomechanical properties in the generation of typical morphologies of intestinal organoids.

A more recent mathematical model, devised by Yan et al., simulates the 3D growth of a colon cancer organoid by explicitly formalizing the dynamics of stem, progenitor, and terminally differentiated cell populations (**Figure 1D**) (Yan et al., 2018). Stem and committed progenitor cells (i.e. undifferentiated cells committed to differentiate) produce self-renewal factors that can be inhibited by additional negative feedback factors secreted by terminal cells (i.e. terminally differentiated cells). The parameters of this model, describing general properties such as cell mobility, adhesion force, cellular mitosis rate, and apoptosis rate as cellular environment parameters, were obtained through numerical experimentation and from the literature (Youssefpour et al., 2012; Gao et al., 2013). Nonetheless, the dynamics of this system lead to diverse growth patterns and suggest that control of the self-renewal capacity of stem cells may cause a more stable organoid growth pattern. The Yan et al. model, implemented in MATLAB, can reproduce the spatial distribution of cell populations and the influence of feedback factors, as well as the dynamics of each cell population in the presence of exogenous factors such as Wnt, BMP, and HGF. The results obtained from their simulations propose a link between cancer metastasis and changes in the microenvironment of a tumor.

Cerebral Organoids

Protocols enabling *in vitro* 3D cell cultures of certain zones of neural tissue have been recently established (Eiraku et al., 2008; Muguruma et al., 2010; Danjo et al., 2011; Eiraku and Sasai, 2012; Mariani et al., 2012; Muguruma and Sasai, 2012). In addition, Knoblich's group was able to produce organoids from human pluripotent stem cells, which differentiate into various cell types and self-organize into distinct brain regions, including the formation of cortical layers with the organizational characteristics of a human brain (Lancaster et al., 2013). Cerebral organoids have made possible the study of early developmental events of the human brain. However, their maturation into adult brains is restricted due to lack of vascularization, which hinders gas exchange, nutrient supply, and waste removal (Sun et al., 2018). Thus, it is important to understand the actual nutrient consumption in cerebral organoids, in order to engineer new ways to provide the essential metabolites required to obtain mature brain tissue models.

McMurtrey employed equation-based models of diffusion to predict the diameter range of cerebral organoids, by using the lower range of reported metabolic rates of oxygen and glucose, and by fitting the experimental cell density and organoid diameter obtained from images of organoids using inverted phase-contrast light microscope and fluorescence imaging (McMurtrey, 2016). These models suggest that oxygen is more of a limiting factor in the growth of organoids than glucose. A multicompartment spherical equation-based model was also developed to represent the higher metabolic consumption that exists in the outer shell of the sphere as compared to the metabolic consumption in the inner shell (**Figure 1E**). The multicompartment model suggest that cerebral organoids achieve their largest growth potential by such a localization mechanism, providing a possible explanation for neural precursor outward migration in avascular neural systems.

Monzel et al. (2017) generated a protocol to produce midbrain-specific organoids (hMOs); later, Berger et al. (2018) explored the response of hMOs to the application of a continuous flow of media, as a method to prevent a necrotic core

by increasing its access to cells located in the organoids' center. In this study, they employed a 3D computational model, built within COMSOL Multiphysics 4.3, to compare the profiles of oxygen concentration in hMO cultures in a 24-well plate with orbital shaking versus cultures in a millifluidic system chamber. Their reaction-diffusion (RD) equation-based model consisted of a solid ellipsoid representing the hMO and an ellipsoidal shell mimicking the gel that supports the organoid, surrounded by a fluid domain (**Figure 1F**). The oxygen consumption of the organoid cells was assumed to be governed by Michaelis–Menten kinetics. The parameters used for oxygen consumption were obtained from the literature (Mattei et al., 2017), and the parameters related to metabolite consumption and production rate were calculated from metabolite concentration in the culture medium. For the model of the millifluidic chamber, an additional influx of oxygen was modeled as the material of the system is gas permeable. Simulation results suggest that there is a higher oxygen concentration inside hMOs cultured in a millifluidic chamber in comparison with hMOs cultured in plates with orbital shaking. While the millifluidic chamber approach still requires modifications to maintain hMOs for extended periods, it promises a more robust culture system for midbrain organoids, which could allow the use of cerebral organoids in the study of degenerative diseases.

Optic-Cup Organoids

Eiraku et al. (2011) reported a stepwise culture method to produce optic-cup organoids from pluripotent stem cells, which recapitulates the optic-cup morphogenesis. Okuda et al. (2018a) developed a 3D vertex model to describe optic-cup multicellular dynamics based on individual-cell behaviors, using custom C++ software. In their model, individual-cell behaviors change dynamically depending on cell differentiation state, from optic vesicle (OV) to neural retina (NR) to retinal pigment epithelium (RPE) (**Figure 1C**). Cells are defined as polyhedrons, and each integrates a mechanical model that defines the spatial dimensions, surface stiffness, and cell cycle dynamics. Okuda et al. obtained some parameters from the literature (Eiraku et al., 2011; Hasegawa et al., 2016) and performed experiments to measure others (then fed into the computational model) such as the thickness of the epithelial sheet; length of apical and basal surfaces; area of OV, NR, and RPE; and cell density. The parameters that were not obtained experimentally were calculated by fitting the known parameters into the system assuming a quasi-static deformation process. The simulations replicated the experimental features and predicted that proper proportions of NR and RPE regions, in addition to frequent cell proliferation, are required to produce NR invagination. Simulation results also suggested that mechanical feedback has an important role in the development of the optic cup. The authors mentioned that this model could also be applied to the study of other multicellular systems. However, it is important to note that the cell differentiation state in this model is defined by the height of the cells; it would be valuable to include other mechanisms, such as signaling pathways, that trigger cell differentiation to examine their effect on pattern formation.

Gastruloids

One of the main questions in developmental biology is how cell fate is acquired during embryogenesis. Pluripotent cells within the developing embryo differentiate intro the three-germ layers (ectoderm, mesoderm, and endoderm) and eventually undergo a series of cell-fate decisions that determine the final adult tissues. Diverse culture systems have been developed to reproduce models of a gastrulating embryo (van den Brink et al., 2014; Warmflash et al., 2014; Tewary et al., 2017; Beccari et al., 2018). These biological models, called gastruloids, recapitulate morphological and patterning events present during gastrulation, producing cell types corresponding to the three germ layers. Cell–cell interactions and intracellular regulatory networks control the formation of multicellular structures from homogenous populations. Mathematical models are valuable for the study of self-organization and creation of patterns during gastrulation, as these mechanisms depend on several signaling pathways that regulate each other in a nonlinear manner. Etoc et al. (2016) proposed a quantitative equation-based model, based on a classical RD system, to formalize the dynamics of essential regulators of cell fate such as pSMAD1, NOGGIN, and BMP4. This model simulates the radial profiles of pSMAD1 in microcolonies to test the effect of NOGGIN induction and receptor re-localization in gastruloids (**Figure 1G**). They found that the continuous expression of NOGGIN provokes a spatial asymmetry of BMP4 signaling, with a stronger inhibition of BMP4 at the center of the micropattern. Their model, fitted to experimental data of pSMAD1 profiles, was able to recapitulate the transport of NOGGIN accumulated at the center of the cell colony and locally inhibiting BMP4, leaving low and elevated concentrations of NOGGIN and free BMP4, respectively, at the edges. Furthermore, their model was able to simulate the resulting gastruloid fate patterns obtained through different signaling profiles. Tewary et al. (2017) developed a stepwise computational model based on a RD and positional information (PI) system to study the mechanisms of fate patterning in gastruloids. In their model, the RD section of the system describes the self-organization of the BMP4 and NOGGIN signaling molecules into asymmetric patterns, while the PI component allows the interpretation of the cell fate patterning acquisition (**Figure 1H**). The model parameters were chosen as in Kondo and Miura (2010), to obtain oscillations of BMP4 and NOGGIN. Tewary et al. obtained similar results to Etoc et al., which suggests the presence of negative-feedback control of BMP and density-dependant re-localization of BMP receptors to produce the micropattern. However, the interpretations of the two studies differ: Tewary et al. explored a larger range of colony sizes and suggested that the receptor re-localization results from the RD-mediated gradient, while Etoc et al. concluded that the RD-mediated gradient was determined by it. The Tewary et al. results indicate that cell fate acquisition is consistent with the PI paradigm and requires the collective work of multiple signaling pathways.

DISCUSSION

All the mathematical models described above have contributed to a deeper quantitative understanding of intrinsic mechanisms that

take place during the development and maintenance of organoids. These findings can be also translated into a better comprehension of the events that occur in their *in vivo* counterparts.

Nonetheless, there are limitations that need to be considered. The majority of intestinal and optic-cup organoid models discussed in this review are agent-based models. These formalisms simulate the properties and behavior of individual cells (agents) and the interactions among agents and the environment and can aid in the understanding of cell–cell interactions, cell–media interactions, and macro-level effects such as growth size and structure. One advantage of these types of models is that they allow the agents to make decisions according to a set of rules and provide realistic heterogeneous patterns, which can be valuable in the study of organoid phenotypes. However, they require significant computation power as compared with aggregate or equation-based models; for instance, the model generated by Langlands et al. (2016) and modified by Almet et al. (2018) required approximately 13 min of CPU time for 100 simulated hours. Additionally, they demand coding skills to generate a customized simulation code or the use of dedicated software frameworks such as CHASTE or CGAL. CHASTE is a simulation library package which has a specialized cell-based library that already contains several defined cell property models; however, it also allows the user to adapt them or to code and implement novel cellular models. Similarly, CGAL is a software project that provides a C++ library of geometric algorithms, which can be implemented to simulate the biomechanical behavior of different cell types in an organoid system. These packages offer some advantages: several biomechanical properties, signaling pathways, and system interactions are already implemented, and models based on previous research studies can be easily accessed. Nevertheless, both CHASTE and CGAL still require familiarity with C++. Agent-based models can also be developed using other programming languages, such as Python or R, but C++ is generally preferred as it allows a simple creation and organization of classes to describe the system components, providing efficient memory management and good performance. Commonly used frameworks include CGAL (Fabri et al., 2000), CellSys (Hoehme and Drasdo, 2010), CHASTE (Pitt-Francis et al., 2009; Mirams et al., 2013), CompuCell3D (Swat et al., 2012), MecaGen (Delile et al., 2014), EmbryoMaker (Marin-Riera et al., 2016), PhysiCell (Ghaffarizadeh et al., 2018), PhisiBoSS (Letort et al., 2018), and ya||a (Germann et al., 2019) (see **Table 1**(II), for source codes).

On the other hand, models developed to date for cerebral organoids and gastruloids are aggregate equation-based models (i.e. constituted by a set of equations that summarize the overall system dynamics), without focusing on individual-cell properties. These models are designed to analyze homogenous populations and tend to be easier to develop, fit, and implement, and faster to simulate. However, these formalisms are not easily able to account for spatially complex dynamics or heterogeneity. MATLAB (2018) is one of the main platforms used to simulate these models; it is user-friendly, and many tutorials exist. However, the assumptions necessary for these reduced-order models may not be a good fit to the underlying cell biology.

There are important experimental aspects of organoid cultures that determine the accuracy and required complexity of the corresponding computational models. For instance, self-organizing systems develop their own endogenous interactions according to the signals received between the elements that constitute the system. This results in heterogeneity in viability, size, and shape of organoids. It is important to understand the rules that govern the self-organization and self-assembly of the cells to improve the accuracy of mathematical models. The agent-based models described here take into account general organoid characteristics as diameter, cell turnover, spatial cell distribution, and growth curves to obtain the necessary parameter values for their simulations. Nonetheless, reliable fits of agent-based organoid models require more detailed information than equation-based models. For example, details of the biomechanics of different cell types can address the suggestion made by some intestinal organoid models about the link between cell biomechanics and growth phenotypes. Furthermore, as mentioned in Yan et al. (2018), the culture microenvironment also contributes to the resulting growth patterns of organoids. Thus, future mathematical models should include the culture mechanical and molecular characteristics to improve their predictive power.

It is worth mentioning that there is another important classification of organoids called tumor organoids. Tumor organoids are cancer-cell-derived organoids that provide a potentially useful tool in the understanding of tumor morphology and gene mutations and in the research of targeted tumor treatment responses. There are many experimental studies capable of biologically modeling the main features of primary tumors in 3D (Sato et al., 2011; Boj et al., 2015; van de Wetering et al., 2015; Hubert et al., 2016; Broutier et al., 2017; Duarte et al., 2018; Lee et al., 2018; Vlachogiannis et al., 2018). The current focus is on the culture of patient cell-derived healthy and tumor organoids to allow an assessment of therapeutic effects for personalized medicine applications (Nagle et al., 2018; Tuveson and Clevers, 2019). Grassi et al. (2019) recently compared the growth and structure of healthy and tumor patient-derived organoids with clear cell renal cancer and showed, in line with the literature (Sato et al., 2011; Gao et al., 2014; Boj et al., 2015; Kashfi et al., 2018), that tumor organoids and healthy organoids present phenotypical differences. Therefore, as this review is focused on mathematical models of organoids that aid in the understanding of the functionality and morphology of specific organs, models that simulate the morphology of tumor organoids are not included in the present review. However, a detailed study by Karolak et al. (2018) reviews computational models that provide insights on tumor development, progression, and response to treatment. These mathematical models include the simulation of acinar structures, tumor multicellular spheroids, preinvasive tumors, vascularized-tumors, and tumor response to anticancer therapies.

Although there are relatively few mathematical and computational models of organoid systems, it is essential to mention that many other models have been generated for similar or more general systems, which could be modified to represent organoid models. For example, Okuda et al. created 3D computational

models that recapitulate general properties of cellular tissue before developing a model focused on the formation of optic-cup organoids. One such model explored the effect of apoptosis in morphogenesis (Okuda et al., 2016). More recently, they developed a mathematical model combining a RD system at the single-cell level and a 3D vertex model to explore the phenomena of patterning and deformation (Okuda et al., 2018b). Applying these frameworks to organoids remains an area for future research.

In conclusion, mathematical and computational models are valuable to understand and explore the intrinsic mechanisms of organoids. Nonetheless, the production of these models is not an easy task and requires the participation of multidisciplinary teams. An all-round model for every organoid type does not currently exist and will be difficult to generate due to all the different cell fates, signaling pathways, and specific self-organization and self-assembly characteristics. It would be worthwhile to explore properties shared across organoid systems, integrate them into a general platform, and contribute to the creation of mathematical and computational models for other organoids, such as the liver, pancreas, and lungs, not considered so far.

AUTHOR CONTRIBUTIONS

SM-O, LM, and MH conceived and designed the study; SM-O performed the literature review and wrote the first draft of the manuscript. All authors contributed to manuscript editing and revision and read and approved the submitted version.

FUNDING

This work was funded through the UK Medical Research Council (grant MR/N021444/1 to LM) and the Mexico Consejo Nacional de Ciencia y Tecnología (CONACYT) PhD scholarship provided to SM-O.

ACKNOWLEDGMENTS

The authors gratefully acknowledge the expertise and guidance provided by Dr Alexander Fletcher from the University of Sheffield, through discussions on the topics covered in this review.

REFERENCES

Almet, A. A., Hughes, B. D., Landman, K. A., Nathke, I. S., Osborne, J. M., Näthke, I. S., et al. (2018). A multicellular model of intestinal crypt buckling and fission. *Bull. Math. Biol.* 80 (2), 335–359. doi: 10.1007/s11538-017-0377-z

Beccari, L., Moris, N., Girgin, M., Turner, D. A., Baillie-Johnson, P., Cossy, A.-C., et al. (2018). Multi-axial self-organization properties of mouse embryonic stem cells into gastruloids. *Nature* 562 (7726), 272–276. doi: 10.1038/s41586-018-0578-0

Berger, E., Magliaro, C., Paczia, N., Monzel, A. S., Antony, P., Linster, C. L., et al. (2018). Millifluidic culture improves human midbrain organoid vitality and differentiation. *Lab. Chip* 18 (20), 3172–3183. doi: 10.1039/C8LC00206A

Boj, S. F., Hwang, C.-I., Baker, L. A., Chio, I. I. C., Engle, D. D., Corbo, V., et al. (2015). Organoid models of human and mouse ductal pancreatic cancer. *Cell* 160 (1–2), 324–338. doi: 10.1016/j.cell.2014.12.021

Broutier, L., Mastrogiovanni, G., Verstegen, M. M., Francies, H. E., Gavarro, L. M., Bradshaw, C. R., et al. (2017). Human primary liver cancer-derived organoid cultures for disease modeling and drug screening. *Nat. Med.* 23 (12), 1424–1435. doi: 10.1038/nm.4438

Buske, P., Galle, J., Barker, N., Aust, G., Clevers, H., and Loeffler, M. (2011). A comprehensive model of the spatio-temporal stem cell and tissue organisation in the intestinal crypt. *PLoS Comput. Biol.* 7 (1), e1001045. doi: 10.1371/journal.pcbi.1001045

Buske, P., Przybilla, J., Loeffler, M., Sachs, N., Sato, T., Clevers, H., et al. (2012). On the biomechanics of stem cell niche formation in the gut—modelling growing organoids. *FEBS J.* 279 (18), 3475–3487. doi: 10.1111/j.1742-4658.2012.08646.x

Dahl-Jensen, S., and Grapin-botton, A. (2017). The physics of organoids: a biophysical approach to understanding organogenesis. *Development* 144 (6), 946–951. doi: 10.1242/dev.143693

Danjo, T., Eiraku, M., Muguruma, K., Watanabe, K., Kawada, M., Yanagawa, Y., et al. (2011). Subregional specification of embryonic stem cell-derived ventral telencephalic tissues by timed and combinatory treatment with extrinsic signals. *J. Neurosci.* 31 (5), 1919–1933. doi: 10.1523/JNEUROSCI.5128-10.2011

Delile, J., Doursat, R., and Peyriéras, N. (2014). "Computational modeling and simulation of animal early embryogenesis with the MecaGen platform," in *Computational systems biology*, Eils, 2nd edn., Eds. A. Kriete and B. T. Eils Roland (Oxford: Academic Press), 359–405. doi: 10.1016/B978-0-12-405926-9.00016-2

Duarte, A. A., Gogola, E., Sachs, N., Barazas, M., Annunziato, S., de Ruiter, J. R., et al. (2018). BRCA-deficient mouse mammary tumor organoids to study cancer-drug resistance. *Nat. Methods* 15 (2), 134–140. doi: 10.1038/nmeth.4535

Dunn, S. J., Appleton, P. L., Nelson, S. A., Näthke, I. S., Gavaghan, D. J., and Osborne, J. M. (2012). A two-dimensional model of the colonic crypt accounting for the role of the basement membrane and pericryptal fibroblast sheath. *PLoS Comput. Biol.* 8 (5), e1002515. doi: 10.1371/journal.pcbi.1002515

Duval, K., Grover, H., Han, L.-H., Mou, Y., Pegoraro, A. F., Fredberg, J., et al. (2017). Modeling physiological events in 2D vs. 3D cell culture. *Physiology* 32 (4), 266–277. doi: 10.1152/physiol.00036.2016

Eiraku, M., and Sasai, Y. (2012). Self-formation of layered neural structures in three-dimensional culture of ES cells. *Curr. Opin. Neurobiol.* 22 (5), 768–777. doi: 10.1016/j.conb.2012.02.005

Eiraku, M., Takata, N., Ishibashi, H., Kawada, M., Sakakura, E., Okuda, S., et al. (2011). Self-organizing optic-cup morphogenesis in three-dimensional culture. *Nature* 472, 51. doi: 10.1038/nature09941

Eiraku, M., Watanabe, K., Matsuo-Takasaki, M., Kawada, M., Yonemura, S., Matsumura, M., et al. (2008). Self-organized formation of polarized cortical tissues from ESCs and its active manipulation by extrinsic signals. *Cell Stem Cell* 3 (5), 519–532. doi: 10.1016/j.stem.2008.09.002

Etoc, F., Metzger, J., Ruzo, A., Kirst, C., Yoney, A., Ozair, M. Z., et al. (2016). A balance between secreted inhibitors and edge sensing controls gastruloid self-organization. *Dev. Cell* 39 (3), 302–315. doi: 10.1016/j.devcel.2016.09.016

Fabri, A., Giezeman, G.-J., Kettner, L., Schirra, S., and Schönherr, S. (2000). On the design of CGAL, a computational geometry algorithms library. *Softw. Pract. Exp.* 30 (11), 1167–1202. doi: 10.1002/1097-024X(200009)30:11<1167::AID-SPE337>3.0.CO;2-B

Gao, D., Vela, I., Sboner, A., Iaquinta, P. J., Karthaus, W. R., Gopalan, A., et al. (2014). Organoid cultures derived from patients with advanced prostate cancer. *Cell* 159 (1), 176–187. doi: 10.1016/j.cell.2014.08.016

Gao, X., McDonald, J. T., Hlatky, L., and Enderling, H. (2013). Acute and fractionated irradiation differentially modulate glioma stem cell division kinetics. *Cancer Res.* 73, 1481 LP– 1490. doi: 10.1158/0008-5472.CAN-12-3429

Germann, P., Marin-Riera, M., and Sharpe, J. (2019). ya||a: GPU-powered spheroid models for mesenchyme and epithelium. *Cell Syst.* 8 (3), 261–266.e3. doi: 10.1016/j.cels.2019.02.007

Ghaffarizadeh, A., Heiland, R., Friedman, S. H., Mumenthaler, S. M., and Macklin, P. (2018). PhysiCell: an open source physics-based cell simulator for 3-D multicellular systems. *PLoS Comput. Biol.* 14 (2), e1005991. doi: 10.1371/journal.pcbi.1005991

Granados-Romero, J. J., Valderrama-Treviño, A. I., Contreras-Flores, E. H., Barrera-Mera, B., Herrera Enríquez, M., Uriarte-Ruíz, K., et al. (2017). Colorectal cancer: a review. *Int. J. Res. Med. Sci.* 5 (11), 4667–4676. doi: 10.18203/2320-6012.ijrms20174914

Grassi, L., Alfonsi, R., Francescangeli, F., Signore, M., De Angelis, M. L., Addario, A., et al. (2019). Organoids as a new model for improving regenerative medicine and cancer personalized therapy in renal diseases. *Cell Death Dis.* 10 (3), 201. doi: 10.1038/s41419-019-1453-0

Hartung, T. (2008). Thoughts on limitations of animal models. *Parkinsonism Relat. Disord.* 14 (Suppl 2), S81–S83. doi: 10.1016/j.parkreldis.2008.04.003

Hasegawa, Y., Takata, N., Okuda, S., Kawada, M., Eiraku, M., and Sasai, Y. (2016). Emergence of dorsal–ventral polarity in ESC-derived retinal tissue. *Development (Cambridge, England)* 143 (21), 3895–3906. doi: 10.1242/dev.134601

Hoehme, S., and Drasdo, D. (2010). A cell-based simulation software for multi-cellular systems. *Bioinformatics* 26 (20), 2641–2642. doi: 10.1093/bioinformatics/btq437

Hubert, C. G., Rivera, M., Spangler, L. C., Wu, Q., Mack, S. C., Prager, B. C., et al. (2016). A three-dimensional organoid culture system derived from human glioblastomas recapitulates the hypoxic gradients and cancer stem cell heterogeneity of tumors found *in vivo*. *Cancer Res.* 76 (8), 2465–2477. doi: 10.1158/0008-5472.CAN-15-2402

Karolak, A., Markov, D. A., McCawley, L. J., and Rejniak, K. A. (2018). Towards personalized computational oncology: from spatial models of tumour spheroids, to organoids, to tissues. *J. R. Soc. Interface* 15 (138), 20170703. doi: 10.1098/rsif.2017.0703

Kashfi, S. M. H., Almozyan, S., Jinks, N., Koo, B.-K., and Nateri, A. S. (2018). Morphological alterations of cultured human colorectal matched tumour and healthy organoids. *Oncotarget* 9 (12), 10572–10584. doi: 10.18632/oncotarget.24279

Kondo, S., and Miura, T. (2010). Reaction-diffusion model as a framework for understanding biological pattern formation. *Science* 329 (5999), 1616–1620. doi: 10.1126/science.1179047

Kriete, A., and Eils, R. (2014). "Introducing computational systems biology," in *Computational systems biology*, 2nd edn., Eds. A. Kriete and B. T. Eils Roland (Oxford: Elsevier Academic Press), 1–8. doi: 10.1016/B978-0-12-405926-9.00001-0

Lancaster, M. A., and Knoblich, J. A. (2014). Organogenesis in a dish: modeling development and disease using organoid technologies. *Science* 345 (6194), 1247125. doi: 10.1126/science.1247125

Lancaster, M. A., Renner, M., Martin, C.-A., Wenzel, D., Bicknell, L. S., Hurles, M. E., et al. (2013). Cerebral organoids model human brain development and microcephaly. *Nature* 501 (7467), 373–379. doi: 10.1038/nature12517

Langlands, A. J., Almet, A. A., Appleton, P. L., Newton, I. P., Osborne, J. M., and Näthke, I. S. (2016). Paneth cell-rich regions separated by a cluster of Lgr5+ cells initiate crypt fission in the intestinal stem cell niche. *PLoS Biol.* 14 (6), e1002491. doi: 10.1371/journal.pbio.1002491

Lee, S. H., Hu, W., Matulay, J. T., Silva, M. V., Owczarek, T. B., Kim, K., et al. (2018). Tumor evolution and drug response in patient-derived organoid models of bladder cancer. *Cell* 173 (2), 515–528.e17. doi: 10.1016/j.cell.2018.03.017

Letort, G., Montagud, A., Stoll, G., Heiland, R., Barillot, E., Macklin, P., et al. (2018). PhysiBoSS: a multi-scale agent-based modelling framework integrating physical dimension and cell signalling. *Bioinformatics* 35 (7), 1188–1196. doi: 10.1093/bioinformatics/bty766

Mariani, J., Simonini, M. V., Palejev, D., Tomasini, L., Coppola, G., Szekely, A. M., et al. (2012). Modeling human cortical development *in vitro* using induced pluripotent stem cells.". *Proc. Natl. Acad. Sci. U.S.A.* 109 (31), 12770–12775. doi: 10.1073/pnas.1202944109

Marin-Riera, M., Brun-Usan, M., Zimm, R., Valikangas, T., and Salazar-Ciudad, I. (2016). Computational modeling of development by epithelia, mesenchyme and their interactions: a unified model. *Bioinformatics* 32 (2), 219–225. doi: 10.1093/bioinformatics/btv527

MATLAB (2018). *Release 2018a (R2018a)*. Natick, Massachusetts: The MathWorks Inc.

Mattei, G., Magliaro, C., Giusti, S., Ramachandran, S. D., Heinz, S., Braspenning, J., et al. (2017). On the adhesion–cohesion balance and oxygen consumption characteristics of liver organoids. *PLoS One* 12 (3), e0173206. doi: 10.1371/journal.pone.0173206

McMurtrey, R. J. (2016). Analytic models of oxygen and nutrient diffusion, metabolism dynamics, and architecture optimization in three-dimensional tissue constructs with applications and insights in cerebral organoids. *Tissue Eng. Part C Methods* 22 (3), 221–249. doi: 10.1089/ten.tec.2015.0375

Mirams, G. R., Arthurs, C. J., Bernabeu, M. O., Bordas, R., Cooper, J., Corrias, A., et al. (2013). Chaste: an open source C++ library for computational physiology and biologyEdited by Andreas Prlic. *PLoS Comput. Biol.* 9 (3), e1002970. doi: 10.1371/journal.pcbi.1002970

Monzel, A. S., Smits, L. M., Hemmer, K., Hachi, S., Moreno, E. L., van Wuellen, T., et al. (2017). Derivation of human midbrain-specific organoids from neuroepithelial stem cells. *Stem. Cell Rep.* 8 (5), 1144–1154. doi: 10.1016/j.stemcr.2017.03.010

Muguruma, K., and Sasai, Y. (2012). In vitro recapitulation of neural development using embryonic stem cells: from neurogenesis to histogenesis. *Dev. Growth Differ.* 54 (3), 349–357. doi: 10.1111/j.1440-169X.2012.01329.x

Muguruma, K., Nishiyama, A., Ono, Y., Miyawaki, H., Mizuhara, E., Hori, S., et al. (2010). Ontogeny-recapitulating generation and tissue integration of ES cell-derived Purkinje cells. *Nat. Neurosci.* 13 (10), 1171–1180. doi: 10.1038/nn.2638

Nagle, P. W., Plukker, J. T. M., Muijs, C. T., van Luijk, P., and Coppes, R. P. (2018). Patient-derived tumor organoids for prediction of cancer treatment response. *Semin. Cancer Biol.* 53, 258–264. doi: 10.1016/j.semcancer.2018.06.005

Nakamura, T., and Sato, T. (2018). Advancing intestinal organoid technology toward regenerative medicine. *Cell Mol. Gastroenterol. Hepatol.* 5 (1), 51–60. doi: 10.1016/j.jcmgh.2017.10.006

Okuda, S., Inoue, Y., Eiraku, M., Adachi, T., and Sasai, Y. (2016). Modeling cell apoptosis for simulating three-dimensional multicellular morphogenesis based on a reversible network reconnection framework. *Biomech. Model Mechanobiol.* 15 (4), 805–816. doi: 10.1007/s10237-015-0724-7

Okuda, S., Miura, T., Inoue, Y., Adachi, T., and Eiraku, M. (2018b). Combining Turing and 3D vertex models reproduces autonomous multicellular morphogenesis with undulation, tubulation, and branching. *Sci. Rep.* 8 (1), 2386. doi: 10.1038/s41598-018-20678-6

Okuda, S., Takata, N., Hasegawa, Y., Kawada, M., Inoue, Y., Adachi, T., et al. (2018a). Strain-triggered mechanical feedback in self-organizing optic-cup morphogenesis. *Sci. Adv.* 4 (11), eaau1354. doi: 10.1126/sciadv.aau1354

Pin, C., Parker, A., Gunning, A. P., Ohta, Y., Johnson, I. T., Carding, S. R., et al. (2015). An individual based computational model of intestinal crypt fission and its application to predicting unrestrictive growth of the intestinal epithelium. *Integr. Biol. (United Kingdom)* 7 (2), 213–228. doi: 10.1039/C4IB00236A

Pitt-Francis, J., Pathmanathan, P., Bernabeu, M. O., Bordas, R., Cooper, J., Fletcher, A. G., et al. (2009). Chaste: a test-driven approach to software development for biological modelling. *Comput. Phys. Commun.* 180 (12), 2452–2471. doi: 10.1016/j.cpc.2009.07.019

Sato, T., Stange, D. E., Ferrante, M., Vries, R. G. J., Van Es, J. H., Van den Brink, S., et al. (2011). Long-term expansion of epithelial organoids from human colon, adenoma, adenocarcinoma, and Barrett's epithelium. *Gastroenterology* 141 (5), 1762–1772. doi: 10.1053/j.gastro.2011.07.050

Sato, T., Vries, R. G., Snippert, H. J., Van De Wetering, M., Barker, N., Stange, D. E., et al. (2009). Single Lgr5 stem cells build crypt–villus structures *in vitro* without a mesenchymal niche. *Nature* 459 (7244), 262–265. doi: 10.1038/nature07935

Shamir, E. R., and Ewald, A. J. (2014). Three-dimensional organotypic culture: experimental models of mammalian biology and disease. *Nat. Rev. Mol. Cell Biol.* 15 (10), 647–664. doi: 10.1038/nrm3873

Shanks, N., Greek, R., and Greek, J. (2009). Are animal models predictive for humans? *Philos. Ethics Humanit. Med.* 4 (1), 1–20. doi: 10.1186/1747-5341-4-2

Sun, A. X., Ng, H.-H., and Tan, E.-K. (2018). Translational potential of human brain organoids. *Ann. Clin. Transl. Neurol.* 5 (2), 226–235. doi: 10.1002/acn3.505

Swat, M. H., Thomas, G. L., Belmonte, J. M., Shirinifard, A., Hmeljak, D., and Glazier, J. A. (2012). Multi-scale modeling of tissues using CompuCell3D. *Methods Cell Biol.* 110, 325–366. doi: 10.1016/B978-0-12-388403-9.00013-8

Szallasi, Z, Stelling J, Periwal V, editors. (2010). *System modeling in cellular biology*. Cambridge, Mass: The MIT Press.

Tewary, M., Ostblom, J., Prochazka, L., Zulueta-Coarasa, T., Shakiba, N., Fernandez-Gonzalez, R., et al. (2017). A stepwise model of reaction-diffusion and positional information governs self-organized human peri-gastrulation-like patterning. *Development* 144 (23), 4298–4312. doi: 10.1242/dev.149658

Thalheim, T., Quaas, M., Herberg, M., Braumann, U. D., Kerner, C., Loeffler, M., et al. (2018). Linking stem cell function and growth pattern of intestinal organoids. *Dev. Biol.* 433 (2), 254–261. doi: 10.1016/j.ydbio.2017.10.013

Tuveson, D., and Clevers, H. (2019). Cancer modeling meets human organoid technology. *Science* 364 (6444), 952 LP–952955. doi: 10.1126/science.aaw6985

Uma, S. (2010). Intestinal stem cells. *Curr. Gastroenterol. Rep.* 12 (5), 340–348. doi: 10.1007/s11894-010-0130-3

van de Wetering, M., Francies, H. E., Francis, J. M., Bounova, G., Iorio, F., Pronk, A., et al. (2015). Prospective derivation of a living organoid biobank of colorectal cancer patients. *Cell* 161 (4), 933–945. doi: 10.1016/j.cell.2015.03.053

van den Brink, S. C., Baillie-Johnson, P., Balayo, T., Hadjantonakis, A.-K., Nowotschin, S., Turner, D. A., et al. (2014). Symmetry breaking, germ layer specification and axial organisation in aggregates of mouse embryonic stem cells. *Development* 141 (22), 4231–4242. doi: 10.1242/dev.113001

Vlachogiannis, G., Hedayat, S., Vatsiou, A., Jamin, Y., Fernandez-Mateos, J., Khan, K., et al. (2018). Patient-derived organoids model treatment response of metastatic gastrointestinal cancers. *Science (New York, N.Y.)* 359 (6378), 920–926. doi: 10.1126/science.aao2774

Wallach, T., and Bayrer, J. R. (2017). Intestinal organoids: new frontiers in the study of intestinal disease and physiology. *J. Pediatr. Gastroenterol. Nutr.* 64 (2), 180–185. doi: 10.1097/MPG.0000000000001411

Warmflash, A., Sorre, B., Etoc, F., Siggia, E. D., and Brivanlou, A. H. (2014). A method to recapitulate early embryonic spatial patterning in human embryonic stem cells. *Nat. Methods* 11 (8), 847–854. doi: 10.1038/nmeth.3016

Yan, H., Konstorum, A., and Lowengrub, J. S. (2018). Three-dimensional spatiotemporal modeling of colon cancer organoids reveals that multimodal control of stem cell self-renewal is a critical determinant of size and shape in early stages of tumor growth. *Bull. Math. Biol.* 80 (5), 1404–1433. doi: 10.1007/s11538-017-0294-1

Yin, X., Mead, B. E., Safaee, H., Langer, R., Karp, J. M., and Levy, O. (2016). Engineering stem cell organoids. *Cell Stem Cell* 18 (1), 25–38. doi: 10.1016/j.stem.2015.12.005

Youssefpour, H., Li, X., Lander, A. D., and Lowengrub, J. S. (2012). Multispecies model of cell lineages and feedback control in solid tumors. *J. Theor. Biol.* 304, 39–59. doi: 10.1016/j.jtbi.2012.02.030

Conflict of Interest Statement: The authors declare that the research was conducted in the absence of any commercial or financial relationships that could be construed as a potential conflict of interest.

frontiers in Cell and Developmental Biology

ORIGINAL RESEARCH
published: 28 November 2019
doi: 10.3389/fcell.2019.00303

Human Cerebral Organoids and Fetal Brain Tissue Share Proteomic Similarities

Juliana Minardi Nascimento[1,2], Verônica M. Saia-Cereda[1], Rafaela C. Sartore[2,3], Rodrigo Madeiro da Costa[2], Clarissa S. Schitine[4,5], Hercules Rezende Freitas[5,6], Michael Murgu[7], Ricardo A. de Melo Reis[5], Stevens K. Rehen[2,4] and Daniel Martins-de-Souza[1,8,9]**

[1] Laboratory of Neuroproteomics, Department of Biochemistry and Tissue Biology, Institute of Biology, University of Campinas (UNICAMP), Campinas, Brazil, [2] D'Or Institute for Research and Education (IDOR), Rio de Janeiro, Brazil, [3] National Institute of Traumatology and Orthopedics, Rio de Janeiro, Brazil, [4] Institute of Biomedical Sciences, Federal University of Rio de Janeiro (UFRJ), Rio de Janeiro, Brazil, [5] Institute of Biophysics, Federal University of Rio de Janeiro (UFRJ), Rio de Janeiro, Brazil, [6] School of Health Sciences, IBMR – University Center, Rio de Janeiro, Brazil, [7] Waters Corporation, Barueri, Brazil, [8] Instituto Nacional de Biomarcadores em Neuropsiquiatria (INBION), Conselho Nacional de Desenvolvimento Científico e Tecnológico, São Paulo, Brazil, [9] Experimental Medicine Research Cluster (EMRC), University of Campinas, Campinas, Brazil

The limited access to functional human brain tissue has led to the development of stem cell-based alternative models. The differentiation of human pluripotent stem cells into cerebral organoids with self-organized architecture has created novel opportunities to study the early stages of the human cerebral formation. Here we applied state-of-the-art label-free shotgun proteomics to compare the proteome of stem cell-derived cerebral organoids to the human fetal brain. We identified 3,073 proteins associated with different developmental stages, from neural progenitors to neurons, astrocytes, or oligodendrocytes. The major protein groups are associated with neurogenesis, axon guidance, synaptogenesis, and cortical brain development. Glial cell proteins related to cell growth and maintenance, energy metabolism, cell communication, and signaling were also described. Our data support the variety of cells and neural network functional pathways observed within cell-derived cerebral organoids, confirming their usefulness as an alternative model. The characterization of brain organoid proteome is key to explore, in a dish, atypical and disrupted processes during brain development or neurodevelopmental, neurodegenerative, and neuropsychiatric diseases.

Keywords: brain organoids, neural cells, proteomics, oligodendrocyte progenitors, stem cells

OPEN ACCESS

Edited by:
Eumorphia Remboutsika, National and Kapodistrian University of Athens, Greece

Reviewed by:
Claudio Cantù, Linköping University, Sweden
Patricia Johansson contributed to the review of Claudio Cantù
Zhiping P. Pang, Rutgers, The State University of New Jersey, United States

***Correspondence:**
Stevens K. Rehen
srehen@lance-ufrj.org
Daniel Martins-de-Souza
dmsouza@unicamp.br

Specialty section:
This article was submitted to Stem Cell Research, a section of the journal Frontiers in Cell and Developmental Biology

Received: *06 August 2019*
Accepted: *08 November 2019*
Published: *28 November 2019*

Citation:
Nascimento JM, Saia-Cereda VM, Sartore RC, Madeiro da Costa R, Schitine CS, Freitas HR, Murgu M, de Melo Reis RA, Rehen SK and Martins-de-Souza D (2019) Human Cerebral Organoids and Fetal Brain Tissue Share Proteomic Similarities. Front. Cell Dev. Biol. 7:303. doi: 10.3389/fcell.2019.00303

INTRODUCTION

Understanding the molecular basis of human diseases is currently one of the main challenges faced in contemporary medicine. Particularly regarding the human central nervous system (CNS), the challenge lies in both its complexity and the reduced accessibility to living tissue. Research with postmortem brains and animal models along with a broader spectrum of tools, such as brain imaging and studies utilizing pluripotent stem cells (PSC) – have all advanced understanding in the field. Differentiating PSC, both human embryonic stem cells (hESC) (Thomson, 1998), and induced pluripotent stem cells (iPSC) (Takahashi et al., 2007), into functional neural cells grown in

2D cultures (Zhang et al., 2001; Chambers et al., 2009), and 3D brain organoid cultures (Eiraku and Sasai, 2012; Lancaster et al., 2013) has become a functional alternative to investigate CNS disorders.

Hence, PSC-derived cerebral organoids have recently become a focus in the complex disorders quest. Upon minimal instructions *in vitro*, cells can self-organize into 3D structures where intrinsic molecular programs are activated to generate diverse neuronal and non-neuronal cell types from CNS specific regions, recapitulating some of the early features of the human brain development (Lancaster et al., 2013; Sasai, 2013; Lancaster and Knoblich, 2014; Quadrato et al., 2017; Sartore et al., 2017). Some recent studies have shown potential for modeling several human disorders using cerebral organoids, such as microcephaly (Lancaster et al., 2013), lissencephaly (Bershteyn et al., 2017), Zika virus infection microcephaly (Cugola et al., 2016; Garcez et al., 2016; Qian et al., 2016), Alzheimer's disease (Raja et al., 2016), and autism spectrum disorders (Mariani et al., 2015). Those modeling applications may lead to new insight into drug discovery and interactions, cell therapy, and basic research (Brennand et al., 2014; Quadrato and Arlotta, 2017).

Advances in 3D cell–cell interaction using cellular and molecular tools have shown a diverse and more advanced cell maturation profile within brain organoids (Paşca et al., 2015; Quadrato et al., 2017; Sloan et al., 2017; Madhavan et al., 2018; Ormel et al., 2018). Notable similarities in cell composition and gene expression profiles between *in vitro* cortical development of human brain organoids and human fetal neocortex were revealed by single-cell RNA sequencing and whole-organoid transcriptomics (Camp et al., 2015; Bershteyn et al., 2017; Xiang et al., 2017). However, oftentimes mRNA levels poorly correlate to cell expression of selected markers, due to divergences in translation (Carlyle et al., 2017). Regarding proteins, only a small number have been identified by immunocytochemistry in brain organoids, most of which are considered regional patterning cell markers (Renner et al., 2017).

However, fundamental organization of the developing brain is orchestrated by thousands of molecules simultaneously. And understanding those broad and complex molecular processes are key to unravel novel targets in disease modeling. As such, mass spectrometry-based proteomics can offer a complementary outlook to mRNA, as a great molecular tool to uncover deeper and more comprehensive large-scale, protein-level data. The possibility of detecting thousands of proteins within a sample at a given moment can reveal functional profiles associated with genes and interaction with their environment.

Here we describe in what ways stem cell-derived cerebral organoids is similar to brain tissue in proteomic terms, defending its use as a robust model to study psychiatric disorders. We present findings on large-scale proteome profiling of human cerebral organoids, using systems level analysis showing initial development of varied cell types leading to a complex neural network. This includes proteins of a wide-range of cellular functions, indicative of active pathways in organoids, including neuritogenesis, dendritic branching and synapse formation, initial gliogenesis, and oligodendrogenesis. The protein data provide a deeper knowledge of the microenvironmental niches governing a network of functional molecules in organoid neocortical development. Molecular information from protein levels, signaling, and pathways of interest can be used to better assess neurodevelopmental abnormalities in further investigations. Complex brain disorders such as schizophrenia, bipolar disorder, autism, and Alzheimer's disease benefit from studies on unbiased cellular and molecular interactions, where models and hypotheses can be further tested to uncover disrupted processes.

MATERIALS AND METHODS

Human Pluripotent Stem Cells and Cerebral Organoids Differentiation

Human embryonic stem cells [hESC; cell line BR1 obtained from the Laboratory for Embryonic Stem Cell Research (LaNCE), University of São Paulo (Fraga et al., 2011)] were cultured in mTeSR1 media (Stemcell Technologies, Vancouver, BC, Canada) on Matrigel (BD Biosciences)-coated cell culture plates. The hESC colonies were manually passaged upon 70% confluence and maintained at 37°C in humidified air with 5% CO_2. The differentiation of PSC into cerebral organoids was performed as previously described (Sartore et al., 2017). Concisely, cells were inoculated in a spinner flask containing mTeSR1 media supplemented with 10 μM Y-27632 (Rho-associated protein kinases inhibitor, iRock) (Merck) under constant rotation (40 rpm). After 24 h, cell culture medium was replaced to initiate embryoid body formation. By day 7, neural induction media [DMEM/F12 1:1 supplemented with N2 (1x) supplement, 2 mM glutamax, 1% MEM-NEAA (Thermo Scientific), and heparin (1 μg/mL, Sigma)] was added. On day 11, cellular aggregates were covered in Matrigel and cultured in differentiation media [DMEM/F12:Neurobasal (1:1), supplemented with N2 (0.5x) and B27 minus vitamin A (1x) supplements, 2 mM glutamax, 0.5% MEM-NEAA 0.2 μM 2-mercaptoethanol (Thermo Scientific), and 2.5 μg/mL insulin (Sigma)] for 4 days. After this period, the medium was replaced with the same formulation, except with 1x B27 containing vitamin A (Thermo Scientific). This final differentiation medium was replaced every week during the complete differentiation process (45 days).

Sample Preparation and Digestion

Two separate hESC (BR1) cultures were harvested at 70–80% confluence. At 45 days in culture, five hESC-derived cerebral organoids were pooled to provide population variability within each experiment. Three different experimental spinner flasks, differentiated by distinct differentiation processes (batches), were analyzed. Cell lysates of either hESC or 45-day organoids were homogenized in extraction buffer containing 7 M urea, 2 M thiourea, 4% CHAPS, 70 mM DTT and EDTA-free protease inhibitor cocktail (Roche). Sample lysates were centrifuged at 10,000 × *g* for 10 min at 4°C. The supernatant was collected and quantified with a Qubit® 3.0 Fluorometer (Thermo Fisher Scientific). Each sample (50 μg) was subjected to an SDS-PAGE gel electrophoresis and *in gel* reduction, alkylation, and

overnight digestion in a 1:50 (trypsin:total protein) solution, at 37°C. Peptides obtained from this process were dried by SpeedVac (Thermo Fisher Scientific) and stored at −80°C prior to quantitative and qualitative analyses by shotgun mass spectrometry.

Liquid Chromatography-Mass Spectrometry

Proteomic analyses were performed on a state-of-the-art 2D-LC-MS/MS system. Peptides were injected into a two-dimensional, liquid chromatographer [Acquity UPLC M-Class System (Waters Corporation, Milford, MA, United States)] coupled to a Synapt G2-S mass spectrometer (Waters Corporation, Milford, MA, United States). In first-dimension reverse-phase chromatography, peptides (5 μg) were loaded onto a M-Class BEH C18 Column (130 Å, 5 μm, 300 μm × 50 mm, Waters Corporation, Milford, MA, United States). Fractionation was performed using ascending concentration steps of acetonitrile (11, 14, 17, 20, and 50% acetonitrile). Peptide loads were directed to second-dimension separation, on a nanoACQUITY UPLC HSS T3 Column (100 Å, 1.8 μm, 75 μm × 150 mm, Waters Corporation, Milford, MA, United States), with an acetonitrile gradient of 7–40% (v/v) over 54 min at a flow rate of 0.4 μL/min directly into a Synapt G2-S. The mass spectrometer acquired data in data-independent mode (DIA) with ion mobility separation (high-definition data-independent mass spectrometry; $HDMS^E$), to distinguish ions with the same intact mass, significantly enhancing the proteome coverage (Distler et al., 2014). Injection was performed using nano-electrospray ionization in positive ion mode, nanoESI (+), with a NanoLock Spray (Waters, Manchester, United Kingdom) ionization source. The lock mass channel was sampled every 30 s. Calibration was performed with an MS/MS spectrum of [Glu1]-Fibrinopeptide B human (Glu-Fib) solution from the reference NanoLock Spray source. Each of the three independent biological samples was run in technical triplicates.

Database Search and Quantification

Raw data was processed with Progenesis® QI for Proteomics, version 3.0 (Waters). Data processing for protein identification and quantification was performed using dedicated algorithms, searching against the Uniprot human proteomic database (version 2017/10), with the default parameters for ion accounting and quantitation (Li et al., 2009). The databases used were reversed "on the fly" during queries and appended to the original database to assess the false-positive identification rate, and false discovery rate (FDR) was set to less than 1%. Other variable parameters set for peptide identification were: up to two missed cleavages for trypsin digestion; variable modifications by oxidation (M) and fixed modifications by carbamidomethyl (C). Identifications not satisfying these criteria were rejected. The quantitative analysis was carried out on the log2-values of the measured intensities. Raw mass spectrometry (MS) files used in this experiment were uploaded to the PRIDE proteomics data repository with the accession number PXD011605.

In silico Analysis

Gene ontology was analyzed using DAVID[1] (Huang et al., 2009a,b) and Panther[2] (Mi et al., 2016) databases. The significant biological functions are based on Fisher's exact test. Gene Analytics[3] and LifeMap[4] were used to search for specific proteins within cell types. Reactome Pathways Knowledgebase[5] (Fabregat et al., 2017) and the KEGG knowledge base[6] (Kanehisa et al., 2016) were used to identify overrepresented pathways. Protein interaction networks were identified using the STRING database[7] (Szklarczyk et al., 2018). Ingenuity® Pathway Analysis (Qiagen Bioinformatics, Redwood, CA, United States) performed a core analysis on diseases and biofunctions. The BrainSpan Atlas of the Developing Human Brain was also consulted for developmental information[8]. The BrainSpan human developmental transcriptome dataset (RNA-Seq Genecode v10 summarized to genes) Log2 values averaged to genes was compared to the proteomics data of this study. As well, the Log2 transformed values of single-cell transcriptomics data of human cerebral organoids accession GSE75140 and GSE82022 (Camp et al., 2015; Luo et al., 2016), using Spearman correlation. The protein level Log2 transformed values of formalin-fixed, paraffin-embedded human brain data at 16–20 gestational weeks (GW) from the study of Djuric et al. (2017) was compared with data of human cerebral organoids of our study.

Oligodendrocyte Progenitor Cell in Cerebral Organoids

Cerebral organoids that had been differentiated for 45 days were used for oligodendrocyte progenitor cell (OPC) isolation and initial differentiation. Approximately five cerebral organoids were mechanically dissociated and plated in 100-mm culture dishes (~5×10^6 cells/dish), previously coated with polyornithine (1.5 μg/mL, Sigma) and laminin (5 μg/mL, Sigma). They were then maintained for 4 days in DMEM/F12 (Invitrogen) supplemented with 1x N2, 0.5x B27, 20 ng/mL of FGF2, and 20 ng/mL of EGF (Thermo Fisher Scientific). After this time, the medium was changed to include 10 ng/mL of platelet-derived growth factor-AA (PDGFA, Thermo Fisher Scientific) and incubated for another week. Upon confluence, cells were passaged, and the medium was replaced with DMEM/F12 containing 0.5x B27, 10 ng/mL PDGFA, 30 ng/mL T3, 10 ng/mL insulin-like growth factor 1 (IGF-1), and 200 μM ascorbic acid (Sigma-Aldrich). This medium was changed every 5 days for another 8 weeks, when OPCs showed initial ramified morphology and were then analyzed by immunolabeling.

[1]https://david.ncifcrf.gov/
[2]http://www.pantherdb.org/
[3]https://geneanalytics.genecards.org/
[4]https://discovery.lifemapsc.com/
[5]https://reactome.org/
[6]http://www.kegg.jp/
[7]https://string-db.org/
[8]http://www.brainspan.org/

Single-Cell Calcium Imaging

Variations of free intracellular calcium ($[Ca^{2+}]i$) levels were evaluated in single cells obtained from dissociated cerebral organoids in culture, following application of KCl or ATP using a method adapted from the protocol of retina cells (Freitas et al., 2016) or cortical astrocytes (Faria et al., 2016). Dissociated organoids (30 and 45-days) were plated onto a 15-mm coverslip (Marienbad, Germany) and maintained for 10 days *in vitro* to allow adhesion and network stabilization. Prior assessment, cells in culture were loaded for 40 min with 5 μM Fura-2/AM (Molecular Probes), 0.1% fatty acid-free bovine serum albumin (BSA), and 0.02% pluronic F-127 (Molecular Probes) in Krebs solution (132 mM NaCl, 4 mM KCl, 1.4 mM $MgCl_2$, 2.5 mM $CaCl_2$, 6 mM glucose, 10 mM HEPES, pH 7.4), in an incubator with 5% CO_2 at 37°C. After a 10-min post-loading period at room temperature in Krebs solution, to obtain a complete hydrolysis of the probe, coverslips with the cells were mounted on a chamber in a PH3 platform (Warner Instruments, Hamden, CT, United States) for rapid perfusion on the stage of an inverted fluorescence microscope (Axiovert 200; Carl Zeiss). Cells were continuously perfused with Krebs solution (273 mOsm) and stimulated with different solutions (50 mM KCl or 100 μM ATP). The solutions were prepared immediately before the assays. Preparing 50 mM KCl (Sigma) 55.9 mg were diluted in 15 mL Krebs, 372 mOsm; while for ATP (Sigma) 92 mg were diluted in 1 mL (preparing a 167 mM stock solution) we then diluted to a 10 mL ATP, to 100 μM, final pH set to 7.4. Solutions were added to the cells by a fast-transition system (approximately 8 s). The variations in $[Ca^{2+}]i$ were evaluated by quantifying the ratio of fluorescence emitted at 510 nm following alternate excitation (750 ms) at 340 and 380 nm, using a Lambda DG4 apparatus (Sutter Instrument, Novato, CA, United States) and a 510 nm long-pass filter (Carl Zeiss) before fluorescence acquisition with a 40X objective by Cool SNAP digital camera (Roper Scientific, Trenton, NJ, United States). Acquired values were processed using MetaFluor software (Universal Imaging Corp., West Chester, PA, United States). Values for Fura-2 fluorescence ratio were calculated based on a 15% increase cutoff of the $[Ca^{2+}]i$ level induced by the stimulus. Cell cultures after single cell imaging were fixed in 4% paraformaldehyde (PFA) for immunolabeling.

Immunohistochemistry and Immunocytochemistry

Cerebral organoids were collected from spinner flasks and fixed in 4% PFA, followed by incubation in sucrose solutions over an increasing gradient (10, 20, and 30%) prepared in phosphate buffered saline (PBS). Organoids were then embedded in optimal cutting temperature compound (OCT) and frozen in liquid nitrogen. The organoids were sectioned with a cryostat (Leica) into 20 μm thick sections.

Dissociated cerebral organoids and OPCs were fixed in 4% PFA. After fixed, cells were washed with PBS, permeabilized in 0.3% Triton-X solution, blocked in a 3% bovine serum albumin solution (BSA), and immunolabeled using primary antibodies: anti-Nestin (1:100, MAB5326, Millipore), anti-Neurofilament 200 (1:400, N0142, Sigma-Aldrich), anti-class III β-tubulin (1:100, MAB1637, Millipore), anti-S100β (1:200, ab52642, Abcam). For isolated and differentiated OPCs, primary antibodies were: anti-BLBP (1:200, AB110099, Abcam), anti-CNPase (1:200, #5664, Cell Signaling), anti-PDGFRA (1:1000, #3174, Cell Signaling), anti-olig2 (1:100, MABN50, Millipore), and anti-PAX6 (1:200, sc-11357, KloneLife). Secondary antibodies Alexa Fluor 488 goat anti-mouse (A11001, Invitrogen) and goat anti-rabbit (A11008), and Alexa Fluor 594 goat anti-mouse (A11032; Invitrogen) were used. DAPI (4′, 6- diamidino-2-phenylindole, 1 mg/mL) was used for nucleus staining. After immunostaining, cerebral organoids and OPCs were visualized using a Leica SP5 confocal microscope or a Leica DM5500B fluorescence microscope (Leica, Germany).

Transmission Electron Microscopy

Organoids were fixed in a solution of 2.5% glutaraldehyde in 0.1 M cacodylate buffer (v/v), post-fixed for 5 min in 1% OsO_4 solution in cacodylate buffer (w/v) containing 5 mM $CaCl_2$ and 0.8% potassium ferricyanide (w/v). Samples were dehydrated in solutions of increasing acetone concentration and embedded in epoxy resin (EMS, PA, United States). Ultra-thin (70 nm) sections were stained with uranyl acetate and lead citrate and observed with a Leo 900 electron microscope at 80 kV (Zeiss, Germany).

RESULTS

Proteome Enrichment of PSC-Derived Cerebral Organoids

To resolve the complex proteome of whole, 45-day cerebral organoids, we used state-of-the-art label-free shotgun proteomics to provide broader coverage of cerebral organoids cultured for 45 days (**Figure 1A**), in which early neuronal network formation already takes place, as previously reported by our group (Sartore et al., 2017). The combined analyses of the organoids identified and quantified 3,073 proteins with at least two unique peptides (**Figure 1B**, and data on **Supplementary Table 1**). Tissue clustering analyses demonstrated enrichment of terms such as fetal brain cortex, epithelium and other brain proteins (**Figure 1C**). Investigating broad biological processes identified in 45-day cerebral organoids, the proteomic profile analyses showed majorly enriched pathways related to metabolic and cellular processes, such as cell–cell adhesion, RNA splicing, ATP metabolism, cerebral cortex development, and cytoskeleton organization. Specific neuronal functions were also seen, such as glutamate secretion, neuron projection development, axonal transport, and dendrite morphogenesis (**Figure 1D**). Regarding cellular compartments, proteome analysis comprehended cytosol, membrane, cytoskeleton and nucleoplasm, general cellular compartments, showing a global overview of the cell, in agreement with our whole-cell proteomics approach. Nevertheless, enriched proteins from extracellular exosome, including synaptic vesicle, axon and postsynaptic density were found, in addition to myelin sheath, cell–cell–adherent junction and focal adhesion proteins (**Figure 1D**).

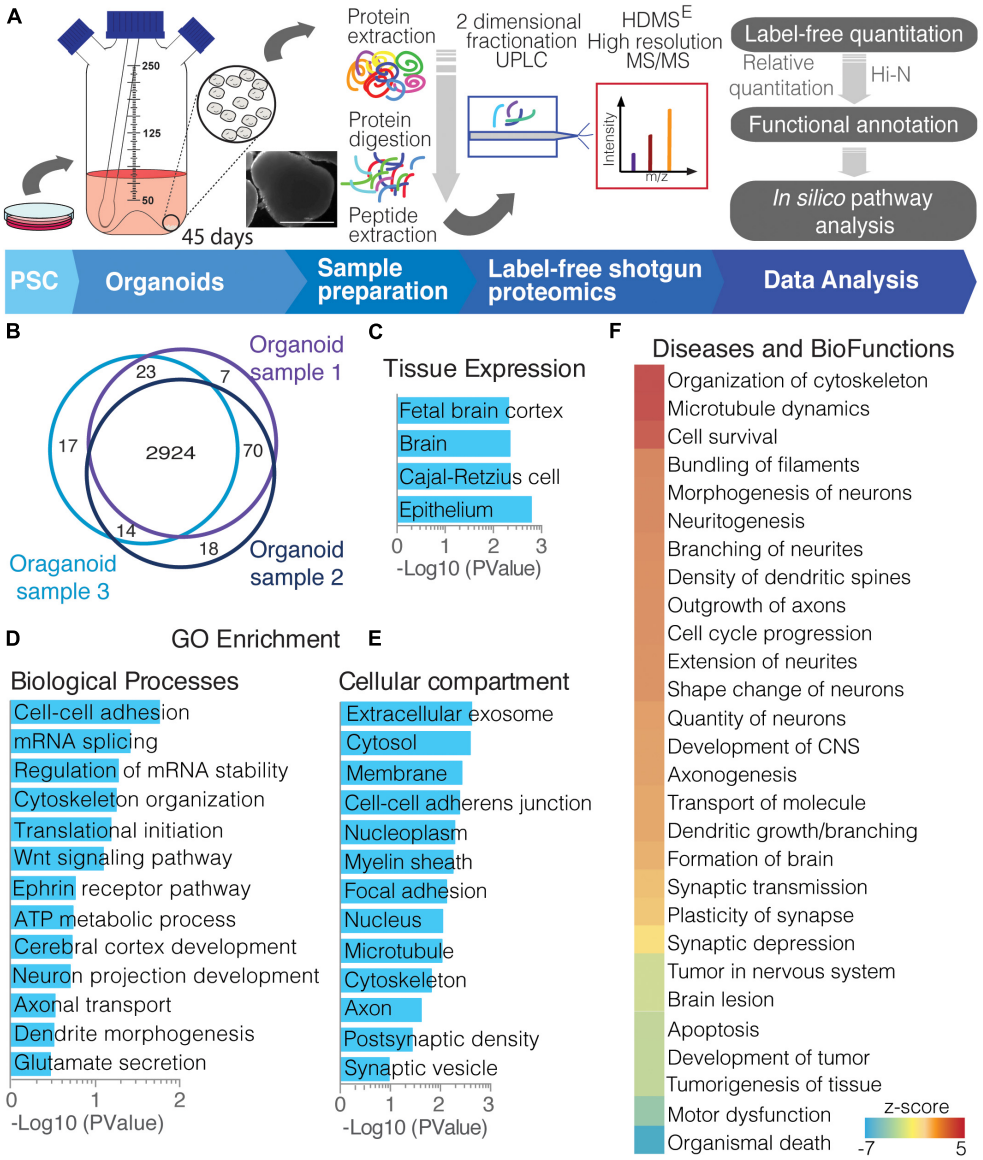

FIGURE 1 | Overview of cerebral organoid protein expression. **(A)** Experimental proteomics workflow, from collecting cerebral organoids and processing to proteomic studies. After sample preparation (extraction and digestion), peptides underwent a 2D-UPLC fractionation and on-line detection using HDMS^E high resolution MS/MS acquisition. The acquired peptides were deconvoluted, identified, and quantified using the software Progenesis, whereupon proteins were identified and quantified. This was followed by functional annotation of protein groups and other *in silico* analyses. **(B)** Venn diagram showing commonly found proteins among cerebral organoids replicates (PSC-derived samples). Functional annotation analyses of proteins commonly found in replicates are clustered by **(C)** tissue expression; gene ontology using **(D)** biological function and **(E)** cellular compartment distribution; and **(F)** diseases and biofunctions activity.

In addition, using downstream effects analysis of those protein functions, we observe proteins related to cytoskeletal organization with filament bundling, indicating activation of neuronal morphogenesis and neuritogenesis. This included proteins for axon outgrowth, branching, and neurite extension (**Figure 1E**). On the other hand, the proteins present have ties with inhibition of organismal death, tumorigenesis and apoptosis, while active cell survival, possibly indicating adaptation to organoid culture growth expansion limitations (**Figure 1F**). These enrichment analyses confirm a global, functional correlation between 45-day whole-brain cerebral organoids and to brain tissue.

Additionally, we compared the proteomes of cerebral organoids with those of fetal human brains with 16–20 GW (Djuric et al., 2017). Djuric et al. (2017) have analyzed the developing human brain in a spatiotemporal manner, specifically the ventricular zone (VZ), intervening intermediate zone (IZ), subplate (SP), and frontal cerebral cortex (Cx). The Spearman correlation of the protein intensities of both datasets [from this study and that of Djuric et al. (2017)], ranged from $r = 0.28–0.35$

($p < 1.24E-26$), with approximately a 40% overlap of proteins among samples (**Supplementary Figure 1A**). Because different methodological approaches were applied in each proteomic study, and as information of fetal brain only as young as 16 GW was available; the overlap range is potentially justified, as cerebral organoids were grown for 45 days, and according to previous mRNA correlation studies (Camp et al., 2015; Luo et al., 2016) are expected to correlate to a younger GW. In addition, the overlapping proteins indicate that cerebral organoids exhibit characteristics from all developing cortical layers, equivalently separated into VZ, IZ, SP, and Cx proteins, as the majority of overlapping proteins are common among them (**Supplementary Figure 1B**). Certain proteins found in common included novel layer markers described by them (Djuric et al., 2017), such as filamin C (FLNC), found mainly in VZ, and cellular retinoic acid binding protein 1 (CRABP1), found in later and more committed neural cells within the VZ during development (**Supplementary Table 1**). These shared proteins over-represent functions related to cell–cell adhesion, mRNA splicing and translation initiation processes, in addition RNA and protein binding molecules, and found to be principally part of the cytosol, exosome, or myelin sheath compartments (**Supplementary Figure 1C**).

Additional markers of development found in organoids are from early events, including forebrain dorsal/ventral pattern formation, such as clusterin (CLU), SPARCL1 (SPARC like protein 1) and TTC21B (tetratricopeptide repeat protein 21B); and hindbrain formation, via HOXA1 (homeobox protein Hox-A1). Retinal proteins such as guanylyl cyclase 2 (GUCY2F), dehydrogenase 1 (ALDH1A1), and alpha-crystallin B chain (CRYAB) were also detected (**Supplementary Table 1**). Evidence of those markers emphasizes the heterogeneity and diversity niches formed by this cerebral organoid model.

We have also compared the cerebral organoid proteomics dataset with that of the BrainSpan fetal transcriptomic dataset[9], with a focus on the 8–37 post-conception week (dorsolateral prefrontal cortex area). The correlation of RNA-protein is lower than that of protein-protein comparisons, ranging from $r = 0.02$-0.06 ($p < 0.003$) (**Supplementary Figure 2A**). On the other hand, the comparison of the proteome of cerebral organoids with the RNA-Seq dataset of similar protocols of differentiation of cortical organoids (Camp et al., 2015; Luo et al., 2016), showed a moderate correlation ranged from $r = 0.19$–0.22 ($p < 5.88E-22$), stronger in older organoids (**Supplementary Figure 2B**). Possible differences are due divergences in translational rates and technical distinctions in mRNA and protein levels during the differentiation process.

Diversity of Cell Types in Cerebral Organoids

A closer look into the proteome of cerebral organoids reveals specific proteins from a wide range of neural cell types related to neurodevelopment. Overall, **Figure 2** (along with **Supplementary Table 1**) depicts how broad the protein dynamics are, and highly abundant cytoskeleton proteins can be observed, such as nestin (NES), tubulin β3 (TUBB3), neurofilaments (NEFL, NEFM, NEFH), microtubule-associated protein 2 (MAP2), and microtubule-associated protein tau (MAPT), and neural cell adhesion molecule 1 (NCAM1). Low-abundance proteins however were more specific to differentiation processes and other neuron-related proteins. This included sodium/potassium-transporting ATPase subunit alpha-3 (ATP1A3), synaptosomal associated protein 25 (SNAP25), and leucine-rich repeat kinase 2 (LRRK2), indicating the presence of both progenitor and neuronal cells. Several of these neural proteins are commonly found in proteomes of human brain tissue (Carlyle et al., 2017). The presence of these neural proteins is widespread in cerebral organoids. Cell proliferation zones are shown in yellow by phospho-H3 protein (PH3), surrounding ventricle-like cavities, and are surrounded by nestin-expressing cells (**Figures 3A–C**). Other neuronal cytoskeleton proteins were found to be widespread throughout cerebral organoids, such as the neurofilament heavy (NEFH, in **Figures 3D–F**), an intermediate filament polypeptide, and the neuronal microtubule protein tubulin (TUBB3, **Figures 3G–I**).

The proteomic analysis of cerebral organoids has also unveiled proteins associated with glial cell types, such as glial fibrillary acidic protein (GFAP), vimentin (VIM), glia maturation factor beta (GMFB), and aldehyde dehydrogenase 1 family member L1 (ALDH1L1). Those proteins are commonly found in astrocytes, and represented here by the S100 protein (**Figures 3J–L**); several astroglial cells were found in the cerebral organoids. Consistently, though to a lesser extent, proteins related to an oligodendroglial phenotype were also present. Which included not only proteins related to OPC stage, such as 2′,3′-cyclic nucleotide 3′phosphodiesterase (CNP) and platelet-derived growth factor receptor alpha (PDGFRA), but also proteins related to more mature oligodendrocyte transitional stages, such as myelin basic protein (MBP), myelin proteolipid protein (PLP1), and myelin oligodendrocyte glycoprotein (MOG). Indeed, although early in development and variable within organoid formation, specific niche environments allow some organoid areas to present initial stages of myelin sheath formation around neurite bundles, in early stages of lamellae formation, as observed in transmission electron microscopy (**Figures 3M–P**). Additionally, myelinating proteins were among those correlated with fetal brains (16–26 weeks) (Djuric et al., 2017) despite the completed process being associated with later developmental stages. According to this data, cerebral organoids are composed mainly of progenitors, including radial glia, and neurons, followed by astroglia and, to a lesser extent, oligodendroglia.

Isolation and Maturation of OPCs From Cerebral Organoids

Due to the presence of oligodendroglial proteins, we hypothesized the possibility of isolating human oligodendrocytes from cerebral organoid cultures. Following a similar approach as previously described for astrocytes (Dezonne et al., 2017), an isolation protocol was developed to extract progenitors, including OPCs from those 45-day cerebral organoids and was followed by 2D maturation *in vitro*. After proliferative progenitors were isolated from the whole organoid, OPC cultures

[9]http://www.brainspan.org/

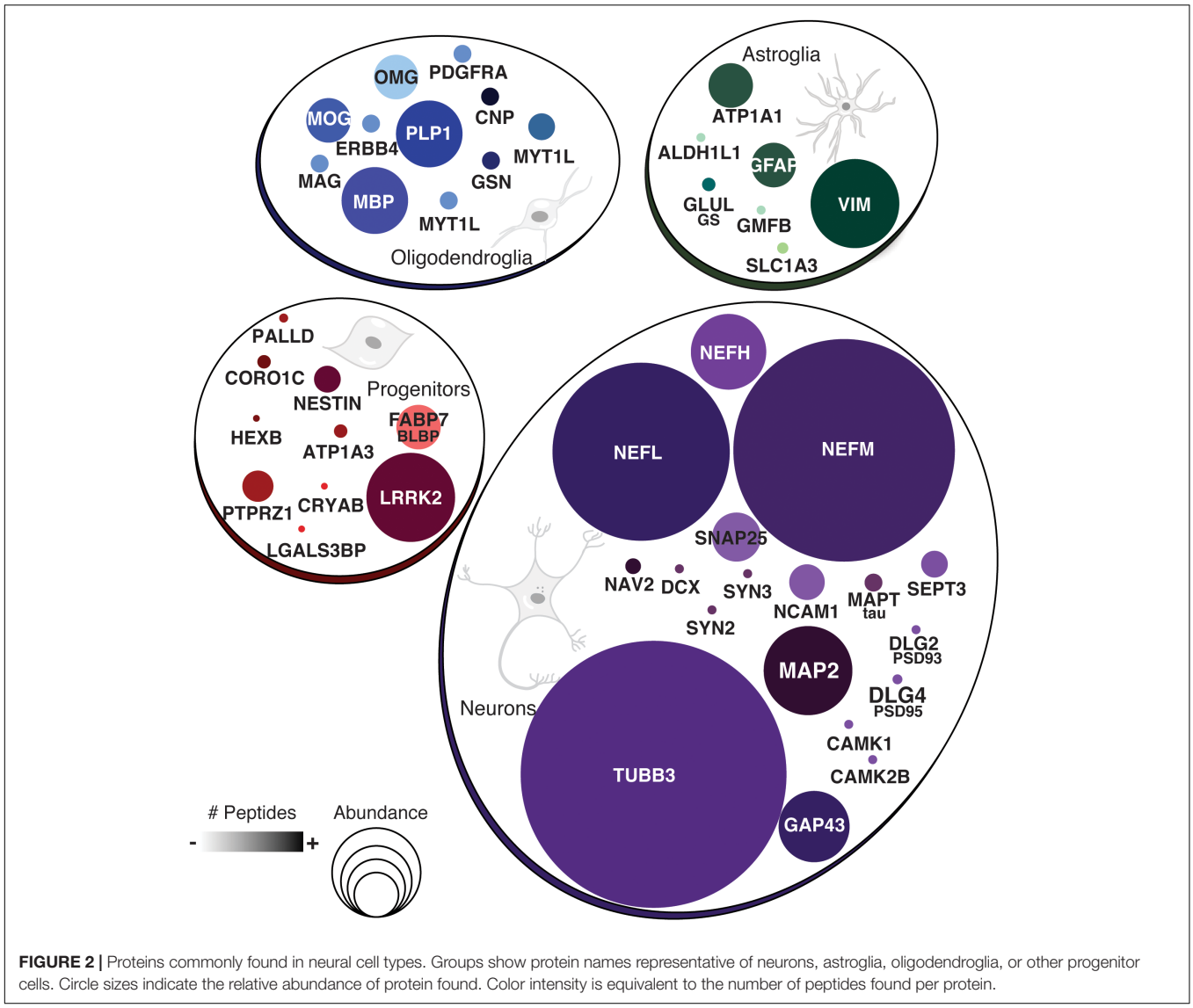

FIGURE 2 | Proteins commonly found in neural cell types. Groups show protein names representative of neurons, astroglia, oligodendroglia, or other progenitor cells. Circle sizes indicate the relative abundance of protein found. Color intensity is equivalent to the number of peptides found per protein.

were further differentiated for up to 60 days (**Figure 4A**). For the length of the culture period, cells with a bipolar morphology composed the majority of OPCs, while some had initiated active cytoplasm ramification toward a multipolar morphology, typical of more mature intermediate oligodendrocytes (**Figure 4B**, arrows). These OPCs in culture, bipolar or multipolar, were labeled with radial glia markers BLBP and PAX6 (**Figures 4E–G**), and early event markers of oligodendrogenesis such as OLIG2, CNPase (CNP) and PDGFRA (**Figures 4C,D,H,I**).

Calcium Signaling Analysis of Neural Cells in PSC-Derived Cerebral Organoids

Based on the identification of proteins associated with axon guidance and neurotransmitter secretion, there is indication of the presence of maturing neurons in cerebral organoids. Here, we used calcium transient imaging to measure neuronal activity of cultured cerebral organoid cells. These neural cells are physiologically balanced by neurotransmitter exocytosis, which is constantly modulated by the levels of intracellular calcium $[Ca^{2+}]i$. Proteomic data have positively identified Cav1.2 (CACNA1C – voltage-dependent L-type calcium channel subunit alpha-1C), in addition to the regulatory subunit CACNA2D3 (voltage-dependent calcium channel subunit alpha-2/delta-3) (**Supplementary Table 1**).

Dissociated human cerebral organoids displayed more flat cells (**Figure 5A**) or neuron-like cells (**Figure 5G**). Their equivalent fluorescence microscopic fields are shown in **Figures 5B,H**, respectively. Additionally, the numbers illustrated in **Figures 5C,I** Fura-2 fluorescence of selected cells, in the same microscopic fields, are regions of interest selected before stimulation with 50 mM KCl or 100 μM ATP; then, single cell calcium variations were evaluated by quantifying the ratio of the fluorescence and later matched with the cell number, showing that most of the responses (cells # 3, 31, 82, 83, 84 were activated by KCl, pink arrows in **Figure 5E**), but not by ATP.

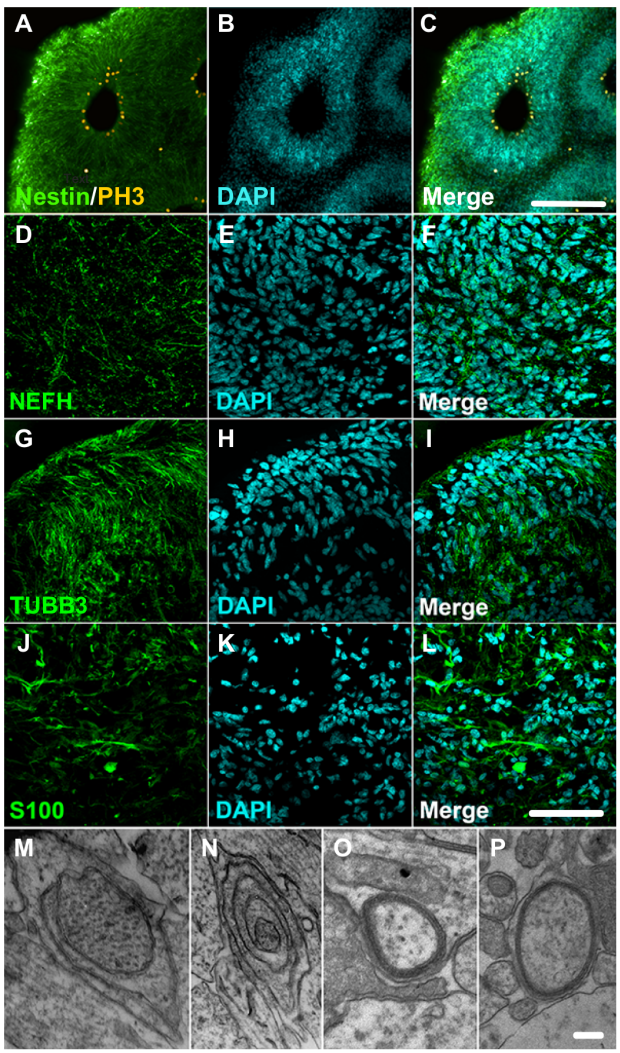

FIGURE 3 | Cerebral organoids expressing neuronal and glial proteins. **(A–C)** Immunostaining of 30-day cerebral organoids with nestin (green) and showing proliferative areas with PH3 (yellow). Immunostaining of 45-day cerebral organoids with neuronal markers **(D–F)** neurofilament 200 (NEFH), and **(G–I)** tubulin βIII (TUBB3), or glial marker **(J–L)** S100 protein in cryosections. Nuclear staining with DAPI. **(M–P)** Transmission electron microscopy images showing myelin sheath formation around some cells of cerebral organoids. Scale bars shown correspond to **(A–C)** 200 μm, **(D–L)** 50 μm, and **(M–P)** 1 μm.

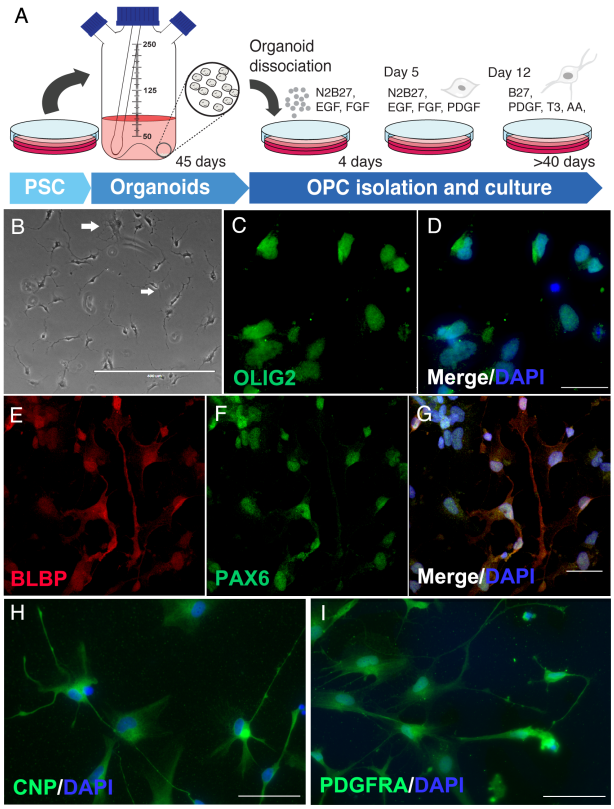

FIGURE 4 | Oligodendrocyte progenitors derived from cerebral organoids. **(A)** Schematic representation of OPC isolation and culture. **(B)** Phase contrast of immature oligodendrocytes with initial ramifications (arrows in white). OPCs were stained for **(C,D)** olig2, oligodendrocyte lineage transcription factor, **(E–G)** BLBP and PAX6 progenitor markers, **(H)** CNPase (CNP), enzyme of early oligodendrocyte formation and myelin precursor, and **(I)** PDGFRA oligodendrocyte lineage marker. Scale bars shown are **(B)** 400 μm, **(D,G)** 30 μm and **(H,I)** 50 μm.

On the other hand, a flat-like cell (#74) – identified by a yellow arrow – is activated by 100 μM ATP (**Figure 5D**) but not by KCl. Several of those cells were labeled by nestin (**Figure 5F**) and TUBB3 (**Figure 5K**), with a few MAP2 positive cells (**Figure 5L**), suggesting they are progenitors and/or neuronal-like cells, which respond to 50 mM KCl (**Figure 5E**). As the organoids mature, coverslips presented neuron-like cells (for example, cells # 21, 36, 38, 40, and 41) and were only responsive to KCl (**Figure 5J**), suggesting those cells express voltage dependent calcium channels. In total, 607 cells were analyzed from 30- and 45-day cerebral organoids, in which 245 cells (40%) were responsive to 50 mM KCl, while only 5 cells (1%) were activated by 100 μM ATP. The area under the curve was quantified for those cultured flat cells (**Figures 5A,M**), or neuron-like cells (**Figures 5G,N**), which responded to 100 μM ATP or 50 mM KCl, as previously done (Freitas et al., 2019). This percentage agrees with the previously addressed protein content, which indicated the presence of more neuronal than glial cells in organoids at this differentiation stage, several of which are young and still unresponsive.

Protein Signals Involved With Neuronal Patterning of Cerebral Organoids

Cells in the differentiating cerebral organoids followed patterns seen in the nervous system to acquire distinct identities. Among the neuronal patterning proteins found in cerebral organoids, we observed downstream reelin pathway proteins (**Figure 6A**), such as FABP7/BLBP (fatty acid binding protein 7, also known as brain lipid-binding protein), and PAFAH1B1 (platelet activating factor acetyl hydrolase 1b regulatory subunit 1, also known as LIS1 - lissencephaly 1 protein), in addition to the surface receptor LRP8 (Low-density lipoprotein receptor-related protein 8, also

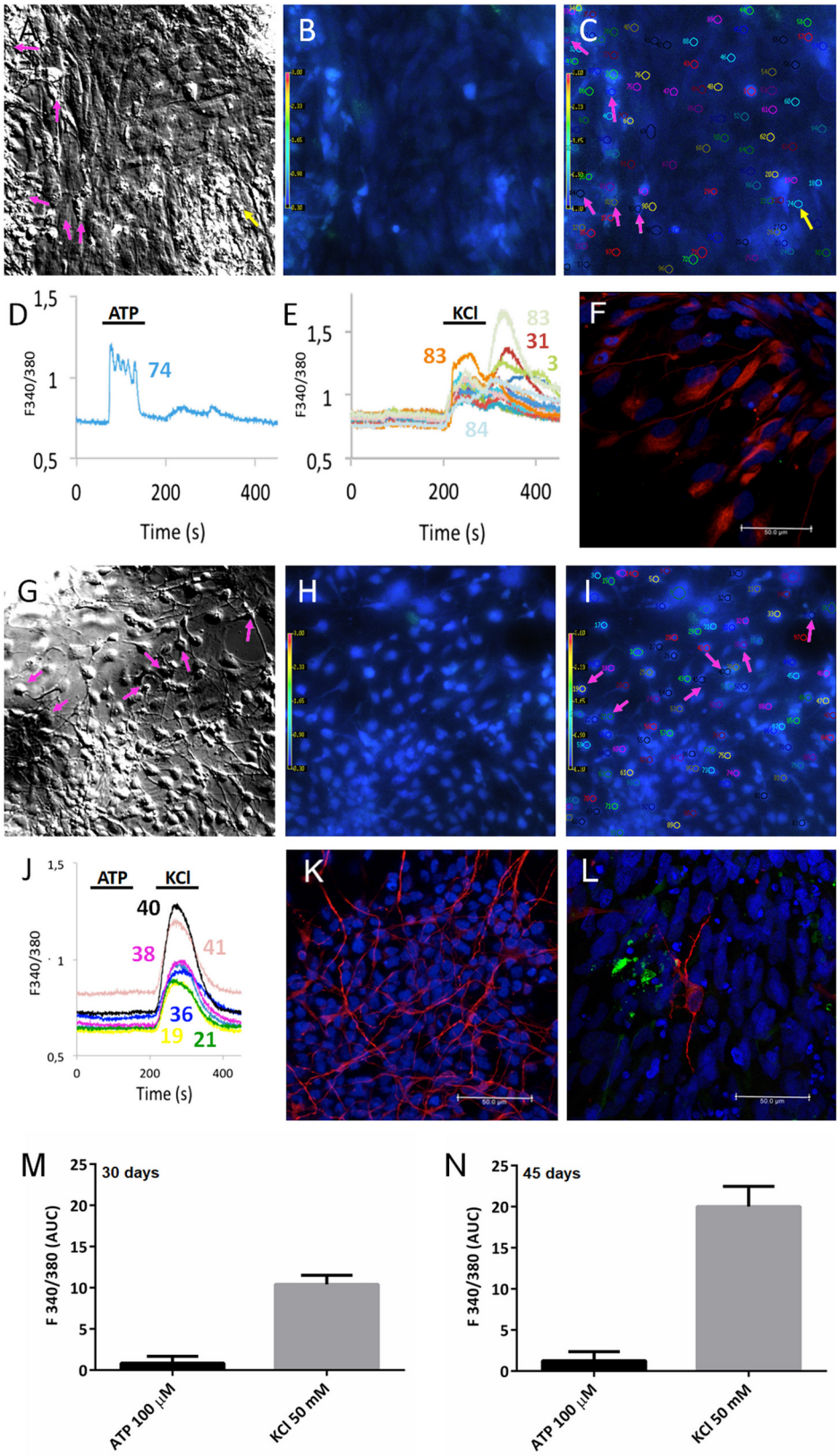

FIGURE 5 | Continued

FIGURE 5 | Calcium response to ATP and KCl stimulation of cerebral organoids. PSC-derived cerebral organoids grown for **(A–C)** 30 or **(G–I)** 45 days had their cells dissociated and plated for 10 days on 15 mm coverslips. Cultured cells shown in **(A,G)** bright field and **(B,H)** under fluorescence. **(C,I)** Selected cells are shown in the same microscope field under fura-2 fluorescence in SCCI experiments. Typical responses are shown for cells when stimulated with **(D)** 100 μM ATP or **(E,J)** 50 mM KCl. As shown in **(C–E)**, only one cell (#74) responded exclusively to ATP (yellow arrow), whereas several cells (# 3, 31, 82, 83, 84) responded to KCl (pink arrows), in 30-day cerebral organoids. As shown in **(I,J)** selected cells (# 21, 36, 38, 40, and 41) were only responsive to 50 mM KCl (pink arrows) in 45-day cerebral organoids. Post-stimulation, coverslips were fixed and cells labeled for **(F)** nestin, **(K)** TUJ1/tubulin βIII (TUBB3), or MAP2 **(L)** scale bars 50 μm. Areas under the curve are representative of calcium responses to ATP or KCl obtained from 30-day **(M)** or 45-day organoids **(N)**.

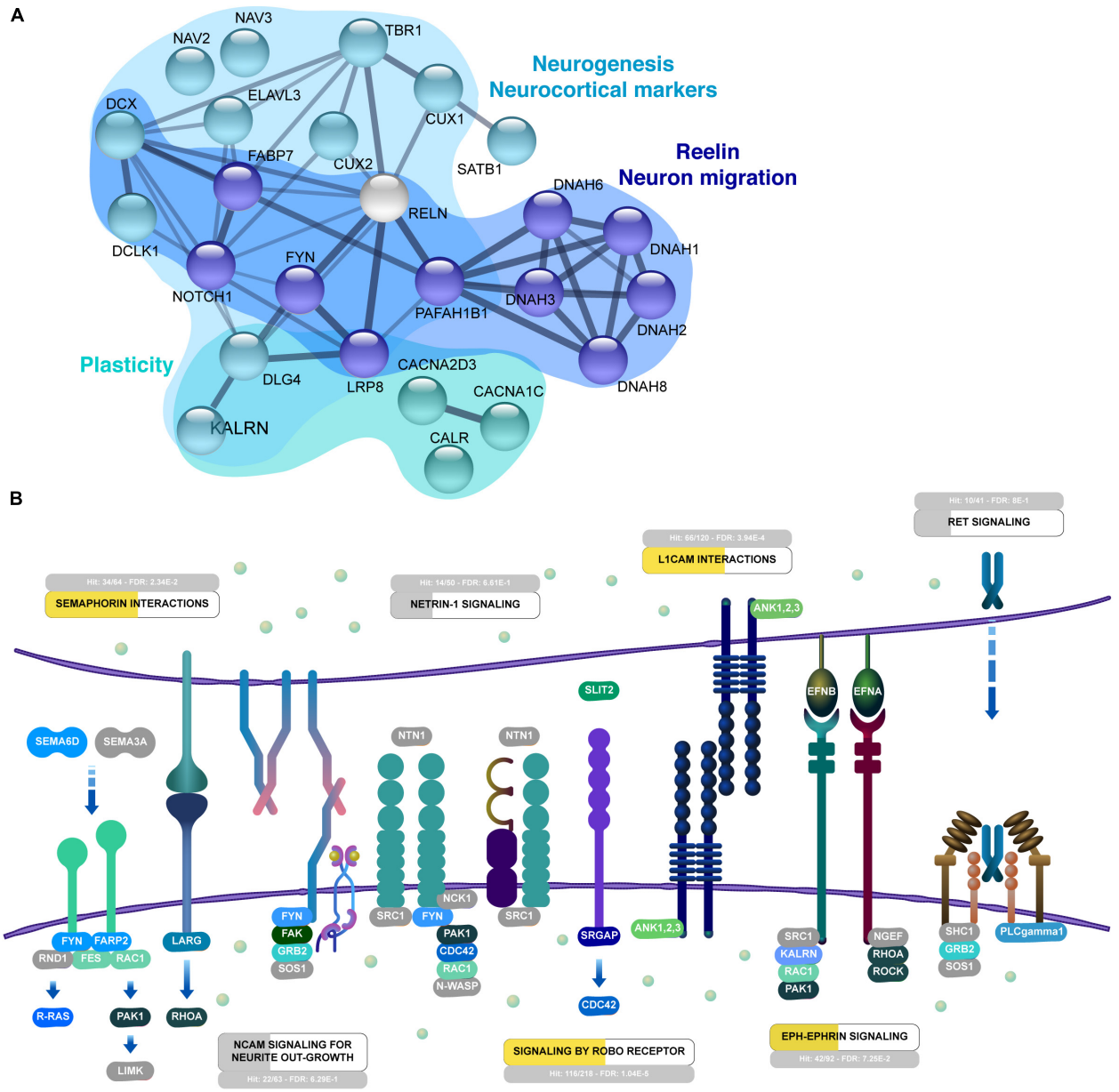

FIGURE 6 | Interactive organization of proteins from 45-day cerebral organoids. **(A)** Network representation of selected proteins related to neurogenesis, reelin and migration of neurons, and synaptogenesis. Networks are based on the STRING database (https://string-db.org/). **(B)** Neuronal guidance is overrepresented in 45-day cerebral organoids (FDR 2.05E-15). Enriched signaling pathways include semaphorin interactions (FDR 5.14E-4), L1CAM interactions (FDR 9.68E-7), signaling by ROBO receptor (FDR 4.9E-9) and Eph-Ephrin signaling (FDR 3.6E-3). Proteins in NCAM signaling for neurite outgrowth, netrin-1, and ret signaling are partially represented. Overrepresentation analyses were performed with Reactome (https://reactome.org/). Proteins found in proteomics analyses of 45-day organoids are colored in shades of blue and green, while gray proteins were not found in the dataset.

known as ApoER2 – apolipoprotein E receptor 2) and dyneins (DNAH1, 2, 3, 6, 8). This pathway is triggered by activation of NOTCH1 (neurogenic locus notch homolog protein 1) and FYN (tyrosine-protein kinase Fyn), which were also detected in cerebral organoids (**Figure 6A**).

These proteins are connected to protein markers of neurogenesis and patterning, including ELAVL3 (ELAV like RNA binding protein 3, also known as HuC – Hu antigen C and paralog to HuD, neuronal-specific RNA-binding proteins), and the special AT-rich DNA-binding protein 1 (SATB1), which plays regulatory roles in neuronal differentiation (**Figure 6A**). In addition, proteins associated with the radial glia scaffold were also present in organoids (**Figure 6A**), such as doublecortin (DCX), DCLK1 (doublecortin-like kinase 1/Serine/threonine-protein kinase DCLK1), the neocortical markers CUX1 and CUX2 (homeobox protein cut-like 1 and 2, respectively), TBR1 (T-box brain protein 1), and neuronal navigator proteins 2 and 3 (NAV2 and NAV3).

These findings indicate plasticity of the model, supported by the presence of calcium-binding protein calretinin (CALB2) in cerebral organoids, a protein that is abundantly found in neurons of the retina and cortical interneurons. This is in addition to the presence of other signaling proteins from the calcium-calmodulin family, such as the calcium/calmodulin-dependent protein kinase type I (CAMK1), type II subunit alpha (CAMK2A), and type II subunit beta (CAMK2B) (**Figure 6A**). Overall, this reflects the different levels cell signaling pathways we are able to capture, and its similarities to the neural developmental *in vivo*.

Development of Axonal Guidance in Cerebral Organoids

The proteins identified in cerebral organoids show an overrepresentation of pathways related to axonal guidance, which includes semaphorin (FDR 2.34E-2), L1CAM signaling (FDR 3.9E-4), Robo receptor signaling (FDR 1.04E-5) and Eph-Ephrin signaling (FDR 7.25E-2) (**Figure 6B**). In regards to semaphorins, protein SEMA6D and the signaling cascade with FYN, FARP2 (FERM_RhoGEF and pleckstrin domain-containing protein 2), and RAC1 (Ras-related C3 botulinum toxin substrate 1) were found (**Figure 6B**). These are common interactors of the CRMP/DPYSL protein family (collapsin response mediator protein/dihydropyrimidinase like), such as DPYSL2-5, which are related to microtubule assembly and growth cone collapse (**Supplementary Figure 3**). Several of the secretory and membrane proteins that are related to semaphorin, netrin, or ephrin signaling are connected to extracellular matrix (ECM) proteins, such as laminin (LAMA1, A3, A4, A5, B1, C1), fibronectin (FN1), and proteoglycans (i.e., basement membrane-specific heparan sulfate proteoglycan core protein - HSPG2). The ECM regulates neuroepithelial growth, signaling via cell-surface integrins alpha-6 and beta-1 (ITGA6 and ITGB1), proteins supporting interconnection of cells in the organoids (**Supplementary Figure 3**).

Regarding pathways controlled by cell adhesion molecules, the L1CAM signaling pathway has possible molecular interactions with ankyrins (ANK1, 2, 3), proteins that play key roles in neurite extension and inter-neuronal adhesion (**Supplementary Figure 3**). Signaling by Robo Receptor – another key developmental axonal guidance pathway, which regulates cell migration, proliferation, and intermediate progenitor transition – is represented by ROBO1 (roundabout homolog 1). It could signal via SRGAP1 and 3 (SLIT-ROBO Rho GTPase-activating protein 1 and 3) and CDC42BPB (CDC42 binding protein kinase beta) (**Figure 6B**). Slit-Robo signaling via netrin-1/DCC on a ROBO1-DCC interaction (netrin receptor DCC) is necessary for appropriate neuronal maturation. Afterward, the Eph-Ephrin pathway, via expression of ephrin (EFNB1) and its preferred receptors EPHB3 and EPHB1, could lead to axonal orientation and subsequent synaptic maturation (**Figure 6B**). EPHB2, EPHA3, and EPHA8, other receptors found in the organoids, are known to regulate dendritic spine development, along with a plethora of signaling molecules, including kalirin (KALRN), RAC1 (Ras-related C3 botulinum toxin substrate 1), and PAK1 (serine/threonine-protein kinase PAK 1) (**Figure 6B**).

Neuronal Subtypes and Synaptogenesis Starting in Cerebral Organoids

Having seen protein networks related to axon guidance and positioning, and previous indications of functional neurons like calcium signaling, we expected to find a diversity of neuronal subtypes. Grouping proteins by their transmission function (glutamatergic, dopaminergic, serotonergic or GABAergic neurons), we found proteins related to two main types of neurons (**Figure 7**) in cerebral organoids. Proteins belonging to dopaminergic (p-value 1.5E-3) and glutamatergic (p-value 1.3E-2) synapse were predominantly enriched within the set of proteins found in the cerebral organoids. Around 41 proteins from the dopamine receptor signaling were found (**Figure 7A** and **Supplementary Table 2**), among them tyrosine hydroxylase (TH, tyrosine 3-monooxygenase), a marker for dopaminergic neurons, and calcium/calmodulin dependent protein kinase II alpha (CAMK2A), a key protein that stimulated dopamine efflux. Post-synaptic signaling molecules, like PSD-95 and SHANK1 (SH3 and multiple ankyrin repeat domains protein 1), were found, supporting the presence of synaptogenesis. And 34 proteins related to the glutamate receptor signaling (**Figure 7B** and **Supplementary Table 2**), including glutamate receptor 4 (GRIA4), a subunit present on AMPA receptors, and others such as metabotropic glutamate receptor 8 (GRIM8, mGluR8). We also identified 17 proteins related to GABAergic synapse, such as CALB2, which is usually found in GABAergic interneurons, as previously mentioned, was also found, however, this pathway was not significantly enriched ($p > 0.05$).

DISCUSSION

Cerebral organoids have emerged as an unparalleled functional model of the human brain, allowing this organ to be studied mainly during neurodevelopmental stages (Lancaster and Knoblich, 2014; Quadrato and Arlotta, 2017). Previous studies (Lancaster et al., 2013, 2017; Qian et al., 2016;

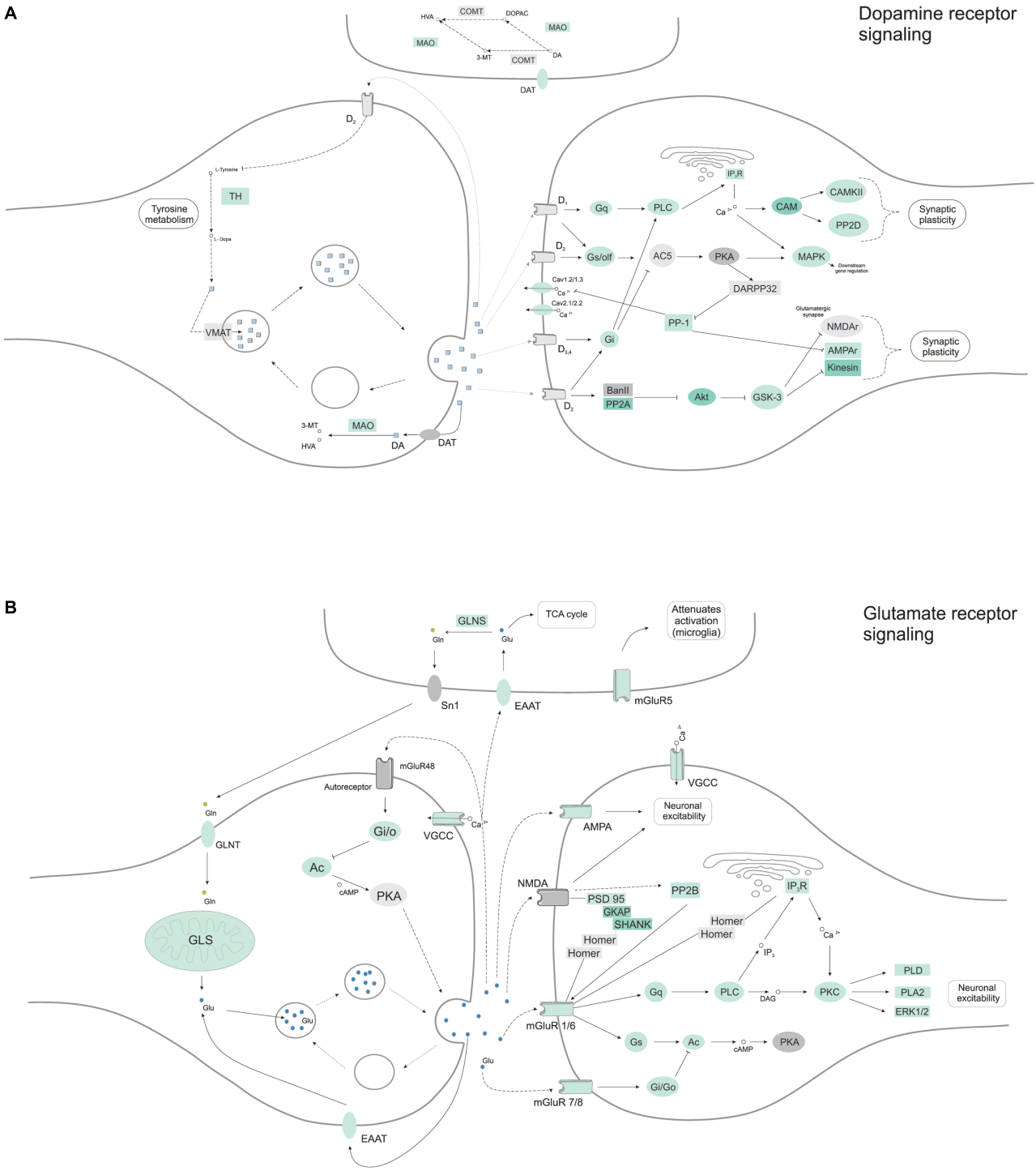

FIGURE 7 | Neuronal molecular pathways indicate glutamate and dopamine receptor signaling, in a representation of 45-day cerebral organoid proteomes. Pathway interactions of **(A)** dopamine and **(B)** glutamate receptor signaling were analyzed from the proteome dataset using the KEGG database (http://www.kegg.jp/). Proteins found in proteomic analyses are colored in green, while gray proteins were not found in the dataset.

Bershteyn et al., 2017; Birey et al., 2017), including from our group (Sartore et al., 2017), have shown that cerebral organoids are self-organizing and that regionalization follows several neurodevelopmental steps, with a variety of heterogeneous micro-niches being present (Renner et al., 2017). Due to extensive cellular variability, self-patterning, and various tissue

architectures, more functional neural networks can be achieved (Quadrato and Arlotta, 2017). Pluripotent stem cell-derived cerebral organoids are still an under-development tool, holding great promise in future studies in the quest of understanding the complexity of the human brain cellular network (Paşca, 2018). Therefore, our effort was to unfold that cell diversity and molecular complexity by investigating the proteome of PSC-derived organoids, providing snapshots of the early developmental stages of neural protein networks, using an unbiased method.

The main efforts to study organoids has been to uncover the typical cellular compositions of neurodevelopmental stages (Lancaster et al., 2013; Camp et al., 2015; Quadrato et al., 2017; Velasco et al., 2019). Using a previously described protocol for whole-cortical organoid (Lancaster et al., 2013; Sartore et al., 2017), cerebral organoids were differentiated for 45 days from human pluripotent stem cells (hPSC) to access their proteome content. At this stage, cerebral organoids present a well-organized structure with ventricle-like cavities, contained cell proliferation zones, and expressed intermediate progenitors followed by early differentiation stage neurons (Sartore et al., 2017). Therefore, while the cytoarchitecture of cerebral organoids has been shown to be complex (Quadrato et al., 2017; Renner et al., 2017), and contains several cell types, when it comes to studies of molecular behavior, there is still much to be discussed. The developmental cues of corticogenesis, including those of a radial glia, are present in the proteome of cerebral organoids. Immature neurons, regulated by the reelin (RELN) signaling pathway, are able to migrate, position, and establish cortical layers to support early synaptic circuits, laminar organization, and further interconnections (Bystron et al., 2006; Sekine et al., 2012). Despite RELN itself not being found in our dataset, downstream proteins of its pathway were present and might contribute to patterning. Several other key developmental pathways of cell migration, proliferation, and axonal guidance follow these signals. Such as Robo receptor signaling, which confers transition of primary to intermediate progenitor via ROBO1 (Borrell and Götz, 2014); or markers such as HuC and SATB1. Moreover, L1CAM signaling pathway participates in the projection neurons crossing the brain midline (Demyanenko et al., 1999), to avoid aberrant axonal trajectories. In addition to neuronal navigator proteins 2 and 3 (NAV2 and NAV3, respectively), proteins previously shown to be connected to neurite outgrowth and axonal elongation upon interaction with the vitamin A metabolite all-trans retinoic acid (atRA) (Merrill et al., 2002; Muley et al., 2008). All of which implicate the organoids into setting early migrating environment, axonal outgrowth, and prone for synapses formation.

The protein–protein interactions observed here indicate intricate mechanisms involved in the migration of progenitor cells, radial glia, or oligodendrocyte progenitors following the neural program. This state-of-the-art proteomics data provided a broader assortment of the prevailing proteins in cerebral organoids, and complements previous studies that have highlighted global and single-cell RNA expression (Camp et al., 2015; Bershteyn et al., 2017; Quadrato et al., 2017). Correlating to protein expression of the human brain, the 45-day-old, whole-brain cerebral organoids depicted representative brain proteins, and a reasonable similarity with *in vivo* human cortex development, shown by revealing their functionality and connecting pathways among those different cell types, already at the early stages. A recent study showed the same similarity between cell-type patterns found in organoids and fetal human brain by comparing scRNA-seq dataset, with about 13% glial cells in 3-month old organoids (Velasco et al., 2019). Glial cells have roles in several steps of remodeling and consolidation, in addition to a carefully orchestrated regulation of transcription factor expression (as reviewed in Allen and Eroglu, 2017). Some of the pathways found overrepresented in cerebral organoids, and which participate in the regulation of neural differentiation, coincide with the genesis of different neuronal cell types and glia cells via cell-to-cell interactions. These include glypican signaling, SPARCL1/hevin and thrompospondin (THBS1), promoting synaptogenesis (Allen and Eroglu, 2017). Several of the cell surface receptors that were found, such as the tyrosine phosphatase family PTPRs, including PTPRD and PTPRS (receptor-type tyrosine-protein phosphatase delta and S), are required for a normal brain development (Coles et al., 2011). They have roles in the pre- and post-synaptic differentiation of neurons, neurite outgrowth driven by ECM stimuli, and glial cell-secreted factors. For instance, PTPRZ1 (receptor-type tyrosine-protein phosphatase zeta) and contactin-1 (CNTN1), which modulates outer radial glia and oligodendrocyte progenitor proliferation, are responsible for maintenance of the stem cell niche (Pollen et al., 2015), and switch to myelinating mature cells to insulate neurons (Lamprianou et al., 2011), and have not been explored.

Most studies of human brain proteomics have been performed on adult postmortem tissue, with only a few on the developing brain, then being predominantly postnatal brain tissue (Carlyle et al., 2017; Djuric et al., 2017). Despite cerebral organoids being a somewhat simpler model of the fetal human brain, it can be adequate to recapitulate several events following directional developmental cues. Additionally, it is an adequate model to study signaling events that are dependent on particular cellular niches within the organoid. Containing separate neuroepithelial layers, the organoids are comprised of a structure similar to cerebral ventricles, with a possible separation of ventricular and subventricular zones, in common with early human brain development. This have been previously shown by the genetic program of previous studies of differentiating organoids (Camp et al., 2015; Luo et al., 2016; Quadrato et al., 2017; Velasco et al., 2019). Our approach revealed major functional proteins expressed at one specific moment; yet, several transcription factors that are often found throughout neurodevelopment – and which are considered markers of regionalization and cell type specification – might not be detected using this total-cell, whole-cerebral organoid, due to their low-abundance and/or discovery limitations inherent to the method. Regardless, this provides a broader understanding of the signaling pathways that are present, consequently predicting phenotypical outcomes.

In accordance with early stages of development, following an orderly formation of neurons and layers, we observe proteins for a proliferative pool of progenitors, neuronal development and the presence of glutamatergic and dopaminergic neuronal subtypes. Those early events indicate functionality at this stage, with signaling processes that regulate migration of neuronal cells, involving changes in Ca^{2+} concentration. As shown here, several of the proteins found in cerebral organoids indicated migration. Others, such as calcium-binding protein calretinin, abundantly found in neurons of the retina and cortical interneurons, or the calcium-calmodulin family, suggest activation of migration, plasticity, and regulation of dendritic spines in cerebral organoids, via NMDA receptor Ca^{2+} influx signaling, when interacting with PSD-95/DLG4 (disk large homolog 4) (Wayman et al., 2008). Neuronal migration has been highlighted by other studies using organoids as a model for neurodevelopment (Quadrato et al., 2017; Renner et al., 2017).

Additionally, as presented here, whole-brain organoids have the potential for gliogenesis and oligodendrogenesis. On a lower level, proteins involved in the switch of producing neuronal cells to glial precursors are present, including GFAP, MBP, and PLP, despite the early stage in development. We have previously shown functional astrocytes derived from glial precursors of cerebral organoids (Dezonne et al., 2017). Here, we demonstrated that CNPase expressing OPCs could be derived from those organoids in culture, providing, at the least, a potential for testing OPC differentiation *in vitro*. In addition, further development of organoids using growth factor specific-stimulation could lead to more diverse subtypes of glial cells, including myelinating oligodendrocytes (Paşca et al., 2015; Bershteyn et al., 2017; Iefremova et al., 2017; Quadrato et al., 2017; Madhavan et al., 2018).

More recently, several groups aimed for more regionalized or cell-specific organoids to understand development and disease modeling. Comprised of particular morphogens and growth factors for patterning, organoids can achieve a more specific regionalization, such as midbrain-like (Jo et al., 2016), and hypothalamus organoids (Qian et al., 2016), fusion of cortical to medial ganglionic eminence organoids (Xiang et al., 2017), and cortico-thalamic fused organoids (Bagley et al., 2017). Several studies have pursued an enrichment of cell types, such as long-term cerebral organoid cultures, increasing astrocyte (Paşca et al., 2015; Sloan et al., 2017), oligodendrocyte (Marton et al., 2019), and microglial cell (Ormel et al., 2018) production within organoids, or achieving neuronal maturation able to achieve muscle contraction (Giandomenico et al., 2019). More homogeneous and reproducible spheroids have also been a modeling idea aiming on cell diversity for drug testing development (Pamies et al., 2017; Madhavan et al., 2018; Velasco et al., 2019). This ultimate opens new paths to better understand and model the human brain.

CONCLUSION

We provide a large-scale protein level evidence of neurodevelopmental processes and pathways occurring within the *in vitro* cerebral organoid model. Here, we have shown some of the main protein interactions related to neocortical development, including those related to proliferation and cell-fate specification, axonal guidance, synapse formation, and beginnings of myelin sheath formation. This provides evidence of the heterogeneity of this model and the robustness of a whole-organoid proteomics approach. We understand that our samples sizes are modest, and that future studies with higher throughput over an expanded time course would be valuable. However, global representation of protein families and networks in cerebral organoids are still scarce. Much of the knowledge presented here validates the organoid model beyond the transcriptional level, as adequate to investigate several brain networks. Proteome-wide information can be particularly important to study human brain development and how diseases might develop when pathways are disrupted. Currently, the challenges are toward developing differentiation strategies to yield disease-relevant organoids and producing selective subpopulations of glial and neuronal cell types in later stages of maturation to address more direct questions. Combining proteomics with recent advances in human PSC-derived organoids widens the possibilities to test different hypotheses, several of which have been generated exclusively from post-mortem brain studies. Specific pathways could also increase translational targets in a protein-driven approach for drug-development and human disease modeling.

DATA AVAILABILITY STATEMENT

The proteomics datasets generated for this study can be found in the PRIDE proteomics data repository (https://www.ebi.ac.uk/pride/archive/) with the accession number PXD011605.

AUTHOR CONTRIBUTIONS

JN, DM-D-S, and SR contributed to the conception and design of the study. JN, VS-C, RS, RMC, CS, HF, MM, and RMR performed the experiments, and collected, assembled, and analyzed the data. JN wrote the first draft of the manuscript. VS-C, RS, RMC, HF, and RMR contributed to the writing of the manuscript. JN, SR, and DM-D-S reviewed the final manuscript. All authors approved the final version of the manuscript.

FUNDING

JN, VS-C, and DM-D-S are supported by the São Paulo Research Foundation (FAPESP) grants 14/21035-0, 16/07332-7, 13/08711-3, and 14/10068-4. CS was recipient of a CAPES-FAPERJ Postdoc fellowship. Other funds are provided by the National Council for Scientific and Technological Development (CNPq), the Instituto Nacional de Ciência e Tecnologia de Neurociência Translacional (INCT-INNT), Foundation for Research Support in the State of Rio de Janeiro (FAPERJ), Coordination for

the Improvement of Higher Education Personnel (CAPES), Brazilian Funding Authority for Studies and Projects (FINEP), and Brazilian Development Bank (BNDES).

ACKNOWLEDGMENTS

We thank Ismael Gomes, Marcelo Costa, Ludmila S. S. Bastos, Paulo Baldasso, Guilherme Reis de Oliveira, and Gabriel Ferraz for their excellent technical support and Bradley Joseph Smith for English proofreading the manuscript. We also thank the support of the Centro Nacional de Biologia Estrutural e Bioimagem (CENABIO) for the use of their electron microscopy facility.

SUPPLEMENTARY MATERIAL

The Supplementary Material for this article can be found online at: https://www.frontiersin.org/articles/10.3389/fcell.2019.00303/full#supplementary-material

REFERENCES

Allen, N. J., and Eroglu, C. (2017). Cell biology of astrocyte-synapse interactions. *Neuron* 96, 697–708. doi: 10.1016/j.neuron.2017.09.056

Bagley, J. A., Reumann, D., Leitner, B., Lévi-Strauss, J., and Knoblich, J. A. (2017). Fused cerebral organoids model interactions between brain regions. *Nat. Methods* 14, 743–751. doi: 10.1038/nmeth.4304

Bershteyn, M., Nowakowski, T. J., Pollen, A. A., Di Lullo, E., Nene, A., Wynshaw-Boris, A., et al. (2017). Human iPSC-derived cerebral organoids model cellular features of lissencephaly and reveal prolonged mitosis of outer radial glia. *Cell Stem Cell* 20:435-449.e4. doi: 10.1016/j.stem.2016.12.007

Birey, F., Andersen, J., Makinson, C. D., Islam, S., Wei, W., Huber, N., et al. (2017). Assembly of functionally integrated human forebrain spheroids. *Nature* 545, 54–59. doi: 10.1038/nature22330

Borrell, V., and Götz, M. (2014). Role of radial glial cells in cerebral cortex folding. Curr Opin Neurobiol. 27, 39–46. doi: 10.1016/j.conb.2014.02.007

Brennand, K., Savas, J. N., Kim, Y., Tran, N., Simone, A., Hashimoto-Torii, K., et al. (2014). Phenotypic differences in hiPSC NPCs derived from patients with schizophrenia. *Mol. Psychiatry* 20, 361–368. doi: 10.1038/mp.2014.22

Bystron, I., Rakic, P., Molnár, Z., and Blakemore, C. (2006). The first neurons of the human cerebral cortex. *Nat. Neurosci.* 9, 880–886. doi: 10.1038/nn1726

Camp, J. G., Badsha, F., Florio, M., Kanton, S., Gerber, T., Wilsch-Bräuninger, M., et al. (2015). Human cerebral organoids recapitulate gene expression programs of fetal neocortex development. *Proc. Natl. Acad. Sci. U.S.A* 112, 15672–15677. doi: 10.1073/pnas.1520760112

Carlyle, B. C., Kitchen, R. R., Kanyo, J. E., Voss, E. Z., Pletikos, M., Sousa, A. M. M., et al. (2017). A multiregional proteomic survey of the postnatal human brain. *Nat. Neurosci.* 20, 1787–1795. doi: 10.1038/s41593-017-0011-2

Chambers, S. M., Fasano, C. A., Papapetrou, E. P., Tomishima, M., Sadelain, M., and Studer, L. (2009). Highly efficient neural conversion of human ES and iPS cells by dual inhibition of SMAD signaling. *Nat. Biotech.* 27, 275–280. doi: 10.1038/nbt.1529

Coles, C. H., Shen, Y., Tenney, A. P., Siebold, C., Sutton, G. C., Lu, W., et al. (2011). Proteoglycan-specific molecular switch for RPTPσ clustering and neuronal extension. *Science* 332, 484–488. doi: 10.1126/science.1200840

Cugola, F. R., Fernandes, I. R., Russo, F. B., Freitas, B. C., Dias, J. L. M., Guimarães, K. P., et al. (2016). The brazilian zika virus strain causes birth defects in experimental models. *Nature* 534, 267–271. doi: 10.1038/nature18296

Demyanenko, G. P., Tsai, A. Y., and Maness, P. F. (1999). Abnormalities in neuronal process extension, hippocampal development, and the ventricular system of L1 knockout mice. *J. Neurosci.* 19, 4907–4920. doi: 10.1523/JNEUROSCI.19-12-04907.1999

Dezonne, R. S., Sartore, R. C., Nascimento, J. M., Saia-Cereda, V. M., Romão, L. F., Alves-Leon, S. V., et al. (2017). Derivation of functional human astrocytes from cerebral organoids. *Sci. Rep.* 7:45091. doi: 10.1038/srep45091

Distler, U., Kuharev, J., Navarro, P., Levin, Y., Schild, H., and Tenzer, S. (2014). Drift time-specific collision energies enable deep-coverage data-independent acquisition proteomics. *Nat. Methods* 11, 167–170. doi: 10.1038/nmeth.2767

Djuric, U., Rodrigues, D. C., Batruch, I., Ellis, J., Shannon, P., and Diamandis, P. (2017). Spatiotemporal proteomic profiling of human cerebral development. *Mol. Cell Proteomics* 16, 1548–1539. doi: 10.1074/mcp.M116.066274

Eiraku, M., and Sasai, Y. (2012). Self-formation of layered neural structures in three-dimensional culture of ES cells. *Curr. Opin. Neurobiol.* 22, 768–777. doi: 10.1016/j.conb.2012.02.005

Fabregat, A., Jupe, S., Matthews, L., Sidiropoulos, K., Gillespie, M., Garapati, P., et al. (2017). The reactome pathway knowledgebase. *Nucleic Acids Res.* 46, D649–D655. doi: 10.1093/nar/gkx1132

Faria, R. X., Reis, R. A. M., Ferreira, L. G. B., Cezar-de-Mello, P. F. T., and Moraes, M. O. (2016). P2X7R large pore is partially blocked by pore forming proteins antagonists in astrocytes. *J. Bioenerg. Biomembr.* 48, 309–324. doi: 10.1016/j.brainres.2005.06.022

Fraga, A. M., Sukoyan, M., Rajan, P., Paes de Almeida Ferreira Braga, D., Iaconelli, A., Jr, Franco, J. G., et al. (2011). Establishment of a brazilian line of human embryonic stem cells in defined medium: implications for cell therapy in an ethnically diverse population. *Cell Trans.* 20, 431–440. doi: 10.3727/096368910X522261

Freitas, H. R., Ferraz, G., Ferreira, G. C., Ribeiro-Resende, V. T., Chiarini, L. B., do Nascimento, J. L. M., et al. (2016). Glutathione-induced calcium shifts in chick retinal glial cells. *PLoS One* 11:e0153677. doi: 10.1371/journal.pone.0153677

Freitas, H. R., Isaac, A. R., Silva, T. M., Diniz, G. O. F., Santos Dabdab dos, Y., Bockmann, E. C., et al. (2019). Cannabinoids induce cell death and promote P2X7 receptor signaling in retinal glial progenitors in culture. *Mol. Neurobiol.* 56, 6472–6486. doi: 10.1007/s12035-019-1537-y

Garcez, P. P., Loiola, E. C., Madeiro da Costa, R., Higa, L. M., Trindade, P., Delvecchio, R., et al. (2016). Zika virus impairs growth in human neurospheres and brain organoids. *Science* 352, 816–818. doi: 10.1126/science.aaf6116

Giandomenico, S. L., Mierau, S. B., Gibbons, G. M., Wenger, L. M. D., Masullo, L., Sit, T., et al. (2019). Cerebral organoids at the air–liquid interface generate diverse nerve tracts with functional output. *Nat. Neurosci.* 22, 669–679. doi: 10.1038/s41593-019-0350-2

Huang, D. W., Sherman, B. T., and Lempicki, R. A. (2009a). Bioinformatics enrichment tools: paths toward the comprehensive functional analysis of large gene lists. *Nucleic Acids Res.* 37, 1–13. doi: 10.1093/nar/gkn923

Huang, D. W., Sherman, B. T., and Lempicki, R. A. (2009b). Systematic and integrative analysis of large gene lists using DAVID bioinformatics resources. *Nat. Protoc.* 4, 44–57. doi: 10.1038/nprot.2008.211

Iefremova, V., Manikakis, G., Krefft, O., Jabali, A., Weynans, K., Wilkens, R., et al. (2017). An organoid-based model of cortical development identifies non-cell-autonomous defects in wnt signaling contributing to miller-dieker syndrome. *Cell Rep.* 19, 50–59. doi: 10.1016/j.celrep.2017.03.047

Jo, J., Xiao, Y., Sun, A. X., Cukuroglu, E., Tran, H. -D., Göke, J., et al. (2016). Midbrain-like organoids from human pluripotent stem cells contain functional dopaminergic and neuromelanin-producing neurons. *Cell Stem Cell* 19, 248–257. doi: 10.1016/j.stem.2016.07.005

Kanehisa, M., Furumichi, M., Tanabe, M., Sato, Y., and Morishima, K. (2016). KEGG: new perspectives on genomes, pathways, diseases and drugs. *Nucleic Acids Res.* 45, D353–D361. doi: 10.1016/j.febslet.2013.06.026

Lamprianou, S., Chatzopoulou, E., Thomas, J. -L., Bouyain, S., and Harroch, S. (2011). A complex between contactin-1 and the protein tyrosine phosphatase PTPRZ controls the development of oligodendrocyte precursor cells. *Proc. Natl. Acad. Sci. U.S.A.* 108, 17498–17503. doi: 10.1073/pnas.1108774108

Lancaster, M. A., and Knoblich, J. A. (2014). Organogenesis in a dish: modeling development and disease using organoid technologies. *Science* 345:1247125. doi: 10.1126/science.1247125

Lancaster, M. A., Corsini, N. S., Wolfinger, S., Gustafson, E. H., Phillips, A. W., Burkard, T. R., et al. (2017). Guided self-organization and cortical plate formation in human brain organoids. *Nat. Biotechnol.* 35, 659–666. doi: 10.1038/nbt.3906

Lancaster, M. A., Renner, M., Martin, C. -A., Wenzel, D., Bicknell, L. S., Hurles, M. E., et al. (2013). Cerebral organoids model human brain development and microcephaly. *Nature* 501, 373–379. doi: 10.1038/nature12517

Li, G. -Z., Vissers, J. P. C., Silva, J. C., Golick, D., Gorenstein, M. V., and Geromanos, S. J. (2009). Database searching and accounting of multiplexed precursor and product ion spectra from the data independent analysis of simple and complex peptide mixtures. *Proteomics* 9, 1696–1719. doi: 10.1002/pmic.200800564

Luo, C., Lancaster, M. A., Castanon, R., Nery, J. R., Knoblich, J. A., and Ecker, J. R. (2016). Cerebral organoids recapitulate epigenomic signatures of the human fetal brain. *Cell Rep.* 17, 3369–3384. doi: 10.1016/j.celrep.2016.break12.001

Madhavan, M., Nevin, Z. S., Shick, H. E., Garrison, E., Clarkson-Paredes, C., Karl, M., et al. (2018). Induction of myelinating oligodendrocytes in human cortical spheroids. *Nat. Methods* 15, 700–706. doi: 10.1038/s41592-018-0081-4

Mariani, J., Coppola, G., Zhang, P., Abyzov, A., Provini, L., Tomasini, L., et al. (2015). FOXG1-dependent dysregulation of GABA/glutamate neuron differentiation in autism spectrum disorders. *Cell* 162, 375–390. doi: 10.1016/j.cell.2015.06.034

Marton, R. M., Miura, Y., Sloan, S. A., Li, Q., Revah, O., Levy, R. J., et al. (2019). Differentiation and maturation of oligodendrocytes in human three-dimensional neural cultures. *Nat. Neurosci.* 22, 484–491. doi: 10.1038/s41593-018-0316-9

Merrill, R. A., Plum, L. A., Kaiser, M. E., and Clagett-Dame, M. (2002). A mammalian homolog of unc-53is regulated by all- transretinoic acid in neuroblastoma cells and embryos. *Proc. Natl. Acad. Sci. U.S.A.* 99, 3422–3427. doi: 10.1016/S0960-9822(02)00509-2

Mi, H., Poudel, S., Muruganujan, A., Casagrande, J. T., and Thomas, P. D. (2016). PANTHER version 10: expanded protein families and functions, and analysis tools. *Nucleic Acids Res.* 44, D336–D342. doi: 10.1038/srep02015

Muley, P. D., McNeill, E. M., Marzinke, M. A., Knobel, K. M., Barr, M. M., and Clagett-Dame, M. (2008). The atRA-responsive gene neuron navigator 2 functions in neurite outgrowth and axonal elongation. *Dev. Neurobio.* 68, 1441–1453. doi: 10.1002/dneu.20670

Ormel, P. R., Vieira de Sá, R., van Bodegraven, E. J., Karst, H., Harschnitz, O., Sneeboer, M. A. M., et al. (2018). Microglia innately develop within cerebral organoids. *Nat. Comms.* 9:4167. doi: 10.1038/s41467-018-06684-2

Pamies, D., Barreras, P., Block, K., Makri, G., Kumar, A., Wiersma, D., et al. (2017). A human brain microphysiological system derived from induced pluripotent stem cells to study neurological diseases and toxicity. *ALTEX* 34, 362–376. doi: 10.14573/altex.1609122

Paşca, A. M., Sloan, S. A., Clarke, L. E., Tian, Y., Makinson, C. D., Huber, N., et al. (2015). Functional cortical neurons and astrocytes from human pluripotent stem cells in 3D culture. *Nat. Meth.* 12, 671–678. doi: 10.1038/nmeth.3415

Paşca, S. P. (2018). The rise of three-dimensional human brain cultures. *Nature* 553, 437–445. doi: 10.1038/nature25032

Pollen, A. A., Nowakowski, T. J., Chen, J., Retallack, H., Sandoval-Espinosa, C., Nicholas, C. R., et al. (2015). Molecular identity of human outer radial glia during cortical development. *Cell* 163, 55–67. doi: 10.1016/j.cell.2015.09.004

Qian, X., Nguyen, H. N., Song, M. M., Hadiono, C., Ogden, S. C., Hammack, C., et al. (2016). Brain-region-specific organoids using mini-bioreactors for modeling ZIKV exposure. *Cell* 165, 1238–1254. doi: 10.1016/j.cell.2016.04.032

Quadrato, G., and Arlotta, P. (2017). Present and future of modeling human brain development in 3D organoids. *Curr. Opin. Cell Biol.* 49, 47–52. doi: 10.1016/j.ceb.2017.11.010

Quadrato, G., Nguyen, T., Macosko, E. Z., Sherwood, J. L., Yang, S. M., Berger, D. R., et al. (2017). Cell diversity and network dynamics in photosensitive human brain organoids. *Nature* 545, 48–53. doi:doi: 10.1038/nature22047

Raja, W. K., Mungenast, A. E., Lin, Y. -T., Ko, T., Abdurrob, F., Seo, J., et al. (2016). Self-organizing 3D human neural tissue derived from induced pluripotent stem cells recapitulate Alzheimer's disease phenotypes. *PLoS One* 11:e0161969. doi: 10.1371/journal.pone.0161969

Renner, M., Lancaster, M. A., Leitner, B., Choi, H., Ku, T., Peer, A., et al. (2017). Self-organized developmental patterning and differentiation in cerebral organoids. *EMBO J.* 36:e201694700. doi: 10.15252/embj.201694700

Sartore, R. C., Cardoso, S. C., Lages, Y. V. M., Paraguassu, J. M., Stelling, M. P., da Costa, R. F. M., et al. (2017). Trace elements during primordial plexiform network formation in human cerebral organoids. *PeerJ* 5:e2927. doi: 10.7287/peerj.preprints.2126v1

Sasai, Y. (2013). Next-generation regenerative medicine: organogenesis from stem cells in 3D culture. *Cell Stem Cell* 12, 520–530. doi: 10.1016/j.stem.2013.04.009

Sekine, K., Kawauchi, T., Kubo, K. -I., Honda, T., Herz, J., Hattori, M., et al. (2012). Reelin controls neuronal positioning by promoting cell-matrix adhesion via inside-out activation of integrin α5β1. *Neuron* 76, 353–369. doi: 10.1016/j.neuron.2012.07.020

Sloan, S. A., Darmanis, S., Huber, N., Khan, T. A., Birey, F., Caneda, C., et al. (2017). Human astrocyte maturation captured in 3D cerebral cortical spheroids derived from pluripotent stem cells. *Neuron* 95:779-790.e6. doi: 10.1016/j.neuron.2017.07.035

Szklarczyk, D., Gable, A. L., Lyon, D., Junge, A., Wyder, S., Huerta-Cepas, J., et al. (2018). STRING v11: protein–protein association networks with increased coverage, supporting functional discovery in genome-wide experimental datasets. *Nucleic Acids Res.* 47, D607–D613. doi: 10.1093/nar/gky1131

Takahashi, K., Tanabe, K., Ohnuki, M., Narita, M., Ichisaka, T., Tomoda, K., et al. (2007). Induction of pluripotent stem cells from adult human fibroblasts by defined factors. *Cell* 131, 861–872. doi: 10.1016/j.cell.2007.11.019

Thomson, J. A. (1998). Embryonic stem cell lines derived from human blastocysts. *Science* 282, 1145–1147. doi: 10.1126/science.282.5391.1145

Velasco, S., Kedaigle, A. J., Simmons, S. K., Nash, A., Rocha, M., Quadrato, G., et al. (2019). Individual brain organoids reproducibly form cell diversity of the human cerebral cortex. *Nature* 570, 523–527. doi: 10.1038/s41586-019-1289-x

Wayman, G. A., Lee, Y. -S., Tokumitsu, H., Silva, A., and Soderling, T. R. (2008). Calmodulin-kinases: modulators of neuronal development and plasticity. *Neuron* 59, 914–931. doi: 10.1016/j.neuron.2008.08.021

Xiang, Y., Tanaka, Y., Patterson, B., Kang, Y. -J., Govindaiah, G., Roselaar, N., et al. (2017). Fusion of regionally specified hPSC-derived organoids models human brain development and interneuron migration. *Cell Stem Cell* 21:383-398.e7. doi: 10.1016/j.stem.2017.07.007

Zhang, S.-C., Wernig, M., Duncan, I. D., Brüstle, O., and Thomson, J. A. (2001). In vitro differentiation of transplantable neural precursors from human embryonic stem cells. *Nat. Biotechnol.* 19, 1129–1133. doi: 10.1038/nbt1201-1129

Conflict of Interest: MM was employed by Waters Corporation.

The remaining authors declare that the research was conducted in the absence of any commercial or financial relationships that could be construed as a potential conflict of interest.

frontiers in Cell and Developmental Biology

OPINION
published: 18 February 2020
doi: 10.3389/fcell.2020.00084

Organoid Models of Human Endometrial Development and Disease

Youssef Hibaoui[1,2]* *and Anis Feki*[2]*

[1] Department of Genetic Medicine and Development, University of Geneva Medical School, Geneva, Switzerland, [2] Service de Gynécologie Obstétrique, HFR Fribourg - Hôpital Cantonal, Fribourg, Switzerland

Keywords: endometrial organoids, iPSCs, endometrial development, embryonic implantation disease modeling, infertility, pregnancy disorders, endometriosis, cancer

INTRODUCTION

The endometrium is a complex multicellular tissue lining the uterus that plays a crucial role in human reproduction. This multi-layered organ is composed of a functionalis layer, adjacent to the uterine lumen and a basalis layer, attached to the myometrium. These layers comprise several cell types including luminal and glandular epithelial cells, endometrial stromal cells, immune cells and vascular cells forming the spiral arterioles (Kobayashi and Behringer, 2003; Roy and Matzuk, 2011; Hart, 2016). This unique tissue undergoes remarkable dynamic remodeling orchestrated by menstrual repair, proliferation and differentiation processes, which are carefully controlled by female sex hormones during the menstrual cycle. The remodeling requires a delicate interplay of cellular and molecular events that enable the endometrium to be receptive for embryo implantation. During the proliferative (or follicular) phase, both the endometrial glands and stroma of the functionalis layer proliferate in response to rising estrogen levels coming from the ovarian follicular. Consequently, the thickness of the endometrium increases. Then, the functionalis layers maturate during the secretory (or luteal) phase with the concomitant presence of secretory and ciliated cells in response to progesterone. In the absence of conception, this tissue sheds before regenerating for a subsequent menstrual cycle (Kobayashi and Behringer, 2003; Roy and Matzuk, 2011). Defects in endometrium remodeling and function can lead to the development of various types of disorders that affect considerable numbers of women. These includes infertility, pregnancy disorders, endometriosis and endometrial cancers (Hart, 2016). For instance, endometriosis a condition in which endometrial tissues proliferate outside the uterus leading to pelvic pain, excessive bleeding and infertility affects between 10 and 15% of all women of reproductive age (Giudice and Kao, 2004; Vercellini et al., 2013). Endometrial cancer, the most common malignancy of the female genital tract, affects ∼3% of women, with the highest rates registered in North America and Europe (Lortet-Tieulent et al., 2017; Urick and Bell, 2019).

Even if progress has been made in the knowledge of the endometrium structure and function, little is known regarding the molecular and the cellular mechanisms involved in this dynamic remodeling in both physiological and pathological conditions. The main obstacle of such studies is the lack of accurate models. Many insights have been provided thanks to studies using mouse models. However, these models do not accurately recapitulate the specificities of human endometrial development and function. As a matter of fact, endometrium decidualization in mice and humans are quite different. Decidualization of the endometrium occurs in rodents exclusively when there is an incoming embryo or in response to mechanical injury, whereas in humans the endometrium undergoes decidualization in a cyclic manner, regardless of the presence of an embryo (Gellersen et al., 2007; Peterse et al., 2018). Therefore, findings obtained with these animals often cannot be directly translated to humans. Immortalized or carcinoma-derived cell lines, such

OPEN ACCESS

Edited by:
Eumorphia Remboutsika, National and Kapodistrian University of Athens, Greece

Reviewed by:
Gianpaolo Papaccio, Second University of Naples, Italy

***Correspondence:**
Youssef Hibaoui
youssef.hibaoui@unige.ch
Anis Feki
anis.feki@h-fr.ch

Specialty section:
This article was submitted to Stem Cell Research, a section of the journal Frontiers in Cell and Developmental Biology

Received: *28 November 2019*
Accepted: *29 January 2020*
Published: *18 February 2020*

Citation:
Hibaoui Y and Feki A (2020) Organoid Models of Human Endometrial Development and Disease. Front. Cell Dev. Biol. 8:84. doi: 10.3389/fcell.2020.00084

as Ishikawa cells (derived from epithelial endometrial cells) or St-T1b cell (derived from stromal endometrial cells) are also available for *in vitro* investigations. While these cells are easily cultured for long periods (**Table 1**), there are general limitations of using such cell lines including their genetic background, the potential changes acquired following transformation and during their establishment in culture (Mannelli et al., 2015). Alternatively, primary endometrial cells can be isolated, but these are difficult to maintain and expand in long term culture. Most of these cells lose their phenotype and hormone responsiveness in culture (Mannelli et al., 2015). Moreover, two dimensional (2D) cell cultures do not faithfully mimic *in vivo* three dimensional (3D) structure and function. These limitations prompted researchers to find novel strategies to model human endometrium. To that end, 3D-culture methods, namely organoids hold promise as models to better mimic *in vivo* human endometrium.

ORGANOIDS DERIVED FROM HUMAN PRIMARY ENDOMETRIUM

Organoids can be defined as 3D *in vitro* tissue models that recapitulate many of the physiologically relevant properties and features of the *in vivo* tissue. Numerous studies have succeeded to derive organoids from various primary tissues such as intestine, liver, pancreas (reviewed in Clevers, 2016). The recent discovery that human endometrial organoids can be generated from primary endometrial cells has opened up new possibilities to investigate biological processes involved in human pregnancy, disease modeling and testing therapeutic compounds for clinical applications (Boretto et al., 2017; Turco et al., 2017). To generate human endometrial organoids, primary endometrial tissue samples are dissociated with enzymatic procedures (collagenase and/or dispase) and resuspended into Matrigel droplets in a defined medium that was shown to promote organoid formation and maintenance from primary tissue or iPSC-derived cells (**Figure 1**). The define medium includes activators of WNT signaling (WNT ligands and R-respondin-1), growth factors (EFG, FGF10), TGFβ inhibitors (A83-01), BMP inhibitor (Noggin) and nicotinamide. Importantly, these organoids can be generated from endometrium biopsies obtained throughout the menstrual cycle phases, as well as from endometrium from pregnant and post-menopausal women. Moreover, these organoids can be extensively passaged (every 7–10 days for more than 6 months in culture) while maintaining genetic and phenotypic stability (Turco et al., 2017). This provides opportunity for cryopreserved bio–banking of these endometrial organoids and easily accessible resource for future investigations.

Endometrial organoids have been shown to recapitulate many features of human endometrium. First, genomic analysis through RNA sequencing reveals that these endometrial organoids cluster more closely to glands than to stroma, which recapitulates the molecular signature of the endometrial glands *in vivo*. Second, these organoids respond to sex hormones in a similar manner to that expected *in vivo*. Organoids treated with progesterone exhibited characteristics of the endometrium in its secretory phase, with an increased folding of the glands with the presence of subnuclear vacuolation in the columnar cells. In line with this, endometrial organoids have the ability to generate the two main endometrial cell types: (i) the secretory cells (progestogen-associated endometrial protein (PAEP) positive) that are present in the *in vivo* secretory endometrium, and (ii) and ciliated cells (acetylated-α-tubulin positive) that are present *in vivo* in the uterine luminal epithelium and in superficial glands (Boretto et al., 2017; Turco et al., 2017). By contrast, organoids treated with estrogen displayed morphologic characteristics of the endometrium during the proliferative phase, as revealed by the presence of pseudostratified glandular epithelium. Cells positive for the TRH (Thyrotropin-releasing hormone) marker were also found in organoids treated with estrogen (Boretto et al., 2017; Turco et al., 2017).

ENDOMETRIUM 3D CULTURE DERIVED FROM HUMAN INDUCED PLURIPOTENT STEM CELLS

Soon after the generation of organoids from human primary endometrium, a method for culturing human endometrial stromal fibroblasts (EMSFs) from induced pluripotent stem cells (iPSCs) was published by Miyazaki et al. (2018) (**Figure 1**). Using embryoid body culture conditions, iPSCs were successively directed into intermediate mesoderm (IM, after 4 days of differentiation) and the Müllerian duct (MD, after 8 days of differentiation), a tissue that gives rise to the female reproductive tract including the uterus, the oviduct and the upper vaginal canal. Thereafter, MD cells were further differentiated into endometrial stromal fibroblasts (EMSFs) using 5′-aza-2′-deoxycytidine (5aza2), CHIR99021, 17β-estradiol (E2), FGF9, and PDGF-BB for another 6 days. As expected for EMSFs, these cells expressed the critical endometrial markers including HOXA10, HOXA11, and PGF genes/proteins (Miyazaki et al., 2018). Interestingly, iPSC-derived EMSFs undergo decidualization in response to an 8 days-treatment with a hormonal-based cocktail containing E2, progestin and 8-bromoadenosine 3′,5′-cyclic adenosine monophosphate (cAMP), recapitulating hormone responsiveness of the endometrial stroma. Markers for decidualization such as *FOXO1*, *HAND2*, *IGFBP1,* and *PRL* were all found to be up-regulated using this approach. Moreover, RNA sequencing analysis of these iPSC-derived EMSFs confirmed a transcriptional signature which recapitulated endometrial stroma (Miyazaki et al., 2018).

ADVANTAGES AND APPLICATIONS OF ENDOMETRIAL ORGANOIDS

It is now widely accepted that 3D organoids more accurately mimic the structural and the functional properties of the *in vivo* tissue compared with its 2D cell culture counterparts. One reason for this is the ability of organoids to recapitulate the physiological, biomechanical, and biochemical microenvironments of the *in vivo* tissue, which is simply not possible in the case of 2D cell culture growing in a homogeneous monolayer. As

TABLE 1 | Comparative advantages and drawbacks of the current *in vitro* endometrial models.

	Immortalized human endometrial cell lines	Organoid culture of human endometrium	Endometrial cells derived from human iPSCs
Rate of initial establishment	Moderate	Moderate	Moderate
Derivation time	2–4 months	∼1 month	2–4 months (including differentiation)
Maintenance in culture	Easy	Not easy	Not easy
Required expertise	Low	High	High
Expansion	Very high	High (but limited)	Very high
Cost	Low	High	High
Endometrial development and disease modeling	No	Yes	Yes
Genetic manipulation	High	High	High
Possibility to generate isogenic controls	Yes	Yes	Yes
Microenvironment of the *in vivo* tissue	No	Yes	Possible using co-culture

such, organoids allow cell-cell interactions and cell-extracellular (ECM) matrix interactions in all the three dimensions, interactions which are very limited, if not impossible, in 2D cell culture (**Table 1**).

A key advantage of endometrial organoid model is the ability to genetically modify the cells, which represents a significant benefit compared with the time and the energy required to create for instance a knock-out mouse model (**Table 1**). These organoids can be manipulated genetically through various means, including both viral (e.g., lentiviral and adeno-associated viral vectors) and non-viral (e.g., electroporation) approaches, lending itself favorably to gene editing and transposon-based gene modification strategies. In this regards, CRISPR/Cas9, the most attractive gene editing technique, has enabled researchers to efficiently manipulate genomic sequences in organoids derived from primary tissue or from iPSCs, repairing for instance putative genetic mutations in patient-derived iPSCs or by introducing genetic mutations in healthy wild type cells (Matano et al., 2015).

Perhaps the most obvious application of endometrial organoids is as an *in vitro* model system for researchers studying endometrial development. As these cultures can incorporate most of the cell types present in the *in vivo* tissue and recapitulate many of the structural and functional properties of the *in vivo* tissue, endometrial organoids constitute a valuable tool for the investigation of the changes and events that occur during the menstrual cycle and during early pregnancy following the establishment of the placenta. Until now, it was not possible to adequately capture these events in a woman. Moreover, endometrial organoids may be an alternative to the existing models used for the investigation of embryo-endometrium interactions (reviewed in Weimar et al., 2013). It allows to study of the initial stages of human embryo implantation *in vitro* and should provide a better understanding of the mechanisms underlying human embryo-endometrium cross-talk. Such studies are a prerequisite for the improvement of assisted reproduction outcomes and for the prevention of early pregnancy loss.

In the last decade, organoid culture has been widely used to model human disease *in vitro* (the so-called "disease in a dish"). Recent progress in generating endometrial organoids from either primary biopsy or iPSCs hold great promise to model endometrial disorders such as infertility, pregnancy disorders, endometrial cancers, endometriosis, Asherman syndrome, and possibly others (**Figure 1**). In this respect, Turco and colleagues have succeeded to derive organoids from endometrial cancer from post-menopausal women (Turco et al., 2017). These organoids phenocopied the morphology of the primary tumor from which it was derived (FIGO grade I endometrioid carcinoma with predominant gland growth, nuclear pleomorphism, and disorganized epithelium with irregular basement membrane), supporting the idea that this model recapitulates the histological organization and phenotype of the endometrial carcinoma. Also, this model allows the comparison of the endometrial carcinoma tissue with the normal adjacent endometrium providing an isogenic control tissue, without the biological "noise" that could result from the variability of an individual's genetic background (Turco et al., 2017). More recently, Boretto et al. derived organoids from patients with low- to high grade endometrial cancers. Interestingly, these organoids capture accurately cancer subtypes, recapitulate disease phenotype and display patient-specific drug responses (Boretto et al., 2019). Patient-derived endometrial organoids can also be exploited for modeling endometriosis, a disease that affects between 10 and 15% of all women of reproductive age and 70% of women with chronic pelvic pain (Giudice and Kao, 2004; Vercellini et al., 2013). When one considers that there is no curative solution for endometriosis (Fadhlaoui et al., 2014), it is hoped that endometrial organoids may help to accelerate the development of novel therapeutics in this area of research.

As alluded to above, a promising avenue for use of endometrial organoids in translational research is the possibility to identify novel therapeutic targets and at the same time, to perform screens of molecules for endometrial diseases (**Figure 1**). Endometrial organoids derived from primary biopsies or from iPSCs can provide a more relevant model for high throughput drug screening than immortalized or carcinoma-derived cell lines. Also, patient-derived endometrial organoids offer a powerful model for predicting efficacy and safety at preclinical stages.

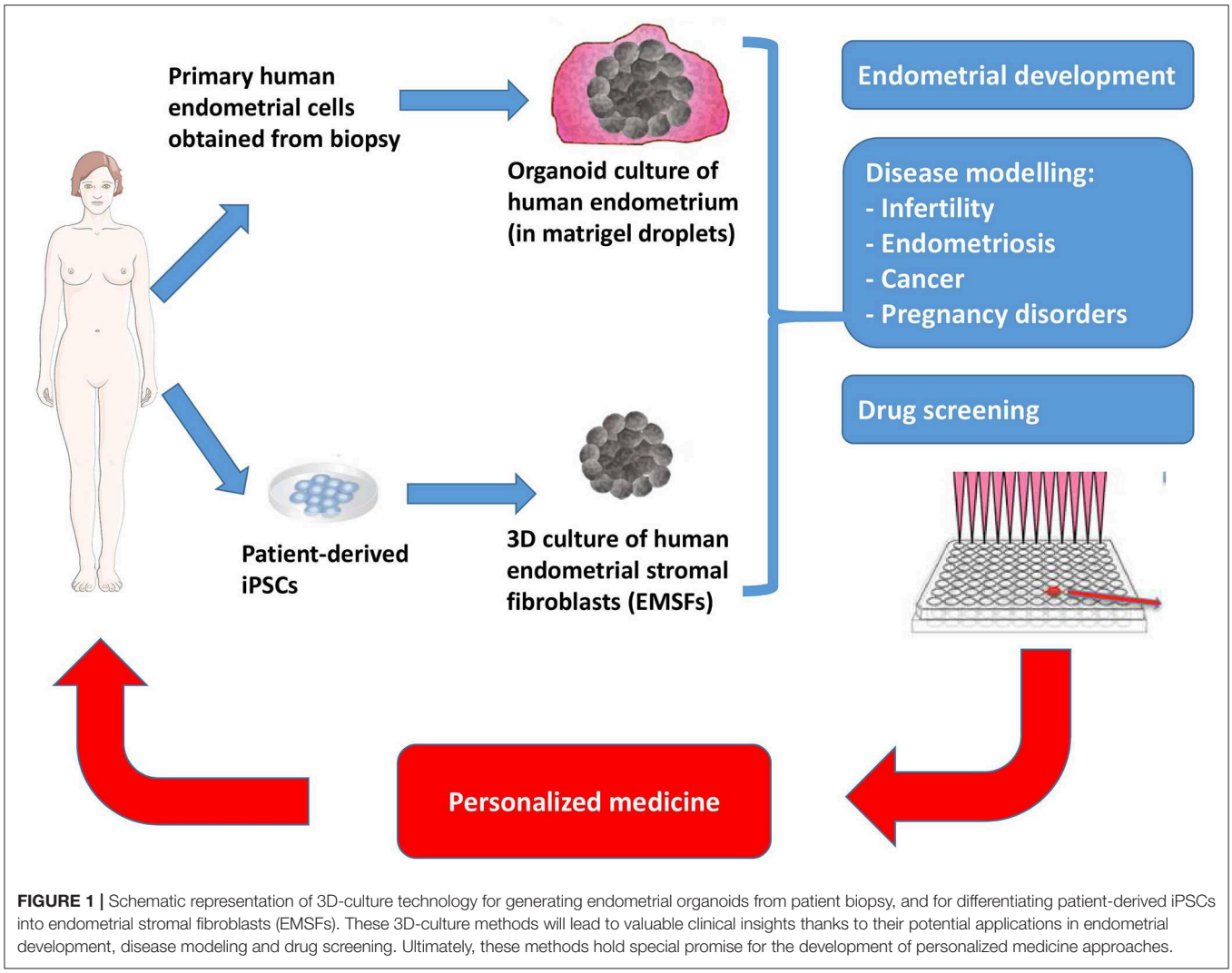

FIGURE 1 | Schematic representation of 3D-culture technology for generating endometrial organoids from patient biopsy, and for differentiating patient-derived iPSCs into endometrial stromal fibroblasts (EMSFs). These 3D-culture methods will lead to valuable clinical insights thanks to their potential applications in endometrial development, disease modeling and drug screening. Ultimately, these methods hold special promise for the development of personalized medicine approaches.

In fact, toxicology testing is one of the most attractive uses of diseased endometrial organoids, given that it is possible to generate healthy controls (matched isogenic and non-isogenic), as well as cells and tissues that are involved in drug metabolism including cholangiocytes, liver or intestine, from patient-derived iPSCs (Takebe et al., 2013; Watson et al., 2014; Sampaziotis et al., 2015). Such a model will undoubtedly improve our understanding of the genetic basis and the molecular mechanisms that govern the side effects of drugs currently used for endometrial diseases.

HURDLES AND CHALLENGES OF ENDOMETRIAL ORGANOIDS

The fact that endometrial organoids recapitulate the temporal progression of endometrial development presents both an advantage and disadvantage. While it offers an unprecedented opportunity for researchers to probe the different stages of human endometrial development, such organoids take a long time to proliferate and mature in culture, elevating cell culture costs and potentially compromising reproducibility (**Table 1**). The latter hurdle arises mainly from the self-organization property of organoids (more particularly for organoids derived from iPSCs). Therefore, researchers should carefully control the proliferation and maturation process of endometrial organoids, while also being critical in discriminating true phenotypes from observations of sporadic events in a dish. Poor control of this process will lead to an inherent variability between organoid samples, making it very difficult to quantitatively assess experiments in an unbiased manner. In order to understand the molecular and cellular mechanisms underlying endometrial development in physiological and pathological conditions, it is essential that every endometrial organoid display near-identical phenotypic characteristics in terms of size, shape, cellular composition, and architecture and similar functional properties.

Because of their 3D nature, the size of all organoids is limited by oxygen and nutrient supply. Viable parts of the organoids are restricted by the physical area over which oxygen and nutrients can diffuse from the surrounding media. Therefore, researchers

should be aware of necrosis in the interior of organoids. Such a hurdle can be overcome introducing vascularization to the organoids. Thus, extensive effort will likely focus on the development of biomaterials and microfluidic systems that can be used to engineer a vascularized network to supply the organoid interior with sufficient oxygen and nutrients (Brassard and Lutolf, 2019).

While the endometrial organoid model is still in its infancy, a long term goal of this technology will be to apply it for cell replacement in regenerative medicine. However, significant improvements regarding the safety will be required in order to derive clinical grade iPSCs. An important concern would be selection of the optimal method for reprograming patient cells into iPSCs, as retroviral- or lentiviral-based methods can cause insertional inactivation of tumor suppressor genes, insertional activation of oncogenes and variability in the differentiation potential of these cells (for review see (Hibaoui and Feki, 2012, 2015). Among the integration-free methods of reprograming, episomal plasmids and Sendai viral vectors appear to be methods of choice for deriving clinical grade iPSCs.

CONCLUDING REMARKS

Endometrial organoids, whether derived from primary human biopsy or from patient-derived iPSCs provide unprecedented opportunity to study the human endometrium. The possibility to derive endometrial and trophoblast organoids from primary biopsies (Boretto et al., 2017; Turco et al., 2017, 2018) together with the capacity to differentiate endometrial cells and trophoblast cells from iPSCs (Hibaoui and Feki, 2013; Horii et al., 2016; Miyazaki et al., 2018) offer new area of investigations. Such organoids can be exploited for disease modeling, drug screening, testing and benchmarking for novel therapeutics, as well as the potential evaluation of personalized therapeutic medicine approaches (**Figure 1**). Finally, considering the progression at which the biopsy-derived and iPSC-derived organoid field has advanced in the past 5 years (Nature Methods, 2018), there is a good reason for optimism that endometrial organoids will enhance our understanding of the molecular and cellular mechanisms involved in endometrial development and disease.

AUTHOR CONTRIBUTIONS

YH and AF conceived, designed, and wrote the manuscript.

ACKNOWLEDGMENTS

The authors would like to especially thank Dr. Marco Alessandrini, Dr. Mauricio Olguin Albuerne, and Dr. Audrey Roussel-Gervais for useful comments and proofreading.

REFERENCES

Boretto, M., Cox, B., Noben, M., Hendriks, N., Fassbender, A., Roose, H., et al. (2017). Development of organoids from mouse and human endometrium showing endometrial epithelium physiology and long-term expandability. *Development* 144, 1775–1786. doi: 10.1242/dev.148478

Boretto, M., Maenhoudt, N., Luo, X., Hennes, A., Boeckx, B., Bui, B., et al. (2019). Patient-derived organoids from endometrial disease capture clinical heterogeneity and are amenable to drug screening. *Nat. Cell Biol.* 21, 1041–1051. doi: 10.1038/s41556-019-0360-z

Brassard, J. A., and Lutolf, M. P. (2019). Engineering stem cell self-organization to build better organoids. *Cell Stem Cell* 24, 860–876. doi: 10.1016/j.stem.2019.05.005

Clevers, H. (2016). Modeling development and disease with organoids. *Cell* 165, 1586–1597. doi: 10.1016/j.cell.2016.05.082

Fadhlaoui, A., Bouquet De La Jolinière, J., and Feki, A. (2014). Endometriosis and infertility: how and when to treat? *Front. Surg.* 1:24. doi: 10.3389/fsurg.2014.00024

Gellersen, B., Brosens, I. A., and Brosens, J. J. (2007). Decidualization of the human endometrium: mechanisms, functions, and clinical perspectives. *Semin. Reprod. Med.* 25, 445–453. doi: 10.1055/s-2007-991042

Giudice, L. C., and Kao, L. C. (2004). Endometriosis. *Lancet* 364, 1789–1799. doi: 10.1016/S0140-6736(04)17403-5

Hart, R. J. (2016). Physiological aspects of female fertility: role of the environment, modern lifestyle, and genetics. *Physiol. Rev.* 96, 873–909. doi: 10.1152/physrev.00023.2015

Hibaoui, Y., and Feki, A. (2012). Human pluripotent stem cells: applications and challenges in neurological diseases. *Front. Physiol.* 3:267. doi: 10.3389/fphys.2012.00267

Hibaoui, Y., and Feki, A. (2013). Human pluripotent stem cells as alternative models to study trophoblast development. *Front. Physiol.* 4:374. doi: 10.3389/fphys.2013.00374

Hibaoui, Y., and Feki, A. (2015). Concise review: methods and cell types used to generate down syndrome induced pluripotent stem cells. *J. Clin. Med.* 4, 696–714. doi: 10.3390/jcm4040696

Horii, M., Li, Y., Wakeland, A. K., Pizzo, D. P., Nelson, K. K., Sabatini, K., et al. (2016). Human pluripotent stem cells as a model of trophoblast differentiation in both normal development and disease. *Proc. Natl. Acad. Sci. U.S.A.* 113, E3882–E3891. doi: 10.1073/pnas.1604747113

Kobayashi, A., and Behringer, R. R. (2003). Developmental genetics of the female reproductive tract in mammals. *Nat. Rev. Gene.* 4, 969–980. doi: 10.1038/nrg1225

Lortet-Tieulent, J., Ferlay, J., Bray, F., and Jemal, A. (2017). International patterns and trends in endometrial cancer incidence, 1978–2013. *J. Natl. Cancer Inst.* 110, 354–361. doi: 10.1093/jnci/djx214

Mannelli, C., Ietta, F., Avanzati, A. M., Skarzynski, D., and Paulesu, L. (2015). Biological tools to study the effects of environmental contaminants at the feto–maternal interface. *Dose-Response* 13:1559325815611902. doi: 10.1177/1559325815611902

Matano, M., Date, S., Shimokawa, M., Takano, A., Fujii, M., Ohta, Y., et al. (2015). Modeling colorectal cancer using CRISPR-Cas9–mediated engineering of human intestinal organoids. *Nat. Med.* 21, 256–262. doi: 10.1038/nm.3802

Miyazaki, K., Dyson, M. T., Coon, V. J. S., Furukawa, Y., Yilmaz, B. D., Maruyama, T., et al. (2018). Generation of progesterone-responsive endometrial stromal fibroblasts from human induced pluripotent stem cells: role of the WNT/CTNNB1 pathway. *Stem Cell Rep.* 11, 1136–1155. doi: 10.1016/j.stemcr.2018.10.002

Nature Methods (2018). Method of the Year 2017: organoids. *Nat Methods* 15:1. doi: 10.1038/nmeth.4575

Peterse, D., Clercq, K. D., Goossens, C., Binda, M. M., Dorien, F. O., Saunders, P., et al. (2018). Optimization of endometrial decidualization in the menstruating mouse model for preclinical endometriosis research. *Reprod. Sci.* 25, 1577–1588. doi: 10.1177/1933719118756744

Roy, A., and Matzuk, M. M. (2011). Reproductive tract function and dysfunction in women. *Nat. Rev. Endocrinol.* 7, 517–525. doi: 10.1038/nrendo.2011.79

Sampaziotis, F., Cardoso De Brito, M., Madrigal, P., Bertero, A., Saeb-Parsy, K., Soares, F., et al. (2015). Cholangiocytes derived from human induced pluripotent stem cells for disease modeling and drug validation. *Nat. Biotechnol.* 33, 845–852. doi: 10.1038/nbt.3275

Takebe, T., Sekine, K., Enomura, M., Koike, H., Kimura, M., Ogaeri, T., et al. (2013). Vascularized and functional human liver from an iPSC-derived organ bud transplant. *Nature* 499, 481–484. doi: 10.1038/nature12271

Turco, M. Y., Gardner, L., Hughes, J., Cindrova-Davies, T., Gomez, M. J., Farrell, L., et al. (2017). Long-term, hormone-responsive organoid cultures of human endometrium in a chemically defined medium. *Nat. Cell Biol.* 19:568. doi: 10.1038/ncb3516

Turco, M. Y., Gardner, L., Kay, R. G., Hamilton, R. S., Prater, M., Hollinshead, M. S., et al. (2018). Trophoblast organoids as a model for maternal–fetal interactions during human placentation. *Nature* 564, 263–267. doi: 10.1038/s41586-018-0753-3

Urick, M. E., and Bell, D. W. (2019). Clinical actionability of molecular targets in endometrial cancer. *Nat. Rev. Cancer* 19, 510–521. doi: 10.1038/s41568-019-0177-x

Vercellini, P., Viganò, P., Somigliana, E., and Fedele, L. (2013). Endometriosis: pathogenesis and treatment. *Nat. Rev. Endocrinol.* 10:261. doi: 10.1038/nrendo.2013.255

Watson, C. L., Mahe, M. M., Múnera, J., Howell, J. C., Sundaram, N., Poling, H. M., et al. (2014). An *in vivo* model of human small intestine using pluripotent stem cells. *Nat. Med.* 20, 1310–1314. doi: 10.1038/nm.3737

Weimar, C. H. E., Post Uiterweer, E. D., Teklenburg, G., Heijnen, C. J., and Macklon, N. S. (2013). *In-vitro* model systems for the study of human embryo–endometrium interactions. *Reprod. Biomed. Online* 27, 461–476. doi: 10.1016/j.rbmo.2013.08.002

Conflict of Interest: The authors declare that the research was conducted in the absence of any commercial or financial relationships that could be construed as a potential conflict of interest.

frontiers in Cell and Developmental Biology

REVIEW
published: 24 March 2020
doi: 10.3389/fcell.2020.00183

Cellular and Molecular Mechanisms of Kidney Development: From the Embryo to the Kidney Organoid

Niloofar Khoshdel Rad[1,2], Nasser Aghdami[3] and Reza Moghadasali[1]†*

[1] Department of Stem Cells and Developmental Biology, Cell Science Research Center, Royan Institute for Stem Cell Biology and Technology, ACECR, Tehran, Iran, [2] Department of Developmental Biology, University of Science and Culture, Tehran, Iran, [3] Department of Regenerative Medicine, Cell Science Research Center, Royan Institute for Stem Cell Biology and Technology, ACECR, Tehran, Iran

OPEN ACCESS

Edited by:
Thimios Mitsiadis, University of Zurich, Switzerland

Reviewed by:
Gianandrea Pasquinelli, University of Bologna, Italy
Ryuji Morizane, Brigham and Women's Hospital, Harvard Medical School, United States

***Correspondence:**
Reza Moghadasali
rezamoghadasali@royaninstitute.org; rezamoghadasali@yahoo.com

†ORCID:
Reza Moghadasali
orcid.org/0000-0001-6933-6344

Specialty section:
This article was submitted to Stem Cell Research, a section of the journal Frontiers in Cell and Developmental Biology

Received: *14 January 2020*
Accepted: *04 March 2020*
Published: *24 March 2020*

Citation:
Khoshdel Rad N, Aghdami N and Moghadasali R (2020) Cellular and Molecular Mechanisms of Kidney Development: From the Embryo to the Kidney Organoid. Front. Cell Dev. Biol. 8:183. doi: 10.3389/fcell.2020.00183

Development of the metanephric kidney is strongly dependent on complex signaling pathways and cell–cell communication between at least four major progenitor cell populations (ureteric bud, nephron, stromal, and endothelial progenitors) in the nephrogenic zone. In recent years, the improvement of human-PSC-derived kidney organoids has opened new avenues of research on kidney development, physiology, and diseases. Moreover, the kidney organoids provide a three-dimensional (3D) *in vitro* model for the study of cell-cell and cell-matrix interactions in the developing kidney. *In vitro* re-creation of a higher-order and vascularized kidney with all of its complexity is a challenging issue; however, some progress has been made in the past decade. This review focuses on major signaling pathways and transcription factors that have been identified which coordinate cell fate determination required for kidney development. We discuss how an extensive knowledge of these complex biological mechanisms translated into the dish, thus allowed the establishment of 3D human-PSC-derived kidney organoids.

Keywords: differentiation, kidney development, organoid, renal progenitors, signaling pathways

Abbreviations: 3D, three-dimensional; AIM, anterior intermediate mesoderm; AP1, activator protein 1; BMP, bone morphogenetic protein; CITED1, Cbp/p300-interacting transactivator 1; CM, cap mesenchyme; DKK1, Dickkopf-1; ECM, extracellular matrix; Ecm1, extracellular matrix 1; EC, endothelial cells; EMX, empty spiracles homolog; EPC, endothelial progenitor cells; ERK, extracellular signal-regulated kinase; Eya1, eyes absent 1; FGF, fibroblast growth factor; FOXD1, forkhead/winged helix transcription factor; FSS, fluid shear stress; GATA, *trans*-acting T-cell-specific transcription factor; Gas1, growth arrest-specific 1; GDNF, glial cell-derived neurotrophic factor; GFRα1, glial cell line derived neurotrophic factor family receptor α1; Hox, homeobox; hPSCs, human pluripotent stem cells; IM, intermediate mesoderm; Kdr/VEGFR2/Flk1, kinase insert domain protein receptor; LHX1, LIM-class homeodomain 1; LTL, lotus tetragonolobus lectin; MCAM, melanoma cell adhesion molecule (CD146); MET, mesenchymal-epithelial-transition; MM, metanephric mesenchyme; MSCs, mesenchymal stem cells; NPCs, nephron progenitor cells; Odd1 or Osr1, odd skipped related 1; PAX, paired box protein; PBX1, Pre-B-cell leukemia transcription factor 1; PDGFRβ, Platelet-derived growth factor receptor beta; PECAM-1/CD31, Platelet/endothelial cell adhesion molecule-1; PIM, posterior intermediate mesoderm; PI3K, Phosphoinositide 3-kinase; PTA, pre-tubular aggregate; RA, retinoic acid; RAR, retinoic acid receptor; RBP-J, recombination signal binding protein for immunoglobulin kappa J region; RV, renal vesicle; SALL1, spalt like transcription factor 1; SCF, stem cell factor; SFRP, secreted frizzled-related proteins; SIX2, sine oculis-related homeobox 2; TGFβ, transforming growth factor beta; UB, ureteric bud; UBPCs, ureteric bud progenitor cells; VEGF, vascular endothelial growth factor; VEGFR, vascular endothelial growth factor receptor; WT1, Wilm's tumor; WNT, wingless-type mouse mammary tumor virus integration site.

INTRODUCTION

The mammalian kidney is one of the most complex organs in the body. The kidney is the major homeostatic organ necessary for pH and electrolyte regulation, and maintenance of overall fluid balance. In addition to these excretory functions, the kidney produces several hormones and humoral factors such as renin, erythropoietin, calcitriol (1,25-dihydroxycholecalciferol) and prostaglandins (Santoro et al., 2015). Kidney function depends on nephrons, the structural and filtration unit of the kidney, that are composed of more than 20 different specialized cells (Al-Awqati and Oliver, 2002). In the human kidney, nephrons are generated only during nephrogenesis and *de novo* nephron formation continues until 36 weeks of gestation (Romagnani et al., 2013; Ahmadi et al., 2019a). *In vitro* re-creation of these complex structural units of the kidney is a challenging issue; however, there has been some success in the past decade. A defined culture system drives the differentiation of human pluripotent stem cells (hPSCs) into kidney organoids by recapitulating the developmental processes. Generation of human PSCs-derived kidney organoids depends on cell–cell communication between multiple distinct progenitor populations that lie adjacent to each other (Morizane et al., 2015; Garreta et al., 2019; Homan et al., 2019). This review focuses on major signaling pathways and transcription factors that coordinate cell fate determination of renal progenitor cells. We intend to discuss the ways in which cell communications between nephron progenitor cells (NPCs), ureteric bud progenitor cells (UBPCs), endothelial and stromal cells during organogenesis lead to a fully patterned and vascularized kidney tissue, and how a deep knowledge of these biological mechanisms translated into the dish, thus allowed the establishment of PSCs-derived kidney organoids.

SPATIAL ORGANIZATION AND EARLY PATTERNING OF THE KIDNEY-FORMING MESODERM

During organogenesis, the intermediate mesoderm (IM) gives rise to three types of excretory organs: pronephros, mesonephros, and metanephros. The metanephric kidney remains for the period after birth and forms the definitive mature organ. Metanephros differentiates as the result of interaction between the metanephric mesenchyme (MM), which is derived from the most posterior intermediate mesoderm (PIM), and the ureteric bud (UB) lineage that includes the collecting system that is derived from a more anterior IM (Taguchi et al., 2014; Takasato and Little, 2015). PIM have a multi-potent precursor population that give rise to nephron segments and interstitial stromal cells. The signals that specify the early kidney field along the body axes have received more attention. Several transcriptional regulators such as homeobox (Hox) paralogs, LIM1 (LIM-class homeodomain1), odd skipped related 1 (OSR1), PAX2/8 (Paired box protein 2/8), and eyes absent 1 (EYA1) have been shown to play major roles in early patterning and specification of the developing kidney (**Figure 1**) (Bouchard et al., 2002). These events lead to the formation of multiple distinct renal progenitor populations within the nephrogenic niche.

The Homeobox (*Hox*) Genes

The *Hox* genes have an important role in anterior-posterior patterning of the body. From these, 28 of the 39 *Hox* genes are expressed in the developing kidney (Patterson and Potter, 2004). Given that the Hox proteins have intrinsically weak DNA-binding affinity, their interaction with cofactors is critical for target selectivity (Gong et al., 2007). Thus, interaction of *Hox* genes with regulatory partners such as Pax2, Eya1, and SMADs [*Caenorhabditis elegans* SMA ("small" worm phenotype) and *Drosophila* MAD ("Mothers Against Decapentaplegic")] is necessary for kidney mesoderm specification (Gong et al., 2007; Preger-Ben Noon et al., 2009). *Hoxb4* plays key roles in the establishment of the kidney morphogenetic field anterior border (Preger-Ben Noon et al., 2009) and nephric duct specification (Attia et al., 2012). Retinoic acid (RA) signaling in the anterior IM stimulate the expression of *Hoxb4*. *Hoxb4* confers competence on IM cells to respond to inductive signals from neighboring tissues. Cooperation of Hoxb4 with SMADs induces expressions of Lim1 and Pax2 in IM cells (Preger-Ben Noon et al., 2009). Another *Hox* gene, *HoxB7,* is expressed from the early stages in the nephric duct to terminal differentiation of UB derivatives, including the ureter, pelvis, calyces, and collecting ducts (Argao et al., 1995; Srinivas et al., 1999). However, the direct downstream targets of Hoxb7 in these cells is unknown. Hoxa11 and Hoxd11 expressions are restricted to the PIM, which develops into MM. Hoxd11 is expressed in both cap mesenchyme (CM) and cortical stroma (Mugford et al., 2008a), and activates several metanephric specific markers, including sine oculis-related homeobox 2 (SIX2) (Mugford et al., 2008a), glial cell-derived neurotrophic factor (GDNF), forkhead/winged helix transcription factor (FOXD1) (Patterson et al., 2001), and pre-B-cell leukemia transcription factor 1 (PBX1) (Moens and Selleri, 2006). Hox11 function is required for generation of NPCs, stromal progenitor cells, and induction of UB branching morphogenesis. Studies have shown that Hox11 paralogs interact with Pax2 and Eya1 to induce transcription of direct downstream targets such as SIX2 and GDNF (Wellik et al., 2002; Gong et al., 2007). Therefore, the spatiotemporal pattern of Hox11 expression indicates that it has a key role in MM patterning. The results of a study have shown that although Hox10 and Hox11 expression patterns mostly overlap, Hox10 displays additional expression in the FOXD1-expressing cortical stromal cells. Hox10 has an essential role in appropriate integration and further differentiation of stromal progenitor cells in the developing metanephric kidney (Yallowitz et al., 2011).

LIM-Class Homeodomain 1 (Lim1)

LIM-class homeodomain 1 (Lim1) is a transcription factor encoded by the *LHX1* gene in humans. Lim1 is an early marker for kidney organogenesis. This gene is a direct downstream target for the RA signaling pathway to IM specification and patterning (Osafune et al., 2002; Cartry et al., 2006; Wingert et al., 2007). During renal development, Lim1 is expressed in different

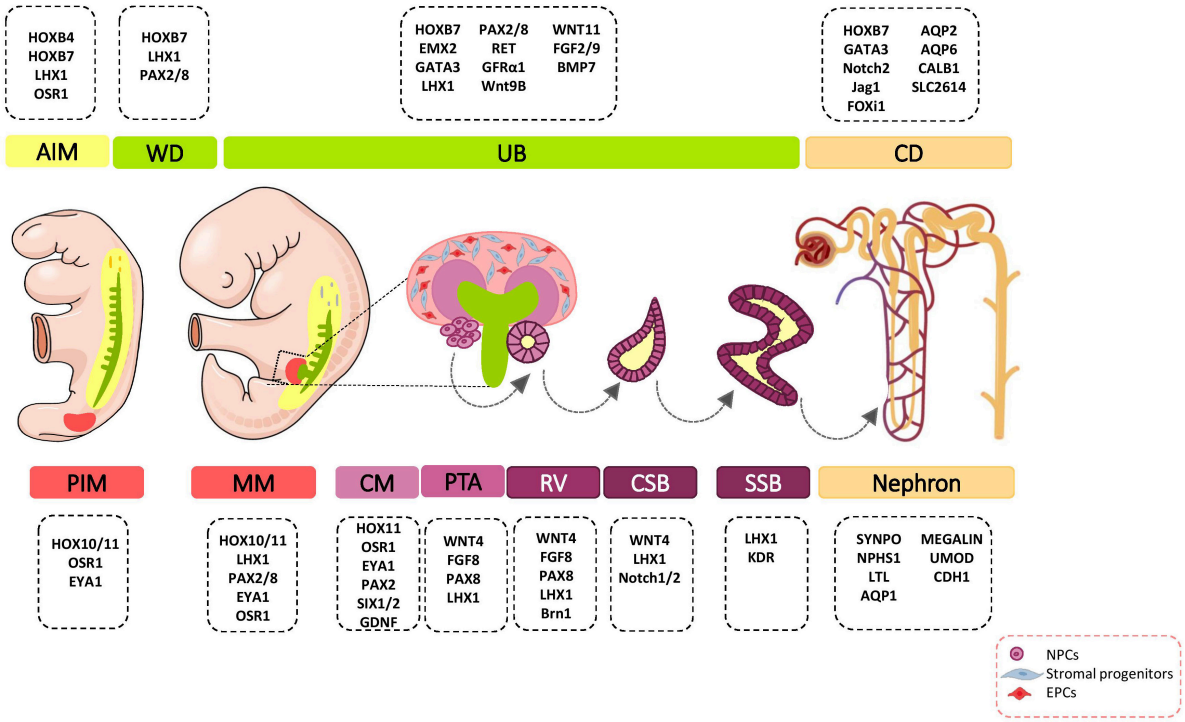

FIGURE 1 | Major genetic markers involved in kidney development. The cell fate decision of renal cells are coordinately controlled with different genetic markers during nephrogenesis. AIM, anterior intermediate mesoderm; AQP, aquaporin; BMP, bone morphogenetic protein; Brn1, Bruno-like1; CALB1, calbindin; CD, Collecting duct; CM, cap mesenchyme; CSB, comma-shaped body; EMX, empty spiracles homolog; Eya1, eyes absent 1; FGF, fibroblast growth factor; FOXi1, forkhead box protein i1; FRS2α, fibroblast growth factor receptor substrate 2α; GATA, *trans*-acting T-cell-specific transcription factor; GDNF, glial cell–derived neurotrophic factor; GFRα1, glial cell line derived neurotrophic factor family receptor α1; Jag1, Jagged 1; HOX, homeobox; IM, intermediate mesoderm; Kdr, kinase insert domain protein receptor; LHX1, LIM-class homeodomain 1; LTL, lotus tetragonolobus lectin; MM, metanephric mesenchyme; NPCs, nephron progenitor cells; NPHS1, nephrosis 1; Osr1, odd skipped related 1; PAX, paired box protein; PI3K, phosphoinositide 3-kinases; PIM, posterior intermediate mesoderm; PTA, pre-tubular aggregate; RV, renal vesicle; SIX2, sine oculis-related homeobox 2; SLC2614, solute carrier 2614; SSB, S-shaped body; SYNPO, synaptopodin; TGFβ, transforming growth factor beta; UB, ureteric bud; UMOD, uromodulin; WNT, wingless-type mouse mammary tumor virus integration site; WD, Wolffian duct.

stages - the IM; nephric duct; pro- and mesonephros; UB; pre-tubular aggregates (PTA); comma- and S-shaped bodies; and podocytes. Its expression pattern suggests that Lim1 has distinct functions in several steps of kidney organogenesis. To this end, Lim1 affects expression of several key genes and regulates cell fate specification. According to research, Lim1 regulates its own expression and the expressions of Pax2, *E*-cadherin, WNT9b, and Ret in the nephric duct, thereby influencing early specification of the IM, nephric duct elongation, and UB outgrowth (Tsang et al., 2000; Kobayashi et al., 2005; Pedersen et al., 2005). This cell fate-specifying transcription factor regulates the patterning of renal vesicles (RV) by transcriptional activation of Brn1 (Bruno-like1) and EphA4 (Chen et al., 2006).

Odd Skipped Related 1 (Odd1 or Osr1)

OSR1 is a zinc-finger DNA-binding protein that is broadly expressed in the IM and MM (James, 2006). OSR1 is one of the earliest genetic markers that is expressed in the MM and UB lineages. OSR1 is specifically required for establishment of the MM. Early OSR1 expressing cells are a multi-potent precursor population that give rise to nephron and interstitial mesenchyme progenitors (Mugford et al., 2008b). In the nephrogenic lineage, OSR1 expression is downregulated from the RV stage (Xu et al., 2014). OSR1 regulates the expressions of several key genes (*LHX1*, *PAX2*, *EYA1*, *SIX2*, *GDNF*, Cbp/p300-interacting transactivator 1 [*CITED1*], and Spalt like transcription factor 1 [*SALL1*]) in the nephrogenic mesenchyme (James, 2006; Xu et al., 2014, 2016). OSR1 interacts synergistically with other factors such as Wilm's tumor (WT1) and SIX2 to regulate MM specification and NPC pool maintenance (Xu et al., 2014, 2016). OSR1-dependent transcriptional activation of LHX1 might regulate expression of foot process and podocyte junction-associated genes that result in podocyte differentiation (Tomar et al., 2014).

Paired Box Proteins (*PAX2/8*)

The paired box proteins (PAX2/8) transcription factors are earlier genetic markers expressed in the IM. RA signaling and low levels of bone morphogenetic protein (BMP) signaling from neighboring tissues induce the expressions of *PAX2/8* genes in the kidney-forming mesoderm (James and Schultheiss, 2005; Cartry et al., 2006; Fleming et al., 2013). PAX2 transcripts and proteins are found in multiple stages of the developing kidney, including the IM, nephric duct, UB, MM, and CM.

Subsequently, its expression in MM derivatives is downregulated (Ryan et al., 1995; Mugford et al., 2008a) and becomes restricted to UB derivatives (Cai et al., 2005). In the early stage of kidney development, PAX8 and PAX2 are co-expressed. As development proceeds, the PAX8 mRNA and protein disappear, and are expressed again in the RV stage (Narlis et al., 2007). PAX2/8 can affect signaling in the developing kidney by transcriptional regulation of *GATA3* (Trans-acting T-cell-specific transcription factor), *LIM1* (Narlis et al., 2007; Boualia et al., 2013), *RET* (Bouchard et al., 2002), *SALL1* (Ranghini and Dressler, 2015), *SIX2*, *GDNF* (Brophy et al., 2001), *WNT4* (Torban et al., 2006), and secreted frizzled-related protein 2 (*SFRP2*) (Brophy et al., 2003) genes during multiple steps. The results of studies indicate that both *PAX2/8* are critical for cell survival, branching morphogenesis, and nephron specification (Bouchard et al., 2002; Narlis et al., 2007).

Eyes Absent Homolog 1 (EYA1)

EYA1 is a transcription regulator with threonine phosphatase activity. EYA1 is expressed in the PIM, MM, and CM. As nephrogenesis proceeds, its expression is gradually decreased (Xu et al., 2015). EYA1 forms a transcriptional complex with homeodomain genes during multiple stages of nephrogenesis. Eya1-Six1-Dach and Eya1-Hox11-Pax2 complexes during the early stages of MM activate expressions of SIX2 and GDNF in the mesenchymal progenitors (Li et al., 2003; Gong et al., 2007; Xu et al., 2015). Thereafter, the SIX2-Eya1-Myc complex is critical for expansion of the multi-potent nephron progenitor pool (Xu et al., 2015).

Early patterning of kidney-forming mesoderm leads to the formation of multiple distinct renal progenitor populations within the nephrogenic niche. Kidney organogenesis depends on cell–cell communication between these populations that lie adjacent to each other.

RENAL PROGENITOR CELLS

Pioneering studies revealed that the renal nephrogenic niche includes at least four major self-renewing, multi-potent progenitor cell populations: UBPCs, NPCs, stromal progenitors, and endothelial progenitor cells (EPCs; **Figure 1**). Kidney organogenesis, like the organogenesis of all other organs, is dependent on the migration of external cells from different embryonic tissues into the developing kidney (Bronner-Fraser and Fraser, 1988; Schmidt-Ott et al., 2006; Guillaume et al., 2009). Spatiotemporal multicellular interactions and precise orchestration of signals between several distinct cell populations have important roles in the successful induction, maintenance, and differentiation of all cell types of the kidney.

Nephron Progenitor Cells (NPCs)

NPCs harbor the capacities of both self-renewal and differentiation to maintain the nephron progenitor pool and generation of all epithelial cells of nephrons. NPCs undergo mesenchymal-epithelial-transition (MET) and sequential morphological alterations to form the PTA that differentiate into RV, comma- and S-shaped bodies, and mature nephrons. One nephron is composed of more than 20 different cell types that include podocyte cells, the proximal tubule, loop of Henle, distal tubule, and connecting tubule cells (Al-Awqati and Oliver, 2002). The modes of proliferation and differentiation of NPCs are coordinately controlled during nephrogenesis. For this purpose, NPCs-specific transcription factors CITED1, PAX2, EYA1, SIX2, SALL1, and WT1 specify cell phenotypes (Lindström et al., 2018). NPCs population in the CM are divided into the self-renewing $CITED1^{+}/SIX2^{+}$ compartment and $CITED1^{-}/SIX2^{+}$ induced compartment that progress toward epithelialization (Brown et al., 2013). SIX2 expression is controlled by upstream signaling proteins such as the Pax2/Eya1/Hox11 complex (Gong et al., 2007). SIX2 maintains the un-differentiated cell state of NPCs, and its expression is progressively decreased in the following steps of kidney organogenesis (Park et al., 2012). Several lines of evidence indicate that SIX2 regulates its own expression and the expressions of LHX1, OSR1, WT1, GDNF, FGF8, and WNT4 in NPCs and thereby regulates cell maintenance and self-renewal (Brodbeck et al., 2004; Self et al., 2006; Park et al., 2012; Xu et al., 2014). WT1 is another transcription factor that is important in regulation of self-renewal, MET, and differentiation of NPCs (Hartwig et al., 2010; Fanni et al., 2011). WT1, by inhibition of BMP7/pSMAD signaling, can repress apoptosis in MM (Motamedi et al., 2014). WT1 directly activates growth arrest-specific 1 (GAS1) transcription and promotes NPCs proliferation via the fibroblast growth factor (FGF) stimulated phosphoinositide 3-kinase (PI3K)-Akt signaling pathway (Kann et al., 2015). FGF16/20 are direct transcriptional targets of WT1 (Motamedi et al., 2014). The three-dimensional (3D) arrangement of NPCs and communication with other cells in the developing nephrogenic zone is critical for the cell fate decisions of these cells (**Figure 2**).

Ureteric Bud Progenitor Cells (UBPCs)

Anterior intermediate mesoderm (AIM) commit to the UB lineage, including the collecting system (Ohmori et al., 2013). The collecting duct have critical roles in electrolyte and fluid balance, and acid-base homeostasis (Costantini and Kopan, 2010). The collecting duct consists of two highly specialized cell types, principal cells and intercalated cells. Both populations are derived from bi-potent UB precursors located at the UB tips (Al-Awqati, 2013). vHNF1 (Garcia-Villalba et al., 2009), EMX2 (Empty spiracles homolog 2) (Miyamoto et al., 1997), PAX2 (Dressler et al., 1990), LHX1 (Karavanov et al., 1998), GATA3 (Grote, 2005; Grote et al., 2008), RET (Pachnis et al., 1993), WNT11 (Majumdar, 2003), and Vsnl1 (Bridgewater et al., 2011) are expressed in the UB tips and they specify its cell fate. Results from studies indicate that a sub-population of UBPCs, which express the ΔNp63 isoform (N-terminus truncated p63) is dedicated to generating cortical intercalated cells (El-dahr et al., 2017). FOXi1 and a disintegrin and metalloproteinase domain 10 (Adam10)/Notch signaling pathway play critical roles in intercalated and principal cell fate decision in the collecting duct, respectively (Al-Awqati and Schwartz, 2004; Jeong et al., 2009; Vidarsson et al., 2009; Guo et al., 2015). In response to paracrine signals from neighboring tissues, UB precursors

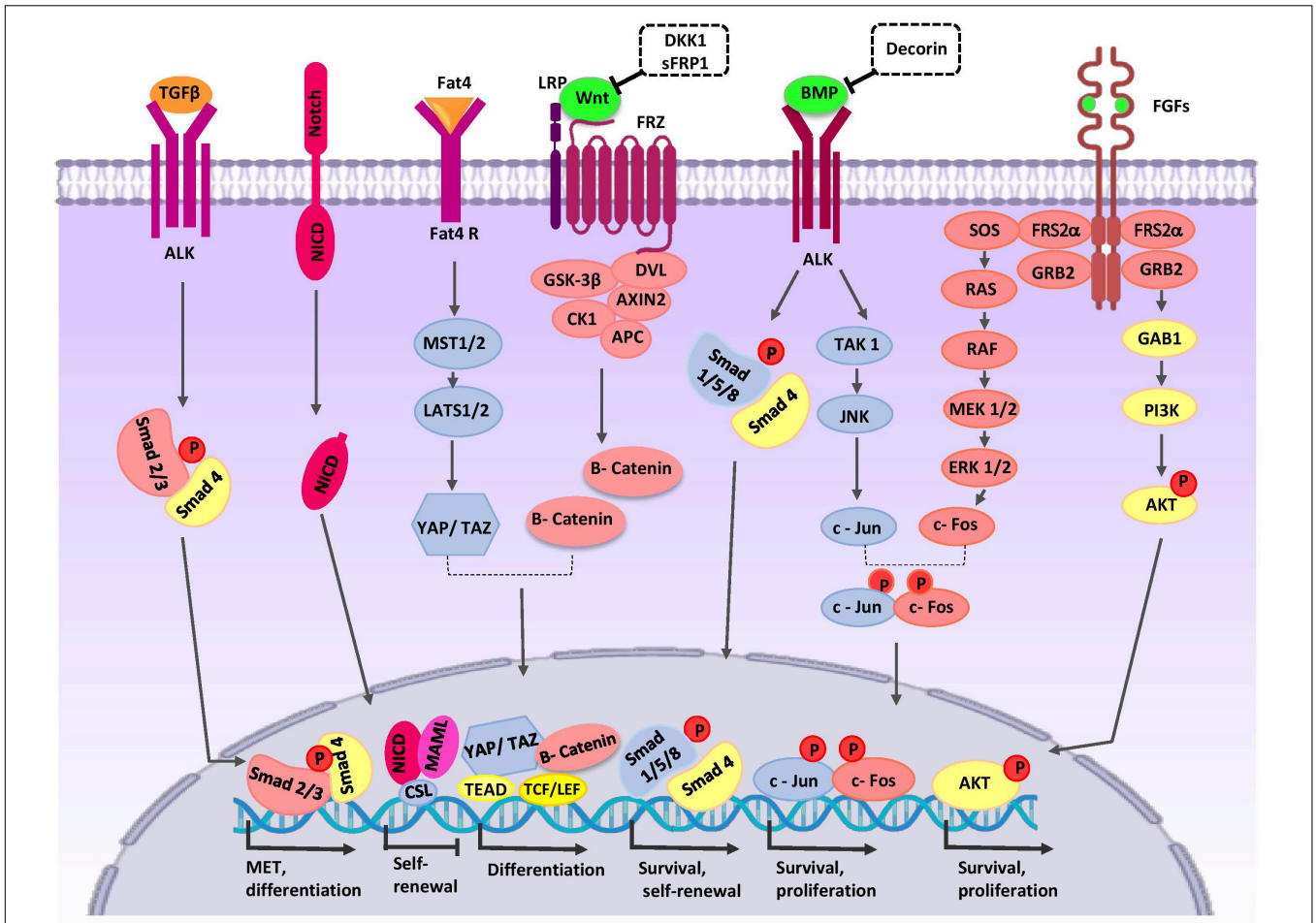

FIGURE 2 | Crosstalk between major signaling pathways during nephron progenitor cell (NPC) differentiation. WNT9b, BMP7, and FGF2/9 are secreted by UB cells (green color). Stromal cells secret Decorin, SFRP1, Fat4, and TGFβ2 (orange color). High levels of WNT9b/β-catenin increase expression of the differentiation-specific genes (*PAX8, C1qdc2,* and *WNT4*) of nephron progenitor cells (NPCs). Fat4/Hippo signaling amplifies β-catenin activity. On the other hand, WNT signaling can be inhibited by SFRP1 and DKK1 to arrive appropriate number of nephrons in a definitive kidney. The BMP7/SMAD1/5 signaling pathway promotes differentiation of NPCs. Decorin antagonizes BMP7/SMAD signaling in NPCs. BMP7 activates proliferation by the TAK1-JNK-JUN cascade. FOS activation is regulated by FGF9. AP1 (a dimeric transcription factor composed of Jun and FOS) acts as a point of collaboration between the BMP7 and FGF9 signaling pathways. AP-1 activates transcription of a variety of genes (*MYC, BCL-2,* and *p53*) related to the cell cycle and anti-apoptotic events; thereby, it regulates survival and proliferation of NPCs. The FGF/RAS-MAPK, FGF/PI3K/AKT signaling pathway promotes survival and proliferation of NPCs. After binding of Notch2 to Notch ligands, NICD is released into the cytoplasm and translocates to the nucleus where the complex decreases self-renewal specific gene expression and primes NPCs for differentiation. TGFβ2 is required for MET-related gene expression during NPCs differentiation. AKT, protein kinase B; ALK, anaplastic lymphoma kinase; AP1, activator protein 1; APC, adenomatous polyposis coli; BMP, bone morphogenetic protein; CK1, casein kinase 1; Csl, CBF1/RBP-J, Su(H), Lag-1, the mammalian, fly, and worm orthologous proteins; DKK1, DKK1, Dickkopf-1; DVL, homologous to drosophila Dishevelled; EC, endothelial cells; ERK, extracellular signal-regulated kinase; Fat4, tumor suppressor homolog 4; FGF, fibroblast growth factor; Frz, Frizzled; GAB1, Grb2-associated binder 1; GSK-3β, glycogen synthase kinase 3β; GRB2, growth factor receptor-bound protein 2; JAK, Janus kinase; JNK, c-Jun N-terminal kinase; LATS1, large tumor suppressor homolog 1; LEF, lymphoid enhancing factor; LRP, low-density lipoprotein receptor-related protein; MAML, mastermind-like; MAPK, mitogen activated protein kinase; MEK, mitogen activated protein kinase; MET, mesenchymal to epithelial transition; MST1/2, Mammalian sterile 20-like kinases; NICD, notch intracellular domain; P, phosphate group; PI3K, phosphatidylinositol 3-kinase; RAS/RAF, Rat sarcoma/rapidly accelerated fibrosarcoma; SFRP1, secreted frizzled-related protein; Smad, Caenorhabditis elegans SMA ("small" worm phenotype) and Drosophila MAD ("Mothers Against Decapentaplegic"); SOS, Son of Sevenless; TAK1, TGF β-activated kinase; TCF, T-cell factor; TEAD, transcription factor family member; TGF-β, transforming growth factor-β; WNT, wingless-type mouse mammary tumor virus integration site; YAP, yes-associated protein.

undergo morphological changes and coordinated cell movements to form the collecting duct (**Figure 3**).

Stromal Progenitor Cells

The interstitial stroma is defined as a heterogeneous population of cells that serve both as a supportive environment and a source of dedicated cells that produce extracellular matrix (ECM) and associated signaling molecules. Stromal progenitors are spindle-shaped cells that encompass the anterior part of NPCs in the MM and later localize around nascent UBs and nephrons. The stromal cells not only provide structural support but also regulate the development of neighboring cells. Cellular origins of the $FOXD1^{+}$ cortical stromal cell lineage arise from multipotential $Osr1^{+}$ cells in the IM (Mugford et al., 2008b). This multipotent

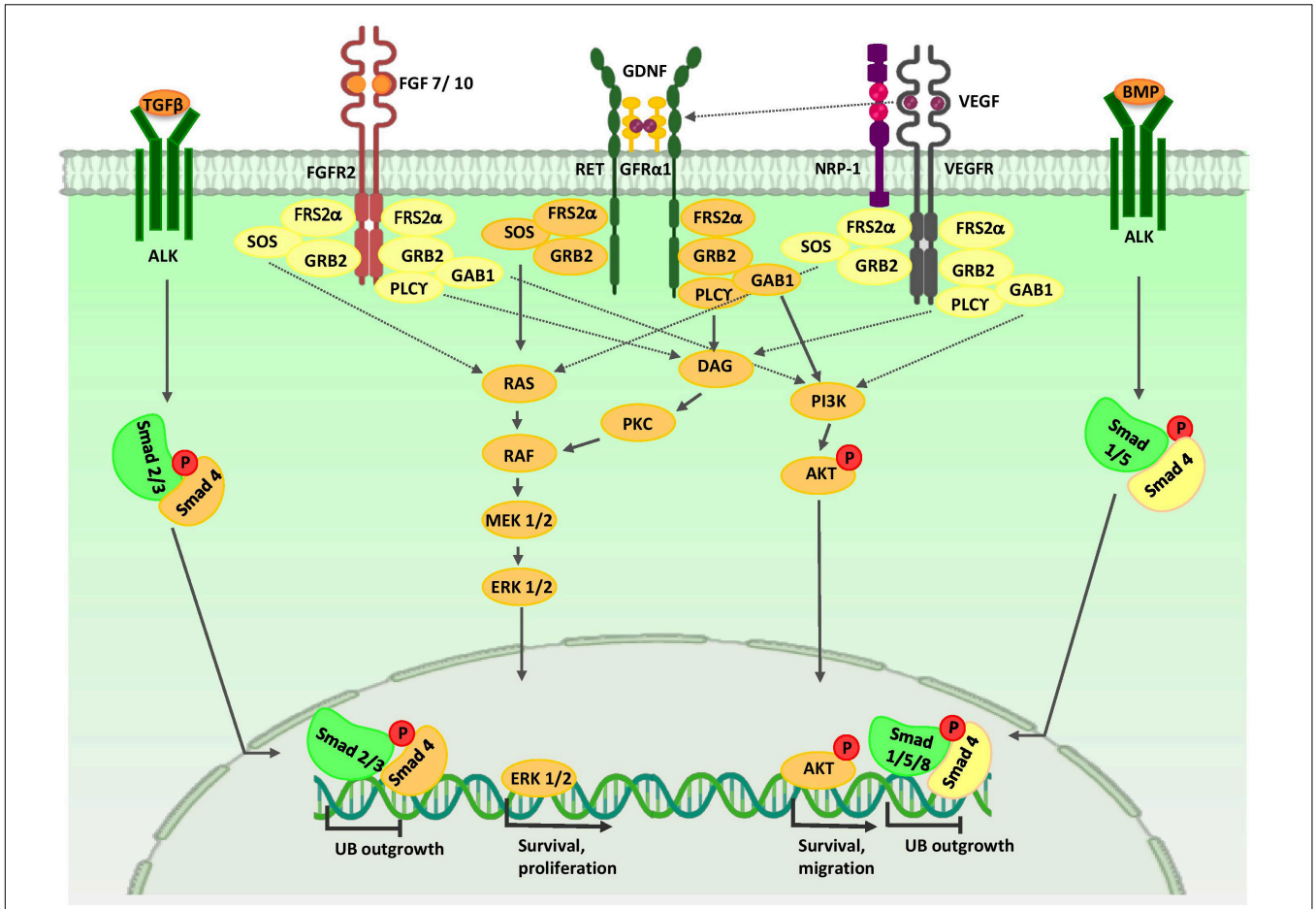

FIGURE 3 | Major signaling pathways in ureteric bud morphogenesis. Branching morphogenesis is tightly regulated by different growth factors such as GDNF, VEGF, and FGFs. GDNF and VEGF are secreted from the MM and FGF7/10 is produced by stromal cells. Binding of these growth factors to their tyrosine kinase receptors activates three major signaling pathways: RAS/MAPK, DAG/PKC/MAPK, and PI3-K/AKT. Thus, they stimulate mitotic proliferation, survival, and migration of UB cells. VEGF-A induces RET activation. Members of the TGF-β super-family, including BMP4 and TGFβ, which are expressed by mesenchymal cells that surround UB, inhibit UB outgrowth in a Smad-dependent manner. AKT, protein kinase B; ALK, anaplastic lymphoma kinase; BMP, bone morphogenetic protein; ERK, extracellular signal-regulated kinase; DAG, diacylglycerol; DVL, homologous to drosophila Dishevelled; EC, endothelial cells; FGF, fibroblast growth factor; FGFR, fibroblast growth factor receptor; FRS2α, fibroblast growth factor receptor substrate 2α; GAB1, Grb2-associated binder 1; GDNF, glial cell-derived neurotrophic factor; GFRα1, glial cell line-derived neurotrophic factor family receptor α1; GRB2, growth factor receptor-bound protein 2; MEK, mitogen activated protein kinase; NRP1, neuropilin 1; P, phosphate group; PI3K, phosphatidylinositol 3-kinase; PKC, protein kinase C; PLC-γ, Phospholipase C-γ; RAS/RAF, Rat sarcoma/rapidly accelerated fibrosarcoma; Smad, Caenorhabditis elegans SMA ("small" worm phenotype) and Drosophila MAD ("Mothers Against Decapentaplegic"); SOS, Son of Sevenless; Smad, Caenorhabditis elegans SMA ("small" worm phenotype) and Drosophila MAD ("Mothers Against Decapentaplegic"); TGF-β, transforming growth factor-β; UB, ureteric bud; VEGF, vascular endothelial growth factor; VEGFR, vascular endothelial growth factor receptor.

stromal progenitor population is characterized by expressions of FOXD1, PBX1, POD1, SALL1, retinoic acid receptors (RARs), and FAT4 (Das et al., 2013; Bagherie-lachidan et al., 2015; Ohmori et al., 2015). Some researchers have demonstrated that renal stromal cells may be derived from migrating cells of other tissues such as paraxial mesoderm and neural crest that integrate into the FOXD1^{+} compartment of the MM (Bronner-Fraser and Fraser, 1988; Guillaume et al., 2009). TBX18 expressing cells are another population of multi-potent mesenchymal progenitors in the metanephric kidney that contribute to the ureteric mesenchyme and renal interstitial cells (Bohnenpoll et al., 2013). Cells derived from mesenchymal progenitors contribute to different types of stromal cells, including interstitial fibroblasts, vascular smooth muscle cells, renin producing cells, pericytes, and mesangial cells (Kobayashi et al., 2014).

Endothelial Progenitor Cells (EPCs)

Renal vasculature plays a significant role in the development and function of the kidney. It has been shown that endothelial cells (EC) are important not only for delivery of oxygen and micronutrients, but also for paracrine signals that are distributed to other cells in the nephrogenic niche that promote kidney organogenesis (Munro et al., 2017). Development of the renal vasculature proceeds synchronously with nephrogenesis and occurs through two main mechanisms, vasculogenesis and angiogenesis (Mukherjee et al., 2017). Sprouting angiogenesis

of pre-existent vessels plays a key role in formation of the major vessels (Nishimura et al., 2016). The renal vasculature arises predominantly from formation of *de novo* vessels via differentiation of endothelial progenitors (angioblasts) (Sequeira-lopez et al., 2015). Results of recent studies suggest that there are different populations of both intra- and extra-renal EPCs (Mugford et al., 2008b; Munro et al., 2017). Previously, a population of FLK1-expressing cells (vascular endothelial growth factor [VEGF]-A receptor, VEGFR2 [FLK1, KDR]) in the periphery of the induced mesenchyme and adjacent to the stalk of the UB have been identified (Robert et al., 2018). These cells are most probably derived from $OSR1^+$ multi-potential progenitors within the IM (Mugford et al., 2008b). In the following stages of development, these KDR^+ cells undergo changes to immature intermediate melanoma cell adhesion molecule ($MCAM^+$, $CD146^+$) cells, and at the end of the developmental period, platelet/endothelial cell adhesion molecule-1 ($PECAM^+$, $CD31^+$) mature vascular cells (Homan et al., 2019). Furthermore, a population of c-Kit^+ endothelial progenitors reside within the cortical stromal compartment. Studies indicate that this progenitor population has migrated from the aorta-gonad-mesonephros (AGM) region to the early MM. UB cells secrete stem cell factor (SCF), a c-Kit ligand and thereby promote survival, migration, and tube formation of EC (Schmidt-Ott et al., 2006; Homan et al., 2019). Another source of endothelial progenitors is a subpopulation of $FOXD1^+$ renal stromal cells that are incorporated into the peritubular capillary. These cells play a critical role in the proper spatial distribution of renal vessels (Sims-lucas et al., 2013; Mukherjee et al., 2017). A subset of $MCAM^+$ progenitors that are derived from a $FOXD1^+$ renal stromal population are incorporated into endothelial structures (Pärssinen et al., 2016). Results of a transcriptomic study have revealed that a subpopulation of $SALL1^+/SIX1^+$ NPCs reside in the second-trimester of human fetal kidneys and co-express the CD31 mature endothelial marker (Low et al., 2019).

REGULATION OF NEPHRON PROGENITOR CELL (NPC) FATE

Many studies identified biological processes and signaling pathways that regulate cell fate decisions of NPCs. We intend to discuss the critical role of the wingless-type mouse mammary tumor virus integration site (Wnt) protein family, FAT4, Hippo, BMPs, FGFs, Notch, and Hedgehog/transforming growth factor beta (TGFβ) signaling pathways and explain how cross-talk between them determines the cell fate of NPCs (**Figure 2**).

Wnt Family Signaling Pathways

WNT9b/β-catenin signaling is one of the major signals that mediate nephron progenitor renewal and differentiation (Karner et al., 2011). The activity of β-catenin in NPCs is controlled by signals from the UB and cortical stroma. Low levels of β-catenin increase expression of self-renewing genes and promote expansion of the NPC pool. High levels stimulate transcription of several differentiation-specific genes such as *PAX8, C1qdc2*, and *WNT4*, resulting in PTA formation (Park et al., 2007; Ramalingam et al., 2018). One signaling pathway that amplifies β-catenin activity is Fat4/Hippo signaling from stromal cells. Fat4, by phosphorylation of YAP/TAZ, stimulates transcription of differentiation-related genes (Das et al., 2013). Fat4 binds to Dchs1 in the CM and regulates the polarity of polarized cells. This process is thought to regulate cell-cell communication and cell fate determination (Saburi et al., 2008; Mao et al., 2015). In the following steps of nephrogenesis, WNT4, through a Ca^{2+}-dependent pathway, stimulates expression of differentiation genes *FGF8, LHX1, PAX8, Notch, RET, ItgA6a, E-cadherin*, and *ZO1* (Valerius and McMahon, 2008; Tanigawa et al., 2011; Park et al., 2012) in the CM and provokes MET in NPCs. WNT11 is expressed in UB tips through non-canonical pathways and regulates the polarity and behavior of NPCs, which ultimately determines the proper nephrogenic program (O'Brien et al., 2018). During nephrogenesis, some molecules act to downregulate WNT signaling to arrive at an appropriate number of nephrons in a definitive kidney. Dickkopf-1 (DKK1) is an inhibitor of the WNT co-receptor LRP5/6 and downstream of LHX1. During nephrogenesis, DKK1 is expressed by PTA cells and their derivatives (Potter et al., 2007). Stromal cells generate SFRP1, a secreted WNT antagonist that blocks canonical WNT signaling, and restricts NPC differentiation (Levinson et al., 2005).

Growth Factor Signaling Cross-Talk

Studies of the role of BMPs in kidney organogenesis indicate that BMP2/4 signaling has a critical role in size determination and patterning of the nephrogenic field (Oxburgh et al., 2014). Likewise, BMP7 promotes survival and self-renewal of NPCs. BMP7 is exclusively expressed in the NPCs and UB tips (Blank et al., 2009; Jeanpierre et al., 2012). UB-derived WNT9b induces NPCs expression of BMP7 (Park et al., 2012). The BMP7/SMAD1/5 signaling pathway promotes susceptibility of NPCs to the differentiation signal of WNT9b/β-catenin (Brown et al., 2013; Muthukrishnan et al., 2015). Furthermore, SMAD1 can bind to β-catenin to form a transcriptional activating complex in the promoter region of MYC, and thereby exhibit synergistic effects with the WNT/β-catenin pathway (Hu and Rosenblum, 2005). Decorin, an ECM protein produced by stromal progenitor cells accumulates in the ECM microenvironment that surrounds the NPCs. Decorin antagonizes BMP7/SMAD signaling in NPCs and represses the differentiation signal of the canonical WNT9b/β-catenin pathway. Therefore, ECM components mediate differentiation of NPCs to epithelial structures (Fetting et al., 2014; Ohmori et al., 2015).

BMP7 activates the proliferative signal mediated by the TAK1-JNK-JUN cascade in self-renewing $CITED1^+/SIX2^+$ NPCs. JUN is a DNA-binding partner in the dimeric AP-1 transcription factor. Besides, the activator protein 1 (AP1) also includes another component named FOS. FOS activation is regulated by FGF9 (Muthukrishnan et al., 2015). FGFs is produced in UB cells. Likewise, FGF9 and FGF20 are exclusively expressed in the CM (Jeanpierre et al., 2012). FGF9 expression in these cells is activated by UB-secreted WNT9b. AP1 acts as a point

of collaboration between BMP7 and FGF9 signaling pathways. AP-1 activates transcription of the target genes *MYC, BCL-2*, and *p53*, and thereby regulates the cell cycle and proliferation of NPCs (Couillard and Trudel, 2009; Muthukrishnan et al., 2015; Saifudeen et al., 2012). When FGF2 and FGF9 bind to their receptors on the NPCs, the RAS-MAPK and PI3K/AKT signaling cascades are activated, which promotes survival and proliferation of CITED1$^+$/SIX2$^+$ NPCs (Brown et al., 2011; Lindström et al., 2015). The use of BMP7 and FGFs in directed differentiation of PSCs promotes both proliferation and differentiation of NPCs *in vitro* (Morizane et al., 2015; Taguchi and Nishinakamura, 2017). Recently, researchers have demonstrated that the activin/GDF11/TGFb-SMAD2/3 signaling cascade showed superior effects to BMP7 in maintenance of hiPSC-derived NPCs (Yamamoto et al., 2019).

Other Signaling Pathways in Nephron Progenitor Cell (NPC) Fate Decision

Notch signaling plays two distinct roles in nephrogenesis. (1) Notch2 downregulates PAX2, SIX2, and GDNF expressions, and thereby primes NPCs for differentiation (Yuri et al., 2015; Chung et al., 2016). (2) Notch is required for accurate segmentation of the nephrons by transcriptional activation of the *LHX1* and *HNF1B* genes (Chung et al., 2017).

The Hedgehog (Hh)/*GLI3R* signaling pathway controls the development of capsular stromal cells by increasing expression of the stromal genes *FOXD1, RALDH2*, and *PBX1*. Furthermore, HH-GLI3R signaling regulates the expression of TGFβ2 and its targets in FOXD1$^+$ stromal cells. TGFβ2 that is secreted from the stroma mediates crosstalk between stromal and nephrogenic compartments. In NPCs, TGFβ2 is required for the expression of MET-related genes such as LHX1(Rowan et al., 2018).

DEVELOPMENTAL EVENTS DURING URETERIC BUD (UB) AND COLLECTING DUCT MORPHOGENESIS

Many studies have revealed the critical roles for growth factors secreted from the MM in UB branching morphogenesis (**Figure 3**). GDNF/RET/glial cell line derived neurotrophic factor family receptor α1 (GFRα1) signaling plays an important role in early developmental events during UB and collecting duct morphogenesis. GDNF secreted from NPCs stimulates cell proliferation and survival in these cells (Pepicelli et al., 1997; Shakya et al., 2005). The positive feedback loop between WNT11 and GDNF/Ret provides for dense packing of the UB branches (Iber et al., 2019). VEGF-A is involved in mitotic proliferation and migration of endothelial and epithelial cells, and may serve to coordinate the formation of blood vessels and kidney tubules during kidney development (Marlier et al., 2008). In the early stages of kidney organogenesis, VEGF-A is produced by NPCs. This molecule influences two adjacent cell populations: Flk1-expressing angioblasts and UB cells (Gao, 2005). In the UB cells, VEGF-A promotes the formation of a Neuropilin 1 and KDR complex, thereby promoting branching morphogenesis in a PKC, ERK1/2, and PI3-K dependent manner (Karihaloo et al., 2005). Furthermore, VEGF-A induces RET activation; therefore, VEGF-A and GDNF have increasing effects on UB cell proliferation and branching morphogenesis (Tufro et al., 2007). These cells send an unknown signal to NPCs to maintain PAX2 and GDNF expressions and, in turn, stimulate branching of the UB (Gao, 2005).

FGF7 and FGF10 are expressed in cortical stromal cells and bind to FGFR2 (IIIb) on UB cells, thereby stimulating UB cell proliferation (Qiao et al., 1999; Ohuchi et al., 2000; Walker et al., 2017). Spatial expression of Ret in the UB branch tips is under the control of stromal-specific transcription factors FOXD1, Rara, Rarb2, and Pod1 (Piscione and Rosenblum, 2002). RA signaling in FOXD1$^+$ stromal cells induces the expression and secretion of the extracellular matrix 1 (Ecm1), which restricts expression of Ret to the UB tips (Paroly et al., 2013). Also, SFRP1 from stromal cells may directly down-regulate WNT11 and restrict branching morphogenesis (Yoshino et al., 2002). Sprouty 1/2 and SLIT2/ROBO2 signals restrict UB formation to the posterior nephric duct (Grieshammer et al., 2004; Licht et al., 2005; Wilhelm et al., 2015). Several factors such as BMP4 and TGFβ inhibit UB elongation (Cain et al., 2005; Lopez-Rios et al., 2007; Sakurai and Nigam, 2017) and can generate a proper definitive renal collecting system structure and position.

ENDOTHELIAL MIGRATION AND PATTERNING DURING RENAL VASCULAR DEVELOPMENT

As mentioned before, NPCs and UB cells produce VEGF-A (Gao, 2005; Marlier et al., 2008). VEGF-A binds to VEGFR-2 (KDR, Flk-1) on the EPC surface and the signal transduction events activate endothelial progenitor mitotic proliferation and migration (Abrahamson et al., 1998). At later stages, presumptive podocytes in the S-shaped bodies express VEGF-A and recruit EC into the developing glomerulus (Mundel et al., 2003; Eremina, 2006). Activation of ECs may involve a signaling pathway independent of VEGF. UB cells secrete SCF, a c-Kit ligand, and thereby promote survival, migration, and tube formation of ECs (**Figure 4**) (Schmidt-ott et al., 1993; Homan et al., 2019). Expressions of WNT7b and WNT9b in the medullary ureteric epithelium regulate capillary lumen formation through modulation of VE-cadherin localization (Roker et al., 2017).

Stromal cells have critical roles in the normal hierarchical pattern of the renal vasculature. It is thought to that adjacent stromal cells secret SFRP1, and thereby induce proliferation, migration and tubulogenesis of ECs (Dufourcq et al., 2002; Yoshino et al., 2002). Recombination signal binding protein for immunoglobulin kappa J region (RBP-J)-mediated Notch signaling regulates vascular patterning by controlling stromal progenitor differentiation into the vascular mural cell layer of the renal arteries and mesangial cells (Lin and Gomez, 2014). At later stages, EC-derived PDGF-β binds to platelet-derived growth factor receptor beta (PDGFRβ) on stromal cells; thereby, ECs are recruited into the glomerulus and generate capillary loops. On the other hand, in stromal cells, PBX1 temporally and

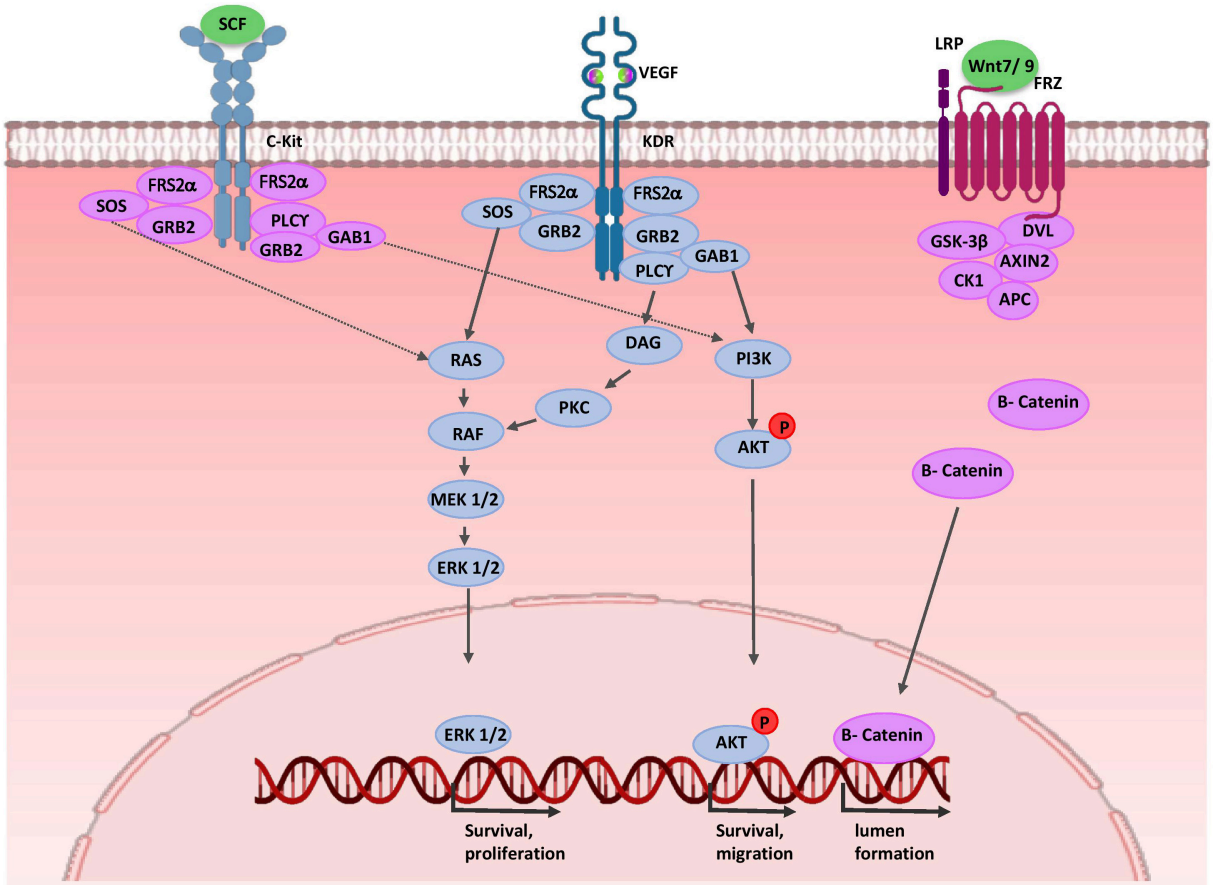

FIGURE 4 | Molecular control of renal endothelial migration and patterning. VEGF is secreted by UB and NPC cells. Binding of VEGF to its tyrosine kinase receptor (KDR) activates three major signaling pathways: RAS/MAPK, DAG/PKC/MAPK, and PI3-K/AKT. Thus, it stimulates mitotic proliferation, survival, and migration of endothelial cells and promotes vascular network formation. UB cells produce SCF and induce survival, migration, and tube formation of endothelial cells. Expressions of WNT7b and WNT9b in the medullary ureteric epithelium regulate capillary lumen formation through modulation of VE-cadherin localization. AKT, protein kinase B; APC, adenomatous polyposis coli; c-Kit, tyrosine-protein kinase KIT (CD117); CK1, casein kinase 1; DAG, diacylglycerol; EC, endothelial cells; ERK, extracellular signal-regulated kinase; FRS2α, fibroblast growth factor receptor substrate 2; Frz, Frizzled; GAB1, Grb2-associated binder 1; GSK-3β, glycogen synthase kinase 3β; GRB2, growth factor receptor-bound protein 2; KDR, kinase insert domain protein receptor; MAPK, mitogen activated protein kinase; MEK, mitogen activated protein kinase; P, phosphate group; PI3K, phosphatidylinositol 3-kinase; PKC, protein kinase C; PLC-γ, phospholipase C-γ; RAS/RAF, Rat sarcoma/rapidly accelerated fibrosarcoma; SCF, stem cell factor; SOS, Son of Sevenless; VEGF, vascular endothelial growth factor; WNT, wingless-type mouse mammary tumor virus integration site.

spatially restrict PDGFRβ expression patterns to cortical domains of the kidney, leading to renal vascular stabilization (Hurtado et al., 2015; Daniel and Cleaver, 2019). Finally, perivascular macrophages in the nephrogenic zone interact with newly forming renal vessels and promote vascular anastomoses. Thus, they play a critical role in proper vessel network formation (Munro et al., 2019).

KIDNEY ORGANOIDS: TRANSLATING DEVELOPMENTAL KNOWLEDGE INTO THE DISH

Many recent efforts have aimed to generate *in vitro* 3D models of both functional tissues and organs to study human developmental and physiological processes, drug screening, disease modeling, and regenerative medicine applications. A defined culture system drives forward the differentiation of human PSCs into kidney organoids by recapitulating the developmental signaling events. Human metanephric kidney formation is initiated during the fifth week of gestation and this corresponds to embryonic day 10.5 (E10.5) for mouse kidney formation (Reidy and Rosenblum, 2009; Costantini and Kopan, 2010). Human PSC-derived kidney organoids, like the developing kidney, should be composed of NPCs, UBPCs, and stromal and EPCs. Recently, scientists have developed protocols that mimic kidney developmental paths *in vivo*. A cocktail of small molecules and growth factors (CHIR99021, Noggin, Activin A, FGF9, and BMP7) are essential for *in vitro* renal lineage differentiation (Morizane et al., 2015; Ahmadi et al., 2019b; Mansoori-moghadam et al., 2019). The stepwise processes of directed differentiation includes

intermediate cell populations: mesendoderm, PIM, RPCs, PTAs, RVs, and the mature kidney. Next, we describe protocols and methods used for the generation of *in vitro* 3D kidney organoids and how developmental knowledge can improve their complexity.

Kidney Organoid Differentiation Protocols and Methods

Takasato and colleagues have reported a protocol that generates human iPSC-derived kidney organoids that consist of both NPCs and UBPCs-derived populations, as well as the $CD31^+/KDR1^+/SOX17^+$ endothelial network, and cortical ($FOXD1^+/MEIS1^+$) and medullary ($FOXD1^+/MEIS1^+$) stromal cells. RNA sequencing analysis indicated that Takasato organoids were very similar to the first trimester kidney (Takasato et al., 2015). Several studies utilized the Takasato protocol to conduct developmental studies (Bantounas et al., 2018), disease modeling (Forbes et al., 2018), *in vivo* transplantation (Koning et al., 2018), and a scale-up of organoid generation (Kumar et al., 2019). Another study was conducted by Bonventre's laboratory. Their method, the Morizane differentiation protocol, enabled 75–92% induction efficiency of NPCs with a shorter differentiation period from hPSCs. However, the nephron derived organoids lacked UB lineages (Morizane and Bonventre, 2017). Wu and colleagues compared the Takasato and Morizane differentiation protocols by using single-cell transcriptomics of hPSCs-derived kidney organoid cells. Their data demonstrated that both protocols generated organoids with at least 12 individual kidney cell types, but with different proportions. Both protocols produced non-renal cells including neurons, muscles, and melanocytes. The Morizane protocol generated only 11% non-renal cells whereas the Takasato organoids contained about 21% of these cells. Although hPSCs-derived kidney organoids expressed some markers of terminal differentiation, they were relatively immature. The Morizane protocol had fewer proliferative cells, and their organoids had more podocyte cells and more differentiated loop of Henle, whereas the Takasato protocol generated more tubular epithelial cell types (Wu et al., 2018).

In another study, hPSCs cultured between two layers of dilute Matrigel (0.2 mg ml), and cavitated epiblast spheroids were produced. To induce the differentiation of the spheroids toward kidney organoids, the researchers used GSK-3β inhibitor CHIR99021 (12 μM) for 1.5 days, and then incubated the spheroids in B27-supplemented media for up to 16 days. The spheroids underwent a sequential epithelial-mesenchymal transition (EMT) and mesenchymal-epithelial transition (MET) process and acquired 3D kidney structures that contained some segments of nephron such as $PODXL^+/WT1^+/SYNPO^+$ podocytes, lotus tetragonolobus lectin $(LTL)^+$ proximal tubules, and immature ECs (Siedlecki et al., 2015). These organoids resembled an immature kidney reminiscent of the late first trimester to mid-second trimester human kidney. Podocyte cells are similar to developing capillary loop stage podocytes *in vivo* (Brooks et al., 2017; Harder et al., 2019) and their nephron-like organoids contain non-renal cells, including ectoderm and lateral plate mesoderm derivatives (Morizane and Bonventre, 2017). In another study, the same protocol was used to generate hPSC-derived organoid plates in microwell formats (high-throughput screening platform) to enhance the differentiation efficiency of the kidney organoids. Single-cell RNA sequencing analysis revealed six major clusters of cell type subpopulations that included proximal tubules, podocytes, early tubules that expressed markers of both proximal and distal tubules and collecting ducts, early podocytes that had characteristics of both $CLDN1^+/PAX8^+$ parietal epithelial cells and podocytes, as well as, stromal and ECs (Czerniecki et al., 2018).

In a recent study, Garreta and colleagues improved the speed and efficiency of maturation by increasing the duration of the 3D culture. They utilized soft hydrogels during the monolayer culture for 4 days to derive IM committed cells that contained both AIM and PIM cell populations. Afterward, the cells were aggregated in a 96-well V-bottom plate to form the 3D structures. Aggregates were cultured in the presence of the induction factors for 16 days to generate the kidney organoids. Their hPSCs-derived kidney organoids contained various kidney cell types, including cell populations with characteristics of proximal tubules, loops of Henle, distal tubules, and glomeruli. The human kidney organoids were transplanted into chick chorioallantoic membrane (CAM) and incubated *in ovo* for 5 days. hPSCs-derived organoid transplants showed more *in vivo*-like characteristics with higher functional differentiation compared to *in vitro* organoids, and transcriptionally, they more closely resembled second trimester human fetal kidneys (Garreta et al., 2019). Hiratsuka et al. (2019) established a new approach that used synthetic mRNAs to generate induced nephron-like organoids (iNephLOs) with some segments of the nephron that were comprised of proximal tubules, distal tubules, and podocytes. They used two sets of synthetic mRNAs encoding transcription factors for 4 days to derive $PAX8^+/LHX1^+$ pretubular aggregate cells, after which the cells were aggregated in 96-well U-bottom plate for up to 14 days to form 3D structures that transcriptionally resembled kidney organoids generated by using growth factor induction (Hiratsuka et al., 2019).

There is a large variation between independent differentiation experiments. The variability may arise from the technical strategies underlying kidney organoids formation such as inter-reagent and inter-batch variability, variation between hPSC lines, and even skill of the experimenter. Moreover, the generation of hPSC-derived kidney organoids faces many remaining challenges including immature renal cell types, nascent vascular network, and lack of connection between nephron segments and collecting duct system in organoids (Miyoshi et al., 2019). Therefore, developing more *in vivo* mimicking structures by biological approaches for reproducible and robust generation of kidney organoid is urgently needed.

Biological Approaches to Improve Kidney Organoid Complexity

Cell-to-cell interactions and signals from the complex microenvironment during embryonic kidney development affect cell behaviors such as proliferation, migration and

differentiation of renal progenitors. Organoids can be generated following the same developmental events that occur in the embryo; thus, consideration for cellular communications and microenvironmental cues in organoids can improve their complexity.

Cell-to-Cell Interactions

Like early organogenesis event, a tightly coordinated crosstalk between NPCs, UBPCs, ECs, and stromal cells during development leads to a higher-order and vascularized kidney organoid (Takasato et al., 2016). Studies have shown that increasing the duration of the 3D culture by enhancing cell–cell and cell–matrix interactions would generate kidney organoids with higher maturity (Garreta et al., 2019). Most studies of kidney organoids have relied on the self-organizing capacity of aggregates derived from uni-lineage progenitors such as hPSCs (Morizane et al., 2015; Takasato et al., 2015; Garreta et al., 2019). However, some studies have developed heterotypic cellular aggregates. Taguchi and Nishinakamura established a protocol for differential induction of mouse NPCs and UBPCs separately, and reaggregated them with the PDGFRa$^+$ stromal progenitors isolated from E11.5 mouse embryonic kidneys. This reassembled kidney organoid had more differentiated nephron structures with overall components and contiguous collecting duct architecture (Taguchi and Nishinakamura, 2017). Many studies, including researches in our laboratory, indicated that when hPSC-derived progenitor cells were combined with mesenchymal stem cells (MSCs) and ECs, the mixture self-organized into 3D structures such as kidney (Takebe et al., 2015), pancreatic (Takebe et al., 2015; Takahashi et al., 2018), cardiac (Varzideh et al., 2018), and liver (Takebe et al., 2014, 2015, 2017) organoids. Data showed that stromal cells produced various cytokines and growth factors that modulated the proliferation and maturation of other cells in the organoids (Takahashi et al., 2018). Myosin IIA expressed by MSCs directed forceful movements of cells and triggered the initiation of self-condensation (Takebe et al., 2015).

Research has shown that ECs are important not only for delivery of oxygen and micronutrients, but also for the paracrine signals that are critical for proper RPCs differentiation and promotion of organoid maturation (Garreta et al., 2019). EC generation in both the Takasato and the Morizane differentiation protocols was very low (0.3% or less of total cells) (Wu et al., 2018). A recent study developed a highly-efficient protocol that used a three-step CHIR treatment to generate a subset of SIX1$^+$/KDR$^+$/PECAM1$^+$ NPCs that contributed to new vessel formation in 3D hPSC-derived kidney organoids. VEGF-A secretion by differentiating podocytes within the organoid supported maturation of the newly formed ECs (Low et al., 2019). Some studies demonstrated that VEGF supplementation during the differentiation process resulted in a significant increase of ECs and a population of stromal cells that expressed the VEGF receptor, FLT1, and maturation and maintenance of organoid vasculature. However, many of these ECs have immature characteristics. These ECs fail to invade the developing podocytes (Czerniecki et al., 2018; Koning et al., 2018). Moreover, organoid transplantation into a highly vascularized site such as the sub-renal capsule and CAM facilitates both vascularization and maturation of organoids (Koning et al., 2018; Varzideh et al., 2018; Garreta et al., 2019; Low et al., 2019).

Microenvironmental Cues

Microenvironmental cues include biochemical and biophysical (oxygen tension, ECM stiffness, and fluid flow) signals during organogenesis regulate cell behavior of different stem cell populations (Vining and Mooney, 2017; Silva et al., 2019). The ECM of the kidney is a complex architectural network that contains collagens, elastin, and several proteoglycans and glycoproteins, which together form basal membranes and the interstitial space. In addition to its biochemical cues, these dynamic structures provide mechanical support and mediate the cell signaling pathways, which are essential for proper kidney development and function (Bülow and Boor, 2019).

Researchers have demonstrated that cells sense the ECM stiffness by mechanoreceptors such as integrins. Thus, the ECM plays a key role in the cell fate decision (Akkerman and Defize, 2017). ECM stiffness regulates differentiation into each germ layer (Zoldan et al., 2011). Researchers have sought to determine if the substrate matrix stiffness may affect self-organization and maturation of the organoids. Takebe and colleagues used a co-culture system by combining hPSC-derived tissue-specific progenitors with MSCs and ECs. This mixture was transferred onto Matrigel with varying degrees of stiffness. Data showed that self-condensation was promoted by soft environmental conditions ($E\sim$ 10 $\sim$ 20 kPa) in their 3D culture system (Takebe et al., 2015). Garreta and colleagues fabricated polyacrylamide hydrogels with varying mechanical properties (1–60 kPa). They investigated whether substrates with mechanical properties similar to native tissues such as CAM could improve organoid maturation. RNA-Seq analysis revealed that the soft substrate ($E\sim$1 kPa) improved the expressions of mesodermal lineage genes *T, PAX2, SALL1, LHX1*, and *Hoxd11*. These organoids had more mature features when compared with rigid conditions (Garreta et al., 2019).

Fluid flow is a mechanical force that plays a key role in the developmental process, including vascularization and differentiation (Ghaffari et al., 2015; Vining and Mooney, 2017). Homan et al. (2019) have investigated the effect of fluid shear stress (FSS) in vascularization and maturation of hPSCs-derived kidney organoids. hPSCs were differentiated into pretubular aggregate cells as previously reported (Morizane et al., 2015). They placed these aggregates onto a gelatin-fibrin (gelbrin) ECM layer within a 3D-printed millifluidic chip that was perfused under varying flow rates for 10 days. Their data showed that gelbrin increased expression of endothelial markers PECAM1 and MCAM. Under high FSS at differentiation day 21, they observed significantly enhanced expansion and differentiation of the KDR$^+$ and PECAM1$^+$ ECs with formation of perfusable vascular anastomosis between the organoids. As the organoid vasculature evolved, PDGFRβ$^+$ pericyte-like cells greatly increased in numbers and were recruited to the vascular network. Accordingly, endothelial-epithelial crosstalk increased the maturation of tubular and glomerular cells within the kidney organoids in comparison to static conditions (Homan et al., 2019).

CONCLUSION AND PERSPECTIVES

Major advances have been made in the understanding of various cellular components and intercellular signaling pathways involved in kidney development. The creation of kidney organoids from hPSCs by assessing the cells at each step of nephrogenesis has also expanded our knowledge of kidney development. Organoids can be generated following the same developmental events that occur in the embryo. Thus, consideration for cellular communications and microenvironmental cues in organoids can improve their complexity. Despite some significant improvements, there are difficult challenges that remain before this technology can be used in modern regenerative medicine. Until now, kidney organoids have been in a relatively immature state comparable to fetal nephrons. Moreover, kidney organoid vasculature is not fully mature, and their nascent ECs fail to invade the glomerular primordial. In the future, kidney organoids combined with recent biotechnological progresses such as microfluidic kidney-on-a-chip, co-culture systems, and 3D bioprinting technology have the potential to revolutionize developmental studies, drug screening, and personalized medicine.

AUTHOR CONTRIBUTIONS

NK contributed to the preparation of this manuscript for writing and conducting the literature review. RM and NA drafted the manuscript and revised it critically for all content.

ACKNOWLEDGMENTS

We would like to express our sincere appreciation to Prof. Hossein Baharvand for his scientific assistance and critical comments.

REFERENCES

Abrahamson, D. R., Robert, B., Hyink, D. P., St John, P. L., and Daniel, T. O. (1998). Origins and formation of microvasculature in the developing kidney. *Kidney Int. Suppl.* 67, S7–S11. doi: 10.1046/j.1523-1755.1998.06702.x

Ahmadi, A., Khoshdel Rad, N. K., Ezzatizadeh, V., and Moghadasali, R. (2019a). Kidney regeneration: stem cells as a new trend. *Curr. Stem Cell Res. Ther.* [E-pub ahead of print].

Ahmadi, A., Moghadasali, R., Ezzatizadeh, V., Taghizadeh, Z., Nasiri, S. M., Vostikolaee, M. A., et al. (2019b). Transplantation of mouse induced pluripotent stem cell-derived podocytes in a mouse model of membranous nephropathy attenuates proteinuria. *Sci. Rep.* 9:15467. doi: 10.1038/s41598-019-51770-0

Akkerman, N., and Defize, L. H. K. (2017). Prospects & overviews dawn of the organoid era. *Bioessays.* 39:1600244. doi: 10.1002/bies.201600244

Al-Awqati, Q. (2013). Cell biology of the intercalated cell in the kidney. *FEBS Lett.* 587, 1911–1914. doi: 10.1016/j.febslet.2013.05.007

Al-Awqati, Q., and Oliver, J. A. (2002). Stem cells in the kidney. *Kidney Int.* 61, 387–395. doi: 10.1046/j.1523-1755.2002.00164.x

Al-Awqati, Q., and Schwartz, G. J. (2004). A fork in the road of cell differentiation in the kidney tubule. *J. Clin. Invest.* 113, 1528–1530. doi: 10.1172/JCI200422029

Argao, E. A., Kern, M. J., Branford, W. W., Scott, W. J., and Potter, S. S. (1995). Malformations of the heart, kidney, palate, and skeleton in alpha-MHC-Hoxb-7 transgenic mice. *Mech. Dev.* 52, 291–303. doi: 10.1016/0925-4773(95)98114-P

Attia, L., Yelin, R., and Schultheiss, T. M. (2012). Analysis of nephric duct specification in the avian embryo. *Development* 139, 4143–4151. doi: 10.1242/dev.085258

Bagherie-lachidan, M., Reginensi, A., Pan, Q., Zaveri, H. P., Scott, D. A., Blencowe, B. J., et al. (2015). Stromal Fat4 acts non-autonomously with Dchs1/2 to restrict the nephron progenitor pool. *Development* 142, 2564–2573. doi: 10.1242/dev.122648

Bantounas, I., Ranjzad, P., Tengku, F., Silajdžić, E., Forster, D., Asselin, M. C., et al. (2018). Generation of functioning nephrons by implanting human pluripotent stem cell-derived kidney progenitors. *Stem Cell Rep.* 10, 766–779. doi: 10.1016/j.stemcr.2018.01.008

Blank, U., Brown, A., Adams, D. C., Karolak, M. J., and Oxburgh, L. (2009). BMP7 promotes proliferation of nephron progenitor cells via a JNK-dependent mechanism. *Development* 136, 3557–3566. doi: 10.1242/dev.036335

Bohnenpoll, T., Bettenhausen, E., Weiss, A. C., Foik, A. B., Trowe, M. O., Blank, P., et al. (2013). Tbx18 expression demarcates multipotent precursor populations in the developing urogenital system but is exclusively required within the ureteric mesenchymal lineage to suppress a renal stromal fate. *Dev. Biol.* 380, 25–36. doi: 10.1016/j.ydbio.2013.04.036

Boualia, S. K., Gaitan, Y., Tremblay, M., Sharma, R., Cardin, J., Kania, A., et al. (2013). A core transcriptional network composed of Pax2/8, Gata3 and Lim1 regulates key players of pro/mesonephros morphogenesis. *Dev. Biol.* 382, 555–566. doi: 10.1016/j.ydbio.2013.07.028

Bouchard, M., Souabni, A., Mandler, M., Neubüser, A., and Busslinger, M. (2002). Nephric lineage specification by Pax2 and Pax8. *Genes Dev.* 16, 2958–2970. doi: 10.1101/gad.240102

Bridgewater, D., Braunewell, K.-H., Perala, N., Immonen, T., Rosenblum, N. D., Chilov, D., et al. (2011). The GDNF target Vsnl1 marks the ureteric tip. *J. Am. Soc. Nephrol.* 22, 274–284. doi: 10.1681/asn.2010030316

Brodbeck, S., Besenbeck, B., and Englert, C. (2004). The transcription factor Six2 activates expression of the Gdnf gene as well as its own promoter. *Mech. Dev.* 121, 1211–1222. doi: 10.1016/j.mod.2004.05.019

Bronner-Fraser, M., and Fraser, S. (1988). Cell lineage analysis reveals multipotency of some avian neural crest cells. *Nature* 335, 161–164. doi: 10.1038/335161a0

Brooks, C. R., McNagny, K. M., Liu, Y., Jing, P., Kim, Y. K., Shankland, S. J., et al. (2017). Gene-edited human kidney organoids reveal mechanisms of disease in podocyte development. *Stem Cells* 35, 2366–2378. doi: 10.1002/stem.2707

Brophy, P. D., Lang, K. M., and Dressler, G. R. (2003). The secreted frizzled related protein 2 (SFRP2) gene is a target of the Pax2 transcription factor. *J. Biol. Chem.* 278, 52401–52405. doi: 10.1074/jbc.M305614200

Brophy, P. D., Ostrom, L., Lang, K. M., and Dressler, G. R. (2001). Regulation of ureteric bud outgrowth by Pax2-dependent activation of the glial derived neurotrophic factor gene. *Development* 128, 4747–4756. doi: 10.3410/f.1002321.26604

Brown, A. C., Adams, D., Caestecker, M., De Yang, X., Friesel, R., and Oxburgh, L. (2011). FGF/EGF signaling regulates the renewal of early nephron progenitors during embryonic development. *Development* 138, 5099–5112. doi: 10.1242/dev.065995

Brown, A. C., Muthukrishnan, S. D., Guay, J. A., Adams, D. C., Schafer, D. A., Fetting, J. L., et al. (2013). Role for compartmentalization in nephron progenitor differentiation. *Proc. Natl. Acad. Sci. U.S.A.* 110, 4640–4645. doi: 10.1073/pnas.1213971110

Bülow, R. D., and Boor, P. (2019). Extracellular matrix in kidney fibrosis: more than just a scaffold. *J. Histochem. Cytochem.* 67, 643–661. doi: 10.1369/0022155419849388

Cai, Q., Dmitrieva, N. I., Ferraris, J. D., Brooks, H. L., van Balkom, B. W. M., and Burg, M. (2005). Pax2 expression occurs in renal medullary epithelial cells in vivo and in cell culture, is osmoregulated, and promotes osmotic tolerance. *Proc. Natl. Acad. Sci. U.S.A.* 102, 503–508. doi: 10.1073/pnas.0408840102

Cain, J. E., Nion, T., Jeulin, D., and Bertram, J. F. (2005). Exogenous BMP-4 amplifies asymmetric ureteric branching in the developing mouse kidney in vitro. *Kidney Int.* 67, 420–431. doi: 10.1111/j.1523-1755.2005.67098.x

Cartry, J., Nichane, M., Ribes, V., Colas, A., Riou, J. F., Pieler, T., et al. (2006). Retinoic acid signalling is required for specification of pronephric cell fate. *Dev. Biol.* 299, 35–51. doi: 10.1016/j.ydbio.2006.06.047

Chen, Y. T., Kobayashi, A., Kwan, K. M., Johnson, R. L., and Behringer, R. R. (2006). Gene expression profiles in developing nephrons using Lim1 metanephric mesenchyme-specific conditional mutant mice. *BMC Nephrol.* 7:1. doi: 10.1186/1471-2369-7-1

Chung, E., Deacon, P., Marable, S., Shin, J., and Park, J. (2016). Notch signaling promotes nephrogenesis by downregulating Six2. *Development* 143, 3907–3913. doi: 10.1242/dev.143503

Chung, E., Deacon, P., and Park, J.-S. (2017). Notch is required for the formation of all nephron segments and primes nephron progenitors for differentiation. *Development* 144, 4530–4539. doi: 10.1242/dev.156661

Costantini, F., and Kopan, R. (2010). Patterning a complex organ: branching morphogenesis and nephron segmentation in kidney development. *Dev. Cell* 18, 698–712. doi: 10.1016/j.devcel.2010.04.008

Couillard, M., and Trudel, M. (2009). c-myc as a modulator of renal stem/progenitor cell population. *Dev. Dyn.* 238, 405–414. doi: 10.1002/dvdy.21841

Czerniecki, S. M., Cruz, N. M., Harder, J. L., Menon, R., Annis, J., Otto, E. A., et al. (2018). High-throughput screening enhances kidney organoid differentiation from human pluripotent stem cells and enables automated multidimensional phenotyping. *Cell Stem Cell* 22, 929–940.e4. doi: 10.1016/j.stem.2018.04.022

Daniel, E., and Cleaver, O. (2019). *Vascularizing Organogenesis: Lessons from Developmental Biology and Implications for Regenerative Medicine*, 1st Edn. Amsterdam: Elsevier Inc. doi: 10.1016/bs.ctdb.2018.12.012

Das, A., Tanigawa, S., Karner, C. M., Xin, M., Lum, L., Chen, C., et al. (2013). Stromal–epithelial crosstalk regulates kidney progenitor cell differentiation. *Nat. Cell Biol.* 15, 1035–1044. doi: 10.1038/ncb2828

Dressler, G. R., Deutsch, U., Chowdhury, K., Nornes, H. O., and Gruss, P. (1990). Pax2, a new murine paired-box-containing gene and its expression in the developing excretory system. *Development* 109, 787–795.

Dufourcq, P., Couffinhal, T., Ezan, J., Barandon, L., Moreau, C., Daret, D., et al. (2002). FrzA, a secreted frizzled related protein, induced angiogenic response. *Circulation* 106, 3097–3103. doi: 10.1161/01.CIR.0000039342.85015.5C

El-dahr, S. S., Li, Y., Liu, J., Gutierrez, E., Hering-smith, K. S., Signoretti, S., et al. (2017). p63 + ureteric bud tip cells are progenitors of intercalated cells. *JCI Insight* 2:e89996. doi: 10.1172/jci.insight.89996

Eremina, V. (2006). Vascular endothelial growth factor a signaling in the podocyte-endothelial compartment is required for mesangial cell migration and survival. *J. Am. Soc. Nephrol.* 17, 724–735. doi: 10.1681/asn.2005080810

Fanni, D., Fanos, V., Monga, G., Gerosa, C., Locci, A., Nemolato, S., et al. (2011). Expression of WT1 during normal human kidney development. *J. Matern. Fetal Neonatal Med.* 24(Suppl. 2), 44–47. doi: 10.3109/14767058.2011.606619

Fetting, J. L., Guay, J. A., Karolak, M. J., Iozzo, R. V., Adams, D. C., Maridas, D. E., et al. (2014). FOXD1 promotes nephron progenitor differentiation by repressing decorin in the embryonic kidney. *Development* 141, 17–27. doi: 10.1242/dev.089078

Fleming, B. M., Yelin, R., James, R. G., and Schultheiss, T. M. (2013). A role for Vg1/Nodal signaling in specification of the intermediate mesoderm. *Development* 140, 1819–1829. doi: 10.1242/dev.093740

Forbes, T. A., Howden, S. E., Lawlor, K., Phipson, B., Maksimovic, J., Hale, L., et al. (2018). Patient-iPSC-derived kidney organoids show functional validation of a ciliopathic renal phenotype and reveal underlying pathogenetic mechanisms. *Am. J. Hum. Genet.* 102, 816–831. doi: 10.1016/j.ajhg.2018.03.014

Gao, X. (2005). Angioblast-mesenchyme induction of early kidney development is mediated by Wt1 and Vegfa. *Development* 132, 5437–5449. doi: 10.1242/dev.02095

Garcia-Villalba, P., Heliot, C., Lokmane, L., Fabre, M., and Cereghini, S. (2009). vHNF1 functions in distinct regulatory circuits to control ureteric bud branching and early nephrogenesis. *Development* 137, 347–357. doi: 10.1242/dev.042226

Garreta, E., Prado, P., Tarantino, C., Oria, R., Fanlo, L., Martí, E., et al. (2019). Fine tuning the extracellular environment accelerates the derivation of kidney organoids from human pluripotent stem cells. *Nat. Mater.* 18, 397–405. doi: 10.1038/s41563-019-0287-6

Ghaffari, S., Leask, R. L., and Jones, E. A. V. (2015). Flow dynamics control the location of sprouting and direct elongation during developmental angiogenesis. *Development* 142, 4151–4157. doi: 10.1242/dev.128058

Gong, K.-Q., Yallowitz, A. R., Sun, H., Dressler, G. R., and Wellik, D. M. (2007). A Hox-Eya-Pax complex regulates early kidney developmental gene expression. *Mol. Cell. Biol.* 27, 7661–7668. doi: 10.1128/mcb.00465-07

Grieshammer, U., Ma, L., Plump, A. S., Wang, F., Tessier-Lavigne, M., and Martin, G. R. (2004). SLIT2-mediated ROBO2 signaling restricts kidney induction to a single site. *Dev. Cell* 6, 709–717. doi: 10.1016/S1534-5807(04)00108-X

Grote, D. (2005). Pax2/8-regulated Gata3 expression is necessary for morphogenesis and guidance of the nephric duct in the developing kidney. *Development* 133, 53–61. doi: 10.1242/dev.02184

Grote, D., Boualia, S. K., Souabni, A., Merkel, C., Chi, X., Costantini, F., et al. (2008). Gata3 acts downstream of β-catenin signaling to prevent ectopic metanephric kidney induction. *PLoS Genet.* 4:e1000316. doi: 10.1371/journal.pgen.1000316

Guillaume, R., Bressan, M., and Herzlinger, D. (2009). Paraxial mesoderm contributes stromal cells to the developing kidney. *Dev. Biol.* 329, 169–175. doi: 10.1016/j.ydbio.2009.02.034

Guo, Q., Wang, Y., Tripathi, P., Manda, K. R., Mukherjee, M., Chaklader, M., et al. (2015). Adam10 mediates the choice between principal cells and intercalated cells in the kidney. *J. Am. Soc. Nephrol.* 26, 149–159. doi: 10.1681/ASN.2013070764

Harder, J. L., Menon, R., Otto, E. A., Zhou, J., Eddy, S., Wys, N. L., et al. (2019). Organoid single cell profiling identifies a transcriptional signature of glomerular disease. *JCI Insight* 4:e122697. doi: 10.1172/jci.insight.122669

Hartwig, S., Ho, J., Pandey, P., Macisaac, K., Taglienti, M., Xiang, M., et al. (2010). Genomic characterization of Wilms ' tumor suppressor 1 targets in nephron progenitor cells during kidney development. *Development* 137, 1189–1203. doi: 10.1242/dev.045732

Hiratsuka, K., Monkawa, T., Akiyama, T., Nakatake, Y., Oda, M., Goparaju, S. K., et al. (2019). Induction of human pluripotent stem cells into kidney tissues by synthetic mRNAs encoding transcription factors. *Sci. Rep.* 9:913. doi: 10.1038/s41598-018-37485-8

Homan, K. A., Gupta, N., Kroll, K. T., Kolesky, D. B., Skylar-Scott, M., Miyoshi, T., et al. (2019). Flow-enhanced vascularization and maturation of kidney organoids in vitro. *Nat. Methods* 16, 255–262. doi: 10.1038/s41592-019-0325-y

Hu, M. C., and Rosenblum, N. D. (2005). Smad1, β -catenin and Tcf4 associate in a molecular complex with the Myc promoter in dysplastic renal tissue and cooperate to control Myc transcription. *Dev. Dis.* 132, 215–225. doi: 10.1242/dev.01573

Hurtado, R., Zewdu, R., Mtui, J., Liang, C., Aho, R., Kurylo, C., et al. (2015). Pbx1-dependent control of VMC differentiation kinetics underlies gross renal vascular patterning. *Development* 142, 2653–2664. doi: 10.1242/dev.124776

Iber, D., Lang, C., Menshykau, D., McMahon, A. P., Conrad, L., and Michos, O. (2019). Image-based modeling of kidney branching morphogenesis reveals GDNF-RET based Turing-type mechanism and pattern-modulating WNT11 feedback. *Nat. Commun.* 10, 239–252. doi: 10.1038/s41467-018-08212-8

James, R. G. (2006). Odd-skipped related 1 is required for development of the metanephric kidney and regulates formation and differentiation of kidney precursor cells. *Development* 133, 2995–3004. doi: 10.1242/dev.02442

James, R. G., and Schultheiss, T. M. (2005). Bmp signaling promotes intermediate mesoderm gene expression in a dose-dependent, cell-autonomous and translation-dependent manner. *Dev. Biol.* 288, 113–125. doi: 10.1016/j.ydbio.2005.09.025

Jeanpierre, C., Kopan, R., Bole-Feysot, C., Ornitz, D. M., Chen, S., Parisot, M., et al. (2012). FGF9 and FGF20 maintain the stemness of nephron progenitors in mice and man. *Dev. Cell* 22, 1191–1207. doi: 10.1016/j.devcel.2012.04.018

Jeong, H., Jeon, U. S., Koo, B., Kim, W., Im, S., Shin, J., et al. (2009). Inactivation of Notch signaling in the renal collecting duct causes nephrogenic diabetes insipidus in mice. *J. Clin. Invest.* 119, 3290–3300. doi: 10.1172/JCI38416.3290

Kann, M., Bae, E., Lenz, M. O., Li, L., Trannguyen, B., Schumacher, V. A., et al. (2015). WT1 targets Gas1 to maintain nephron progenitor cells by modulating FGF signals. *Development* 142, 1254–1266. doi: 10.1242/dev.119735

Karavanov, A. A., Karavanova, I., Perantoni, A., and Dawid, I. B. (1998). Expression pattern of the rat Lim-1 homeobox gene suggests a dual role during kidney development. *Int. J. Dev. Biol.* 42, 61–66.

Karihaloo, A., Karumanchi, S. A., Cantley, W. L., Venkatesha, S., Cantley, L. G., and Kale, S. (2005). Vascular endothelial growth factor induces branching morphogenesis/tubulogenesis in renal epithelial cells in a neuropilin-dependent fashion. *Mol. Cell. Biol.* 25, 7441–7448. doi: 10.1128/MCB.25.17.7441

Karner, C. M., Das, A., Ma, Z., Self, M., Chen, C., Lum, L., et al. (2011). Canonical Wnt9b signaling balances progenitor cell expansion and differentiation during kidney development. *Development* 138, 1247–1257. doi: 10.1242/dev.057646

Kobayashi, A., Kwan, K., Carroll, T. J., Mcmahon, A. P., Mendelsohn, C. L., and Behringer, R. R. (2005). Distinct and sequential tissue-specific activities of the LIM-class homeobox gene Lim1 for tubular morphogenesis during kidney development. *Development* 132, 2809–2823. doi: 10.1242/dev.01858

Kobayashi, A., Mugford, J. W., Krautzberger, A. M., Naiman, N., Liao, J., and Mcmahon, A. P. (2014). Identification of a multipotent self-renewing stromal progenitor population during mammalian kidney organogenesis. *Stem Cell Rep.* 3, 650–662. doi: 10.1016/j.stemcr.2014.08.008

Koning, M., Leuning, D. G., Vanslambrouck, J. M., van den Berg, C. W., Ritsma, L., Rabelink, T. J., et al. (2018). Renal subcapsular transplantation of PSC-derived kidney organoids induces Neo-vasculogenesis and significant glomerular and tubular maturation in vivo. *Stem Cell Rep.* 10, 751–765. doi: 10.1016/j.stemcr.2018.01.041

Kumar, S. V., Er, P. X., Lawlor, K. T., Motazedian, A., Scurr, M., Ghobrial, I., et al. (2019). Kidney micro-organoids in suspension culture as a scalable source of human pluripotent stem cell-derived kidney cells. *Development* 146:dev172361. doi: 10.1242/dev.172361

Levinson, R. S., Batourina, E., Choi, C., Vorontchikhina, M., Kitajewski, J., and Mendelsohn, C. L. (2005). Foxd1-dependent signals control cellularity in the renal capsule, a structure required for normal renal development. *Development* 132, 529–539. doi: 10.1242/dev.01604

Li, X., Oghi, K. A., Zhang, J., Krones, A., Bush, K. T., Glass, C. K., et al. (2003). Eya protein phosphatase activity regulates Six1–Dach–Eya transcriptional effects in mammalian organogenesis. *Nature* 426, 247–254. doi: 10.1038/nature02083

Licht, J. D., Basson, M. A., Wilson, P. D., Costantini, F. D., Simon, R., Akbulut, S., et al. (2005). Sprouty1 is a critical regulator of GDNF/RET-mediated kidney induction. *Dev. Cell* 8, 229–239. doi: 10.1016/j.devcel.2004.12.004

Lin, E. E., and Gomez, R. A. (2014). RBP-J in FOXD1 renal stromal progenitors is crucial for the proper development and assembly of the kidney vasculature and glomerular mesangial cells. *Am. J. Physiol. Renal Physiol.* 306, F249–F258. doi: 10.1152/ajprenal.00313.2013

Lindström, N. O., Carragher, N. O., and Hohenstein, P. (2015). The PI3K pathway balances self-renewal and differentiation of Nephron progenitor cells through β-catenin signaling. *Stem Cell Rep.* 4, 551–560. doi: 10.1016/j.stemcr.2015.01.021

Lindström, N. O., Guo, J., Kim, A. D., Tran, T., Guo, Q., Brandine, G. D. S., et al. (2018). Conserved and divergent features of mesenchymal progenitor cell types within the cortical nephrogenic niche of the human and mouse kidney. *J. Am. Soc. Nephrol.* 29, 806–824. doi: 10.1681/ASN.2017080890

Lopez-Rios, J., Naillat, F., Vainio, S., Michos, O., Zeller, R., Tiecke, E., et al. (2007). Reduction of BMP4 activity by gremlin 1 enables ureteric bud outgrowth and GDNF/WNT11 feedback signalling during kidney branching morphogenesis. *Development* 134, 2397–2405. doi: 10.1242/dev.02861

Low, J. H., Li, P., Guo, E., Chew, Y., Foo, J. N., Carlos, J., et al. (2019). Generation of human PSC-Derived Kidney Organoids with Patterned Nephron Segments and a De Novo Vascular Network. *Cell Stem Cell* 25, 373– 387.e9. doi: 10.1016/j.stem.2019.06.009

Majumdar, A. (2003). Wnt11 and Ret/Gdnf pathways cooperate in regulating ureteric branching during metanephric kidney development. *Development* 130, 3175–3185. doi: 10.1242/dev.00520

Mansoori-moghadam, Z., Totonchi, M., Hesaraki, M., Aghdami, N., Baharvand, H., and Moghadasali, R. (2019). Programming of ES cells and reprogramming of fibroblasts into renal lineage-like cells. *Exp. Cell Res.* 379, 225–234. doi: 10.1016/j.yexcr.2019.04.011

Mao, Y., Francis-West, P., and Irvine, K. D. (2015). Fat4/Dchs1 signaling between stromal and cap mesenchyme cells influences nephrogenesis and ureteric bud branching. *Development* 142, 2574–2585. doi: 10.1242/dev.122630

Marlier, A., Schmidt-ott, K. M., Gallagher, A., Barasch, J., and Karihaloo, A. (2008). Vegf as an epithelial cell morphogen modulates branching morphogenesis of embryonic kidney by directly acting on the ureteric bud. *Mech. Dev.* 126, 91–98. doi: 10.1016/j.mod.2008.12.003

Miyamoto, N., Yoshida, M., Kuratani, S., Matsuo, I., and Aizawa, S. (1997). Defects of urogenital development in mice lacking Emx2. *Development* 124, 1653–1664.

Miyoshi, T., Hiratsuka, K., Saiz, E. G., and Morizane, R. (2019). Kidney organoids in translational medicine: disease modeling and regenerative medicine. *Dev. Dyn.* 249, 34–45. doi: 10.1002/dvdy.22

Moens, C. B., and Selleri, L. (2006). Hox cofactors in vertebrate development. *Dev. Biol.* 291, 193–206. doi: 10.1016/j.ydbio.2005.10.032

Morizane, R., and Bonventre, J. V. (2017). Kidney organoids: a translational journey. *Trends Mol. Med.* 23, 246–263. doi: 10.1016/j.molmed.2017.01.001

Morizane, R., Lam, A. Q., Freedman, B. S., Kishi, S., Valerius, M. T., and Bonventre, J. V. (2015). Nephron organoids derived from human pluripotent stem cells model kidney development and injury. *Nat. Biotechnol.* 33, 1193–1200. doi: 10.1038/nbt.3392

Motamedi, F. J., Badro, D. A., Clarkson, M., Lecca, M. R., Bradford, S. T., Buske, F. A., et al. (2014). WT1 controls antagonistic FGF and BMP-pSMAD pathways in early renal progenitors. *Nat. Commun.* 5:4444. doi: 10.1038/ncomms5444

Mugford, J. W., Sipilä, P., Kobayashi, A., Behringer, R. R., and McMahon, A. P. (2008a). Hoxd11 specifies a program of metanephric kidney development within the intermediate mesoderm of the mouse embryo. *Dev. Biol.* 319, 396–405. doi: 10.1016/j.ydbio.2008.03.044

Mugford, J. W., Sipilä, P., Mcmahon, J. A., and Mcmahon, A. P. (2008b). Osr1 expression demarcates a multi-potent population of intermediate mesoderm that undergoes progressive restriction to an Osr1-dependent nephron progenitor compartment within the mammalian kidney. *Dev. Biol.* 324, 88–98. doi: 10.1016/j.ydbio.2008.09.010.Osr1

Mukherjee, E., Maringer, K. V., Papke, E., Bushnell, D. S., Schaefer, C. M., Kramann, R., et al. (2017). Endothelial markers expressing stromal cells are critical for kidney formation. *Am. J. Physiol. Renal Physiol.* 313, F611–F620. doi: 10.1152/ajprenal.00136.2017

Mundel, P., Huber, S., Schröppel, B., Schlöndorff, D., Horster, M., Kretzler, M., et al. (2003). Detection of multiple vascular endothelial growth factor splice isoforms in single glomerular podocytes. *Kidney Int.* 54, S159–S161. doi: 10.1046/j.1523-1755.1998.06733.x

Munro, D. A., Wineberg, Y., Tarnick, J., Vink, C. S., Li, Z., Pridans, C., et al. (2019). Macrophages restrict the nephrogenic field and promote endothelial connections during kidney development. *Elife* 8:e43271. doi: 10.7554/eLife.43271

Munro, D. A. D., Hohenstein, P., and Davies, J. A. (2017). Cycles of vascular plexus formation within the nephrogenic zone of the developing mouse kidney. *Sci. Rep.* 7:3273. doi: 10.1038/s41598-017-03808-4

Muthukrishnan, S. D., Yang, X., Friesel, R., and Oxburgh, L. (2015). Concurrent BMP7 and FGF9 signalling governs AP-1 function to promote self-renewal of nephron progenitor cells. *Nat. Commun.* 6:10027. doi: 10.1038/ncomms10027

Narlis, M., Grote, D., Gaitan, Y., Boualia, S. K., and Bouchard, M. (2007). Pax2 and Pax8 regulate branching morphogenesis and nephron differentiation in the developing kidney. *J. Am. Soc. Nephrol.* 18, 1121–1129. doi: 10.1681/ASN.2006070739

Nishimura, Y., Hsu, H. H., and Wang, P. C. (2016). Detection of initial angiogenesis from dorsal aorta into metanephroi and elucidation of its role in kidney development. *Regen. Ther.* 4, 27–35. doi: 10.1016/j.reth.2016.01.003

O'Brien, L. L., Combes, A. N., Short, K. M., Lindström, N. O., Whitney, P. H., Cullen-McEwen, L. A., et al. (2018). Wnt11 directs nephron progenitor polarity and motile behavior ultimately determining nephron endowment. *Elife* 7:e40392. doi: 10.7554/eLife.40392

Ohmori, T., Sharmin, S., Ogawa, M., Taguchi, A., Nishinakamura, R., Sasaki, H., et al. (2013). Redefining the in vivo origin of metanephric nephron progenitors enables generation of complex kidney structures from pluripotent stem cells. *Cell Stem Cell* 14, 53–67. doi: 10.1016/j.stem.2013.11.010

Ohmori, T., Tanigawa, S., Kaku, Y., and Fujimura, S. (2015). Sall1 in renal stromal progenitors non-cell autonomously restricts the excessive expansion of nephron progenitors. *Sci. Rep.* 5:15676. doi: 10.1038/srep15676

Ohuchi, H., Hori, Y., Yamasaki, M., Harada, H., Sekine, K., Kato, S., et al. (2000). FGF10 acts as a major ligand for FGF receptor 2 IIIb in mouse multi-organ development. *Biochem. Biophys. Res. Commun.* 277, 643–649. doi: 10.1006/bbrc.2000.3721

Osafune, K., Nishinakamura, R., and Komazaki, S. (2002). In vitro induction of the pronephric duct in *Xenopus* explants. *Dev. Growth Differ.* 44, 161–167. doi: 10.1046/j.1440-169x.2002.00631.x

Oxburgh, L., Brown, A. C., Muthukrishnan, S. D., and Fetting, J. L. (2014). Bone morphogenetic protein signaling in nephron progenitor cells. *Pediatr. Nephrol.* 29, 531–536. doi: 10.1007/s00467-013-2589-2

Pachnis, V., Mankoo, B., and Costantini, F. (1993). Expression of the c-ret proto-oncogene during mouse embryogenesis. *Development* 119, 1005–1017.

Park, J. S., Ma, W., O'Brien, L. L., Chung, E., Guo, J. J., Cheng, J. G., et al. (2012). Six2 and Wnt regulate self-renewal and commitment of nephron progenitors through shared gene regulatory networks. *Dev. Cell* 23, 637–651. doi: 10.1016/j.devcel.2012.07.008

Park, J.-S., Valerius, M. T., and McMahon, A. P. (2007). Wnt/beta-catenin signaling regulates nephron induction during mouse kidney development. *Development* 134, 2533–2539. doi: 10.1242/dev.006155

Paroly, S. S., Wang, F., Spraggon, L., Merregaert, J., Batourina, E., Tycko, B., et al. (2013). Stromal protein Ecm1 regulates ureteric bud patterning and branching. *PLoS One* 8:e84155. doi: 10.1371/journal.pone.0084155

Pärssinen, H. E., Koivunen, P., Sims-Lucas, S., Junttila, S. M., Saarela, U., Quaggin, S., et al. (2016). CD146 + cells are essential for kidney vasculature development. *Kidney Int.* 90, 311–324. doi: 10.1016/j.kint.2016.02.021

Patterson, L. T., Pembaur, M., and Potter, S. S. (2001). Hoxa11 and Hoxd11 regulate branching morphogenesis of the ureteric bud in the developing kidney. *Development* 128, 2153–2161.

Patterson, L. T., and Potter, S. S. (2004). Atlas of hox gene expression in the developing kidney. *Dev. Dyn.* 229, 771–779. doi: 10.1002/dvdy.10474

Pedersen, A., Skjong, C., and Shawlot, W. (2005). Lim1 is required for nephric duct extension and ureteric bud morphogenesis. *Dev. Biol.* 288, 571–581. doi: 10.1016/j.ydbio.2005.09.027

Pepicelli, C. V., Kispert, A., Rowitch, D. H., and McMahon, A. P. (1997). Rapid communication: GDNF induces branching and increased cell proliferation in the ureter of the mouse. *Dev. Biol.* 192, 193–198. doi: 10.1006/dbio.1997.8745

Piscione, T. D., and Rosenblum, N. D. (2002). The molecular control of renal branching morphogenesis: current knowledge and emerging insights. *Differentiation* 70, 227–246. doi: 10.1046/j.1432-0436.2002.700602.x

Potter, S. S., Hartman, H. A., Kwan, K. M., Behringer, R. R., and Patterson, L. T. (2007). Laser capture-microarray analysis of lim1 mutant kidney development. *Genesis* 45, 432–439. doi: 10.1002/dvg

Preger-Ben Noon, E., Barak, H., Guttmann-Raviv, N., and Reshef, R. (2009). Interplay between activin and hox genes determines the formation of the kidney morphogenetic field. *Development* 136, 1995–2004. doi: 10.1242/dev.035592

Qiao, J., Uzzo, R., Obara-Ishihara, T., Degenstein, L., Fuchs, E., and Herzlinger, D. (1999). FGF-7 modulates ureteric bud growth and nephron number in the developing kidney. *Development* 126, 547–554. doi: 10.1006/dbio.2000.9623

Ramalingam, H., Fessler, A. R., Das, A., Valerius, M. T., Basta, J., Robbins, L., et al. (2018). Disparate levels of beta-catenin activity determine nephron progenitor cell fate. *Dev. Biol.* 440, 13–21. doi: 10.1016/j.ydbio.2018.04.020

Ranghini, E. J., and Dressler, G. R. (2015). Evidence for intermediate mesoderm and kidney progenitor cell specification by Pax2 and PTIP dependent mechanisms. *Dev. Biol.* 399, 296–305. doi: 10.1016/j.ydbio.2015.01.005

Reidy, K. J., and Rosenblum, N. D. (2009). Cell and molecular biology of kidney development. *Semin. Nephrol.* 29, 321–337. doi: 10.1016/j.semnephrol.2009.03.009

Robert, B., John, L. S. T., and John, L. S. (2018). Evidence that embryonic are intrinsic, vasculogenic kidney cells expressing angioblasts flk-1. *Am. J. Physiol.* 271(3 Pt 2), F744–F753. doi: 10.1152/ajprenal.1996.271.3.F744

Roker, L. A., Nemri, K., and Yu, J. (2017). Wnt7b signaling from the ureteric bud epithelium regulates medullary capillary development. *J. Am. Soc. Nephrol.* 28, 250–259. doi: 10.1681/ASN.2015111205

Romagnani, P., Lasagni, L., and Remuzzi, G. (2013). Renal progenitors: an evolutionary conserved strategy for kidney regeneration. *Nat. Rev. Nephrol.* 9, 137–146. doi: 10.1038/nrneph.2012.290

Rowan, C. J., Li, W., Martirosyan, H., Erwood, S., Kim, Y., Sheybani-deloui, S., et al. (2018). Hedgehog-GLI signaling in Foxd1- positive stromal cells promotes nephrogenesis via TGFβ signaling. *Development* 145:dev159947. doi: 10.1242/dev.159947

Ryan, G., Steele-Perkins, V., Morris, J. F., Rauscher, F. J., and Dressler, G. R. (1995). Repression of Pax-2 by WT1 during normal kidney development. *Development* 121, 867–875.

Saburi, S., Hester, I., Fischer, E., Pontoglio, M., Eremina, V., Gessler, M., et al. (2008). Loss of Fat4 disrupts PCP signaling and oriented cell division and leads to cystic kidney disease. *Nat. Genet.* 40, 1010–1015. doi: 10.1038/ng.179

Saifudeen, Z., Liu, J., Dipp, S., Yao, X., Li, Y., Mclaughlin, N., et al. (2012). A p53-Pax2 pathway in kidney development: implications for nephrogenesis. *PLoS One* 7:e44869. doi: 10.1371/journal.pone.0044869

Sakurai, H., and Nigam, S. K. (2017). Transforming growth factor-beta selectively inhibits branching morphogenesis but not tubulogenesis. *Am. J. Physiol. Physiol.* 272, F139–F146. doi: 10.1152/ajprenal.1997.272.1.f139

Santoro, D., Caccamo, D., Lucisano, S., Buemi, M., Sebekova, K., Teta, D., et al. (2015). Interplay of Vitamin D, erythropoiesis, and the renin-angiotensin system. *Biomed Res. Int.* 2015:145828. doi: 10.1155/2015/145828

Schmidt-Ott, K. M., Chen, X., Paragas, N., Levinson, R. S., Mendelsohn, C. L., and Barasch, J. (2006). C-kit delineates a distinct domain of progenitors in the developing kidney. *Dev. Biol.* 299, 238–249. doi: 10.1016/j.ydbio.2006.07.026

Schmidt-ott, K. M., Yang, J., Chen, X., Wang, H., Paragas, N., Mori, K., et al. (1993). Novel regulators of kidney development from the tips of the ureteric bud. *J. Am. Soc. Nephrol.* 16, 1993–2002. doi: 10.1681/ASN.2004121127

Self, M., Lagutin, O. V., Bowling, B., Hendrix, J., Cai, Y., Dressler, G. R., et al. (2006). Six2 is required for suppression of nephrogenesis and progenitor renewal in the developing kidney. *EMBO J.* 25, 5214–5228. doi: 10.1038/sj.emboj.7601381

Sequeira-lopez, M. L. S., Lin, E. E., Li, M., Hu, Y., Sigmund, C. D., and Gomez, R. A. (2015). The earliest metanephric arteriolar progenitors and their role in kidney vascular development. *Am. J. Physiol. Regul. Integr. Comp. Physiol.* 308, R138–R150. doi: 10.1152/ajpregu.00428.2014

Shakya, R., Wu, Z., Costantini, F., D'Agati, V., Burke, R., Kholodilov, N., et al. (2005). The role of GDNF in patterning the excretory system. *Dev. Biol.* 283, 70–84. doi: 10.1016/j.ydbio.2005.04.008

Siedlecki, A. M., Lerou, P. H., Valerius, M. T., McNagny, K. M., Lam, A. Q., Musunuru, K., et al. (2015). Modelling kidney disease with CRISPR-mutant kidney organoids derived from human pluripotent epiblast spheroids. *Nat. Commun.* 6:8715. doi: 10.1038/ncomms9715

Silva, T. P., Cotovio, J. P., Bekman, E., Carmo-fonseca, M., Cabral, J. M. S., and Fernandes, T. G. (2019). Design principles for pluripotent stem cell-derived organoid engineering. *Stem Cells Int.* 2019:4508470. doi: 10.1155/2019/4508470

Sims-lucas, S., Schaefer, C., Bushnell, D., Ho, J., and Logar, A. (2013). Endothelial progenitors exist within the kidney and lung mesenchyme. *PLoS One* 8:e659938. doi: 10.1371/journal.pone.0065993

Srinivas, S., Watanabe, T., Goldberg, M. R., D'Agati, V., Al-Awqati, Q., and Costantini, F. (1999). Expression of green fluorescent protein in the ureteric bud of transgenic mice: a new tool for the analysis of ureteric bud morphogenesis. *Dev. Genet.* 24, 241–251. doi: 10.1002/(SICI)1520-6408199924

Taguchi, A., Kaku, Y., Ohmori, T., Sharmin, S., Ogawa, M., Sasaki, H., et al. (2014). Redefining the in vivo origin of metanephric nephron progenitors enables generation of complex kidney structures from pluripotent stem cells. *Cell Stem Cell* 14, 53–67. doi: 10.1016/j.stem.2013.11.010

Taguchi, A., and Nishinakamura, R. (2017). Higher-order kidney organogenesis from pluripotent stem cells. *Cell Stem Cell* 21, 730–746.e6. doi: 10.1016/j.stem.2017.10.011

Takahashi, Y., Takebe, T., and Taniguchi, H. (2018). Methods for generating vascularized islet-like organoids via self-condensation. *Curr. Protoc. Stem Cell Biol.* 45:e49. doi: 10.1002/c.49

Takasato, M., Er, P. X., Chiu, H. S., and Little, M. H. (2016). Generation of kidney organoids from human pluripotent stem cells. *Nat. Protoc.* 11, 1681–1692. doi: 10.1038/nprot.2016.098

Takasato, M., Er, P. X., Chiu, H. S., Maier, B., Baillie, G. J., Ferguson, C., et al. (2015). Kidney organoids from human iPS cells contain multiple lineages and model human nephrogenesis. *Nature* 526, 564–568. doi: 10.1038/nature15695

Takasato, M., and Little, M. H. (2015). The origin of the mammalian kidney: implications for recreating the kidney in vitro. *Development* 142, 1937–1947. doi: 10.1242/dev.104802

Takebe, T., Enomura, M., Yoshizawa, E., Kimura, M., Koike, H., and Ueno, Y. (2015). Vascularized and complex organ buds from diverse short article vascularized and complex organ buds from diverse tissues via mesenchymal cell-driven condensation. *Cell Stem Cell* 16, 556–565. doi: 10.1016/j.stem.2015.03.004

Takebe, T., Sekine, K., Kimura, M., Yoshizawa, E., Ayano, S., Koido, M., et al. (2017). Massive and reproducible production of liver buds entirely from human

pluripotent stem cells report massive and reproducible production of liver buds entirely from human pluripotent stem cells. *Cell Rep.* 21, 2661–2670. doi: 10.1016/j.celrep.2017.11.005

Takebe, T., Zhang, R., Koike, H., Kimura, M., Yoshizawa, E., Enomura, M., et al. (2014). Generation of a vascularized and functional human liver from an iPSC-derived organ bud transplant. *Nat. Protoc.* 9, 396–409. doi: 10.1038/nprot.2014.020

Tanigawa, S., Wang, H., Yang, Y., Sharma, N., Tarasova, N., Ajima, R., et al. (2011). Wnt4 induces nephronic tubules in metanephric mesenchyme by a non-canonical mechanism. *Dev. Biol.* 352, 58–69. doi: 10.1016/j.ydbio.2011.01.012

Tomar, R., Mudumana, S. P., Pathak, N., Hukriede, N. A., and Drummond, I. A. (2014). osr1 is required for podocyte development downstream of wt1a. *J. Am. Soc. Nephrol.* 25, 2539–2545. doi: 10.1681/ASN.2013121327

Torban, E., Dziarmaga, A., Iglesias, D., Chu, L. L., Vassilieva, T., Little, M., et al. (2006). PAX2 activates WNT4 expression during mammalian kidney development. *J. Biol. Chem.* 281, 12705–12712. doi: 10.1074/jbc.M513181200

Tsang, T. E., Shawlot, W., Kinder, S. J., Kobayashi, A., Kwan, K. M., Schughart, K., et al. (2000). Lim1 activity is required for intermediate mesoderm differentiation in the mouse embryo. *Dev. Biol.* 223, 77–90. doi: 10.1006/dbio.2000.9733

Tufro, A., Teichman, J., Banu, N., and Villegas, G. (2007). Crosstalk between VEGF-A/VEGFR2 and GDNF/RET signaling pathways. *Biochem. Biophys. Res. Commun.* 358, 410–416. doi: 10.1016/j.bbrc.2007.04.146

Valerius, M. T., and McMahon, A. P. (2008). Transcriptional profiling of Wnt4 mutant mouse kidneys identifies genes expressed during nephron formation. *Gene Expr. Patterns* 8, 297–306. doi: 10.1016/j.gep.2008.02.001

Varzideh, F., Pahlavan, S., Ansari, H., Halvaei, M., and Kostin, S. (2018). Human cardiomyocytes undergo enhanced maturation in embryonic stem cell-derived organoid transplants. *Biomaterials* 192, 537–550. doi: 10.1016/j.biomaterials.2018.11.033

Vidarsson, H., Westergren, R., Heglind, M., Blomqvist, S. R., Breton, S., and Enerbäck, S. (2009). The forkhead transcription factor Foxi1 is a master regulator of vacuolar H+-ATPase proton pump subunits in the inner ear, kidney and epididymis. *PLoS One* 4:e4471. doi: 10.1371/journal.pone.0004471

Vining, K. H., and Mooney, D. J. (2017). Mechanical forces direct stem behaviour in development and cell regeneration. *Nat. Rev. Mol. Cell Biol.* 18, 728–742. doi: 10.1038/nrm.2017.108

Walker, K. A., Sims-lucas, S., and Bates, C. M. (2017). Fibroblast growth factor receptor signaling in kidney and lower urinary tract development. *Pediatr. Nephrol.* 31, 885–895. doi: 10.1007/s00467-015-3151-1

Wellik, D. M., Hawkes, P. J., and Capecchi, M. R. (2002). Hox11 paralogous genes are essential for metanephric kidney induction. *Genes Dev.* 16, 1423–1432. doi: 10.1101/gad.993302

Wilhelm, D., Combes, A. N., Koopman, P., Wainwright, E. N., and Little, M. H. (2015). ROBO2 restricts the nephrogenic field and regulates Wolffian duct–nephrogenic cord separation. *Dev. Biol.* 404, 88–102. doi: 10.1016/j.ydbio.2015.05.023

Wingert, R. A., Selleck, R., Yu, J., Song, H. D., Chen, Z., Song, A., et al. (2007). The cdx genes and retinoic acid control the positioning and segmentation of the zebrafish pronephros. *PLoS Genet.* 3:e189. doi: 10.1371/journal.pgen.0030189

Wu, H., Uchimura, K., Donnelly, E. L., Kirita, Y., Morris, S. A., and Humphreys, B. D. (2018). Comparative analysis and refinement of human PSC-derived kidney organoid differentiation with single-cell transcriptomics. *Cell Stem Cell* 23, 869–881.e8. doi: 10.1016/j.stem.2018.10.010

Xu, J., Liu, H., Chai, O. H., Lan, Y., and Jiang, R. (2016). Osr1 interacts synergistically with Wt1 to regulate kidney organogenesis. *PLoS One* 11:e0159597. doi: 10.1371/journal.pone.0159597

Xu, J., Liu, H., Park, J.-S., Lan, Y., and Jiang, R. (2014). Osr1 acts downstream of and interacts synergistically with Six2 to maintain nephron progenitor cells during kidney organogenesis. *Development* 141, 1442–1452. doi: 10.1242/dev.103283

Xu, J., Wong, E. Y. M., Cheng, C., Li, J., Sharkar, M. T. K., Xu, C. Y., et al. (2015). Eya1 interacts with Six2 and Myc to regulate expansion of the nephron progenitor pool during nephrogenesis. *Dev. Cell* 31, 434–447. doi: 10.1016/j.devcel.2014.10.015

Yallowitz, A. R., Hrycaj, S. M., Short, K. M., Smyth, I. M., and Wellik, D. M. (2011). Hox10 genes function in kidney development in the differentiation and integration of the cortical stroma. *PLoS One* 6:e23410. doi: 10.1371/journal.pone.0023410

Yamamoto, T., Taguchi, A., and Nishinakamura, R. (2019). Activin is superior to BMP7 for efficient maintenance of human iPSC-derived nephron progenitors. *Stem Cell Rep.* 13, 322–337. doi: 10.1016/j.stemcr.2019.07.003

Yoshino, K., Rubin, J. S., Higinbotham, K. G., Aykut, U., Anest, V., Plisov, S. Y., et al. (2002). Secreted frizzled-related proteins can regulate metanephric development. *Mech. Dev.* 102, 45–55. doi: 10.1016/s0925-4773(01)00282-9

Yuri, S., Nishikawa, M., Yanagawa, N., and Jo, O. D. (2015). Maintenance of mouse nephron progenitor cells in aggregates with gamma-secretase inhibitor. *PLoS One* 10:e0129242. doi: 10.1371/journal.pone.0129242

Zoldan, J., Karagiannis, E. D., Lee, C. Y., Anderson, D. G., Langer, R., and Levenberg, S. (2011). The influence of scaffold elasticity on germ layer specification of human embryonic stem cells. *Biomaterials* 32, 9612–9621. doi: 10.1016/j.biomaterials.2011.09.012

Conflict of Interest: The authors declare that the research was conducted in the absence of any commercial or financial relationships that could be construed as a potential conflict of interest.

frontiers in Cell and Developmental Biology

ORIGINAL RESEARCH
published: 14 May 2020
doi: 10.3389/fcell.2020.00304

Urine Sample-Derived Cerebral Organoids Suitable for Studying Neurodevelopment and Pharmacological Responses

*Victor J. T. Lin, Jiangnan Hu, Ashwini Zolekar, Liang-Jun Yan and Yu-Chieh Wang**

Department of Pharmaceutical Sciences, UNT System College of Pharmacy, University of North Texas Health Science Center, Fort Worth, TX, United States

Cerebral organoids (COs) developed from human induced pluripotent stem cells (hiPSCs) have been noticed for their potential in research and clinical applications. While skin fibroblast-derived hiPSCs are proficient at forming COs, the cellular and molecular features of COs developed using hiPSCs generated from other somatic cells have not been systematically examined. Urinary epithelial cells (UECs) isolated from human urine samples are somatic cells that can be non-invasively collected from most individuals. In this work, we streamlined the production of COs using hiPSCs reprogrammed from urine sample-derived UECs. UEC-derived hiPSC-developed COs presented a robust capacity for neurogenesis and astrogliogenesis. Although UEC-derived hiPSCs required specific protocol optimization to properly form COs, the cellular and transcriptomic features of COs developed from UEC-derived hiPSCs were comparable to those of COs developed from embryonic stem cells. UEC-derived hiPSC-developed COs that were initially committed to forebrain development showed cellular plasticity to transition between prosencephalic and rhombencephalic fates *in vitro* and *in vivo*, indicating their potential to develop into the cell components of various brain regions. The opposite regulation of AKT activity and neural differentiation was found in these COs treated with AKT and PTEN inhibitors. Overall, our data reveal the suitability, advantage, and possible limitations of human urine sample-derived COs for studying neurodevelopment and pharmacological responses.

Keywords: urinary epithelial cells, hiPSCs, hESCs, neurodevelopment, cerebral organoids

OPEN ACCESS

Edited by:
Eumorphia Remboutsika, National and Kapodistrian University of Athens, Greece

Reviewed by:
Elisa Cimetta, University of Padova, Italy
Panagiotis Politis, Biomedical Research Foundation of the Academy of Athens (BRFAA), Greece

***Correspondence:**
Yu-Chieh Wang
yu-chieh.wang@unthsc.edu

Specialty section:
This article was submitted to Stem Cell Research, a section of the journal Frontiers in Cell and Developmental Biology

Received: *21 December 2019*
Accepted: *07 April 2020*
Published: *14 May 2020*

Citation:
Lin VJT, Hu J, Zolekar A, Yan L-J and Wang Y-C (2020) Urine Sample-Derived Cerebral Organoids Suitable for Studying Neurodevelopment and Pharmacological Responses. Front. Cell Dev. Biol. 8:304. doi: 10.3389/fcell.2020.00304

INTRODUCTION

Recent progress in stem cell research and culture techniques has enabled human organoid models that better mimic the development, structure, and function of human organs (Huch et al., 2017; Rossi et al., 2018; Takahashi, 2019). In particular, human cerebral organoids (COs) offer exciting opportunities to mechanistically investigate brain development and pathogenesis in human cell-based, self-organized, and defined conditions (Lancaster et al., 2013; Quadrato and Arlotta, 2017; Arlotta, 2018).

Human pluripotent stem cells (hPSCs), including human embryonic stem cells (hESCs) and induced pluripotent stem cells (hiPSCs), are often used as starting materials to generate COs.

Many recent studies have leveraged COs and made important discoveries regarding developmental biology, disease mechanisms, and pharmacological responses in the central nervous system (Lancaster et al., 2013; Pasca et al., 2015; Bershteyn et al., 2017; Dakic et al., 2017; Lee et al., 2017; Quadrato et al., 2017; Watanabe et al., 2017; Trujillo and Muotri, 2018; Kanton et al., 2019; Pollen et al., 2019; Velasco et al., 2019; Zhang et al., 2019). Transcriptomic profiling has revealed that cortical cells generated in human COs use gene expression programs highly similar to those of the human fetal neocortex to organize into cerebral cortex-like regions (Camp et al., 2015). This similarity highlights the suitability of COs for studying the molecular and cellular features of human cortical development at an early stage. Although hiPSCs reprogrammed from dermal fibroblasts can develop into COs as revealed by many studies (Lancaster et al., 2013; Bershteyn et al., 2017; Velasco et al., 2019; Xu et al., 2019; Zhang et al., 2019), the capacity of hiPSCs reprogrammed from other somatic cells to generate COs has not been systematically characterized.

Many types of somatic cells, including dermal fibroblasts, peripheral blood mononuclear cells, hair follicle keratinocytes, and urinary epithelial cells (UECs), have been used in cell reprogramming to acquire hiPSCs (Takahashi et al., 2007; Zhou et al., 2012; Streckfuss-Bomeke et al., 2013; Wen et al., 2016). Among them, UECs can be harvested from an individual's urine samples that represent a non-invasive source for obtaining human somatic cells. A major advantage of using urine samples to acquire UECs for cell reprogramming is that procedures for urine collection could be easily applied to virtually all individuals and may be performed by personnel without advanced training. In effect, harvesting somatic cells from this sample source can be achieved in any cohort with minimal concerns. Thus, COs generated using urine sample-derived hiPSCs would be a highly useful platform for studying human disease such as genetic disorders that involve brain developmental defects.

Here, we streamlined the production of COs using hiPSCs reprogrammed from urine sample-derived UECs as well as characterized the cellular and molecular features of these COs during development and in response to the treatment of small molecules. Our results indicate that urine samples are highly practical biospecimens to enable the generation of personalized COs. Viable and reprogrammable human UECs can be readily isolated using centrifugation-based and filtration-based methods. COs developed from the UEC-derived hiPSCs with a normal karyotype highly resemble COs developed from normal hESCs that have shown a robust capacity for neurogenesis and CO formation in this and previous studies (Lancaster et al., 2013; Renner et al., 2017). In addition, COs that were developed from the UEC-derived hiPSCs and initially committed to forebrain development present cellular plasticity for the induced transition from a prosencephalic fate into a mesencephalic or rhombencephalic fate. Upon transplantation into the mouse brain, the COs develop distinctively in response to the different transplanted regions.

Although UEC-derived hiPSCs may have intrinsic features that require specific protocol optimization for the successful production of COs, UEC-derived hiPSC-developed COs are similar to hESC-developed COs at cellular and molecular levels. The versatility of urine sample-derived COs as a useful model for the investigation of neurodevelopment and pharmacological responses *in vitro* and *in vivo* is also revealed in our work.

RESULTS

Urine Sample-Derived hiPSCs With Cellular and Molecular Features Similar to WA09 hESCs

In contrast to fibroblasts isolated from skin-biopsy samples, UECs isolated from human urine samples can be readily obtained from a completely non-invasive procedure. From the collection of 200–400 ml urine from each individual (**Figure 1A**), we established primary cultures of UECs from different human subjects. Viable UECs (**Figure 1B**) can be obtained from the samples through either centrifugation-based or filtration-based isolation. To gauge how long a urine sample may be preserved without affecting the viability of isolated UECs, we tested cell isolation in urine samples stored under various conditions. As expected, the freshly collected samples (samples subjected to cell isolation within 20 min of post-collection) gave rise to the most viable, proliferative UEC colonies in culture. The prolonged storage of urine samples at room temperature largely diminished the viability of isolated UECs (**Figure 1C**). Although the number of cell colonies from the urine kept at 4°C was also reduced due to prolonged storage, the low-temperature condition partially preserved the viability of UECs in urine up to 48 h (**Figure 1C**). While failing to obtain any colony from urine samples stored for 72 h in all the tested conditions, our results indicate the feasibility of applying this sample-collection method to harvesting viable cells from individuals in different geographic locations that require a short period of sample storage and/or transportation prior to cell isolation. For filtration-based isolation, we filtered urine samples using sterilized membranes made of different materials. By directly culturing cells that remained on the filter membranes, the isolation of proliferative UECs was achievable using polycarbonate (PC) membranes with a pore size of 10 μm (**Figure 1D**).

Morphological heterogeneity was frequently seen in cells isolated from urine. This heterogeneity was observed even in the cells derived from the same individual (**Figure 1E**), indicating that distinct cell types may exist in each collection of urine samples. Although we cannot pinpoint which type(s) of cells from each urine sample was reprogrammed and gave rise to hiPSCs, regardless of the UEC heterogeneity, we have obtained hPSC-like cells from four different individuals by cell reprogramming with retrovirus-mediated delivery of POU5F1, SOX2, KLF4, and MYC. Similar to WA09 hESCs and UEC715i-501 hiPSCs that were generated by Sendai virus-mediated reprogramming in the UECs from another individual, the feeder-free cultures of UEC001i-009 and UEC001i-010 hiPSCs had typical hPSC morphology (**Figure 2A**) and a normal karyotype (**Figure 2B**). These UEC-derived hiPSCs expressed multiple biomarkers for cellular pluripotency (**Figure 2C**). Like WA09 hESCs, the

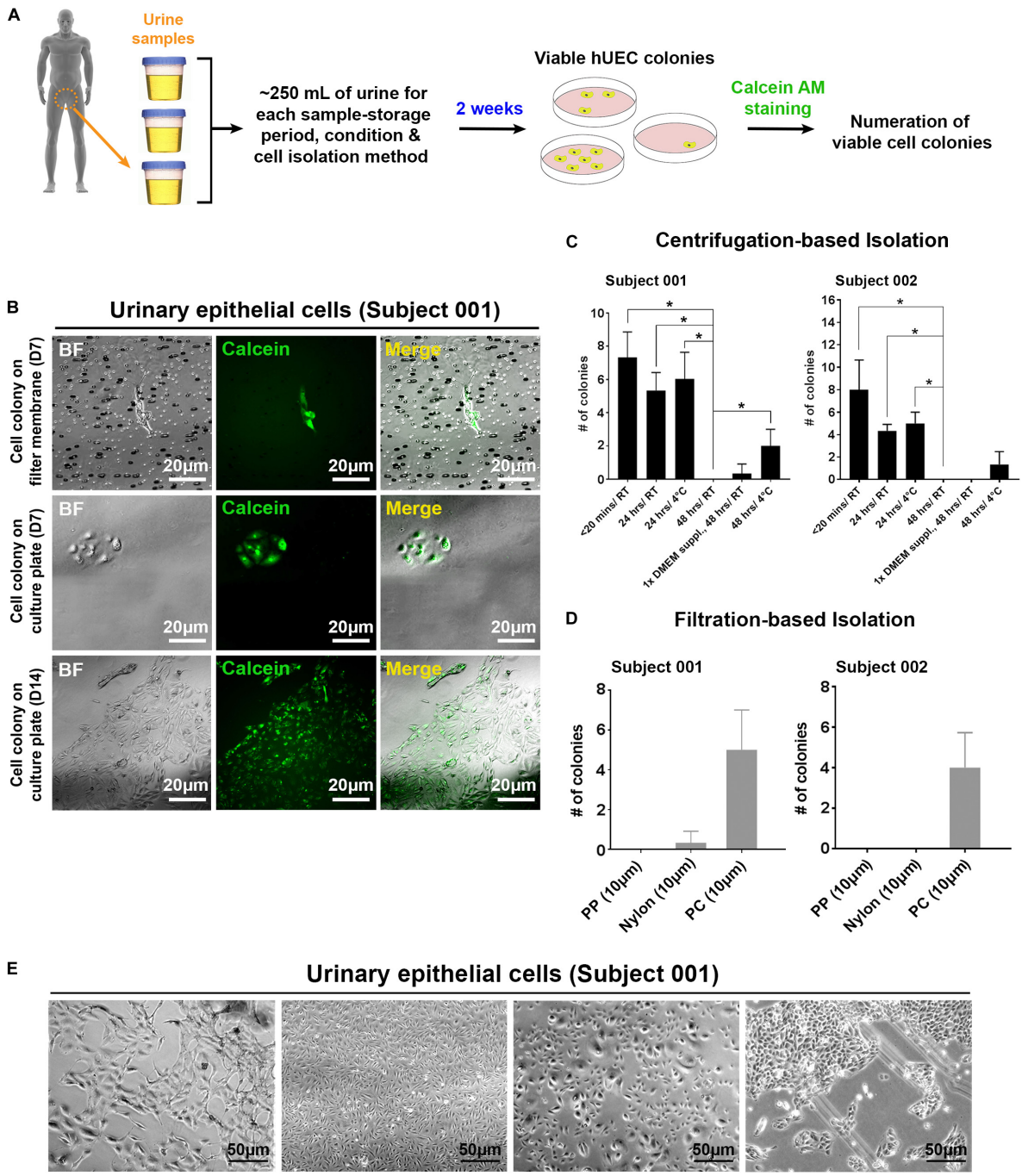

FIGURE 1 | The isolation of proliferative UECs from human urine samples by centrifugation and filtering approaches. **(A)** A schematic illustration of the procedure to isolate UECs from human urine samples. **(B)** Proliferative UECs isolated from two human subjects. **(C)** The efficiencies of UEC isolation in urine samples from the two subjects preserved under the indicated conditions prior to centrifugation (mean ± SD; $n = 3$, $^*p < 0.05$, t-test). 1× DMEM suppl: 10× DMEM spiked into urine sample at the final concentration of 10%. **(D)** The efficiencies of UEC isolation in urine samples from the two subjects using the filtration-based approach with filter membranes (pore size: 10 μm) made of distinct materials (mean ± SD; $n = 3$). PP: polypropylene. PC: polycarbonate. **(E)** The morphological features of different UEC subpopulations isolated from the subject 001.

UEC-derived hiPSCs formed embryoid bodies (EBs) that contain cells belonging to three-germ-layer lineages (**Figures 2D,E**). When they were examined by the PluriTest (Muller et al., 2011), similar to WA09 hESCs, all the tested UEC-derived hiPSCs showed transcriptomic features unique to other *bona fide* hPSCs samples (**Figure 2F**). The expression levels of POU5F1 and NANOG in the UEC-derived hiPSCs were comparable to those in WA09 hESCs (**Figure 2G**). These data demonstrated that,

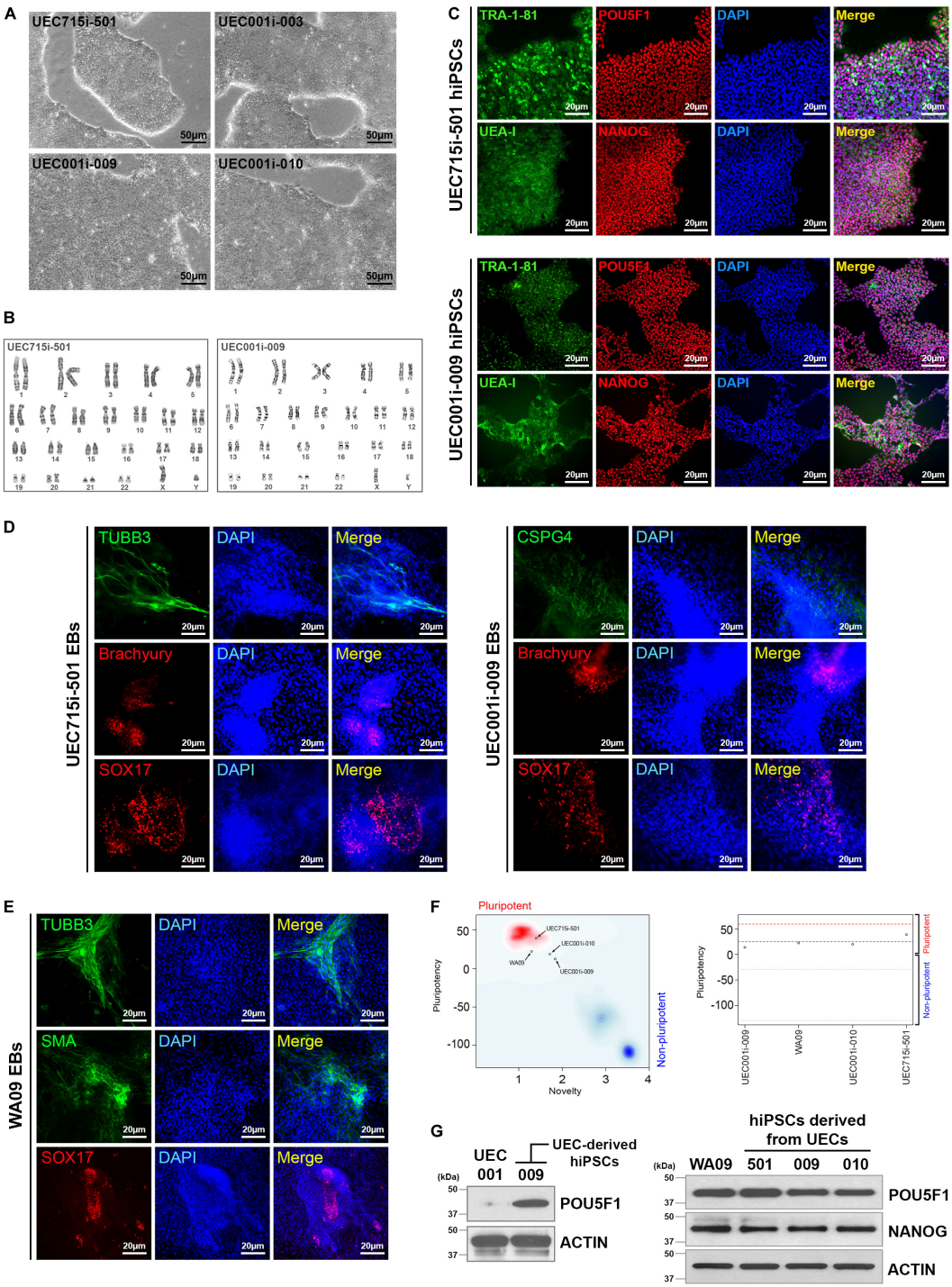

FIGURE 2 | Normal hiPSCs established by cell reprogramming in UECs isolated from urine samples. **(A)** The pluripotent cell morphology of UEC-derived hiPSCs. UEC715i-501 hiPSCs were generated using a Sendai virus-mediated, non-integrative reprogramming method. UEC001i-003, UEC001i-009, and UEC001i-010 hiPSCs were generated using retrovirus-mediated delivery of expression vectors for transcription factors POU5F1, SOX2, KLF4, and MYC. **(B)** UEC715i-501 and UEC001i-009 hiPSCs (passage numbers 19 and 16, respectively) showed apparently normal karyotypes (46, XY). **(C)** The UEC-derived hiPSCs were positive of cellular pluripotency markers TRA-1-81, UEA-I, POU5F1, and NANOG. **(D)** UEC-derived hiPSCs formed embryoid bodies (EBs) containing cells relevant to all three germ-layer lineages. TUBB3 and CSPG4: ectoderm. Brachyury: mesoderm. SOX17: endoderm. **(E)** WA09 hESCs used in this study also formed EBs containing cells relevant to all three germ-layer lineages. TUBB3 and CSPG4: ectoderm. SMA: mesoderm. SOX17: endoderm. **(F)** The Pluritest results of undifferentiated WA09 hESCs and UEC-derived hiPSCs revealed that their transcriptomic features are highly similar to those of the pluripotent samples included in the Pluritest database. **(G)** POU5F1 and NANOG were expressed similarly in undifferentiated WA09, UEC715i-501, UEC001i-003, UEC001i-009, UEC001i-010 cells. UEC001: proliferative UECs isolated from the subject 001.

regardless of cell reprogramming methods, hiPSCs similar to WA09 hESCs can be generated using UECs collected from different individuals.

COs Developed From Urine Sample-Derived hiPSCs

WA09 hESC-derived COs have been used in several studies (Lancaster et al., 2013; Camp et al., 2015; Renner et al., 2017; Watanabe et al., 2017; Matsui et al., 2018; Kanton et al., 2019). Because the capacity of WA09 hESCs to form COs was previously confirmed and characterized, we used WA09 hESCs as a standard to compare against UEC-derived hiPSCs for organoid formation.

Based on the protocol illustrated in **Figure 3A**, we reproducibly developed COs from undifferentiated WA09 hESCs. Despite minor variations, most WA09 cell aggregates gave rise to compact spheroids (**Figure 3B**) in response to suspension culture for 6 days in an FGF2-free neural induction medium that contains 10 μM SB431542 (a TGFβ receptor inhibitor) and 3 μM IWR-1-endo (an AXIN1/2 stabilizer). The structure of these cell spheroids often remained densely packed with a clear and smooth border before their transition into the N2-containing differentiation medium I for an additional culture period of 6–7 days, where the cells were further committed to the neuroectoderm lineage and continued developing into healthy spheres with translucent outer layers of neuroepithelial cells prior to matrigel embedding (**Figure 3B**). Most of the WA09 neuroepithelial spheres embedded in matrigel droplets kept developing in the N2/B27-containing differentiation medium II and retinoic acid (RA)-containing differentiation medium III to allow neurogenesis, gliogenesis, and neural cell maturation. Along this process, the neuroepithelial cell layers continued to enlarge, invaginate, and form crest-like structures. Similar morphological changes were observed during CO development initiated using the neural induction medium that contains 0.1 μM LDN193189 (a BMP receptor inhibitor) and 0.5 μM A83-01 (an ALK4/5/7 inhibitor) for dual SMAD inhibition in WA09 hESC aggregates (**Figures 3C,D**).

While the aggregates of UEC001i-009, UEC001i-010, and UEC715i-501 hiPSCs developed into multicellular structures that were morphologically similar to the WA09 neuroepithelial spheres (**Figure 3D** and **Supplementary Figure S1**) in the LDN193189/A83-01-containing induction medium, most UEC-derived hiPSC aggregates cultured in the SB431542/IWR-1-containing induction medium developed into neuroepithelial spheres with poor structural stability (**Figure 3B** and **Supplementary Figure S1**). When matrigel embedding was attempted with the defective spheres, they often failed to continuously develop (**Figure 3B**). These findings suggest that, though capable of CO formation, UEC-derived hiPSCs appear to have unique intrinsic features that require specific treatment for the successful development of COs.

Neural Cells in COs Developed From Urine Sample-Derived hiPSCs

As shown in **Figure 4**, multiple types of cells indicated by the expression of distinct markers were found in COs developed from the UEC-derived hiPSCs. The major cell types found in these COs included cells that express neural progenitor markers (SOX2, p-VIM, TBR2, OTX2, and HOPX), neuronal markers (TUBB3, DCX, TBR1, BCL11B, and SATB2), and an astroglial marker (GFAP). Different types of cells showed their unique distribution and organization that resemble specific layers and anatomical structures, which can be seen in the developing brain. In addition, the pervasive presence of FOXG1-positive cells in these COs indicated that they were committed to the development of the telencephalon-like tissue. By monitoring the presence of TUBB3 + and GFAP + cells in the samples collected at different time points (**Supplementary Figure S2**), we confirmed that astrogliogenesis followed neurogenesis in the COs developed from UEC-derived hiPSCs, resembling the temporal sequence of normal cortical development in mammals (Sauvageot and Stiles, 2002).

Array-based transcriptomic profiling followed by non-supervised clustering analysis revealed that, despite some variations in COs formed by UEC-derived hiPSCs and WA09 hESCs at the early stage (day 6 to day 40) of development, the gene expression profiles of the hESC- and hiPSC-developed COs were highly similar after 80 days of development and segregated away from those of the undifferentiated hPSCs (**Figure 5A**). Gene ontology and pathway analysis on the differentially expressed genes ($p < 0.05$, fold change ≥ 5) in day-80 COs and undifferentiated hPSCs indicated that these differentially expressed genes are strongly relevant to the biological process and signaling pathways of nervous system development, neurogenesis, and neuron projection development (**Figure 5B**). These molecular features further highlight the neural lineage and similarity of COs developed from UEC-derived hiPSCs and WA09 hESCs.

Gene-Expression Features Associated With the Distinct Responses of UEC-Derived hiPSCs and WA09 hESCs in Neural Induction for CO Development

Compared with undifferentiated WA09 hESCs, undifferentiated UEC-derived hiPSCs appeared to present a distinct expression pattern of certain genes (**Figure 5A** and **Supplementary Figure S3A**). The differential expression of a panel of selected genes in three UEC-derived hiPSC lines and WA09 hESCs were confirmed by qRT-PCR (**Supplementary Figure S3B**). It is possible that the genes that are intrinsically hyper- or hypo-expressed in the UEC-derived hiPSCs may contribute to their preference for the LDN193189/A83-01-containing induction medium in forming COs (**Figure 3**).

Through differential expression analysis ($p < 0.05$) between WA09 hESC and UEC-derived hiPSC samples, around 2250 gene probes were identified (**Figure 5C**). Gene ontology and pathway analysis revealed that multiple signaling pathways, including WNT signaling, gonadotropin-releasing hormone (GnRH) receptor signaling, and integrin signaling pathways, are enriched by these differentially expressed genes (**Figure 5D**). Because WNT, BMP, and TGFβ signaling pathways have frequent crosstalk and are highly relevant to the regulation of

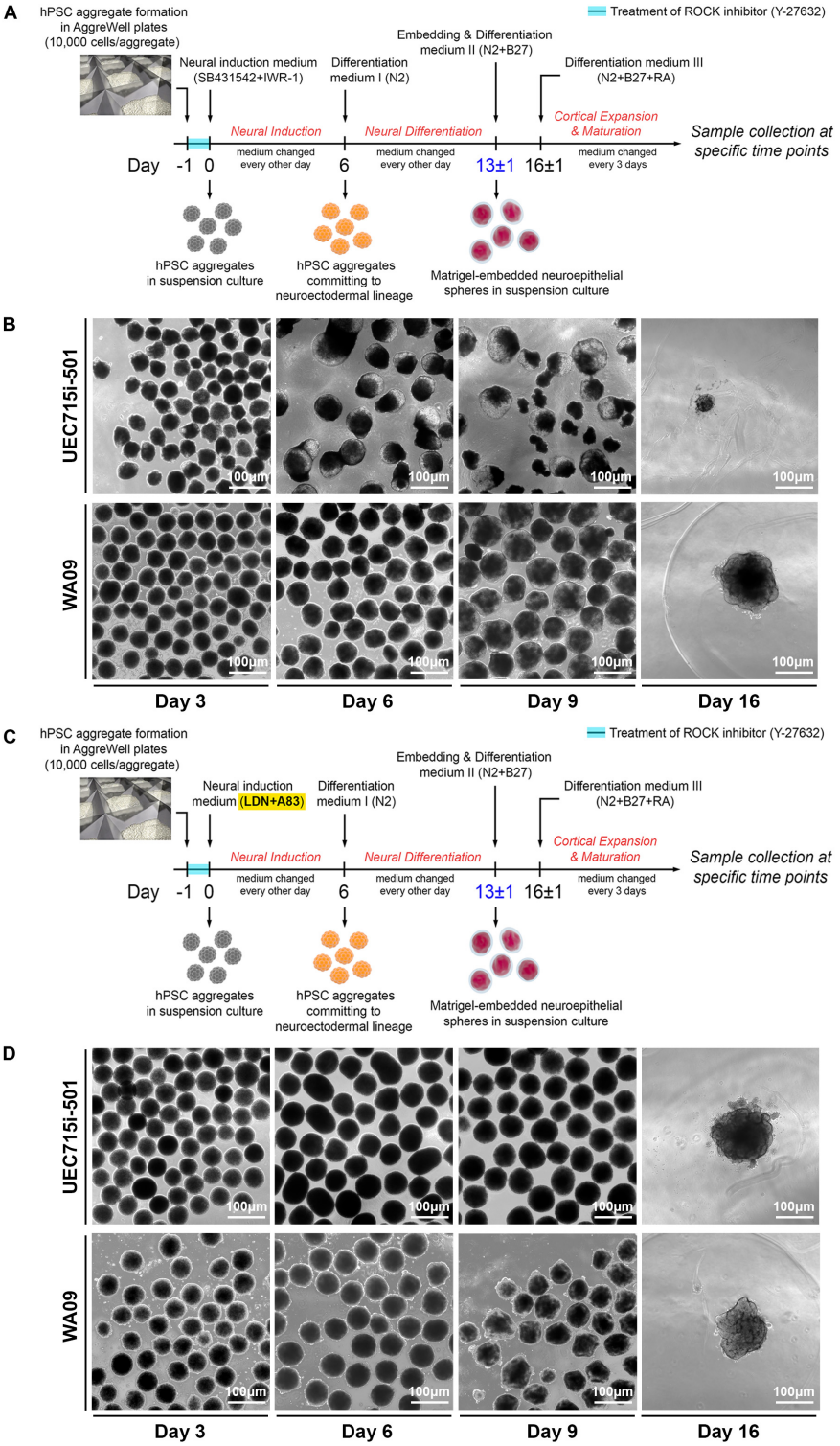

FIGURE 3 | The differential development of COs from UEC-derived hiPSCs and WA09 hESCs. **(A)** A schematic illustration of the procedure that generated COs from the hiPSCs and hESCs by inhibition of TGFβ and WNT signaling to induce their neuroectodermal commitment. **(B)** The morphological representations at the indicated time points of the COs that were developed in response to inhibition of TGFβ and WNT signaling. Within 2 weeks after the induction of neuroectodermal commitment, the disintegration was observed in most organoids developed from UEC715i-501 hiPSCs. **(C)** A schematic illustration of the procedure that generated COs from the hiPSCs and hESCs by inhibition of TGFβ and BMP signaling to induce their neuroectodermal commitment. **(D)** The morphological representations at the indicated time points of the COs that were developed in response to inhibition of TGFβ and BMP signaling. Two weeks after the induction of neuroectodermal commitment, most organoids developed from UEC715i-501 hiPSCs remained intact and continued to grow.

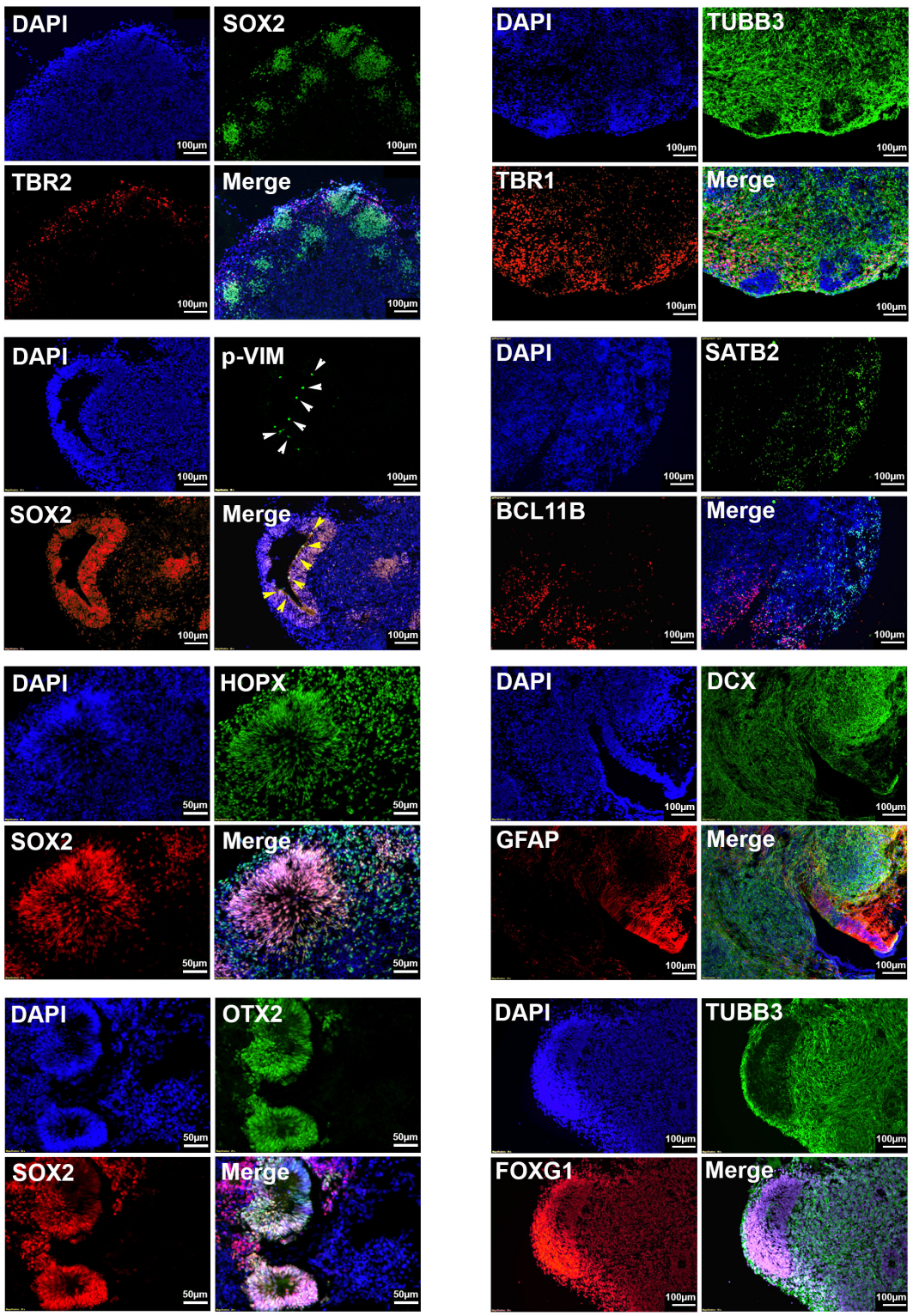

FIGURE 4 | Neural lineage markers were expressed by the cells in COs developed from UEC-derived hiPSCs. **(A)** The expression of multiple markers for neural progenitor cells in the COs collected at day 40 of development. **(B)** The expression of multiple markers for neuronal and astroglial cells in the COs collected at day 80 of development. The development of these CO samples was based on the procedure that inhibited TGFβ and BMP signaling to induce neuroectodermal commitment.

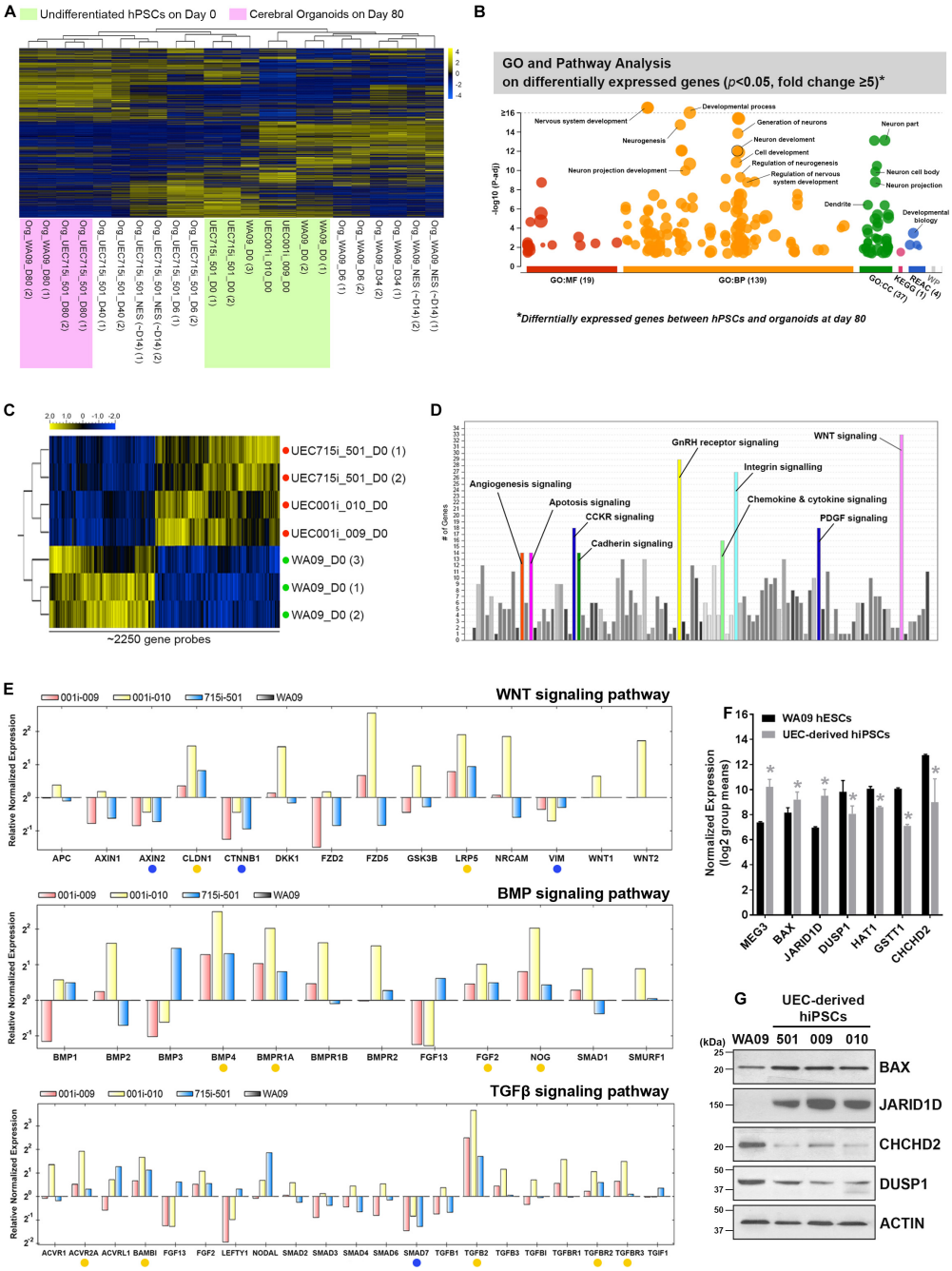

FIGURE 5 | The molecular features of gene expression in COs developed from UEC-derived hiPSCs. **(A)** The heatmap representation of non-supervised clustering based on the global gene-expression profiles in the hPSC and their CO samples. The gene expression profiles in the organoids developed for 80 days from UEC715i-501 hiPSCs and WA09 hESCs were clustered together and segregated away from others, supporting the molecular similarity of COs developed from UEC-derived hiPSCs and WA09 hESCs. **(B)** The result of gene ontology and pathway analysis of differentially expressed genes identified through comparing the samples of undifferentiated WA09 hESCs and UEC715i-501 hiPSCs with the day-80 samples of COs developed from these hPSCs. The differentially expressed genes were found significantly involved in the biological processes of development and neurogenesis. **(C)** The heatmap representation of ∼2250 probes that measured the relative expression levels of differentially expressed genes ($p < 0.05$, *t*-test) in the UEC-derived hiPSC and WA09 hESC samples without differentiation. *Red dots:* UEC-derived hiPSCs. *Green dots:* WA09 hESCs. **(D)** Gene ontology and pathway analysis revealed the signaling pathways that are highly relevant to the differentially expressed genes identified between the sample groups of undifferentiated UEC-derived hiPSCs and WA09 hESCs. **(E)** The expression of the selected genes relevant to the regulation of WNT, BMP, and TGFβ signaling was examined using qRT-PCR array analysis. *Yellow dots:* genes hyperexpressed in UEC-derived hiPSCs. *Blue dots:* genes hypoexpressed in UEC-derived hiPSCs. **(F)** The expression of representative genes that are differentially expressed in UEC-derived hiPSCs and WA09 hESCs as well as involved in the regulation of cellular responses to stimuli, epigenetic control, or protein posttranslational modifications (mean ± SD; $n = 4$ for hiPSC samples, $n = 3$ for hESC samples, $^*p < 0.05$, *t*-test), according to gene expression array analysis. **(G)** The protein expression of the selected genes detected by western blotting confirmed their differential expression in UEC-derived hiPSCs and WA09 hESCs.

neurodevelopment and morphogenesis (Munji et al., 2011; Bond et al., 2012; Dias et al., 2014), we examined the expression of selected genes involved in these signaling pathways using qRT-PCR arrays. Compared with the gene expression in WA09 hESCs, multiple genes, including *AXIN2*, *CLDN1*, *CTNNB1*, *LRP5*, *VIM*, *BMP4*, *BMPR1A*, *FGF2*, *NOG*, *ACVR2A*, *BAMBI*, *SMAD7*, *TGFB2*, *TGFBR2*, *TGFBR3*, were either hypoexpressed or hyperexpressed consistently in the UEC-derived hiPSC lines that were analyzed (**Figure 5E**). In addition, we found the hyperexpression of the *MEG3*, *BAX*, *JARID1D* genes and the hypoexpression of the *DUSP1*, *HAT1*, *GSTT1*, and *CHCHD2* genes in the UEC-derived hiPSCs (**Figures 5F,G**).

CHCHD2 is a mitochondria-associated protein that can function as an apoptosis inhibitor by promoting the interaction of BCL-XL and BAX and limiting the activation of BAX (Liu et al., 2015). Having the hypoexpression of the *CHCHD2* gene and the hyperexpression of the *BAX* gene identified in the UEC-derived hiPSCs, we examined whether the low expression of CHCHD2 and the activation of BAX may be involved in the challenge of CO development based on SB431542/IWR-1-mediated neural induction in the UEC-derived hiPSCs. Cell aggregates cultured parallelly in the LDN193189/A83-01-containing and SB431542/IWR-1-containing induction media were compared. Indicated by cleaved CASP3, enhanced apoptosis occurred in the aggregates of UEC001i-009 and UEC715i-501 hiPSCs, but not in the aggregates of WA09 hESCs, that were cultured in the SB431542/IWR-1-containing medium (**Figure 6A**). BAX multimerization was also enhanced in the aggregates of the UEC-derived hiPSCs (**Figure 6B**). While BCL-XL was similarly expressed in the aggregates of the UEC-derived hiPSCs and WA09 hESCs (**Figure 6A**), reduced interaction between BAX and BCL-XL was found in the aggregates of the UEC-derived hiPSCs (**Figure 6C**), in parallel with their hypoexpression of CHCHD2 (**Figure 6A**).

These findings support that UEC-derived hiPSCs and WA09 hESCs have intrinsic differences in signaling networks likely to affect responses to growth factors, neurogenesis, apoptotic propensity, and CO formation.

Cellular Plasticity That Permits Cell-Fate Conversion in COs Developed by UEC-Derived hiPSCs

Based on a published protocol (Muguruma et al., 2015), we generated cerebellar organoids from UEC-derived hiPSCs and analyzed their gene expression. These cerebellar organoids showed the downregulation of a forebrain marker (FOXG1) and the upregulation of hindbrain markers (GBX2, HOXA2, and HOXB4) during development (**Supplementary Figure S4A**), suggesting that cell signaling for the development of the hindbrain tissue in response to patterning stimuli properly functions in the UEC-derived hiPSCs.

Having the capacity of forming cerebellar organoids determined in UEC-derived hiPSCs, we subsequently tested cellular plasticity in COs through potential conversion from their prosencephalic fate into a rhombencephalic fate. COs formed by UEC-derived hiPSCs and WA09 hESCs in response to three methods for cerebral patterning (**Supplementary Figure S4B**)

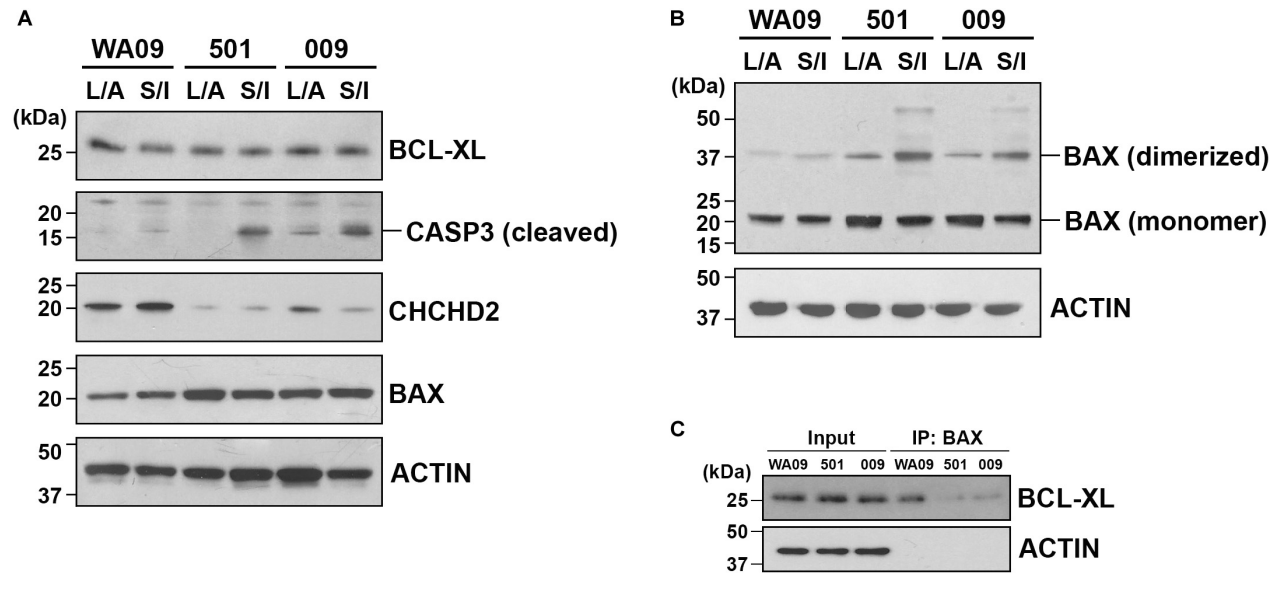

FIGURE 6 | The expression of CHCHD2, the dimerization of BAX, and the interaction between BCL-XL and BAX in the aggregates of UEC-derived hiPSCs and WA09 hESCs that were cultured in LDN193189/A83-01-containing and SB431542/IWR-1-containing media. **(A)** The expression and activation of CHCHD2, BAX, BCL-XL, and CASP3 were revealed by western blotting in the indicated cell aggregate samples that were cultured in the indicated media. **(B)** Dimerized BAX (∼40 kDa) with electromobility shift from BAX monomer (∼20 kDa) was detected by western blotting in the cell aggregate samples. **(C)** BCL-XL interacted and co-immunoprecipitated with BAX in the cell aggregate samples cultured in the SB431542/IWR-1-containing medium was detected by western blotting. 501: UEC715i-501 hiPSCs. 009: UEC001i-009 hiPSCs. L/A: LDN193189/A83-01-containing medium. S/I: SB431542/IWR-1-containing medium. All the cell aggregates were cultured in the indicated media for 6 days prior to sample collection and analysis.

consistently showed the upregulation of FOXG1 during the initial 35 days of development (**Figure 7**). In addition, the repression of GBX2, HOXA2 and HOXB4 was found in these COs (**Figure 7**). These findings were expected and relevant to the normal prosencephalic development of COs. After being transferred into the conversion media that contain SB431542, FGF2, and FGF19, the organoids with conversion started during the initial 14 days of development (**Supplementary Figure S4B**) showed downregulated FOXG1 accompanied by the upregulation of GBX2, HOXA2, and HOXB4, independent of hPSC sources and the methods for their initial cerebral patterning (**Figure 7**). These findings indicate that, like hESC-developed COs, COs developed from UEC-derived hiPSCs possess cellular plasticity that permits conversion between prosencephalic and rhombencephalic fates.

The Distinct Response of COs Formed by UEC-Derived hiPSCs to Different Transplanted Regions in the Mouse Brain

To study the continued development of COs formed by UEC-derived hiPSCs *in vivo*, the organoids that went through the initial 14 days of *in vitro* development were transplanted to the anterior and posterior brain regions of adult mice with severe combined immunodeficiency ($n = 6$). Independent of the transplanted regions (**Figure 8A**), the CO-developed tissue was vascularized (**Figure 8B**), indicating that the transplanted COs survived and continued to develop in the animal brain. Three weeks after implantation, three anterior implants developed visible pigmented areas (**Figure 8B**). In contrast, pigmented cells were not observed in any implant in the posterior brain regions of the same mice (**Figure 8C**). By the end of 6 weeks after implantation, pigmented areas were visible in four anterior and one posterior implants (**Figure 8C**). The distinct frequencies of pigmented cells present in the anterior and posterior implants suggest that the microenvironments of different brain regions may substantially affect the continued development of the transplanted COs. Immunofluorescence staining revealed that, compared with the anterior implants, the posterior implants contained cells with the hypoexpression of FOXG1 and the upregulation of GBX2, HOXA2, and HOXB4 (**Figure 8D**). Our findings reveal that conversion from a prosencephalic fate to a rhombencephalic fate in COs developed by UEC-derived hiPSCs is likely to occur *in vivo* and be driven by the microenvironment and niche signaling in the host's hindbrain tissue.

The Opposite Responses of AKT Signaling and Neural Differentiation in COs Developed From UEC-Derived hiPSCs Treated With AKT and PTEN Inhibitors

To further test how COs developed from UEC-derived hiPSCs may be affected by small molecules, we exposed UEC-derived hiPSC–developed COs to PTEN and AKT inhibitors (**Figure 9A**). VO-OHpic and afuresertib were used as representative inhibitors for PTEN and AKT, respectively. As expected, COs treated with VO-OHpic during their development showed the hyperactivation of AKT signaling, indicated by the enhanced phosphorylation of AKT substrates in the COs (**Figure 9B**). The upregulation of MKI67, SOX2, TBR2, and HOPX accompanied by the downregulation of TUBB3 and RBFOX3 was observed in the VO-OHpic-treated COs (**Figures 9C,D**). Moreover, the treatment of afuresertib led to the opposite regulation of these markers (**Figures 9C,D**). Our results indicate that UEC-derived hiPSC-developed COs can respond normally to the small molecule-mediated regulation of cell signaling that is strongly involved in differentiation, neurogenesis, and cerebral development.

DISCUSSION

Human iPSC-developed COs emerge as a powerful platform for paradigm-shifting research in neural development and pathogenesis. Although COs can be developed using hiPSCs reprogrammed from dermal fibroblasts, little is known about the capacity and features of hiPSCs reprogrammed from other somatic cells in CO formation. The optimization and characterization of COs developed from different types of hiPSCs is expected to contribute substantially to the basic science and translational research of the human brain. In this work, we have studied the development of COs using hiPSCs reprogrammed from urine sample-derived UECs.

Within 48 h after urine collection, proliferative human UECs can be obtained from urine samples through either centrifugation-based or filtration-based isolation (**Figures 1C,D**). Thus, this non-invasive method to obtain proliferative somatic cells from many individuals could be implemented easily by researchers or supporting staff with minimal training required. Although the subtype identity of the collected UECs that were reprogrammed and gave rise to hiPSCs from heterogenous UECs remains elusive, we were able to establish hiPSCs from the urine sample-derived UECs of multiple individuals with different ages and ethnic backgrounds. Nevertheless, the high heterogeneity of urine sample-derived UECs (**Figure 1E**) that could exist among different individuals may lead to the variable efficiency of cell reprogramming and hiPSC establishment in different samples. Further characterizing these UECs by single cell-based analysis in a future study is also expected to help address the cell-heterogeneity issue.

Because unique features may be associated with different hiPSCs reprogrammed from the same type of somatic cells using distinct methods (Schlaeger et al., 2015), we included UEC-derived hiPSCs generated using integrative and non-integrative systems to be tested in our studies. Despite the variations associated with sample donors and different methods for cell reprogramming, all the UEC-derived hiPSCs that we examined can develop into COs (**Figure 3D** and **Supplementary Figure S1**). Non-supervised clustering of samples based on their transcriptomic profiles revealed that the COs developed from UEC-derived hiPSCs and WA09 hESCs share highly similar features in gene expression after they pass the dynamic transition phase for commitment to the neural lineage (**Figure 5A**). Since

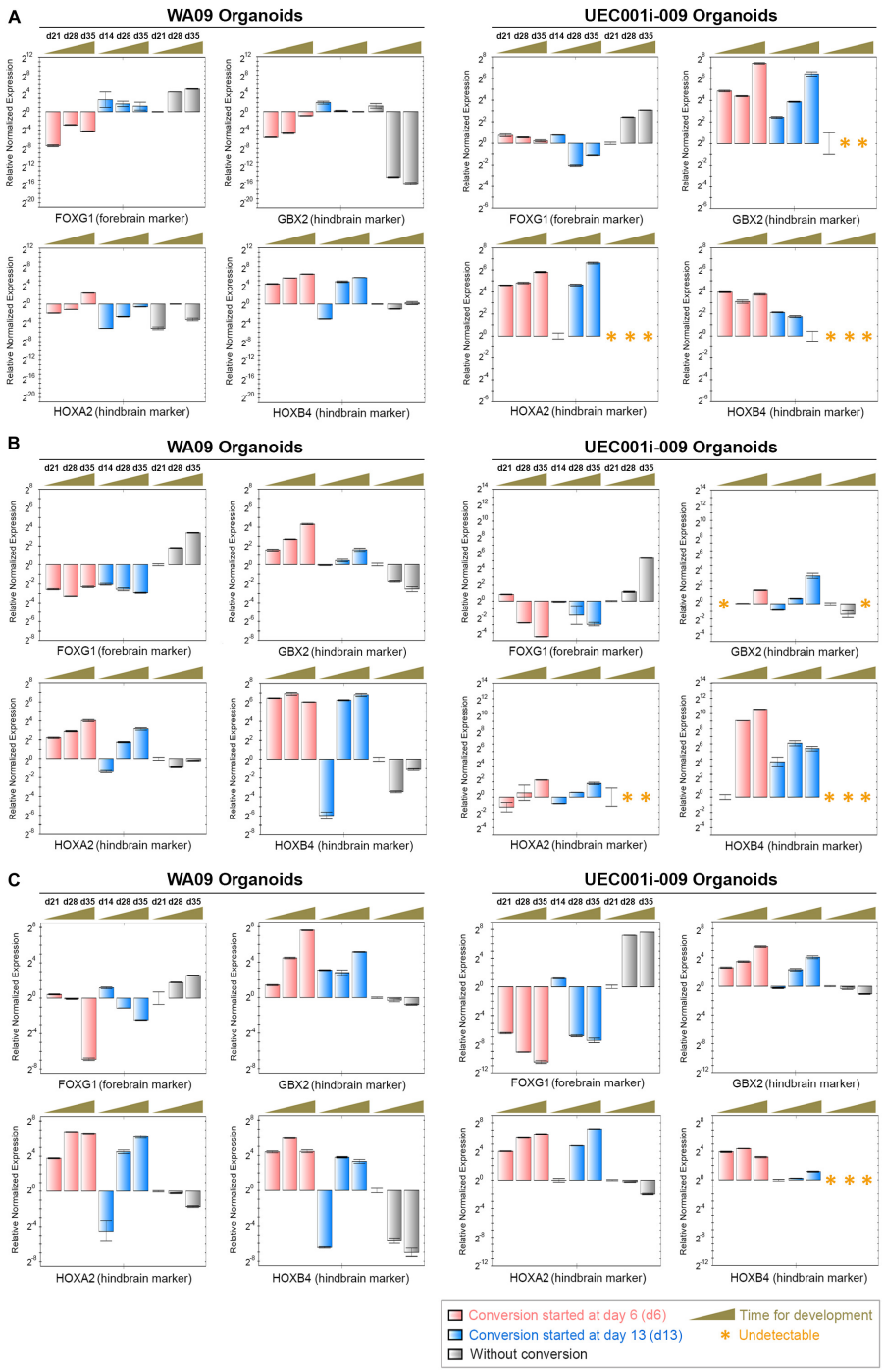

FIGURE 7 | The gene expression alterations of forebrain and hindbrain markers due to the exposure of COs to FGF2, FGF19, and CHIR99021 (a WNT-signaling activator). **(A)** The expression of the *FOXG1*, *GBX2*, *HOXA2*, and *HOXB4* genes (marker genes) was determined by qRT-PCR analysis in the indicated organoid samples (n = 3 at each indicated time point for sample collection) that were developed through the procedure of cerebral induction 1 with and without the conversion treatment depicted in **Supplementary Figure S4**. The upregulation of FOXG1 as well as the suppression of GBX2, HOXA2, and HOXB4 in COs were reversed in the COs with rhombencephalic conversion mediated by the treatment of FGF2, FGF19, and CHIR99021. **(B)** The expression of the marker genes was determined by qRT-PCR analysis in the indicated organoid samples (n = 3 at each indicated time point for sample collection) that were developed through the procedure of cerebral induction 2 with and without the conversion treatment depicted in **Supplementary Figure S4**. The upregulation of FOXG1 as well as the suppression of GBX2, HOXA2, and HOXB4 in COs were reversed in the COs with the conversion treatment. **(C)** The expression of the marker genes was determined by qRT-PCR analysis in the indicated organoid samples (n = 3 at each indicated time point for sample collection) that were developed through the procedure of cerebral induction 3 with and without the conversion treatment depicted in **Supplementary Figure S4**. The upregulation of FOXG1 as well as the suppression of GBX2, HOXA2, and HOXB4 in COs were reversed in the COs with the conversion treatment. Time points for sample collection relevant to each experimental setting are presented in the days (d) of development. All data represent mean ± SD.

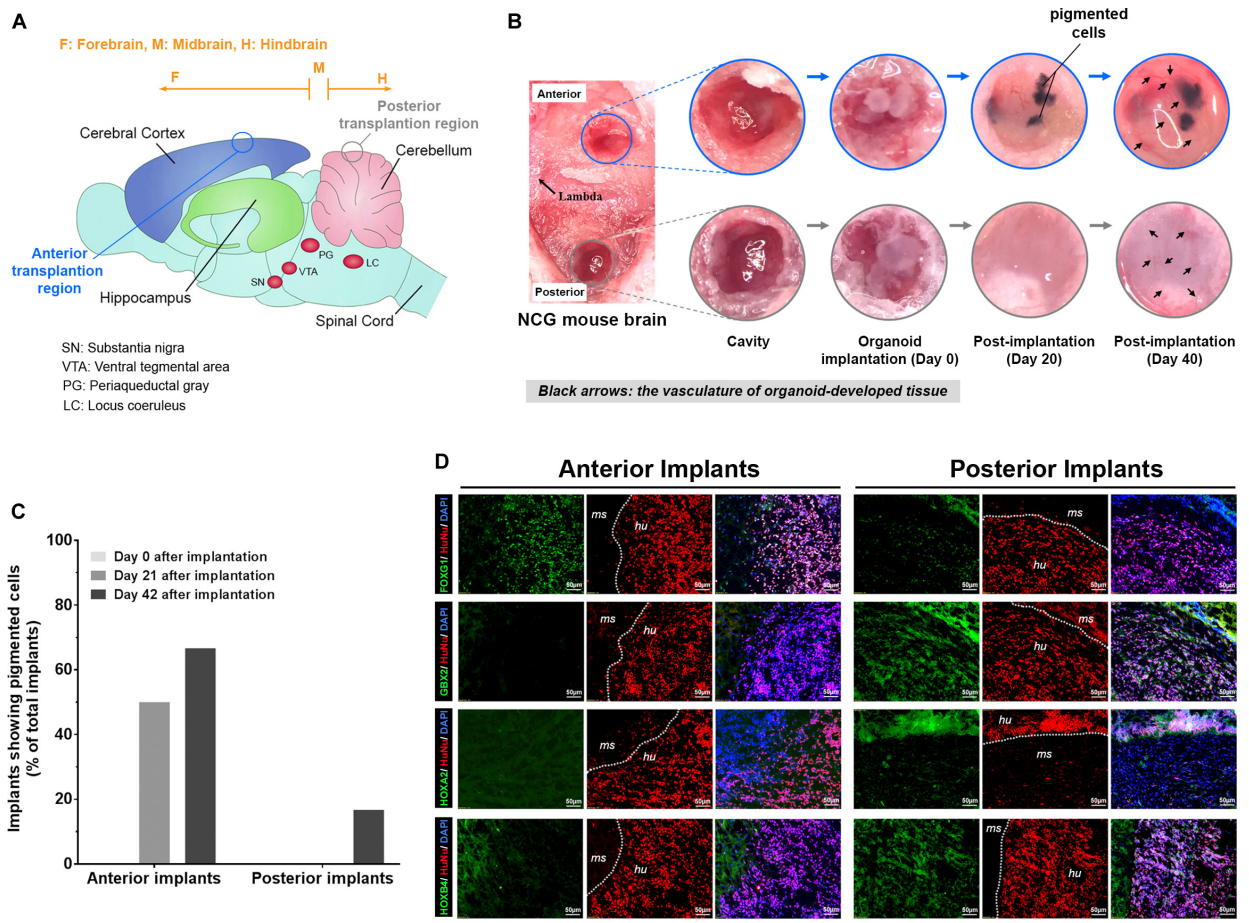

FIGURE 8 | The transplantation of COs developed from UEC-derived hiPSCs into the cerebral cortex and cerebellum of the mouse brain led to the continuation of distinctive neural development in the organoids at these transplantation sites. **(A)** The schematic illustration of regions in the mouse brain for the anterior and posterior transplantation of the COs developed from UEC001i-009 hiPSCs. **(B)** The continued development of the implanted COs was monitored periodically through a cranial window under a surgical stereomicroscope. The vascularization of the tissue formed by the implanted COs was clearly visible at day 40 of post-implantation. **(C)** The percentage of the implanted organoids (n = 6) that developed into tissue with pigmented cells. **(D)** In contrast to the anterior implants (i.e., the tissue formed by the COs transplanted in the cerebral cortex of the mouse brain), the posterior implants (i.e., the tissue formed by the COs transplanted in the cerebellum of the mouse brain) presented with cells that showed the lower expression of FOXG1 and the higher expression of GBX2, HOXA2, and HOXB4 detected by immunofluorescence staining. HuNu: human nuclear antigen. ms: mouse tissue. hu: human tissue. The brain samples with organoid implants were harvested at day 42 of post-implantation.

the cortical cells found in WA09 hESC-developed COs use gene expression programs that resemble those of the human fetal neocortex to organize into cerebral cortex-like regions (Camp et al., 2015), the similarity between the gene expression of COs developed from UEC-derived hiPSCs and WA09 hESCs suggests that COs developed from UEC-derived hiPSCs may also recapitulate the developmental features of the human fetal neocortex. While transcriptomic features were similar in the day-80 COs developed from UEC-derived hiPSCs and WA09 hESCs, noticeable variations existed in the COs at earlier time points (**Figure 5A**). These variations may reflect different kinetics and efficiencies for neural commitment that are likely due to variable susceptibility to patterning signals in different cells and caused by their intrinsic variations (**Figure 5C**).

Though pluripotent, hiPSCs generated using distinct reprogramming methods and from different individuals' UECs consistently encountered a problem with the inhibition of TGFβ and WNT signaling, but tolerated the inhibition of TGFβ and BMP signaling well for neural induction during CO formation (**Supplementary Figure S1**). Both approaches to induce neural differentiation were previously used for developing COs (Kadoshima et al., 2013; Bershteyn et al., 2017; Qian et al., 2018; Cederquist et al., 2019; Zhang et al., 2019) and tolerated well by WA09 hESCs in this study. Thus, the differential responses of UEC-derived hiPSCs and WA09 hESCs to the inhibition of TGFβ and WNT signaling during CO development would be irrelevant to the differences of individuals and cell reprogramming methods but rather reflecting molecular features that exist commonly in UEC-derived hiPSCs.

From gene expression profiling, we discovered the differential expression of multiple genes involved in the regulation of WNT, BMP, and TGFβ signaling pathways in UEC-derived hiPSCs

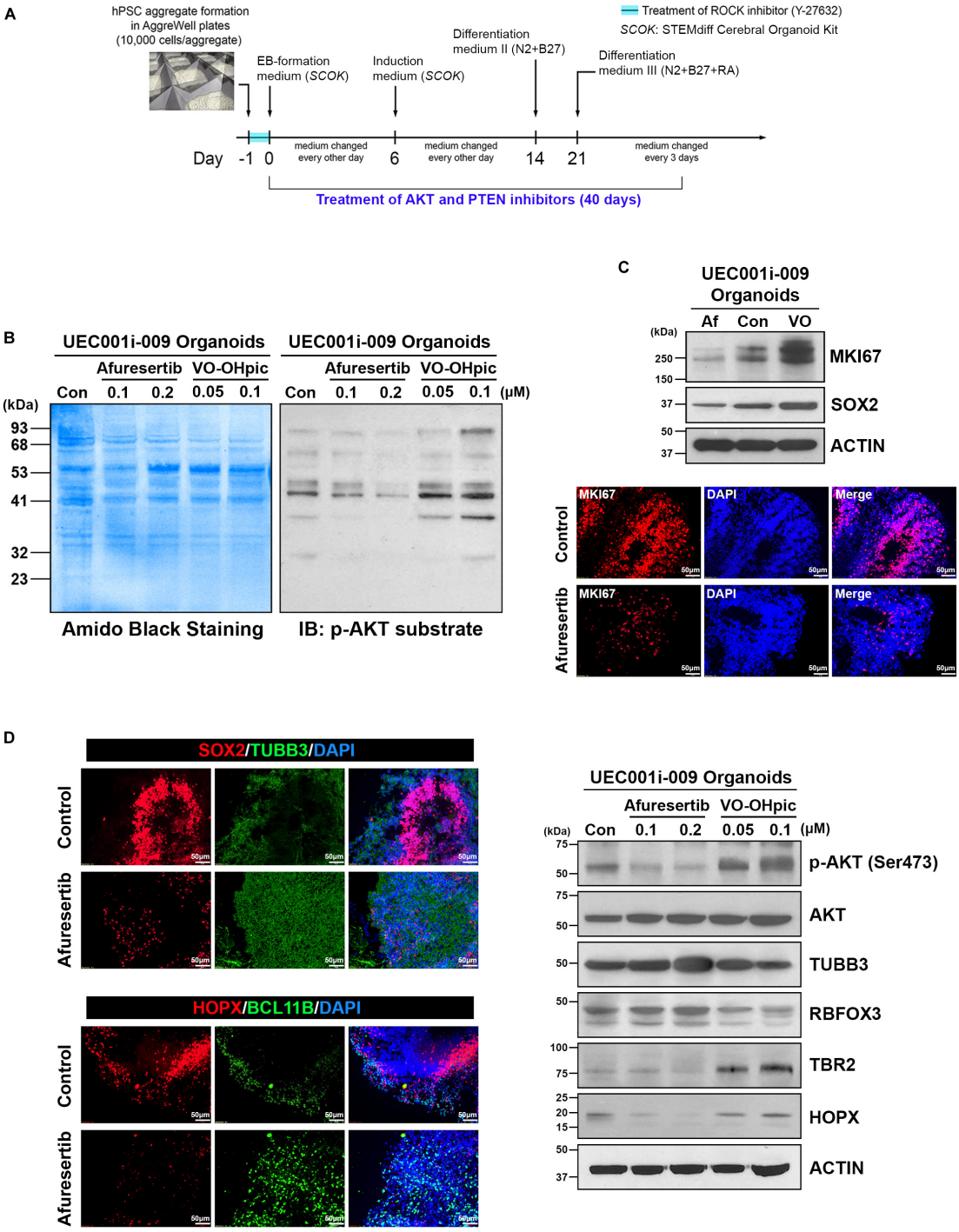

FIGURE 9 | AKT and PTEN inhibitors led to the opposite regulation of AKT activity, cell proliferation, and neural differentiation in cerebral organoids developed from UEC-derived hiPSCs. **(A)** A schematic illustration of the procedure for generating cerebral organoids that were treated with AKT- and PTEN-inhibitory small molecules. **(B)** The phosphorylated AKT substrate was detected by western blotting in the lysates of the cerebral organoids treated with afuresertib (an AKT inhibitor) and VO-OHpic (a PTEN inhibitor) at the indicated concentrations along with their development for 40 days. Con: DMSO-treated organoids. **(C)** The expression of MKI67 (a marker for proliferative cells) and SOX2 (a marker for neural progenitors) was detected by western blotting and immunofluorescence staining in the organoids treated with afuresertib (Af, 0.2 μM) and VO-OHpic (VO, 0.1 μM) along with their development for 40 days. *Upper panel:* Protein expression detected by western blotting. Con: DMSO-treated organoids. *Lower panel:* The immunofluorescence staining of MKI67 in control (DMSO-treated) and afuresertib-treated organoids. **(D)** The expression of multiple markers for neural differentiation was detected by immunofluorescence staining and western blotting in the inhibitor-treated organoids. *Left panel:* The immunofluorescence staining of markers for neural progenitors (SOX2 and HOPX), a pan-neuronal marker (TUBB3) and a marker for early-born neurons (BCL11B) in control and 0.2 μM afuresertib-treated organoids. *Right panel:* Protein expression of phosphorylated AKT, AKT, pan-neuronal markers (TUBB3 and RBFOX3) and markers for neural progenitors (HOPX and TBR2) detected by western blotting. Con: DMSO-treated organoids.

and WA09 hESCs (**Figures 5D,E**). The hyperexpression of pro-apoptotic protein BAX and the hypoexpression of CHCHD2 were also found in all the UEC-derived hiPSC samples compared with WA09 hESCs (**Figures 5F,G**). Notably, CHCHD2 primes the potential of neuroectodermal differentiation in hPSCs and enhances the viability of their differentiated derivatives through modulating SMAD4 (Zhu et al., 2016). It has also been reported as an apoptosis inhibitor by promoting the binding of BCL-XL to BAX and limiting the activation of BAX (Liu et al., 2015). Although the knockdown of CHCHD2 appears to show a negligible effect on the neuroectoderm differentiation of hPSCs in monolayer culture (Markouli et al., 2019), in parallel with CHCHD2 hypoexpression in the UEC-derived hiPSCs, the attenuated interaction of BCL-XL and BAX was found in the aggregates of UEC-derived hiPSCs with suspension culture in the SB431542/IWR-1-containing medium (**Figure 6C**). Compared with LDN193189/A83-01-mediated neural induction, SB431542/IWR-1-mediated neural induction caused a higher propensity for apoptosis that was evidenced by the enhanced activation of CASP3 and BAX in the aggregates of UEC-derived hiPSCs (**Figures 6A,B**). With the concomitant treatment of Y-27632, a ROCK inhibitor with anti-apoptotic effects in hPSCs (Kurosawa, 2012), during SB431542/IWR-1-mediated neural induction (**Supplementary Figure S4**), some aggregates of UEC-derived hiPSCs can form healthy neuroepithelial spheres and continue to develop FOXG1-expressing COs after matrigel embedding (**Figure 7B**). Thus, the challenge of CO development initiated by the inhibition of TGFβ and WNT signaling in UEC-derived hiPSCs could be, at least partially, due to their apoptotic propensity resulted from the low expression of CHCHD2 and overcome by the treatment of anti-apoptosis agents.

Several genes that mediate epigenetic regulation (e.g., *MEG3*, JARID1D, and *HAT1*) or protein posttranslational modification (e.g., *DUSP1*) that are involved in developmental programs (Yang et al., 2012; Nagarajan et al., 2013; Yen et al., 2018) also showed distinct expression patterns in the UEC-derived hiPSCs (**Figures 5F,G**). Since the *JARID1D* gene is a Y-linked gene, the high expression of JARID1D in the male hiPSC lines that we analyzed, compared with WA09 hESCs established from a normal female blastocyst (Thomson et al., 1998), was expected. Although additional studies will be required to functionally determine the critical factors that mediate the different responses of UEC-derived hiPSCs and WA09 hESCs to the inhibition of TGFβ and WNT signaling during CO formation, our discoveries reveal that unique signaling-network features may frequently exist in UEC-derived hiPSCs and underlie their specific responses to different methods for the induction of CO development.

Given the knowledge that FGF2 and FGF19 signaling is critical for cerebellar development (Muguruma et al., 2015) and that the activation of WNT signaling promotes caudalization (Takata et al., 2017), we challenged COs developed from UEC-derived hiPSCs to potentially convert from a prosencephalic fate to a rhombencephalic fate through the activation of FGF2, FGF19, and WNT signaling together with the suppression of TGFβ signaling during CO formation. Regardless of the different methods initially used for neural induction, the upregulation of FOXG1 and the downregulation of several hindbrain markers (**Figure 7**) suggest that cells in the COs were driven to a prosencephalic fate. Upon exposure to conversion media that contain SB431542, FGF2, CHIR99021, and FGF19, the expression patterns of forebrain and hindbrain markers can be effectively reversed if the conversion treatment begins in the initial 2 weeks of CO development. Evidenced by the significant downregulation of POU5F1 and the upregulation of FOXG1 within the initial 2 weeks of regular CO development (**Supplementary Figure S5**), most cells in COs, if not all, have lost their cellular pluripotency and begun to commit to a prosencephalic fate at that time. Although we cannot fully exclude a possibility that the upregulation of hindbrain markers detected in the converted organoids may be due to the selective induction of a rhombencephalic program in residual pluripotent cells, the likelihood of having the residual pluripotent cells solely responsible for the reversal of forebrain and hindbrain marker expression in the converted organoids is low. Our findings support that cellular plasticity is present in COs developed from UEC-derived hiPSCs.

Cerebral organoids developed from UEC-derived hiPSCs continued developing and were vascularized after transplantation into the mouse brain (**Figure 8B**). The high frequency of having pigmented cells in the anterior implants but not in the posterior implants (**Figures 8B,C**) indicates that the development of the transplanted organoids may respond differentially to distinct microenvironments in the cerebral cortex and cerebellum. The hypoexpression of a forebrain marker and the upregulation of hindbrain markers (**Figure 8D**) observed in the posterior implants compared with the anterior implants further suggest that the cellular plasticity observed in the COs (**Figure 7**) may be leveraged to generate cell components of various brain regions based on the organoids patterned by unique niche signaling at different transplanted locations *in vivo*.

Similar to hyperactive AKT found in the COs developed from WIBR3 hESCs with PTEN mutation for modeling human macrocephaly (Li et al., 2017), our COs treated with a PTEN inhibitor during their development showed the enhanced phosphorylation of AKT substrates (**Figure 9B**). The upregulation of MKI67, SOX2, TBR2, and HOPX accompanied by the downregulation of TUBB3 and RBFOX3 found in the COs with PTEN mutation (Li et al., 2017) was also observed in the PTEN inhibitor-treated COs (**Figures 9C,D**). Moreover, the treatment of an AKT inhibitor led to the opposite regulation of these markers (**Figures 9C,D**). Since the treatment of other two AKT inhibitors, ipatasertib and MK-2206, also attenuates overexpansion as well as normalizes cell proliferation and neural gene expression in the PTEN-mutant COs (Li et al., 2017), the similar molecular features caused by the inactivation of PTEN and AKT in hESC-developed and UEC-derived hiPSC-developed COs suggest the suitability and potential use of UEC-derived hiPSCs in CO production for disease modeling and drug screening.

As a potential platform for investigating the development and pathogenesis of the human brain, the improved reproducibility and quality of COs are critical for neurological research based on the organoid system. Although the establishment of cells

enriched in the cerebral cortex appears to emerge reproducibly from COs generated with different cell origins and growth environments (Velasco et al., 2019), the unique responses of UEC-derived hiPSCs to different protocols for CO development (**Figure 3** and **Supplementary Figure S1**) indicate that variations among different cell origins can largely affect the efficacy of CO development under certain conditions. Thus, the production of COs may still require specific optimization for different hPSCs to permit robust results in each CO-based study.

Summarized in **Supplementary Table S1**, our work demonstrates the suitability, advantage, and potential challenge of using COs developed from UEC-derived hiPSCs to study cerebral development and pharmacological responses. COs generated with this unique stem cell source represent a valuable platform that could be easily adopted and further optimized to facilitate a variety of brain research.

MATERIALS AND METHODS

Isolation of UECs From Urine Samples

The sterile sample cups were provided to each subject enrolled in the study for collection of minimal 250 ml of their midstream urine from one visit. The urine samples from eight adults (six males and two females) who were healthy at the time of sample collection were used in this study. The age of the sample donors ranged from 24 to 65 at the time of sample collection. For centrifugation-based isolation, UECs in around 250 ml of the urine samples from each individual were pelleted by centrifugation at 500 $\times$ *g* for 5 min in an ultracentrifuge (Beckman Coulter, Indianapolis, IN, United States). The cell pellets were resuspended in 25 ml of phosphate-buffered saline (PBS) containing 5% heat-inactivated fetal bovine serum (FBS), pelleted, resuspended in 2 ml of the urinary cell medium, and placed into a well of six-well cell culture plate. For filtration-based isolation, the urine samples were filtered through sterilized membrane filters made of polypropylene (Tisch Scientific, North Bend, OH, United States), nylon (Tisch Scientific, North Bend, OH, United States), and PC (Isopore^{TM}; MilliporeSigma, Burlington, MA, United States) with 10 μm pore size in a reusable bottle top filtering device. The membranes were retrieved from the device and placed into a cell culture dish to directly culture UECs on each membrane. The detailed information relevant to the urinary cell medium is provided as part of **Supplementary Materials and Methods**.

Cell Culture

WA09 hESCs were obtained from the WiCell Stem Cell Bank (WiCell Research Institute, Madison, WI, United States). UEC715i-501 hiPSCs were established using CytoTune Sendai Reprogramming Kit (Thermo Fisher Scientific, Carlsbad, CA, United States) and kindly provided by Dr. Jeanne Loring from The Scripps Research Institute. UEC001i-003, UEC001i-009, and UEC001i-010 hiPSCs were established through retroviral vector-mediated cell reprogramming by the method described previously (Wang et al., 2011). Except the use of TeSR-E8 medium (Stemcell Technologies, Vancouver, BC, Canada) and EDTA hPSC passaging solution (Thermo Fisher Scientific, Carlsbad, CA, United States) in this study, we generally followed the reported method (Wang et al., 2011) for culturing undifferentiated hPSCs in a feeder cell-free condition with 0.5 mg/ml growth factor-reduced matrigel (Corning, Tewksbury, MA, United States) in a DMEM/F12 medium for plate coating. All the hPSCs were routinely subcultured when cell density reached 80–90% in culture plates. The passage numbers of the hiPSCs used in our experiments were spanning across 25–70. Additional information relevant to cells used in this study is summarized in **Supplementary Table S2**. The experiments using hPSCs were performed in compliance with the guidelines and approval of the institutional biosafety committee at UNTHSC. All cells were periodically tested using the MycoAlert mycoplasma detection kit (Lonza, Walkersville, MD, United States) and free of mycoplasma.

Karyotyping

Chromosomal analysis in UEC-derived hiPSCs by counting 20 metaphase spreads for each sample was performed using a contract research service provided by Molecular Diagnostic Services (San Diego, CA, United States).

Cerebral Organoid Formation

The protocols for the development of COs from WA09 hESCs and UEC-derived hiPSCs are illustrated schematically in **Figure 3**. The detailed information relevant to the protocols is summarized in **Supplementary Materials and Methods**.

Cerebellar Organoid Formation and Rhombencephalic Conversion in Cerebral Organoids

The generation of cerebellar organoids from UEC-derived hiPSCs was based on a protocol reported previously (Muguruma et al., 2015). For the conversion of COs from its prosencephalic fate into a rhombencephalic fate, the organoids were transferred into conversion media I, II, and III at the specific time points illustrated schematically in **Supplementary Figure S4B**. The detailed information relevant to the protocols is summarized in **Supplementary Materials and Methods**.

Treatment of AKT and PTEN Inhibitors

Afuresertib was obtained from Cayman Chemical (Ann Arbor, MI, United States). VO-OHpic was obtained from Tocris (Minneapolis, MN, United States). The small-molecule inhibitors dissolved in DMSO as stock solutions were diluted in media and applied to COs during the time period illustrated schematically in **Figure 9A**.

Immunofluorescence Staining

The general procedure for antibody-mediated fluorescence staining was previously described (Wang et al., 2011) and provided as part of **Supplementary Materials and Methods**. The detailed information of primary antibodies used in this study is summarized in **Supplementary Table S3**.

Immunoprecipitation

The cell lysates were prepared using M-PER mammalian protein extraction reagent (Thermo Fisher Scientific, Carlsbad, CA, United States) containing EDTA-free protease inhibitor and phosphatase inhibitor cocktails (Millipore Sigma, St. Louis, MO, United States). Anti-BAX mouse IgG (MA5-14003; Thermo Fisher Scientific, Carlsbad, CA, United States) was pre-coated onto Dynabeads M-280 sheep anti-mouse IgG (Thermo Fisher Scientific, Carlsbad, CA, United States) at 4°C. The paramagnetic beads pre-coated with the antibody were mixed with cell lysates (80 μg total protein per lysate sample as an input) in PBS with the reaction volume of 400 μl at 4°C overnight, prior to the magnet-mediated separation of bead-bound proteins from the rest of the sample. The bead-bound proteins eluted off the beads were analyzed by immunoblotting with antibodies against specific targets.

Immunoblotting

The general procedure for immunoblotting was described in a previously published report (Wang et al., 2008), except that cell lysates were prepared using M-PER mammalian protein extraction reagent (Thermo Fisher Scientific, Carlsbad, CA, United States) containing EDTA-free protease inhibitor and phosphatase inhibitor cocktails (Millipore Sigma, St. Louis, MO, United States). To detect multimerized BAX, cell lysates were prepared using a hypotonic buffer that contains 20 mM HEPES, 10 mM potassium chloride, and the protease inhibitor and phosphatase inhibitor cocktails. Bismaleimidohexane (Thermo Fisher Scientific, Carlsbad, CA, United States) was added into the lyates at the final concentration of 5 mM to stabilize oligomerized proteins through crosslinking. The detailed information of primary antibodies used in this study is summarized in **Supplementary Table S3**. HRP-conjugated secondary antibodies were from Jackson ImmunoResearch Laboratories (West Grove, PA, United States). For detecting targets in the bead-bound proteins from immunoprecipitation, TrueBlot HRP-conjugated secondary antibodies (Rockland Immunochemicals, Limerick, PA, United States) were used to specifically recognize the non-reduced form of primary antibodies.

Gene Expression Analysis by qRT-PCR and Microarrays

The procedures for microarray analysis in this study are provided as part of **Supplementary Materials and Methods**. The test of cellular pluripotency based on the transcriptomic features of cell samples was performed using the PluriTest[1] (Muller et al., 2011). Multiplex qRT-PCR was performed using cDNA generated from the RNA samples and Taqman assays for the *BMP4*, *BMPR1A*, *CTNNB1, LRP5, SMAD7, FOXG1, GBX2, HOXA2*, *HOXB4, POU5F1,* and *ACTB* (internal control) genes (assay ID# Hs00370078_m1, Hs01034913_g1, Hs00355049_m1, Hs00182031_m1, Hs00998193_m1, Hs01850784_s1, Hs00230965_m1, Hs00534579_m1, Hs00256884_m1, Hs00999632_g1, and Hs03023943_g1; Thermo Fisher Scientific, Carlsbad, CA, United States), according to the manufacturer's instructions. The customized qRT-PCR arrays with primer sets from PrimePCR target-list panels for detection of the selected human WNT, TGFβ, and BMP signaling targets and reference genes (*ACTB* and *GAPDH*) were obtained from Bio-Rad (Hercules, CA, United States). The SYBR Green-based qRT-PCR reactions on the arrays were performed according to the manufacturer's instructions.

[1] www.pluritest.org

In vivo Studies

The procedures for organoid transplantation in this study are provided as part of **Supplementary Materials and Methods**.

Statistical Analysis

Quantitative data reported in this work were reproducible in at least three biological replicates and presented as mean ± standard deviation. The significance of differences in comparisons was primarily determined by the two-tailed Student's *t*-test for a two-group comparison or by the multivariate analysis of variance for testing variables in three or more groups.

Study Approval

The collection of urine samples from human subjects and the isolation of UECs from the urine samples for experiments were performed in compliance with the guidelines and approval of the Institutional Review Board Committee at the University of North Texas Health Science Center (UNTHSC). All experimental procedures and protocols utilizing mice were approved by the Institutional Animal Care and Use Committee at UNTHSC.

DATA AVAILABILITY STATEMENT

The gene expression array data have been deposited and linked to an accession number GSE131562 in the Gene Expression Omnibus (GEO). Other data included in the article to demonstrate our findings are available from the corresponding author upon reasonable request. The biological samples used in this study may be distributed upon request and under institutional material transferring agreements or a licensing process.

ETHICS STATEMENT

The studies involving human participants were reviewed and approved by the Institutional Review Board Committee at University of North Texas Health Science Center. The patients/participants provided their written informed consent to participate in this study. The animal study was reviewed and approved by the Institutional Animal Care and Use Committee at University of North Texas Health Science Center.

AUTHOR CONTRIBUTIONS

VL, AZ, and JH contributed to the study concept, data collection and analysis, and manuscript preparation. L-JY contributed to the data collection and analysis for the animal

studies. Y-CW supervised the study, coordinated research efforts, and contributed to the study concept and design, data analysis, and manuscript writing. All authors reviewed and approved the manuscript.

FUNDING

This work was supported by the UNTHSC Start-up Fund for Stem Cell Laboratory and Faculty Pilot Grant FY15 (RI6182) to Y-CW, NIH Research Project Grant (R01NS079792) and UNTHSC grants (RI10039 and RI10015) to L-JY. VL was supported by the NIH NRSA Institutional Predoctoral Training Grant (T32 AG020494), Glenn/AFAR Scholarship for Research in the Biology of Aging, and AOA/SOMA Research Fellowship. JH was supported by the AHA Predoctoral Fellowship (19PRE34380114).

SUPPLEMENTARY MATERIAL

The Supplementary Material for this article can be found online at: https://www.frontiersin.org/articles/10.3389/fcell.2020.00304/full#supplementary-material

REFERENCES

Arlotta, P. (2018). Organoids required! A new path to understanding human brain development and disease. *Nat. Methods* 15, 27–29. doi: 10.1038/nmeth.4557

Bershteyn, M., Nowakowski, T. J., Pollen, A. A., Di Lullo, E., Nene, A., Wynshaw-Boris, A., et al. (2017). Human iPSC-derived cerebral organoids model cellular features of lissencephaly and reveal prolonged mitosis of outer radial glia. *Cell Stem Cell* 20, 435.e4–449.e4. doi: 10.1016/j.stem.2016.12.007

Bond, A. M., Bhalala, O. G., and Kessler, J. A. (2012). The dynamic role of bone morphogenetic proteins in neural stem cell fate and maturation. *Dev. Neurobiol.* 72, 1068–1084. doi: 10.1002/dneu.22022

Camp, J. G., Badsha, F., Florio, M., Kanton, S., Gerber, T., Wilsch-Brauninger, M., et al. (2015). Human cerebral organoids recapitulate gene expression programs of fetal neocortex development. *Proc. Natl. Acad. Sci. U.S.A.* 112, 15672–15677. doi: 10.1073/pnas.1520760112

Cederquist, G. Y., Asciolla, J. J., Tchieu, J., Walsh, R. M., Cornacchia, D., Resh, M. D., et al. (2019). Specification of positional identity in forebrain organoids. *Nat. Biotechnol.* 37, 436–444. doi: 10.1038/s41587-019-0085-3

Dakic, V., Minardi Nascimento, J., Costa Sartore, R., Maciel, R. M., De Araujo, D. B., Ribeiro, S., et al. (2017). Short term changes in the proteome of human cerebral organoids induced by 5-MeO-DMT. *Sci. Rep.* 7:12863. doi: 10.1038/s41598-017-12779-5

Dias, J. M., Alekseenko, Z., Applequist, J. M., and Ericson, J. (2014). Tgfbeta signaling regulates temporal neurogenesis and potency of neural stem cells in the CNS. *Neuron* 84, 927–939. doi: 10.1016/j.neuron.2014.10.033

Huch, M., Knoblich, J. A., Lutolf, M. P., and Martinez-Arias, A. (2017). The hope and the hype of organoid research. *Development* 144, 938–941. doi: 10.1242/dev.150201

Kadoshima, T., Sakaguchi, H., Nakano, T., Soen, M., Ando, S., Eiraku, M., et al. (2013). Self-organization of axial polarity, inside-out layer pattern, and species-specific progenitor dynamics in human ES cell-derived neocortex. *Proc. Natl. Acad. Sci. U.S.A.* 110, 20284–20289. doi: 10.1073/pnas.1315710110

Kanton, S., Boyle, M. J., He, Z., Santel, M., Weigert, A., Sanchis-Calleja, F., et al. (2019). Organoid single-cell genomic atlas uncovers human-specific features of brain development. *Nature* 574, 418–422. doi: 10.1038/s41586-019-1654-9

Kurosawa, H. (2012). Application of Rho-associated protein kinase (ROCK) inhibitor to human pluripotent stem cells. *J. Biosci. Bioeng.* 114, 577–581. doi: 10.1016/j.jbiosc.2012.07.013

Lancaster, M. A., Renner, M., Martin, C. A., Wenzel, D., Bicknell, L. S., Hurles, M. E., et al. (2013). Cerebral organoids model human brain development and microcephaly. *Nature* 501, 373–379. doi: 10.1002/mds.25740

Lee, C. T., Chen, J., Kindberg, A. A., Bendriem, R. M., Spivak, C. E., Williams, M. P., et al. (2017). CYP3A5 mediates effects of cocaine on human neocorticogenesis: studies using an *in vitro* 3D self-organized hPSC model with a single cortex-like unit. *Neuropsychopharmacology* 42, 774–784. doi: 10.1038/npp.2016.156

Li, Y., Muffat, J., Omer, A., Bosch, I., Lancaster, M. A., Sur, M., et al. (2017). Induction of expansion and folding in human cerebral organoids. *Cell Stem Cell* 20, 385.e3–396.e3. doi: 10.1016/j.stem.2016.11.017

Liu, Y., Clegg, H. V., Leslie, P. L., Di, J., Tollini, L. A., He, Y., et al. (2015). CHCHD2 inhibits apoptosis by interacting with Bcl-x L to regulate Bax activation. *Cell Death Diff.* 22, 1035–1046. doi: 10.1038/cdd.2014.194

Markouli, C., Couvreu De Deckersberg, E., Regin, M., Nguyen, H. T., Zambelli, F., Keller, A., et al. (2019). Gain of 20q11.*21* in human pluripotent stem cells impairs TGF-beta-dependent neuroectodermal commitment. *Stem Cell Rep.* 13, 163–176. doi: 10.1016/j.stemcr.2019.05.005

Matsui, T. K., Matsubayashi, M., Sakaguchi, Y. M., Hayashi, R. K., Zheng, C., Sugie, K., et al. (2018). Six-month cultured cerebral organoids from human ES cells contain matured neural cells. *Neurosci. Lett.* 670, 75–82. doi: 10.1016/j.neulet.2018.01.040

Muguruma, K., Nishiyama, A., Kawakami, H., Hashimoto, K., and Sasai, Y. (2015). Self-organization of polarized cerebellar tissue in 3D culture of human pluripotent stem cells. *Cell Rep.* 10, 537–550. doi: 10.1016/j.celrep.2014.12.051

Muller, F. J., Schuldt, B. M., Williams, R., Mason, D., Altun, G., Papapetrou, E. P., et al. (2011). A bioinformatic assay for pluripotency in human cells. *Nat Methods* 8, 315–317. doi: 10.1038/nmeth.1580

Munji, R. N., Choe, Y., Li, G., Siegenthaler, J. A., and Pleasure, S. J. (2011). Wnt signaling regulates neuronal differentiation of cortical intermediate progenitors. *J. Neurosci.* 31, 1676–1687. doi: 10.1523/JNEUROSCI.5404-10.2011

Nagarajan, P., Ge, Z., Sirbu, B., Doughty, C., Agudelo Garcia, P. A., Schlederer, M., et al. (2013). Histone acetyl transferase 1 is essential for mammalian development, genome stability, and the processing of newly synthesized histones H3 and H4. *PLoS Genet.* 9:e1003518. doi: 10.1371/journal.pgen.1003518

Pasca, A. M., Sloan, S. A., Clarke, L. E., Tian, Y., Makinson, C. D., Huber, N., et al. (2015). Functional cortical neurons and astrocytes from human pluripotent stem cells in 3D culture. *Nat. Methods* 12, 671–678. doi: 10.1038/nmeth.3415

Pollen, A. A., Bhaduri, A., Andrews, M. G., Nowakowski, T. J., Meyerson, O. S., Mostajo-Radji, M. A., et al. (2019). Establishing cerebral organoids as models of human-specific brain evolution. *Cell* 176, 743.e17–756.e17. doi: 10.1016/j.cell.2019.01.017

Qian, X., Jacob, F., Song, M. M., Nguyen, H. N., Song, H., and Ming, G. L. (2018). Generation of human brain region-specific organoids using a miniaturized spinning bioreactor. *Nat. Protoc.* 13, 565–580. doi: 10.1038/nprot.2017.152

Quadrato, G., and Arlotta, P. (2017). Present and future of modeling human brain development in 3D organoids. *Curr. Opin. Cell Biol.* 49, 47–52. doi: 10.1016/j.ceb.2017.11.010

Quadrato, G., Nguyen, T., Macosko, E. Z., Sherwood, J. L., Min Yang, S., Berger, D. R., et al. (2017). Cell diversity and network dynamics in photosensitive human brain organoids. *Nature* 545, 48–53. doi: 10.1038/nature22047

Renner, M., Lancaster, M. A., Bian, S., Choi, H., Ku, T., Peer, A., et al. (2017). Self-organized developmental patterning and differentiation in cerebral organoids. *EMBO J.* 36, 1316–1329. doi: 10.15252/embj.201694700

Rossi, G., Manfrin, A., and Lutolf, M. P. (2018). Progress and potential in organoid research. *Nat. Rev. Genet.* 19, 671–687. doi: 10.1038/s41576-018-0051-9

Sauvageot, C. M., and Stiles, C. D. (2002). Molecular mechanisms controlling cortical gliogenesis. *Curr. Opin. Neurobiol.* 12, 244–249. doi: 10.1016/s0959-4388(02)00322-7

Schlaeger, T. M., Daheron, L., Brickler, T. R., Entwisle, S., Chan, K., Cianci, A., et al. (2015). A comparison of non-integrating reprogramming methods. *Nat. Biotechnol.* 33, 58–63.

Streckfuss-Bomeke, K., Wolf, F., Azizian, A., Stauske, M., Tiburcy, M., Wagner, S., et al. (2013). Comparative study of human-induced pluripotent stem cells

derived from bone marrow cells, hair keratinocytes, and skin fibroblasts. *Eur. Heart J.* 34, 2618–2629. doi: 10.1093/eurheartj/ehs203

Takahashi, K., Tanabe, K., Ohnuki, M., Narita, M., Ichisaka, T., Tomoda, K., et al. (2007). Induction of pluripotent stem cells from adult human fibroblasts by defined factors. *Cell* 131, 861–872. doi: 10.1016/j.cell.2007.11.019

Takahashi, T. (2019). Organoids for drug discovery and personalized medicine. *Annu. Rev. Pharmacol. Toxicol.* 59, 447–462. doi: 10.1146/annurev-pharmtox-010818-021108

Takata, N., Sakakura, E., Eiraku, M., Kasukawa, T., and Sasai, Y. (2017). Self-patterning of rostral-caudal neuroectoderm requires dual role of Fgf signaling for localized Wnt antagonism. *Nat. Commun.* 8:1339. doi: 10.1038/s41467-017-01105-2

Thomson, J. A., Itskovitz-Eldor, J., Shapiro, S. S., Waknitz, M. A., Swiergiel, J. J., Marshall, V. S., et al. (1998). Embryonic stem cell lines derived from human blastocysts. *Science* 282, 1145–1147. doi: 10.1101/sqb.2008.73.038

Trujillo, C. A., and Muotri, A. R. (2018). Brain organoids and the study of neurodevelopment. *Trends Mol. Med.* 24, 982–990.

Velasco, S., Kedaigle, A. J., Simmons, S. K., Nash, A., Rocha, M., Quadrato, G., et al. (2019). Individual brain organoids reproducibly form cell diversity of the human cerebral cortex. *Nature* 570, 523–527. doi: 10.1038/s41586-019-1289-x

Wang, Y. C., Kulp, S. K., Wang, D., Yang, C. C., Sargeant, A. M., Hung, J. H., et al. (2008). Targeting endoplasmic reticulum stress and Akt with OSU-03012 and gefitinib or erlotinib to overcome resistance to epidermal growth factor receptor inhibitors. *Cancer Res.* 68, 2820–2830. doi: 10.1158/0008-5472.CAN-07-1336

Wang, Y. C., Nakagawa, M., Garitaonandia, I., Slavin, I., Altun, G., Lacharite, R. M., et al. (2011). Specific lectin biomarkers for isolation of human pluripotent stem cells identified through array-based glycomic analysis. *Cell Res.* 21, 1551–1563. doi: 10.1038/cr.2011.148

Watanabe, M., Buth, J. E., Vishlaghi, N., De La Torre-Ubieta, L., Taxidis, J., Khakh, B. S., et al. (2017). Self-organized cerebral organoids with human-specific features predict effective drugs to combat zika virus infection. *Cell Rep.* 21, 517–532. doi: 10.1016/j.celrep.2017.09.047

Wen, W., Zhang, J. P., Xu, J., Su, R. J., Neises, A., Ji, G. Z., et al. (2016). Enhanced generation of integration-free iPSCs from human adult peripheral blood mononuclear cells with an optimal combination of episomal vectors. *Stem Cell Rep.* 6, 873–884. doi: 10.1016/j.stemcr.2016.04.005

Xu, R., Brawner, A. T., Li, S., Liu, J. J., Kim, H., Xue, H., et al. (2019). OLIG2 drives abnormal neurodevelopmental phenotypes in human iPSC-based organoid and chimeric mouse models of down syndrome. *Cell Stem Cell* 24, 908.e8–926.e8. doi: 10.1016/j.stem.2019.04.014

Yang, S. H., Kalkan, T., Morrisroe, C., Smith, A., and Sharrocks, A. D. (2012). A genome-wide RNAi screen reveals MAP kinase phosphatases as key ERK pathway regulators during embryonic stem cell differentiation. *PLoS Genet.* 8:e1003112. doi: 10.1371/journal.pgen.1003112

Yen, Y. P., Hsieh, W. F., Tsai, Y. Y., Lu, Y. L., Liau, E. S., Hsu, H. C., et al. (2018). Dlk1-Dio3 locus-derived lncRNAs perpetuate postmitotic motor neuron cell fate and subtype identity. *eLife* 7:e38080.

Zhang, W., Yang, S. L., Yang, M., Herrlinger, S., Shao, Q., Collar, J. L., et al. (2019). Modeling microcephaly with cerebral organoids reveals a WDR62-CEP170-KIF2A pathway promoting cilium disassembly in neural progenitors. *Nat. Commun.* 10:2612. doi: 10.1038/s41467-019-10497-2

Zhou, T., Benda, C., Dunzinger, S., Huang, Y., Ho, J. C., Yang, J., et al. (2012). Generation of human induced pluripotent stem cells from urine samples. *Nat. Protoc.* 7, 2080–2089. doi: 10.1038/nprot.2012.115

Zhu, L., Gomez-Duran, A., Saretzki, G., Jin, S., Tilgner, K., Melguizo-Sanchis, D., et al. (2016). The mitochondrial protein CHCHD2 primes the differentiation potential of human induced pluripotent stem cells to neuroectodermal lineages. *J. Cell. Biol.* 215, 187–202. doi: 10.1083/jcb.201601061

Conflict of Interest: The authors declare that the research was conducted in the absence of any commercial or financial relationships that could be construed as a potential conflict of interest.

frontiers in Cell and Developmental Biology

ORIGINAL RESEARCH
published: 02 June 2020
doi: 10.3389/fcell.2020.00307

In vitro Neo-Genesis of Tendon/Ligament-Like Tissue by Combination of Mohawk and a Three-Dimensional Cyclic Mechanical Stretch Culture System

Kensuke Kataoka[1,2], Ryota Kurimoto[1], Hiroki Tsutsumi[1], Tomoki Chiba[1], Tomomi Kato[1], Kana Shishido[1], Mariko Kato[1], Yoshiaki Ito[1,3], Yuichiro Cho[4], Osamu Hoshi[4], Ayako Mimata[3], Yuriko Sakamaki[3], Ryo Nakamichi[1,5], Martin K. Lotz[5], Keiji Naruse[6] and Hiroshi Asahara[1,5,7]**

[1] Department of Systems BioMedicine, Tokyo Medical and Dental University, Tokyo, Japan, [2] Research Fellow of Japan Society for the Promotion of Science, Tokyo, Japan, [3] Research Core, Tokyo Medical and Dental University, Tokyo, Japan, [4] Anatomy and Physiological Science, Tokyo Medical and Dental University, Tokyo, Japan, [5] Department of Molecular Medicine, The Scripps Research Institute, La Jolla, CA, United States, [6] Department of Cardiovascular Physiology, Graduate School of Medicine, Dentistry and Pharmaceutical Sciences, Okayama University, Okayama, Japan, [7] AMED-CREST, Japan Agency for Medical Research and Development, Tokyo, Japan

OPEN ACCESS

Edited by:
Atsushi Asakura,
University of Minnesota Twin Cities, United States

Reviewed by:
Motohiro Komaki,
Kanagawa Dental University, Japan
So-Ichiro Fukada,
Osaka University, Japan

***Correspondence:**
Keiji Naruse
knaruse@md.okayama-u.ac.jp
Hiroshi Asahara
asahara@scripps.edu;
asahara.syst@tmd.ac.jp

Specialty section:
This article was submitted to Stem Cell Research, a section of the journal Frontiers in Cell and Developmental Biology

Received: 24 September 2019
Accepted: 07 April 2020
Published: 02 June 2020

Citation:
Kataoka K, Kurimoto R, Tsutsumi H, Chiba T, Kato T, Shishido K, Kato M, Ito Y, Cho Y, Hoshi O, Mimata A, Sakamaki Y, Nakamichi R, Lotz MK, Naruse K and Asahara H (2020) In vitro Neo-Genesis of Tendon/Ligament-Like Tissue by Combination of Mohawk and a Three-Dimensional Cyclic Mechanical Stretch Culture System. Front. Cell Dev. Biol. 8:307. doi: 10.3389/fcell.2020.00307

Tendons and ligaments are pivotal connective tissues that tightly connect muscle and bone. In this study, we developed a novel approach to generate tendon/ligament-like tissues with a hierarchical structure, by introducing the tendon/ligament-specific transcription factor Mohawk (MKX) into the mesenchymal stem cell (MSC) line C3H10T1/2 cells, and by applying an improved three-dimensional (3D) cyclic mechanical stretch culture system. In our developed protocol, a combination of stable *Mkx* expression and cyclic mechanical stretch synergistically affects the structural tendon/ligament-like tissue generation and tendon related gene expression. In a histological analysis of these tendon/ligament-like tissues, an organized extracellular matrix (ECM), containing collagen type III and elastin, was observed. Moreover, we confirmed that *Mkx* expression and cyclic mechanical stretch, induced the alignment of structural collagen fibril bundles that were deposited in a fibripositor-like manner during the generation of our tendon/ligament-like tissues. Our findings provide new insights for the tendon/ligament biomaterial fields.

Keywords: Mohawk, tendon, ligament, tissue engineering, mechanical-stress

INTRODUCTION

Tendons and ligaments are pivotal connective tissues that connect muscle to bone, and bone to the bone in joints. Tendons and ligaments mainly constitute the "tendon/ligament proper" and the "tendon/ligament sheath." Tendon/ligament proper comprises highly oriented tendon/ligament cells and extracellular matrix (ECM), which contains about 70–80% of collagens and approximately 20–30% of tendon/ligament ECM associated proteins such as elastin and proteoglycans in dry mass. Tendon/ligament sheaths are connective tissues that cover tendon/ligament surfaces and contain collagen type III (Bland and Ashhurst, 1996; Killian et al., 2012; Thorpe et al., 2013; Docheva et al., 2015). Due to its ECM complexity and the poor vascularized system of the tissue, tendon/ligament

injuries are one of the major issues among orthopedic diseases (Vailas et al., 1978; Liu et al., 2011; Mall et al., 2014).

To aim generating structural tendon/ligament like tissue, tissue engineering is one of promising approach. In order to recapitulate native tendon/ligament tissue structure, various methods such as cell sheets, biomaterials, and decellularized tissues have been developed as artificial substitutes for tendon/ligament tissue (Rodrigues et al., 2012). Recently, many studies have reported on the development of artificial tissues using cells such as mesenchymal stem cells (MSCs), embryonic tendon cells, or *Scleraxis* (*Scx*)–over-expressing embryonic stem cells (ESCs) (Kapacee et al., 2008, 2010; Chen et al., 2012; Breidenbach et al., 2015).

To construct structural tendon/ligament-like tissue via a three-dimensional (3D) culture, we focused on the developmental process of tendons and ligaments. Mechanical stress is indispensable for the growth and development of the musculoskeletal system (Dook et al., 1997; Couppé et al., 2008). For instance, mechanical stress expressing the synthesis of the cartilage ECM during development (Zuscik et al., 2008).

Furthermore, mechanical stress is essential for maintaining musculoskeletal system function. In fact, when mechanical stress is reduced, muscles show various pathologies such as atrophy (Sakuma et al., 2014).

These observations led us to investigate the synergetic effects between a 3D-culture and mechanical stress to generate structural tendon/ligament tissue. We previously showed that the tendon/ligament-specific transcription factor Mohawk (encoded by *Mkx*) is essential for the mechanical load response in tendons and ligaments. *Mkx* expression depends on mechanical stress both *in vivo* and *in vitro* and induces the expression of tendon/ligament-related genes (Kayama et al., 2016; Suzuki et al., 2016). Additionally, *MKX* differentiates the mesenchymal stem cell line C3H10T1/2 cells into tendon/ligament-like cells (Nakamichi et al., 2016).

Here, to develop a novel method to generate structural tendon/ligament-like tissue, we introduced for the first time an improved 3D cell culture and stretch system, in which various cell-stretching conditions could be adjusted. We used a stable *Mkx*-expressing C3H10T1/2 cells, which can be used for tendon/ligament-like tissue generation, as the source of tenocytes (Nakamichi et al., 2016). Combination of these strategies successfully allowed us to generate a tendon/ligament-like tissue with a highly organized collagen hieratical structure. Our findings provide new insights in the tendon/ligament biomaterial fields.

RESULTS

Production of Tenocyte-Like Cells From Mesenchymal Stem Cells by *Mkx* Introduction

Preparation of tenocytes in adequate amounts is challenging because tenocyte sources and the number of tenocytes obtained from each tissue are limited. In addition, primary cultured tenocytes can easily lose their phenotype in a few passages (Yao, 2006; Shukunami, 2018). Therefore, to achieve the aim of making tendon/ligament-like tissue, we need to prepare cells that have the cell stability for cells and synthetic ability of tendon/ligament tissues. In this regard, C3H10T1/2 cells are ideal for our experiential system. It is known that the most of tendons/ligaments cells are originated from *Scx* and SRY-Box transcription factor 9 (*Sox9*) expressing progenitor cells (Sugimoto, 2013). C3H10T1/2 cells show expressing *Scx*/*Sox9* and also show MSC like multipotent differentiate capacity (Zehentner et al., 1999; Zhao et al., 2009; Shukunami, 2018).

Furthermore, previous studies reported that the tendon/ligament-specific transcription factor *Mkx* induces differentiation of the mesenchymal stem cell line C3H10T1/2 cells into abundant and uniform tenocytes-like cells (Liu, 2015; Nakamichi et al., 2016).

Therefore, we used C3H10T1/2 cells to produce tenocytes-like cells that maintained their phenotype in the long-term. In this study, we prepared *Venus-Mkx*–expressing C3H10T1/2 cells and *Venus* (Mock)-expressing C3H10T1/2 cells as the control (Mock) (Nakamichi et al., 2016; **Figure 1**).

Development of Improved Mechanical Cell Stretch System for 3D Cell Culture

Previous studies showed that mechanical stress is critical for tendon/ligament maturation (Wang, 2006; Kayama et al., 2016) and that mechanical stress under *Mkx* expression could induce critical tendon-related gene expressions (Kayama et al., 2016; Suzuki et al., 2016).

This evidence prompted us to test whether *Mkx*-expressing MSCs, combined with mechanical stress, may potentiate the generation of tendon/ligament-like tissues *in vitro*. When mechanical stress is applied to cells under two-dimensional (2D) culture conditions, cell morphology vertically orients against the cell stretching direction (Yao, 2006; Morita et al., 2013; Shukunami, 2018).

On the other hand, 3D-culture systems of tendon cells with hydrogels are recognized to provide an environment closer to that experienced by tendon cells *in vivo* (Yeung, 2015).

Thus, we utilized a 3D-culture condition to generate tendon/ligament-like tissues. *Venus-Mkx*–expressing C3H10T1/2 cells embedded in a 3D chamber by gelation of the collagen gel (**Table 1**). This 3D culture system aims to create an *in vivo* culture environment *in vitro*. However during long-term culture, the embedded cells undergo apoptosis because there are no blood vessels that supply nutrients and oxygen in the deep layer of this artificial culture system (data not shown). To promote cell survival under 3D and mechanical stress culture conditions (Frisch and Ruoslahti, 1997), we introduced a cocktail of pro-survival factors (Laflamme et al., 2007) into the collagen gel (**Table 1** and **Figure 1**). We also prepared 3D-cultured *Venus* (Mock)-expressing C3H10T1/2 cells as the control.

In our previous studies, we observed that that appropriate mechanical stress is beneficial for promoting tendon-related gene expression (Kayama et al., 2016; Suzuki et al., 2016).

To deliver appropriate mechanical stress on 3D-cultured tenocyte-like cells, we modified our former mechanical cell

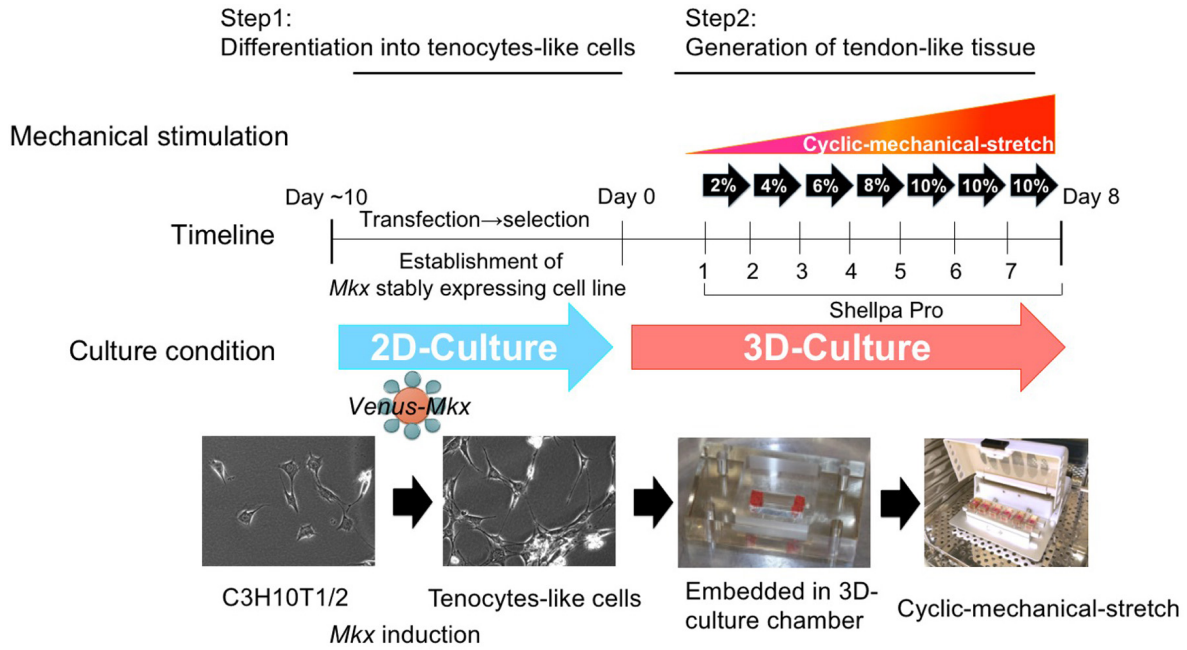

FIGURE 1 | The tendon/ligament-like tissue generation protocol. Schematic illustration of the tendon/ligament-like tissue generation strategy.

stretch system (Naruse et al., 1998). This improved mechanical cell stretch system allows us to adjust three parameters: stretch pattern (square wave, sine wave, sine wave with retention, and a combination of two types of square waves), stretch ratio [1%–20% elongation (in 1% steps)], and stretch frequency (1/600–2 Hz) (**Supplementary Figure S1**). Following cell embedding in the 3D-culture chamber, the samples were set to a mechanical cell stretch system. First, we have tested several different stress patterns, however, by applying too high a strain [static strain 10% at all incubation period (day 1 to day 7)] or too low a strain [static strain 2% at all incubation period (day 1 to day 7)] we were not able to generate a tissue like structure. High strain was caused to happen unintended tissue broken and low strain were not enough to accomplish collagen gel organize by embedded cell. After these testing which parameter set was best in obtaining tendon/ligament-like tissues (data not shown), we chose the following protocol: cyclic mechanical stretch was performed for one week with a gradually increasing stretch loading rate with sine wave pattern; 2% (day 1), 4% (day 2), 5% (day 3), 8% (day 4), and 10% (day 5–7) (**Figure 1**).

Generation of Tendon/Ligament-Like Tissue From 3D-Cultured *Venus-Mkx*–Expressing C3H10T1/2 Cells Using Cyclic Mechanical Stretch Load

Using the cyclic mechanical stretch conditions described above, we generated tendon/ligament-like tissues from *Venus-Mkx*–expressing C3H10T1/2 cells. To confirm the synergistic effects between *Mkx* and cyclic mechanical stretch, tendon/ligament-like tissues were generated under four different experimental conditions: *Venus-Mkx*–expressing C3H10T1/2 cells undergoing cyclic mechanical stretch (VMS+), *Venus-Mkx* without cyclic mechanical stretch (VMS−), *Venus* (Mock) –expressing C3H10T1/2 undergoing cyclic mechanical stretch (VS+), and *Venus* (Mock) –expressing C3H10T1/2 without cyclic mechanical stretch (VS−). As shown in **Figure 2A**, the tendon/ligament-like tissue generated in VMS+ condition is relatively thick comparing other conditions (**Figure 2A**). Next, to check the orientation of the cells, we performed Phalloidin staining. As a result, the orientation of actin filaments labeled with Phalloidin was observed in the stretching direction (**Supplementary Figure S2**).

Additionally, we examined tendon-related gene expression in each sample. The expression levels of the basic helix-loop-helix (BHLH) transcription factor *Scx*, which is highly expressed in tendon/ligament cells; collagen type I alpha 1 chain (*Col1a1*), which is the main component of tendon proper; and decorin (*Dcn*), which is involved in collagen fibrosis, were synergistically increased in the VMS + condition. Collagen type III alpha 1 chain (*Col3a1*) expression levels tend to increase depending on the cyclic mechanical stretch load but not with *Mkx* expression (**Figure 2B**).

Histological Analysis of Tendon/Ligament-Like Tissue

Histological analysis with hematoxylin and eosin (H&E) staining of the tendon/ligament-like tissue generated using VMS + condition showed that the nuclei, eosinophilic connective tissue (**Figure 3A**). Collagen fibers were stained in picrosirius red, and the fibers were oriented parallel to the direction of the cyclic mechanical stretch load (**Supplementary Figure S3**).

TABLE 1 | Tendon/ligament-like tissue 3D-culture cocktail.

Tendon/ligament-like tissue 3D-culture protocol	For 1sample	
Cellmatrix (Type1-A, nitta gelatin) (final concentration: 2 mg/mL)	32.27	ul
Collagen neutralize buffer (Type1-A, nitta gelatin) (final concentration: 1 ×)	5	
0.05mg/ml Bcl-Xl BH4 4-23 (197217-1MG, Calbiochem) (final concentration: 100 nM)	0.38	
10mM Z-VAD-FMK (G723A, PROMEGA) (final concentration: 100 μM)	0.5	
0.2mg/ml Ciclosporin A (039-16301, wako) (final concentration: 400 nM)	0.12	
100ng/μl Murine IGF-1 (250-19, PeoroTech) (final concentration: 200 ng/mL)	0.1	
10mg/ml Pinacidil monohydrate (sc-203198, ChemCruz) (final concentration: 100 μM)	0.13	
5		
100 × NEAA (11140-050, gibco) (final concentration: 1 v/v%)	0.5	
100 × GlutaMAX (35050-061, gibco) (final concentration: 1 v/v%)	0.5	
100 × Penicillin/Streptomycin (15140-122, gibco) (final concentration: 1 v/v%)	0.5	
↓		
Suspending 5 × 10^5 cells into above mixture		
↓		
Gelation into geltrex (A1413302, Thermo) coated three-dimensional stretch culture chamber (STB-3.5GS, STREX) and incubated at 37°C, 5% CO2 for 60 min		
↓		
Added to the medium [final concentration of 1 × MEMα (12000-063, gibco), 10 v/v% FBS, 1 v/v% 100 × NEAA (11140-050, gibco),1 v/v% 100 × GlutaMAX (35050-061, gibco), 55 uM 2-mercaptoethanol (21985-023, gibco), 1 v/v% 100 × Penicillin/Streptomycin (15140-122, gibco)] to the chamber	1500	ul
↓		
Further incubation was carried out at 37°C, 5% CO2 for 18 h to gelation completely		

It has been shown approximately 70–80% of the protein of the tendon dry mass is composed of collagens, whereas approximately 1–10% of elastin (Thorpe et al., 2013), which was not included in the cell-embedding gel. These two extracellular molecules have different physical properties: collagen is rigid and elastin is elastic (Schoen and Levy, 1999).

We next tested whether the tendon/ligament-like tissues were composed of elastin by Elastica van Gieson (EVG) elastic fiber staining. The tissue generated using *Venus-Mkx*–expressing C3H10T1/2 cells showed a strong signal over the entire section (**Figure 3B**), whereas other samples showed relatively weak staining. Additionally, we performed elastin immunohistochemical staining on each sample and confirmed that the tissues generated by *Venus-Mkx*–expressing C3H10T1/2 cells displayed relatively strong staining (**Figures 3C,D**). We also performed EVG staining in a mouse achilles tendon as a comparison with our tendon like tissue. We harvested two different developmental stages from the tendon tissue: neonate (postnatal day 14: P14) and adult (3 month old: 3M). We found clear reddish fuchsin acid staining, which represents high content of collagens in the adult mouse tendon tissue proper. However, the neonate achilles tendon tissue proper showed purplish red staining, which represents a moderate amount of collagen and elastin (**Supplementary Figure S4**). Comparing these results, we found that mouse achilles tendon tissue, derived from the neonate, showed a similar staining pattern than our artificial tissue (VMS+ and VMS−) (**Figure 3B** and **Supplementary Figure S4**). These results suggested that *Mkx* expression and cyclic mechanical stretch cooperatively affect elastin-containing ECM remodeling during tendon/ligament-like tissue generation.

Tendons and ligaments mainly comprise the "tendon/ligament proper" and "tendon/ligament sheath. We examined whether the sheath-like structure was reproduced in the tendon/ligament-like tissues. In all samples, tissue morphology on the surface layer is different from that in the rest of the tissue. Tendon/ligament proper is composed of highly oriented tendon/ligament cells and oriented collagens, which consists of 90−95% collagen type I. On the contrary, the tendon/ligament sheath, the connective tissue that covers the tendon/ligament surface, mainly contains other type of collagens such as collagen type III (Bland and Ashhurst, 1996; Docheva et al., 2015; Marqueti et al., 2018; Taye et al., 2020). Consistent with their reports, we were able to observe the tendon sheath's specific expression of collagen type III in mouse tendon tissue (**Supplementary Figure S4**).

Immunohistochemistry for collagen type III showed that VMS + C3H10T1/2 cells displayed strong and thick signal intensity at the surface layer compared with other samples (**Figure 3E**). VMS− and VS + condition also showed thick signal intensity at the surface of tissue but signal intensity is about less than half of VMS + condition (**Figure 3F**). VS− condition showed higher signal intensity comparing than VMS− and VM + but it hasn't thick signal intensity at the surface of tissue (**Figures 3E,F**). This tendency was different from *Col3a1* expression in **Figure 2B**. Although these might indicate a discrepancy between mRNA and protein expression, it is difficult to directly comparing differences of mRNA expression level and protein tissue distribution in the section.

Ultra-Structure Analysis of Surface and Inner Tissue of the Tendon/Ligament-Like Tissue

We found a difference in the staining patterns between the tissue surface layer and the remaining tissue from our histological analysis (**Figure 3**). Therefore, we further focused on these two areas. To achieve a detailed analysis tendon/ligament-like tissue morphology, we performed a scanning electron microscopy analysis.

For the surface layer, the tendon/ligament-like tissue of the VMS + condition showed that the surface layer structure was uniform and thick compared with that of other samples (**Figures 4A,B**). An image of the same sample taken at a different angle clearly depicted the multi-layered structure of the

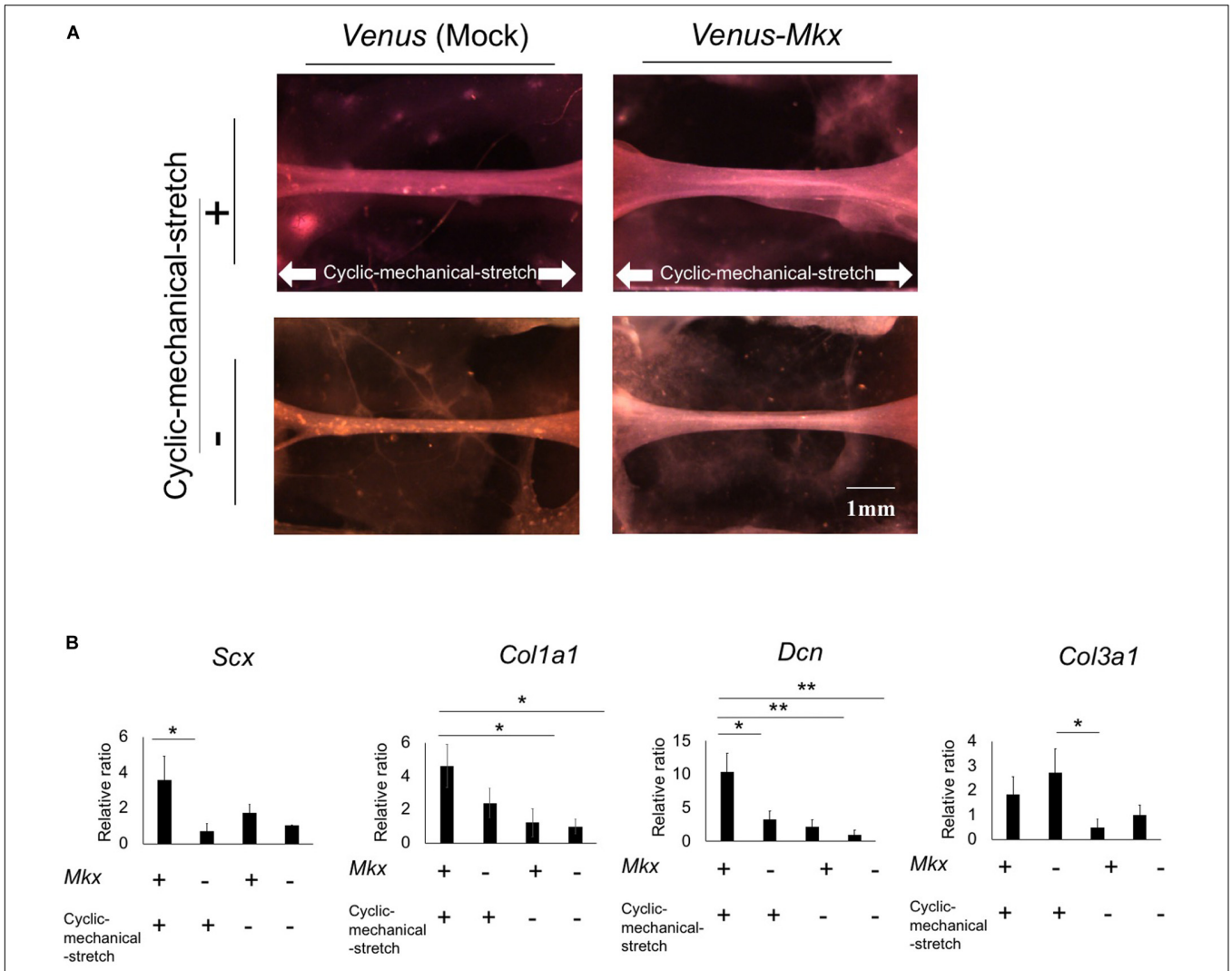

FIGURE 2 | Morphology and gene expression analysis of the tendon/ligament-like tissue under four different culture conditions. **(A)** The tendon/ligament-like tissue. These tissues were generated under four different culture conditions: *Venus-Mkx*–expressing mesenchymal stem cell (MSC) line C3H10T1/2 cells undergoing cyclic mechanical stretch (right top) (VMS+), *Venus-Mkx*–expressing C3H10T1/2 cells without cyclic mechanical stretch (right bottom) (VMS–), *Venus* (Mock)-expressing C3H10T1/2 cells undergoing cyclic mechanical stretch (left top) (VS+), and *Venus* (Mock)-expressing C3H10T1/2 cells without cyclic mechanical stretch (left bottom) (VS–) ($n = 3$). The direction of the cyclic mechanical stretch load is represented by white arrows. Scale bar: 1 mm. **(B)** Quantitative real-time quantitative reverse transcription polymerase chain reaction (qRT-PCR) analysis of the expression of *Scx*, *Col1a1*, *Col3a1*, and *Dcn*. Gene expression levels are normalized to the reference gene (*Gapdh*). Error bars show the mean ± standard deviation ($n = 3$). An asterisk represents the statistical significance calculated by Bonferroni test: $^{*}p < 0.05$ (for expression of *Scx*) and Tukey's honestly significant difference (HSD) test: $^{*}p < 0.05$ and $^{**}p < 0.01$ (for expression of *Col1a1*, *Col3a1*, and *Dcn*).

tendon/ligament-like tissue (**Figure 4B**). These results suggested that *Mkx* expression and cyclic mechanical stretch have a synergistic effect in remodeling tendon/ligament sheath-like structures containing collagen type III. For the inner layer, the tendon/ligament-like tissue of VMS + condition showed a uniformly horizontal orientation of the collagen fibril compared with that of other samples (**Figure 4C**). We analyzed the 3D orientation of these fibrils using scanning electron microscopy and analyzed the interior of the tendon/ligament-like tissue (**Figure 4C**). The orientation of the collagen fibril bundle was mostly parallel to the direction of the cyclic mechanical stretch in *Venus-Mkx*–expressing C3H10T1/2 cells (**Figures 4D,E**).

Analysis of Collagen Fibril Structure in the Tendon/Ligament-Like Tissue

Next, we assessed the collagen fibril bundle diameter of the VMS + condition. Transmission electron microscopy (**Figure 5A**) confirmed that the diameter of the collagen fibrils increased uniformly with the cyclic mechanical stretch load (**Figures 5B,C**).

Altogether, these results confirmed that the cooperative effect of *Mkx* expression and cyclic mechanical stretch results not only in increasing the number of collagen fibril bundles, but also in aligning their orientation during the tendon/ligament-like tissue generation process.

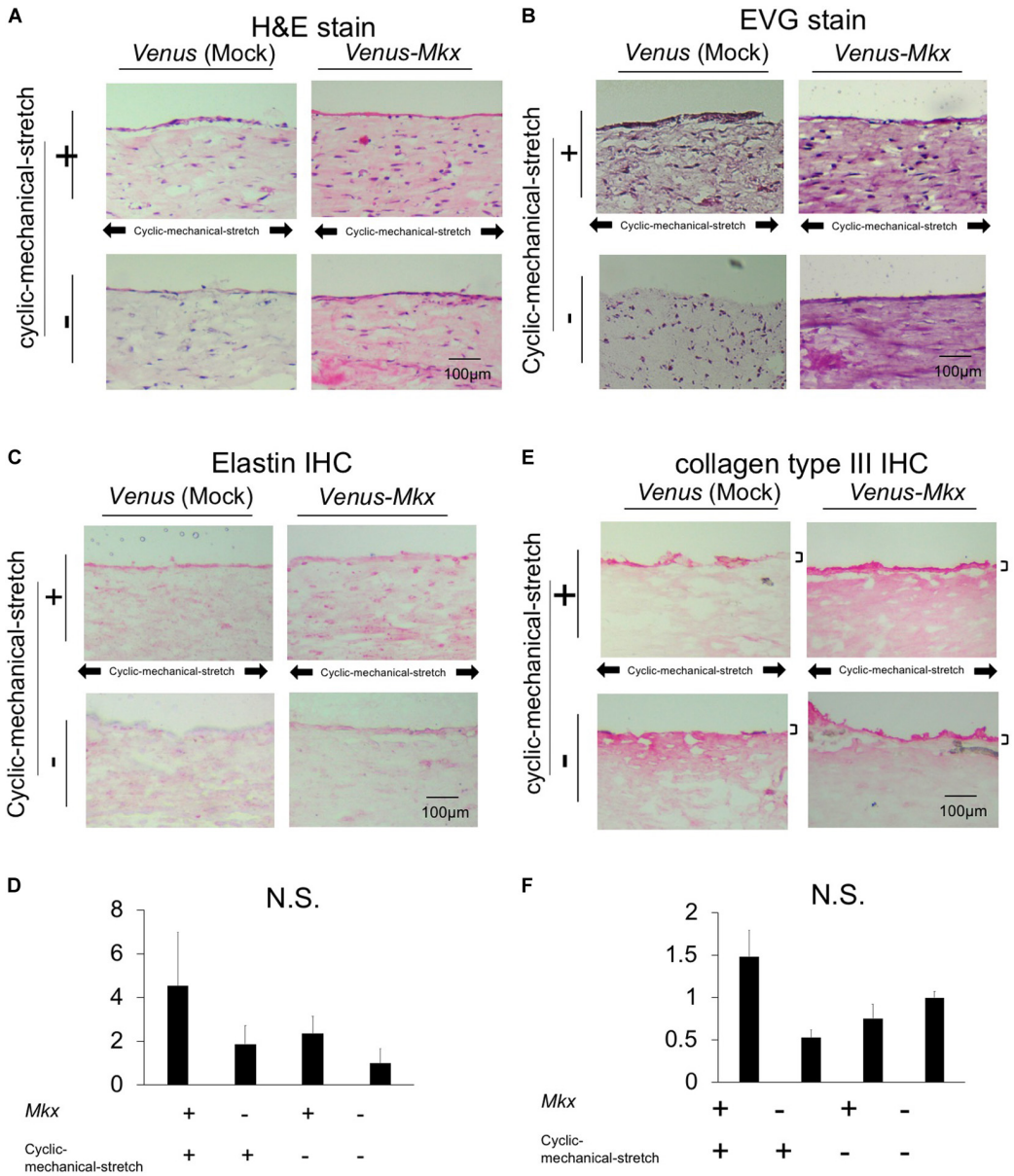

FIGURE 3 | Histological and immunohistochemical analysis of the tendon/ligament-like tissue. Histological **(A,B)** and immunohistochemical (IHC) **(C,D)** analyses. These tissues were generated under four different culture conditions: VMS+ (right top), VMS– (right bottom), VS+ (left top), and VS– (left bottom) (n = 3). The direction of the cyclic mechanical stretch load is represented by black arrows. Scale bar: 100 μm. **(A)** Representative micrographs of hematoxylin and eosin (H&E)-stained tissue sections. **(B)** Representative micrographs of Elastica Van Gieson (EVG)-stained tissue sections. **(C)** Representative micrographs of immunohistochemical staining for elastin in each tissue section. **(D)** Relative quantitative data of panel **(C)**. **(E)** Immunohistochemical analysis of the sectioned tendon/ligament-like tissue. Representative micrographs of immunohistochemical stain of collagen type III in each tissue section. Black bars depict collagen type III staining of the surface layer of the tendon/ligament-like tissue obtained from VMS + condition (n = 3). Scale bar: 100 μm. **(F)** Relative quantitative data of panel **(E)**.

Collagen Fibril Bundle Formation in Fibripositor-Like Manner Depends on *Mkx* Expression and Cyclic Mechanical Stretch Load

The results which we have presented previously strongly suggested that the *Venus-Mkx*–expressing C3H10T1/2 cells autonomously secrete collagen fibrils and generate oriented collagen fibril bundles upon 3D cyclic mechanical stretch. Therefore, to confirm this hypothesis, we further analyzed the electron microscopy images.

If the cells are autonomously generating oriented collagen fibril bundles, the collagen fibrils in the proximity of the cells would be mature compared with those far from the cells. To test whether the cells remodel the ECM, we defined the "cell proximal region" as within 1 μm of the plasma membrane, and the

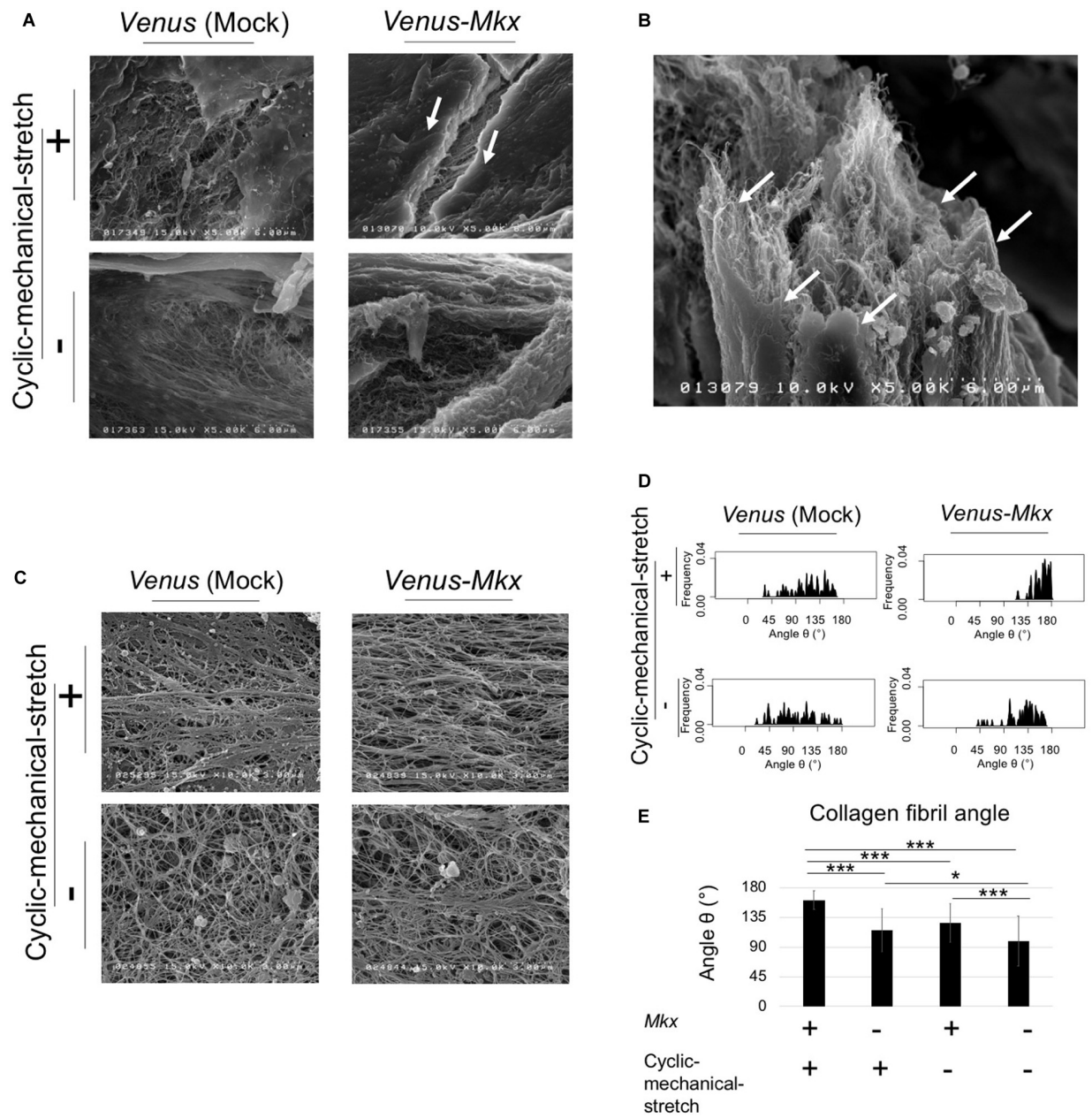

FIGURE 4 | SEM analysis revealed the ultra-structure of surface and fibril arrangement of inner tissue. **(A–E)** The tendon/ligament-like tissue. These tissues were generated under four different culture conditions: VMS+ (right top), VMS– (right bottom), VS+ (left top), and VS– (left bottom). The direction of the cyclic mechanical stretch load is represented by black arrows. **(A)** Scanning electron microscopy (SEM) images of the surface layer of tendon/ligament-like tissues. The white arrow shows the surface layer of the tendon/ligament-like tissue obtained from VMS + condition (n = 3). Scale bar: 6 μm. **(B)** SEM image of the section illustrated in panel **(A)** taken from a different angle. The white arrow shows the surface layer of the tendon/ligament-like tissue. Scale bar: 6 μm. **(C–E)** Analysis of collagen fibril arrangement. **(C)** SEM images of the tendon/ligament-like tissue. **(D)** Kernel Density Plots of collagen fibril arrangements. Data were calculated from 60 collagen fibrils in three different fields of view. The collagen fibril angle (θ) was calculated by comparing the direction of the horizontal axis and the orientation of the collagen fiber axis. **(E)** Calculated mean collagen fibril arrangement of each sample. The collagen fibril angle (θ) was calculated by comparing the direction of the horizontal axis and the orientation of the collagen fiber axis. The mean diameter of 60 collagen fibrils from three different fields of view was calculated: for VMS + condition (right top), mean angle 161°; for VMS– condition (right bottom), mean angle 126°; VS+ condition (left top), mean angle 115°; for VS– condition (left bottom), mean angle 99°. Error bars show the mean ± standard deviation. An asterisk represents statistical significance calculated by Bonferroni test:* $p < 0.05$ and *** $p < 0.001$.

"cell distal region" as greater than 1 μm from the plasma membrane; then, the length of the collagen fibril bundles in each region was measured.

The results showed that the lengths of the collagen fibril bundles were longer in the proximal area of the cell than they were far from the cell (**Figures 6A–D**). Furthermore,

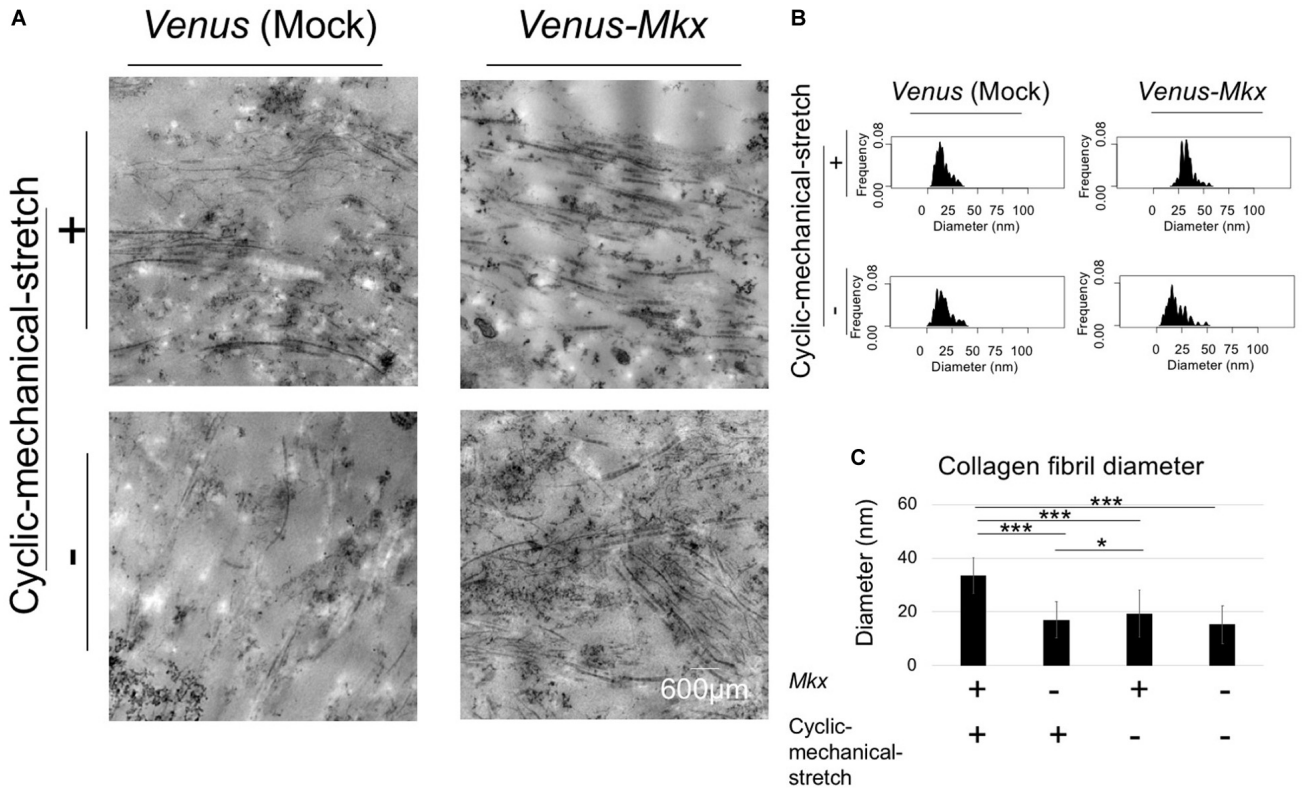

FIGURE 5 | Combination of mechanical stress and *Mkx* expressing has synergistic effect for thickness of collagen fibril diameter of tendon/ligament-like tissue. **(A–C)** Analysis of collagen fibril diameter. **(A)** Vertical section of transmission electron microscopy (TEM) images of tendon/ligament-like tissue. These tissues were generated under four different culture conditions: VMS + (right top), VMS– (right bottom), VS + (left top), and VS– (left bottom) (n = 3). Scale bar: 600 μm. **(B)** Kernel Density Plots of collagen fibril diameters. Data were calculated from 60 collagen fibrils in three different fields of view. **(C)** Calculated mean collagen fibril diameter from each sample. The mean diameter of 60 collagen fibrils from three different fields of view was calculated: for VMS + condition (right top), mean diameter 34 nm; for VMS– condition (right bottom), mean diameter 19 nm; for VS + condition (left top), mean diameter 17 nm; for VS– condition (left bottom), mean diameter 15 nm. Error bars show the mean ± standard deviation. An asterisk represents the statistical significance calculated by Tukey's honestly significant difference (HSD) test: $^{*}p < 0.05$ and $^{***}p < 0.001$.

statistical analysis of the collagen fibril bundle length in the "cell proximal region" revealed significantly longer bundles (Bonferroni test; $p < 0.01$ compared with the VMS− condition, $p < 0.001$ compared with the VS + condition and VS− condition) in VMS + condition than those in the other samples (**Figure 6B**). These results suggest that *Mkx* expressing and applying mechanical stretch have a synergistic effect with regard to collagen length (**Figures 6A–F**).

To determine the mechanisms of collagen maturation in *Venus-Mkx*–expressing C3H10T1/2 cells during cyclic mechanical stretch, we analyzed collagen secretion. A detailed analysis of the transmission electron microscopy images of VMS + C3H10T1/2 cells showed that the cells secrete mature collagen bundles directly into the plasma membrane (**Figure 6E**), which resembles fibripositors (Canty et al., 2004). A previous report showed that cellular fibripositor protrusions contain collagen fibrils (Canty et al., 2004; Kapacee et al., 2008). Interestingly, the VMS + C3H10T1/2 cells showed a typical fibripositor lumen-like structure (**Figure 6F**).

These results revealed that, in samples subjected to cyclic mechanical stretch and stably express *Mkx*, the cells autonomously secrete collagen fibril bundles in a fibripositor-like manner.

DISCUSSION

In this study, we developed a novel artificial tendon/ligament-like tissue generation method by coupling the expression of the tendon/ligament-specific transcription factor MKX with a 3D cyclic mechanical stretch culture system. Specifically, we embedded cells that stably express *Mkx* in a collagen gel and cultured them in three dimensions under a gradually increasing cyclic mechanical stretch load to mimic tendon/ligament development conditions.

However, how to generate structures that closely mimic the ECM in the *in vivo* tendon/ligament environment, which comprise several ECM-related proteins, such as collagen type I, collagen type III, and elastin (Thorpe et al., 2013; Docheva et al., 2015), could not be established.

To overcome these difficulties, we used cells that were stably transfected with a vector expressing the transcription factor

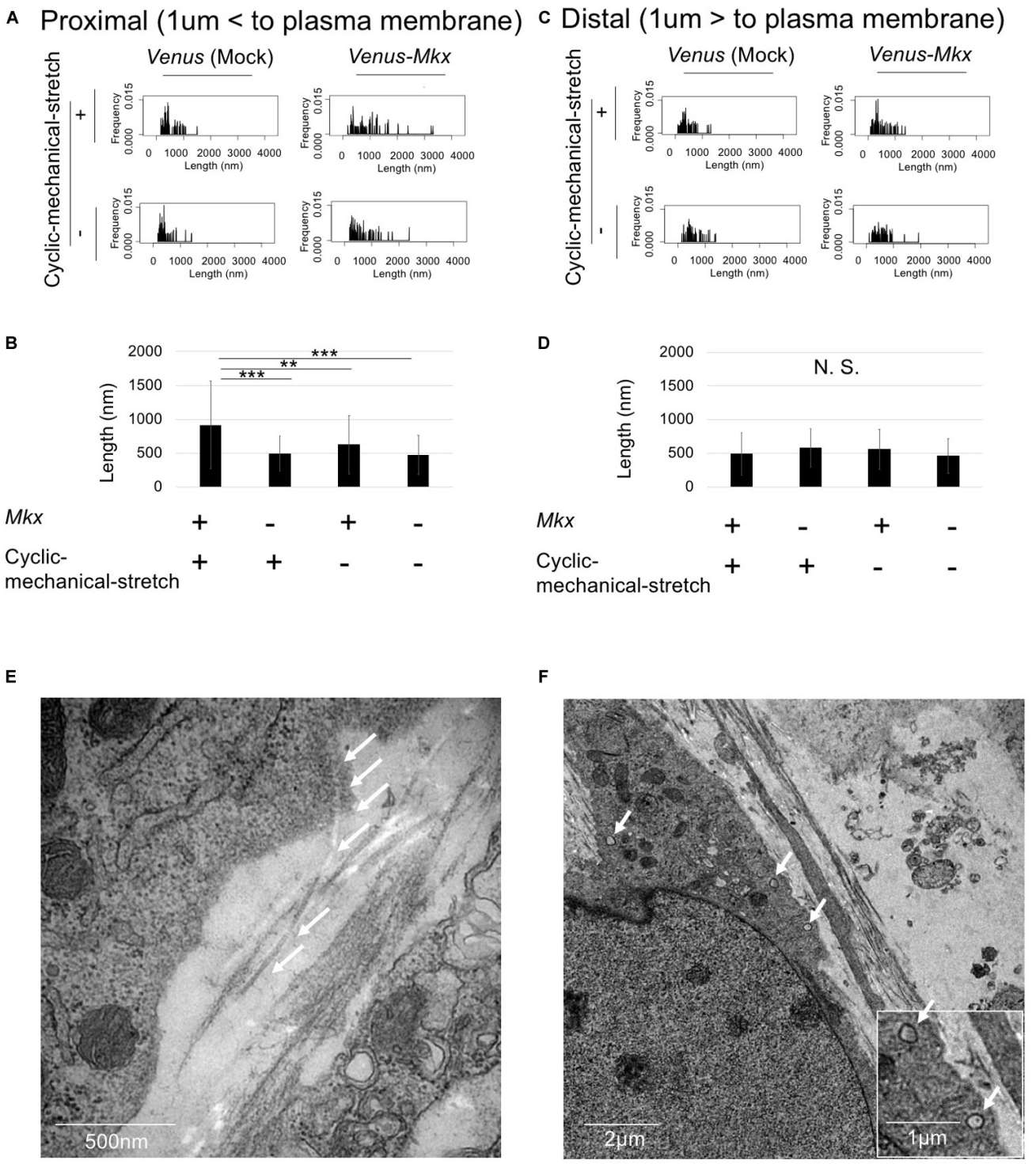

FIGURE 6 | Cells autonomously remodel the extracellular matrix during tendon/ligament-like tissue generation. **(A–D)** Analysis of collagen fibril length. These tissues were generated under four different culture conditions: VMS + (right top), VMS– (right bottom), VS + (left top), and VS– (left bottom) (n = 2). The "cell proximal region" was defined as within 1 μm of the plasma membrane, and the "cell distal region" as more than 1 μm from the plasma membrane. The length of collagen fibril bundles in each region was measured. **(A)** Kernel Density Plots of collagen fibril length in the "cell proximal region." Data were calculated from 60 collagen fibrils in three different fields of view. **(B)** Calculated mean collagen fibril length in the "cell proximal region" from each sample. The mean diameter of 60 collagen fibrils from

(Continued)

FIGURE 6 | Continued

three different fields of view was calculated: for VMS + condition, mean length 915 nm; for VMS– condition (right bottom), mean length 625 nm; for VS + condition (left top), mean length 495 nm; for VS– condition (left bottom), mean length 473 nm. Error bars show the mean ± standard deviation. An asterisk represents the statistical significance calculated by Bonferroni test: $^{**}p < 0.01$ and $^{***}p < 0.001$. **(C)** Kernel Density Plots of collagen fibril length in the "cell distal region." Data were calculated from 60 collagen fibrils in three different fields of view. **(D)** Calculated mean collagen fibril length in the "cell proximal region" from each sample. The mean diameter of 60 collagen fibrils from three different fields of view was calculated: for VMS + condition, mean length 489 nm; for VMS– condition (right bottom), mean length 560 nm; for VS + condition (left top), mean length 495 nm; for VS– condition (left bottom), mean length 460 nm. Error bars show the mean ± standard deviation. Statistical significance calculated by one-way analysis of variance (ANOVA). **(E,F)** Deposition of collagen fibrils in a fibripositor-like manner ($n = 2$). **(E)** Direct secretion of collagen fibrils through the plasma membrane into the extracellular matrix. The white arrow indicates the collagen fibril. Scale bar: 500 nm. **(F)** Intracellular lumen of the fibripositor-like structure. The white arrow indicates the fibripositor-like lumen structure. Scale bar: 2 μm. The bottom panel shows a higher magnification of the fibripositor-like lumen structure. The white arrow indicates fibripositor-like lumen structure. Scale bar: 1 μm.

MKX, which has the ability to promote collagen maturation and arrangement. The analysis of our electron microscope images confirmed that horizontal orientation of the collagen fibril bundles occurred exclusively in the cells that stably expressing *Mkx* and were subjected to cyclic mechanical stretch. The oriented collagen fibrils were secreted in a fibripositor-like manner similar to specific collagen secretion in the embryonic tendon development process (Canty et al., 2004). This phenotype was not observed in the control sample [*Venus* (Mock)-expressing C3H10T1/2 cells] or in samples not subjected to cyclic mechanical stretch, demonstrating the synergistic effects between MKX and cyclic mechanical stretch on collagen fibril bundle secretion and remodeling processes.

Importantly, we confirmed the presence of an organized ECM structure in the tendon/ligament-like tissue, similar to that of actual tendon tissues. The result of EVG staining showed that our artificial tissue (VMS+ and VMS−) has a similar staining pattern to neonatal mouse achilles tendon tissue (**Figure 3B** and **Supplementary Figure S4**). Analysis of the tendon/ligament-like tissue section confirmed that collagen type III aligned to the surface layer and that the tendon proper contained elastin. This organized ECM was rarely observed in the control sample [*Venus* (Mock)-expressing C3H10T1/2 cells] or in samples without cyclic mechanical stretch, which confirmed the synergistic effects between MKX and cyclic mechanical stretch in the remodeling and organization of the ECM. Previous reports have shown that collagen type III is specifically expressed in the tendon sheath, suggesting that collagen type III is among the "morphological marker proteins" of the tendon and ligament tissue (Docheva et al., 2015; Marqueti et al., 2018; Taye et al., 2020). Consistent with previous reports, we could observe the tendon sheath's specific expression of collagen type III in mouse tendon tissue (**Supplementary Figure S4**). We also observed the specific collagen type III distribution in the tendon/ligament-like tissue surface layer (**Figure 3E**), suggesting that the surface layer of an artificial tendon might possess tendon sheath characters.

The cell senses mechanical stress via a specific mechanical sensing receptor and a mechanical stress specific signal transduction. A previous report showed that *Mkx* and its upstream GTF2IRD is involving tendon mechanical sensing (Kayama et al., 2016). It has also been shown that MKX has the ability to maintain tenocyte identity via repressed cartilage specific transcription factor SOX9 (Suzuki et al., 2016). These reports indicate that *MKX* has dual role in tendon development: respond to the mechanical stress and maintain tendon tissue. This dual effect of *MKX* might be involved in generating the most constructive structure at the VMS+ condition.

With an aim to recapitulate the *in vivo* mechanical environment, various cell stretching devices have been developed and marketed (Naruse et al., 1998; Matheson et al., 2006; Chen et al., 2012; Kreutzer et al., 2014; Mihic et al., 2014; Breidenbach et al., 2015). In this study, we improved on our previously published mechanical cell stretch system (Naruse et al., 1998). The advantage of this new system is that it allows the configuration of detailed stretching conditions by setting three main parameters (1) stretch pattern, (2) stretch ratio, and (3) stretch frequency. By altering the stretch pattern (square wave, sine wave, sine wave with retention, or a combination of two types of square waves); stretch ratio [1–20% elongation (in 1% steps)]; and stretch frequency (1/600–2 Hz), this system could be configured to mimic the dynamic environment inside the human body and could be used to generate other tissues/organs requiring cyclic mechanical stretch.

In summary, we developed a novel system and method to generate structural tendon/ligament-like tissues containing elastin, oriented collagen type III, and collagen fibril bundles deposited in a fibripositor-like manner. By changing the shape of the 3D-culture chamber, it could be possible to prepare various fibrous tissues such as intervertebral disc-like artificial tissue and rotator cuff-like artificial tissue.

Our findings provide new insights in the tendon/ligament biomaterial fields.

MATERIALS AND METHODS

Cell Culture and Retrovirus Infection

C3H10T1/2 culture, retrovirus transfection, and establishment of *Venus*- (Nagai et al., 2002) or *Venus-Mkx* C3H10T1/2 cells were performed as previously described (Nakamichi et al., 2016). Briefly, C3H10T1/2 cells were cultured in alpha minimal essential medium (MEMα) with 10 v/v% fetal bovine serum (FBS) and 1 v/v% penicillin/streptomycin (15140-122, Gibco, MA, United States). Retrovirus infection was performed in the supernatant of retrovirus vector (pMIGR/*Venus*, pMIGR/*Venus-Mkx*) transfected PLAT-E cells. In order to clearly observe the cell

shape, we simultaneously introduced *mCherry* in both cell lines using the supernatant of pMIGR/*mCherry*-transfected PLAT-E cells. Stable cell lines were established by 1 μg/mL puromycin (ant-pr-1, InvivoGen, CA, United States) and 10 μg/mL blasticidin S (026-18711, FUJIFILM Wako Pure Chemical Corp., Osaka, JAPAN) selection for 1 week.

Isolation of Mouse Tendon and Fixation

Achilles tendons were harvested from neonate (postnatal day 14: P14) or adult (3 month old: 3M) C57BL/6N mice (Sankyo Labo Service Corporation, Tokyo, Japan). All mice were kept in specific pathogen-free facilities. After euthanizing anesthetized mice through cervical dislocation, both achilles tendons were removed. All tendons were fixed with 4% paraformaldehyde, dehydrated with 30% sucrose and embedded with OCT (Sakura Finetek, Torrance, CA, USA), and frozen at −80°C before section. All animal experiments were performed according to protocols approved by the Institutional Animal Care and Use Ethical Committee at the Tokyo Medical and Dental University (Approval No. A2018-096A).

3D-Culture

The cells were embedded in a 3D-culture cocktail (**Table 1**). The 3D-culture cocktail was constructed by mixing collagen gel [final concentrations: 2 mg/mL Cellmatrix (Type I-A, Nitta Gelatin Inc., Osaka, JAPAN) and 1 × collagen neutralization buffer (Type I-A, Nitta Gelatin Inc.)], pro-survival cocktail according to Laflamme et al. (2007) final concentrations: 100 nM B-cell lymphoma extra-large (Bcl-Xl) BH4 4-23 (197217-1MG, Calbiochem), 100 μM carbobenzoxy-valyl-alanyl-aspartyl-[O-methyl]-fluoromethylketone (Z-VAD-FMK) (G723A, Promega, WI, United States), 400 nM cyclosporin A (039-16301, FUJIFILM Wako Pure Chemical Corp.), 200 ng/mL murine insulin-like growth factor 1 (IGF-1) (250-19, PeproTech, NJ, United States), and 100 μM pinacidil monohydrate (sc-203198, ChemCruz, TX, United States), and medium [final concentration: 1 × MEMα (12000-063, Gibco), 10 v/v% FBS (2916154, MP Biomedical), 1 v/v% 100 × non-essential amino acid solution (NEAA) (11140-050, Gibco), 1 v/v% 100 × GlutaMAX (35050-061, Gibco), and 1 v/v% 100 × penicillin/streptomycin (15140-122, Gibco)].

To avoid irregular adhesion between the bottom of the 3D chamber and the 3D-culture cocktail, the bottom of the 3D stretch culture chamber (STB-3.5GS, STREX Inc., Osaka, JAPAN) was coated with 40 μL of Geltrex (A1413302, Thermo, MA, United States) and incubated at 37°C, 5% CO_2 for 30 min to allow Geltrex gelation. This step is important because irregular adhesion with the 3D chamber may hinder the structuring of the tendon/ligament-like tissue. The 3D-culture cocktail and cell mixture were transferred to the Geltrex-coated 3D stretch culture chamber and incubated at 37°C, 5% CO_2 for 60 min for gelation. Following gelation, MEMα medium containing 10 v/v% FBS, 1 v/v% 100 × penicillin/streptomycin (15140-122, Gibco), 1 v/v% 100 × GlutaMAX (35050-061, Gibco), 1 v/v% 100 × NEAA (Gibco 11140 - 050), and 55 μM 2-mercaptoethanol (21985-023, Gibco) was added to the chamber. Further incubation was carried out at 37°C, 5% CO_2 for 18 h for complete gelation.

Mechanical Stimulation

Following gelation, the 3D-cultured samples were set into a mechanical cell stretch system device (Shellpa Pro, Menicon Co., Ltd./Life Science Department, Aichi, Japan). Cyclic mechanical stretch was performed for one week, with a gradually increasing stretch loading rate to mimic the tendon/ligament development process: 2% (day 1), 4% (day 2), 5% (day 3), 8% (day 4), and 10% (day 5–7). The stretch loading rate was defined according to the following formula.

Stretch loading rate (%) = (width of the 3D stretch culture before stretching – width of the 3D stretch culture after stretching)/(width of the 3D stretch culture before stretch × 100). The cyclic mechanical stretch was programed at 0.25 Hz for 18 h/day, followed by resting for 6 h/day at 37°C, 5% CO_2. Samples which were appropriately anchored with a 3D chamber sponge and which had no irregular adhesion to the chamber side-wall were assayed in this study.

Histological and Immunohistochemical Analysis

Tendon/ligament-like tissue or mouse achilles tendon was fixed in 4% paraformaldehyde overnight at 4°C, washed in 1 × phosphate-buffered saline (PBS), cryo-preserved in 20% sucrose overnight, and embedded in optimal cutting temperature (OCT) compound (45833, Sakura Finetek Japan Co., Ltd., Tokyo, Japan). Then, the tendon/ligament-like tissue was cryo-sectioned at 10 μm and desiccated by air-drying overnight. Histological staining using hematoxylin (131-09665, FUJIFILM Wako Pure Chemical Corp.) and eosin (051-06515, FUJIFILM Wako Pure Chemical Corp.), Picrosirius red staining kit (24901-500, Polysciences, Inc., PA, United States), and Elastica Van Gieson (EVG) staining kit (1.15974.0002, Merck Millipore, Burlington, MA, United States) was performed according to the manufacturers' instructions. Immunohistochemical staining was performed using a Vectastain ABC-AP Rabbit IgG Kit (AK-5001, VECTOR LABORATORIES, INC., CA, United States) and Vector Red (SK-5100, VECTOR LABORATORIES, INC.) according to the manufacturer's instructions. Anti-Collagen III (1/500 dilution) (ab7778, Abcam plc, Cambridge, United Kingdom) and Anti-Elastin antibodies (1/500 dilution) (ab217356, Abcam plc) were used as the primary antibodies. We quantified the images using Image J software (NIH). In brief, the image was split into three colors (red, green, and blue), and only red colored images were picked up (red − blue). All images stained and photographed at the same time were set to the same threshold. The relative ratio of the area that exceeded the threshold from three different fields of view was calculated. To stain F-Actin, Alexa Fluor 594-phalloidin (A12381, Life technology) staining was performed according to the manufacturer's instructions. DAPI (VECTASHIELD with DAPI, H-1200, funakoshi) was used for nuclear staining.

RNA Isolation and qRT-PCR

RNA was isolated in ISOGEN (319-90211, NIPPON GENE CO., LTD., Toyama, Japan) using a teflon homogenizer and was

reverse-transcribed using a ReverTra Ace (TRT-101, TOYOBO CO., LTD., Osaka, Japan) according to the manufacturer's instructions. Complementary DNA was quantitated by qRT-PCR using a Thunderbird SYBR mix (QPS-201, TOYOBO CO., LTD.). *Gapdh* expression served as the control for mRNA expression. Changes in gene expression were quantified using the $\Delta\Delta$CT method (Livak and Schmittgen, 2001). Primer sequences are listed in **Supplementary Table S1**.

Statistical Analysis and Image Quantification

All statistical analyses were performed using R version 3.4.3 (R Core Team, 2017). First, significance of variance among samples was calculated by Bartlett's test using the command "bartlett.test." Secondly, if the samples had equal variance, one-way ANOVA was conducted using the command "aov," if samples had no equal variance, Kruskal-Wallis rank sum test was conducted using the command "kruskal.test."

Finally, if the samples rejected the null hypothesis of one-way ANOVA, the significant of each sample was calculated with *post hoc* comparisons by Tukey's honest significant difference (HSD) test using the command "TukeyHSD," and if the samples rejected the null hypothesis of the Kruskal-Wallis rank sum test, the significance of each sample was calculated with *post hoc* comparisons by Bonferroni using the command "pairwise.*t*.test (p.adjust.method = "bonferroni")." $p < 0.05$ was considered significant in all statistical analyses. The command "density" was used to calculate and depict the Kernel Density Plots. The diameter and arrangement of collagen fibrils were analyzed using the ImageJ software (Schneider et al., 2012). The collagen fibril angle (θ) was calculated by comparing the direction of the horizontal axis and the orientation of the collagen fiber axis.

Electron Microscopy

Tendon/ligament-like tissues were dissected and fixed in 2.5% glutaraldehyde in 0.1 M phosphate buffer (PB) overnight. For transmission electron microscopy (TEM), the specimens ($n = 3$) were washed with 0.1 M PB, post-fixed in 1% osmium buffered with 0.1 M PB for 2 h, and dehydrated in a graded series of ethanol. Then, the specimens were embedded in Epon 812, sliced into ultrathin sections (70 nm), collected on copper grids, and double-stained with uranyl acetate and lead citrate. The specimens were observed using TEM (H-7100, Hitachi, Ltd., Tokyo, Japan). For scanning electron microscopy (SEM), the specimens ($n = 2$) were dried in a critical-point drying apparatus (HCP-2, Hitachi, Ltd.) with liquid CO_2 and were spatter-coated with platinum. Then, the specimens were observed using SEM (S-4500, Hitachi, Ltd.).

DATA AVAILABILITY STATEMENT

All the data required to reproduce this study are included in this published article and **Supplementary Information**. The raw data required to reproduce these findings are available from the corresponding author on reasonable request.

ETHICS STATEMENT

The animal study was reviewed and approved by the Institutional Animal Care and Use Ethical Committee at the Tokyo Medical and Dental University (Approval No. A2018-096A).

AUTHOR CONTRIBUTIONS

KK, TC, YI, RN, ML, and HA designed all of the experiments. KN contributed refinement of the mechanical cell stretch system and advised on tendon/ligament-like tissue generation. KK performed the 3D-culture with cyclic mechanical stretching, qRT-PCR of tendon/ligament-like tissue, and all statistical analyses. KK, RK, HT, TK, KS, and MK performed all the histological/immuno-histochemical analyses. AM and YS performed the sample preparation of transmission/scanning electron microscope. KK, RK, HT, TK, KS, MK, YC, and OH performed the analysis of the scanning electron microscope. KK, RK, HT, TK, and KS performed the analysis of the transmission electron microscope. KK, TC, and HA interpreted all the experimental data and wrote the manuscript. ML and HA supervised the laboratory and all experiments.

FUNDING

This work was supported by JSPS KAKENHI (Grant Nos.: 26113008, 15H02560, 15K15544, 18K196013, and 19KK0227 to HA, 26220203 to KN, and 18J13487 to KK), Core Research for the Evolutionary Science and Technology (CREST) funding from the Japan Science and Technology Agency and AMED-CREST (Grant Nos.: JP15gm0410001 and JP19gm0810008 to HA), and grants from the NIH (Grant Nos.: AR050631 and AR065379 to HA). KN was supported by the Menicon Co., Ltd., Aichi, Japan.

ACKNOWLEDGMENTS

We thank Dr. Naoko Nakamura, Dr. Tsuyoshi Kimura, and Prof. Akio Kishida from the Department of Material-Based Medical Engineering, Tokyo Medical and Dental University, Tokyo, Japan for their critical discussions. We also thank all the members of the Department of Systems BioMedicine in Tokyo Medical and Dental University for their support. We would like to thank Editage (www.editage.jp) for the English language editing.

SUPPLEMENTARY MATERIAL

The Supplementary Material for this article can be found online at: https://www.frontiersin.org/articles/10.3389/fcell.2020.00307/full#supplementary-material

REFERENCES

Bland, Y. S., and Ashhurst, D. E. (1996). Changes in the distribution of fibrillar collagens in the collateral and cruciate ligaments of the rabbit knee joint during fetal and postnatal development. *Histochem. J.* 28, 325–334. doi: 10.1007/bf02331395

Breidenbach, A. P., Dyment, N. A., Lu, Y., Rao, M., Shearn, J. T., Rowe, D. W., et al. (2015). Fibrin gels exhibit improved biological, structural, and mechanical properties compared with collagen gels in cell-based tendon tissue-engineered constructs. *Tissue Eng. Part A* 21, 438–450. doi: 10.1089/ten.TEA.2013.0768

Canty, E. G., Lu, Y., Meadows, R. S., Shaw, M. K., Holmes, D. F., and Kadler, K. E. (2004). Coalignment of plasma membrane channels and protrusions (fibripositors) specifies the parallelism of tendon. *J. Cell Biol.* 165, 553–563. doi: 10.1083/jcb.200312071

Chen, X., Yin, Z., Chen, J. L., Shen, W. L., Liu, H. H., Tang, Q. M., et al. (2012). Force and scleraxis synergistically promote the commitment of human ES cells derived MSCs to tenocytes. *Sci. Rep.* 2:977. doi: 10.1038/srep00977

Couppé, C., Kongsgaard, M., Aagaard, P., Hansen, P., Bojsen-Moller, J., Kjaer, M., et al. (2008). Habitual loading results in tendon hypertrophy and increased stiffness of the human patellar tendon. *J. Appl. Physiol.* 105, 805–810. doi: 10.1152/japplphysiol.90361.2008

Docheva, D., Müller, S. A., Majewski, M., and Evans, C. H. (2015). Biologics for tendon repair. *Adv. Drug Deliv. Rev.* 84, 222–239. doi: 10.1016/j.addr.2014.11.015

Dook, J. E., James, C., Henderson, N. K., and Price, R. I. (1997). Exercise and bone mineral density in mature female athletes. *Med. Sci. Sports Exerc.* 29, 291–296. doi: 10.1097/00005768-199703000-00002

Frisch, S. M., and Ruoslahti, E. (1997). Integrins and anoikis. *Curr. Opin. Cell Biol.* 9, 701–706.

Kapacee, Z., Richardson, S. H., Lu, Y., Starborg, T., Holmes, D. F., Baar, K., et al. (2008). Tension is required for fibripositor formation. *Matrix Biol.* 27, 371–375.

Kapacee, Z., Yeung, C. Y., Lu, Y., Crabtree, D., Holmes, D. F., and Kadler, K. E. (2010). Synthesis of embryonic tendon-like tissue by human marrow stromal/mesenchymal stem cells requires a three-dimensional environment and transforming growth factor β3. *Matrix Biol.* 29, 668–677. doi: 10.1016/j.matbio.2010.08.005

Kayama, T., Mori, M., Ito, Y., Matsushima, T., Nakamichi, R., Suzuki, H., et al. (2016). Gtf2ird1-dependent mohawk expression regulates mechanosensing properties of the tendon. *Mol. Cell. Biol.* 36, 1297–1309. doi: 10.1128/MCB.00950-15

Killian, M. L., Cavinatto, L., Galatz, L. M., and Thomopoulos, S. (2012). The role of mechanobiology in tendon healing. *J. Shoulder Elbow Surg.* 21, 228–237.

Kreutzer, J., Ikonen, L., Hirvonen, J., Pekkanen-Mattila, M., Aalto-Setälä, K., and Kallio, P. (2014). Pneumatic cell stretching system for cardiac differentiation and culture. *Med. Eng. Phys.* 36, 496–501. doi: 10.1016/j.medengphy.2013.09.008

Laflamme, M. A., Chen, K. Y., Naumova, A. V., Muskheli, V., Fugate, J. A., Dupras, S. K., et al. (2007). Cardiomyocytes derived from human embryonic stem cells in pro-survival factors enhance function of infarcted rat hearts. *Nat. Biotechnol.* 25, 1015–1024. doi: 10.1038/nbt1327

Liu, C. F., Aschbacher-Smith, L., Barthelery, N. J., Dyment, N., Butler, D., and Wylie, C. (2011). What we should know before using tissue engineering techniques to repair injured tendons: a developmental biology perspective. *Tissue Eng. Part B Rev.* 17, 165–176. doi: 10.1089/ten.TEB.2010.0662

Liu, H. (2015). Mohawk promotes the tenogenesis of mesenchymal stem cells through activation of the TGFβ signaling pathway. *Stem Cells* 33, 443–455. doi: 10.1002/stem.1866

Livak, K. J., and Schmittgen, T. D. (2001). Analysis of relative gene expression data using real-time quantitative PCR and the 2(-Delta Delta C(T)) Method. *Methods* 25, 402–408. doi: 10.1006/meth.2001.1262

Mall, N. A., Chalmers, P. N., Moric, M., Tanaka, M. J., Cole, B. J., Bach, B. R. Jr., et al. (2014). Incidence and trends of anterior cruciate ligament reconstruction in the United States. *Am. J. Sports Med.* 42, 2363–2370. doi: 10.1177/0363546514542796

Marqueti, R. C., Durigan, J. L. Q., Oliveira, A. J. S., Mekaro, M. S., Guzzoni, V., Aro, A. A., et al. (2018). Effects of aging and resistance training in rat tendon remodeling. *FASEB J.* 32, 353–368. doi: 10.1096/fj.201700543R

Matheson, L. A., Fairbank, N. J., Maksym, G. N., Paul Santerre, J., and Labow, R. S. (2006). Characterization of the Flexcell Uniflex cyclic strain culture system with U937 macrophage-like cells. *Biomaterials* 27, 226–233. doi: 10.1016/j.biomaterials.2005.05.070

Mihic, A., Li, J., Miyagi, Y., Gagliardi, M., Li, S. H., Zu, J., et al. (2014). The effect of cyclic stretch on maturation and 3D tissue formation of human embryonic stem cell-derived cardiomyocytes. *Biomaterials* 35, 2798–2808. doi: 10.1016/j.biomaterials.2013.12.052

Morita, Y., Watanabe, S., Ju, Y., and Xu, B. (2013). Determination of optimal cyclic uniaxial stretches for stem cell-to-tenocyte differentiation under a wide range of mechanical stretch conditions by evaluating gene expression and protein synthesis levels. *Acta Bioeng. Biomech.* 15, 71–79.

Nagai, T., Ibata, K., Park, E. S., Kubota, M., Mikoshiba, K., and Miyawaki, A. (2002). A variant of yellow fluorescent protein with fast and efficient maturation for cell-biological applications. *Nat. Biotechnol.* 20, 87–90. doi: 10.1038/nbt0102-87

Nakamichi, R., Ito, Y., Inui, M., Onizuka, N., Kayama, T., Kataoka, K., et al. (2016). Mohawk promotes the maintenance and regeneration of the outer annulus fibrosus of intervertebral discs. *Nat. Commun.* 7:12503. doi: 10.1038/ncomms12503

Naruse, K., Yamada, T., and Sokabe, M. (1998). Involvement of SA channels in orienting response of cultured endothelial cells to cyclic stretch. *Am. J. Physiol. Hear. Circ. Physiol.* 43, 1532–1538. doi: 10.1152/ajpheart.1998.274.5.H1532

R Core Team (2017). *R: A Language and Environment for Statistical Computing*. Vienna: R Foundation for Statistical Computing.

Rodrigues, M. T., Reis, R. L., and Gomes, M. E. (2012). Engineering tendon and ligament tissues: present developments towards successful clinical products. *J. Tissue Eng. Regen. Med.* 7, 673–686. doi: 10.1002/term.1459

Sakuma, K., Aoi, W., and Yamaguchi, A. (2014). The intriguing regulators of muscle mass in sarcopenia and muscular dystrophy. *Front. Aging Neurosci.* 29:230. doi: 10.3389/fnagi.2014.00230

Schneider, C. A., Rasband, W. S., and Eliceiri, K. W. (2012). NIH Image to ImageJ: 25 years of image analysis. *Nat. Methods* 9, 671–675. doi: 10.1038/nmeth.2089

Schoen, F. J., and Levy, R. J. (1999). Tissue heart valves: current challenges and future research perspectives. *J. Biomed. Mater. Res.* 47, 439–465. doi: 10.1002/(sici)1097-4636(19991215)47:4<439::aid-jbm1>3.0.co;2-o

Shukunami, C. (2018). Scleraxis is a transcriptional activator that regulates the expression of Tenomodulin, a marker of mature tenocytes and ligamentocytes. *Sci. Rep.* 8:3155. doi: 10.1038/s41598-018-21194-3

Sugimoto, Y. (2013). Scx+/Sox9+ progenitors contribute to the establishment of the junction between cartilage and tendon/ligament. *Development* 140, 2280–2288. doi: 10.1242/dev.096354

Suzuki, H., Ito, Y., Shinohara, M., Yamashita, S., Ichinose, S., Kishida, A., et al. (2016). Gene targeting of the transcription factor Mohawk in rats causes heterotopic ossification of Achilles tendon via failed tenogenesis. *Proc. Natl. Acad. Sci. U.S.A.* 113, 7840–7845. doi: 10.1073/pnas.1522054113

Taye, N., Karoulias, S. Z., and Hubmacher, D. (2020). The "other" 15-40%: the role of non-collagenous extracellular matrix proteins and minor collagens in tendon. *J. Orthop. Res.* 38, 23–35. doi: 10.1002/jor.24440

Thorpe, C. T., Birch, H. L., Clegg, P. D., and Screen, H. R. (2013). The role of the non-collagenous matrix in tendon function. *Int. J. Exp. Pathol.* 94, 248–259. doi: 10.1111/iep.12027

Vailas, A. C., Tipton, C. M., Laughlin, H. L., Tcheng, T. K., and Matthes, R. D. (1978). Physical activity and hypophysectomy on the aerobic capacity of ligaments and tendons. *J. Appl. Physiol. Respir. Environ. Exerc. Physiol.* 44, 542–546. doi: 10.1152/jappl.1978.44.4.542

Wang, J. H. (2006). Mechanobiology of tendon. *J. Biomech.* 39, 1563–1582.

Yao, L. (2006). Phenotypic drift in human tenocyte culture. *Tissue Eng.* 12, 1843–1849.

Yeung, C. Y. (2015). Chick tendon fibroblast transcriptome and shape depend on whether the cell has made its

own collagen matrix. *Sci. Rep.* 5:13555. doi: 10.1038/srep 13555

Zehentner, B. K., Dony, C., and Burtscher, H. (1999). The transcription factor Sox9 is involved in BMP-2 signaling. *J. Bone Miner. Res.* 14, 1734–1741. doi: 10.1359/jbmr.1999.14.10.1734

Zhao, L., Li, G., Chan, K. M., Wang, Y., and Tang, P. F. (2009). Comparison of multipotent differentiation potentials of murine primary bone marrow stromal cells and mesenchymal stem cell line C3H10T1/2. *Calcif. Tissue Int.* 84, 56–64. doi: 10.1007/s00223-008-9189-3

Zuscik, M. J., Hilton, M.-J., Zhang, X., Chen, D., and O'Keefe, R.-J. (2008). Regulation of chondrogenesis and chondrocyte differentiation by stress. *J. Clin. Invest.* 118, 429–438. doi: 10.1172/JCI34174

Conflict of Interest: The authors declare that the research was conducted in the absence of any commercial or financial relationships that could be construed as a potential conflict of interest.

frontiers in Cell and Developmental Biology

OPINION
published: 04 June 2020
doi: 10.3389/fcell.2020.00419

Dissecting the Niche for Alveolar Type II Cells With Alveolar Organoids

Danying Liao[1] *and Huaibiao Li*[2]*

[1] Department of Haematology, Union Hospital, Tongji Medical College, Huazhong University of Science and Technology, Wuhan, China, [2] Institute of Reproductive Health, Tongji Medical College, Huazhong University of Science and Technology, Wuhan, China

Keywords: lung, alveolar epithelium, alveolar type II epithelial cell, alveolar stem cell, alveolar organoid, Wnt pathway, FGF pathway, coronavirus

INTRODUCTION

The self-renewal and differentiation of tissue stem cells are dictated by the microenvironment in which they reside, the so-called stem cell niche (Scadden, 2006; de Cuevas and Matunis, 2011; Chacón-Martínez et al., 2018; Pinho and Frenette, 2019). To date, the importance of the niche in maintaining tissue homeostasis is increasingly appreciated, given the capability of stem cells to restore normal tissue function upon injury (Wabik and Jones, 2015). With the advent of new techniques, such as *in vivo* imaging, lineage tracing models and single-cell sequencing, our understanding of the interaction between stem cells and the niche under both normal physiological and pathological conditions is broadened (Zepp et al., 2017; Joost et al., 2018; Nguyen and Currie, 2018). However, the complexity and dynamics of the niche within the tissue, which are difficult to recapitulate in 2D culture, compound the effort to pinpoint the contribution of each niche component to stem cell function. Here, we discuss how to deconvolute the complexity of the stem cell niche with organotypic culture methods using alveolar stem cells within the lung as an example.

The alveoli in the distal regions of the lung are the primary sites for gas exchange (Brody and Williams, 1992). The alveolar epithelia mainly consist of type II (AEC2) and type I (AEC1) epithelial cells (**Figure 1A**; Brody and Williams, 1992). The latter are squamous cells responsible for gas exchange, covering most of the surface area of alveoli (Brody and Williams, 1992). AEC2 cells have cuboidal shape and maintain the stability of alveoli through synthesis and secretion of surfactant proteins (reviewed in detail by Fehrenbach, 2001; Beer and Moodley, 2017). In addition to these characteristics, AEC2 cells are proposed to be the stem cells within the alveolar epithelia (Fehrenbach, 2001; Barkauskas et al., 2013). This is supported by results from lineage tracing studies (Barkauskas et al., 2013; Desai et al., 2014; Zacharias et al., 2018). Within the normal lung, AEC2 cells are able to differentiate into AEC1 cells, albeit at a very low turnover rate (Barkauskas et al., 2013; Desai et al., 2014). Injuries to the lung trigger the rapid proliferation of AEC2 cells, followed by differentiation to AEC1 cells to restore the normal function of the lung (Barkauskas et al., 2013; Desai et al., 2014; Nabhan et al., 2018; Zacharias et al., 2018). Of note, single-cell sequencing and lineage tracing studies have unraveled the heterogeneity of AEC2 cells that display differential capacity of proliferation and differentiation in both homeostatic and regenerative states (Desai et al., 2014; Treutlein et al., 2014; Nabhan et al., 2018; Zacharias et al., 2018; Riemondy et al., 2019). Therefore, a subpopulation of AEC2 cells might serve as the stem/progenitor cells to maintain the homeostasis of the alveoli in the lung (Hogan et al., 2014).

OPEN ACCESS

Edited by:
Eumorphia Remboutsika, National and Kapodistrian University of Athens, Greece

Reviewed by:
Hani N. Alsafadi, Lund University, Sweden

***Correspondence:**
Huaibiao Li
lihuaibiao@hust.edu.cn

Specialty section:
This article was submitted to Stem Cell Research, a section of the journal Frontiers in Cell and Developmental Biology

Received: *20 March 2020*
Accepted: *06 May 2020*
Published: *04 June 2020*

Citation:
Liao D and Li H (2020) Dissecting the Niche for Alveolar Type II Cells With Alveolar Organoids. Front. Cell Dev. Biol. 8:419. doi: 10.3389/fcell.2020.00419

THE NICHE OF AEC2 CELLS

Within the alveolar epithelia, AEC2 cells are in contact with AEC1 cells via cell junctions (Fehrenbach, 2001). There are several types of stromal cells in the interstitial region, including mesenchymal cells, pericytes, endothelial cells, and immune cells (Hogan et al., 2014; Tan and Krasnow, 2016; Endale et al., 2017). Together with extracellular matrix (ECM), these cells constitute the "putative" niche for AEC2 cells (**Figure 1A**; Hogan et al., 2014). How the niche modulates the behavior of AEC2 cells starts to unfold, driven by lineage tracing models. Nabhan and colleagues showed that a subpopulation of AEC2 cells are Axin2-positive; these cells localize at close proximity to Wnt-expressing fibroblasts (Nabhan et al., 2018). The "juxtacrine" Wnt signal maintains the stemness of Axin2+AEC2 cells, whereas the loss-of-contact with the niche promotes their differentiation to AEC1 cells (Nabhan et al., 2018). Using single-cell RNA sequencing and reporter mouse lines, five subpopulations of mesenchymal cells are identified, based on the levels of PDGFRα, Wnt2, and Axin2 (Zepp et al., 2017). Spatial distance mapping further revealed that PDGFRα-Axin2 double-positive mesenchymal cells localize closer to AEC2 cells than other subpopulations (Zepp et al., 2017). Collectively, these results support the notion that mesenchymal cells in close contact with AEC2 cells are critical components of the alveolar stem cell niche.

Deconvolution of the niche complexity requires a reductionist system through which the contribution of a single niche component to AEC2 behavior can be examined. Organotypic culture appears to suit this purpose, in which the interaction between the stem cell and the niche can be interrogated (Kretzschmar and Clevers, 2016; Murrow et al., 2017). AEC2 cells have been cocultured with various types of stromal cells in Matrigel to form spheroids, including lung fibroblasts, endothelial cells and macrophages (**Figures 1B,C**, **Supplementary Table 1**; McQualter et al., 2010; Chen et al., 2012; Barkauskas et al., 2013; Lee et al., 2014; Lechner et al., 2017). With the support of mesenchymal cells, AEC2 cells grow into spheroids with multiple layers of cells, in which AEC1 cells are lined along the inner lumen surface, surrounded by AEC2 cells, referred to as alveolar organoids (**Figure 1B**; Chen et al., 2012; Barkauskas et al., 2013, 2017). It seems that the presence of mesenchymal cells promotes both the self-renewal and differentiation of AEC2 cells (Barkauskas et al., 2013). One of the tempting explanations is the proximity of AEC2 cells to mesenchymal cells, as suggested by the *in vivo* data. Indeed, when cultured on top of mesenchymal cells, the differentiation of AEC2 cells is blocked (Sucre et al., 2018). Furthermore, the capacity of organoid induction by subpopulations of mesenchymal cells is evaluated via the organotypic coculture system, among which PDGFRα-Axin2 double-positive populations show the highest efficiency (Zepp et al., 2017). Overall, the application of alveolar organoid facilitates the examination of the role of stromal cells in regulating the fate of AEC2 cells.

SIGNALS FROM THE NICHE DIRECTING THE FATE OF AEC2 CELLS

Niche-derived paracrine signals modulate the behavior of AEC2 cells, among which FGF signaling is of particular importance (**Figure 1A**). It has been demonstrated that FGF ligands secreted by lung fibroblasts are pivotal to AEC2 proliferation and differentiation, e.g., FGF7 and FGF10 (Fehrenbach, 2001). Deletion of FGFR2 receptor, which is highly expressed in AEC2 cells, results in loss of AEC2 cells, thereby leading to lung fibrosis (Dorry et al., 2019). In agreement with previous findings, the supplementation of FGF7 in the medium of organotypic coculture dramatically enhances the formation and size of alveolar organoids (Zepp et al., 2017). Nevertheless, FGF7 alone is insufficient to induce alveolar organoid formation in mesenchymal cell-free organotypic culture (Shiraishi et al., 2019a), implying that additional factors from mesenchymal cells are necessary to activate the proliferation of AEC2 cells. Analysis of putative ligand-receptor interactions between mesenchymal and AEC2 cells has identified the TGF-β, BMP, Wnt, and Notch pathways as those that regulate alveologenesis (Zepp et al., 2017; Shiraishi et al., 2019a). Results from organotypic coculture systems demonstrate that these pathways have distinct roles in alveologenesis. Activation of the Wnt pathway enhances the self-renewal of AEC2 cells and blocks their differentiation to AEC1 cells (Nabhan et al., 2018), while addition of BMP4 to the medium inhibits AEC2 proliferation and promotes their differentiation (Zepp et al., 2017; Chung et al., 2018).

Prior work has shown that vascular endothelium is essential for alveolization during lung development and regeneration (McGrath-Morrow et al., 2005; Ding et al., 2011; Lazarus et al., 2011), indicating that endothelial cells and pericytes are important niche components of AEC2 cells (Hogan et al., 2014; Mammoto and Mammoto, 2019), apart from mesenchymal cells. In organotypic coculture, endothelial cells also stimulate the formation of alveolar organoids (**Figure 1B**), through the secretion of thrombospondin-1 (Lee et al., 2014). Although not tested yet, pericytes likely have a similar effect in organotypic coculture of AEC2 cells as other cellular components, since pericytes are also sources of HGF, Wnt11, TGF-β, and BMP4 ligands (Kato et al., 2018). Similar to FGF ligands, HGF is a potent mitogen for AEC2 cells, when added in organotypic coculture (McQualter et al., 2010).

The impact of immune cells on the proliferation and differentiation of AEC2 cells has attracted increasing attention since they are recruited to the lung and release a variety of cytokines to initiate inflammatory response upon lung injury (Fehrenbach, 2001; Cohen et al., 2018). Targeted cytokine screenings with the organotypic coculture of AEC2 cells have identified cytokines that have distinct influences on alveolar organoid formation (Katsura et al., 2019; Glisinski et al., 2020). Specifically, IL-13 treatment disrupts the differentiation of AEC2 cells and reprograms the alveolar cells toward bronchiolar-like cells (Glisinski et al., 2020). In contrast, other cytokines,

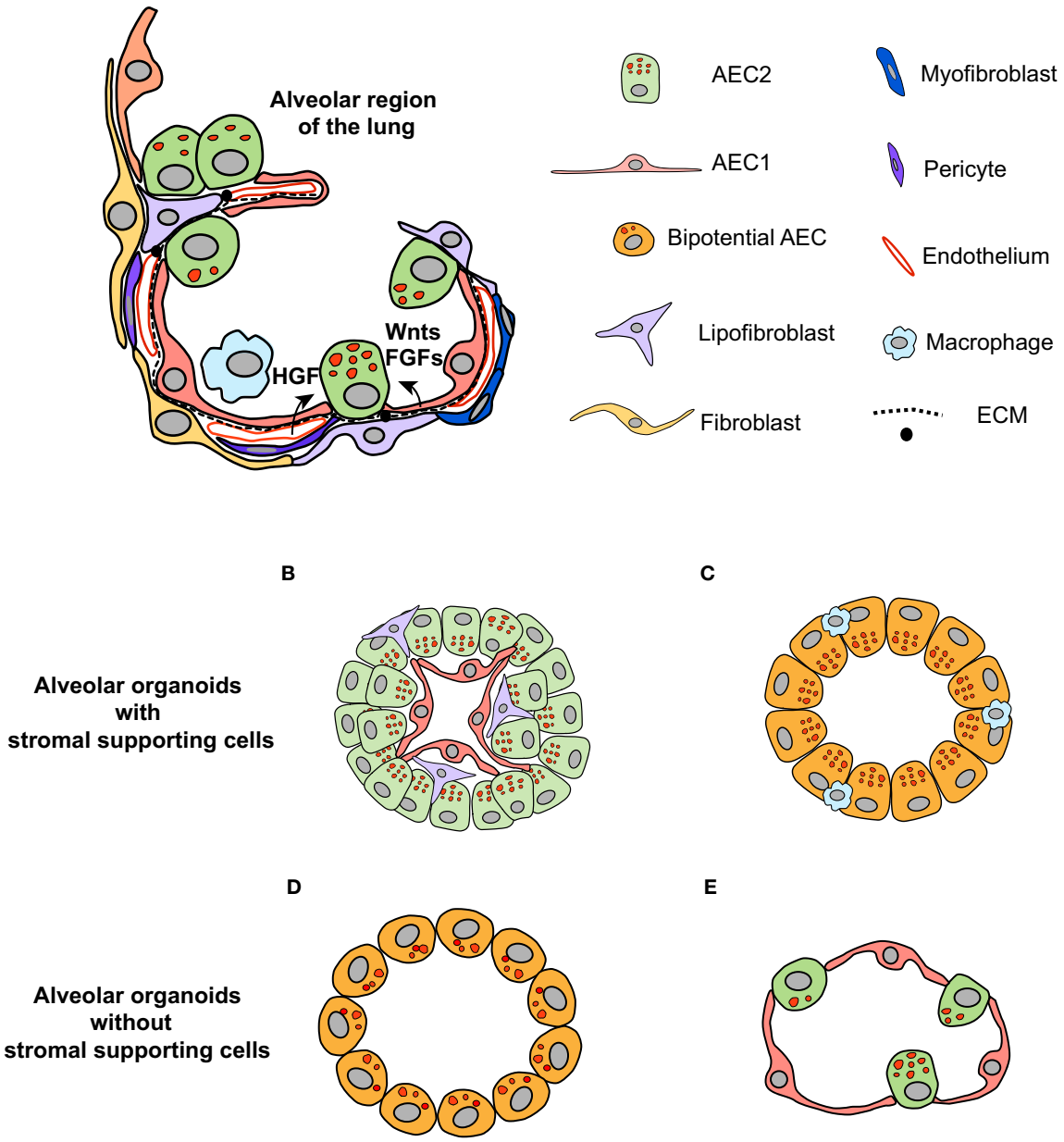

FIGURE 1 | Organotypic culture to dissect the role of the niche in regulating the fate of AEC2 cells. **(A)** The microenvironment in which AEC2 cells inhabit composes of different types of stromal cells within the alveoli regions of the lung, including fibroblasts, endothelial cells, pericytes, and immune cells (adapted from Barkauskas et al., 2017 with modifications). Together with AEC1 cells and ECM components, these stromal cells form the niche for AEC2 cells. The paracrine signals generated by stromal cells regulate the behavior of AEC2 stem cells during homeostasis and regeneration states. **(B,C)** Organotypic coculture of AEC2 cells with stromal cells give rise to alveolar organoids. The alveolar organoids supported by mesenchymal cells or endothelial cells have similar structure, in which AEC1 cells are surrounded by AEC2 cells, with stromal cells mingled with alveolar epithelial cells **(B)**. The alveolar organoids promoted by macrophages is mainly composed of cells positive for both the AEC2 marker (SPC) and the AEC1 marker (RAGE), suggesting that these organoids might originate from the bipotential cells **(C)**. **(D)** The alveolar organoids induced by defined culture medium, independent of stromal supporting cells. The cells within this type of organoids exhibit overlapped signals of SPC and AQP5 (the marker for AEC1 cell). **(E)** Based on the knowledge of pathways that promote AEC2 proliferation and differentiation, we propose that alveolar organoids that are similar in structure to alveoli of the lung can be stimulated by defined growth factors in a stepwise manner.

including IL-1, IL-6, and TNF-α, enhance the proliferation of AEC2 cells without inhibiting their differentiation, thereby increasing the growth of alveolar organoids (Zepp et al., 2017; Katsura et al., 2019). The presence of mesenchymal cells in coculture compounds the effort to determine whether the effects of these cytokines on AEC2 behavior are direct or

indirect. Therefore, the role of cytokines in modulating AEC2 behavior can be further verified through mesenchymal cell-free alveolar organoids.

Recently, progress has been made to use defined growth factors and inhibitors to stimulate the growth of alveolar organoids (**Supplementary Table 1**; Shiraishi et al., 2019a,b; Weiner et al., 2019). The supplementation of Notch ligands (Jagged1 and Noggin), KGF, GSK-β inhibitor (CHIR-99021), and ALK5 inhibitor (SB431542) in the culture medium replaces the mesenchymal cells to stimulate alveolar organoid formation (**Figure 1D**; Shiraishi et al., 2019a,b). Of note, the cells within these organoids display overlapped signals of the AEC2 marker SPC and the AEC1 marker AQP5 (Shiraishi et al., 2019a). One explanation is that the cocktail of growth factors and inhibitors reprograms the AEC2 cells to a bipotential state (Treutlein et al., 2014). Furthermore, the AEC2-like cells isolated from these organoids are unable to differentiate to AEC1 cells when transplanted into bleomycin-injured lung (Weiner et al., 2019), suggesting that simultaneous modulation of multiple pathways likely impairs the differentiation capacity of AEC2 cells. Thus, the composition of culture medium requires further optimization for supporting cell-free organotypic culture in the future. On the other hand, mesenchymal-free organotypic culture of AEC2 cells implies that it is feasible to stimulate the growth of alveolar organoids that are similar in structure to alveoli within the lung (**Figure 1E**). We propose that the expansion of AEC2 cells can be initially activated by mitogens, such as FGFs and HGF, followed by activation of the BMP pathway to promote the differentiation of AEC2 cells (Chung et al., 2018).

MODELING THE INTERACTION BETWEEN AEC2 CELLS AND THE NICHE WITH ALVEOLAR ORGANOIDS

Alveolar organoids can be employed to elucidate the reciprocal interaction between AEC2 cells and the niche in a pathological context (Fiorini et al., 2020; Li et al., 2020). For instance, the dysfunction of AEC2 cells is regarded as the driver of pulmonary fibrosis, in which aberrant deposition of collagen produced by the mesenchymal cells is one of the main manifestations (Martinez et al., 2017; Parimon et al., 2020). Apart from ECM, the cellular composition of the niche also changes in the fibrotic lung, in which seven subtypes of mesenchymal cell are identified by single-cell sequencing, with increased percentage of matrix fibroblasts, compared to the normal lung (Booth et al., 2012; Xie et al., 2018). How do these changes impact the function of AEC2 cells? Alveolar organoids allow us to examine the contribution of a niche component to AEC2 dysfunction by adding the fibrosis-associated niche components into the housing matrix. To date, Matrigel, the main component of which is laminin, collagen IV, and entactin (Li et al., 2016), is widely used as the housing matrix for organotypic culture of AEC2 cells (**Supplementary Table 1**). The laminin-rich Matrigel can promote the growth of integrin-high AEC2 cells to form alveolar organoids (Chapman et al., 2011). Thus, to minimize variation due to the heterogeneity of AEC2 cells, it is recommended to also examine the change in AEC2 behavior through reseeding alveolar organoids in a housing matrix containing fibrosis-associated niche components. Additionally, the experimental reproducibility can be affected by the lot-to-lot variability of Matrigel that is produced from mouse sarcoma (Murrow et al., 2017). In this respect, well-defined synthetic matrix, such as PEG-based hydrogel, can replace Matrigel as the starting housing matrix for alveolar organoids.

Moreover, how AEC2 cells influence the niche in response to lung injury can be explored with alveolar organoids. One example is the immune response from AEC2 cells elicited by microbial infections, such as *M. tuberculosis* and coronavirus (Qian et al., 2013; Ryndak and Laal, 2019; Li et al., 2020). The current outbreak of COVID-19 highlights the importance of understanding the development of coronavirus-caused pneumonia (Malta et al., 2020; Zhou et al., 2020). A recent report shows that, upon infecting the lung explant, SARS-CoV induces the expression of IFNs in 48 h, but not SARS-CoV-2, despite that the replication of SARS-CoV-2 is more efficient than SARS-CoV (Chu et al., 2020). These results lead to a question: what could be the underlying mechanism for the differential immune responses to these two coronaviruses, which share 79% sequence identity and infect AEC2 cells (Chu et al., 2020; Zhou et al., 2020)? In addition, it remains unclear how coronaviruses exit the cell (Fehr and Perlman, 2015). The secretory system for surfactant proteins in AEC2 cells could be utilized by SARS-CoV-2; Alternatively, the virus may have a unique pathway for exit, leading to reduced production of surfactant proteins and destruction of alveolar homeostasis. Alveolar organoids would be useful models to address these questions and to study the development of COVID-19 *in vitro,* complementary to animal models. Several reports have shown that airway organoids and intestinal organoids are successfully infected with influenza virus and MERS-CoV, respectively, by incubating the virus with organoids or microinjection of the virus into the inner lumen (Zhou et al., 2017, 2018; Hui et al., 2018; Bui et al., 2019; Sachs et al., 2019). We anticipate that similar methodology can be applied with alveolar organoids to investigate how AEC2 cells respond to coronavirus infection and reshape the niche.

CONCLUDING REMARKS

Although not every aspect of alveoli within the lung can be fully recapitulated in organotypic culture, alveolar organoids help to dissect the role of the niche in AEC2 self-renewal and differentiation, thereby bridging the gap between *in vivo* model and *in vitro* culture. We envision that application of these model systems in combination will bring more insight to the development of lung diseases.

AUTHOR CONTRIBUTIONS

DL and HL conceived, designed, and wrote the manuscript.

FUNDING

This work was funded through the Independent Innovation Research Fund of HUST (5003519003 to HL).

ACKNOWLEDGMENTS

We would like to thank the reviewer for his constructive comments and suggestions.

SUPPLEMENTARY MATERIAL

The Supplementary Material for this article can be found online at: https://www.frontiersin.org/articles/10.3389/fcell.2020.00419/full#supplementary-material

REFERENCES

Barkauskas, C. E., Chung, M. I., Fioret, B., Gao, X., Katsura, H., and Hogan, B. L. (2017). Lung organoids: current uses and future promise. *Development* 144, 986–997. doi: 10.1242/dev.140103

Barkauskas, C. E., Cronce, M. J., Rackley, C. R., Bowie, E. J., Keene, D. R., Stripp, B. R., et al. (2013). Type 2 alveolar cells are stem cells in adult lung. *J. Clin. Invest.* 123, 3025–3036. doi: 10.1172/JCI68782

Beer, M. F., and Moodley, Y. (2017). When is an alveolar type 2 cell an alveolar type 2 cell? A conundrum for lung stem cell biology and regenerative medicine. *Am. J. Respir. Cell Mol. Biol.* 57, 18–27. doi: 10.1165/rcmb.2016-0426PS

Booth, A. J., Hadley, R., Cornett, A. M., Dreffs, A. A., Matthes, S. A., Tsui, J. L., et al. (2012). Acellular normal and fibrotic human lung matrices as a culture system for *in vitro* investigation. *Am. J. Respir. Crit.Care Med.* 186, 866–876. doi: 10.1164/rccm.201204-0754OC

Brody, J. S., and Williams, M. C. (1992). Pulmonary alveolar epithelial cell differentiation. *Annu. Rev. Physiol.* 54, 351–371. doi: 10.1146/annurev.ph.54.030192.002031

Bui, C. H. T., Chan, R. W. Y., Ng, M. M. T., Cheung, M. C., Ng, K. C., Chan, M. P. K., et al. (2019). Tropism of influenza B viruses in human respiratory tract explants and airway organoids. *Eur. Respir. J.* 54:1900008. doi: 10.1183/13993003.00008-2019

Chacón-Martínez, C. A., Koester, J., and Wickström, S. A. (2018). Signaling in the stem cell niche: regulating cell fate, function and plasticity. *Development* 145:dev165399. doi: 10.1242/dev.165399

Chapman, H. A., Li, X., Alexander, J. P., Brumwell, A., Lorizio, W., Tan, K., et al. (2011). Integrin α6β4 identifies an adult distal lung epithelial population with regenerative potential in mice. *J. Clin. Invest.* 121, 2855–2862. doi: 10.1172/JCI57673

Chen, H., Matsumoto, K., Brockway, B. L., Rackley, C. R., Liang, J., Lee, J. H., et al. (2012). Airway epithelial progenitors are region specific and show differential responses to bleomycin-induced lung injury. *Stem Cells* 30, 1948–1960. doi: 10.1002/stem.1150

Chu, H., Chan, J. F., Wang, Y., Yuen, T. T., Chai, Y., Hou, Y., et al. (2020). Comparative replication and immune activation profiles of SARS-CoV-2 and SARS-CoV in human lungs: an *ex vivo* study with implications for the pathogenesis of COVID-19. *Clin. Infect. Dis.* doi: 10.1093/cid/ciaa410. [Epub ahead of print].

Chung, M. I., Bujnis, M., Barkauskas, C. E., Kobayashi, Y., and Hogan, B. (2018). Niche-mediated BMP/SMAD signaling regulates lung alveolar stem cell proliferation and differentiation. *Development* 145:dev163014. doi: 10.1242/dev.163014

Cohen, M., Giladi, A., Gorki, A. D., Solodkin, D. G., Zada, M., Hladik, A., et al. (2018). Lung single-cell signaling interaction map reveals basophil role in macrophage imprinting. *Cell* 175, 1031–1044. doi: 10.1016/j.cell.2018.09.009

de Cuevas, M., and Matunis, E. L. (2011). The stem cell niche: lessons from the *Drosophila* testis. *Development* 138, 2861–2869. doi: 10.1242/dev.056242

Desai, T. J., Brownfield, D. G., and Krasnow, M. A. (2014). Alveolar progenitor and stem cells in lung development, renewal and cancer. *Nature* 507, 190–194. doi: 10.1038/nature12930

Ding, B. S., Nolan, D. J., Guo, P., Babazadeh, A. O., Cao, Z., Rosenwaks, Z., et al. (2011). Endothelial-derived angiocrine signals induce and sustain regenerative lung alveolarization. *Cell* 147, 539–553. doi: 10.1016/j.cell.2011.10.003

Dorry, S. J., Ansbro, B. O., Ornitz, D. M., Mutlu, G. M., and Guzy, R. D. (2019). FGFR2 is required for AEC2 homeostasis and survival following bleomycin-induced lung injury. *Am. J. Respir. Cell Mol. Biol.* 62, 608–621. doi: 10.1165/rcmb.2019-0079OC

Endale, M., Ahlfeld, S., Bao, E., Chen, X., Green, J., Bess, Z., et al. (2017). Temporal, spatial, and phenotypical changes of PDGFRα expressing fibroblasts during late lung development. *Dev. Biol.* 425, 161–175. doi: 10.1016/j.ydbio.2017.03.020

Fehr, A. R., and Perlman, S. (2015). Coronaviruses: an overview of their replication and pathogenesis. *Methods Mol. Biol.* 1282, 1–23. doi: 10.1007/978-1-4939-2438-7_1

Fehrenbach, H. (2001). Alveolar epithelial type II cell: defender of the alveolus revisited. *Respir. Res.* 2, 33–46. doi: 10.1186/rr36

Fiorini, E., Veghini, L., and Corbo, V. (2020). Modeling cell communication in cancer with organoids: making the complex simple. *Front. Cell Dev. Biol.* 8:166. doi: 10.3389/fcell.2020.00166

Glisinski, K. M., Schlobohm, A. J., Paramore, S. V., Birukova, A., Moseley, M. A., Foster, M. W., et al. (2020). Interleukin-13 disrupts type 2 pneumocyte stem cell activity. *JCI Insight* 5:e131232. doi: 10.1172/jci.insight.131232

Hogan, B. L., Barkauskas, C. E., Chapman, H. A., Epstein, J. A., Jain, R., Hsia, C. C., et al. (2014). Repair and regeneration of the respiratory system: complexity, plasticity, and mechanisms of lung stem cell function. *Cell Stem Cell* 15, 123–138. doi: 10.1016/j.stem.2014.07.012

Hui, K. P. Y., Ching, R. H. H., Chan, S. K. H., Nicholls, J. M., Sachs, N., Clevers, H., et al. (2018). Tropism, replication competence, and innate immune responses of influenza virus: an analysis of human airway organoids and *ex-vivo* bronchus cultures. *Lancet Respir. Med.* 6, 846–854. doi: 10.1016/S2213-2600(18)30236-4

Joost, S., Jacob, T., Sun, X., Annusver, K., La Manno, G., Sur, I., et al. (2018). Single-cell transcriptomics of traced epidermal and hair follicle stem cells reveals rapid adaptations during wound healing. *Cell Rep.* 25, 585–597. doi: 10.1016/j.celrep.2018.09.059

Kato, K., Diéguez-Hurtado, R., Park, D. Y., Hong, S. P., Kato-Azuma, S., Adams, S., et al. (2018). Pulmonary pericytes regulate lung morphogenesis. *Nat. Commun.* 9:2448. doi: 10.1038/s41467-018-04913-2

Katsura, H., Kobayashi, Y., Tata, P. R., and Hogan, B. L. M. (2019). IL-1 and TNFα contribute to the inflammatory niche to enhance alveolar regeneration. *Stem Cell Rep.* 12, 657–666. doi: 10.1016/j.stemcr.2019.02.013

Kretzschmar, K., and Clevers, H. (2016). Organoids: modeling development and the stem cell niche in a dish. *Dev. Cell.* 38, 590–600. doi: 10.1016/j.devcel.2016.08.014

Lazarus, A., Del-Moral, P. M., Ilovich, O., Mishani, E., Warburton, D., and Keshet, E. (2011). A perfusion-independent role of blood vessels in determining branching stereotypy of lung airways. *Development* 138, 2359–2368. doi: 10.1242/dev.060723

Lechner, A. J., Driver, I. H., Lee, J., Conroy, C. M., Nagle, A., Locksley, R. M., et al. (2017). Recruited monocytes and type 2 immunity promote lung regeneration following pneumonectomy. *Cell Stem Cell* 21, 120–134. doi: 10.1016/j.stem.2017.03.024

Lee, J. H., Bhang, D. H., Beede, A., Huang, T. L., Stripp, B. R., Bloch, K. D., et al. (2014). Lung stem cell differentiation in mice directed by endothelial cells via a BMP4-NFATc1-thrombospondin-1 axis. *Cell* 156, 440–455. doi: 10.1016/j.cell.2013.12.039

Li, Q., Uygun, B. E., Geerts, S., Ozer, S., Scalf, M., Gilpin, S. E., et al. (2016). Proteomic analysis of naturally-sourced biological scaffolds. *Biomaterials* 75, 37–46. doi: 10.1016/j.biomaterials.2015.10.011

Li, Y., Wu, Q., Sun, X., Shen, J., and Chen, H. (2020). Organoids as a powerful model for respiratory diseases. *Stem Cells Int*. 2020:5847876. doi: 10.1155/2020/5847876

Malta, M., Rimoin, A. W., and Strathdee, S. A. (2020). The coronavirus 2019-nCoV epidemic: is hindsight 20/20? *EClinicalMedicine* 20:100289. doi: 10.1016/j.eclinm.2020.100289

Mammoto, A., and Mammoto, T. (2019). Vascular niche in lung alveolar development, homeostasis, and regeneration. *Front. Bioeng. Biotechnol.* 7:318. doi: 10.3389/fbioe.2019.00318

Martinez, F. J., Collard, H. R., Pardo, A., Raghu, G., Richeldi, L., Selman, M., et al. (2017). Idiopathic pulmonary fibrosis. *Nat. Rev. Dis. Primers* 3:17074. doi: 10.1038/nrdp.2017.74

McGrath-Morrow, S. A., Cho, C., Cho, C., Zhen, L., Hicklin, D. J., and Tuder, R. M. (2005). Vascular endothelial growth factor receptor 2 blockade disrupts postnatal lung development. *Am. J. Respir. Cell Mol. Biol.* 32, 420–427. doi: 10.1165/rcmb.2004-0287OC

McQualter, J. L., Yuen, K., Williams, B., and Bertoncello, I. (2010). Evidence of an epithelial stem/progenitor cell hierarchy in the adult mouse lung. *Proc. Natl. Acad. Sci. U. S. A.* 107, 1414–1419. doi: 10.1073/pnas.0909207107

Murrow, L. M., Weber, R. J., and Gartner, Z. J. (2017). Dissecting the stem cell niche with organoid models: an engineering-based approach. *Development* 144, 998–1007. doi: 10.1242/dev.140905

Nabhan, A. N., Brownfield, D. G., Harbury, P. B., Krasnow, M. A., and Desai, T. J. (2018). Single-cell Wnt signaling niches maintain stemness of alveolar type 2 cells. *Science* 359, 1118–1123. doi: 10.1126/science.aam6603

Nguyen, P. D., and Currie, P. D. (2018). *In vivo* imaging: shining a light on stem cells in the living animal. *Development* 145:dev150441. doi: 10.1242/dev.150441

Parimon, T., Yao, C., Stripp, B. R., Noble, P. W., and Chen, P. (2020). Alveolar epithelial type II cells as drivers of lung fibrosis in idiopathic pulmonary fibrosis. *Int. J. Mol. Sci.* 21:E2269. doi: 10.3390/ijms21072269

Pinho, S., and Frenette, P. S. (2019). Haematopoietic stem cell activity and interactions with the niche. *Nat. Rev. Mol. Cell Biol.* 20, 303–320. doi: 10.1038/s41580-019-0103-9

Qian, Z., Travanty, E. A., Oko, L., Edeen, K., Berglund, A., Wang, J., et al. (2013). Innate immune response of human alveolar type II cells infected with severe acute respiratory syndrome-coronavirus. *Am. J. Respir. Cell Mol. Biol.* 48, 742–748. doi: 10.1165/rcmb.2012-0339OC

Riemondy, K. A., Jansing, N. L., Jiang, P., Redente, E. F., Gillen, A. E., Fu, R., et al. (2019). Single cell RNA sequencing identifies TGFβ as a key regenerative cue following LPS-induced lung injury. *JCI Insight* 5:e123637. doi: 10.1172/jci.insight.123637

Ryndak, M. B., and Laal, S. (2019). *Mycobacterium tuberculosis* primary infection and dissemination: a critical role for alveolar epithelial cells. *Front. Cell Infect. Microbiol.* 9:299. doi: 10.3389/fcimb.2019.00299

Sachs, N., Papaspyropoulos, A., Zomer-van Ommen, D. D., Heo, I., Böttinger, L., Klay, D., et al. (2019). Long-term expanding human airway organoids for disease modeling. *EMBO J.* 38:e100300. doi: 10.15252/embj.2018100300

Scadden, D. T. (2006). The stem-cell niche as an entity of action. *Nature* 441, 1075–1079. doi: 10.1038/nature04957

Shiraishi, K., Nakajima, T., Shichino, S., Deshimaru, S., Matsushima, K., and Ueha, S. (2019a). *In vitro* expansion of endogenous human alveolar epithelial type II cells in fibroblast-free spheroid culture. *Biochem. Biophys. Res. Commun.* 515, 579–585. doi: 10.1016/j.bbrc.2019.05.187

Shiraishi, K., Shichino, S., Ueha, S., Nakajima, T., Hashimoto, S., Yamazaki, S., et al. (2019b). Mesenchymal-epithelial interactome analysis reveals essential factors required for fibroblast-free alveolosphere formation. *iScience* 11, 318–333. doi: 10.1016/j.isci.2018.12.022

Sucre, J., Jetter, C. S., Loomans, H., Williams, J., Plosa, E. J., Benjamin, J. T., et al. (2018). Successful establishment of primary type II alveolar epithelium with 3D organotypic coculture. *Am. J. Respir. Cell Mol. Biol.* 59, 158–166. doi: 10.1165/rcmb.2017-0442MA

Tan, S. Y., and Krasnow, M. A. (2016). Developmental origin of lung macrophage diversity. *Development* 143, 1318–1327. doi: 10.1242/dev.129122

Treutlein, B., Brownfield, D. G., Wu, A. R., Neff, N. F., Mantalas, G. L., Espinoza, F. H., et al. (2014). Reconstructing lineage hierarchies of the distal lung epithelium using single-cell RNA-seq. *Nature* 509, 371–375. doi: 10.1038/nature13173

Wabik, A., and Jones, P. H. (2015). Switching roles: the functional plasticity of adult tissue stem cells. *EMBO J.* 34, 1164–1179. doi: 10.15252/embj.201490386

Weiner, A. I., Jackson, S. R., Zhao, G., Quansah, K. K., Farshchian, J. N., Neupauer, K. M., et al. (2019). Mesenchyme-free expansion and transplantation of adult alveolar progenitor cells: steps toward cell-based regenerative therapies. *NPJ Regen. Med.* 4:17. doi: 10.1038/s41536-019-0080-9

Xie, T., Wang, Y., Deng, N., Huang, G., Taghavifar, F., Geng, Y., et al. (2018). Deconvolution of fibroblast heterogeneity in mouse pulmonary fibrosis. *Cell Rep.* 22, 3625–3640. doi: 10.1016/j.celrep.2018.03.010

Zacharias, W. J., Frank, D. B., Zepp, J. A., Morley, M. P., Alkhaleel, F. A., Kong, J., et al. (2018). Regeneration of the lung alveolus by an evolutionarily conserved epithelial progenitor. *Nature* 555, 251–255. doi: 10.1038/nature25786

Zepp, J. A., Zacharias, W. J., Frank, D. B., Cavanaugh, C. A., Zhou, S., Morley, M. P., et al. (2017). Distinct mesenchymal lineages and niches promote epithelial self-renewal and myofibrogenesis in the lung. *Cell* 170, 1134–1148. doi: 10.1016/j.cell.2017.07.034

Zhou, J., Li, C., Sachs, N., Chiu, M. C., Wong, B. H., Chu, H., et al. (2018). Differentiated human airway organoids to assess infectivity of emerging influenza virus. *Proc. Natl. Acad. Sci. U.S.A.* 115, 6822–6827. doi: 10.1073/pnas.1806308115

Zhou, J., Li, C., Zhao, G., Chu, H., Wang, D., Yan, H. H., et al. (2017). Human intestinal tract serves as an alternative infection route for middle east respiratory syndrome coronavirus. *Sci. Adv.* 3:eaao4966. doi: 10.1126/sciadv.aao4966

Zhou, P., Yang, X. L., Wang, X. G., Hu, B., Zhang, L., Zhang, W., et al. (2020). A pneumonia outbreak associated with a new coronavirus of probable bat origin. *Nature* 579, 270–273. doi: 10.1038/s41586-020-2012-7

Conflict of Interest: The authors declare that the research was conducted in the absence of any commercial or financial relationships that could be construed as a potential conflict of interest.

frontiers in Cell and Developmental Biology

ORIGINAL RESEARCH
published: 02 July 2020
doi: 10.3389/fcell.2020.00375

Congruence of Transcription Programs in Adult Stem Cell-Derived Jejunum Organoids and Original Tissue During Long-Term Culture

*Bart van der Hee[1,2], Ole Madsen[3], Jacques Vervoort[4], Hauke Smidt[2] and Jerry M. Wells[1]**

[1] Host-Microbe Interactomics Group, Department of Animal Sciences, Wageningen University & Research, Wageningen, Netherlands, [2] Laboratory of Microbiology, Wageningen University & Research, Wageningen, Netherlands, [3] Animal Breeding and Genomics, Department of Animal Sciences, Wageningen University & Research, Wageningen, Netherlands, [4] Laboratory of Biochemistry, Wageningen University & Research, Wageningen, Netherlands

The emergence of intestinal organoids, as a stem cell-based self-renewable model system, has led to many studies on intestinal development and cell-cell signaling. However, potential issues regarding the phenotypic stability and reproducibility of the methodology during culture still needs to be addressed for different organoids. Here we investigated the transcriptomes of jejunum organoids derived from the same pig as well as batch-to-batch variation of organoids derived from different pigs over long-term passage. The set of genes expressed in organoids closely resembled that of the tissue of origin, including small intestine specific genes, for at least 17 passages. Minor differences in gene expression were observed between individual organoid cultures. In contrast, most small intestine-specific genes were not expressed in the jejunum cell line IPEC-J2, which also showed gene expression consistent with cancer phenotypes. We conclude that intestinal organoids provide a robust and stable model for translational research with clear advantages over transformed cells.

Keywords: intestinal organoids, porcine organoids, gastrointestinal, organoid stability, IPEC-J2

OPEN ACCESS

Edited by:
Eumorphia Remboutsika, National and Kapodistrian University of Athens, Greece

Reviewed by:
Masayuki Fujii, Keio University, Japan
Claudio Cantù, Linköping University, Sweden

***Correspondence:**
Jerry M. Wells
jerry.wells@wur.nl

Specialty section:
This article was submitted to Stem Cell Research, a section of the journal Frontiers in Cell and Developmental Biology

Received: *24 January 2020*
Accepted: *27 April 2020*
Published: *02 July 2020*

Citation:
van der Hee B, Madsen O, Vervoort J, Smidt H and Wells JM (2020) Congruence of Transcription Programs in Adult Stem Cell-Derived Jejunum Organoids and Original Tissue During Long-Term Culture. Front. Cell Dev. Biol. 8:375. doi: 10.3389/fcell.2020.00375

INTRODUCTION

The intestinal epithelium plays an essential role in the digestion and absorption of nutrients while also maintaining homeostasis with symbiotic microbiota (Van Der Flier and Clevers, 2009; Wells et al., 2011; Bron et al., 2012). The physical containment of microbes to the lumen and homeostasis of tolerance and immunity depends on the functions of different lineages of intestinal epithelial cells (Van Der Flier and Clevers, 2009; Wells et al., 2011). For decades, scientists have exploited the replicative potential of immortalized intestinal cells as enterocyte models to study host-pathogen interactions and intestinal functions *in vitro*. Such monotypic cell models have led to important discoveries but have notable limitations. Immortalized cell lines can undergo significant genotypic alterations within a few passages *in vitro* which are potential threats to data reproducibility (Gillet et al., 2013; Gisselsson et al., 2018; Liu et al., 2019). Furthermore, cell lines often have altered pathway expression compared to primary cells (Gillet et al., 2013).

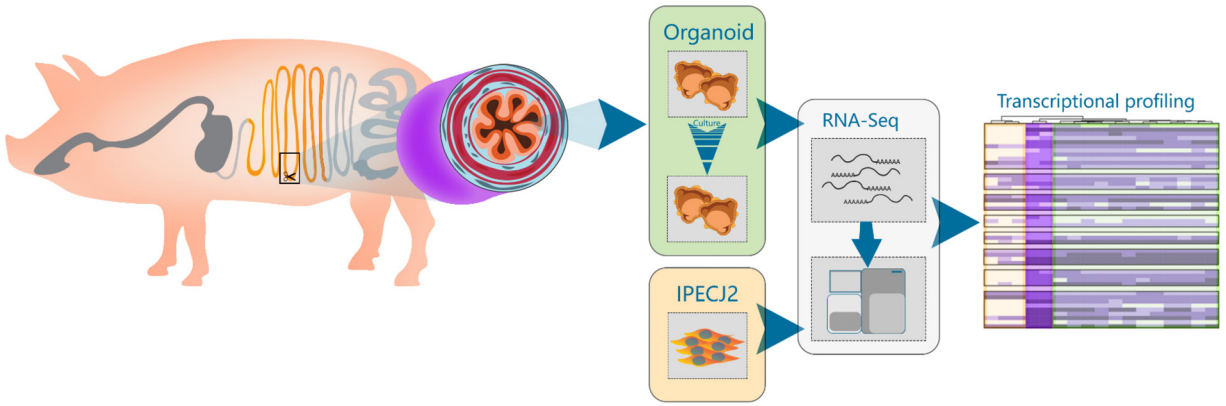

GRAPHICAL ABSTRACT | Porcine intestinal organoids show batch-independent homogeneity to their derived host and stability during long-term culture, as well as profound benefits over transformed cell cultures.

Since 2009, when it was shown that intestinal adult leucine-rich repeat-containing G protein-coupled receptor 5 (LGR5+) stem cells (Barker et al., 2007) could be grown into organotypic cultures and propagated in 3D culture (Ootani et al., 2009; Sato et al., 2009), there has been much interest in employing intestinal organoids as advanced models. A distinct advantage of organoids is the development of a crypt-villus axis with a similar spatial organization of the heterotypic cell lineages found in the tissue of origin. Additionally, methods for generating polarized monolayers of organoids cells (Moon et al., 2014) have been optimized (van der Hee et al., 2018) to improve the versatility of the models, e.g., to study transport, and differential responses to luminal or basolateral stimulants. Another favorable property of organoids generated from adult intestinal stem cells is that they express specific functions associated with their original intestinal location (Middendorp et al., 2014). This means that location-specific functions of different parts of the intestine are intrinsically programmed in adult stem cells.

In the future we can expect intestinal organoids to be increasingly adopted as intestinal models for humans and other mammals. However, there are some unresolved issues that need to be addressed to ensure reliability and reproducibility of results in this emerging field. As organoids contain different cell types there is potential for variability and problems with reproducibility which may compromise their application to phenotype individuals. To address this issue, we assessed the transcriptional stability of intestinal organoids differentiated from the same crypt batch and between organoids from different pigs (*Sus scrofa domesticus*) over long-term passage. Furthermore, we compared expressed genes and pathways in organoids, the original epithelial tissue from which the organoids were derived, and IPEC-J2, a porcine cell line derived from the jejunum. The results show that intestinal organoids derived from adult stem cells generally resemble the epithelial tissue of origin in terms of expressed genes and provide a reference for researchers wishing to investigate specific small intestinal functions not present in IPEC-J2.

MATERIALS AND METHODS

Intestinal Organoid Generation

Jejunum tissue segments were obtained from control piglets used for another study, following guidelines of the animal ethics committee of Wageningen University. Two 5-week-old piglets were used for generating organoids following procedures previously described (Sato et al., 2011; van der Hee et al., 2018). Briefly, a 2 cm section of the mid-jejunum was dissected and placed in ice-cold PBS. After opening the sections longitudinally, jejunum segments were washed three times in ice-cold PBS and villi removed by carefully scraping with a scalpel. Small sections of the mucosa were cut from the muscle layer, divided into small cubes, and transferred into ice-cold PBS containing 30 mM EDTA and incubated with rotation at room temperature for 15 min. The PBS – EDTA was then replaced and incubation continued for 10 min at 37°C. After washing in ice-cold DMEM supplemented with 5% penicillin/streptomycin (Gibco, Thermo Fisher Scientific), the crypts were dissociated by rigorous vortexing and passed through a 100 μm strainer into cold DMEM containing 5% fetal bovine serum (FBS, v/v). Crypts were pelleted by centrifugation at 300 × *g* for 5 min, and suspended in Matrigel (Basement Membrane, Growth factor reduced, REF 356231, Corning, Bedford, MA, United States). To improve surface tension, empty 24-well plates were pre-incubated overnight at 37°C. Seven drops of Matrigel containing crypts were placed in each well (approx. 35 μl per well) and inverted to polymerize at 37°C. After polymerization, 600 μl F12 cell culture medium (Gibco) was added, supplemented with 100 μg/ml primocin (Invivogen), 10 mM HEPES (HyClone), 1 × B-27 (Gibco), 1.25 mM *N*-acetylcysteine (Sigma), 50 ng/ml human epidermal growth factor (R&D systems), 15 nM gastrin, 10 mM nicotinamide, 10 μM p38 MAPK inhibitor (Sigma), 600 nM TGFβ receptor inhibitor A83-01, and conditioned media for recombinant Noggin (15% v/v), Spondin (15% v/v), and Wnt3A (30% v/v) provided by Dr. Kuo and Hubrecht Institute (Utrecht, Netherlands). Organoids were passaged at a 1:5 ratio every 5 days using ice-cold DMEM by mechanical dissociation,

centrifugation at 500 × *g* for 5 min, and plating in fresh Matrigel matrix droplets as previously described (van der Hee et al., 2018). For measuring transport of amino acids (AAs), two-dimensional organoids were generated as previously described (van der Hee et al., 2018). 3D organoids were dissociated into single cells by TrypLE digestion and seeded on Matrigel (0.5% v/v) precoated transwells (Falcon BD). After reaching confluence, the apical medium was replaced with DMEM (Gibco) and basolateral medium with HBSS (Gibco). After incubation, the basolateral AA composition was measured using triple quadrupole mass spectrometry (TQMS).

Culturing Methods and RNA Isolation

Directly after crypt isolation, organoid cultures were separated into three batches per animal and grown independently for 17 passages. Jejunum organoids were grown for 3 and 12 weeks (4–17 passages) and extracted using ice-cold PBS. After washing twice in PBS, intact organoids were pelleted at 300 × g for 5 min and suspended in RLT lysis buffer and stored at −80°C prior to RNA isolation. Porcine jejunum epithelial cell line IPEC-J2 (ACC-701) was grown in DMEM F12 medium supplemented with 10% FBS and 5% penicillin/streptomycin (P/S, Gibco) in 75 cm^2 culture flasks. Data for one IPEC-J2 (p67) transcriptome was kindly provided by Dr. Richard Crooijmans, via the Functional Annotation of ANimal Genomes (FAANG, BioSamples accession SAMEA4447551) (Giuffra et al., 2018). For the analysis of the remaining two lines, IPEC-J2 at passage 87 and 91 were seeded at 5×10^4 cells/well in 24-well plates and grown to confluence within 48 h with reduced P/S (1%). The monolayers were subsequently left to differentiate for 5 days, lysed using RLT-buffer, and stored at −80°C prior to RNA isolation. For RNA extraction of tissue, 0.5 mg of whole jejunum cross section per animal was added to a gentleMACS M tube (Miltenyi Biotec, Germany) and dissociated in 2 ml RLT lysis buffer using a gentleMACS Dissociator for 30 s. Subsequently, 100 μl of homogenized tissue suspension was added to 500 μl fresh RLT buffer, homogenized using pipetting with a p200 pipette, and stored at −80°C until extraction. Total RNA was extracted using a RNeasy Mini Kit (Qiagen) following manufacturer's instructions including a 15 min on-column DNAse step. Preliminary tRNA concentrations, contamination and degradation were identified using Qubit (Thermo-Fisher) and gel-electrophoresis. The quantity and integrity of RNA was measured using a Bioanalyzer 2100 (Agilent).

RNA-Sequencing Procedures and Data Handling

A minimum of 1 μg total RNA in 50 μl was used for library preparation using the TruSeq RNA sample preparation kit (Illumina) following the manufacturer's protocol at Novogene. Briefly, total RNA samples were depleted for ribosomal RNA using the RiboZero kit and enriched for mRNA using oligo(dT) beads, fragmented, and synthesized into cDNA using mRNA template and hexamer primers. Custom second strand-synthesis buffer (Illumina), dNTP's, RNAse H and DNA Polymerase I were added for second strand synthesis initiation. Furthermore, following a series of terminal repair, cDNA library construction was completed with size selection and PCR enrichment. Samples were sequenced using an Illumina Hi-Seq 4000 (Novogene, Hong Kong) at 9 GB raw data/sample with 150 bp paired-end reads.

Raw sequencing reads were checked for quality using FastQC [v0.11.5; (Andrews, 2017)] and trimmed using trim-galore for adaptors and quality [v0.4.4 (Krueger, 2017)]. Only paired-end reads longer than 35 bp were included for further downstream analysis. Sequences were aligned against Ensembl *Sus scrofa* reference genome and annotation 11.1.91 (Zerbino et al., 2018) using Tophat [v2.1.1 (Trapnell et al., 2012)]. Transcriptomes were assembled with 5 bp intron overhang tolerance, merged, normalized, and analyzed using the Cufflinks package [v2.2.1 (Trapnell et al., 2012)]. Differential expression was analyzed with 0.01 false discovery rate (FDR) using cuffdiff with bias and weight correction and visualized in R using CummeRbund [v2.7.2 (Trapnell et al., 2012)]. Mapping analytics can be found in **Supplementary Table S1**. Fragments per kilobase million (FPKM) were calculated and log-transformed for downstream analysis. The sequencing data was also processed using CLC Genomics Workbench 11 (Qiagen) using identical reference genome, annotation and settings for identification of insertions/deletions, breakpoints, structural variants, and track generation. Output was filtered for genes <1 FPKM to establish expression.

Data Availability

All data are available for download through the gene expression omnibus under GEO accession number GSE146408. This data also contains the merged transcriptome file for cufflinks analysis and detailed analysis. The FPKM value data table is available as **Supplementary File S1**.

Functional Analysis and Pathway Expression

Differentially expressed genes were clustered by k-means into seven clusters using CummeRbund. Due to limited analysis methods for further downstream functional analysis in pig, databases for human genomes were used as a background. Differentially expressed genes were analyzed for functional enrichment and ontologies using the TOPPfun suite (Chen et al., 2009), and gene list enrichment and candidate prioritization were evaluated with a threshold <0.05 for *P*- and *Q*-value adjusted for FDR with the Benjamini-Hochberg procedure (B&H). Ingenuity Pathway Analysis (IPA, Qiagen) was used for determining overlapping networks of expressed genes between tissue and organoids, and overall expression of molecular and cellular development of organoids between time-points. Genes for elevated tissue-specific expression were acquired from the human protein atlas for specific mRNA transcription in the small intestine, and porcine orthologs were identified to determine tissue and group enriched genes (Fagerberg et al., 2014).

Histological Analysis

Whole mount imaging was performed as previously described with small modifications (Dow et al., 2015). Organoids grown

in 8-well chambered slides (Millicell EZ slide, Merck) were fixed in 4% paraformaldehyde (PFA) for 2 h at RT. PFA-fixed organoids were stained using FITC-conjugated UEA-1 antibody (1:250, FL-1061, Vector Laboratories, United States) for 2 h and counterstained with Hoechst (0.5 μg/ml, 33342, Thermo Fisher) for 10 min at room temperature. Z-stacks of whole organoids were imaged on a confocal microscope (Zeiss). Immunohistochemical analysis for Mucin-2 was performed following procedures previously described (Loonen et al., 2014; van der Hee et al., 2018). Organoids were retrieved from Matrigel using ice-cold PBS, pelleted, and fixed overnight using 1% PFA at 4°C. After pelleting, organoids were suspended in 2% agarose gel, dehydrated and embedded in paraffin blocks. After cutting 5 μM-thick sections and subsequent drying on glass slides, sections were rehydrated, blocked in 5% normal goat serum, and stained using anti-MUC2 antibody (1:200, AB_1950958, GeneTex) overnight. After addition of secondary FITC-antibody (Thermo-Fisher), sections were counterstained using Hoechst and imaged using a DM6 microscope fitted with DFC365 camera at 40x magnification.

RESULTS

Comparative Analysis of the Transcriptome of Organoids, Tissue and a Cell Line Derived From the Porcine Jejunum

Jejunum tissue was isolated from two euthanized 5-week-old piglets for generating organoids and isolation of RNA from epithelial cells (**Figure 1A**). Triplicate batches of each organoid were separately cultured for 12 weeks by passaging approximately every 5 days. After 3- and 12-weeks continuous culture (4–17 passages) RNA was isolated from the organoids for RNA sequencing (**Figure 1A**). Within the first two passages after isolation, the organoids acquired a budding phenotype, which might be attributed to whole crypt isolation also containing transit amplifying cells in differentiation stages; as opposed to basal culture after 2 weeks forming a more cyst-like phenotype. After 2 weeks continuous culture the organoids formed spheroids (**Figure 1B**) but maintained different cell lineages, as shown with UEA-1 staining for secretory cell lineages (**Figure 1C** and **Supplementary Figure S1**). Similarly, RNA was isolated from the porcine jejunum cell line IPEC-J2 at passage number 67, 87, and 91. RNA sequencing data was analyzed using a customized analysis pipeline and CLC genomics workbench 11. Multidimensional scaling showed the transcriptomes of the organoids clustered closely together, despite 12-weeks continuous passage and isolation from different pigs (**Figure 1D**). It was also evident that the transcriptomes of the tissue and organoid samples were most similar, not separating in the first dimension, whereas IPEC-J2 separated from tissue in both dimensions. A correlation matrix of transcriptomic data from all samples revealed highest similarity for replicate samples of the same origin (**Figure 1E**).

The hierarchical clustering of gene expression (**Figure 1F**) further revealed that the transcriptome of organoids more closely resembled that of jejunum epithelial tissue than the IPEC-J2 cell line. The two tissue samples clustered under the same branch, where organoids showed consistent homogenous expression derived from different pigs than between 3 and 12- week cultures of replicate samples of the same organoid batch. Furthermore, organoid transcriptomes showed better correlation to tissue ($r = 0.77$) than IPEC-J2 ($r = 0.73$), whereas between tissue and IPEC-J2 correlation is lower ($r = 0.57$) (**Supplementary Figure S2**).

Organoid Transcriptomes Closely Resemble Gene Expression Signatures Associated With Their Tissue of Origin

Of the 24912 annotated genes in the pig genome, 11099 (44.6%) were not expressed in the dataset (<1 FPKM). All samples shared expression of 9117 genes, and a large set of genes was commonly expressed between organoids and tissue exclusively (1762 genes; **Figure 2A**). Genes associated with different overlapping areas of the Venn diagram were categorized by gene ontology using TOPPfun (**Supplementary File S2**).

However, the dataset for expressed genes in organoids still contained 1304 genes not annotated denoted with an unknown gene ID, and after conversion to human orthologs using g:profiler (Reimand et al., 2016), only 121 of these unknown ID's with unknown function acquired a gene annotation. Nevertheless, after conversion most of the 1304 genes did contain a description (80.6%), but no gene ortholog name to identify specific function. It is therefore evident that further curation of the porcine ontology database is necessary to generate a more comprehensive reference genome for transcriptomics research.

The top clusters of all pathways, based on all expressed genes, in organoids are involved in basal molecular and cellular function as well as physiological system development, reflecting the interactions with extracellular factors and self-organization of organoid microanatomy (**Figure 2B**). Pathways of particular relevance for using organoid models in host-microbe interactions, such as homeostasis and innate immunity, were highly expressed. Cellular homeostatic signaling or activation pathways included integrin, mTOR, Sirtuin, PPARα, and RXRα, with typically more than 40% of genes in the annotation being expressed (**Figure 2C**). Immunity- pathways included important cytokine and cytokine receptor signaling pathways (e.g., *TNFR1, IL8, JAK/STAT, PKR*) and innate immune signaling (*NF-kB, ERK/MAPK, iNOS*).

Ingenuity pathway analysis of the 1762 expressed genes shared only between organoids and tissues revealed pathways associated with GPCR and Ephrin signaling, which is associated with processes such as cell migration and stem cell differentiation (**Figure 2D**). Pathways associated with the endocrine functions of cells were also identified including signaling via tryptophan derived melatonin and serotonin. Other pathways specific to organoids and tissue included pathways linked to cytokine, MAP-kinase and other signaling pathways, which are altered in various disease states. Genes encoding complement factors

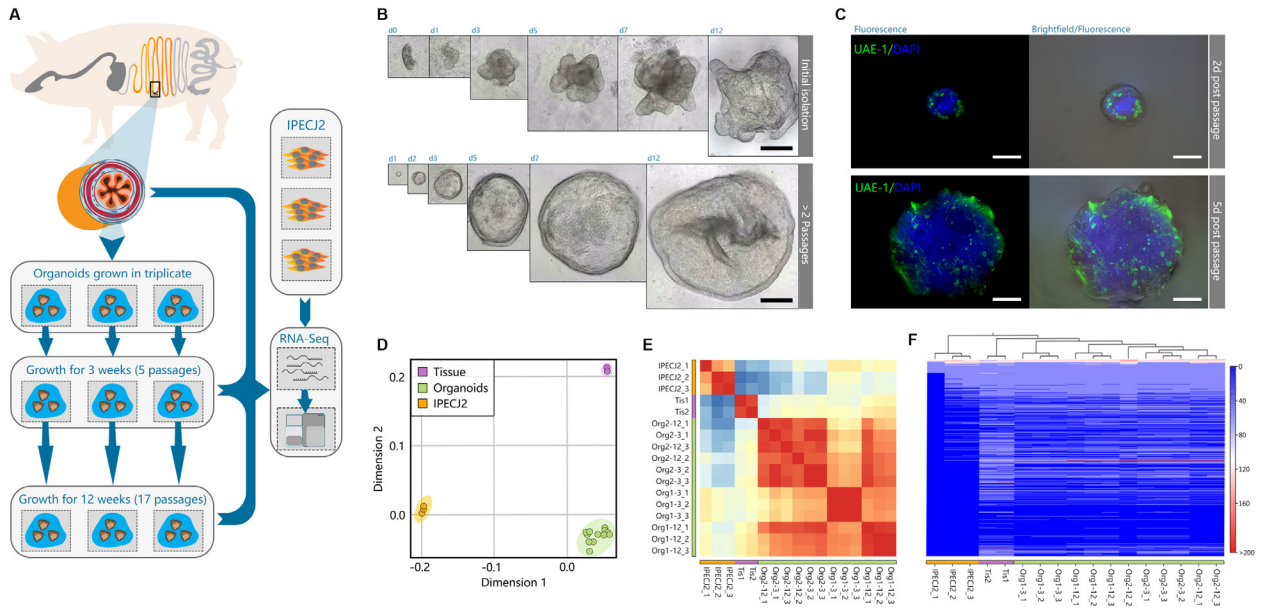

FIGURE 1 | Porcine intestinal organoid culture and transcriptome sequencing overview. **(A)** graphical overview of the study design. Organoids were generated from the jejunum of two individual pigs, directly divided into triplicate organoid cultures per animal, and passaged for 12 weeks. Total RNA of tissue, organoids, and jejunum cell line IPEC-J2 was extracted and sequenced by RNA-seq. **(B)** Initially after isolation, intestinal crypts form budding organ-like structures *in vitro*. Within 2 weeks of passaging, organoids form more spheroid-resembling structures for the remainder of the experiment, indicating more long-term reproducibility after a short-term series of passaging. **(C)** After 12 weeks of growth, spheroids still retain secretory cell lineage differentiation early post-passaging (green: stained with UEA-1). **(D)** Multidimensional scaling of transcriptomic data showed separation of organoids, tissue and IPEC-J2, where organoids and tissue show separation in only one dimension. **(E)** Correlation matrix of all samples show high correlation among individual organoid batches, and strong correlation between tissue. **(F)** Heat map and hierarchical clustering of all expressed genes (>1 FPKM) in the dataset.

were also specifically expressed in tissue and organoids. Recent studies integrating intestinal transcriptomes deposited in public databases suggest that intestinal expression of complement pathways plays a homeostatic role, being upregulated by inflammatory challenges to control microbial invasion or colonization (Sina et al., 2018; Benis et al., 2019). From this data it is evident that many complement factors are expressed in organoids and tissue (**Figure 2E**). A key difference between IPEC-J2 and organoid or tissue was the specific expression of hormones associated with Enteroendocrine cells, such as *CCK* which induces secretion of digestive enzymes and *PYY*, a satiety hormone (**Figure 2F**).

Genes which are specific for the different cell lineages found in the small intestinal epithelium (Grun et al., 2015), were generally highly expressed in organoids (**Figure 3A**) but largely absent in IPEC-J2. Surprisingly IPEC-J2 lacked expression of some genes commonly associated with mature absorptive enterocytes, even though cultures of this cell line are reported to differentiate into functional epithelium (Vergauwen, 2015). Initially our dataset suggested lack of mucin 2 (*MUC2*) gene expression using Ensembl gene annotation. However, we identified a high number of RNA-seq reads from organoids and tissue mapping to the chromosomal locus associated with *MUC2* in the NCBI database (XM_021082584, Chromosome 2, bp 689,363–719,542) (**Figure 3B**). We verified the expression of *MUC2* in porcine organoids and tissue using histology confirming mucin production and secretion as described previously (Sato et al., 2011; van der Hee et al., 2018). The genes identified in the human protein atlas to be enriched in the small intestine (i.e., jejunum) (Berglund et al., 2008; Fagerberg et al., 2014) were checked for expression in porcine jejunum tissue, jejunum and ileum organoids, and IPEC-J2 cells (**Supplementary File S3**). Most of the porcine orthologs (65% in tissue samples) were indeed expressed in epithelial tissue from the pig jejunum (**Figure 3C**). Moreover, between 74 and 86% of the porcine jejunum tissue-specific genes were also expressed in jejunum organoids, while this number was lower in ileum-derived organoids (52%). Furthermore, only 32% of small intestine-specific genes were expressed in IPEC-J2 cells. Genes associated with general digestion (*SI*, *FABP1*), absorption (solute-carriers; *SLC*-genes), or immunity (*IL22RA1*) were exclusively expressed in the tissue and jejunum organoids. Some of the genes associated with secreted peptides for immunity and digestion were not expressed in organoids and IPEC-J2 (i.e., *MEP1A*, *MEP1B*, *AQP10*, *CCL11*). It was shown that the intestinal epithelium is intrinsically programmed to differentiate into location specific organoid cultures (Middendorp et al., 2014). To investigate this for our organoid lines, we identified overlapping and exclusively expressed genes between jejunum and ileum-derived organoids. Both organoid types shared a large set of genes (10601), but several genes were identified for jejunum (1685) or ileum (481) only (**Figure 3D**). These

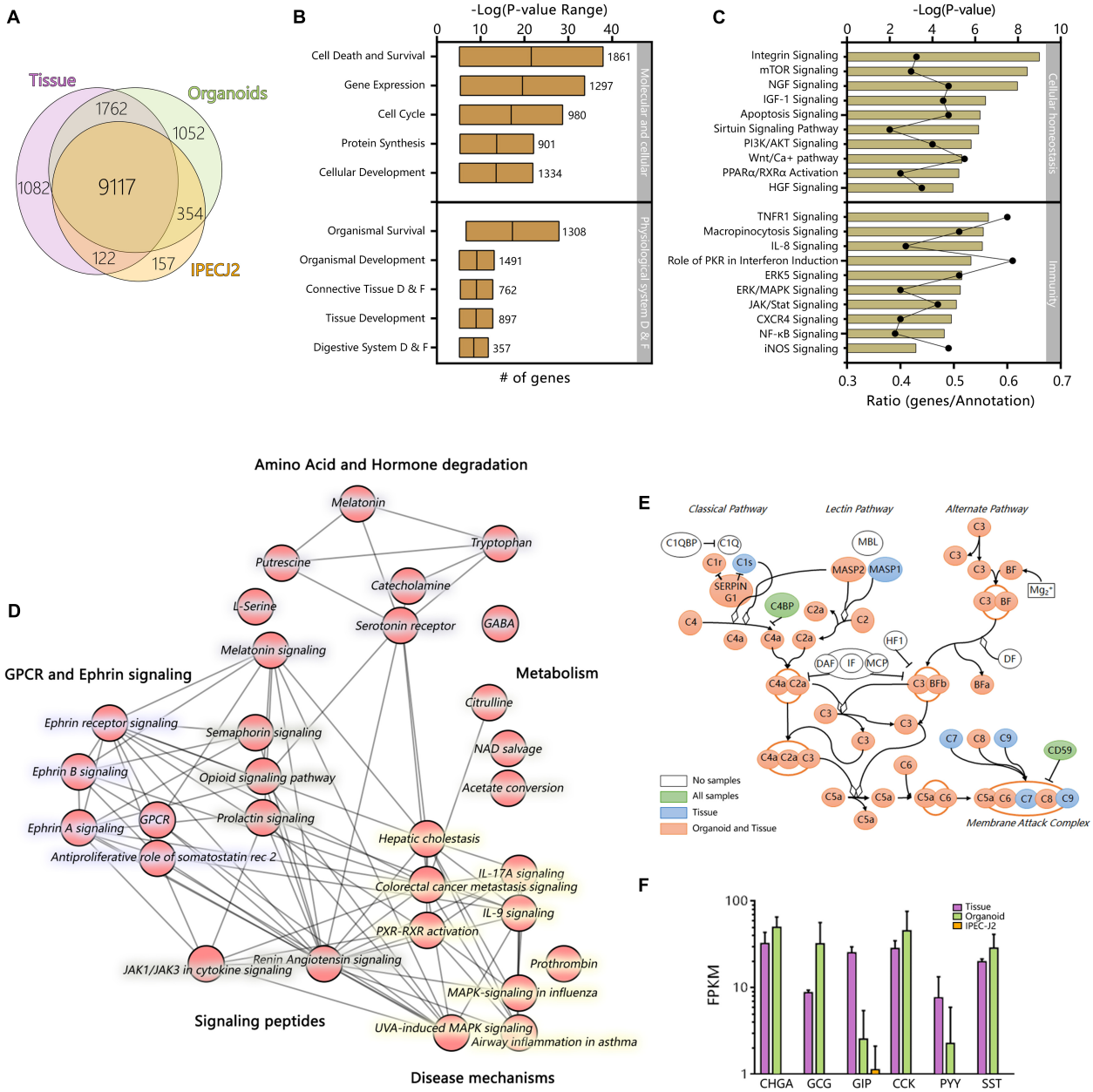

FIGURE 2 | The transcriptome of jejunum organoids exhibits strong similarity to its derived tissue transcriptome, including a distinct group of overlapping genes not expressed in IPEC-J2. Averages of all expressed genes were compared between sample type and **(A)** can be viewed in the weighted Venn-diagram. All genes expressed in organoids after 12 weeks of culture were analyzed using Ingenuity pathway analysis. **(B)** Molecular, cellular, and physiological system development and function shows many genes involved in basic cellular and tissue specific processes. More than >400 pathways were expressed in the organoid RNA-seq dataset. **(C)** The top 10 cellular homeostasis and immunity related pathways; –logP values indicate statistical probability of pathway expression; ratio, indicates number of expressed genes divided by number of annotated genes in the pathway. Testing the RNA-seq dataset for overlapping genes revealed a set of 1762 genes exclusively expressed in tissue and organoids. **(D)** Top 30 connected canonical pathways of these 1762 genes from ingenuity pathway analysis, which showed subdivision into metabolic, disease, GPCR/Ephrin signaling, and small molecule degradation pathways. **(E)** Expression of genes involved in the complement pathway are expressed in organoids and tissue (Pink), Tissue only (Blue), organoids tissue and IPEC-J2 (Green), or not found to be expressed (White). **(F)** Expression patterns of genes involved in Enteroendocrine signaling [CHGA, Chromogranin A; GCG, Glucagon; GIP, Gastric inhibitory polypeptide; CCK, Cholecystokinin; PYY, Peptide YY; SST, Somatostatin; Purple, Tissue; Green, Organoid; Orange, IPEC-J2, data shown as Log(FPKM)].

genes were subsequently analyzed for gene set function using TOPPfun. Jejunum exclusively expressed genes associated with transmembrane transport, like solute-carrier transporters (SLC), and digestion (e.g., FABP1 and 2) (See **Supplementary File S4** for output and gene lists). Ileum expressed genes associated with immune function, e.g., type 1 interferon responses by

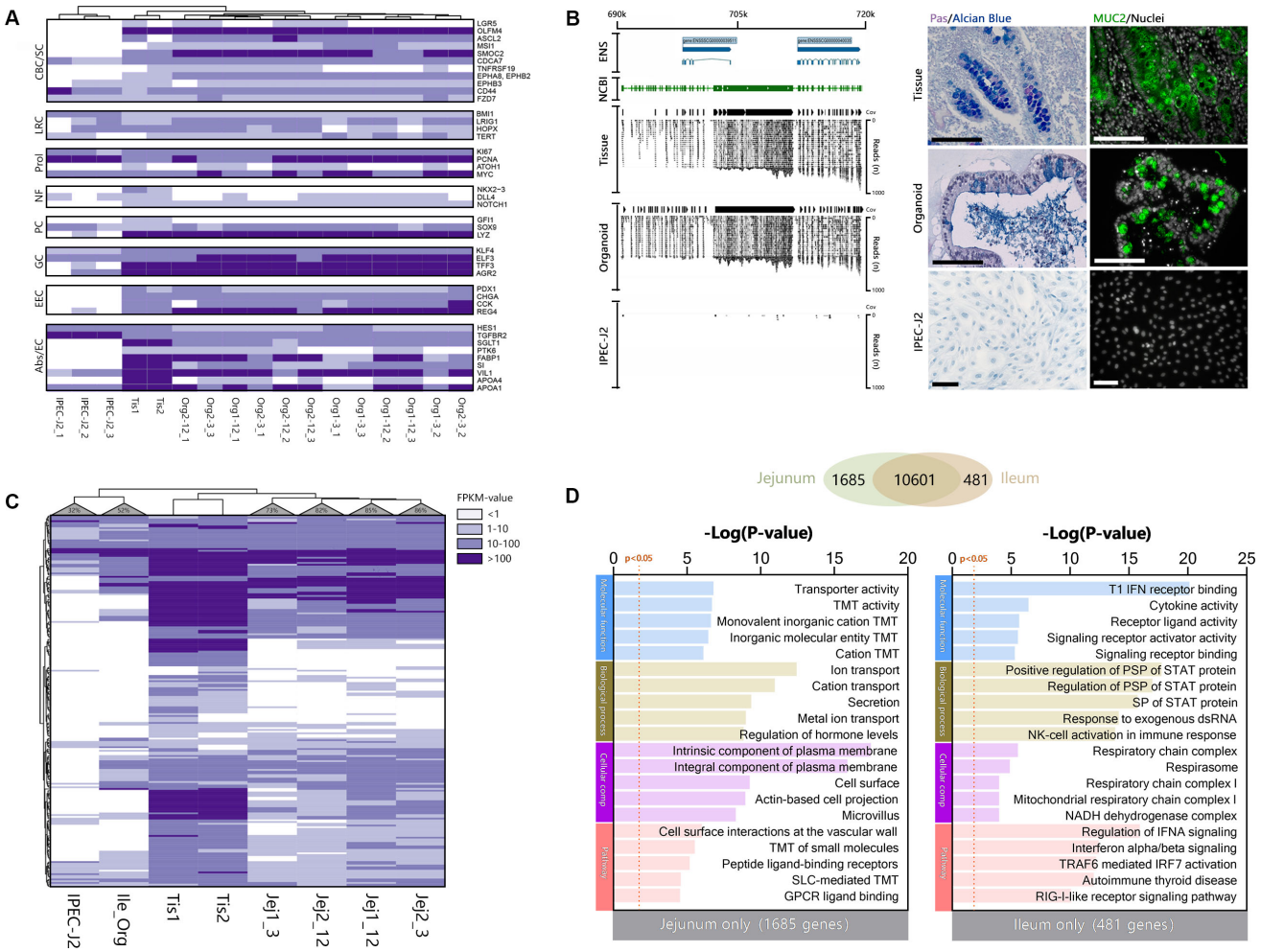

FIGURE 3 | Organoids derived from adult intestinal stem cells show intrinsic programming to differentiate into different epithelial cell lineages and express small intestine-specific genes. **(A)** Cell type-specific transcripts for Crypt Base Columnar *(CBC)* and Stem cells, Label-retaining *(LRC)* +4 cells, Proliferation (Prol), Niche factors (NF), Paneth cells (PC), Goblet cells (GC), Enteroendocrine cells (EEC), and Absorptive cells or enterocytes (Abs/EC). **(B)** Overlaying the NCBI gene tracks of MUC2 NC_010444.4 on chromosome 2 at location 689363–719542bp (green area), shows identical overlap with the mapped reads and coverage (Cov) from organoid and tissue samples, but not in IPEC-J2 (ENS; Ensembl reference genome). To confirm MUC2 protein translation and subsequent mucus formation, Carnoy fixed tissue, organoid, and IPEC-J2 samples were stained with PAS/Alcian blue (left) and porcine anti-MUC2 (right; black and white size bars indicate 100 μm). **(C)** Most small intestine-specific genes identified in the human protein atlas are also expressed in porcine jejunum tissue and their derived organoids (>74%), whereas fewer are expressed in ileum organoids (52%). IPEC-J2 only expressed 32% of the small intestine-specific genes. **(D)** Organoid transcriptomes from jejunum and ileum were compared to identify differences in expressed genes, showing large overlap of genes (Venn), but also some differences. The different genes were analyzed using TOPPfun to identify putative differences in gene ontology and pathways (TMT, Transmembrane transport; PSP, Peptidyl-serine phosphorylation).

interferon alpha genes, as well as fucosyltransferase activity (FUT1 and FUT2).

Cluster Analysis of Differentially Expressed Genes (DEGs)

Genes which were differentially expressed in tissue, organoids or IPEC-J2 ($P < 0.05$), were categorized by K means clustering and represented as biological processes and pathways (**Figures 4A–C**). The genes expressed only in tissue ($n = 141$) are mostly involved in immune pathways e.g., T cell and leukocyte functions, suggesting they might be due to presence of lamina propria immune cells in the tissue sample (**Figure 4A**). Genes related to extracellular matrix (ECM) or muscle contraction pathways were also differentially expressed in tissue compared to organoids and IPEC-J2.

The cluster of genes expressed at higher levels in tissue and IPEC-J2 ($n = 52$) compared to organoids comprise of processes related to cell morphology, proliferation, movement, remodeling of the ECM as well as integrin and ECM signaling pathways (**Figure 4B**). Altered expression of some of these pathways has been reported in cancer (Jorissen et al., 2009; Viana et al., 2013). The low or absent expression of the ECM genes in organoids may be due to provision of Matrigel acting as a basement membrane

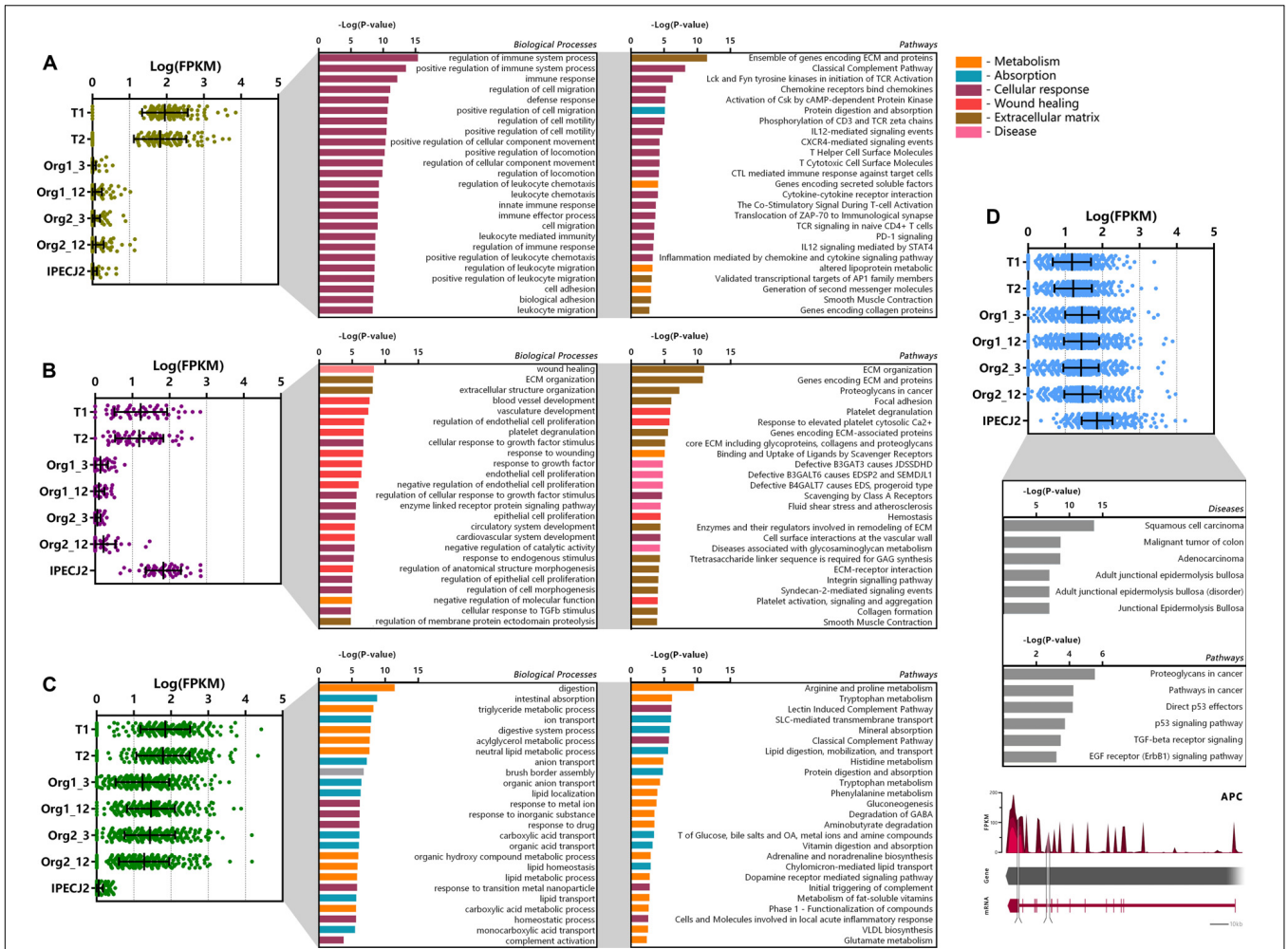

FIGURE 4 | Cluster analysis of differentially expressed genes (DEGs). DEGs were clustered according to their expression pattern using k-means clustering, and subsequently analyzed for functional enrichment using TOPPfun. **(A)** Cluster of genes (n = 141) showing increased expression in tissue only and low expression in organoids and IPEC-J2. **(B)** Cluster of genes (n = 52) showing high expression in tissue and IPEC-J2, with low expression in organoids. **(C)** Cluster of genes (n = 299) with increased expression in tissue and organoids, with low expression in IPECJ-2 (data represented in Log(FPKM) or –Log(P-value), P and $q < 0.05$). **(D)** Cluster of genes (n = 841) expressed more highly in IPEC-J2 than tissue and organoids which were associated with diseases and pathways involved in tumor formation. A common mutation in colon cancer is inactivation of adenomatous polyposis coli (APC) gene where IPEC-J2 shows an insertion (217 bp, tandem duplication) in the protein coding region and splice site deletion (331 bp, cross mapped breakpoints; bottom).

substrate. Furthermore, there may be components present in the intestinal ECM capable of inducing cell integrin signaling which are not present in Matrigel. Clustering genes transcribed in significantly higher amounts in IPEC-J2 show gene-list enrichment in disease processes and pathways associated with cancer (**Figure 4D**). Furthermore, one of our IPEC-J2 cultures showed an insertion in the protein coding region and a large deletion in the splicing site of the adenomatous polyposis coli (*APC*) gene, which is a tumor suppressor often inactivated in colon cancer (Sakai et al., 2018).

The cluster of genes with higher expression in organoids and tissue (n = 299) compared to IPEC-J2 involve nutrient transport and metabolic processes such as lipid digestion and transport, protein digestion and AA metabolism (**Figure 4C**). Examples include metabolism of tryptophan, arginine, proline, histidine, phenylalanine and transport of glucose, bile salts, fatty acids, lipids, and vitamins.

Congruence of the Transcriptome in Individual Organoids During Passage

Comparison of transcriptomes of organoid cultures over time and between batches indicated high correlation in expression values (r = 0.906–0.910, **Figure 5A**). After long-term passage there were 199 genes in organoid 1 and 172 genes in organoid 2 which were significantly increased in expression (**Figure 5B**; n = 3 per group). All differentially expressed genes were distributed across nine common ontologies (**Figure 5B**) and consisted of only 1.93–3.67% of the annotated genes in each biological process. This included processes such as

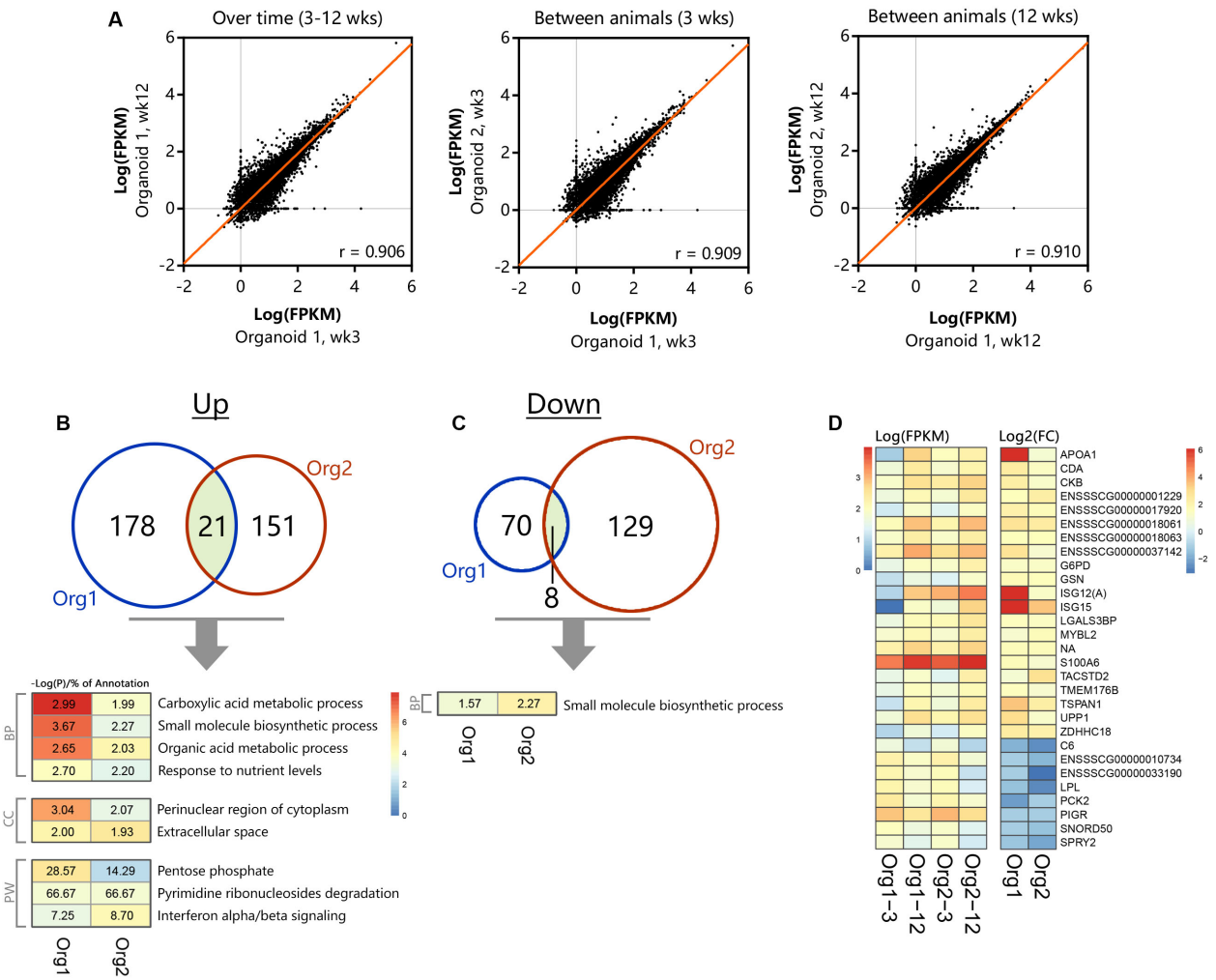

FIGURE 5 | Differential gene- and pathway expression in organoids shows stable transcription over time. The two separate organoid cultures (n = 3 per group) were tested for expression differences between 3 and 12 weeks of culturing, **(A)** showing representative correlations over time within an organoid line and between different animals (n = 13813 genes with at least 1 sample >1 FPKM). Significant ($p < 0.05$) up- **(B)** and down-regulation **(C)** of genes and their corresponding overlapping pathways when tested individually using TOPPfun (overlapping area shows similar genes between organoid types, BP, Biological processes; CC, Cellular component; PW, Pathway). **(D)** Overlapping up- and down-regulated genes between 3 and 12 weeks of culturing in actual expression values [Log(FPKM)] and their corresponding fold change [Log2(FC)].

small molecule biosynthesis, organic acid metabolic processes and response to nutrient levels. Variation in expression of genes in organoid cultures over time may therefore be due to differences in nutrient abundance in culture medium, and replicative activity, rather than permanent loss or gain of functions. Long-term passage also resulted in differential down regulation of 78 and 137 genes in organoids 1 and 2, respectively (n = 3 per group, **Figure 5C**). The only common ontology found for these genes was small molecule biosynthetic process, which was also included in genes upregulated after long term passage (**Figure 5B**). This suggests that culture dependent conditions result in variation in a small percentage of genes in this ontology group, perhaps due to variation in number or activity of several cell types in low abundance.

The heatmap in **Figure 5D** shows expression or fold change in genes that were commonly differentially expressed in organoids 1 and 2 after long-term passage. Although being significantly differentially regulated, a group of genes with significantly reduced fold change in expression after 12 weeks passage was seen to be overall reduced in transcript abundance (FPKM) and appeared to be involved in unrelated processes when tested for gene ontology. Differences between organoid 1 and 2 are likely to reflect individual variation and the most striking differences were for apolipoprotein A1 (*APOA1*), *ISG12*(A), and *ISG15*.

Small Molecule Transport by Intestinal Organoids

Determining cellular function by gene expression could result in biased interpretation. For this, functional assays can be used to

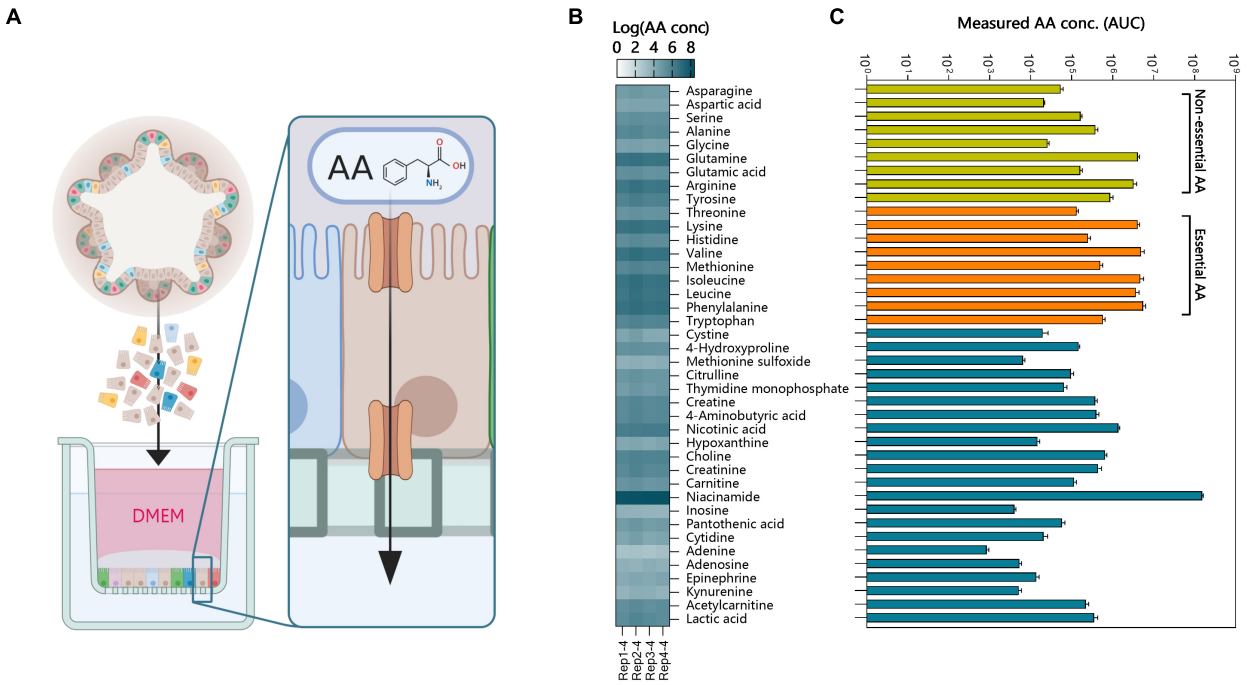

FIGURE 6 | Functional amino acid transport assay using intestinal organoid monolayers. **(A)** 3-Dimensional organoids were dissociated into single cells and plated on Matrigel precoated (0.5% v/v) Transwell inserts. The monolayers were grown to confluence for 1 or 4 days and generated TEER values >750 Ω/cm2. The apical medium was replaced with DMEM and basolateral medium with HBSS. Amino acids (AA) and other molecules were measured in the basal compartment using TQMS. **(B)** AA concentrations (Log values) of individual amino acids and other molecules for 4 replicate Transwell inserts of ileum organoids. **(C)** AA concentrations in the basolateral compartment show increased transport of essential AA's (orange).

determine cellular function *in vitro*. The luminal compartment of 3D organoids is in the center, preventing access for apical stimulation with compounds. Methods have been developed to inject compounds into organoids (**Supplementary Figure 3A**), but this temporarily disrupts the barrier, and injection of multiple organoids is laborious. We demonstrated basolateral efflux of compounds by adding celltracker red dye to 3D organoids and monitoring transport into the lumen (**Supplementary Figure 3B**). It was evident this was an active transport process, as the dye rapidly accumulated in the center of the organoids and was as inhibited by 200 nM zosuquidar, an inhibitor of the P-glycoprotein efflux pump, involved in multi-drug resistance. To make the apical side of the organoid epithelium more accessible for transport studies we generated 2-dimensional monolayers of polarized organoid cells that still retain their differentiated features (van der Hee et al., 2018) (schematic overview; **Figure 6A**). This allowed us to demonstrate the AA transport function of intestinal organoids (**Figure 6**). The individual AA's present in DMEM were transported across the intact monolayer in sufficient concentrations to be measured by TQMS (**Figure 6B**). We observed low variability in AA transport between replicates when the cell monolayers had TEER values >300 Ω/cm^2. To ensure integrity of the monolayers we used Transwell filters with *Trans*-epithelial electrical resistance (TEER) values between 750 and 850 Ω/cm^2 (Srinivasan et al., 2015). In addition to AA we showed that a variety of other molecules such as vitamin B5, choline, and epinephrine were transported from the apical to basolateral side. A high amount of niacinamide was measured in the basal compartment, which could be attributed to free NAD$^+$ (Belenky et al., 2007). Thus, polarized monolayers of small intestinal organoids provide a model for testing several compound transport mechanisms.

DISCUSSION

(non-)Transformed and cancer cell lines commonly display aneuploidy and mutations affecting cellular physiology, which may further change during long-term passage. Intestinal organoids are considered an attractive alternative to cell lines, but there are no studies evaluating the variability of the transcriptome in different batches of organoids generated from the same crypts and the effect of long-term culture on genomic stability and the transcriptome.

In this study, we compared gene expression in the porcine jejunum cell line IPEC-J2, organoids derived from adult stem cells of the porcine jejunum and the intestinal tissue from which they were derived. The genes highly expressed in tissue, but not organoids or IPEC-J2, were mostly involved in immune cell, ECM or muscle contraction pathways. This is most likely due to the presence of elements of the (sub)mucosa, including lamina propria immune cells in the tissue sample. Porcine intestinal organoids possessed the different epithelial cell lineages found in tissue for at least 17 passages. An interesting observation

in organoids was the high expression of *LYZ* which is often associated with Paneth cells. Until recently Paneth cells were considered to be absent in the porcine small intestine (Dekaney et al., 1997; Gonzalez et al., 2013). Paneth cells facilitate regeneration of the intestinal mucosa after metaplasia and produce high amounts of *LYZ* in presence of intestinal disease or damage (Brentnall et al., 2009; Sarvestani et al., 2018).

The set of genes expressed in organoids closely resembled that of the tissue of origin, a characteristic reported for other types of organoids (Huch et al., 2015; Matano et al., 2015). Moreover, jejunum organoids expressed the majority of gene orthologs (>74%) that are specifically expressed in the human small intestine for at least 17 passages, showing that the adult stem cells retain small intestine-associated gene expression over long-term culture (Middendorp et al., 2014; Haber et al., 2017). Interestingly, fewer small intestine-specific genes were expressed in ileum-derived organoids (52%), indicating location-specific differences. We also noticed that ileum organoids expressed the fucosyltransferase-1 (FUT1) and FUT2 genes, which were absent in our jejunum organoid transcriptome. A polymorphism in these genes has been associated with decreased susceptibility to infection with specific pathogens (Meijerink et al., 2000), further highlighting the importance of selecting the correct tissue origin when studying specific host-pathogen interactions.

Overall the batch to batch variation in organoids from the same animal was low, which may have been aided by concurrent passage and consequently differentiation state. The functions of genes which significantly altered expression between organoids from different animals or different cultures suggests they arise from differences in abundance of nutrients in culture medium or replicative activity, rather than permanent loss or gain of functions.

The main described benefits of the jejunum cell line IPEC-J2 are its non-cancerous origin and stability for more than 98 passages (Geens and Niewold, 2011; Vergauwen, 2015). However, we observed multiple indications of increased expression of genes associated with cancer or tumors in IPEC-J2 (passage 67–91). For example, these included *ANXA1* and *CALD1* (De Marchi et al., 2016), as well as insertions and deletions in the tumor suppressor *APC* (Sakai et al., 2018). We conclude that porcine jejunum organoids more closely resemble jejunum tissue than IPEC-J2 and provide a robust model for gene expression studies for at least 12 weeks of culture. As such they provide an advanced model for mechanistic studies on host-microbe interactions and intestinal physiology (Li et al., 2018). Organoids are also likely to avoid changes in glycosylation patterns seen in cancer or (non-)transformed cell models, however, timepoints extending further than 3 months could still be investigated. Motivation not to do so in this study, was the assumption that researchers would utilize the model within the tested timeframe. The RNA-seq data provides a valuable resource for researchers to assess the suitability of intestinal organoids for studying specific pathways or biological processes, as well as providing a comprehensive transcriptional map of expressed genes in IPEC-J2, formerly mainly available from microarray studies.

Previous studies have shown that organoids express proteins involved in nutrient sensing, like fructose or glucose, as well as transport by several transporters, like GLUT5, SGLT1, or PEPT1 (Zietek et al., 2015; Kishida et al., 2017). We verified the ability of 3-dimensional organoids to transport small molecules into the lumen within a short amount of time. However, studying transport over the epithelial barrier requires apical stimulation with compounds. The spatial nature of 3-dimensional organoids prevents easy access to the apical surface, but can be overcome by injection or monolayer formation. We have recently shown that apical stimulation of small intestinal organoids with various protein rich ingredients elicit specific metabolic responses, like altered lipid metabolism (Kar et al., 2020). In that study, predicted putative pathways were verified using protein-detection assays, showing the ability to measure gene-predicted responses in organoids. Transport of AAs is an essential function of the small intestine, and by measuring individual AA concentrations in a monolayer Transwell system enabled us to identify the rate at which different AAs cross the epithelial barrier. In the future, such a model could be used to identify specific transporter genes and their activity using CRISPR-Cas9 gene editing methods or transport inhibitors (Zietek et al., 2015; Schwank and Clevers, 2016).

Pig organoids can be rapidly generated from left over slaughter material without requirement for ethical approval. Thus, they have potential to be used to identify new phenotypes and investigate the role of genetic polymorphisms in susceptibility to enteric infections or other production traits. Furthermore, porcine intestinal physiology is considered to closely resemble that of humans increasing the potential for translational *in vitro* studies. Moreover, recent progress in developing robust methods for generating 2D monolayers from 3D organoid cultures facilitates apical exposure to test substances and also opens up possibilities for studying epithelial transport (Wang et al., 2017; van der Hee et al., 2018).

DATA AVAILABILITY STATEMENT

The datasets generated for this study can be found in the Gene expression omnibus GSE146408.

ETHICS STATEMENT

The animal study was reviewed by the Animal Ethics committee of Wageningen University and approved by the National Central Authority for Scientific Procedures on Animals (CCD) according to the legal and ethical requirements (No. AVD104002016515).

AUTHOR CONTRIBUTIONS

JW, BH, and HS conceptualized the study. BH performed the experiments, curated, analyzed, and visualized the data. JW and HS advised on the analysis methods and design of the figures. OM set up the sequencing contact and developed the analysis pipeline. JV performed the QTMS measurements and analyzed the data. JW and BH developed the methodology and wrote the initial draft of the manuscript. JW, HS, OM, JV, and BH reviewed and edited the final manuscript. All authors contributed to the article and approved the submitted version.

FUNDING

This research is financed by the Applied and Engineering Sciences Division of the Netherlands Organization for Scientific Research NWO (project number 14935), the Ministry of Economic Affairs, and DSM Nutritional Products.

ACKNOWLEDGMENTS

This manuscript has been released as a pre-print at bioRxiv by Van Der Hee et al. (2019). We would like to thank Anja Taverne-Thiele, Nico Taverne, and Linda Loonen for their practical assistance and helpful discussions. Furthermore, we appreciate the provision of one IPEC-J2 RNA-seq dataset (IPEC-J2 – 67; BioSamples database: SAMEA4447551) by Dr. Richard Crooijmans, Animal Breeding and Genomics, Wageningen University & Research, Netherlands, under the FAANG data sharing agreement (http://data.faang.org/home), as well as jejunum tissue from Raka Choudhury and Prof. Dr. Michiel Kleerebezem, Dr. Sabine Middendorp, Wilhelmina Children's Hospital, Utrecht, Netherlands, for initial guidance setting up organoid cultures, Dr. Kuo, Stanford University, United States, for providing the R-Spondin 1 transfected cell line for conditioned medium. Cell lines for Noggin and WNT3A conditioned medium were provided by the Hubrecht Institute, Utrecht, Netherlands, and Dr. Arie Kies for critically reading our manuscript and helpful suggestions. We would also like to thank Dr. Alfred Schinkel at the Netherlands Cancer Institute for helpful discussion about drug transporters in intestinal epithelium and for providing the inhibitor zosuquidar.

SUPPLEMENTARY MATERIAL

The Supplementary Material for this article can be found online at: https://www.frontiersin.org/articles/10.3389/fcell.2020.00375/full#supplementary-material

REFERENCES

Andrews, S. (2017). *FastQC: A Quality Control Tool for High Throughput Sequence Data*. Available online at: http://www.bioinformatics.babraham.ac.uk/projects/fastqc/

Barker, N., Van, J. H., Kuipers, J., Kujala, P., van den Born, M., Cozijnsen, M., et al. (2007). Identification of stem cells in small intestine and colon by marker gene Lgr5. *Nature* 449, 1003–1007. doi: 10.1038/nature06196

Belenky, P., Bogan, K. L., and Brenner, C. (2007). NAD+ metabolism in health and disease. *Trends Biochem. Sci.* 32, 12–19. doi: 10.1016/j.tibs.2006.11.006

Benis, N., Wells, J. M., Smits, M. A., Kar, S. K., van der Hee, B., Dos Santos, V., et al. (2019). High-level integration of murine intestinal transcriptomics data highlights the importance of the complement system in mucosal homeostasis. *BMC Genomics* 20:1028.

Berglund, L., Bjoerling, E., Oksvold, P., Fagerberg, L., Asplund, A., Szigyarto, C. A. K., et al. (2008). A Genecentric human protein atlas for expression profiles based on antibodies. *Mol. Cell Proteomics* 7, 2019–2027. doi: 10.1074/mcp.r800013-mcp200

Brentnall, T. A., Pan, S., Bronner, M. P., Crispin, D. A., Mirzaei, H., Cooke, K., et al. (2009). Proteins that underlie neoplastic progression of ulcerative colitis. *Proteom. Clin. Appl.* 3, 1326–1337. doi: 10.1002/prca.200900061

Bron, P. A., Van Baarlen, P., and Kleerebezem, M. (2012). Emerging molecular insights into the interaction between probiotics and the host intestinal mucosa. *Nat. Rev. Microbiol.* 10, 66–90.

Chen, J., Bardes, E. E., Aronow, B. J., and Jegga, A. G. (2009). ToppGene Suite for gene list enrichment analysis and candidate gene prioritization. *Nucleic Acids Res.* 37, W305–W311.

De Marchi, T., Timmermans, A. M., Smid, M., Look, M. P., Stingl, C., Opdam, M., et al. (2016). Annexin-A1 and caldesmon are associated with resistance to tamoxifen in estrogen receptor positive recurrent breast cancer. *Oncotarget* 7, 3098–3110. doi: 10.18632/oncotarget.6521

Dekaney, C. M., Bazer, F. W., and Jaeger, L. A. (1997). Mucosal morphogenesis and cytodifferentiation in fetal porcine small intestine. *Anat. Record.* 249, 517–523. doi: 10.1002/(sici)1097-0185(199712)249:4<517::aid-ar12>3.0.co;2-r

Dow, L. E., O'Rourke, K. P., Simon, J., Tschaharganeh, D. F., van Es, J. H., Clevers, H., et al. (2015). Apc restoration promotes cellular differentiation and reestablishes crypt homeostasis in colorectal cancer. *Cell* 161, 1539–1552. doi: 10.1016/j.cell.2015.05.033

Fagerberg, L., Hallstrom, B. M., Oksvold, P., Kampf, C., Djureinovic, D., Odeberg, J., et al. (2014). Analysis of the human tissue-specific expression by genome-wide integration of transcriptomics and antibody-based proteomics. *Mol. Cell Proteomics* 13, 397–406. doi: 10.1074/mcp.m113.035600

Geens, M. M., and Niewold, T. A. (2011). Optimizing culture conditions of a porcine epithelial cell line IPEC-J2 through a histological and physiological characterization. *Cytotechnology* 63, 415–423. doi: 10.1007/s10616-011-9362-9

Gillet, J. P., Varma, S., and Gottesman, M. M. (2013). The clinical relevance of cancer cell lines. *J. Natl. Cancer Inst.* 105, 452–458. doi: 10.1093/jnci/djt007

Gisselsson, D., Lichtenzstejn, D., Kachko, P., Karlsson, J., Manor, E., and Mai, S. (2018). Clonal evolution through genetic bottlenecks and telomere attrition: potential threats to in vitro data reproducibility. *Genes Chromosomes Cancer* 58, 452–461. doi: 10.1002/gcc.22685

Giuffra, E., Tuggle, C. K., and The, F. C. (2018). Functional annotation of animal genomes (FAANG): current achievements and roadmap. *Ann. Rev. Anim. Biosci.* 7, 65–88. doi: 10.1146/annurev-animal-020518-114913

Gonzalez, L. M., Williamson, I., Piedrahita, J. A., Blikslager, A. T., and Magness, S. T. (2013). Cell lineage identification and stem cell culture in a porcine model for the study of intestinal epithelial regeneration. *PLoS One* 8:e66465. doi: 10.1371/journal.pone.0066465

Grun, D., Lyubimova, A., Kester, L., Wiebrands, K., Basak, O., Sasaki, N., et al. (2015). Single-cell messenger RNA sequencing reveals rare intestinal cell types. *Nature* 525, 251–255. doi: 10.1038/nature14966

Haber, A. L., Biton, M., Rogel, N., Herbst, R. H., Shekhar, K., Smillie, C., et al. (2017). A single-cell survey of the small intestinal epithelium. *Nature* 551, 333–339.

Huch, M., Gehart, H., van Boxtel, R., Hamer, K., Blokzijl, F., Verstegen, M. M. A., et al. (2015). Long-term culture of genome-stable bipotent stem cells from adult human liver. *Cell* 160, 299–312. doi: 10.1016/j.cell.2014.11.050

Jorissen, R. N., Gibbs, P., Christie, M., Prakash, S., Lipton, L., Desai, J., et al. (2009). Metastasis-associated gene expression changes predict poor outcomes in patients with dukes stage b and c colorectal cancer. *Clin. Cancer Res.* 15, 7642–7651. doi: 10.1158/1078-0432.ccr-09-1431

Kar, S. K., van der Hee, B., Loonen, L. M. P., Taverne, N., Taverne-Thiele, J. J., Schokker, D., et al. (2020). Effects of undigested protein-rich ingredients on polarised small intestinal organoid monolayers. *J. Anim. Sci. Biotechnol.* 11:51.

Kishida, K., Pearce, S. C., Yu, S., Gao, N., and Ferraris, R. P. (2017). Nutrient sensing by absorptive and secretory progenies of small intestinal stem cells. *Am. J. Physiol. Gastrointest Liver Physiol.* 312, G592–G605.

Krueger, F. (2017). *Trim Galore: A Wrapper Around Cutadapt and FastQC to Consistently Apply Adapter and Quality Trimming to FastQ Files*. Available online at: https://www.bioinformatics.babraham.ac.uk/projects/trim_galore/

Li, L., Fu, F., Guo, S., Wang, H., He, X., Xue, M., et al. (2018). Porcine intestinal enteroids: a new model for studying enteric coronavirus PEDV infection and the host innate response. *J. Virol.* 93:e01682-18.

Liu, Y., Mi, Y., Mueller, T., Kreibich, S., Williams, E. G., Van Drogen, A., et al. (2019). Multi-omic measurements of heterogeneity in HeLa cells across laboratories. *Nat. Biotechnol.* 37, 314–322. doi: 10.1038/s41587-019-0037-y

Loonen, L. M. P., Stolte, E. H., Jaklofsky, M. T. J., Meijerink, M., Dekker, J., van Baarlen, P., et al. (2014). REG3 gamma-deficient mice have altered mucus distribution and increased mucosal inflammatory responses to the microbiota and enteric pathogens in the ileum. *Mucosal Immunol.* 7, 939–947. doi: 10.1038/mi.2013.109

Matano, M., Date, S., Shimokawa, M., Takano, A., Fujii, M., Ohta, Y., et al. (2015). Modeling colorectal cancer using CRISPR-Cas9-mediated engineering of human intestinal organoids. *Nat. Med.* 21, 256–262. doi: 10.1038/nm.3802

Meijerink, E., Neuenschwander, S., Fries, R., Dinter, A., Bertschinger, H. U., Stranzinger, G., et al. (2000). A DNA polymorphism influencing alpha(1,2)fucosyltransferase activity of the pig FUT1 enzyme determines susceptibility of small intestinal epithelium to *Escherichia coli* F18 adhesion. *Immunogenetics* 52, 129–136. doi: 10.1007/s002510000263

Middendorp, S., Schneeberger, K., Wiegerinck, C. L., Mokry, M., Akkerman, R. D. L., van Wijngaarden, S., et al. (2014). Adult stem cells in the small intestine are intrinsically programmed with their location-specific function. *Stem Cells* 32, 1083–1091. doi: 10.1002/stem.1655

Moon, C., VanDussen, K. L., Miyoshi, H., and Stappenbeck, T. S. (2014). Development of a primary mouse intestinal epithelial cell monolayer culture system to evaluate factors that modulate IgA transcytosis. *Mucosal Immunol.* 7, 818–828. doi: 10.1038/mi.2013.98

Ootani, A., Li, X. N., Sangiorgi, E., Ho, Q. T., Ueno, H., Toda, S., et al. (2009). Sustained in vitro intestinal epithelial culture within a Wnt-dependent stem cell niche. *Nat. Med.* 15, 701–706. doi: 10.1038/nm.1951

Reimand, J., Arak, T., Adler, P., Kolberg, L., Reisberg, S., Peterson, H., et al. (2016). g:Profiler-a web server for functional interpretation of gene lists (2016 update). *Nucleic Acids Res.* 44, W83–W89.

Sakai, E., Nakayama, M., Oshima, H., Kouyama, Y., Niida, A., Fujii, S., et al. (2018). Combined mutation of Apc, Kras, and Tgfbr2 effectively drives metastasis of intestinal cancer. *Cancer Res.* 78, 1334–1346. doi: 10.1158/0008-5472.can-17-3303

Sarvestani, S. K., Signs, S. A., Lefebvre, V., Mack, S., Ni, Y., Morton, A., et al. (2018). Cancer-predicting transcriptomic and epigenetic signatures revealed for ulcerative colitis in patient-derived epithelial organoids. *Oncotarget* 9, 28717–28730. doi: 10.18632/oncotarget.25617

Sato, T., Stange, D. E., Ferrante, M., Vries, R. G., Van Es, J. H., Van den Brink, S., et al. (2011). Long-term expansion of epithelial organoids from human colon, adenoma, adenocarcinoma, and Barrett's epithelium. *Gastroenterology* 141, 1762–1772. doi: 10.1053/j.gastro.2011.07.050

Sato, T., Vries, R. G., Snippert, H. J., van de Wetering, M., Barker, N., Stange, D. E., et al. (2009). Single Lgr5 stem cells build crypt-villus structures in vitro without a mesenchymal niche. *Nature* 459, 262–265. doi: 10.1038/nature07935

Schwank, G., and Clevers, H. (2016). CRISPR/Cas9-mediated genome editing of mouse small intestinal organoids. *Methods Mol. Biol.* 1422, 3–11. doi: 10.1007/978-1-4939-3603-8_1

Sina, C., Kemper, C., and Derer, S. (2018). The intestinal complement system in inflammatory bowel disease: shaping intestinal barrier function. *Sem. Immunol.* 37, 66–73. doi: 10.1016/j.smim.2018.02.008

Srinivasan, B., Kolli, A. R., Esch, M. B., Abaci, H. E., Shuler, M. L., and Hickman, J. J. (2015). TEER measurement techniques for in vitro barrier model systems. *J. Lab. Autom.* 20, 107–126. doi: 10.1177/2211068214561025

Trapnell, C., Roberts, A., Goff, L., Pertea, G., Kim, D., Kelley, D. R., et al. (2012). Differential gene and transcript expression analysis of RNA-seq experiments with TopHat and Cufflinks. *Nat. Protoc.* 7, 562–578. doi: 10.1038/nprot.2012.016

Van Der Flier, L. G., and Clevers, H. (2009). Stem cells, self-renewal, and differentiation in the intestinal epithelium. *Annu. Rev. Physiol.* 71, 241–260. doi: 10.1146/annurev.physiol.010908.163145

van der Hee, B., Loonen, L. M. P., Taverne, N., Taverne-Thiele, J. J., Smidt, H., and Wells, J. M. (2018). Optimized procedures for generating an enhanced, near physiological 2D culture system from porcine intestinal organoids. *Stem Cell Res.* 28, 165–171. doi: 10.1016/j.scr.2018.02.013

Van Der Hee, B., Madsen, O., Smidt, H., and Wells, J. M. (2019). Congruence of location-specific transcriptional programs in intestinal organoids during long-term culture. *bioRxiv*. [Preprint]. doi: 10.1101/600940

Vergauwen, H. (2015). "The IPEC-J2 Cell Line," in *The Impact of Food Bioactives on Health: In Vitro and Ex Vivo Models*, eds K. Verhoeckx, P. Cotter, I. Lopez-Exposito, C. Kleiveland, T. Lea, A. Mackie, et al. (Cham: Springer), 125–134. doi: 10.1007/978-3-319-16104-4_12

Viana, L. D., Affonso, R. J., Silva, S. R. M., Denadai, M. V. A., Matos, D., de Souza, C. S., et al. (2013). Relationship between the Expression of the Extracellular Matrix Genes SPARC, SPP1, FN1, ITGA5 and ITGAV and clinicopathological parameters of tumor progression and colorectal cancer dissemination. *Oncol. Basel.* 84, 81–91. doi: 10.1159/000343436

Wang, Y., DiSalvo, M., Gunasekara, D. B., Dutton, J., Proctor, A., Lebhar, M. S., et al. (2017). Self-renewing monolayer of primary colonic or rectal epithelial cells. *Cell Mol. Gastroenterol. Hepatol.* 4:165–82.e7.

Wells, J. M., Rossi, O., Meijerink, M., and van Baarlen, P. (2011). Epithelial crosstalk at the microbiota-mucosal interface. *Proc. Natl. Acad. Sci. U.S.A.* 108, 4607–4614. doi: 10.1073/pnas.1000092107

Zerbino, D. R., Achuthan, P., Akanni, W., Amode, M. R., Barrell, D., Bhai, J., et al. (2018). Ensembl 2018. *Nucleic Acids Res.* 46, D754–D761.

Zietek, T., Rath, E., Haller, D., and Daniel, H. (2015). Intestinal organoids for assessing nutrient transport, sensing and incretin secretion. *Sci. Rep.* 5: 16831.

Conflict of Interest: The authors declare that the research was conducted in the absence of any commercial or financial relationships that could be construed as a potential conflict of interest.

frontiers in Cell and Developmental Biology

BRIEF RESEARCH REPORT
published: 07 October 2020
doi: 10.3389/fcell.2020.567454

Modeling Klinefelter Syndrome Using Induced Pluripotent Stem Cells Reveals Impaired Germ Cell Differentiation

Olivier Botman[1,2†], Youssef Hibaoui[3,4†], Maria G. Giudice[1,2], Jérôme Ambroise[5], Catherine Creppe[6], Anis Feki[3,4] and Christine Wyns[1,2*]*

[1] Gynecology Unit, Institut de Recherche Expérimentale et Clinique (IREC), Université catholique de Louvain, Brussels, Belgium, [2] Department of Gynecology-Andrology, Cliniques Universitaires Saint-Luc, Brussels, Belgium, [3] Stem Cell Research Laboratory, Department of Obstetrics and Gynecology, Geneva University Hospitals, Geneva, Switzerland, [4] Department of Obstetrics and Gynecology, Hôpital Fribourgeois (HFR) Fribourg, Hôpital Cantonal, Fribourg, Switzerland, [5] Center for Applied Molecular Technologies (CTMA), Institut de Recherche Expérimentale et Clinique (IREC), Université catholique de Louvain, Brussels, Belgium, [6] Groupe Interdisciplinaire de Génoprotéomique Appliquée (GIGA)-Signal Transduction, C.H.U. Sart Tilman, University of Liège, Liège, Belgium

OPEN ACCESS

Edited by:
Eumorphia Remboutsika, National and Kapodistrian University of Athens, Greece

Reviewed by:
Alexander Goedel, Karolinska Institutet (KI), Sweden
Seyed Ehsan Enderami, Mazandaran University of Medical Sciences, Iran

***Correspondence:**
Youssef Hibaoui
youssef.hibaoui@unifr.ch
Christine Wyns
christine.wyns@uclouvain.be

[†]These authors share first authorship

Specialty section:
This article was submitted to Stem Cell Research, a section of the journal Frontiers in Cell and Developmental Biology

Received: *29 May 2020*
Accepted: *03 September 2020*
Published: *07 October 2020*

Citation:
Botman O, Hibaoui Y, Giudice MG, Ambroise J, Creppe C, Feki A and Wyns C (2020) Modeling Klinefelter Syndrome Using Induced Pluripotent Stem Cells Reveals Impaired Germ Cell Differentiation. Front. Cell Dev. Biol. 8:567454. doi: 10.3389/fcell.2020.567454

Klinefelter syndrome (KS), with an incidence between 1/600 and 1/1,000, is the main genetic cause of male infertility. Due to the lack of an accurate study model, the detailed pathogenic mechanisms by which this X chromosome aneuploidy leads to KS features remain unknown. Here, we report the generation and characterization of induced pluripotent stem cells (iPSCs) derived from a patient with KS: 47XXY-iPSCs. In order to compare the potentials of both 47XXY-iPSCs and 46XY-iPSCs to differentiate into the germ cell lineage, we developed a directed differentiation protocol by testing different combinations of factors including bone morphogenetic protein 4 (BMP4), glial-derived neurotrophic factor (GDNF), retinoic acid (RA) and stem cell factor (SCF) for 42 days. Importantly, we found a reduced ability of 47XXY-iPSCs to differentiate into germ cells when compared to 46XY-iPSCs. In particular, upon germ cell differentiation of 47XXY-iPSCs, we found a reduced proportion of cells positive for BOLL, a protein required for germ cell development and spermatogenesis, as well as a reduced proportion of cells positive for MAGEA4, a spermatogonia marker. This reduced ability to generate germ cells was not associated with a decrease of proliferation of 47XXY-iPSC-derived cells but rather with an increase of cell death upon germ cell differentiation as revealed by an increase of LDH release and of capase-3 expression in 47XXY-iPSC-derived cells. Our study supports the idea that 47XXY-iPSCs provides an excellent *in vitro* model to unravel the pathophysiology and to design potential treatments for KS patients.

Keywords: induced pluripotent stem cells, primordial germ cells, germ cell differentiation, post-meiotic cells, Klinefelter syndrome, Klinefelter syndrome iPSCs

INTRODUCTION

Klinefelter syndrome (KS), with an incidence between 1/600 and 1/1,000, is the main genetic cause of male infertility as KS represent 11% of azoospermic men and 4% of infertile men (Van Assche et al., 1996). The vast majority of KS patients (80–90%) are non-mosaic with a 47XXY karyotype whereas 10–20% of KS patients are mosaic forms of the disorder (with 47XXY and 46XY karyotype)

or higher grade of aneuploidy (48XXXY karyotype) (Lanfranco et al., 2004; Gravholt et al., 2018). Histological analysis of testes from KS patients reveals an extensive fibrosis and hyalinization of the seminiferous tubules with a progressive decline in germ cells, starting before puberty, intensifying at puberty, and ultimately leading to azoospermia (Wikström et al., 2007). Sertoli cells (SCs) which support germ cells, not only decrease in number but also show impaired function with attenuated maturation (Aksglæde et al., 2011) while Leydig cells (LCs) exhibit hyperplasia (Bojesen et al., 2011). A dysfunctional somatic compartment with reduced expression of androgen receptor in SCs and of INSL3 in LCs, both as maturation markers was recently reported (Giudice et al., 2019). Although KS is associated with male infertility, the pathogenic process by which the extra copy of X chromosome leads to these defects remains unknown. Transgenic mouse models of KS have evidenced a decrease in primordial germ cell (PGC) populations during migration through the epiblastic crest (Mroz et al., 1999) providing a number of insights in KS pathogenesis. However, these models do not accurately recapitulate the human condition.

The discovery that human pluripotent stem cells (PSCs) can be reprogrammed from somatic cells to further differentiate into germ-like cells provided new opportunities to investigate germ cell development and function (Clark et al., 2004; Kee et al., 2009; Park et al., 2009; Panula et al., 2010; Eguizabal et al., 2011; Easley et al., 2012; Medrano et al., 2012; Ramathal et al., 2014; Mahabadi et al., 2018; Li et al., 2020). Also, these cells make excellent *in vitro* models, replicating disease-associated phenotypes (Hibaoui and Feki, 2012; Botman and Wyns, 2014). Recent studies have been successful in generating induced pluripotent stem cells from patients with KS (Ma et al., 2012; Shimizu et al., 2016; Panula et al., 2019). In the present study, we have generated iPSCs from a patient with KS: 47XXY-iPSC line#11 and 47XXY-iPSC line#16. A 46XY-iPSC line generated from a healthy individual was used as control (Grad et al., 2011; Hibaoui et al., 2014). We evaluated the multilineage potential of these iPSCs *in vivo* by teratoma formation when these iPSCs were injected intramuscularly into immunodeficient SCID mice. In order to study KS pathogenesis, we developed a germ cell differentiation protocol by testing different combinations of factors, including bone morphogenetic protein 4 (BMP4), glial-derived neurotrophic factor (GDNF), retinoic acid (RA), and stem cell factor (SCF) for 42 days. The potentials of both 47XXY-iPSCs and 46XY-iPSCs to differentiate into germ cell lineage was also investigated.

MATERIALS AND METHODS

iPSC Derivation and Culture

Skin fibroblasts were isolated from a 20-years-old infertile KS patient. These 47XXY-fibroblasts were used to generate 47XXY-iPSCs by transducing the parental fibroblasts with the polycistronic lentiviral vector, carrying the pluripotent genes *OCT4*, *KLF4*, *SOX2*, and *c-MYC* as we previously described (Grad et al., 2011; Hibaoui et al., 2014). A 46XY-iPSC line derived from a healthy individual with the same method of reprogramming was used as a control (Grad et al., 2011; Hibaoui et al., 2014). Among the 47XXY-iPSC lines generated from the parental 47XXY-fibroblasts, 47XXY-iPSC line#11 and 47XXY-iPSC line#16 were used for the present study. Theses iPSC lines were cultured on primary human foreskin fibroblasts (iHFF 106-05n, ECACC Culture Collections Public Health England, Salisbury, United Kingdom) that were mitotically inactivated by irradiation at 25 Gy. They were maintained with daily changes in knockout (KO)-DMEM medium supplemented with 20% serum replacement, 2 mmol/L GlutaMAX, 50 U/mL penicillin, 50 mg/mL streptomycin, 100 μmol/L β-mercaptoethanol, 100 μmol/L non-essential amino acids (all from Life Technologies, Carlsbad CA, United States) and 100 ng/mL β-fibroblast growth factor (β-FGF from Prospec, Ness-Ziona, Israel). The cell lines were then passaged mechanically in the presence of 10 μM ROCK-inhibitor Y-27632 (Sigma-Aldrich, St. Louis, MO, United States). Alternatively, these iPSCs were maintained in feeder-free conditions, on matrigel-coated dishes in StemFlex medium supplemented with 50 U/mL penicillin and 50 mg/mL streptomycin (Life Technologies, Carlsbad CA, United States) with media changes every 2 days. All cell lines were kept at 37°C in 5% CO_2.

Spontaneous Differentiation Into Three Germ Layers

Whole iPSC colonies were collected and seeded onto ultra-low attachment dishes (Sigma-Aldrich, St Louis MO, United States) in KO-DMEM supplemented with 20% newborn calf serum, 2 mmol/L glutaMAX, 50 U/mL penicillin, 50 mg/mL streptomycin 1% non-essential amino acid (all from Life Technologies, Carlsbad CA, United States) and 0.1 mmol/L β-mercaptoethanol (Sigma-Aldrich, St Louis MO, United States). Within 24 h, the cells had aggregated into EBs. After 7 days of suspension, these EBs were seeded onto gelatin-coated glass slides for an additional 14 days to allow the cells to differentiate. Medium was changed every 2 days.

Germ Cell Lineage Differentiation

The iPSC colonies were dissociated with cell dissociation medium (Sigma-Aldrich, St. Louis MO, United States), centrifuged for 5 min at 1,000 rpm and resuspended in iPSC proliferation medium containing 2 μM ROCK inhibitor Y-27632 to improve cell survival. Then, these cells were allowed to aggregate in Aggrewell^{TM} dishes for 24 h in order to obtain size-calibrated EBs containing 4,000 cells. These EBs were transferred into low attachment wells (Costar, Corning Life Sciences) for 5 days in differentiation medium supplemented or not with 20 ng/mL BMP4 (Life Technologies, Carlsbad CA, United States) as outlined in **Figure 3A**. Approximately 30 EBs (∼120,000 cells) were seeded onto a glass slide coated with gelatin in one well of a 4-well plate and 4 different media were used to culture them over 16 additional days, as shown in **Figure 3A**. For the following 14 days, only retinoic acid (RA) (2 μM, Sigma) was added, and before including stem cell factor (SCF) (100 ng/mL, Life Technologies) from day 35 to day 42. EBs were retrieved for characterization after 5, 21, and 42 days of differentiation (**Figure 3A**).

Karyotyping

Karyotyping was performed on at least 20 metaphase spreads using the GTG-banding method. Briefly, iPSCs were incubated in culture medium, supplemented with 0.2 mg/mL colcemid (Roche, Bâle, Switzerland) at 37°C for 20 min and washed three times in 2 mL PBS containing Ca^{2+} and Mg^{2+} (Life Technologies, Carlsbad CA, United States). A minimum of 15 colonies were collected in 2 mL 1 × trypsin-EDTA (Life Technologies, Carlsbad CA, United States) and incubated at 37°C for 5 min. Trypsin activity was then stopped and the cells were centrifuged at 300 g for 10 min. The pellet obtained was resuspended and incubated in 1 mL pre-warmed potassium chloride solution (KCl, 0.075 M) for 10 min at 37°C. The cells were subsequently pre-fixed in 1 mL Carnoy fixative solution (methanol/acetic acid = 3/1) at −20°C before immediate centrifugation at 1,800 g for 10 min. Finally, the supernatant was discarded and the pellet was once again suspended in Carnoy fixative solution and prepared for analyses.

Alkaline Phosphatase Staining

iPSC colonies were fixed in 4% paraformaldehyde in PBS and treated with 0.1% Triton X-100 in PBS. The colonies were stained with alkaline phosphatase solution as described in the alkaline phosphatase substrate kit III manual (Vector Laboratories Ltd., Peterborough, United Kingdom) for 30–45 min at 37°C.

Immunohistochemistry

Briefly, iPSCs and embryoïd bodies were fixed in 4% paraformaldehyde in phosphate buffered saline (PBS) for 30 min, permeabilized with 0.2% Triton X-100 for 30 min, and blocked with 5% bovine serum albumin in PBS for 1 h at room temperature (RT). Cells were incubated with primary antibody overnight at 4°C, washed with PBS and incubated with secondary antibody for 1 h at RT. The antibodies used for immunohistochemical staining are listed in **Supplementary Table S1**. The cells were finally with Vectashield mounting medium containing DAPI for nuclei identification. Images of immunostained cells were captured on a Mirax Midi fluorescence scanner (Zeiss MicroImaging GmbH, Jena, Germany) in automation. All immunostaining analyses were performed at least in triplicate and analyzed with ImageJ software (National Institutes of Health). For negative controls, primary antibodies were replaced with corresponding immunoglobulin serotypes. The proportion of positive cells was calculated by the difference observed between cells positive for primary antibodies and total cells identified by DAPI. All counting results were expressed as a percentage.

Cytotoxicity Assays

Cell damage was evaluated by measuring lactate dehydrogenase (LDH) release into the medium by means of a UV assays on a Cobas Integra analyzer using the LDHI2 kit (Roche, Bâle, Switzerland). Briefly, 4 μL of supernatant was pipetted at different time points in iPSC differentiation (5, 21, 35, and 42 days) in each condition. Sample absorbance was measured at 340/659 nm and the results were expressed in IU/L.

RNA Extraction, Non-quantitative, and Quantitative Real Time Polymerase Chain Reaction

Total RNA was extracted from iPSC-derived cells (2 wells of a 4-well plate were pooled) using the Qiagen RNeasy mini kit (Qiagen, Venlo, Netherlands) according to the manufacturer's protocol. RNA quantities were assessed with a Nanodrop 2000 analyzer (Thermo Fisher Scientific, Waltham, MA, United States) and RNA integrity Number (RIN) analyses were conducted with the Agilent RNA 6000 nano kit (Agilent Technologies, Santa Clara, United States). Five-Hundred nanograms of RNA was reversed-transcribed with ThermoScript reverse transcriptase following the manufacturer's instructions (Life Technologies, Carlsbad CA, United States). cDNA was amplified by real-time polymerase chain reaction (RT-PCR) in a Light Cycler 480 (Roche) using the Power SYBRGreen PCR master mix (Life Technologies, Carlsbad CA, United States). For amplification, the program used was 50°C for 2 min, 95°C for 10 min, 40 cycles of 95°C for 15 s and 60°C for 1 min. A mean quantity was calculated from duplicate PCR reactions for each sample, and this quantity was normalized against the *GAPDH* housekeeping gene. Each PCR reaction was performed at least in triplicate with negative controls and mean quantities were calculated in each case. For non-quantitative PCR, reactions were performed in a Biometra thermocycler (Göttingen, Germany), using the above program of amplification, with a RedTaq polymerase mix (Sigma-Aldrich, St. Louis, MO, United States), 250 nM primers and 1 μL of cDNA. Primer sequences used for non-quantitative and quantitative RT-PCR are listed in **Supplementary Tables S2, S3**.

Teratoma Formation Assays

In vivo differentiation was investigated by teratoma formation as previously described (Hibaoui et al., 2014). All the procedures involving animals were conducted in accordance with the Swiss Federal Veterinary Office's guidelines, based on the Swiss Federal Law on Animal Welfare and approved by the Ethics Review Board and the Committee on Animal Research of the Catholic University of Louvain. Briefly, 5×10^6 cells were harvested from each iPSC and injected intramuscularly into SCID mice. After 8 weeks, the resulting teratomas were excised, fixed in 4% formaldehyde, and embedded in paraffin for immunohistochemistry analysis with horseradish peroxidase (HRP) using the Ventana Discovery automated staining system (Ventana Medical Systems, Tucson, AZ, United States). Ventana reagents were utilized for the entire procedure. No antigen retrieval pretreatment was required for either SMA or AFP antibodies. After automatic deparaffinization, slides were incubated for 30 min at 37°C SMA 1/300 (M0851, Dako, Baar, Switzerland) and AFP 1/750 (NCL-AFPp, Novocastra Laboratories Ltd, Newcastle upon Tyne, United Kingdom) with primary antibodies in antibody diluent from Dako (S2022; Glostrup, Denmark). For nestin antigen retrieval, the section was heated in CC1 cell conditioning solution for 36 min (EDTA antigen retrieval solution pH 8.4) using a standard protocol. Anti-nestin antibodies (MAB1259,

R&D systems, Inc.) were applied at a dilution of 1/1,000 and also incubated for 30 min at 37°C. Detection of primary antibodies was carried out using secondary universal biotinylated antibody reagent and the amplified DAB map kit (Ventana Medical Systems, Tucson, AZ, United States), based on conversion of diaminobenzidine to a dye with multimeric HRP. For negative controls, AFP antibodies were replaced with rabbit IgG and SMA and nestin antibodies were replaced by mouse IgG serotypes.

Statistical Analysis

For all experiments, comparisons between groups were conducted using regression models taking into account the effect of treatment and of cell lines, with 46XY-iPSCs serving as a reference. For some outcomes, log transformation was applied in order to satisfy assumptions of normality. $P \leq 0.05$ were considered significant. When the treatment effect was evaluated on multiple outcomes, the Benjamini-Hochberg correction procedure was used to correct *p*-values (convert to *q*-values) and maintain a false discovery rate of 0.05. All statistical analyses were performed with R statistical software (version 3.1.2, R Statistical Computing, Vienna) and data are presented in bar and scatterplot graphs showing variance around the mean according to the new standard of data presentation (Weissgerber et al., 2015).

Ethics Statement

Skin fibroblasts were isolated from patients after obtaining written informed consent with the approval of the ethics committee of the Cliniques Universitaires Saint-Luc.

RESULTS

Generation and Characterization of 47XXY-iPSCs

47XXY-fibroblasts were isolated from a patient with Klinefelter syndrome (KS) and used to establish 47XXY-iPSCs using *OCT4*, *SOX2*, *KLF4*, and *c-MYC* genes as we previously described (Grad et al., 2011; Hibaoui et al., 2014). Among the 47XXY-iPSC lines generated from the parental 47XXY-fibroblasts, 47XXY-iPSC line#11 and 47XXY-iPSC line#16 were used for the present study. A 46XY-iPSC line generated with the same method of reprogramming was used as a control line (**Figure 1A**; Grad et al., 2011; Hibaoui et al., 2014). Then, these iPSCs were evaluated to confirm the genotype of the parental somatic cells. As revealed by GTG banding analysis, the 47XXY-iPSC lines showed a supernumerary X chromosome while 46XY-iPSCs had a normal karyotype (**Figure 1B**). RT-PCR analysis demonstrated expression of endogenous pluripotent transcription factors including *OCT4*, *NANOG*, *KLF4*, and *LIN28* in the generated 47XXY-iPSC lines in contrast with their parental fibroblasts (**Figure 1C**). This analysis also confirmed the expression of *OCT4*, *NANOG*, *KLF4*, and *LIN28* in the 46XY-iPSCs as in the human embryonic stem cell line H1 (H1-ESCs) (**Figure 1C**). As expected for cells that have acquired a pluripotent state, transgene silencing of exogenous factors after expansion of approximately ten passages of 47XXY-iPSC lines was demonstrated by RT-PCR (**Supplementary Figure S1A**). In line with this, all iPSC lines expressed markers of pluripotent stem cells including OCT4, NANOG, and TRA1-60 (**Figure 1D**) and showed alkaline phosphatase activity (**Supplementary Figure S1B**).

Moreover, both 47XXY-iPSCs and 46XY-iPSCs were evaluated for their developmental potential *in vivo* by injecting these iPSCs intramuscularly into immunodeficient SCID mice. Immunohistochemistry analysis revealed that these iPSC lines formed teratoma with all embryonic germ layers as detected by the expression of the ectodermal marker β3-tubulin, the mesodermal marker α-smooth muscle actin (α-SMA) and the endodermal marker α-fetoprotein (AFP) (**Figure 1E**). 47XXY-iPSCs and 46XY-iPSCs were also characterized to confirm their multi-lineage differentiation potentials *in vitro* into embryoïd bodies (EBs) (**Figure 2A**). As expected, upon 3 weeks of spontaneous *in vitro* differentiation, both 47XXY-iPSCs and 46XY-iPSCs exhibited a decreased expression of the pluripotent genes *OCT4* and *NANOG* (**Figure 2B**). Concomitantly, we found a significant induction of the ectodermal marker *TUBB3* (fold change = 3.31), the mesodermal marker *ACTA2* (fold change = 23.9) and the endodermal marker *AFP* (fold change = 1,319) in both 47XXY-iPSCs and 46XY-iPSCs as demonstrated by quantitative RT-PCR analysis (**Figure 2B**). Immunofluorescence analysis revealed that these iPSC lines differentiated in derivatives of all embryonic germ layers upon 3 weeks of spontaneous *in vitro* differentiation, as detected by the expression of the ectodermal marker β3-tubulin, the mesodermal marker α-SMA and the endodermal marker AFP (**Figure 2C**).

iPSC Capacity to Differentiate Into Germ Cell Lineage

After 21 days of spontaneous *in vitro* differentiation, between 1 and 3.4% of cells derived from 47XXY-iPSCs and 46XY-iPSCs expressed VASA, a protein primarily found in germ cells (**Figure 2D**). Quantitative RT-PCR analysis revealed a significant decrease (fold change = 0.06) in the expression of *DAZL*, a very early marker of germ cells whereas the expression of *TEKT1* was significantly increased (fold change = 20.99) in cells derived from both iPSCs after 21 days of spontaneous differentiation. No difference was observed between cell lines (**Figure 2E**).

Given the critical roles of bone morphogenetic protein 4 (BMP4), glial-derived neurotrophic factor (GDNF), retinoic acid (as a meiosis-inducing factor) and stem cell factor (SCF) on germ cell differentiation (Kee et al., 2006; West et al., 2009; Spinnler et al., 2010; Singh et al., 2017; Teletin et al., 2017; Li et al., 2020; Mahabadi et al., 2020a,b), we tested different combinations of these factors to enhance germ cell differentiation of iPSCs as outlined in **Figure 3A**. After 21 days of differentiation, we observed a 2.4-fold increase of BOLL positive cells and a 2-fold increase of MAGEA4-positive cells when 46XY-iPSCs were treated with BMP4 compared to control

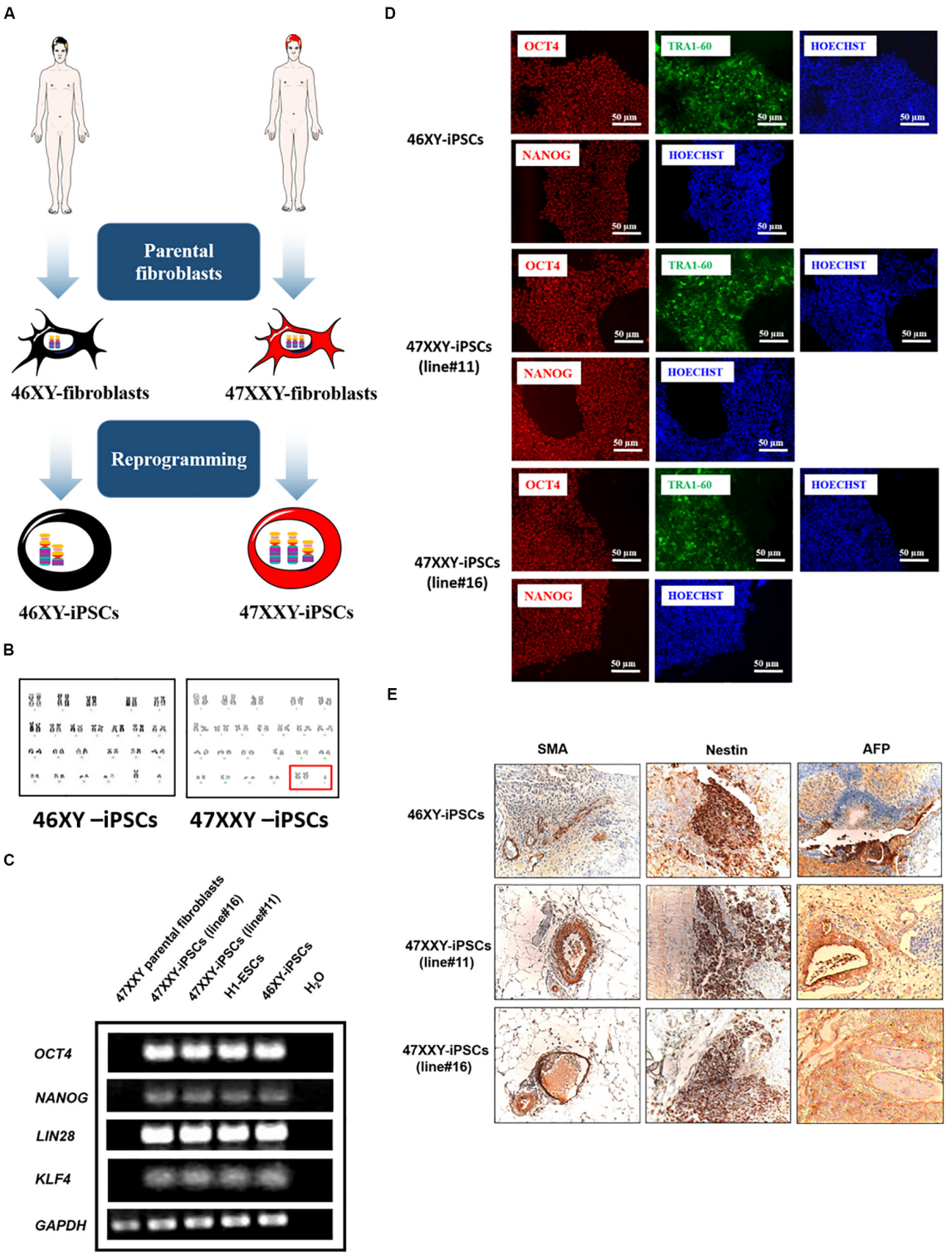

FIGURE 1 | 46XX-iPSCs and 47XXY-iPSCs exhibit markers of pluripotency. **(A)** Schematic representation for the reprogramming of 46XY and 47XXY parental fibroblasts into 46XY-iPSCs and 47XXY-iPSCs using *OCT4*, *SOX2*, *KLF4*, and *c-MYC* genes **(B)** Karyotypes of 46XY-iPSCs and 47XXY-iPSCs are 46, XY and 47, XXY, respectively. **(C)** RT-PCR of pluripotency-related genes *NANOG*, *OCT4*, *KLF4*, and *LIN28* in 46XY-iPSCs and 47XXY-iPSCs. The human embryonic stem cell line H1 (H1-ESCs) and the 47XXY parental fibroblasts were used as positive and negative controls for *OCT4*, *NANOG*, *KLF4*, and *LIN28* expression, respectively. **(D)** Immunofluorescence staining of 46XY-iPSC and 47XXY-iPSC lines for the pluripotency markers NANOG, OCT4 and TRA1-60. **(E)** Immunohistochemistry analysis of teratoma sections generated after intramuscular injection of 46XY-iPSC and 47XXY-iPSC lines into SCID mice. These teratomas expressed α-SMA (mesoderm), AFP (endoderm) and β3-tubulin (ectoderm).

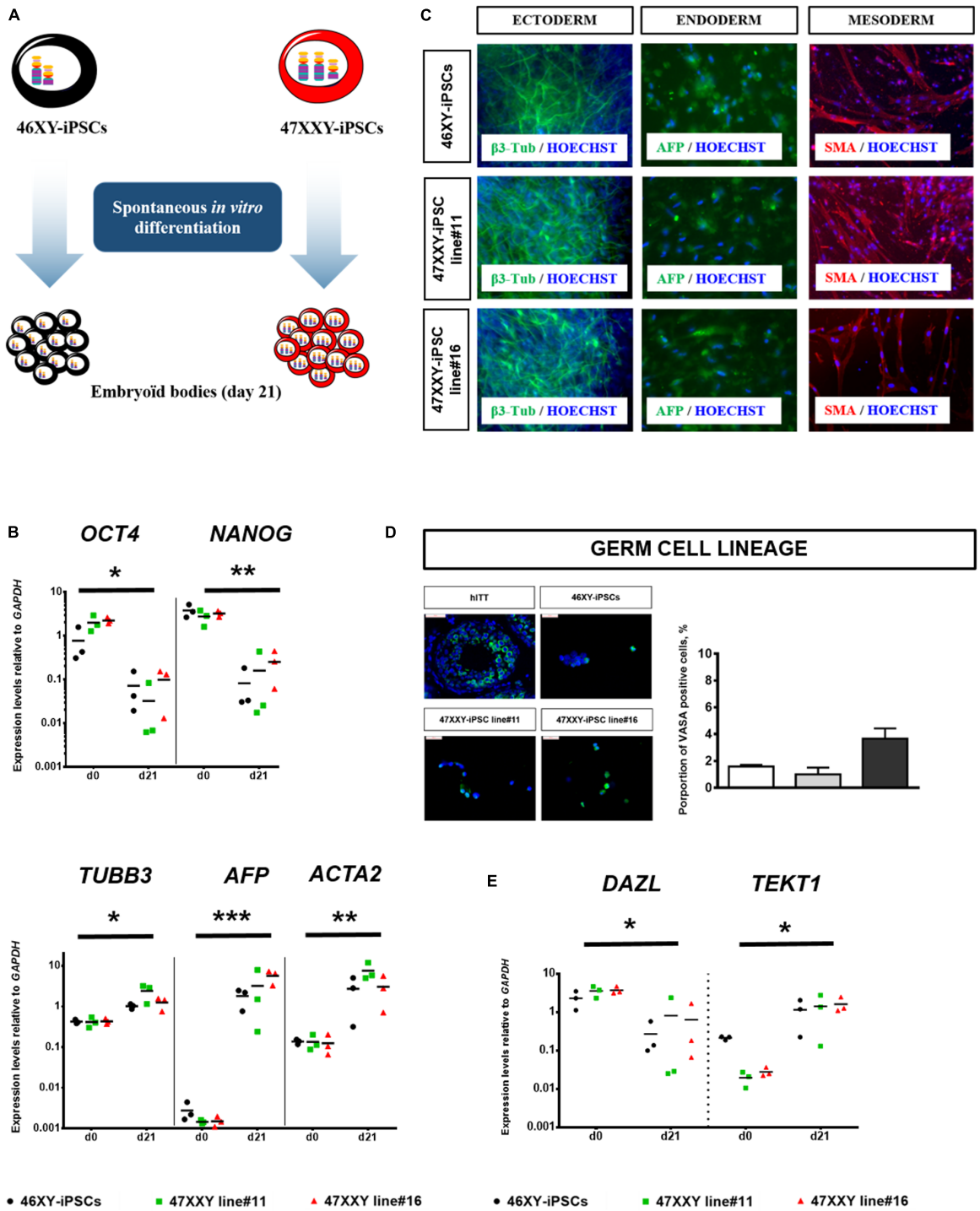

FIGURE 2 | Spontaneous *in vitro* differentiation of 46XX-iPSCs and 47XXY-iPSCs. **(A)** Schematic representation for spontaneous *in vitro* differentiation of 46XY-iPSCs and 47XXY-iPSCs into the three embryonic germ layers as embryoïd bodies (EBs) in suspension culture for 4 days and as adherent cells for an additional 17 days. **(B)** Quantitative RT-PCR of pluripotency-related genes (*NANOG* and *OCT4*) and of markers for mesoderm (*ACTA2*), endoderm (*AFP*), and ectoderm (*TUBB3*). Expression levels are expressed relative to *GAPDH*. **(C)** Immunofluorescence staining of 46XY-iPSC and 47XXY-iPSC lines upon spontaneous *in vitro* differentiation, for markers of mesoderm (α-SMA), endoderm (AFP) and ectoderm (β3-tubulin). **(D)** Immunofluorescence staining of 46XY-iPSC and 47XXY-iPSC lines upon spontaneous *in vitro* differentiation for the germ cell marker VASA. Quantitative analysis of the proportion of VASA positive cells after 21 days of spontaneous *in vitro* differentiation. Human immature testicular tissue (hITT) was used as a positive control (scale = 50 μM). **(E)** Quantitative RT-PCR analysis of markers of germ cell development (*DAZL* and *TEKT1*) upon spontaneous *in vitro* differentiation of 46XY-iPSC and 47XXY-iPSC lines. Expression levels are expressed relative to *GAPDH*. Data are represented as variance around mean, $*p < 0.05$, $**p < 0.01$ and $***p < 0.001$ between day 0 and day 21 from $n = 3$ independent experiments.

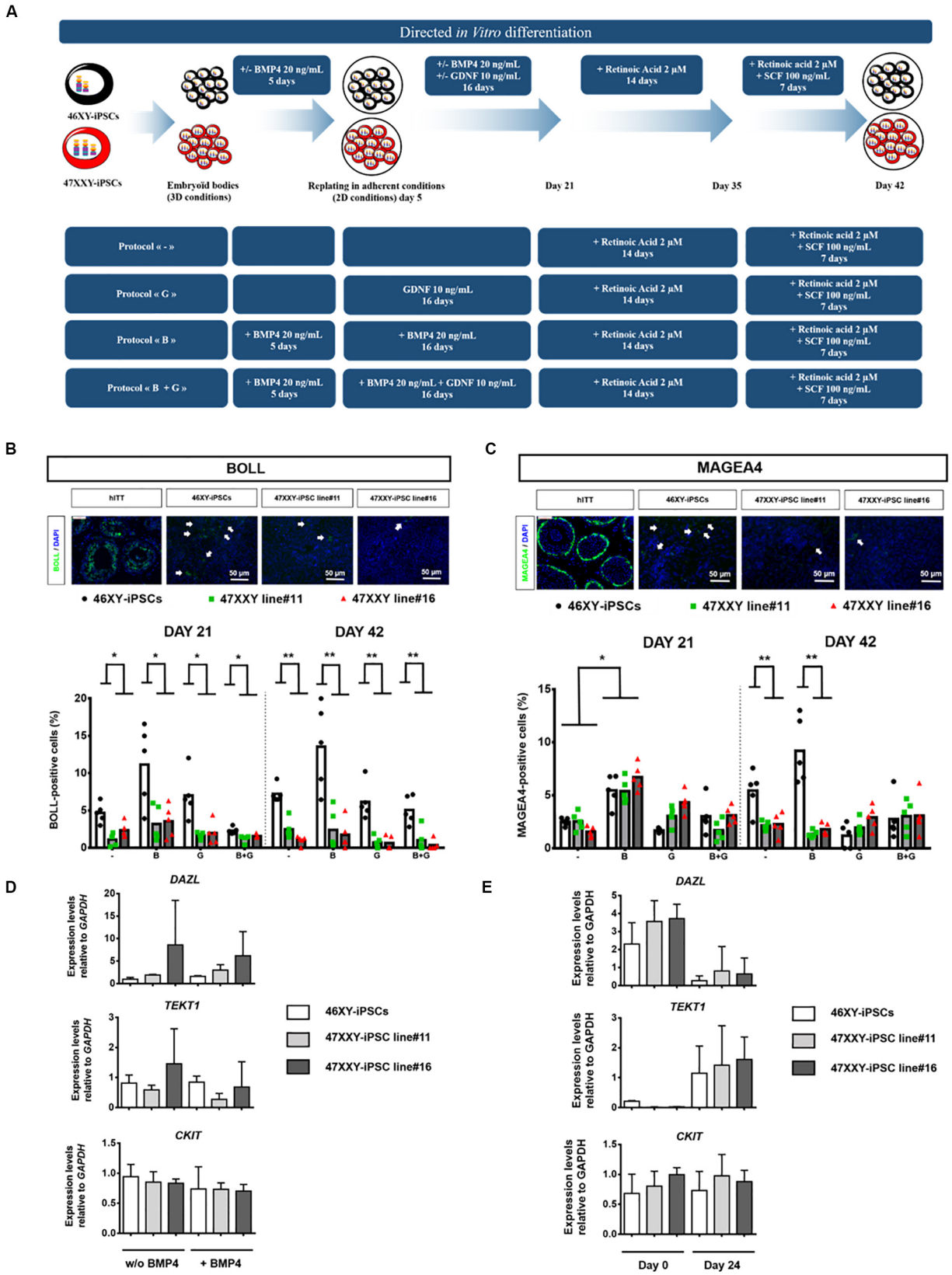

FIGURE 3 | Directed *in vitro* differentiation of 46XX-iPSCs and 47XXY-iPSCs into germ cell lineage. **(A)** Schematic representation of the 4 different protocols used for iPSC differentiation into germ cell lineage. These protocols differed only in the first steps of the differentiation; with or without 20 ng/mL BMP4 in the 5 first days of

(Continued)

FIGURE 3 | Continued
differentiation and the presence or not of 10 ng/mL GDNF between day 5 and day 21 of differentiation. The last step of the protocols is identical with the presence of 2 μM retinoic acid between day 21 and day 35 and the presence of 2 μM retinoic acid + 100 ng/mL SCF between day 35 and day 42. **(B)** Immunofluorescence staining of 46XY-iPSC- and 47XXY-iPSC-derived cells for the germ cell marker BOLL. Representative images of 46XY-iPSC- and 47XXY-iPSC-derived cells at day 42 are represented. Human immature testicular tissue (hITT) was used as a positive control for BOLL expression (scale = 50 μM). Quantitative analysis of the proportion of BOLL positive cells for each protocol at day 21 and day 42 of germ cell differentiation. Data are represented as variance around mean, $*p < 0.05$ and $**p < 0.01$ between 46XY-iPSCs and 47XXY-iPSC line#11 and 47XXY-iPSC line#16 at day 21 and at day 42 from $n = 5$ independent experiments. **(C)** Immunofluorescence staining of 46XY-iPSC- and 47XXY-iPSC-derived cells for the germ cell marker MAGEA4. Representative images of 46XY-iPSC- and 47XXY-iPSC-derived cells at day 42 are represented. Human immature testicular tissue (hITT) was used as a positive control for MAGEA4 expression (scale = 50 μM). Quantitative analysis of the proportion of MAGEA4 positive cells for each protocol at day 21 and day 42 of germ cell differentiation. Data are represented as variance around mean, $*p < 0.05$ and $**p < 0.01$ between 46XY-iPSCs and 47XXY-iPSC line#11 and 47XXY-iPSC line#16 at day 21 and day 42 from $n = 5$ independent experiments. **(D)** Quantitative RT-PCR analysis of *DAZL*, *TEKT1*, and *CKIT* upon germ cell induction with or without 20 ng/mL BMP4 in the 5 first days. Expression levels are expressed relative to *GAPDH*. Data are represented from $n = 3$ independent experiments. **(E)** Quantitative RT-PCR analysis of *DAZL*, *TEKT1*, and *CKIT* upon germ cell differentiation of 46XY-iPSC and 47XXY-iPSC lines at day 0 and day 21. Expression levels are expressed relative to *GAPDH*. Data are represented from $n = 3$ independent experiments.

conditions, although this increase was less marked after 42 days of differentiation: 1.9- and 1.7-fold increase for BOLL-positive cells and MAGEA4-positive cells, respectively (**Figure 3B**). After 42 days of differentiation, the proportion of MAGEA4 positive cells and BOLL positive cells had a tendency to be higher in BMP4-treated compared to control conditions but failed to reach significance (**Figures 3B,C**). Approximately, 13.55 and 9.2% of cells derived from 46XY-iPSCs expressed BOLL and MAGEA4, respectively (**Figures 3B,C**). Of note, upon this BMP4-treated protocol, we also found trophectoderm, mesoderm and endoderm derivatives as revealed by immunofluorescence staining and RT-PCR analysis (**Supplementary Figure S2**). To test whether the greater proportion of BOLL and MAGEA4 positives at day 21 in BMP4-treated compared to control conditions is due to differences in early germ cell induction, we further analyzed the expression of *DAZL*, *TEKT1*, and *CKIT* at day 5 of germ cell differentiation by RT-PCR (**Figure 3D**). No difference in the expression of these genes was found in 46XY-iPSC-derived cells regardless the presence or not of BMP4 (**Figure 3D**). However, in the presence of BMP4, we found a down regulation of *DAZL* and an upregulation of *TEKT1* between day 0 and day 21 of germ cell differentiation (**Figure 3E**).

Reduced Ability of 47XXY-iPSCs to Differentiate Into Germ Cell Lineage

When 46XY-iPSCs and 47XXY-iPSCs were induced to differentiate into germ cell lineage, we found a reduced proportion of BOLL positive cells at day 21 in 47XXY-iPSC-derived cells (**Figure 3B**). By contrast, no difference was found for the proportion of MAGEA4 positive cells at this earlier step of differentiation (**Figure 3C**). Next, we assessed whether the reduced ability of 47XXY-iPSCs to generate BOLL positive cells is due to proliferation failure and/or increased cell death of 47XXY-iPSC-derived cells. As shown in **Figure 4A**, the proportion of Ki-67 positive cells was similar between 47XXY-iPSC-derived cells and 46XY-iPSC-derived cells at day 21, consistent with similar proliferation properties of these cells (**Figure 4A**). However, an overall increase of LDH release was found in 47XXY-iPSC-derived cells compared with 46XY-iPSC-derived cells at day 21, indicating a higher cell death in 47XXY-iPSC-derived cells (**Figure 4B** and **Supplementary Figure S3**). Then, to test which cells derived from 47XXY-iPSCs are responsible for this increase of cell death, we performed co-staining with BOLL or MAGEA4 and cleaved caspase-3 antibodies of 47XXY-iPSC-derived cells at day 21 (**Figures 4C,D**). Importantly, we found a greater proportion of BOLL and cleaved caspase-3 double positive cells (**Figure 4C**) and of MAGEA4 and cleaved caspase-3 double positive cells (**Figure 4D**) upon germ cell differentiation of 47XXY-iPSCs compared to 46XY-iPSCs, consistent with an increase of apoptosis of these cells. Of note, we also found a higher proportion of BOLL negative (or MAGEA4 negative) that were also cleaved caspase-3 positive cells, indicating an overall increase of apoptosis of 47XXY-iPSC-derived cells (**Figures 4C,D**).

Moreover, further differentiation of these iPSCs until day 42 revealed a reduced proportion of BOLL positive cells at day 42 in 47XXY-iPSC-derived cells compared with 46XY-iPSCs (**Figure 3B**). In line with this, we found a significant decrease in the proportion of MAGEA4 positive cells at day 42 in 47XXY-iPSC-derived cells compared to 46XY-iPSCs in both BMP4-treated and control conditions (**Figure 3B**), although this decrease appeared more important in the BMP4-treated (∼4.2-fold decrease) than in control conditions (∼2.4-fold decrease) (**Figure 3B**). These effects were not associated with a proliferation deficit as similar proportions of Ki-67 positive cells were found between 47XXY-iPSC-derived cells and 46XY-iPSC-derived cells at day 42 (**Figure 4A**). Furthermore, these effects could not be attributed to cell death differences as similar LDH release was found in both iPSC-derived cells at day 42 (**Figure 4A** and **Supplementary Figure S3**).

DISCUSSION

A major challenge in the field of Klinefelter syndrome (KS) research has been to recapitulate the disease phenotype and to understand the cellular and molecular mechanisms by which the extra copy of X chromosome leads to KS abnormalities (Lanfranco et al., 2004; Gravholt et al., 2018). In order to recapitulate the disease *in vitro*, iPSCs have been generated from patients with KS (Ma et al., 2012; Shimizu et al., 2016; Panula et al., 2019). However, to the best of our knowledge our study

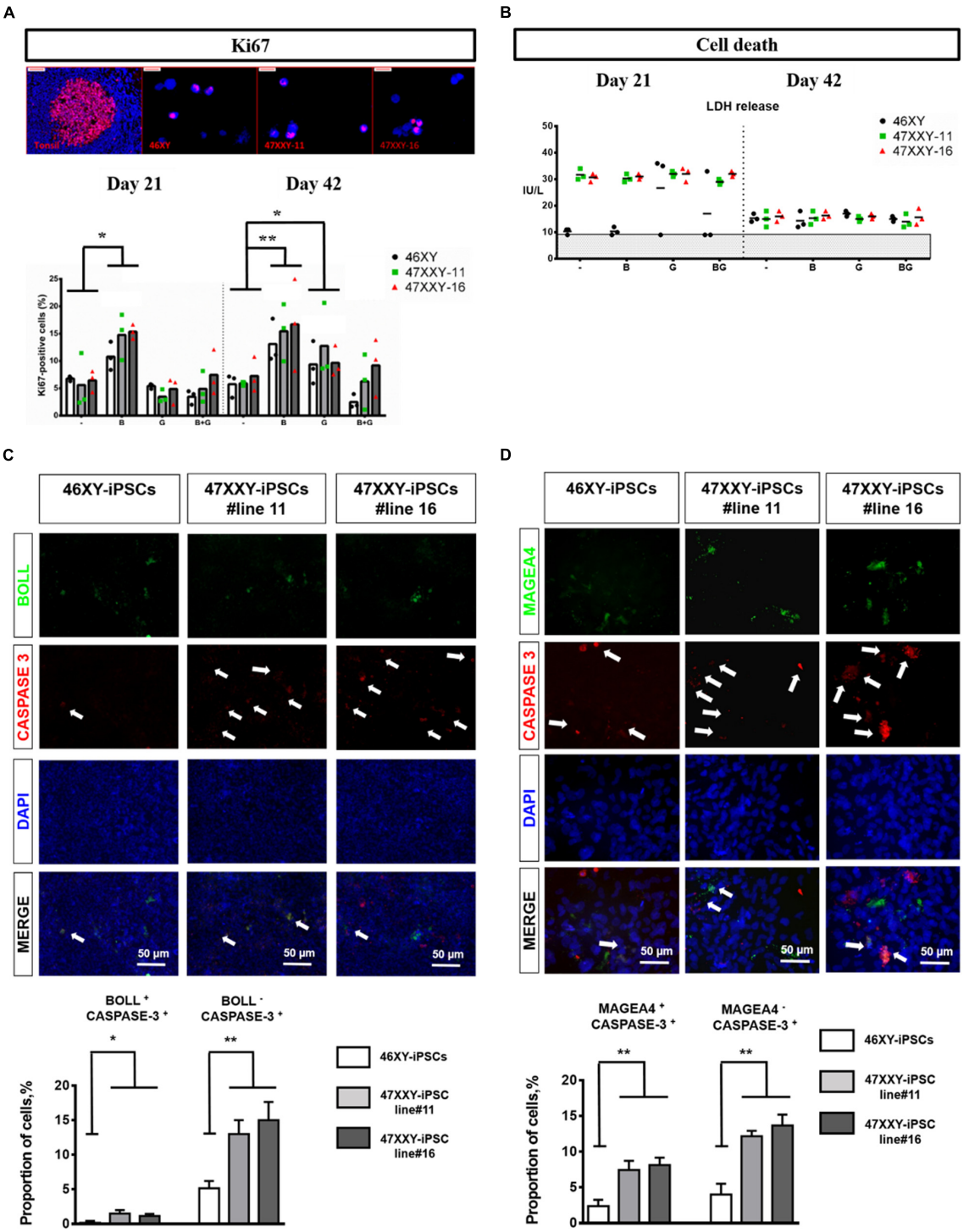

FIGURE 4 | Cell proliferation and cell death analysis of 46XX-iPSCs and 47XXY-iPSCs upon germ cell differentiation. **(A)** Cell proliferation analysis by Ki-67 staining of 46XY-iPSC- and 47XXY-iPSC-derived cells for each protocol after day 21 and day 42 of differentiation. **(B)** Cell death analysis by LDH release by 46XY-iPSC- and 47XXY-iPSC-derived cells for each protocol after day 21 and day 42 of differentiation. Data are represented as variance around mean, $*p < 0.05$ and $**p < 0.01$ between 46XY-iPSCs and 47XXY-iPSC line#11 and 47XXY-iPSC line#16 at day 21 and day 42, from $n = 3$ independent experiments. **(C)** Immunofluorescence co-staining of 46XY-iPSC- and 47XXY-iPSC-derived cells for the germ cell marker BOLL and the marker of apoptosis cleaved caspase-3. Quantitative analysis of the proportion of BOLL and cleaved caspase-3 double positive cells and the proportion of BOLL negative and cleaved caspase-3 positive cells at day 21 of germ cell differentiation. **(D)** Immunofluorescence staining of 46XY-iPSC- and 47XXY-iPSC-derived cells for the germ cell marker MAGEA4 and the marker of apoptosis cleaved caspase-3. Quantitative analysis of the proportion of MAGEA4 and cleaved caspase-3 double positive cells and the proportion of BOLL negative and cleaved caspase-3 positive cells, at day 21 of germ cell differentiation. Data are represented from $n = 3$ independent experiments.

is the first investigating the differentiation potentials of iPSCs derived from a patient with KS (47XXY-iPSCs) into germ cell lineage using a directed differentiation protocol.

Several observations and findings arise from the current study investigating the abilities of 47XXY-iPSCs to differentiate into germ cell lineage when compared with 46XY-iPSCs. Consistent with previous reports (Clark et al., 2004; Chen et al., 2006; Panula et al., 2010), spontaneous *in vitro* differentiation of iPSCs as embryoïd bodies resulted in limited proportions of cells differentiated into germ like cells (between 1 and 3.4%). Therefore, in order to enhance germ cell differentiation of iPSCs, we used combinations of several factors, such as bone morphogenetic protein 4 (BMP4), glial-derived neurotrophic factor (GDNF), retinoic acid (as a meiosis-inducing factor), and stem cell factor (SCF) influencing germ cell differentiation (Kee et al., 2006; West et al., 2009; Spinnler et al., 2010; Singh et al., 2017; Teletin et al., 2017; Li et al., 2020; Mahabadi et al., 2020a,b), as outlined in **Figure 3A**. First, we found that certain key combinations of these factors increased germ cell differentiation compared to spontaneous *in vitro* differentiation protocol. This directed differentiation protocol recapitulates the main steps of germ cell development with the first 3 weeks devoted to obtain a germline and the last 3 weeks that were common across the protocols (2 μM retinoic acid for the first 2 weeks and 2 μM retinoic acid + SCF 100 ng/mL for the last week) to reach the first stages of post-meiotic development. Among the combinations used in our protocols, addition of BMP4 in the early steps of differentiation (the first 21 days) led to a ∼2-fold increase proportion of BOLL positive cells at day 21 and day 42. Similar results were found for MAGEA4 positive cells at day 21, but at day 42 the greater proportion of MAGEA4 positive cells in the presence of BMP4 failed to reach significance. Thus, we did not find any effect of BMP4 addition on gene expression of *VASA*, *CKIT*, and *DAZ1* after 5 days of differentiation. Conflicting results have been published regarding the requirement of BMP4 to start germ cell differentiation (Kee et al., 2006; West et al., 2009; Panula et al., 2010; Eguizabal et al., 2011). The concentrations of BMP4 used or the presence of co-culture systems may account for these discrepancies.

Given that GDNF is a key player of cell fate decision of spermatogonial cells regulating spermatogonial self-renewal and differentiation (Meng et al., 2000; Naughton et al., 2006; Oatley and Brinster, 2008), we tested whether addition of GDNF between day 5 and day 21 improved germ cell differentiation. However, neither the addition of GDNF nor the combination of BMP4 and GDNF improved the proportion of MAGEA4 or BOLL positive cells. We found in particular that the addition of GDNF did not improve proliferation but instead increased cytotoxicity in iPSC-derived cells. In line with these results, Meng and collaborators have shown that mice overexpressing *GDNF* exhibited an increase of GDNF production by Sertoli cells leading to the accumulation of undifferentiated spermatogonia by favoring self-renewing instead of differentiation (Meng et al., 2000). Whether the concentration of GDNF used in our study favors self-renewing instead of differentiation of iPSC-derived cells deserves further investigations.

Collectively, our results suggest an improved germ cell differentiation protocol for iPSCs than spontaneous *in vitro* differentiation. Consistent with previous reports, *DAZL* was down-regulated after 21 days of differentiation (Clark et al., 2004; Geijsen et al., 2004). This is of special interest as *DAZL* encodes RNA binding proteins required for germ cell development in several species and is considered as an early marker of mouse and human germ cell development (Ruggiu et al., 1997; Clark et al., 2004; Geijsen et al., 2004). As expected for efficient germ cell differentiation, after 21 days of germ cell differentiation, we found an upregulation of *TEKT1*, which is a specific marker of germ cells during their later stages of migration when they enter the gonads and progress through meiosis and gamete morphogenesis (Larsson et al., 2000; Clark et al., 2004). Finally, after 42 days of differentiation, approximately 9.2% of the cells were positive for MAGEA4, a pre-spermatogonia marker and 13.55% of the cells were positive for BOLL, a protein required for the germ cell development and spermatogenesis. Of note, we compared our protocol to the one recently established by Zhao and colleagues (Zhao et al., 2018). Importantly, after 21 days of germ cell differentiation, this latter protocol gives rise to ∼23.2% of BOLL positive cells and ∼22.8% of MAGEA4 positive cells (**Supplementary Figures S4, S5**), consistent with a better efficiency of this protocol to generate germ cells from iPSCs. Whether this increased efficiency can be maintained in long term culture remains to be determined.

Another major finding of this study is the reduced ability of 47XXY-iPSCs to differentiate into germ cell lineage compared to 46XY-iPSCs. We found in particular a reduced proportion of MAGEA4 positive cells after 42 days of differentiation of 47XXY-iPSCs regardless of the presence or not of BMP4 in the first 21 days of differentiation. In line with this, we found a reduced proportion of BOLL positive cells after 42 days of differentiation of 47XXY-iPSCs. This decrease of MAGEA4 positive cells and BOLL positive cells could not be attributed to proliferation failure but rather and most likely to an increase of cell death at day 42. This increase of cell death was observed regardless of the addition of BMP4 during the early steps of differentiation. Our results are in contrast with those of Ma and colleagues as they found an aberrant transcriptome of 47XXY-iPSCs at the undifferentiated state but exhibit similar expression of germ cell lineage markers as 46XY-iPSCs (Ma et al., 2012). In accordance with our results, several studies have pointed out an increase of cell death affecting germ cells upon differentiation and maturation as a main mechanism leading to KS testis dysfunction (Aksglæde et al., 2005; D'Aurora et al., 2015, 2017). The molecular mechanisms by which the extra copy of X chromosome leads to this increase of apoptosis in germ cells from patients with KS are poorly understood. The main obstacle for genotype-phenotype correlation studies for KS is that approximately 15% of X chromosomal genes escapes X chromosomal inactivation and 10% of X chromosomal genes shows tissue specific expression (Carrel and Willard, 1999, 2005; Balaton et al., 2015). Some

X chromosomal genes have been proposed to contribute directly or indirectly to the KS phenotype including *SHOX* (Ottesen et al., 2010), *XIST* (Ma et al., 2012; Belling et al., 2017; Winge et al., 2017; Panula et al., 2019), *AKAP17A* (Belling et al., 2017; Winge et al., 2017; Skakkebæk et al., 2018; Panula et al., 2019), *SLC25A6* (Zitzmann et al., 2015; Belling et al., 2017; Skakkebæk et al., 2018; Panula et al., 2019), *HDHD1* (Zitzmann et al., 2015; Panula et al., 2019), *NLGN4X* (Winge et al., 2017; Panula et al., 2019), *PLCXD1* (Belling et al., 2017; Panula et al., 2019), and *LDOC1* (Salemi et al., 2016). Among those genes, *SHOX* has been shown to trigger the lysosomial pathway of apoptosis (Hristov et al., 2013) while *LDOC1* has been shown to inhibit cell proliferation and promote apoptosis (Zhao et al., 2015). Whether these genes contribute to the greater apoptosis of 47XXY-iPSC-derived cells upon germ cell differentiation deserves further investigations.

CONCLUSION

In conclusion, the generation of iPSCs from patients with KS provide an innovative model to study the effect of the supernumerary X chromosome on KS features. Importantly, 47XXY-iPSCs exhibited a reduced ability to differentiate into germ cells compared with 46XY-iPSCs. Our results further emphasize that this defect is more related to an increased cell death at day 21 of differentiation than a proliferation deficit of 47XXY-iPSC-derived cells. Although post-meiotic germ cell differentiation from 47XXY-iPSCs was shown in our study, another aspect that was not investigated but can be of interest for further investigations is the analysis of the ploidy of the germ cells differentiated from 47XXY-iPSCs. This could help to close the debate on the ability of KS germ cells to enter meiosis given that it was suggested that only diploid XY germ cells are competent to engage in meiosis in patients with KS and mouse model of KS (Mroz et al., 1999; Sciurano et al., 2009).

DATA AVAILABILITY STATEMENT

All datasets generated for this study are included in the article/**Supplementary Material**, further inquiries can be directed to the corresponding author.

ETHICS STATEMENT

The animal study was reviewed and approved by the Ethics Review Board and the Committee on Animal Research of the Catholic University of Louvain.

AUTHOR CONTRIBUTIONS

OB contributed to fund raising, designed and performed research, data analysis and interpretation, figure preparation, and manuscript writing. YH performed some of the research data analysis and interpretation, figure preparation, and manuscript writing. MG participated to critical review of the manuscript. JA performed data analysis. CC performed some of the research. AF performed final approval of the manuscript. CW designed research, contributed to data analysis and interpretation, manuscript writing, fund raising, and final approval of the manuscript.

ACKNOWLEDGMENTS

We thank the Salus Sanguinis Foundation (Avenue Mounier 50, 1200 Brussels, Belgium) for financial support.

SUPPLEMENTARY MATERIAL

The Supplementary Material for this article can be found online at: https://www.frontiersin.org/articles/10.3389/fcell.2020.567454/full#supplementary-material

REFERENCES

Aksglæde, L., Skakkebæk, N. E., Almstrup, K., and Juul, A. (2011). Clinical and biological parameters in 166 boys, adolescents and adults with nonmosaic Klinefelter syndrome: a Copenhagen experience. *Acta Paediatr.* 100, 793–806. doi: 10.1111/j.1651-2227.2011.02246.x

Aksglæde, L., Wikström, A. M., Meyts, E. R.-D., Dunkel, L., Skakkebæk, N. E., and Juul, A. (2005). Natural history of seminiferous tubule degeneration in Klinefelter syndrome. *Hum. Reprod. Upd.* 12, 39–48. doi: 10.1093/humupd/dmi039

Balaton, B. P., Cotton, A. M., and Brown, C. J. (2015). Derivation of consensus inactivation status for X-linked genes from genome-wide studies. *Biol. Sex Differ.* 6, 35–35.

Belling, K., Russo, F., Jensen, A. B., Dalgaard, M. D., Westergaard, D., Rajpert-De Meyts, E., et al. (2017). Klinefelter syndrome comorbidities linked to increased X chromosome gene dosage and altered protein interactome activity. *Hum. Mol. Genet.* 26, 1219–1229. doi: 10.1093/hmg/ddx014

Bojesen, A., Hertz, J. M., and Gravholt, C. H. (2011). Genotype and phenotype in Klinefelter syndrome – impact of androgen receptor polymorphism and skewed X inactivation. *Int. J. Androl.* 34, e642–e648.

Botman, O., and Wyns, C. (2014). Induced pluripotent stem cell potential in medicine, specifically focused on reproductive medicine. *Front Surg* 1:5. doi: 10.3389/fsurg.2014.00005

Carrel, L., and Willard, H. F. (1999). Heterogeneous gene expression from the inactive X chromosome: an X-linked gene that escapes X inactivation in some human cell lines but is inactivated in others. *Proc. Natl. Acad. Sci. U.S.A.* 96, 7364–7369. doi: 10.1073/pnas.96.13.7364

Carrel, L., and Willard, H. F. (2005). X-inactivation profile reveals extensive variability in X-linked gene expression in females. *Nature* 434, 400–404. doi: 10.1038/nature03479

Chen, H.-F., Kuo, H.-C., Chien, C. L., Shun, C. T., Yao, Y. L., Ip, P. L., et al. (2006). Derivation, characterization and differentiation of human embryonic stem cells: comparing serum-containing versus serum-free media and evidence of germ cell differentiation. *Hum. Reprod.* 22, 567–577. doi: 10.1093/humrep/del412

Clark, A. T., Bodnar, M. S., Fox, M., Rodriquez, R. T., Abeyta, M. J., Firpo, M. T., et al. (2004). Spontaneous differentiation of germ cells from human embryonic stem cells in vitro. *Hum. Mol. Genet.* 13, 727–739. doi: 10.1093/hmg/ddh088

D'Aurora, M., Ferlin, A., Di Nicola, M., Garolla, A., De Toni, L., Franchi, S., et al. (2015). Deregulation of sertoli and leydig cells function in patients

with klinefelter syndrome as evidenced by testis transcriptome analysis. *BMC Genomics* 16:156. doi: 10.1186/s12864-015-1356-0

D'Aurora, M., Ferlin, A., Garolla, A., Franchi, S., D'onofrio, L., Trubiani, O., et al. (2017). Testis transcriptome modulation in Klinefelter patients with hypospermatogenesis. *Sci. Rep.* 7:45729.

Easley, C. A. IV, Phillips, B. T., McGuire, M. M., Barringer, J. M., Valli, H., and Hermann, B. P. (2012). Direct differentiation of human pluripotent stem cells into haploid spermatogenic cells. *Cell Rep.* 2, 440–446. doi: 10.1016/j.celrep.2012.07.015

Eguizabal, C., Montserrat, N., Vassena, R., Barragan, M., Garreta, E., Garcia-Quevedo, L., et al. (2011). Complete meiosis from human induced pluripotent stem cells. *Stem Cell.* 29, 1186–1195. doi: 10.1002/stem.672

Geijsen, N., Horoschak, M., Kim, K., Gribnau, J., Eggan, K., and Daley, G. Q. (2004). Derivation of embryonic germ cells and male gametes from embryonic stem cells. *Nature* 427, 148–154. doi: 10.1038/nature02247

Giudice, M. G., Vermeulen, M., and Wyns, C. (2019). Blood testis barrier and somatic cells impairment in a series of 35 adult Klinefelter syndrome patients. *Int. J. Mol. Sci.* 20:5717. doi: 10.3390/ijms20225717

Grad, I., Hibaoui, Y., Jaconi, M., Chicha, L., Bergström-Tengzelius, R., Sailani, M. R., et al. (2011). NANOG priming before full reprogramming may generate germ cell tumours. *Eur. Cell Mater.* 22, 258–274. doi: 10.22203/ecm.v022a20

Gravholt, C. H., Chang, S., Wallentin, M., Fedder, J., Moore, P., and Skakkebæk, A. (2018). Klinefelter syndrome: integrating genetics, neuropsychology, and endocrinology. *Endocr. Rev.* 39, 389–423. doi: 10.1210/er.2017-00212

Hibaoui, Y., and Feki, A. (2012). Human pluripotent stem cells: applications and challenges in neurological diseases. *Front Physiol.* 3:267. doi: 10.3389/fphys.2012.00267

Hibaoui, Y., Grad, I., Letourneau, A., Sailani, M. R., Dahoun, S., Santoni, F. A., et al. (2014). Modelling and rescuing neurodevelopmental defect of Down syndrome using induced pluripotent stem cells from monozygotic twins discordant for trisomy 21. *EMBO Mol. Med.* 6, 259–277.

Hristov, G., Marttila, T., Durand, C., Niesler, B., Rappold, G. A., and Marchini, A. (2013). SHOX triggers the lysosomal pathway of apoptosis via oxidative stress. *Hum. Mol. Genet.* 23, 1619–1630. doi: 10.1093/hmg/ddt552

Kee, K., Angeles, V. T., Flores, M., Nguyen, H. N., and Reijo Pera, R. A. (2009). Human DAZL, DAZ and BOULE genes modulate primordial germ-cell and haploid gamete formation. *Nature* 462, 222–225. doi: 10.1038/nature08562

Kee, K., Gonsalves, J. M., Clark, A. T., and Reijo Pera, R. A. (2006). Bone morphogenetic proteins induce germ cell differentiation from human embryonic stem cells. *Stem Cell. Dev.* 15, 831–837. doi: 10.1089/scd.2006.15.831

Lanfranco, F., Kamischke, A., Zitzmann, M., and Nieschlag, E. (2004). Klinefelter's syndrome. *The Lancet* 364, 273–283.

Larsson, M., Norrander, J., Gräslund, S., Brundell, E., Linck, R., Ståhl, S., et al. (2000). The spatial and temporal expression of Tekt1, a mouse tektin C homologue, during spermatogenesis suggest that it is involved in the development of the sperm tail basal body and axoneme. *Eur. J. Cell Biol.* 79, 718–725. doi: 10.1078/0171-9335-00097

Li, L., Yang, R., Yin, C., and Kee, K. (2020). Studying human reproductive biology through single-cell analysis and in vitro differentiation of stem cells into germ cell-like cells. *Hum. Reprod. Upd.* 26, 670-688.

Ma, Y., Li, C., Gu, J., Tang, F., Li, C., Li, P., et al. (2012). Aberrant gene expression profiles in pluripotent stem cells induced from fibroblasts of a Klinefelter syndrome patient. *J. Biol. Chem.* 287, 38970–38979. doi: 10.1074/jbc.m112.380204

Mahabadi, J. A., Karimian, M., Aghighi, F., Enderami, S. E., Seyyed Hosseini, E., Talaei, S. A., et al. (2020a). Retinoic acid and 17β-estradiol improve male germ cell differentiation from mouse-induced pluripotent stem cells. *Andrologia* 52:e13466.

Mahabadi, J. A., Sabzalipoor, H., Kehtari, M., Enderami, S. E., Soleimani, M., and Nikzad, H. (2018). Derivation of male germ cells from induced pluripotent stem cells by inducers: a review. *Cytotherapy* 20, 279–290. doi: 10.1016/j.jcyt.2018.01.002

Mahabadi, J. A., Tameh, A. A., Talaei, S. A., Karimian, M., Rahiminia, T., Enderami, S. E., et al. (2020b). Retinoic acid and/or progesterone differentiate mouse induced pluripotent stem cells into male germ cells in vitro. *J. Cell. Biochem.* 121, 2159–2169. doi: 10.1002/jcb.29439

Medrano, J. V., Ramathal, C., Nguyen, H. N., Simon, C., and Reijo Pera, R. A. (2012). Divergent RNA-binding proteins, DAZL and VASA, induce meiotic progression in human germ cells derived in vitro. *Stem Cell.* 30, 441–451. doi: 10.1002/stem.1012

Meng, X., Lindahl, M., Hyvönen, M. E., Parvinen, M., De Rooij, D. G., Hess, M. W., et al. (2000). Regulation of cell fate decision of undifferentiated spermatogonia by GDNF. *Science* 287, 1489–1493. doi: 10.1126/science.287.5457.1489

Mroz, K., Carrel, L., and Hunt, P. A. (1999). Germ cell development in the XXY mouse: evidence that X Chromosome reactivation is independent of sexual differentiation. *Dev. Biol.* 207, 229–238. doi: 10.1006/dbio.1998.9160

Naughton, C. K., Jain, S., Strickland, A. M., Gupta, A., and Milbrandt, J. (2006). Glial cell-line derived neurotrophic factor-mediated RET signaling regulates Spermatogonial stem cell fate1. *Biol. Reprod.* 74, 314–321. doi: 10.1095/biolreprod.105.047365

Oatley, J. M., and Brinster, R. L. (2008). Regulation of spermatogonial stem cell self-renewal in mammals. *Annu. Rev. Cell Dev. Biol.* 24, 263–286. doi: 10.1146/annurev.cellbio.24.110707.175355

Ottesen, A. M., Aksglaede, L., Garn, I., Tartaglia, N., Tassone, F., Gravholt, C. H., et al. (2010). Increased number of sex chromosomes affects height in a nonlinear fashion: a study of 305 patients with sex chromosome aneuploidy. *Am. J. Med. Genet. A* 152A, 1206–1212. doi: 10.1002/ajmg.a.33334

Panula, S., Kurek, M., Kumar, P., Albalushi, H., Padrell Sánchez, S., Damdimopoulou, P., et al. (2019). Human induced pluripotent stem cells from two azoospermic patients with Klinefelter syndrome show similar X chromosome inactivation behavior to female pluripotent stem cells. *Hum. Reprod.* 34, 2297–2310. doi: 10.1093/humrep/dez134

Panula, S., Medrano, J. V., Kee, K., Bergström, R., Nguyen, H. N., Byers, B., et al. (2010). Human germ cell differentiation from fetal- and adult-derived induced pluripotent stem cells. *Hum. Mol. Genet.* 20, 752–762. doi: 10.1093/hmg/ddq520

Park, T. S., Galic, Z., Conway, A. E., Lindgren, A., Van Handel, B. J., Magnusson, M., et al. (2009). Derivation of primordial germ cells from human embryonic and induced pluripotent stem cells is significantly improved by coculture with human fetal gonadal cells. *Stem Cell.* 27, 783–795. doi: 10.1002/stem.13

Ramathal, C., Durruthy-Durruthy, J., Sukhwani, M., Arakaki, J. E., Turek, P. J., and Orwig, K. E. (2014). Fate of iPSCs derived from Azoospermic and fertile men following Xenotransplantation to murine seminiferous tubules. *Cell Rep.* 7, 1284–1297. doi: 10.1016/j.celrep.2014.03.067

Ruggiu, M., Speed, R., Taggart, M., Mckay, S. J., Kilanowski, F., Saunders, P., et al. (1997). The mouse Dazla gene encodes a cytoplasmic protein essential for gametogenesis. *Nature* 389, 73–77. doi: 10.1038/37987

Salemi, M., Condorelli, R. A., Longo, G., Bullara, V., Romano, C., Campagna, C., et al. (2016). LDOC1 gene expression in men with Klinefelter syndrome. *J. Clin. Lab. Anal.* 30, 408–410. doi: 10.1002/jcla.21870

Sciurano, R. B., Luna Hisano, C. V., Rahn, M. I., Brugo Olmedo, S., Rey Valzacchi, G., Coco, R., et al. (2009). Focal spermatogenesis originates in euploid germ cells in classical Klinefelter patients. *Hum. Reprod.* 24, 2353–2360. doi: 10.1093/humrep/dep180

Shimizu, T., Shiohara, M., Tai, T., Nagao, K., Nakajima, K., and Kobayashi, H. (2016). Derivation of integration-free iPSCs from a Klinefelter syndrome patient. *Reprod. Med. Biol.* 15, 35–43. doi: 10.1007/s12522-015-0213-9

Singh, D., Paduch, D. A., Schlegel, P. N., Orwig, K. E., Mielnik, A., Bolyakov, A., et al. (2017). The production of glial cell line-derived neurotrophic factor by human sertoli cells is substantially reduced in sertoli cell-only testes. *Hum. Reprod.* 32, 1108–1117. doi: 10.1093/humrep/dex061

Skakkebæk, A., Nielsen, M. M., Trolle, C., Vang, S., Hornshøj, H., Hedegaard, J., et al. (2018). DNA hypermethylation and differential gene expression associated with Klinefelter syndrome. *Sci. Rep.* 8:13740.

Spinnler, K., Köhn, F. M., Schwarzer, U., and Mayerhofer, A. (2010). Glial cell line-derived neurotrophic factor is constitutively produced by human testicular peritubular cells and may contribute to the spermatogonial stem cell niche in man. *Hum. Reprod.* 25, 2181–2187. doi: 10.1093/humrep/deq170

Teletin, M., Vernet, N., Ghyselinck, N. B., and Mark, M. (2017). "Chapter Seven - Roles of Retinoic Acid in Germ Cell Differentiation," in *Current Topics in Developmental Biology*, eds D. Forrest, and S. Tsai (Amsterdam: Academic Press), 191–225. doi: 10.1016/bs.ctdb.2016.11.013

Van Assche, E., Bonduelle, M., Tournaye, H., Joris, H., Verheyen, G., Devroey, P., et al. (1996). Cytogenetics of infertile men. *Hum Reprod* 11(Suppl. 4), 1-24.

Weissgerber, T. L., Milic, N. M., Winham, S. J., and Garovic, V. D. (2015). Beyond bar and line graphs: time for a new data presentation paradigm. *PLOS Biol.* 13:e1002128. doi: 10.1371/journal.pbio.1002128

West, F. D., Roche-Rios, M. I., Abraham, S., Rao, R. R., Natrajan, M. S., Bacanamwo, M., et al. (2009). KIT ligand and bone morphogenetic protein signaling enhances human embryonic stem cell to germ-like cell differentiation. *Hum. Reprod.* 25, 168–178. doi: 10.1093/humrep/dep338

Wikström, A. M., Hoei-Hansen, C. E., Dunkel, L., and Rajpert-De Meyts, E. (2007). Immunoexpression of androgen receptor and nine markers of maturation in the testes of Adolescent boys with Klinefelter syndrome: evidence for degeneration of germ cells at the onset of meiosis. *J. Clin. Endocrinol. Metab.* 92, 714–719. doi: 10.1210/jc.2006-1892

Winge, S. B., Dalgaard, M. D., Jensen, J. M., Graem, N., Schierup, M. H., Juul, A., et al. (2017). Transcriptome profiling of fetal Klinefelter testis tissue reveals a possible involvement of long non-coding RNAs in gonocyte maturation. *Hum. Mol. Genet.* 27, 430–439. doi: 10.1093/hmg/ddx411

Zhao, S., Wang, Q., Li, Z., Ma, X., Wu, L., Ji, H., et al. (2015). LDOC1 inhibits proliferation and promotes apoptosis by repressing NF-κB activation in papillary thyroid carcinoma. *J. Exp. Clin. Cancer Res.* 34:146.

Zhao, Y., Ye, S., Liang, D., Wang, P., Fu, J., Ma, Q., et al. (2018). In vitro modeling of human germ cell development using pluripotent stem cells. *Stem Cell Rep.* 10, 509–523. doi: 10.1016/j.stemcr.2018.01.001

Zitzmann, M., Bongers, R., Werler, S., Bogdanova, N., Wistuba, J., Kliesch, S., et al. (2015). Gene expression patterns in relation to the clinical phenotype in klinefelter syndrome. *J. Clin. Endocrinol. Metab.* 100, E518–E523.

Conflict of Interest: The authors declare that the research was conducted in the absence of any commercial or financial relationships that could be construed as a potential conflict of interest.

frontiers in Cell and Developmental Biology

MINI REVIEW
published: 12 October 2020
doi: 10.3389/fcell.2020.590119

Brain Organoids as Model Systems for Genetic Neurodevelopmental Disorders

Simona Baldassari[1†], Ilaria Musante[1,2†], Michele Iacomino[1], Federico Zara[1,2], Vincenzo Salpietro[2,3,4] and Paolo Scudieri[1,2]*

[1] Medical Genetics Unit, IRCSS Giannina Gaslini Institute, Genoa, Italy, [2] Department of Neurosciences, Rehabilitation, Ophthalmology, Genetics, Maternal and Child Health (DiNOGMI), University of Genoa, Genoa, Italy, [3] Pediatric Neurology and Muscular Diseases Unit, IRCSS Giannina Gaslini Institute, Genoa, Italy, [4] Department of Neuromuscular Diseases, UCL Queen Square Institute of Neurology, London, United Kingdom

Neurodevelopmental disorders (NDDs) are a group of disorders in which the development of the central nervous system (CNS) is disturbed, resulting in different neurological and neuropsychiatric features, such as impaired motor function, learning, language or non-verbal communication. Frequent comorbidities include epilepsy and movement disorders. Advances in DNA sequencing technologies revealed identifiable genetic causes in an increasingly large proportion of NDDs, highlighting the need of experimental approaches to investigate the defective genes and the molecular pathways implicated in abnormal brain development. However, targeted approaches to investigate specific molecular defects and their implications in human brain dysfunction are prevented by limited access to patient-derived brain tissues. In this context, advances of both stem cell technologies and genome editing strategies during the last decade led to the generation of three-dimensional (3D) *in vitro*-models of cerebral organoids, holding the potential to recapitulate precise stages of human brain development with the aim of personalized diagnostic and therapeutic approaches. Recent progresses allowed to generate 3D-structures of both neuronal and non-neuronal cell types and develop either whole-brain or region-specific cerebral organoids in order to investigate *in vitro* key brain developmental processes, such as neuronal cell morphogenesis, migration and connectivity. In this review, we summarized emerging methodological approaches in the field of brain organoid technologies and their application to dissect disease mechanisms underlying an array of pediatric brain developmental disorders, with a particular focus on autism spectrum disorders (ASDs) and epileptic encephalopathies.

Keywords: brain organoids, *in vitro* models, stem cells, 3D-culture, neurodevelopmental disorders, autism spectrum disorders, epilepsy

OPEN ACCESS

Edited by:
Eumorphia Remboutsika, National and Kapodistrian University of Athens, Greece

Reviewed by:
Matthias Carl, University of Trento, Italy
Stavros Malas, University of Nicosia, Cyprus

***Correspondence:**
Vincenzo Salpietro
v.salpietro@ucl.ac.uk

† These authors have contributed equally to this work

Specialty section:
This article was submitted to Stem Cell Research, a section of the journal Frontiers in Cell and Developmental Biology

Received: *31 July 2020*
Accepted: *18 September 2020*
Published: *12 October 2020*

Citation:
Baldassari S, Musante I, Iacomino M, Zara F, Salpietro V and Scudieri P (2020) Brain Organoids as Model Systems for Genetic Neurodevelopmental Disorders. Front. Cell Dev. Biol. 8:590119. doi: 10.3389/fcell.2020.590119

INTRODUCTION

Neurodevelopmental disorders (NDDs) encompass a range of frequently co-existing conditions that include intellectual disability (ID), developmental delay (DD), and autism spectrum disorders (ASDs) (Heyne et al., 2018; Salpietro et al., 2019). ASDs represent a complex set of behaviorally defined phenotypes, characterized by impairments in social interaction, communication and

restricted or stereotyped behaviors (Chen et al., 2018). Epilepsy and NDDs frequently occur together, and when refractory seizures are accompanied by cognitive slowing or regression, patients are considered to have an epileptic encephalopathy (EE) (Scheffer et al., 2017). Both ID and ASDs are clinically and etiologically heterogeneous and a unifying pathophysiology has not yet been identified for either the disorder as a whole or its core behavioral components (Myers et al., 2020). Family and twin studies suggest high (0.65–0.91) heritability (Chen et al., 2018) and genetic dissection of the complex molecular architecture of ID/ASD is revealing contributions from both coding and non-coding DNA changes (Williams et al., 2019). Chromosomal microarray and next-generation sequencing (NGS) led over the last decade to the identification of a number of *de novo* and inherited variants implicated in the molecular etiology of ID/ASD variably associated with epilepsy (Wang et al., 2019). Deleterious variants in the same genes are often implicated in multiple NDDs characterized by autistic features and other comorbidities such ID, seizures or developmental epileptic encephalopathies, and neuropsychiatric conditions including schizophrenia and attention-deficit/hyperactivity disorder (O'Donovan and Owen, 2016). Defining the full spectrum of defective molecular pathways will help diagnose, monitor and accelerate treatment development in genetic NDDs (Lombardi et al., 2015). Currently, susceptibility and major mendelian alleles identified in NDDs explain only a small percentage of risk, and most of the work is still ahead to uncover the complex genetics of these disorders.

Also, assessing the pathophysiological mechanism(s) underlying brain developmental disorders is historically challenging due to limitations in accessing human brain and the complexity of the central nervous system (CNS). Studies on animal models, particularly mice, gained insight to various genetic and environmental conditions impacting neurodevelopment and neuronal functions, but rarely achieved to recapitulate precisely the most complex human neurological phenotypes. This could be attributed to human brain complexity and size with many features that are species-specific; as instance, the human cerebral cortex is over 1.000 times larger in terms of area and number of neurons (Leung and Jia, 2016) and extensive differences exist between homologous brain regions in humans and mice, including marked alterations in cell types proportions, distributions, morphology, and gene expression (Hodge et al., 2019). These features unique to humans highlight the importance of investigating the human brain by accurate models capable to recapitulate its development at different stages.

Several recent advances in biotechnology, including stem cells culture and cell reprogramming methods, CRISPR-Cas9-based genome editing, biomaterials, optogenetics, and single-cell transcriptomics, allowed the generation and the fine characterization of complex 3D-models, i.e., the cerebral (or brain) organoids. These *in vitro* 3D-models, with respect to rodent models, may facilitate investigation of complex neurodevelopmental human diseases by combining different important determinants of the human features. In particular, brain organoids generated from human pluripotent stem cells (hPSC) preserve the human genomic context, allowing to study the pathogenetic mechanisms of diseases associated with monogenic as well as polygenic genomic alterations. Moreover, brain organoids recapitulates species-specific developmental timing *in vitro*, such as cell cycle dynamics, duration of neurogenic period, rate and pattern of cell migration (Mariani et al., 2015; Toma et al., 2016). Brain organoids represent also an obvious advance with respect to 2D cell cultures, enabling studying more complex phenotypes involving different neuronal networks, tissue architecture, and organ morphogenesis.

In this review, we focused on the most recent advances in cerebral organoids technology, and on its application to the study of genetic NDDs, particularly ASDs and epilepsy.

BRAIN ORGANOIDS AND TECHNOLOGIES

Brain organoids are self-organized 3D-aggregates generated from hPSC or induced pluripotent stem cells (iPSC) with cell types and cytoarchitectures resembling the embryonic human brain (Eiraku et al., 2008; Kadoshima et al., 2013; Lancaster et al., 2013; Paşca et al., 2015). Multiple brain organoid protocols and techniques have been exploited in the last 5–10 years, ranging from the development of region-specific organoids to more complex whole-brain organoids that recapitulate cell interactions and interconnectivity between multiple brain regions (Lancaster and Knoblich, 2014a,b; Paşca, 2018; Xiang et al., 2020a).

Generally, approaches to generate brain organoids can be categorized in two major classes: unguided and guided methods (**Figure 1A**). Unguided methods rely on spontaneous morphogenesis and intrinsic differentiation capacities of hPSC aggregates (Lancaster et al., 2013; Renner et al., 2017). In the original protocol developed by the Knoblich's lab, embryoid bodies derived from hPSC aggregates are embedded in droplets of Matrigel (to mimic extracellular matrix) and then transferred to a spinning bioreactor to enhance nutrient absorption and, thus, facilitate tissue expansion and neural differentiation (Lancaster et al., 2013; Lancaster and Knoblich, 2014b). With minimal external influence, this method produces large (up to 2–4 mm diameter) and heterogeneous cerebral tissue displaying discrete, but interdependent, brain regions (forebrain, midbrain, and hindbrain) and subregions (various cortical lobes, choroid plexus, and retina) (Lancaster et al., 2013). Single-cell transcriptomic approaches confirmed the heterogeneous cellular population of unguided cerebral organoids, revealing the presence of neural progenitors, excitatory and inhibitory neurons, astrocytes and oligodendrocyte precursor cells, and photosensitive cells (Quadrato et al., 2017; Kanton et al., 2019, 2020; Tanaka et al., 2020). Despite this high cellular and spatial complexity offers the opportunity to model the interactions between different brain regions, the stochastic nature of spontaneous neural differentiation often results in high variability across batches of differentiated organoids that makes quantitative studies challenging. Many modifications of this pioneer protocol have been devised in order to guide the development of more reproducible region-specific organoids or to control different organoid features through bioengineering approaches.

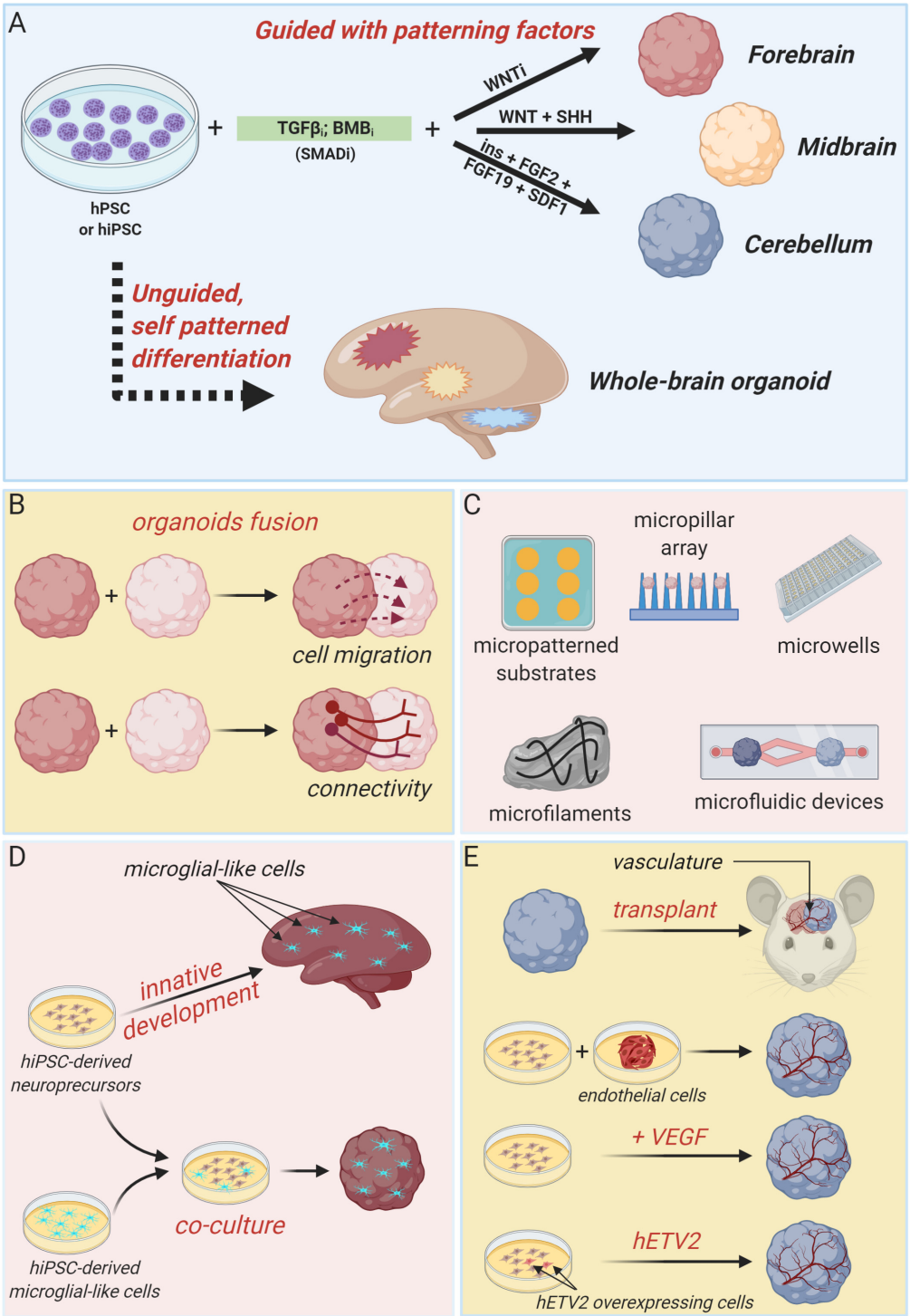

FIGURE 1 | Brain organoid technologies. **(A)** Schematic summary of guided and unguided methods to generate different types of cerebral organoids. Guided approaches allow the generation of region-specific brain organoids resembling discrete parts of the developing human brain, such as forebrain, midbrain or cerebellum. Unguided approaches, instead, result in the generation of organoids resembling the whole-human brain. **(B)** Region-specific organoids can be fused to each other to model regional-interactions, such as cellular migration and long-range connectivity. **(C)** Summary of bioengineering tools to regulate brain organoids morphology and structure. **(D)** Cartoon illustrating two independent strategies to develop microglia-containing brain organoids. Microglial-like cells can innately develop within unguided-whole brain organoids or can be introduce by co-culture methods. **(E)** Different attempts to obtain organoid vascularization, including organoids transplantation in nude mice, co-culture with iPSC-derived endothelial cell precursors and co-differentiation of neuronal and endothelial cells by VEGF administration or hETV2 overexpression (created with biorender.com).

Guided strategies direct regional fate specification by using patterning factors such as morphogens and small molecules (Eiraku et al., 2008; Danjo et al., 2011; Kadoshima et al., 2013). Indeed, self-patterning of organoids precursors can be restricted to forebrain fate by inhibiting TGF-β, BMP, and WNT pathways (**Figure 1A**; Eiraku et al., 2008; Kadoshima et al., 2013). By supplying additional patterning factors (such as WNT3A, SHH, insulin, and BMP7), forebrain fate can be further confined to produce organoids resembling any discrete part of the forebrain region, including cerebral cortex, optic cup, hippocampal, choroid plexus, subpallium, thalamus, and hypothalamus (Wataya et al., 2008; Eiraku et al., 2011; Nakano et al., 2012; Germain et al., 2013; Kadoshima et al., 2013; Liu et al., 2013; Maroof et al., 2013; Nicholas et al., 2013; Mariani et al., 2015; Sakaguchi et al., 2015; Qian et al., 2016; Shiraishi et al., 2017; Kim et al., 2019b; Xiang et al., 2020a). Midbrain organoids are generated by combining TGF-β and BMP inhibition with WNT and SHH activation, and FGF8 treatment (Jo et al., 2016; Kim et al., 2019a), whereas cerebellum organoids are produced by timed and combinatory treatment with a series of patterning factors, including TGF-β and BMP inhibitors, insulin, FGF2, FGF19, and SDF1 (**Figure 1A**; Muguruma et al., 2015).

Interestingly, regionally specified cerebral organoids can be fused to each other to model the interaction between distinct brain regions and to assess fundamental features of brain development and disease, such as cell migration and long-range connectivity (**Figure 1B**; Bagley et al., 2017; Birey et al., 2017; Mich et al., 2017; Xiang et al., 2017, 2018, 2019). For example, dorsal and ventral forebrain organoids can be assembled *in vitro* to recapitulate the typical saltatory migration and integration into cortical circuits of interneurons observed in the fetal brain (Birey et al., 2017). Instead, the creation of reciprocal thalamocortical axon projections, which establishment is critically involved in sensory-motor processing and attention, can be modeled *in vitro* by fusing thalamic and cortical organoids (Xiang et al., 2019).

A series of advances in brain organoids technology have been achieved by integrating organoids culture with bioengineering methodologies, particularly biomaterials, microfabricated, and microfluidic devices, in order to enable a better spatiotemporal control of cellular differentiation and organoid morphogenesis (**Figure 1C**). Indeed, inceptive hPSC aggregates and embryoid bodies dimension and morphology can be easily standardized by using micropatterned substrates, micropillar array or microwells, increasing brain organoid generation reliability, and reproducibility (Knight et al., 2015; Zhu et al., 2017; Haremaki et al., 2019; Velasco et al., 2019; Yoon et al., 2019). Alternatively, fiber microfilaments have been used as a floating scaffold to generate elongated embryoid bodies (Lancaster et al., 2017). The resulting microfilament engineered cerebral organoids (enCORs) were characterized by enhanced neuroectoderm formation and improved cortical development (Lancaster et al., 2017). Others efforts to better control the morphology of developing organoids include the employ of hydrogels or microfabricated culture chambers with defined microscale dimensions (Karzbrun et al., 2018; McNulty et al., 2019). Carefully designed microfluidic devices could be useful to generate morphogen gradients in order to guide organoids patterning (Manfrin et al., 2019).

Additional fundamental aspects of recent advances in brain organoids technology include attempts to incorporate non-neuronal components, such as microglia and vasculature, that are of primary importance in brain development and disease (**Figures 1D,E**; Obermeier et al., 2013; Beggs and Salter, 2016).

Cells with typical microglial morphology, molecular phenotype and function can innately develop within unguided and self-patterned cerebral organoids, as demonstrated by Ormel et al. (2018). Otherwise, microglial component can be integrated in region-specific organoids by co-culture with human induced PSC-derived microglial-like cells (Song et al., 2019).

As depicted in **Figure 1E**, several strategies have been explored also to achieve cerebral organoids vascularization. Indeed, formation of a mature vascular system is essential to sustain organoids growth capacity during long-term cultures and to better recapitulate *in vitro* the complex processes happening *in vivo*, and involving the simultaneous and integrated development of organs and vasculature. Vascularized cerebral organoids have been initially obtained by organoids transplantation into the brain of immunodeficient mice (Mansour et al., 2018) or by co-culture with endothelial cells or their progenitors during organoids formation (Pham et al., 2018). More recently, cerebral organoids have been co-differentiated with endothelial-like cells by supplementation of VEGF during organoids derivation (Ham et al., 2019) or by targeted overexpression of the transcription factor hETV2 in a small subset of initial hPSC population (Cakir et al., 2019). In both cases, a functional vascular-like system appeared without reducing neural morphogenesis, rather favoring a better organoid maturation (Cakir et al., 2019).

BRAIN ORGANOIDS IN AUTISM SPECTRUM DISORDERS

Autism spectrum disorders are defined as a combination of neurodevelopmental diseases (Hodges et al., 2020). Symptoms are characterized by lack of development of social and emotional relationships, difficulties in the use of language, apathy, rigidity in movements and repetitive and maniac behaviors. So far, it has been hard to well define a diagnosis because ASD marks are often associated with other psychiatric features as well as ID, epilepsy, and attention-deficit hyperactivity disorder (Moreno-De-Luca et al., 2013). Genetic variants and environmental factors are known to play important roles in the pathogenesis of ASD (Buxbaum et al., 2007). For instance, genetic variants involving synaptic genes are emerging as recurrent causative factors in the etiology of ASDs (Südhof, 2008; Zoghbi and Bear, 2012; Salpietro et al., 2019). Moreover, different authors speculate on the role of the unbalance between excitatory and inhibitory circuits in the pathogenesis of these disorders (Casanova et al., 2003; Rubenstein, 2010). Recently, genomic data and gene networks analysis suggested a common cause for ASDs during the embryonic development of the cerebral cortex (Parikshak et al., 2013; Willsey et al.,2013). In this context, 3D *in vitro* models are increasing our capability to study neuropsychiatric diseases (Yang and Shcheglovitov, 2020).

As a first example, Mariani and co-workers studied the early cortical development in patients with idiopathic ASD characterized by increased head/brain size (macrocephaly), that is one of the most common sign in ASDs phenotypes (Courchesne et al., 2001; Mariani et al., 2015). Transcriptomic and cellular studies on iPSC-derived forebrain organoids from autism patients revealed alterations in cell-cycle and in synaptic growth (**Figure 2**). Notably, ASD organoids showed an increased production of inhibitory neurons caused by increased expression of the transcription factor *FOXG1*, highlighting the role of this gene as a molecular signature of idiopathic ASD and a potential therapeutic target (Mariani et al., 2015; Hou et al., 2020).

Growing knowledge on ASD risk variants and on gene networks involved at different time points and in different cell types during neurodevelopment process suggest that ASD pathologies may arise from combined deficiencies during early stages of cortical development (Parikshak et al., 2013; Willsey et al., 2013). Indeed, Schafer et al. (2019) by combining transcriptomic analysis, cerebral organoids generation and direct iPSCs-to-neuron conversion demonstrated how autism-related neurodevelopmental alterations are triggered by temporal dysregulation of specific gene networks and morphological growth acceleration occurring during early neural development. Interestingly, while ASD alterations were recapitulated on forebrain organoids generated from idiopathic ASD patients-derived iPSCs, the direct conversion of ASD iPSCs to mature neurons abolished ASD-associated phenotypes (Schafer et al., 2019). These findings indicate that some ASD-associated anomalies are likely to be the consequence of pathological events triggered during neural stem cells stages, and possibly involving epigenetic changes (Schafer et al., 2019).

BRAIN ORGANOIDS AND EPILEPSY

Timothy syndrome (TS) represents a successful application of brain organoids technology to the investigation of human brain development disorders and epilepsy. This disorder is caused by mutations in *CACNA1C*, the gene encoding the L-type calcium channel Cav1.2 α subunit, producing abnormal inhibitory neurons. The generation of cerebral organoids derived from TS-iPSC, gained insight to inhibitory neurons migration pattern during brain development (Birey et al., 2017). Indeed, live imaging of TS-forebrain assembloids (fusion between cerebral organoids resembling dorsal and ventral forebrain) revealed a cell-autonomous defect consisting in overall delayed migration of inhibitory neurons from the ventral to the dorsal forebrain (**Figure 2**; Birey et al., 2017). Importantly, this phenotype was rescued by blocking the activity of L-type calcium channels by nimodipine (Birey et al., 2017). Importantly, this study was the first example of fused organoid approach to *in vitro* modeling of neuronal circuits involving distinct brain regions (Birey et al., 2017; Koo et al., 2019).

Given the limited access to subjects with rare epilepsy mutations, brain organoid technology combined with CRISPR/Cas9 genome editing methods can be particularly useful to investigate the effects of rare patient-specific variants in an isogenic control background.

Tuberous sclerosis complex (TSC) disease is an autosomal dominant disorder associated with epilepsy, ID, and benign tumors of the brain, heart, skin, and kidney. TSC is caused by mutations in the *TSC1* or *TSC2* genes. The proteins encoded by these genes form a heterodimeric complex that negatively regulates mechanistic target of rapamycin complex 1 (mTORC1) signaling (Saxton and Sabatini, 2017). The origins of the neurological aspects of TSC are largely unknown. However, patients present with characteristic malformations, called cortical tubers, which are macroscopic regions of disorganized and dysmorphic cells in the cortex (Crino, 2013). The proposed model of cortical tuber formation is that somatic "second-hit" mutations in patients with heterozygous germ line mutations result in loss of function of the TSC1-TSC2 complex and hyperactivation of mTORC1 signaling in a subset of cortical progenitor cells (Magri and Galli, 2013; Crino, 2016). Recently, Blair and colleagues combined brain organoid and CRISPR/Cas9 gene editing methods as a means to investigate the "two-hit" hypothesis of cortical tuber development (**Figure 2**; Blair et al., 2018; Saber and Sahin, 2020). Homozygous, but not heterozygous, loss of *TSC1* or *TSC2* disrupts the developmental suppression of mTORC1 signaling providing strong support for the two-hit hypothesis of TSC pathophysiology. They also showed that early rapamycin treatment of the brain organoids prevented development of the abnormal phenotypes (Blair et al., 2018; Niu and Parent, 2019).

Lately, iPSCs from patients carrying mutations in *DCSH1* and *FAT4* genes were used to model periventricular heterotopia (PH), a disorder of neuronal migration, using self-patterned brain organoids (Klaus et al., 2019). While analyzing the impact of the *DCSH1* and *FAT4* mutations on organoids generation, the authors found defective radial progenitor cells, which should guide the neurons to the correct final destination (**Figure 2**). In addition, scRNA-seq analysis revealed a specific subpopulation of neurons with an altered navigation system, which changed their migratory dynamics and led to compromised equipment for synaptic signaling (Klaus et al., 2019).

Angelman syndrome (AS) is a debilitating neurological disorder caused by mutation of the E3A ubiquitin protein ligase (*UBE3A*) gene. Although, AS mice showed impaired synaptic connectivity and altered plasticity associated with abnormal behavior, the pathological mechanisms underlying epilepsy, as well as the biological substrate of UBE3A, remained unknown. Recently, by using brain organoids, Sun et al. (2019) demonstrated that UBE3A suppresses neuronal hyperexcitability via ubiquitin-mediated degradation of calcium and voltage-dependent big potassium (BK) channels. Consequently, neuronal excitability can be normalized and seizure susceptibility ameliorated by antagonizing BK channels (Sun et al., 2019).

Rett syndrome and Bosch-Boonstra-Schaaf optic atrophy syndrome (BBSOAS) are two additional examples of recent studies in which brain organoids have been successfully used. Rett syndrome (RTT) is a severe X-linked dominant NDD affecting females caused primarily by mutations in *MECP2*, which encodes

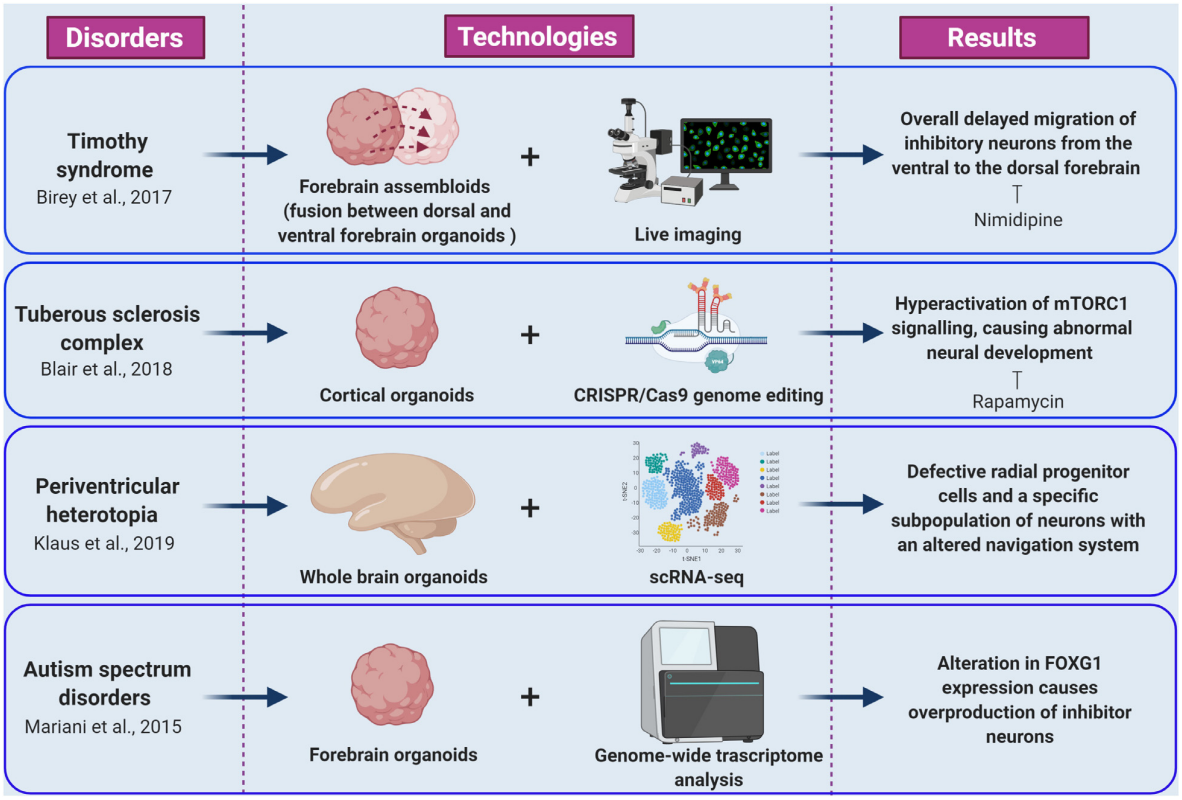

FIGURE 2 | Cellular and molecular phenotypes revealed by brain organoid models of epilepsy and ASDs. The figure summarize how integration of brain organoids technology (forebrain assembloids, cortical organoids, whole brain organoids, and forebrain organoids) with multiple experimental approaches (including live imaging, CRISPR/Cas9 genome editing, scRNA-seq, and genome wide transcriptome analysis) allowed the understanding of various molecular mechanisms underlying epileptic and autism spectrum disorders (created with biorender.com).

a multifunctional epigenetic regulator. Mellios et al. (2018) used *MECP2*-deficient and patient-derived cerebral organoids to identify defects in neurogenesis, neuronal differentiation, and migration. Xiang et al. (2020b) revealed cell-type-specific transcriptome impairment in *MeCP2* mutant region-specific brain organoids.

Bosch-Boonstra-Schaaf optic atrophy syndrome is a recently described autosomal dominant disorder, caused by loss-of-function mutations of the transcriptional regulator *NR2F1*. Cerebral organoids with reduced NR2F1 levels displayed altered neurogenesis and expression of *PAX6*, a gene that has a crucial role in neurogenesis in the developing cortex (Bertacchi et al., 2020).

CONCLUSION AND PERSPECTIVES

Brain organoids technology represent a tremendous breakthrough for the study of brain development, function, evolution and disorders and is still in his infancy. Continuous advances of 3D-culture systems and their integration with state-of-the-art biotechnology and bioengineering approaches, including single-cell transcriptomics, genome-editing, cell reprogramming and biomaterials, will lead the cerebral organoids to probably become the best *in vitro* model system for neurodevelopment studies in humans. Particularly, further advances will be necessary to standardize organoids generation protocols in order to increase their reproducibility and, hopefully, to reduce their costs. The development of new experimental procedures and functional assays will be important to explore the brain organoids ability to mimic even more complex processes involved in human neurodevelopment in health and diseases, and, therefore, to increase the translational value of this technology and its relevance in clinical applications and precision medicine approaches.

AUTHOR CONTRIBUTIONS

SB, IM, VS, and PS wrote the manuscript and prepared the figures. MI, VS, FZ, and PS revised the manuscript. VS and PS coordinated the preparation of the review. All authors contributed to the article and approved the submitted version.

FUNDING

This work was supported by the Compagnia di San Paolo (grant number 9934 to FZ).

REFERENCES

Bagley, J. A., Reumann, D., Bian, S., Lévi-Strauss, J., and Knoblich, J. A. (2017). Fused cerebral organoids model interactions between brain regions. *Nat. Methods* 14, 743–751. doi: 10.1038/nmeth.4304

Beggs, S., and Salter, M. W. (2016). SnapShot: microglia in disease. *Cell* 165:1294. doi: 10.1016/j.cell.2016.05.036

Bertacchi, M., Romano, A. L., Loubat, A., Mau-Them, F. T., Willems, M., Faivre, L., et al. (2020). NR2F1 regulates regional progenitor dynamics in the mouse neocortex and cortical gyrification in BBSOAS patients. *EMBO J.* 39:e104163. doi: 10.15252/embj.2019104163

Birey, F., Andersen, J., Makinson, C. D., Islam, S., Wei, W., Huber, N., et al. (2017). Assembly of functionally integrated human forebrain spheroids. *Nature* 545, 54–59. doi: 10.1038/nature22330

Blair, J. D., Hockemeyer, D., and Bateup, H. S. (2018). Genetically engineered human cortical spheroid models of tuberous sclerosis. *Nat. Med.* 24, 1568–1578. doi: 10.1038/s41591-018-0139-y

Buxbaum, J. D., Cai, G., Chaste, P., Nygren, G., Goldsmith, J., Reichert, J., et al. (2007). Mutation screening of the PTEN gene in patients with autism spectrum disorders and macrocephaly. *Am. J. Med. Genet. B Neuropsychiatr. Genet.* 144B, 484–491. doi: 10.1002/ajmg.b.30493

Cakir, B., Xiang, Y., Tanaka, Y., Kural, M. H., Parent, M., Kang, Y.-J., et al. (2019). Engineering of human brain organoids with a functional vascular-like system. *Nat. Methods* 16, 1169–1175. doi: 10.1038/s41592-019-0586-5

Casanova, M. F., Buxhoeveden, D., and Gomez, J. (2003). Disruption in the inhibitory architecture of the cell minicolumn: implications for autism. *Neuroscientist* 9, 496–507. doi: 10.1177/1073858403253552

Chen, S., Fragoza, R., Klei, L., Liu, Y., Wang, J., Roeder, K., et al. (2018). An interactome perturbation framework prioritizes damaging missense mutations for developmental disorders. *Nat. Genet.* 50, 1032–1040. doi: 10.1038/s41588-018-0130-z

Courchesne, E., Karns, C. M., Davis, H. R., Ziccardi, R., Carper, R. A., Tigue, Z. D., et al. (2001). Unusual brain growth patterns in early life in patients with autistic disorder: an MRI study. *Neurology* 57, 245–254. doi: 10.1212/wnl.57.2.245

Crino, P. B. (2013). Evolving neurobiology of tuberous sclerosis complex. *Acta Neuropathol.* 125, 317–332. doi: 10.1007/s00401-013-1085-x

Crino, P. B. (2016). The mTOR signalling cascade: paving new roads to cure neurological disease. *Nat. Rev. Neurol.* 12, 379–392. doi: 10.1038/nrneurol.2016.81

Danjo, T., Eiraku, M., Muguruma, K., Watanabe, K., Kawada, M., Yanagawa, Y., et al. (2011). Subregional specification of embryonic stem cell-derived ventral telencephalic tissues by timed and combinatory treatment with extrinsic signals. *J. Neurosci.* 31, 1919–1933. doi: 10.1523/JNEUROSCI.5128-10.2011

Eiraku, M., Takata, N., Ishibashi, H., Kawada, M., Sakakura, E., Okuda, S., et al. (2011). Self-organizing optic-cup morphogenesis in three-dimensional culture. *Nature* 472, 51–56. doi: 10.1038/nature09941

Eiraku, M., Watanabe, K., Matsuo-Takasaki, M., Kawada, M., Yonemura, S., Matsumura, M., et al. (2008). Self-organized formation of polarized cortical tissues from ESCs and its active manipulation by extrinsic signals. *Stem Cell* 3, 519–532. doi: 10.1016/j.stem.2008.09.002

Germain, N. D., Banda, E. C., Becker, S., Naegele, J. R., and Grabel, L. B. (2013). Derivation and isolation of NKX2.1-positive basal forebrain progenitors from human embryonic stem cells. *Stem Cells Dev.* 22, 1477–1489. doi: 10.1089/scd.2012.0264

Ham, O., Jin, Y. B., Kim, J., and Lee, M.-O. (2019). Blood vessel formation in cerebral organoids formed from human embryonic stem cells. *Biochem. Biophys. Res. Commun.* 521, 84–90. doi: 10.1016/j.bbrc.2019.10.079

Haremaki, T., Metzger, J. J., Rito, T., Ozair, M. Z., Etoc, F., and Brivanlou, A. H. (2019). Self-organizing neuruloids model developmental aspects of Huntington's disease in the ectodermal compartment. *Nat. Biotechnol.* 37, 1198–1208. doi: 10.1038/s41587-019-0237-5

Heyne, H. O., Singh, T., Stamberger, H., Jamra, A. R., Caglayan, H., Craiu, D., et al. (2018). *De-novo* variants in neurodevelopmental disorders with epilepsy. *Nat. Genet.* 50, 1048–1053. doi: 10.1038/s41588-018-0143-7

Hodge, R. D., Bakken, T. E., Miller, J. A., Smith, K. A., Barkan, E. R., Graybuck, L. T., et al. (2019). Conserved cell types with divergent features in human versus mouse cortex. *Nature* 573, 61–68. doi: 10.1038/s41586-019-1506-7

Hodges, H., Fealko, C., and Soares, N. (2020). Autism spectrum disorder: definition, epidemiology, causes, and clinical evaluation. *Transl. Pediatr.* 9, S55–S65. doi: 10.21037/tp.2019.09.09

Hou, P. S., hAilín, D. Ó, Vogel, T., and Hanashima, C. (2020). Transcription and beyond: delineating FOXG1 function in cortical development and disorders. *Front. Cell. Neurosci.* 14:35. doi: 10.3389/fncel.2020.00035

Jo, J., Xiao, Y., Sun, A. X., Cukuroglu, E., Tran, H.-D., Göke, J., et al. (2016). Midbrain-like organoids from human pluripotent stem cells contain functional dopaminergic and neuromelanin-producing neurons. *Cell Stem Cell* 19, 248–257. doi: 10.1016/j.stem.2016.07.005

Kadoshima, T., Sakaguchi, H., Nakano, T., Soen, M., Ando, S., Eiraku, M., et al. (2013). Self-organization of axial polarity, inside-out layer pattern, and species-specific progenitor dynamics in human ES cell-derived neocortex. *Proc. Natl. Acad. Sci. U.S.A.* 110, 20284–20289. doi: 10.1073/pnas.1315710110

Kanton, S., Boyle, M. J., He, Z., Santel, M., Weigert, A., Sanchís-Calleja, F., et al. (2019). Organoid single-cell genomic atlas uncovers human-specific features of brain development. *Nature* 574, 418–422. doi: 10.1038/s41586-019-1654-9

Kanton, S., Treutlein, B., and Camp, J. G. (2020). Single-cell genomic analysis of human cerebral organoids. *Methods Cell Biol.* 159, 229–256. doi: 10.1016/bs.mcb.2020.03.013

Karzbrun, E., Kshirsagar, A., Cohen, S. R., Hanna, J. H., and Reiner, O. (2018). Human brain organoids on a chip reveal the physics of folding. *Nat. Phys.* 14, 515–522. doi: 10.1038/s41567-018-0046-7

Kim, H., Park, H. J., Choi, H., Chang, Y., Park, H., Shin, J., et al. (2019a). Modeling G2019S-LRRK2 sporadic parkinson's disease in 3D midbrain organoids. *Stem Cell Rep.* 12, 518–531. doi: 10.1016/j.stemcr.2019.01.020

Kim, H., Xu, R., Padmashri, R., Dunaevsky, A., Liu, Y., Dreyfus, C. F., et al. (2019b). Pluripotent stem cell-derived cerebral organoids reveal human oligodendrogenesis with dorsal and ventral origins. *Stem Cell Rep.* 12, 890–905. doi: 10.1016/j.stemcr.2019.04.011

Klaus, J., Kanton, S., Kyrousi, C., Ayo-Martin, A. C., Di Giaimo, R., Riesenberg, S., et al. (2019). Altered neuronal migratory trajectories in human cerebral organoids derived from individuals with neuronal heterotopia. *Nat. Med.* 25, 561–568. doi: 10.1038/s41591-019-0371-0

Knight, G. T., Sha, J., and Ashton, R. S. (2015). Micropatterned, clickable culture substrates enable in situ spatiotemporal control of human PSC-derived neural tissue morphology. *Chem. Commun.* 51, 5238–5241. doi: 10.1039/c4cc08665a

Koo, B., Choi, B., Park, H., and Yoon, K.-J. (2019). Past, present, and future of brain organoid technology. *Mol. Cells.* 42, 617–627. doi: 10.14348/molcells.2019.0162

Lancaster, M. A., Corsini, N. S., Wolfinger, S., Gustafson, E. H., Phillips, A. W., Burkard, T. R., et al. (2017). Guided self-organization and cortical plate formation in human brain organoids. *Nat. Biotechnol.* 35, 659–666. doi: 10.1038/nbt.3906

Lancaster, M. A., and Knoblich, J. A. (2014a). Organogenesis in a dish: modeling development and disease using organoid technologies. *Science* 345, 1247125. doi: 10.1126/science.1247125

Lancaster, M. A., and Knoblich, J. A. (2014b). Generation of cerebral organoids from human pluripotent stem cells. *Nat. Protoc.* 9, 2329–2340. doi: 10.1038/nprot.2014.158

Lancaster, M. A., Renner, M., Martin, C. A., Wenzel, D., Bicknell, L. S., Hurles, M. E., et al. (2013). Cerebral organoids model human brain development and microcephaly. *Nature* 501, 373–379. doi: 10.1038/nature12517

Leung, C., and Jia, Z. (2016). Mouse genetic models of human brain disorders. *Front. Genet.* 7:40. doi: 10.3389/fgene.2016.00040

Liu, Y., Liu, H., Sauvey, C., Yao, L., Zarnowska, E. D., and Zhang, S.-C. (2013). Directed differentiation of forebrain GABA interneurons from human pluripotent stem cells. *Nat. Protoc.* 8, 1670–1679. doi: 10.1038/nprot.2013.106

Lombardi, L. M., Baker, S. A., and Zoghbi, H. Y. (2015). MECP2 disorders: from the clinic to mice and back. *J Clin. Inves.* 125, 2914–2923. doi: 10.1172/JCI78167

Magri, L., and Galli, R. (2013). mTOR signaling in neural stem cells: from basic biology to disease. *Cell. Mol. Life Sci.* 70, 2887–2898. doi: 10.1007/s00018-012-1196-x

Manfrin, A., Tabata, Y., Paquet, E. R., Vuaridel, A. R., Rivest, F. R., Naef, F., et al. (2019). Engineered signaling centers for the spatially controlled patterning of human pluripotent stem cells. *Nat. Methods* 16, 640–648. doi: 10.1038/s41592-019-0455-2

Mansour, A. A., Gonçalves, J. T., Bloyd, C. W., Li, H., Fernandes, S., Quang, D., et al. (2018). An in vivo model of functional and vascularized human brain organoids. *Nat. Biotechnol.* 36, 432–441. doi: 10.1038/nbt.4127

Mariani, J., Coppola, G., Zhang, P., Abyzov, A., Provini, L., Tomasini, L., et al. (2015). FOXG1-dependent dysregulation of GABA/glutamate neuron differentiation in autism spectrum disorders. *Cell* 162, 375–390. doi: 10.1016/j.cell.2015.06.034

Maroof, A. M., Keros, S., Tyson, J. A., Ying, S.-W., Ganat, Y. M., Merkle, F. T., et al. (2013). Directed differentiation and functional maturation of cortical interneurons from human embryonic stem cells. *Cell Stem Cell* 12, 559–572. doi: 10.1016/j.stem.2013.04.008

McNulty, J. D., Marti-Figueroa, C., Seipel, F., Plantz, J. Z., Ellingham, T., Duddleston, L. J. L., et al. (2019). Micro-injection molded, poly(vinyl alcohol)-calcium salt templates for precise customization of 3D hydrogel internal architecture. *Acta Biomater.* 95, 258–268. doi: 10.1016/j.actbio.2019.04.050

Mellios, N., Feldman, D. A., Sheridan, S. D., Ip, J. P. K., Kwok, S., Amoah, S. K., et al. (2018). MeCP2-regulated miRNAs control early human neurogenesis through differential effects on ERK and AKT signaling. *Mol. Psychiatry* 23, 1051–1065. doi: 10.1038/mp.2017.86

Mich, K., Close, J. L., and Levi, B. P. (2017). Putting two heads together to build a better brain. *Cell Stem Cell* 21, 289–290. doi: 10.1016/j.stem.2017.08.017

Moreno-De-Luca, A., Myers, S. M., Challman, T. D., Moreno-De-Luca, D., Evans, D. W., and Ledbetter, D. H. (2013). Developmental brain dysfunction: revival and expansion of old concepts based on new genetic evidence. *Lancet Neurol.* 12, 406–414. doi: 10.1016/S1474-4422(13)70011-5

Muguruma, K., Nishiyama, A., Kawakami, H., Hashimoto, K., and Sasai, Y. (2015). Self-organization of polarized cerebellar tissue in 3D culture of human pluripotent stem cells. *Cell Rep.* 10, 537–550. doi: 10.1016/j.celrep.2014.12.051

Myers, S. M., Challman, T. D., Bernier, R., Bourgeron, T., Chung, W. K., Constantino, J. N., et al. (2020). Insufficient evidence for "autism-specific" genes. *Am J Hum Genet.* 106, 587–595. doi: 10.1016/j.ajhg.2020.04.004

Nakano, T., Ando, S., Takata, N., Kawada, M., Muguruma, K., Sekiguchi, K., et al. (2012). Self-formation of optic cups and storable stratified neural retina from human ESCs. *Cell Stem Cell* 10, 771–785. doi: 10.1016/j.stem.2012.05.009

Nicholas, C. R., Chen, J., Tang, Y., Southwell, D. G., Chalmers, N., Vogt, D., et al. (2013). Functional maturation of hPSC-derived forebrain interneurons requires an extended timeline and mimics human neural development. *Cell Stem Cell* 12, 573–586. doi: 10.1016/j.stem.2013.04.005

Niu, W., and Parent, J. M. (2019). Modeling genetic epilepsies in a dish. *Dev. Dyn.* 249, 56–75. doi: 10.1002/dvdy.79

Obermeier, B., Daneman, R., and Ransohoff, R. M. (2013). Development, maintenance and disruption of the blood-brain barrier. *Nat. Med.* 19, 1584–1596. doi: 10.1038/nm.3407

O'Donovan, M. C., and Owen, M. J. (2016). The implications of the shared genetics of psychiatric disorders. *Nat. Med.* 22, 1214–1219. doi: 10.1038/nm.4196

Ormel, P. R., de Sá, R., van Bodegraven, E. J., Karst, H., Harschnitz, O., Sneeboer, M. A. M., et al. (2018). Microglia innately develop within cerebral organoids. *Nat. Commun.* 9, 4167. doi: 10.1038/s41467-018-06684-2

Parikshak, N. N., Luo, R., Zhang, A., Won, H., Lowe, J. K., Chandran, V., et al. (2013). Integrative functional genomic analyses implicate specific molecular pathways and circuits in autism. *Cell* 155, 1008–1021. doi: 10.1016/j.cell.2013.10.031

Paşca, A. M., Sloan, S. A., Clarke, L. E., Tian, Y., Makinson, C. D., Huber, N., et al. (2015). Functional cortical neurons and astrocytes from human pluripotent stem cells in 3D culture. *Nat. methods* 12, 671–678. doi: 10.1038/nmeth.3415

Paşca, S. P. (2018). The rise of three-dimensional human brain cultures. *Nature* 553, 437–445. doi: 10.1038/nature25032

Pham, M. T., Pollock, K. M., Rose, M. D., Cary, W. A., Stewart, H. R., Zhou, P., et al. (2018). Generation of human vascularized brain organoids. *Neuroreport* 29, 588–593. doi: 10.1097/WNR.0000000000001014

Qian, X., Nguyen, H. N., Song, M. M., Hadiono, C., Ogden, S. C., Hammack, C., et al. (2016). Brain-region-specific organoids using mini-bioreactors for modeling ZIKV exposure. *Cell* 165, 1238–1254. doi: 10.1016/j.cell.2016.04.032

Quadrato, G., Nguyen, T., Macosko, E. Z., Sherwood, J. L., Min Yang, S., Berger, D. R., et al. (2017). Cell diversity and network dynamics in photosensitive human brain organoids. *Nature* 545, 48–53. doi: 10.1038/nature22047

Renner, M., Lancaster, M. A., Bian, S., Choi, H., Ku, T., Peer, A., et al. (2017). Self-organized developmental patterning and differentiation in cerebral organoids. *EMBO J.* 36, 1316–1329. doi: 10.15252/embj.201694700

Rubenstein, J. L. (2010). Three hypotheses for developmental defects that may underlie some forms of autism spectrum disorder. *Curr. Opin. Neurol.* 23, 118–123. doi: 10.1097/WCO.0b013e328336eb13

Saber, W. A., and Sahin, M. (2020). Recent advances in human stem cell-based modeling of tuberous sclerosis complex. *Mol. Autism* 11, 16. doi: 10.1186/s13229-020-0320-2

Sakaguchi, H., Kadoshima, T., Soen, M., Narii, N., Ishida, Y., Ohgushi, M., et al. (2015). Generation of functional hippocampal neurons from self-organizing human embryonic stem cell-derived dorsomedial telencephalic tissue. *Nat. Commun.* 6, 8896. doi: 10.1038/ncomms9896

Salpietro, V., Malintan, N. T., Llano-Rivas, I., Spaeth, C. G., Efthymiou, S., Striano, P., et al. (2019). Mutations in the neuronal vesicular SNARE VAMP2 affect synaptic membrane fusion and impair human neurodevelopment. *Am. J. Hum. Genet.* 104, 721–730. doi: 10.1016/j.ajhg.2019.02.016

Saxton, R. A., and Sabatini, D. M. (2017). mTOR signaling in growth, metabolism and disease. *Cell* 168, 960–976. doi: 10.1016/j.cell.2017.02.004

Schafer, S. T., Paquola, A., Stern, S., Gosselin, D., Ku, M., Pena, M., et al. (2019). Pathological priming causes developmental gene network heterochronicity in autistic subject-derived neurons. *Nat. Neurosci.* 22, 243–255. doi: 10.1038/s41593-018-0295-x

Scheffer, I. E., Berkovic, S., Capovilla, G., Connolly, M. B., French, J., Guilhoto, L., et al. (2017). ILAE classification of the epilepsies: position paper of the ILAE commission for classification and terminology. *Epilepsia* 58, 512–521. doi: 10.1111/epi.13709

Shiraishi, A., Muguruma, K., and Sasai, Y. (2017). Generation of thalamic neurons from mouse embryonic stem cells. *Development* 144, 1211–1220. doi: 10.1242/dev.144071

Song, L., Yuan, X., Jones, Z., Vied, C., Miao, Y., Marzano, M., et al. (2019). Functionalization of brain region-specific spheroids with isogenic microglia-like cells. *Sci. Rep.* 9:11055. doi: 10.1038/s41598-019-47444-6

Südhof, T. C. (2008). Neuroligins and neurexins link synaptic function to cognitive disease. *Nature* 455, 903–911. doi: 10.1038/nature07456

Sun, A. X., Yuan, Q., Fukuda, M., Yu, W., Yan, H., Lim, G. G. Y., et al. (2019). Potassium channel dysfunction in human neuronal models of Angelman syndrome. *Science* 366, 1486–1492. doi: 10.1126/science.aav5386

Tanaka, Y., Cakir, B., Xiang, Y., Sullivan, G. J., and Park, I.-H. (2020). Synthetic analyses of single-cell transcriptomes from multiple brain organoids and fetal brain. *Cell Rep.* 30, 1682–1689. doi: 10.1016/j.celrep.2020.01.038

Toma, K., Wang, T. C., and Hanashima, C. (2016). Encoding and decoding time in neural development. *Dev. Growth Differ.* 58, 59–72. doi: 10.1111/dgd.12257

Velasco, S., Kedaigle, A. J., Simmons, S. K., Nash, A., Rocha, M., Quadrato, G., et al. (2019). Individual brain organoids reproducibly form cell diversity of the human cerebral cortex. *Nature* 570, 523–527. doi: 10.1038/s41586-019-1289-x

Wang, W., Corominas, R., and Lin, G. N. (2019). De novo mutations from whole exome sequencing in neurodevelopmental and psychiatric disorders: from discovery to application. *Front. Genet.* 10:258. doi: 10.3389/fgene.2019.00258

Wataya, T., Ando, S., Muguruma, K., Ikeda, H., Watanabe, K., Eiraku, M., et al. (2008). Minimization of exogenous signals in ES cell culture induces rostral hypothalamic differentiation. *Proc. Natl. Acad. Sci. U.S.A.* 105, 11796–11801. doi: 10.1073/pnas.0803078105

Williams, S. M., An, J. Y., Edson, J., Watts, M., Murigneux, V., Whitehouse, A. J. O., et al. (2019). An integrative analysis of non-coding regulatory DNA variations associated with autism spectrum disorder. *Mol. Psychiatry* 24, 1707–1719. doi: 10.1038/s41380-018-0049-x

Willsey, A. J., Sanders, S. J., Li, M., Dong, S., Tebbenkamp, A. T., Muhle, R. A., et al. (2013). Coexpression networks implicate human midfetal deep cortical projection neurons in the pathogenesis of autism. *Cell* 155, 997–1007. doi: 10.1016/j.cell.2013.10.020

Xiang, Y., Cakir, B., and Park, I.-H. (2020a). Deconstructing and reconstructing the human brain with regionally specified brain organoids. *Semin. Cell Dev. Biol.* doi: 10.1016/j.semcdb.2020.05.023 [Epub ahead of print].

Xiang, Y., Tanaka, Y., Cakir, B., Patterson, B., Kim, K.-Y., Sun, P., et al. (2019). hESC-derived thalamic organoids form reciprocal projections when fused with cortical organoids. *Cell Stem Cell* 24, 487–497. doi: 10.1016/j.stem.2018.12.015

Xiang, Y., Tanaka, Y., Patterson, B., Hwang, S.-M., Hysolli, E., Cakir, B., et al. (2020b). Dysregulation of BRD4 function underlies the functional abnormalities of MeCP2 mutant neurons. *Mol. Cell.* 79, 84–98. doi: 10.1016/j.molcel.2020.05.016

Xiang, Y., Tanaka, Y., Patterson, B., Kang, Y.-J., Govindaiah, G., Roselaar, N., et al. (2017). Fusion of regionally specified hPSC-derived organoids models human brain development and interneuron migration. *Cell Stem Cell* 21, 383–398. doi: 10.1016/j.stem.2017.07.007

Xiang, Y., Yoshiaki, T., Patterson, B., Cakir, B., Kim, K.-Y., Cho, Y. S., et al. (2018). Generation and fusion of human cortical and medial ganglionic eminence brain organoids. *Curr. Protoc. Stem Cell Biol.* 47:e61. doi: 10.1002/cpsc.61

Yang, G., and Shcheglovitov, A. (2020). Probing disrupted neurodevelopment in autism using human stem cell-derived neurons and organoids: an outlook into future diagnostics and drug development. *Dev. Dyn.* 249, 6–33. doi: 10.1002/dvdy.100

Yoon, S.-J., Elahi, L. S., Paşca, A. M., Marton, R. M., Gordon, A., Revah, O., et al. (2019). Reliability of human cortical organoid generation. *Nat. Methods* 16, 75–78. doi: 10.1038/s41592-018-0255-0

Zhu, Y., Wang, L., Yu, H., Yin, F., Wang, Y., Liu, H., et al. (2017). In situ generation of human brain organoids on a micropillar array. *Lab Chip* 17, 2941–2950. doi: 10.1039/c7lc00682a

Zoghbi, H. Y., and Bear, M. F. (2012). Synaptic dysfunction in neurodevelopmental disorders associated with autism and intellectual disabilities. *Cold Spring Harb. Perspect. Biol.* 4:a009886. doi: 10.1101/cshperspect.a009886

Conflict of Interest: The authors declare that the research was conducted in the absence of any commercial or financial relationships that could be construed as a potential conflict of interest.

frontiers in Physiology

REVIEW
published: 04 November 2020
doi: 10.3389/fphys.2020.563981

Kidney Organoids as Disease Models: Strengths, Weaknesses and Perspectives

*Ricardo Romero-Guevara[1], Adonis Ioannides[1] and Christodoulos Xinaris[1,2]**

[1] University of Nicosia Medical School, Nicosia, Cyprus, [2] Istituto di Ricerche Farmacologiche Mario Negri IRCCS, Centro Anna Maria Astori, Science and Technology Park Kilometro Rosso, Bergamo, Italy

Chronic kidney disease is a major global health problem, as it affects 10% of the global population and kills millions of patients every year. It is therefore of the utmost importance to develop models that can help us to understand the pathogenesis of CKD and improve our therapeutic strategies. The discovery of human induced pluripotent stem cells (hiPSCs) and, more recently, the development of methods for the generation of 3D organoids, have opened the way for modeling human kidney development and disease *in vitro*, and testing new drugs directly on human tissue. In this review we will discuss the most recent advances in the field of kidney organoids for modeling disease, as well as the prospective applications of these models for drug screening. We will also emphasize the impact of CRISPR/cas9 genome engineering on the field, point out the current limitations of the existing organoid technologies, and discuss a set of technical developments that may help to overcome limitations and facilitate the incorporation of these exciting tools into basic biomedical research.

Keywords: stem cells, kidney, organoid, 3D cell culture, hiPSC, disease modeling

OPEN ACCESS

Edited by:
Eumorphia Remboutsika, National and Kapodistrian University of Athens, Greece

Reviewed by:
Konstantinos Zarbalis, University of California, Davis, United States
Cristina Porcheri, University of Zurich, Switzerland

****Correspondence:***
Christodoulos Xinaris
xinaris.c@unic.ac.cy;
christodoulos.xinaris@marionegri.it

Specialty section:
This article was submitted to Craniofacial Biology and Dental Research, a section of the journal Frontiers in Physiology

Received: *20 May 2020*
Accepted: *06 October 2020*
Published: *04 November 2020*

Citation:
Romero-Guevara R, Ioannides A and Xinaris C (2020) Kidney Organoids as Disease Models: Strengths, Weaknesses and Perspectives. Front. Physiol. 11:563981. doi: 10.3389/fphys.2020.563981

INTRODUCTION

Chronic Kidney Disease (CKD) is causing an emerging global healthcare crisis (Couser et al., 2011). 10% of the population worldwide is affected by this disease, and millions die each year because they do not have access to affordable treatment. CKD often leads to end stage renal disease (ESRD), for which patients require either hemodialysis or kidney transplantation in order to survive. However, both renal replacement therapies are insufficient: dialysis substitutes only a small percentage of renal function and does not correct the compromised endocrine functions of the kidney, while the usefulness of transplantation is limited by the shortage of donor organs and the subsequent need for lifelong immunosuppressive therapy. Considering the globally increasing prevalence and annual incidence of CKD, more efficient therapeutic options are urgently needed.

Being able to engineer human organoids in a dish would significantly improve our ability to cure and manage kidney diseases, and fundamentally change the way we conduct biomedical research. First, it would allow scientists to study the disease and explore new therapies directly on human tissue, which would significantly improve the translatability of candidate drugs. Second, organoids could be used to model normal human development and diseases in a personalized manner. Finally and most importantly, organoids could be used in replacement therapies, which would make possible the unlimited production of transplantable tissues and would solve the problem of organ shortages once and for all. However, how far organoids are from fulfilling these expectations remains unclear because of significant technical limitations.

In this paper we will provide an overview of the current progress in the field of kidney organoids, with specific emphasis on the use of organoids for disease modeling and drug testing. We will also discuss how the current organoid technologies can be exploited, analyze the existing limitations, and propose technical improvements that may help to overcome limitations and ultimately facilitate the incorporation of these exciting tools in biomedical research.

THE STRENGTHS OF KIDNEY ORGANOIDS

Organoids have significant advantages compared with animal models and traditional 2D cultures. First, compared with animal models, organoids allow more opportunities for experimental manipulations, as they are isolated multicellular systems, are amenable to real-time imaging techniques, and, most importantly, enable the study of human developmental processes and pathogenetic pathways that are not easily or accurately replicated in animal models (**Figure 1**). Compared with monolayer traditional cultures, organoids contain more than one cell type. This enables more "physiological" modeling, as they can replicate various aspects of the disease, especially when the pathogenesis involves interactions between different cell types – as commonly occurs in kidney diseases. Normal renal function depends not only on cellular homeostasis, but also critically depends on the architecture of both the individual cells and the organ. The nephrons (the filtering units of the kidney) work through a complex multi-step process, which involves a specialized microvascular bed (containing fenestrated endothelial cells, highly specialized podocytes, and mesangial cells) that produces the primary filtrate, and an epithelial tubule that returns needed substances to the blood and pulls out additional waste. Studying the mechanisms (or even only some aspects of the mechanisms) governing these processes would require multicellular systems with a high degree of organization. For instance, classic 2D cultures could not model certain glomerulopathies as efficiently as organoids because of the multifactorial etiopathogenesis of the disease, which involves interactions between these different cell types and alterations in tissue organization. Thus, it is sound to assume that the more an experimental model replicates the above processes, the more efficient it would be for modeling human diseases and more reliable mechanistic studies. Therefore in view of the complexity of the kidney, organoids are the most complete *in vitro* experimental model that is currently available.

Importantly, organoid cells maintain genome stability and phenotype better compared with primary cultures, which makes them suitable for biobanking and high-throughput screens. Organoids display a higher degree of organization, specialization and maturation compared to their 2D culture counterparts. For instance, it has been shown that tubular cells in organoids mature sufficiently to uptake fluorescent dextrans from the

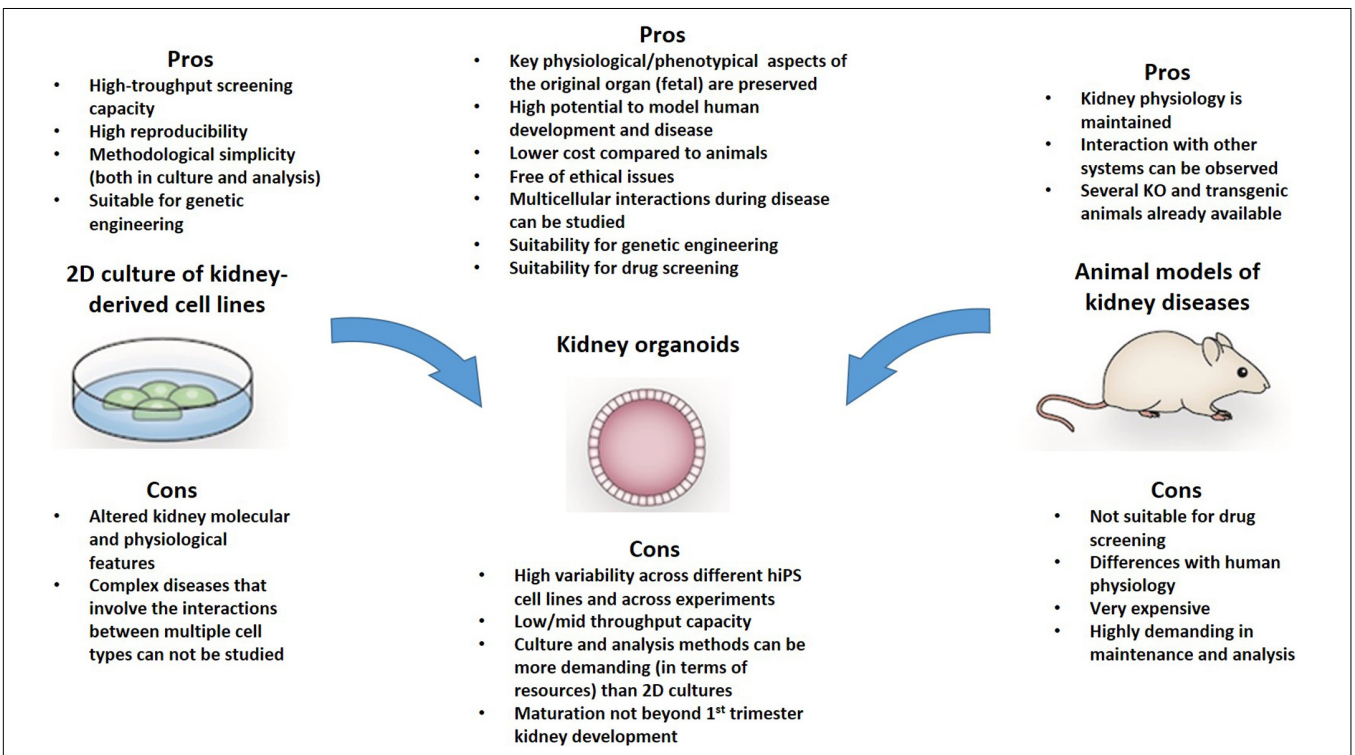

FIGURE 1 | The Pros and cons of kidney organoids for modeling human disease are highlighted in this figure. It is possible that some of the limitations of this system may be overcome with modern technics for miniaturization and culture in microfluidic devices that allow a physiological assessment of podocytes and tubular cells.

lumen of tubules (Freedman et al., 2015; Takasato et al., 2015; Li et al., 2016), in contrast with the loss of cellular polarity and low or absent expression of drug transporters observed in immortalized kidney tubular cell lines (Jenkinson et al., 2012; Nieskens and Sjogren, 2019). In fact, a comparison of primary cultures of proximal tubular epithelial cells, immortalized kidney cell lines and renal tissue showed that several enzymes and receptors that are involved in the xenobiotic metabolism are missing from cultured cells (Van Der Hauwaert et al., 2014). The expression of these metabolic genes plays an important role in tubular function and nephrotoxicity, and this lessens the applicability and robustness of cell culture models in toxicity screens. Moreover, primary cultures of tubular cells exhibited limited proliferation capacity, while the expression of drug metabolism genes decreases quickly during culture (Lash et al., 2008), limiting their application in drug screening.

Significant advances have also been made in attempts to generate glomeruli from hiPSCs. Several studies have shown that podocytes in organoids are organized in glomerular structures containing endothelial cells, and nephrin-positive podocytes with immature foot process and apico-basal polarity of tight junction proteins (Kim et al., 2017; Yoshimura et al., 2019), as well as having a basic filtering capacity when transplanted *in vivo* (Van Den Berg et al., 2018). Another important feature of organoids – that is particularly useful for toxicity studies and disease modeling – is their ability to respond to stress by expressing and/or releasing injury markers in specific cell types, as observed in kidney tissue. For example, in hiPSC-organoids treated with gentamycin or cisplatin, KIM1 was specifically expressed in tubular epithelial cells (Freedman et al., 2015; Morizane et al., 2015). Interestingly, LTL + cells also expressed cleaved caspase 3 (CASP3) following cisplatin treatment, and this effect was only observable in proximal tubular cells of day 18 organoids and not at earlier time points or in other cell types (Takasato et al., 2015). Altogether, these features highlight the higher level of maturity of organoids vs. traditional 2D culture models, which can be exploited for disease modeling, drug screening and toxicological studies.

Nowadays, there are several protocols for generating kidney organoids using embryonic stem cells (ESCs) or hiPSCs that can be derived from patients or healthy donors. These protocols include one or more steps of Wnt activation (by CHIR99021) and a cocktail of secreted factors that can yield organoids with various kidney structures and cell types (**Table 1**; Taguchi et al., 2014; Taguchi and Nishinakamura, 2017; Howden et al., 2019).

Alternatively organoids can also be derived from embryonic kidney progenitors (Xinaris et al., 2012) or adult tissue cells (Schutgens et al., 2019). Interestingly, the recently developed protocols for the generation of tubuloids from Wilms tumors allowed for the establishment of an organoid biobank for childhood kidney cancers and identifying patient-specific drug sensitivities (Calandrini et al., 2020). In addition, with the emergence of genome engineering technologies such as CRISPR/Cas9, hiPSCs can be modified to introduce

TABLE 1 | Main protocols for generating kidney organoids from human pluripotent stem cells: differentiation stages and times, and characterization of final observed cells.

Kidney organoid differentiation protocols

References	Differentiation stages	Length	Cells obtained
Melissa H. Little group Takasato et al., 2014; Takasato et al., 2015; Forbes et al., 2018; Howden et al., 2019	Induction of primitive streak through CHIR99021, followed by FGF9 treatment to induce intermediate mesoderm and MM, plus 3D culture for generating organoids.	18–24 days	Proximal and distal tubule cells, podocytes, and collecting duct cells.
Nishinakamura group Taguchi et al., 2014; Taguchi and Nishinakamura, 2017; Yoshimura et al., 2019	The protocol starts with the formation of embryoid bodies in the presence of BMP4, followed by early mesoderm induction with Activin and Fgf2, and then a cocktail of BMP4, CHIR99021, Retinoic acid to induce intermediate mesoderm and MM. NPCs were then expanded with Fgf9 and CHR99021. For nephron maturation, 3D aggregation and coculture with mouse embryonic spinal cord was used. For inducing the ureteric bud specifically, after the initial mesoderm induction cells were treated with blockers of BMP/Activin signaling LDN193189 and SB43152. In both protocols UB or MM progenitors are sorted for further maturation in 3D culture.	22 days	Glomeruli with podocytes, proximal and distal tubule cells. In Taguchi and Nishinakamura, 2017, UB-derived collecting duct cells were generated.
Izpisua-Belmonte group Xia et al., 2014; Li et al., 2016; Low et al., 2019	These protocols are composed of an initial stage in monolayer with intermittent CHIR99021 treatment to induce intermediate mesoderm, followed by Fgf9 and CHIR99021 for NPCs induction. Then in a second stage, 3D culture of sorted SIX2 + NPCs with Fgf9 and CHIR is maintained, followed by basal media without growth factors. Ureteric bud differentiation is induced by monolayer culture in Fgf2 and Bmp4, followed by Bmp2, Activin A and retinoic acid.	21 days	Glomeruli with podocytes, proximal and distal tubule cells, as well as endothelial cells.
Bonventre and Freedman group Freedman et al., 2015; Morizane et al., 2015; Morizane and Bonventre, 2017	Primitive streak is induced by CHIR treatment in monolayer culture. Then Activin is added to induce intermediate mesoderm, and NPCs are expanded at the presence of Fgf9. Finally cells are aggregated and cultured for 3 days at the presence of Fgf9 and CHIR99021, and then switched to basic media without growth factors and inhibitors.	28–35 days	Podocytes, proximal and distal tubule like cells were observed.
Przepiorski et al., 2018	This protocol is based on the formation and growth of embryoid bodies from hiPSCs, in a bioreactor culture system, The only supplemented used is CHIR99021. The expansion of NPCs within the embryoid bodies is achieved with Knockout serum replacement media instead of Fgf9 as the majority of the differentiation protocols.	14–26 days	Podocytes, proximal and distal tubules, and stromal cells.

disease-specific mutations, correct them, or introduce genetic reporters that are useful for drug screening. Given all these achievements, it is reasonable to ask how we can we use kidney organoids in routine biomedical research.

CURRENT APPLICATIONS

The nearest use of kidney organoids in biomedical research is for studying the mechanisms of kidney diseases, drug discovery and toxicological studies. Despite the great interest in using organoids for disease modeling, so far few human diseases have been successfully modeled in kidney organoids. Nevertheless, the examples described below suffice to provide concrete proof-of-concept for the potential of kidney organoids in biomedical research.

Disease Modeling

Ciliopathies

In one of the earliest examples of using organoids to model polycystic kidney disease (PKD), Freedman et al. (2015) knocked out the *PKD1* and *PKD2* genes in hiPSCs using CRISPR/Cas9 genome editing technology and used these cells to construct kidney organoids. After 35 days in culture, cysts spontaneously formed within the tubules of biallelic *PKD1*-/-, *PKD2*-/- hiPSCs-derived organoids but not in isogenic controls, validating the organoid culture to model PKD. One limitation of this study was the low frequency of cystogenesis (only 6% of organoids developed cysts). In a follow-up study, cystogenesis was improved (up to 75% of organoids developed cysts) by growing organoids in suspension culture compared to adherent conditions (Cruz et al., 2017). Organoids may also help unravel the complex molecular and cellular events that underlie the pathogenesis of PKD and, in doing so, help identify novel targets for disease modulation and therapy. The same group adapted this platform to identify modifiers of PKD, and showed that the non-muscle myosin II inhibitor blebbistatin promotes cystogenesis in this disease model, potentially implicating the myosin pathway and the regulation of actin-myosin activation in these conditions (Czerniecki et al., 2018). In many cells, non-muscle myosin has been involved in adhesion, cell polarity, migration and endocytosis and exocytosis but its specific function in tubular cells has not been elucidated yet (Noris and Remuzzi, 2012). Thus, this study is a paradigm of how these tools can be used to investigate novel aspects of the pathogenesis of as complex a genetic disease as PKD (Czerniecki et al., 2018).

Although gene-edited knockout (KO) hiPSCs exhibited a remarkable ability to form cysts, PKD patient-derived hiPSCs exhibited dramatic line-to-line variability in their abilities to form organoids containing cysts, regardless of PKD genotype and organoid differentiation protocol (Cruz et al., 2017). The morphology of tubular structures also varied noticeably between different lines. Nonetheless in a recent publication, the same group also generated hiPSCs from a patient affected by autosomal recessive PKD (ARPKD). As with PKD KO cells, the ARPKD patient-derived organoids also developed cysts upon exposure to cAMP agonists (Low et al., 2019), proving the concept for modeling PKD in the same genotype as the patient. It remains to be seen if such a culture methods can also efficiently induce cystogenesis in other genotypes from different patients.

Establishing robust protocols for the generation of kidney organoids from hiPSCs of patients with Autosomal Dominant PKD (ADPKD) could create an excellent opportunity to study genotype-phenotype correlation. The majority of cases of ADPKD are caused by pathogenic mutations in the *PKD1* gene and these patients have, on average, an earlier age at diagnosis and onset of ESRD than patients with *PKD2*-associated ADPKD. It is worth noting that there is variation in disease severity amongst patients with different *PKD1* mutations. In keeping with their loss-of-function effect, truncating mutations cause more severe disease compared to non-truncating ones and there is variation within the latter group, depending on the impact on protein structure and function (Heyer et al., 2016; Hwang et al., 2016). More severe disease, including embryonic lethality, intrauterine onset of cystogenesis and diagnosis in childhood, can be caused by biallelic mutations in either the *PKD1* or *PKD2* genes. Personalized genotype-specific organoids will be of crucial significance for studying the molecular mechanisms that govern the different clinical phenotypes, and developing self-tailored approaches to disease monitoring and management.

Other mutations that are associated with the formation of renal cysts have also been studied in hiPSC-derived kidney organoids. Przepiorski and colleagues generated hiPSCs-derived kidney organoids with point mutations to knockout *HNF1B* that could phenocopy nephron defects observed in *Hnf1b* conditionally deficient mice. Nevertheless, these organoids did not develop renal cysts (as happen in $Hnf1b^{-/-}$ mice and individuals with heterozygous mutations in *HNF1B*) highlighting the key phenotypical and mechanistic differences between organoid models and the *in vivo* patho-biology of the disease (Przepiorski et al., 2018).

Another recent example in which a congenital disease has been modeled in organoids is a case of IFT140 nephronophthisis-related ciliopathy (Forbes et al., 2018). In this study, the authors generated hiPSC-derived organoids from a patient with *IFT140* mutations and isogenic mutation-corrected hiPSCs, and showed that *IFT140* mutations can cause defects in primary cilia and alter apico-basal polarity in tubular cells. Interestingly, these alterations were consistent with ciliary defects observed earlier in *Ift140* knockout mouse (Miller et al., 2013).

Mucin 1 Kidney Disease

Proteinopathies are caused by the intracellular accumulation of misfolded proteins, activating several stress response pathways, such as unfolded protein response (UPR), endoplasmic reticulum stress and ultimately cell death. One of such pathologies, mucin1 kidney disease (MKD), is the result of a frame shift mutation in the *MUC1* gene (*MUC1-fs*), which introduces a premature stop codon and leads to the synthesis of a shortened mutant protein that is accumulated in the cytoplasm (Kirby et al., 2013). Greka's lab recently used complementary organoid and *in vivo* models to study this proteinopathy, and demonstrated an intracellular accumulation of mutant MUC1 transmembrane protein in tubular cells of mutant transgenic mice, as well as

in human MKD samples and hiPSC-derived organoids from patients (Dvela-Levitt et al., 2019). In addition, the effectiveness of the BRD4780 compound, selected from a primary screen using mutant *MUC1-fs* immortalized tubular epithelial cells, was demonstrated in the three experimental models by targeting mutant protein to lysosomal degradation.

Podocytopathies

Another important milestone has been the use of patient-derived organoids to study the pathogenesis of congenital nephrotic syndrome. In the Tanigawa et al. (2018), hiPSC-derived organoids from a patient with nephrotic syndrome caused by *NPHS1* mutations were transplanted under the kidney capsules of immunodeficient mice and used to study and identify slit diaphragm abnormalities in podocytes. Moreover, the use of CRISPR/cas9 gene editing technology to correct the *NPHS1* mutation restored the podocyte transcriptional profile and rescued the disease phenotype. hiPSC-derived organoids have also been used to model *NPHS1*-related nephrotic syndrome in the study by Hale et al. (2018) and revealed hyperthrophied podocytes cell bodies and reduced levels of the podocytes proteins nephrin and podocin (Hale et al., 2018).

hiPSC-derived organoids have also been used to study the role of podocalyxin in kidney development (Freedman et al., 2015; Kim et al., 2017). Podocalyxin is important for maintaining the foot process, and knockout mice die soon after birth (Doyonnas et al., 2001). In human organoids, it was shown that podocalyxin plays an important role in providing a negative charge to the cell surface of podocytes that is necessary for epithelial lumen formation and the organization of the podocyte's tight junctions, and it is necessary for microvilli formation (Freedman et al., 2015; Kim et al., 2017). Interestingly, key structural alterations in podocalyxin-deficient mice are partially phenocopied in human kidney organoids with defective podocalyxin, stressing the similarity between organoids and *in vivo* system. It should be pointed out, however, that null mutations in the *PODXL* gene have not been definitively associated with human kidney disease, though a missense variant of unknown significance that affects the podocalyxin transmembrane domain has been identified in a family with focal and segmental glomerulosclerosis (Barua et al., 2014). Still, existing data suggest that kidney organoids can be used to study the role of podocalyxin in normal organogenesis and *PODXL*-associated developmental defects. A summary of the human diseases modeled in organoids is presented in **Table 2**.

Nephrotoxicity Testing

Kidney organoids can potentially be used in toxicological studies as well (**Table 3**). Unlike classic kidney cell lines, organoids can provide a platform for evaluating the different responses of the various cell types simultaneously and following secondary intercellular responses after nephrotoxic injuries. In addition, the higher level of maturity of organoids compared to immortalized cell lines, allow us to obtain more physiologically relevant data. For example, nephrotoxic drugs such as cisplatin, which mainly target the proximal tubules *in vivo*, have also shown specific toxicity for proximal tubular cells in organoids (Freedman et al., 2015; Morizane et al., 2015). Moreover, tubular toxicity was stronger in organoids at day 18 than in less mature organoids on

TABLE 2 | The main outcomes, limitations and future perspectives of the hiPSCs-derived organoids models of kidney diseases are described.

Kidney organoid models of disease

Model-disease type and references	Outcomes	Limitations and challenges	Future perspectives
Mucin 1 kidney disease (MKD) Dvela-Levitt et al., 2019	Human iPSC-derived organoids from MKD patients exhibited Muc1 protein mislocalization in tubular cells. Organoid cells responded to the drug BRD90 in a similar manner as in mouse models and patients with MKD.	No functional assays, such as tubular absorption, were carried out in MKD organoids.	Developing semi-automated culture systems and analysis approaches can make this system a valuable drug testing tool for MKD.
Polycystic kidney disease (PKD) Freedman et al., 2015; Cruz et al., 2017; Czerniecki et al., 2018; Low et al., 2019	These human organoids from PKD1/PKD2 KO hiPSCs extensively formed cysts *in vitro* and can be adapted to high-throughput screening. Using this culture format, a potential involvement of non-muscle myosin in cystogenesis was identified.	PKD patient-derived hiPSCs did not sufficiently form cysts, hampering the application of this organoid system to study the genotypes of patients.	Optimizing culture conditions to induce cysts in patient-derived organoids will provide a highly useful assay for studying disease pathogenesis and developing personalized therapeutic strategies.
ITF40 Nephronophthisis ciliopathic renal disease Forbes et al., 2018	Somatic cells from a patient with compound heterozygous mutations in *IFT140* were reprogrammed and corrected with CRISPR/Cas9. Primary cilia and apico-basal defects were observed in tubular cells of patient-derived kidney organoids but not in gene-corrected isogenic controls.	Primary cilia and spheroid polarity defects were not present in all organoids, which limits the potential use of the system in drug screening applications.	Generation of iPSC-derived organoids from patients with different mutations in NPHP genes will help to elucidate the mechanisms of Nephronophthisis pathogenesis and explain the differences between the clinical phenotypes.
Podocalyxin deficiency Kim et al., 2017	Knockout of podocalyxin demonstrated its importance for microvilli formation and podocyte spacing. Podocalyxin-KO organoids phenocopied, to some degree, the pathological features of the kidney in podocalyxin knockout mice, validating the use of organoids for understanding human podocyte development.	Podocalyxin deficiency is not compatible with life, and newborns with such defects are rarely reported. Therefore, although podocalyxin-deficient organoids can be used to study the role of podocalyxin in early steps of organogenesis, are less useful for studies in adult human diseases.	A mutation variant of unknown significance in *PODXL* has been identified in humans, the generation of patient-specific hiPSCs and their differentiation could be a valuable tool to investigate the pathogenesis of *PODXL* mutations in humans.

TABLE 3 | The proof-of-concept studies in which hiPSCs-derived kidney organoids have been developed as potential models for nephrotoxicity and drug screening are presented, highlighting the main outcomes, limitations and future areas of improvement for these models.

Drug screening and toxicity assays applications of kidney organoids			
Organoid application/references	**Outcomes**	**Limitations and challeges**	**Future perspectives**
Genetic reporters for podocyte differentiation and toxicity Sharmin et al., 2016; Borestrom et al., 2018; Hale et al., 2018; Vanslambrouck et al., 2019; Yoshimura et al., 2019	The use of genome editing made it possible to knock in fluorescent proteins in the NPHS1 and MAFB loci. Their expression during podocyte differentiation in organoids was used to improve differentiation conditions and to establish a proof of concept for doxorubicin and PAN nephrotoxicity studies.	These studies did not carry out functional assays in podocytes following PAN and doxorubicin treatment.	These reporter cell lines could be shared through an international repository to accelerate the use of organoids in toxicology and drug screening. More sensitive reporters of podocyte damage could be developed with CRISPR/Cas9, to mark, for example, alterations on the localization of slit diaphragm proteins, and not only the total fluorescence. These lines could also be combined with microfluidic devices to generate more physiological models of podocyte and drug-induced toxicity.
Toxicity assays in organoid-derived tubular cells Freedman et al., 2015; Morizane et al., 2015; Takasato et al., 2015	In Morizane's and Freedman's work, KIM1 was upregulated in proximal and distal tubular cells of hiPSC-organoids in response to gentamycin and cisplatin treatment. KIM1 mRNA expression was upregulated in a dose-dependent manner. In Takasato's work the activation of CASP3 was observed specifically in tubular cells following cisplatin exposure.	These organoid protocols have not been tested in a high-throughput toxicology setting. Additional iPSC lines and nephrotoxic agents and different iPSC lines are needed to validate the reproducibility of the protocols. Drug transporters will need to be analyzed (qualitatively and quantitatively) to assess similarities and differences with *in vivo* models.	To improve the applicability of organoids in toxicology, KIM1 reporter hiPSC lines could be generated to allow real-time observation of acute kidney injury and drug effect. Tubules assembled in microfluidic devices could also improve some structural functional features of tubular cells that are important for the toxic injury and repair response.

day 11 (Takasato et al., 2015). These data suggest that organoids could be used to study the differential effect of nephrotoxic drugs on renal cells on the basis of their phenotypical (functional and structural) characteristics and differentiation state.

As with tubular cells hiPSC-derived podocytes in organoids are more similar to human podocytes than immortalized podocyte cell lines (Hale et al., 2018; Yoshimura et al., 2019). Gene expression analysis shows that immortalized cell lines lack important mature podocyte markers, have decreased functional capacities, such as albumin uptake, and decreased sensitivity to doxorubicin insult compared with hiPSC-derived podocytes (Musah et al., 2017; Rauch et al., 2018; Yoshimura et al., 2019). In addition, 3D culture of glomeruli-enriched organoids induces the expression of genes associated with slit diaphragm, renal filtration function and glomerular development compared with differentiated immortalized cell lines (Hale et al., 2018). These features make organoids potential candidates for podocyte toxicity studies and functional assays. To this end, the Little group knocked in a fluorescent reporter *BFP2* under the control of the podocyte marker *MAFB* in hiPSCs to generate glomeruli-enriched organoids, which were used to establish a model of doxorubicin-induced toxicity – a classical nephrotoxic drug that causes glomerular damage *in vivo* (Hale et al., 2018) – that allowed for fluorescence-based evaluation of toxicity in a dose-dependent manner.

In a similar approach Nishinakamura group (Yoshimura et al., 2019), used a NPHS1-GFP reporter cell line to optimize the differentiation conditions toward podocyte organoids and to perform toxicity studies. Puromycin aminonucleoside (PAN)-treated podocytes exhibited a significant and specific reduction of slit diaphragm proteins NEPH1 and Podocin at sub-lethal doses, while other podocyte markers remained unchanged, showing that organoid can be used to evaluate podocyte-specific drug toxicity.

In summary, the above studies highlight the potential of kidney organoids for toxicological screening of both tubular and glomerular structures. It is important to mention that 9% of safety failures of new drugs can be attributed to kidney toxicity in humans (Cook et al., 2014). Using human organoids for preclinical toxicity studies may increase the likelihood of candidate drugs succeeding in the clinical setting and at the same time reduce the costs of drug development.

Nonetheless, in order to fully exploit the organoid system in toxicity screens, it is necessary to generate large panels of organoids in an automated and miniaturized format. In a model of PKD, Czerniecki et al. (2018) provided proof-of-concept of how an organoid disease model can be adapted for drug screening. However, when miniaturizing their cultures, they observed a decrease in cystogenesis (20–40%) compared with their previous large-scale culture conditions (75%), highlighting the challenges of adapting organoid models into efficient drug screening formats. A summary of the different organoid toxicity assays is presented in **Table 3**.

THE WEAKNESSES OF KIDNEY ORGANOIDS

Although organoids have significant advantages compared with classical cultures, they still have crucial insufficiencies when compared to the original organs (Xinaris, 2019). Organoids lack vasculature. This means that they are limited in terms of how much they can grow without cell death. However, following transplantation under the mouse kidney capsule, hiPSC-derived

organoids have shown signs of growth, integration with the host circulatory system and further maturation, including the formation of the glomerular basement membrane (GBM), and maturation of the slit diaphragm in podocytes and brush border in tubular cells (Van Den Berg et al., 2018). Notably, hiPSC-derived organoids do not mature as well as transplanted embryonic kidney primordia (Rogers and Hammerman, 2004; Xinaris et al., 2012, 2016; Imberti et al., 2015). In addition, organoids also lack immune cells and therefore cannot be used to study processes that require this key component of human physiology, such as the inflammatory responses accompanying many nephropathies.

In addition, there are important defects in the cell composition of lab-grown organoids compared to the original organs. For example, in the analysis performed by Wu and collaborators using RNA sequencing, it was shown that organoids contain 10–20% off-target cells, such as neurons. The amount of each kidney cell type significantly varies according to the cell line and protocol that were pursued to generate organoids (Wu et al., 2018). According to Wu's findings, the podocyte cluster was approximately 4% following Takasato's differentiation protocol (Takasato et al., 2015), while 28% of cells were podocytes when Morizane's was used (Morizane et al., 2015). Therefore, the efficiency and reproducibility of the differentiation protocol to produce specific cell types such as podocytes is an important aspect to consider when modeling human disease.

Another important limitation of kidney organoids is the limited ability to grow and mature *in vitro*. Several studies using single-cell RNA sequencing and immunofluorescence of kidney markers have shown that organoids do not mature further than an embryonic kidney does during the first trimester, even if maintained for long periods in culture (Takasato et al., 2015; Kim et al., 2017; Wu et al., 2018). This could be a limitation when aiming to model adult-onset diseases with organoids.

As existing culturing methods cannot faithfully replicate *in vivo* organogenesis conditions, organoids display important anatomic and structural insufficiencies. Organoids floating in media or embedded in artificial matrices *in vitro* lack the normal directional cues (both biochemical and mechanical) that drive the correct organization of cells within the organ. As a result, when kidney organoids self-assemble, tissues are developed somewhat randomly throughout the organoids. When the ureteric bud (UB; the precursor of the kidney's collecting duct system) is absent or has developed randomly, the cortical-medullary differences in tissue organization that would normally be imposed by such a tree are missing. Anatomic malformations observed in human pluripotent stem cell-derived organoids, such as nephron-nephron connections and multi-branched nephrons may, in fact, be associated with this deficiency.

Important steps to generate more physiological kidney organoids have recently been taken, by differentiating UB progenitors and metanephric mesenchyme (MM; which gives origin to glomeruli and tubules) simultaneously or assembled in the same cell aggregate (Takasato et al., 2015; Taguchi and Nishinakamura, 2017). Since both populations of progenitors are derived from the intermediate mesoderm, Takasato et al. (2015) developed a differentiation protocol in which both UB and MM are generated in the same culture by varying the length of exposure to the Wnt agonist CHIR99021 and FGF9. They showed that these two populations gave rise to highly complex organoid structures composed of collecting ducts (GATA3+), nephron segments (podocytes, distal and proximal tubular cells), as well as endothelial and interstitial cells (Takasato et al., 2014, 2015). However, in later studies, Wu and collaborators (Wu et al., 2018) raised doubts about the presence of UB in these organoids. Based on a comparison of GATA3 clusters with adult kidney cell types, Wu concluded that GATA3 cells in Takasato's organoids are metanephric mesenchyme-derived distal tubular cells rather than UB progenitors. More recently, Nishinakamura's team took an important step toward solving the "UB hard problem" (Taguchi and Nishinakamura, 2017). The authors integrated UB and MM-derived cells into a 3D culture system to construct a quasi-physiological kidney organoid. Remarkably, branching morphogenesis of ureteric bud progenitors was observed and, when combined with nephron progenitor cells (NPCs), those cluster around the tips of the developing collecting-tree. Nonetheless, the branching morphogenesis of the collecting tree was more elaborated using mouse embryonic stem cells (mESC)-derived cells than in hiPSCs, stressing the differences between species and the need for further optimization when adapting the culture conditions from one cell type to the other (Taguchi and Nishinakamura, 2017).

Finally, hiPSC-derived organoids display commensurately high variability. Variability in organoids exists at many levels—between different starting cell lines or clones, between different genotypes, between batches of organoids, or even between areas of the same organoid itself (because of different local mircro-environmnets). Evaluation of the variability of organoids made by Takasato's protocol showed that, although individual organoids are transcriptionally correlated, there is a significant variation between experimental batches, particularly in genes associated with temporal maturation (Phipson et al., 2019).

The variability across different cell lines or across different organoid preparations plagues the development of the organoid field because it limits its potential to incorporate other technologies, including computational science and bioengineering, which are required for developing high-throughput systems and mathematical models that can be used for phenotypic, toxicological and drug screens. Protocols for generating organoids are based on the knowledge of kidney development, but the accurate timing and amount of the different signaling molecules that are required for correct organogenesis remain mainly empirical. In order to better understand the *in vitro* development of organoids and to improve differentiation conditions, different research teams have generated reporter cell lines to observe in real-time the activation of specific developmental programs and renal cell markers (Kim et al., 2017; Vanslambrouck et al., 2019; Yoshimura et al., 2019). Using these tools, we could control the differentiation process by providing the appropriate spatiotemporal cues necessary for the efficient induction of specific cell types, tissue organization and maturation. This work can be further facilitated by CRISPR/Cas9 gene editing technology. Genome engineering is likely to be very useful for demystifying key mechanisms of

human kidney organogenesis, as it will allow the generation of knockout lines, correct mutations in patient-derived hiPSCs, and a multitude of gene expression reporters. In addition, the use of CRISPR/Cas9 can facilitate the generation of reporter hiPSC lines (Sharmin et al., 2016; Borestrom et al., 2018; Howden et al., 2019; Vanslambrouck et al., 2019), which could be used to study developmental mechanisms, quantitatively the nephrotoxicity, de-differentiation of renal cells, fibrosis and other injury-associated molecular changes.

KEY TECHNICAL MILESTONES TO BE ACHIEVED

This review so far highlighted the advantages of kidney organoids for disease modeling and drug discovery, but also the challenges that must be addressed. We will now discuss a set of key technical milestones that in our opinion can help to circumvent the existing limitations, and strengthen organoids' potential in biomedical research.

The first will be the generation of more hiPSC lines covering a wide range of kidney diseases, from genetic to sporadic diseases, postnatal to late onset diseases. Increasing the repertoire of disease-specific organoids will allow us to understand the role of the genotype in the disease process, and to uncover whether common or divergent disease mechanisms exist in patients with the same diagnosis and different genetic background. Moreover, by integrating high content analysis technologies such as RNA-seq and proteomics into organoid technologies we could identify the molecular networks that are altered in disease and govern organogenesis.

The implementation of microfluidic devices and microfabrication are a technological milestone that will help in the maturation of the organoid system. Homan et al., for instance, have shown that growing organoids in microfluidic devices increases the size of kidney organoids compared to static culture conditions (Homan et al., 2019). Chips designed to emulate tubular absorption *in vitro* have also been engineered (Weber et al., 2016; Vedula et al., 2017); these chips can be very useful for studying tubulogenesis and tubular function and testing drugs. Similar devices have recently been constructed to replicate glomerular filtration using different types of podocytes and endothelial cells (Petrosyan et al., 2019). If these technological improvements are combined with the advances made in the generation of podocyte-enriched organoids (Hale et al., 2018; Yoshimura et al., 2019), more physiological models of nephrons could be established on a larger scale for drug screening.

Bioengineering and 3D bioprinting approaches can be used to guide engineered tissues to pattern, differentiate and morph into more realistic organoids. Moreover, bioengineering the structural and physiological features that are necessary for modeling specific aspects of the organ separately can significantly minimize the inherent variability of self-organizing systems and facilitate the development of robust human models for comparative and quantitative drug testing studies. Indeed, three-dimensional printed polydimethylsiloxane (PDMS) scaffolds have been successfully used to grow complex kidney tubules with predefined architectures with remarkable reproducibility (Benedetti et al., 2018). This system was used to engineer patient-specific tubules, to model PKD and test drug efficacy, and to identify new therapeutic compounds for PKD. Moreover, this system has been applied to construct UB-like tubules from healthy individuals and a patient with a *PAX2* mutation and to study normal UB developmental processes and patient-specific defects. A different approach has shown that the local application of signals (e.g., bead-releasing morphogenetic factors) (Mills et al., 2017) or technical manipulations of engineered tissues (e.g., assembly of previously engineered organ component tissues) (Taguchi and Nishinakamura, 2017) could be used to add key missing information to self-organizing tissue to produce more anatomically realistic organoids.

In summary, the technological advances taking place in the organoid field, such as the generation of gene expression reporters, the increasing number of patient-derived hiPSC lines, the construction of microdevices to better mimic kidney function, bioengineering methods, are very promising developments for the study of kidney diseases and drug screening.

AUTHOR CONTRIBUTIONS

All authors contributed equally to the design and writing of this work.

FUNDING

This work was co-funded by the European Regional Development Fund and the Republic of Cyprus through the Research and Innovation Foundation (Project: POST-DOC/0916/0109). CX research is also funded by Euronanomed (an ERA-NET grant; 736/8221).

ACKNOWLEDGMENTS

The authors wish to thank Rubina Novelli for comments on the text and Kerstin Mierke for excellent editing work on the manuscript.

REFERENCES

Barua, M., Shieh, E., Schlondorff, J., Genovese, G., Kaplan, B. S., and Pollak, M. R. (2014). Exome sequencing and in vitro studies identified podocalyxin as a candidate gene for focal and segmental glomerulosclerosis. *Kidney Int.* 85, 124–133. doi: 10.1038/ki.2013.354

Benedetti, V., Brizi, V., Guida, P., Tomasoni, S., Ciampi, O., Angeli, E., et al. (2018). Engineered kidney tubules for modeling patient-specific diseases and drug discovery. *EBioMedicine* 33, 253–268. doi: 10.1016/j.ebiom.2018.06.005

Borestrom, C., Jonebring, A., Guo, J., Palmgren, H., Cederblad, L., Forslow, A., et al. (2018). A CRISP(e)R view on kidney organoids allows generation of an induced

pluripotent stem cell-derived kidney model for drug discovery. *Kidney Int.* 94, 1099–1110. doi: 10.1016/j.kint.2018.05.003

Calandrini, C., Schutgens, F., Oka, R., Margaritis, T., Candelli, T., Mathijsen, L., et al. (2020). An organoid biobank for childhood kidney cancers that captures disease and tissue heterogeneity. *Nat. Commun.* 11:1310. doi: 10.1038/s41467-020-15155-6

Cook, D., Brown, D., Alexander, R., March, R., Morgan, P., Satterthwaite, G., et al. (2014). Lessons learned from the fate of AstraZeneca's drug pipeline: a five-dimensional framework. *Nat. Rev. Drug Discov.* 13, 419–431. doi: 10.1038/nrd4309

Couser, W. G., Remuzzi, G., Mendis, S., and Tonelli, M. (2011). The contribution of chronic kidney disease to the global burden of major noncommunicable diseases. *Kidney Int.* 80, 1258–1270. doi: 10.1038/ki.2011.368

Cruz, N. M., Song, X., Czerniecki, S. M., Gulieva, R. E., Churchill, A. J., Kim, Y. K., et al. (2017). Organoid cystogenesis reveals a critical role of microenvironment in human polycystic kidney disease. *Nat. Mater.* 16, 1112–1119. doi: 10.1038/nmat4994

Czerniecki, S. M., Cruz, N. M., Harder, J. L., Menon, R., Annis, J., Otto, E. A., et al. (2018). High-throughput screening enhances kidney organoid differentiation from human pluripotent stem cells and enables automated multidimensional phenotyping. *Cell Stem Cell* 22, 929–940.e4. doi: 10.1016/j.stem.2018.04.022

Doyonnas, R., Kershaw, D. B., Duhme, C., Merkens, H., Chelliah, S., Graf, T., et al. (2001). Anuria, omphalocele, and perinatal lethality in mice lacking the CD34-related protein podocalyxin. *J. Exp. Med.* 194, 13–27. doi: 10.1084/jem.194.1.13

Dvela-Levitt, M., Kost-Alimova, M., Emani, M., Kohnert, E., Thompson, R., Sidhom, E. H., et al. (2019). Small molecule targets TMED9 and promotes Lysosomal degradation to reverse proteinopathy. *Cell* 178, 521–535.e23. doi: 10.1016/j.cell.2019.07.002

Forbes, T. A., Howden, S. E., Lawlor, K., Phipson, B., Maksimovic, J., Hale, L., et al. (2018). Patient-iPSC-derived kidney organoids show functional validation of a ciliopathic renal phenotype and reveal underlying pathogenetic mechanisms. *Am. J. Hum. Genet.* 102, 816–831. doi: 10.1016/j.ajhg.2018.03.014

Freedman, B. S., Brooks, C. R., Lam, A. Q., Fu, H., Morizane, R., Agrawal, V., et al. (2015). Modelling kidney disease with CRISPR-mutant kidney organoids derived from human pluripotent epiblast spheroids. *Nat. Commun.* 6:8715. doi: 10.1038/ncomms9715

Hale, L. J., Howden, S. E., Phipson, B., Lonsdale, A., Er, P. X., Ghobrial, I., et al. (2018). 3D organoid-derived human glomeruli for personalised podocyte disease modelling and drug screening. *Nat. Commun.* 9:5167. doi: 10.1038/s41467-018-07594-z

Heyer, C. M., Sundsbak, J. L., Abebe, K. Z., Chapman, A. B., Torres, V. E., Grantham, J. J., et al. (2016). Predicted mutation strength of nontruncating PKD1 mutations aids genotype-phenotype correlations in autosomal dominant polycystic kidney disease. *J. Am. Soc. Nephrol.* 27, 2872–2884. doi: 10.1681/ASN.2015050583

Homan, K. A., Gupta, N., Kroll, K. T., Kolesky, D. B., Skylar-Scott, M., Miyoshi, T., et al. (2019). Flow-enhanced vascularization and maturation of kidney organoids in vitro. *Nat. Methods* 16, 255–262. doi: 10.1038/s41592-019-0325-y

Howden, S. E., Vanslambrouck, J. M., Wilson, S. B., Tan, K. S., and Little, M. H. (2019). Reporter-based fate mapping in human kidney organoids confirms nephron lineage relationships and reveals synchronous nephron formation. *EMBO Rep.* 20:e47483. doi: 10.15252/embr.201847483

Hwang, Y. H., Conklin, J., Chan, W., Roslin, N. M., Liu, J., He, N., et al. (2016). Refining genotype-phenotype correlation in autosomal dominant polycystic kidney disease. *J. Am. Soc. Nephrol.* 27, 1861–1868. doi: 10.1681/ASN.2015060648

Imberti, B., Corna, D., Rizzo, P., Xinaris, C., Abbate, M., Longaretti, L., et al. (2015). Renal primordia activate kidney regenerative events in a rat model of progressive renal disease. *PLoS One* 10:e0120235. doi: 10.1371/journal.pone.0120235

Jenkinson, S. E., Chung, G. W., Van Loon, E., Bakar, N. S., Dalzell, A. M., and Brown, C. D. (2012). The limitations of renal epithelial cell line HK-2 as a model of drug transporter expression and function in the proximal tubule. *Pflugers Arch.* 464, 601–611. doi: 10.1007/s00424-012-1163-2

Kim, Y. K., Refaeli, I., Brooks, C. R., Jing, P., Gulieva, R. E., Hughes, M. R., et al. (2017). Gene-edited human kidney organoids reveal mechanisms of disease in podocyte development. *Stem Cells* 35, 2366–2378. doi: 10.1002/stem.2707

Kirby, A., Gnirke, A., Jaffe, D. B., Baresova, V., Pochet, N., Blumenstiel, B., et al. (2013). Mutations causing medullary cystic kidney disease type 1 lie in a large VNTR in MUC1 missed by massively parallel sequencing. *Nat. Genet.* 45, 299–303. doi: 10.1038/ng.2543

Lash, L. H., Putt, D. A., and Cai, H. (2008). Drug metabolism enzyme expression and activity in primary cultures of human proximal tubular cells. *Toxicology* 244, 56–65. doi: 10.1016/j.tox.2007.10.022

Li, Z., Araoka, T., Wu, J., Liao, H. K., Li, M., Lazo, M., et al. (2016). 3D culture supports long-term expansion of mouse and human nephrogenic progenitors. *Cell Stem Cell* 19, 516–529. doi: 10.1016/j.stem.2016.07.016

Low, J. H., Li, P., Chew, E. G. Y., Zhou, B., Suzuki, K., Zhang, T., et al. (2019). Generation of human PSC-derived kidney organoids with patterned nephron segments and a de novo vascular network. *Cell Stem Cell* 25, 373–387.e9. doi: 10.1016/j.stem.2019.06.009

Miller, K. A., Ah-Cann, C. J., Welfare, M. F., Tan, T. Y., Pope, K., Caruana, G., et al. (2013). Cauli: a mouse strain with an Ift140 mutation that results in a skeletal ciliopathy modelling Jeune syndrome. *PLoS Genet.* 9:e1003746. doi: 10.1371/journal.pgen.1003746

Mills, C. G., Lawrence, M. L., Munro, D. A. D., Elhendawi, M., Mullins, J. J., and Davies, J. A. (2017). Asymmetric BMP4 signalling improves the realism of kidney organoids. *Sci. Rep.* 7:14824. doi: 10.1038/s41598-017-14809-8

Morizane, R., and Bonventre, J. V. (2017). Generation of nephron progenitor cells and kidney organoids from human pluripotent stem cells. *Nat. Protoc.* 12, 195–207. doi: 10.1038/nprot.2016.170

Morizane, R., Lam, A. Q., Freedman, B. S., Kishi, S., Valerius, M. T., and Bonventre, J. V. (2015). Nephron organoids derived from human pluripotent stem cells model kidney development and injury. *Nat. Biotechnol.* 33, 1193–1200. doi: 10.1038/nbt.3392

Musah, S., Mammoto, A., Ferrante, T. C., Jeanty, S. S. F., Hirano-Kobayashi, M., Mammoto, T., et al. (2017). Mature induced-pluripotent-stem-cell-derived human podocytes reconstitute kidney glomerular-capillary-wall function on a chip. *Nat. Biomed. Eng.* 1:0069. doi: 10.1038/s41551-017-0069

Nieskens, T. T. G., and Sjogren, A. K. (2019). Emerging in vitro systems to screen and predict drug-induced kidney toxicity. *Semin. Nephrol.* 39, 215–226. doi: 10.1016/j.semnephrol.2018.12.009

Noris, M., and Remuzzi, G. (2012). Non-muscle myosins and the podocyte. *Clin. Kidney J.* 5, 94–101. doi: 10.1093/ckj/sfs032

Petrosyan, A., Cravedi, P., Villani, V., Angeletti, A., Manrique, J., Renieri, A., et al. (2019). A glomerulus-on-a-chip to recapitulate the human glomerular filtration barrier. *Nat. Commun.* 10:3656. doi: 10.1038/s41467-019-11577-z

Phipson, B., Er, P. X., Combes, A. N., Forbes, T. A., Howden, S. E., Zappia, L., et al. (2019). Evaluation of variability in human kidney organoids. *Nat. Methods* 16, 79–87. doi: 10.1038/s41592-018-0253-2

Przepiorski, A., Sander, V., Tran, T., Hollywood, J. A., Sorrenson, B., Shih, J. H., et al. (2018). A simple bioreactor-based method to generate kidney organoids from pluripotent stem cells. *Stem Cell Rep.* 11, 470–484. doi: 10.1016/j.stemcr.2018.06.018

Rauch, C., Feifel, E., Kern, G., Murphy, C., Meier, F., Parson, W., et al. (2018). Differentiation of human iPSCs into functional podocytes. *PLoS One* 13:e0203869. doi: 10.1371/journal.pone.0203869

Rogers, S. A., and Hammerman, M. R. (2004). Prolongation of life in anephric rats following de novo renal organogenesis. *Organogenesis* 1, 22–25. doi: 10.4161/org.1.1.1009

Schutgens, F., Rookmaaker, M. B., Margaritis, T., Rios, A., Ammerlaan, C., Jansen, J., et al. (2019). Tubuloids derived from human adult kidney and urine for personalized disease modeling. *Nat. Biotechnol.* 37, 303–313. doi: 10.1038/s41587-019-0048-8

Sharmin, S., Taguchi, A., Kaku, Y., Yoshimura, Y., Ohmori, T., Sakuma, T., et al. (2016). Human induced pluripotent stem cell-derived podocytes mature into vascularized glomeruli upon experimental transplantation. *J. Am. Soc. Nephrol.* 27, 1778–1791. doi: 10.1681/ASN.2015010096

Taguchi, A., Kaku, Y., Ohmori, T., Sharmin, S., Ogawa, M., Sasaki, H., et al. (2014). Redefining the in vivo origin of metanephric nephron progenitors enables generation of complex kidney structures from pluripotent stem cells. *Cell Stem Cell* 14, 53–67. doi: 10.1016/j.stem.2013.11.010

Taguchi, A., and Nishinakamura, R. (2017). Higher-order kidney organogenesis from pluripotent stem cells. *Cell Stem Cell* 21, 730–746.e6. doi: 10.1016/j.stem.2017.10.011

Takasato, M., Er, P. X., Becroft, M., Vanslambrouck, J. M., Stanley, E. G., Elefanty, A. G., et al. (2014). Directing human embryonic stem cell differentiation towards a renal lineage generates a self-organizing kidney. *Nat. Cell Biol.* 16, 118–126. doi: 10.1038/ncb2894

Takasato, M., Er, P. X., Chiu, H. S., Maier, B., Baillie, G. J., Ferguson, C., et al. (2015). Kidney organoids from human iPS cells contain multiple lineages and model human nephrogenesis. *Nature* 526, 564–568. doi: 10.1038/nature15695

Tanigawa, S., Islam, M., Sharmin, S., Naganuma, H., Yoshimura, Y., Haque, F., et al. (2018). Organoids from nephrotic disease-derived iPSCs identify impaired NEPHRIN localization and slit diaphragm formation in kidney podocytes. *Stem Cell Rep.* 11, 727–740. doi: 10.1016/j.stemcr.2018.08.003

Van Den Berg, C. W., Ritsma, L., Avramut, M. C., Wiersma, L. E., Van Den Berg, B. M., Leuning, D. G., et al. (2018). Renal subcapsular transplantation of PSC-derived kidney organoids induces neo-vasculogenesis and significant glomerular and tubular maturation in vivo. *Stem Cell Rep.* 10, 751–765. doi: 10.1016/j.stemcr.2018.01.041

Van Der Hauwaert, C., Savary, G., Buob, D., Leroy, X., Aubert, S., Flamand, V., et al. (2014). Expression profiles of genes involved in xenobiotic metabolism and disposition in human renal tissues and renal cell models. *Toxicol. Appl. Pharmacol.* 279, 409–418. doi: 10.1016/j.taap.2014.07.007

Vanslambrouck, J. M., Wilson, S. B., Tan, K. S., Soo, J. Y., Scurr, M., Spijker, H. S., et al. (2019). A toolbox to characterize human induced pluripotent stem cell-derived kidney cell types and organoids. *J. Am. Soc. Nephrol.* 30, 1811–1823. doi: 10.1681/ASN.2019030303

Vedula, E. M., Alonso, J. L., Arnaout, M. A., and Charest, J. L. (2017). A microfluidic renal proximal tubule with active reabsorptive function. *PLoS One* 12:e0184330. doi: 10.1371/journal.pone.0184330

Weber, E. J., Chapron, A., Chapron, B. D., Voellinger, J. L., Lidberg, K. A., Yeung, C. K., et al. (2016). Development of a microphysiological model of human kidney proximal tubule function. *Kidney Int.* 90, 627–637. doi: 10.1016/j.kint.2016.06.011

Wu, H., Uchimura, K., Donnelly, E. L., Kirita, Y., Morris, S. A., and Humphreys, B. D. (2018). Comparative analysis and refinement of human PSC-derived kidney organoid differentiation with single-cell transcriptomics. *Cell Stem Cell* 23, 869–881.e8. doi: 10.1016/j.stem.2018.10.010

Xia, Y., Sancho-Martinez, I., Nivet, E., Esteban, C. R., Campistol, J. M., Izpisua Belmonte, J. C. (2014). The generation of kidney organoids by differentiation of human pluripotent cells to ureteric bud progenitor-like cells. *Nat. Protoc.* 9, 2693–2704. doi: 10.1038/nprot.2014.182

Xinaris, C. (2019). Organoids for replacement therapy: expectations, limitations and reality. *Curr. Opin. Organ Transplant.* 24, 555–561. doi: 10.1097/MOT.0000000000000680

Xinaris, C., Benedetti, V., Novelli, R., Abbate, M., Rizzo, P., Conti, S., et al. (2016). Functional human podocytes generated in organoids from amniotic fluid stem cells. *J. Am. Soc. Nephrol.* 27, 1400–1411. doi: 10.1681/ASN.2015030316

Xinaris, C., Benedetti, V., Rizzo, P., Abbate, M., Corna, D., Azzollini, N., et al. (2012). In vivo maturation of functional renal organoids formed from embryonic cell suspensions. *J. Am. Soc. Nephrol.* 23, 1857–1868. doi: 10.1681/ASN.2012050505

Yoshimura, Y., Taguchi, A., Tanigawa, S., Yatsuda, J., Kamba, T., Takahashi, S., et al. (2019). Manipulation of nephron-patterning signals enables selective induction of podocytes from human pluripotent stem cells. *J. Am. Soc. Nephrol.* 30, 304–321. doi: 10.1681/ASN.2018070747

Conflict of Interest: The authors declare that the research was conducted in the absence of any commercial or financial relationships that could be construed as a potential conflict of interest.

frontiers in Cell and Developmental Biology

ORIGINAL RESEARCH
published: 06 January 2021
doi: 10.3389/fcell.2020.593106

Modeling Poliovirus Infection Using Human Engineered Neural Tissue Enriched With Motor Neuron Derived From Embryonic Stem Cells

Érika Cosset[1], *Youssef Hibaoui*[2], *Sten Ilmjärv*[2], *Pierre-Yves Dietrich*[1], *Caroline Tapparel*[3*†] *and Karl-Heinz Krause*[2*†]

[1] Laboratory of Tumor Immunology, Department of Oncology, Center for Translational Research in Onco-Hematology, Geneva University Hospitals, University of Geneva, Geneva, Switzerland, [2] Service de Gynécologie et Obstétrique, HFR Fribourg -Hôpital Cantonal, Fribourg, Switzerland, [3] Department of Microbiology and Molecular Medicine, Medical School, University of Geneva, Geneva, Switzerland

OPEN ACCESS

Edited by:
Eumorphia Remboutsika, National and Kapodistrian University of Athens, Greece

Reviewed by:
Zi-Bing Jin, Capital Medical University, China
Antal Nógrádi, University of Szeged, Hungary

***Correspondence:**
Caroline Tapparel
caroline.tapparel@unige.ch
Karl-Heinz Krause
karl-heinz.krause@unige.ch

†These authors have contributed equally to this work

Specialty section:
This article was submitted to Stem Cell Research, a section of the journal Frontiers in Cell and Developmental Biology

Received: *09 August 2020*
Accepted: *23 November 2020*
Published: *06 January 2021*

Citation:
Cosset É, Hibaoui Y, Ilmjärv S, Dietrich P-Y, Tapparel C and Krause K-H (2021) Modeling Poliovirus Infection Using Human Engineered Neural Tissue Enriched With Motor Neuron Derived From Embryonic Stem Cells. Front. Cell Dev. Biol. 8:593106. doi: 10.3389/fcell.2020.593106

Poliomyelitis is caused by poliovirus (PV), a positive strand non-enveloped virus. Since its discovery in the 1950s, several cell culture and molecular methods have been developed to detect and characterize the various strains of PV. Here, we provide an accurate and standardized protocol to differentiate human embryonic stem cells (hESCs) toward engineered neural tissue enriched with motor neurons (MN ENTs). These MN ENTs expressed markers of motor neuron CHAT and Hb-9 as revealed by immunofluorescence staining and quantitative RT-PCR. Interestingly, our results suggest that motor neurons are responsible for the permissiveness of poliovirus within the MN ENTs. Moreover, our study revealed the molecular events occurring upon PV-3 infection in the MN ENTs and highlighted the modulation of a set of genes involved in EGR-EP300 complex. Collectively, we report the development of a reliable *in vitro* model to investigate the pathophysiology of PV infection, allowing to both design and assess novel therapeutic approaches against PV infection.

Keywords: poliovirus type III, human embryonic stem cells, tissue engineering, motor neuron differentiation, neural differentiation, disease modeling, pluripotent stem cells

INTRODUCTION

Poliovirus (PV) is a small non-enveloped virus with a single-strand positive genomic RNA classified in the *Enterovirus C* species of the *Picornaviridae* family (Couderc et al., 1989). Due to its fecal-oral transmission route, PV infection is most often present in high density population with subpar sanitation systems (Falconer and Bollenbach, 2000). PV specifically infects the gray matter of the anterior horn of the spinal cord, from which its name derived (Greek polios = gray, myelos = matter). Indeed, in 1–2% of infected individuals, the virus enters the central nervous system (CNS) and replicates in motor neurons (MN) within the spinal cord, brain stem, or motor cortex (Kew et al., 2005; Racaniello, 2006). The motor function impairment leads to muscle paralysis, also known as acute flaccid paralysis, and even death. Consequently, survivors of poliomyelitis often remain disabled (Mueller et al., 2005). Since the 1950's, major vaccination campaigns allowed to decrease the incidence of poliomyelitis (Cochi et al., 2016). Despite few reported cases of poliomyelitis, several reports acknowledge the possible eradication of PV in the next decade

(Kennedy et al., 2015). To date, no efficient antiviral treatments are available for PV infection despite significant efforts (Arita et al., 2011; van der Sanden et al., 2016). Frequently explored antiviral targets are the viral capsid proteins and non-structural proteins (2A, 2C, 3C, and 3D). Host-targeting antiviral strategies are also being investigated, such as those targeting factors necessary for PV replication, namely eIF4A, GBF1, and VCP/p97 (Molla et al., 1993; Shimizu et al., 2000; de Palma et al., 2008; Arita et al., 2012).

Even though neurological symptoms are rare complications of the PV infection, the molecular mechanisms underlying poliomyelitis occurrence are poorly understood. This is remarkable considering that PV represents one of most thoroughly studied and best-understood virus models. The mouse models have been widely used to gain insights into PV infection processes however, genetic, immune, and physiological differences between humans and mice limit their value (Jubelt et al., 1980). Moreover, mice are only susceptible to certain adapted strains of PV, and transgenic mice expressing the PV receptor CD155 cannot be infected orally and thus require infection via nasal or intramuscular routes to induce paralytic disease (Crotty et al., 2002). Alternatively, non-human primates such as Bonnet Monkeys have been extensively used to study PV pathogenesis, as infection of these monkeys results in a limb paralysis that mimics in some extent human paralytic poliomyelitis both clinically and pathologically (John et al., 1992). Unfortunately, these models cannot accurately recapitulate the specificities of PV infection in the human brain.

The discovery that human pluripotent stem cells (PSCs) can be differentiated into 3D culture systems including engineered neural tissues (ENTs) and organoids has provided unprecedented opportunities to investigate diseases affecting the CNS (Hibaoui and Feki, 2012; Lancaster et al., 2013; Cosset et al., 2015). Several studies have been successful in generating ENTs and organoids from disease-specific induced pluripotent stem cells (iPSCs) or human embryonic stem cells (hESCs), providing excellent *in vitro* models for pathophysiology and drug screening (Hibaoui and Feki, 2012; Cosset et al., 2015; Giandomenico et al., 2019). In this context, ENTs and organoids derived from human PSCs have also proven to be reliable models for studying infectious diseases (Cosset et al., 2015; D'Aiuto et al., 2019), including the use of cerebral organoids to model microcephaly caused by Zika virus infection (Cugola et al., 2016; Garcez et al., 2016; Qian et al., 2016).

We report herein the development of an *in vitro* model of human ENT enriched with motor neurons from hESCs. Using this model, we sought to better understand the mechanisms underlying PV-3 tropism and the molecular events following viral infection in this *in vitro* model.

MATERIALS AND METHODS

Maintenance of hESCs

hESC cell lines H1 and H9 (supplied by WiCell Research Institute) were cultured in feeder-free conditions as described previously (Cosset et al., 2015, 2016), and maintained in a humidified 37°C, 5% CO2 incubator. These hESCs were plated onto pre-coated Matrigel (CELLstartTM, Invitrogen) and cultured in Nutristem medium (Stemcell Biotechnologies) with media changes every 2 days.

Engineered Neural Tissue Enriched With Motor Neurons (MN ENTs)

ENTs were generated as previously described (Cosset et al., 2015, 2016), with some modifications to direct toward a motor neuron fate. hESC were dissociated with accutase (Gibco, Thermo Fisher Scientific), resuspended in medium containing 2 μM ROCK inhibitor (Y-27632) (Abcam Biochemicals) to improve cell survival, and allowed to aggregate in Aggrewell™ dishes for 24 h. Then, these aggregates were transferred into low attachment wells (Costar, Corning Life Sciences) in N2B27 neural medium consisting in equal parts of DMEM-F12 and Neurobasal, 0.5% N2, 1% B27, and 2 mM L-glutamine, 10 μM β-mercaptoethanol, 1% non-essential amino acids, 50 U/ml penicillin, and 50 μg/ml streptomycin (all from Gibco, Thermo Fisher Scientific). As outlined in **Supplementary Figure 1B**, and from the first day to day 5, N2B27 medium was supplemented with the Dual-Smad cocktail: SB431542 (10 nM) and LDN (4 nM) (from Cell Guidance). From day 5 to day 12, N2B27 medium was supplemented with 1 μM retinoic acid (RA). From day 12 to day 18, N2B27 medium was supplemented with 1 μM RA and 100 ng/mL sonic hedgehog (shh). From day 18 to day 26, N2B27 medium was supplemented with 10 ng/mL glial cell-derived neurotrophic factor (GDNF), 10 ng/mL brain-derived neurotrophic factor (BDNF), 10 ng/mL insulin growth factor (IGF-1), and 100 ng/mL shh (all from R&D Systems, Inc.,). At day 26, N2B27 medium was supplemented with 1 μM CpE, a γ-secretase inhibitor, (from Cell Guidance) for 1 day. At day 27, these aggregates were plated on a hydrophilic polytetrafluoroethylene (PTFE) membrane (6 mm diameter, 0.4 lm; BioCellInterface) for 2 weeks in N2B27 medium with media changes every 2 days.

Non-directed Late Neural Engineered Neural Tissues (lnENTs)

Neural ENTs were generated as previously described (Cosset et al., 2016), with some minor modifications. hESC were dissociated with accutase (Gibco, Thermo Fisher Scientific), resuspended in medium containing 2 μM ROCK inhibitor (Y-27632) (Abcam Biochemicals) to improve cell survival, and allowed to aggregate in Aggrewell™ dishes for 24 h. Then, these aggregates were transferred into low attachment wells (Costar, Corning Life Sciences) in N2B27 neural medium consisting in equal parts of DMEM-F12 and Neurobasal, 0.5% N2, 1% B27, and 2 mM L-glutamine, 10 μM β-mercaptoethanol, 1% non-essential amino acids, 50 U/ml penicillin, and 50 μg/ml streptomycin (all from Gibco, Thermo Fisher Scientific). As outlined in **Supplementary Figure 1C**, from the first day to day 5, N2B27 medium was supplemented with the dual-Smad cocktail: SB431542 (10 nM) and LDN (4 nM) (from Cell Guidance). From day 5 to day 12, N2B27 medium was supplemented with 10 ng/mL EGF and 10 ng/mL FGF (all from R&D Systems, Inc.,). From day 12 to day 19, N2B27 medium was supplemented

10 ng/mL GDNF and 10 ng/mL BDNF (all from R&D Systems, Inc.,). From day 19 to day 26, N2B27 medium was supplemented with 10 ng/mL GDNF, 10 ng/mL BDNF, and 1 μM CpE (from Cell Guidance). At day 26, these aggregates were plated on a hydrophilic polytetrafluoroethylene (PTFE) membrane (6 mm diameter, 0.4 lm; BioCellInterface) for 2 weeks in N2B27 medium with media changes every 2 days.

Non-directed Early Neural Engineered Neural Tissues (enENTs)

Immature ENT, named enENT, were generated as previously described (Cosset et al., 2015).

Viruses

PV-3 (Sabin strain) was propagated on Vero cells in a 5% CO_2-containing atmosphere in DMEM (Gibco) supplemented with 2 mM L-glutamine, 100 μg/ml penicillin-streptomycin, 1 μg/ml amphotericin B, 100 μg/ml gentamicin, 10% FCS, 0.2% $NaHCO_3$ and 2% Hepes. EV-71 was propagated as previously described (Tseligka et al., 2018). PV-3 was inoculated on cells for 1 h at 37°C, then the inoculum was removed. Cells were washed once with PBS and left at 37°C until the appearance of a strong cytopathic effect. Viral supernatant was collected, clarified by centrifugation (5′, 1,500 RPM at 4°C), aliquoted and frozen at −80°C. The cell culture infective dose 50 (CCID50)/mL was determined for each viral stock using the Karber method (G, 1931). Infection was performed at a MOI of 1 by addition of diluted viral supernatant directly into the medium for monolayer cultures, or on the top of the ENT for three dimensional cultures over 2 h. Medium exchange was performed every 2 days.

Immunofluorescence and Immunochemistry

Immunofluorescence and immunochemistry were performed as previously described (Cosset et al., 2015, 2016). The following primary antibodies were used: mouse anti-neuronal nuclei-specific protein (NeuN) (Chemicon;MAB377), rabbit anti-βIII-tubulin (Covance;PRB435P), goat anti-ChaT (Chemicon; AB144P), rabbit anti-HB-9 (Abcam; ab922606), rabbit anti-ISLET1 (Abcam; ab22450), goat anti-GALR3 (Abcam), mouse anti-EV-71 (Abcam; ab36367), and mouse anti-PV-3 (Abcam; ab22450). Alexa Fluor (555 and 488)-labeled antibodies from goat or donkey against mouse, goat, or rabbit (Molecular Probes) were used as secondary antibodies. Cell nuclei were stained with DAPI (4, 6-diamidino-2-phenylindole). For IHC, biotin-conjugated anti-rabbit IgG or anti-goat IgG were used and developed using avidin-biotin peroxidase detection system (Vector Labs) with 3,3′-diaminobenzidine substrate (DAB, Sigma-Aldrich) after 2 min of incubation.

Quantitative Real-Time PCR

RNA extraction and cDNA synthesis were, respectively, performed using the Rneasy Mini Kit (Qiagen) and Takara Kit for cDNA synthesis primed with Oligo(dt) and Random Primers according to manufacturer's instructions. SYBRGreen reagent was used for Real-time PCR on the ABI Prism 7000 sequence detection system (Applied Biosystems) according to the manufacturer's instructions. ALAS1 and EEF1 were used as housekeeping genes. The results were analyzed using the 2-ΔΔCt method. Primer sequences are provided in the **Supplementary Table 1**. All experiments were performed, at least, in triplicate.

Real-Time (RT)-PCR Screening for the Presence of PV-3

PV-3 infected and non-infected ENT were screened for the presence of PV-3 with the Entero/Ge/08 real-time PCR (Racaniello, 2006). After tissue homogenization, 400 ul of supernatant were collected for RNA extraction with easyMAG (bioMérieux). Taqman Universal Mastermix (Applied Biosystems) was used to perform the Real-time PCR screening using the StepOne thermocycler (Applied Biosystems).

PCR Screening for the Presence of PSC, NSC, and MN Markers

For non-quantitative PCR, reactions were performed in a Biometra thermocycler (Göttingen, Germany), with RedTaq polymerase mix (Sigma-Aldrich, St. Louis, MO, USA), 250 nM primers and 2 μL of cDNA. The primer sequences used for non-quantitative RT-PCR are listed in **Supplementary Table 1**.

Microarray

The Illumina TotalPrep RNA amplification kit was used to synthetize the first and second strand cDNA, as well as cDNA and cRNA purification according to the manufacturer's instructions. The microarray was performed on human HT-12 v3.0 Illumina microarrays. Preprocessing consisted of a background correction, a log2 transformation and quantile normalization, as previously described (Cosset et al., 2015). Then, the limma package from Bioconductor was used to identify the differentially expressed genes (Gentleman et al., 2004). Finally, g:profiler was used for enriched functional annotation analysis (Raudvere et al., 2019).

Statistical Analysis

All quantitative data presented are the mean ± SEM. Samples used and the respective n values refer to the number of independent experiments and are listed in the figure legends. Statistical analyses were performed with the students t-test and ANOVA where $p < 0.05$ was considered significant.

RESULTS

Generation and Characterization of Engineered Neural Tissue Enriched With Motor Neuron (MN ENTs)

Given the known tropism of poliovirus for MNs, we developed a protocol to enrich engineered neural tissues with motor neurons (MN ENTs), as outlined in **Supplementary Figure 1A**. To initiate MN differentiation, colonies of undifferentiated hESCs, expressing *OCT4*, and *NANOG* (**Figures 1A,B**), were dissociated into single cells and re-aggregated in multiwell plates for 24 h to allow size-calibrated neurospheres (**Supplementary Figures 1A–E**). As previously described (Chambers et al., 2009; Kriks et al., 2011), dual-smad inhibition

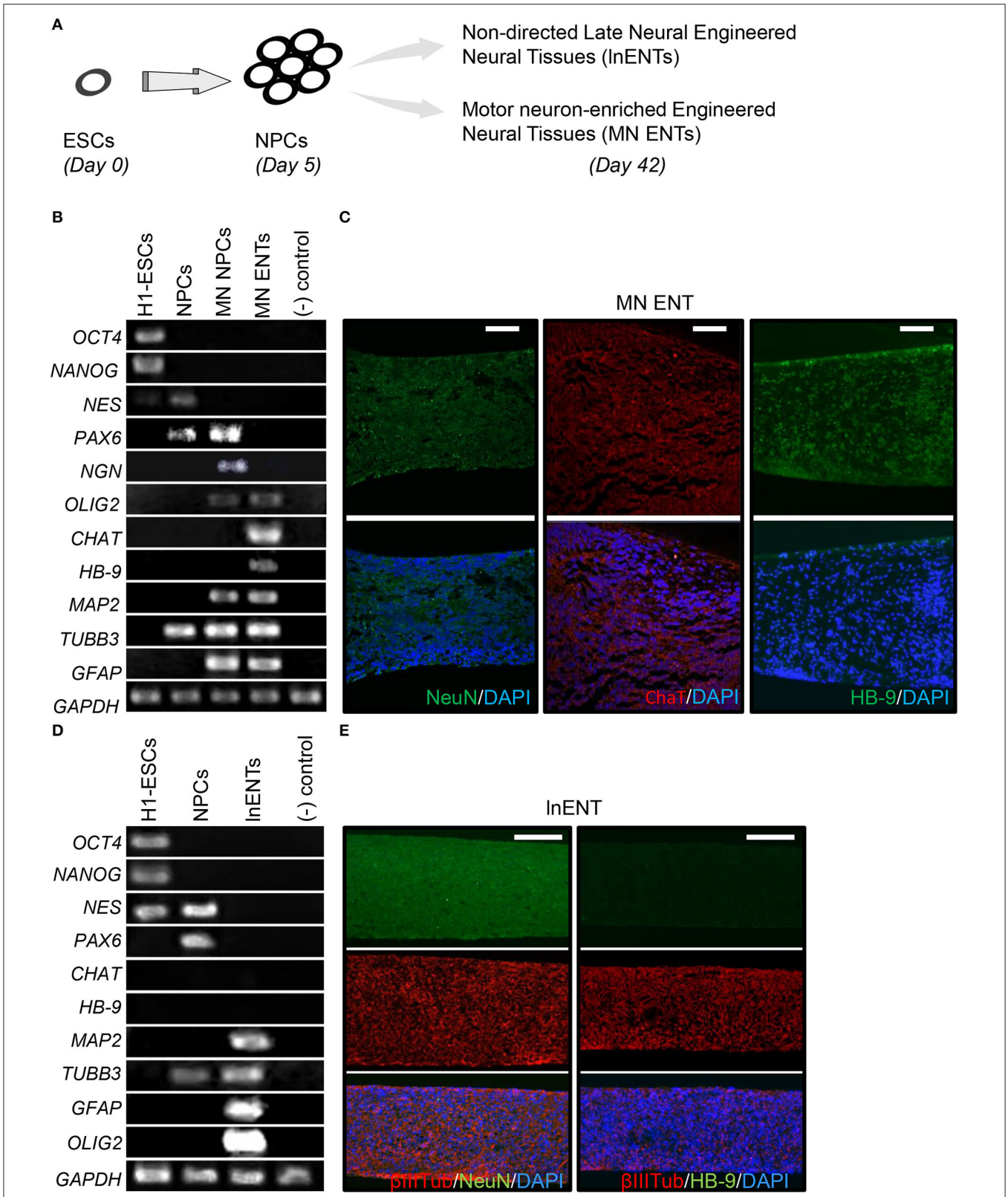

FIGURE 1 | MN ENT generation and characterization. **(A)** Schematic representation of hESC differentiation toward lnENTs and MN ENT. **(B)** RT-PCR analysis of the expression of pluripotency (*OCT4* and *NANOG*), neuroprogenitor cells NPCs (*NES* and *PAX6*), motor neuron progenitor cells (MN NPCs) (*NGN*, *PAX6*, and *OLIG2*),

(Continued)

FIGURE 1 | motor neuron enriched ENTs (*CHAT* and *HB9*), and markers for neuronal, astroglial and oligodendroglial cells (*MAP2*, *TUBB3*, *GFAP*, and *OLIG2*). Human lymphocytes B were used as negative controls. **(C)** Immunofluorescence showed NeuN, CHAT, and HB-9-immunoreactive cells present in the whole MN ENT. Scale bar = 50 μm. **(D)** RT-PCR analysis of the expression of pluripotency (*OCT4* and *NANOG*), neuroprogenitor cells NPCs (*NES* and *PAX6*), and non-directed late neural ENTs (*MAP2*, *TUBB3*, *GFAP*, and *OLIG2*). Human lymphocytes B were used as negative controls. **(E)** Immunofluorescence showed βIII-Tubulin, NeuN, and HB-9-immunoreactive cells present, or not, in the lnENT. Scale bar = 100 μm.

was used to improve neural induction during the initial days of culture (**Supplementary Figure 1A**) (Chambers et al., 2009; Kriks et al., 2011). As illustrated in **Supplementary Figures 1A,B**, these spheres were induced to differentiate into neuroprogenitor cells (NPCs) in suspension culture (**Supplementary Figure 1C**). Thereafter, the addition of retinoic acid (RA), known to induce caudalization after the initial neuralization, quickly oriented neural cells toward MN neural progenitors (MN NPCs), expressing *PAX6*, *NGN*, and *OLIG2* (**Figure 1B**, **Supplementary Figures 1A,C,D**). In response to shh, MN sphere NPCs further differentiated into MN expressing HB-9 and CHAT (**Figure 1B**). Then, GDNF, BDNF, IGF-1 and shh promoted the final differentiation. To improve neural maturation, the γ-secretase inhibitor compound E was added during the final step of the neural maturation phase (**Supplementary Figure 1A**). Thereafter, these MN NPCs were placed on a semipermeable PTFE membrane to facilitate the final maturation of MN engineered neural tissue (MN ENT) on an air–liquid interface over 2 weeks (**Supplementary Figure 1E**). To better characterize the model, MN ENTs were analyzed, stained and compared to non-directed late neural ENT (lnENT, enriched for differentiated neurons and astrocytes), for MN and different neuronal markers (**Figures 1A–C**) (**Supplementary Figure 1F**). As expected in MN ENTs, we observed an induction of *HB-9* and *CHAT* mRNA detected by RT-PCR (**Figure 1B**). These MN markers were also expressed in MN ENTs at the protein level as shown by the immunofluorescence analysis (**Figure 1C**). Such induction of *HB-9* and *CHAT* genes was not observed in lnENTs (**Figure 1D**). Similarly, lnENTs did not show any expression of HB-9 and CHAT proteins (**Supplementary Figure 1F**). Moreover, as lnENTs, MN ENTs expressed markers for astroglial and oligodendroglial cells (*GFAP* and *OLIG2*) and general markers for neurons such as *TUBB3*, *MAP2* as shown by RT-PCR (**Figures 1B,D,E**). Collectively, our results suggest an efficient enrichment of MN in MN ENTs.

Motor Neurons Promote the Spread of Poliovirus Infection in MN ENTs

The permissiveness of cells is defined by their potential to support the viral life cycle. Therefore, we sought to investigate PV-3 permissiveness in 2D and 3D culture. We first evaluated PV-3 infection at different stages of hESC differentiation toward MN namely: (i) at the undifferentiated state, (ii) at the NPC level and (iii) in MN. We thus infected all cells by adding PV-3 at a multiplicity of infection (MOI) of 1 over 1 h, then replaced the medium and maintained the cells in culture for 24 h. Our results showed that MNs were highly permissive to PV-3 infection, as evidence by the high proportion of HB-9 positive cells co-stained for PV-3 (**Figure 2A**). hESCs were less permissive to PV-3 infection, whereas NPCs had none or very few PV-3 immunoreactive cells (**Figure 2A**). We then compared the permissiveness and spread of PV-3 infection in MN ENTs and in two distinct neural ENT models at day 7 after infection. To do so, we generated both non-directed early neuronal ENTs (enENTs) that resemble the early developing brain and exhibit radially organized cells positive for nestin, musashi, and Pax6; (Cosset et al., 2015) and lnENTs (**Figure 1E**) (Cosset et al., 2016). On day 7 after infection, we noticed a striking dissemination of PV-3 virus in MN ENTs, whereas lnENTs and enENTs were only weakly infected (**Figures 2B,C**) (**Supplementary Figure 2A**). Therefore, differentiation of ENTs into a motor neuron phenotype substantially enhances permissiveness for PV-3 infection. Next, we performed the same infections using enterovirus-71 (EV-71), a neurotropic EV from the A species, known to more generally infect neurons and glial cells (Tseligka et al., 2018). Infection with this virus showed a much more pronounced tropism for lnENTs, while it infected the MN ENTs rather weakly (**Supplementary Figure 2B**). Similarly, the enENT showed a relatively weak pattern of EV-71 infection (**Supplementary Figure 2A**). The enENTs were even less permissive to PV-3, with only a few infected cells (**Supplementary Figure 2A**). Altogether, these results demonstrate an evident permissiveness of MN ENTs for PV-3 infection due to the presence of MN within the tissue.

Features of Poliovirus Infection in MN ENTs

We first evaluated the kinetics of viral proliferation within MN ENTs at day 1, 3, 5, and 7 after PV-3 infection by quantitative RT-PCR (**Figure 3A**). As shown in **Figure 3B**, PV-3 expression increased by 100-, 160-, 1,650-, and 4,200-fold at day 1, 3, 5, and 7 after infection, respectively. In line with this, the immunohistological analysis of PV-3 infected MN ENTs revealed that PV-3 was able to penetrate deep into the tissue, suggesting that tissue organization and extracellular matrix do not impede viral infection and dissemination (**Figure 3C**). A time course of PV-3 infection revealed viral multiplication, at days 2–3 and presence in the entire tissue by days 5 and 7 after infection, as detected by both immunochemistry and quantitative RT-PCR, respectively (**Figures 3B,C**). We also observed a tissue damage starting from day 5 to 7 after infection (**Figure 3C**). Of note, immunofluorescence analysis revealed the co-staining of PV-3 with markers of MN within MN ENTs including CHAT, HB-9, and ISLET1, supporting the notion that MNs within MN ENTs are responsible for the permissiveness to PV-3 infection (**Figure 3D**) (**Supplementary Figure 3A**).

Differentiated Neurons Are More Permissive and Sensitive to PV-3 Infection

We next investigated the kinetics of RNA levels of selected markers for neural progenitors (*NES* for nestin) and for markers of mature neurons (*TUBB3* and *RBFOX3* for β3-tubulin and

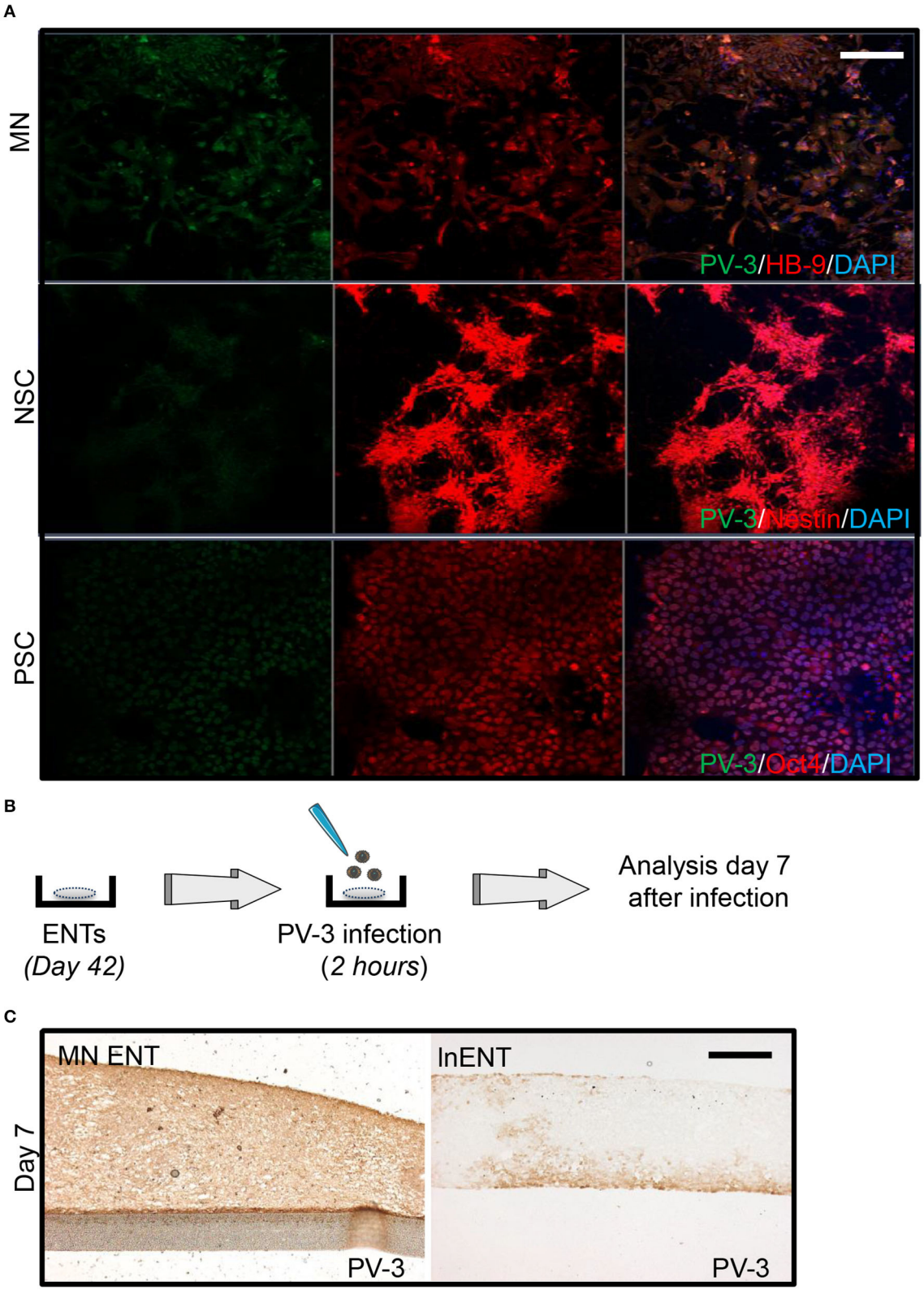

FIGURE 2 | MN ENT shows a greater permissiveness for PV-3 compare to lnENT. **(A)** Infection of motor neurons (MN), neural progenitors (NPC), and human embryonic stem cells (hESCs) by PV-3. Immunofluorescence showed PV-3 (green), HB-9, Nestin, and Oct4 (all in red) in MN, NPC, and PSC, respectively. Scale bar = 50 μm. **(B)** Schematic representation of PV-3 and EV-71 infection of ENTs. **(C)** Immunohistochemistry showing PV-3-immunoreactive cells within MN ENTs (left panel) and lnENT (right panel).

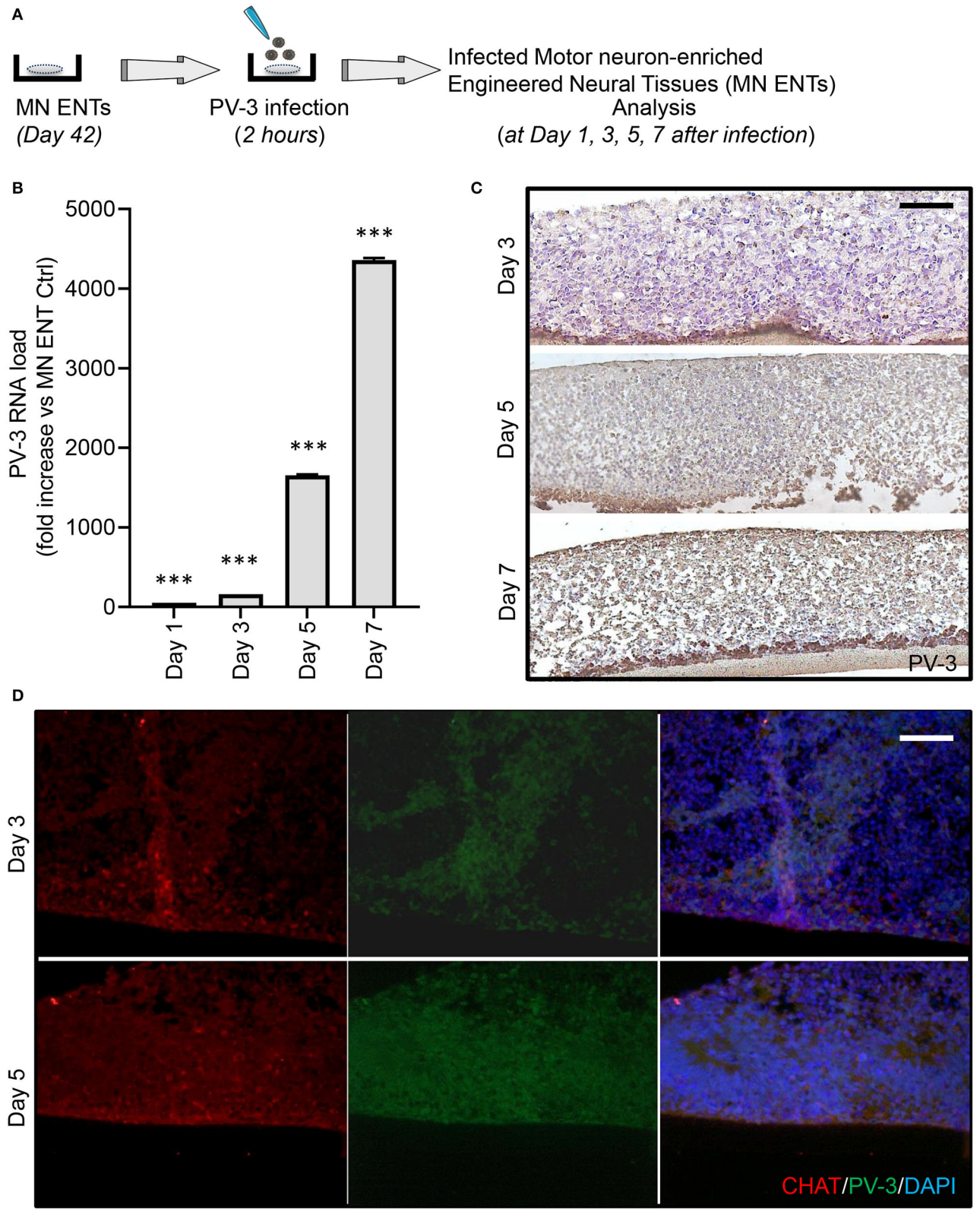

FIGURE 3 | PV-3 preferentially infects motor neurons in MN ENTs. **(A)** Schematic representation of PV-3 infection of MN ENTs. **(B)** Quantitative RT-PCR of mRNA of PV-3 in PV-3-infected MN ENTs at day 1, 3, 5, and 7. Data are normalized to housekeeping genes; mean ± SEM with $^{***}p < 0.01$ for $n = 3$ independent experiments. **(C)** MN ENTs were fixed at 3, 5, and 7 days after PV-3 infection, sectioned, stained by immunohistochemistry with antibodies against PV-3. Scale bar = 50 μm. **(D)** MN ENTs were fixed at 3, and 5 days after PV-3 infection, sectioned, and stained with antobodies against PV-3 (in green), CHAT (in red) and with DAPI (in blue). Scale bar = 50 μm.

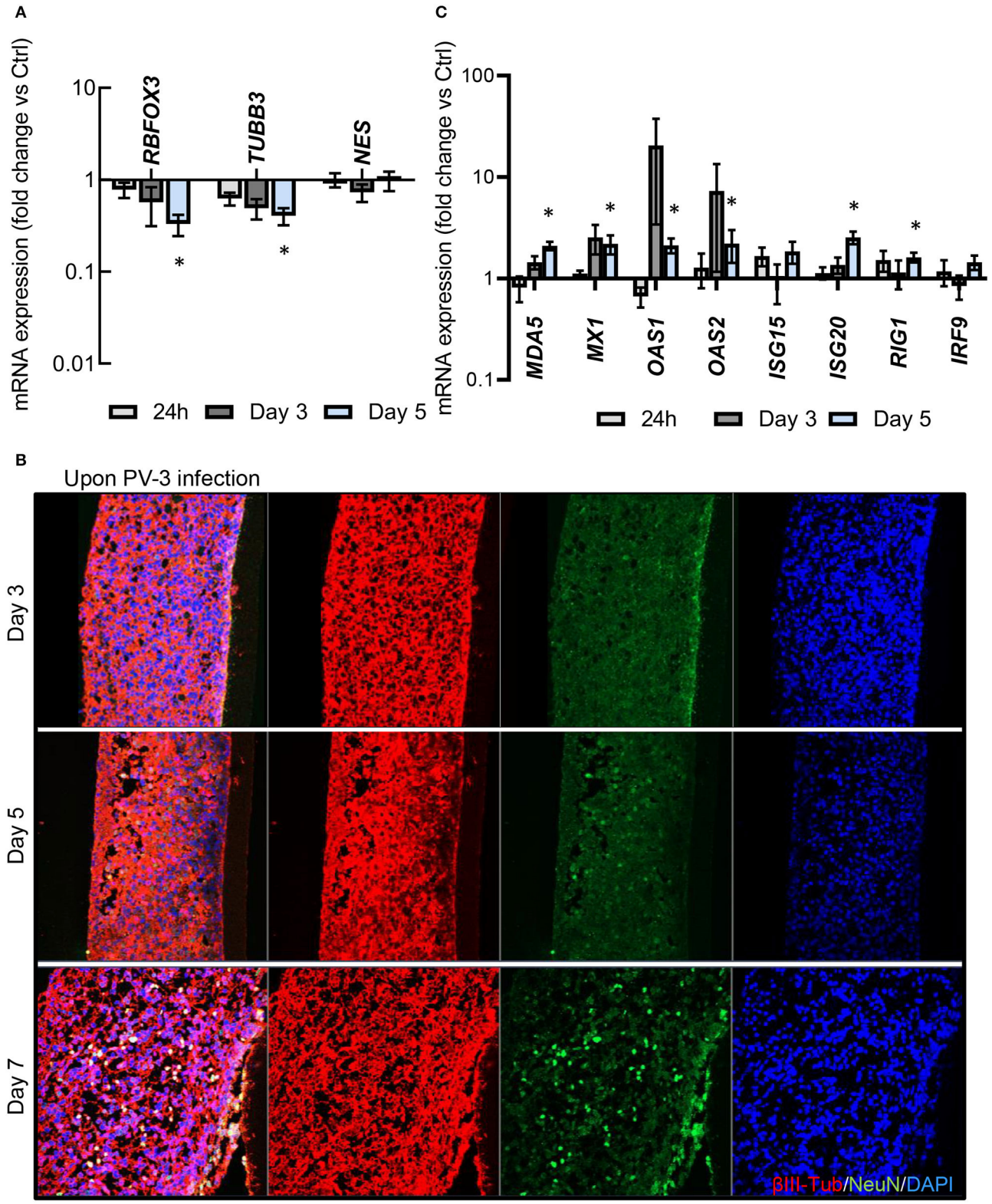

FIGURE 4 | PV-3 infection also affects neural progenitors and induces an innate antiviral response. **(A)** *RBFOX3, NES, and TUBB3* mRNA expression was determined by qPCR in PV-3-infected MN ENT at day 1, 3, and 5. **(B)** Immunofluorescence showing βIII-Tubulin, and NeuN -immunoreactive cells within the MN ENTs at day 3, 5, and 7. **(C)** Quantitative RT-PCR analysis of interferon-related or interferon stimulated mRNA expression in by qPCR in PV-3-infected MN ENTs at day 1, 3, and 5. Data are represented as mean ($n = 3$) ± SEM (*$p < 0.05$).

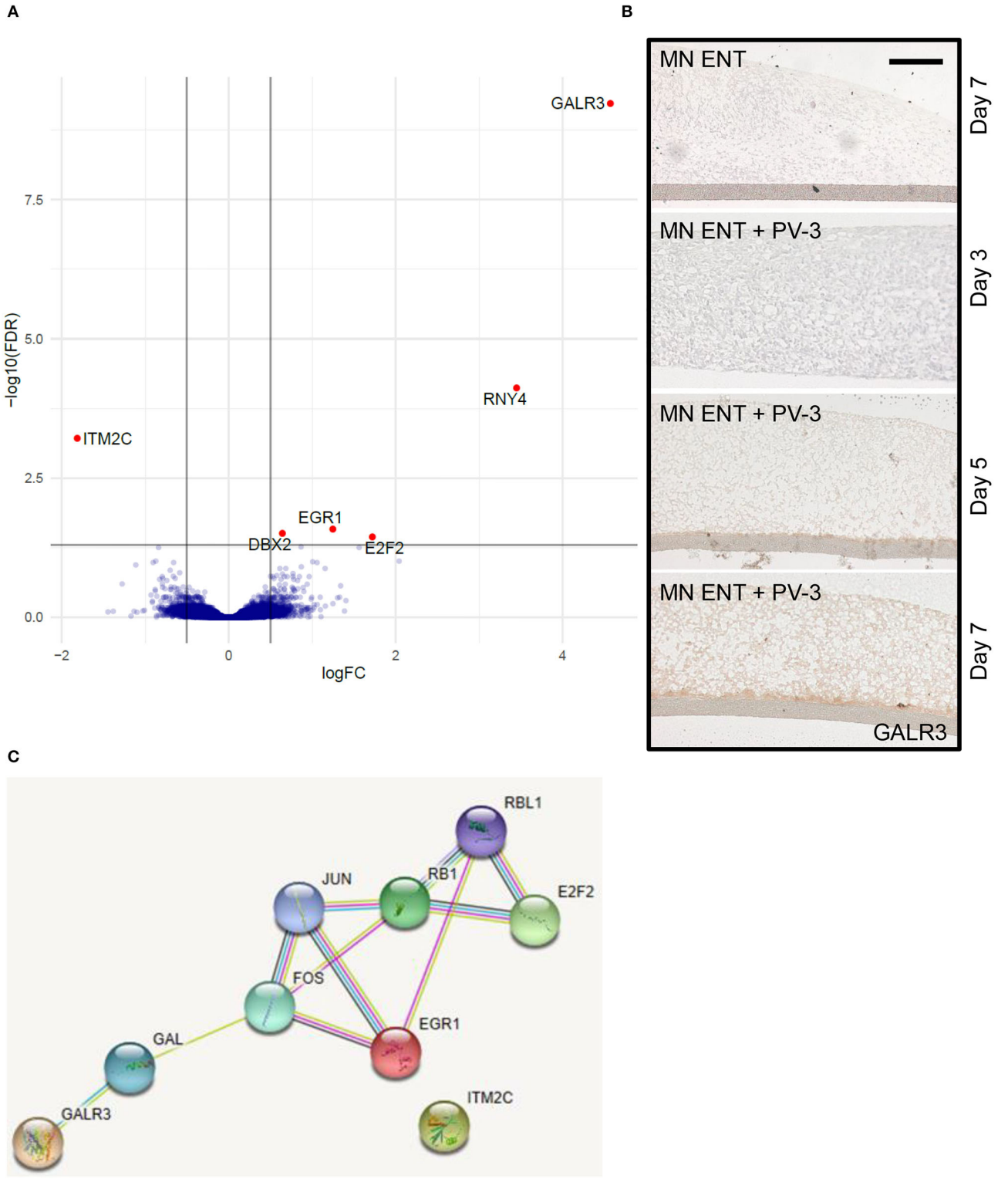

FIGURE 5 | PV-3 infection induces the expression of genes involved in EGR-EP300 complex. **(A)** Volcano plot representing the differentially expressed genes upon PV-3 infection at day 5. **(B)** Immunohistochemistry showed GALR3-immunoreactive cells present in uninfected MN ENT (top panel) and infected MN ENT at day 3, 5, and 7. **(C)** String analysis shows known and predicted interactions between identified genes expressed upon PV-3 infection.

NeuN, respectively) at 24 h, day 3 and 5 after infection, detected by quantitative RT-PCR (**Figure 4A**). Our results revealed a time-dependent decrease of *RBFOX3* and *TUBB3* expression following PV-3 infection, while *NES* expression remained unchanged (**Figures 4A,B**) (**Supplementary Figure 4A**). The results thus indicate that mature neurons are more sensitive to PV-3 infection than neural progenitors. Given that interferon (IFN) signaling has been shown to control tissue tropism and pathogenicity of PV (Ida-Hosonuma et al., 2005), we further investigated the kinetics of RNA levels of IFN-related and -stimulated genes, in response to PV-3 infection by quantitative RT-PCR (**Figure 4C**). Interestingly, *MDA-5* (for melanoma differentiation-associated gene 5), *MX1* (for myxovirus resistance 1), *OAS1* (for oligoadenylate synthetase 1), *ISG20* (for Interferon Stimulated Exonuclease Gene 20) and *RIG-1* (for reticnoic acide-inducible gene 1) were up-regulated at day 5 after infection (**Figure 4C**). This is a notable finding since these genes are recognized as being interferon-inducible antiviral effectors (Sadler and Williams, 2008). Collectively, these results indicated that the MN ENT model recapitulates the innate immune response and probably the first line of defense against viral infection. Surprinsingly though, this response appears rather late, at a moment where a substantial number of mature neurons are already damaged (**Figures 3B**, **4B**; bottom panel).

Transcriptomic Analysis of PV-3 Infected MN ENTs

To get more insight into the molecular mechanisms following PV-3 infection in MN ENTs, we compared the transcriptomic gene expression profiles of MN ENTs infected with PV-3 to non-infected controls. Microarray analysis revealed a set of six differentially expressed genes with five upregulated genes (*GALR3*, for galanin receptor type 3; *RNY4*, for RNA Ro-associated Y4; *EGR1*, for early growth response 1; *DBX2*, for developing brain homeobox 2; *E2F2*, for E2F transcription factor 2) and one downregulated gene (*ITM2C*, for integral membrane protein 2C) (**Figure 5A**) (**Supplementary Table 2**). Immunostaining of MN ENTs confirmed the increased expression of GALR3 in infected MN ENTs over time (**Figure 5B**). Gene ontology enrichment analysis (https://biit.cs.ut.ee/gprofiler/gost) provided evidence that suggests expression of genes involved in the EGR-EP300 complex. STRING analysis (https://string-db.org/), presenting known and predicted protein-protein direct or indirect interactions, showed interactions between E2F2, EGR1, and GALR3 (**Figure 5C**). However, gene expression changes through PV were highly selective for a few genes, and consequently multidimensional scaling analysis confirmed a high similarity between PV-3 infected and control MN ENT (**Supplementary Figure 4B**).

DISCUSSION

The discovery that human embryonic and induced pluripotent stem cells can be differentiated into engineered neural tissues has provided unique opportunities to study diseases and infections affecting the CNS. In our previous study, by using *in vitro* ENTs and biopsy samples from infected fetal brains, we could establish that human cytomegalovirus (HCMV) shows a high tropism for early migrating neurons, providing strong evidence that ENT is a suitable physiological model for studying viral infection. Here, we similarly show that human ENTs enriched with motor neuron can be used as a reliable and relevant model for studying PV infection. We demonstrate that motor neurons are required for a high level ENT infection by PV. Following infection, a decrease in mature motor neurons was observed, suggesting motor neuron cytotoxicity due to PV infection. Transcriptomic analysis revealed highly significant changes in expression of a limited number of genes, rather than a massive gene dysregulation.

A striking finding from our study is the extent of viral infection and virion release. Immunohistochemistry showed a large majority of cells within MN ENTs to be positive for viral antigens. This is in contrast to one of our previous reports using HCMV, where only a small minority of cell was infected (Cosset et al., 2015). Similarly, quantitative RT-PCR of virion release revealed large amounts of viral RNA, far above values that we observed previously with CMV. Thus, not only is our tissue model highly permissive to PV infection, it also provides a means to investigate the aggressive nature of viral dissemination in the appropriate tissue context.

Surprisingly, despite the widespread infection with the virus, changes in the transcriptome remained limited to only a few genes: *GALR3*, *EGR1*, *E2F2*, *RNY4*, *DBX2* were found upregulated, and *ITM2C* was downregulated. Among those, *GALR3*, encodes a G-protein-coupled receptor with widespread distribution in the brain. It plays a role in several physiologic processes (such as sensory/pain processing, hormone secretion, cognition/memory, and feeding behavior) (Lang et al., 2007). There are indications that GALR3 might be involved in CNS infection, since a selective increase in galanin-positive neurons has been shown in a mouse model of sensory ganglia infection with herpes simplex virus (HSV1 and HSV2) (Henken and Martin, 1992a,b). It remains to be seen whether this upregulation of GALR3 expression is part of the host response or due to manipulation of the host tissue by viruses.

E2F2 and *EGR1* are both involved in the EGR-EP300 complex. The latter encodes for a transcription factor (EGR1), which will

TABLE 1 | Comparison of the various responses of ENT following viral infection.

		HCMV	Poliovirus	Enterovirus-71
Immature neural tissue		+++	(+)	(+)
Mature neural tissue	Non-directed neural differentiation	n.d.	+	+++
	Motor neuron differentiation	n.d.	+++	+
Changes in gene expression		+++	+	n.d.
Cell death		+	+++	+

This table presents the difference in terms of virus infection/propagation from elevated +++ to low (+) in the various ENTs. Changes in gene expression and cell death are shown at day 5 and 7 after infection, respectively. n.d., not determined.

form a complex with EP300 and ultimately lead to expression of various target genes, including *E2F2*. Notably, EP300 regulates transcription via chromatin remodeling and is important in cell proliferation and differentiation processes. EP300 is a target of several viruses, including PV, which has been shown to affect the CREB-dependent pathway (Yalamanchili et al., 1997). EP300 knock-down has also been suggested to improve production of PV vaccine (van der Sanden et al., 2016).

In this study, we also documented upregulated genes associated with cellular host responses to viral infection, more specifically the type I interferons, IFNα/β (Desmyter et al., 1968). Of note, previous studies have reported that PV interferes with IFN responses by cleaving the host MDA5 and MAVS proteins, two RIG-I-like receptors (Feng et al., 2014). Given that MDA5 and MAVS are key players in the innate antiviral response, we analyzed their gene expression and identified a significant increase of these genes at day 5 after infection. Thus, while PV does not completely prevent the upregulation of RLRs, it appears to induce a delay in the cellular host response, which is sufficient for the virus to replicate and destroy mature motor neurons.

It is a more general goal of our research team to improve the understanding of viral infections of the CNS by using pluripotent stem cell-derived engineered neural tissues. We have previously investigated CMV infection, and with this study, we report novel data on PV and EV-71 infection, for which the Sabin vaccine strain was used due to biosafety reasons. A comparison among the three highlights important differences (**Table 1**). The type of neural tissue which is sensitive to a given virus is well-correlated with known clinical features. Poliovirus leads to a paralysis through destruction of motor neurons, a patho-mechanism which is evidently confirmed in our *in vitro* model. HCMV infection occurs mainly in the fetal brain, consistent with the infection of immature neural tissues in our *in vitro* model (Cosset et al., 2015). However, there is a striking phenomenon that requires further investigation: HCMV predominantly infects a small subgroup of early migrating neurons, but leads to substantial changes in gene expression. In contrast, in MN ENT, PV leads to a massive infection and cell death; however, there is a very selective and highly specific impact on expression of a limited number of genes.

In summary, we have established a pluripotent stem cell-based model of PV infection. The increase in permissiveness upon motor neuron enrichment of engineered neural tissue provides strong validation of our model, as does the induction of cell death. The restricted gene expression profile and delayed innate immune response are notable findings of PV infection, which may provide intriguing clues and opportunities to potential future therapies. Thus, our MN ENT model provides an extremely useful screening tool for therapy development. Despite the availability of a very efficient vaccine, poliomyelitis is yet to be completely eradicated. As noted by World Health Organization: "failure to eradicate polio from these last remaining strongholds could result in as many as 200,000 new cases every year, within 10 years" (https://www.who.int/news-room/fact-sheets/detail/poliomyelitis).

DATA AVAILABILITY STATEMENT

The datasets presented in this study can be found in online repositories. The names of the repository/repositories and accession number(s) can be found below: Accession number: E-MTAB-9525 Repository: ArrayExpress https://www.ebi.ac.uk/arrayexpress/experiments/E-MTAB-9525/.

AUTHOR CONTRIBUTIONS

ÉC designed and supervised the study, designed and carried out experiments, analyzed and interpreted data, and wrote the paper. YH gave conceptual advice provided critical feedback on the study and the manuscript and carried out experiments. SI analyzed the microarray data. P-YD provided critical feedback on the study and the manuscript. CT and K-HK provided critical feedback and gave conceptual advice. All authors proofread the manuscript. All authors contributed to the article and approved the submitted version.

FUNDING

K-HK was supported by SNF 31003A-179478 and CT was supported by SNF 310030_184777.

ACKNOWLEDGMENTS

The authors thank Dr. Mayra Yebra and Dr. Marco Alessandrini for proofreading the paper. We thank the personel of the Genomic core facility of the faculty of medicine (University of Geneva), in particular Isabelle Durussel, Christelle Barracloug, and Didier Chollet for their help in samples preparation, microarray, and qRT-PCR. The authors also thank the Histology core facility of the faculty of medicine (University of Geneva), in particular Marie Ebrahim Malek and Laura De Luca for their help in samples preparation.

SUPPLEMENTARY MATERIAL

The Supplementary Material for this article can be found online at: https://www.frontiersin.org/articles/10.3389/fcell.2020.593106/full#supplementary-material

Supplementary Figure 1 | (A) Schematic representation of air–liquid interface culture principle for MN ENT. The hESCs **(B)** were cultured on Matrigel then aggregated in microwell plates **(C)**. 4-week-old neurospheres **(D)** were plated onto PTFE membrane **(E)** for two additional weeks at the end of which PV-3 infection occurred. **(F)** Immunohistochemistry showed CHAT, HB-9, and ISLET1-immunoreactive cells present in the whole MN ENT (left panel) and lnENT (right panel). Scale bar = 100 μm. **(G)** Schematic representation of air–liquid interface culture principle for neural ENT (lnENT).

Supplementary Figure 2 | (A) Immunohistochemistry showed enENT infected by EV-71 (left panel) or PV-3 (right panel). Scale bar = 100 μm. Uninfected motor neurons (MN), neural progenitors (NPC), and human pluripotent stem cell (PSC). Immunofluorescence showed PV-3 (green), HB-9, Nestin, and Oct4 (all in red) in MN, NPC, and PSC, respectively. Scale bar = 50μm.

Supplementary Figure 3 | (C) MN ENT were fixed 5 days after PV-3 infection, sectioned, and double immunostainings were performed with antibodies against PV-3 (green) and CHAT, motor neuron markers (in red). Nuclei were counterstained with DAPI. Scale bar = 50 μm.

Supplementary Figure 4 | (A) Immunofluorescence showed βIII-Tubulin, and NeuN-immunoreactive cells present in the uninfected MN ENT at day 3 (top panel) and the negative control (mouse and rabbit secondary antibodies; bottom panel). **(B)** MDS plot showing separation of individual samples for uninfected MN ENT (Ctrl MN_5d) and infected MN ENT (PV-3_5d) at day 5 after infection.

Supplementary Table 1 | List of primers used for quantitative RT-PCR and RT-PCR.

Supplementary Table 2 | List of the differentially expressed gene between PV-3 infected vs. uninfected MN ENT.

REFERENCES

Arita, M., Kojima, H., Nagano, T., Okabe, T., Wakita, T., and Shimizu, H. (2011). Phosphatidylinositol 4-kinase III beta is a target of enviroxime-like compounds for antipoliovirus activity. *J. Virol.* 85, 2364–2372. doi: 10.1128/JVI.02249-10

Arita, M., Wakita, T., and Shimizu, H. (2012). Valosin-containing protein (VCP/p97) is required for poliovirus replication and is involved in cellular protein secretion pathway in poliovirus infection. *J. Virol.* 86, 5541–5553. doi: 10.1128/JVI.00114-12

Chambers, S. M., Fasano, C. A., Papapetrou, E. P., Tomishima, M., Sadelain, M., and Studer, L. (2009). Highly efficient neural conversion of human ES and iPS cells by dual inhibition of SMAD signaling. *Nat. Biotechnol.* 27, 275–280. doi: 10.1038/nbt.1529

Cochi, S. L., Hegg, L., Kaur, A., Pandak, C., and Jafari, H. (2016). The global polio eradication initiative: progress, lessons learned, and polio legacy transition planning. *Health Aff.* 35, 277–283. doi: 10.1377/hlthaff.2015.1104

Cosset, E., Martinez, Y., Preynat-Seauve, O., Lobrinus, J. A., Tapparel, C., Cordey, S., et al. (2015). Human three-dimensional engineered neural tissue reveals cellular and molecular events following cytomegalovirus infection. *Biomaterials* 53, 296–308. doi: 10.1016/j.biomaterials.2015.02.094

Cosset, E., Petty, T., Dutoit, V., Tirefort, D., Otten-Hernandez, P., Farinelli, L., et al. (2016). Human tissue engineering allows the identification of active miRNA regulators of glioblastoma aggressiveness. *Biomaterials* 107, 74–87. doi: 10.1016/j.biomaterials.2016.08.009

Couderc, T., Christodoulou, C., Kopecka, H., Marsden, S., Taffs, L. F., Crainic, R., et al. (1989). Molecular pathogenesis of neural lesions induced by poliovirus type 1. *J. Gen. Virol.* 70, 2907–2918. doi: 10.1099/0022-1317-70-11-2907

Crotty, S., Hix, L., Sigal, L. J., and Andino, R. (2002). Poliovirus pathogenesis in a new poliovirus receptor transgenic mouse model: age-dependent paralysis and a mucosal route of infection. *J. Gen. Virol.* 83, 1707–1720. doi: 10.1099/0022-1317-83-7-1707

Cugola, F. R., Fernandes, I. R., Russo, F. B., Freitas, B. C., Dias, J. L., Guimaraes, K. P., et al. (2016). The Brazilian Zika virus strain causes birth defects in experimental models. *Nature* 534, 267–271. doi: 10.1038/nature18296

D'Aiuto, L., Bloom, D. C., Naciri, J. N., Smith, A., Edwards, T. G., McClain, L., et al. (2019). Modeling herpes simplex virus 1 infections in human central nervous system neuronal cells using two- and three-dimensional cultures derived from induced pluripotent stem cells. *J. Virol.* 93:e00111–19. doi: 10.1128/JVI.00111-19

de Palma, A. M., Heggermont, W., Lanke, K., Coutard, B., Bergmann, M., Monforte, A. M., et al. (2008). The thiazolobenzimidazole TBZE-029 inhibits enterovirus replication by targeting a short region immediately downstream from motif C in the nonstructural protein 2C. *J. Virol.* 82, 4720–4730. doi: 10.1128/JVI.01338-07

Desmyter, J., Melnick, J. L., and Rawls, W. E. (1968). Defectiveness of interferon production and of rubella virus interference in a line of African green monkey kidney cells (Vero). *J. Virol.* 2, 955–961. doi: 10.1128/JVI.2.10.955-961.1968

Falconer, M., and Bollenbach, E. (2000). Late functional loss in nonparalytic polio. *Am. J. Phys. Med. Rehabil.* 79, 19–23. doi: 10.1097/00002060-200001000-00006

Feng, Q., Langereis, M. A., Lork, M., Nguyen, M., Hato, S. V., Lanke, K., et al. (2014). Enterovirus 2Apro targets MDA5 and MAVS in infected cells. *J. Virol.* 88, 3369–3378. doi: 10.1128/JVI.02712-13

Garcez, P. P., Loiola, E. C., Madeiro da Costa, R., Higa, L. M., Trindade, P., Delvecchio, R., et al. (2016). Zika virus impairs growth in human neurospheres and brain organoids. *Science* 352, 816–818. doi: 10.1126/science.aaf6116

Gentleman, R. C., Carey, V. J., Bates, D. M., Bolstad, B., Dettling, M., Dudoit, S., et al. (2004). Bioconductor: open software development for computational biology and bioinformatics. *Genome Biol.* 5:R80. doi: 10.1186/gb-2004-5-10-r80

Giandomenico, S. L., Mierau, S. B., Gibbons, G. M., Wenger, L. M. D., Masullo, L., Sit, T., et al. (2019). Cerebral organoids at the air-liquid interface generate diverse nerve tracts with functional output. *Nat. Neurosci.* 22, 669–679. doi: 10.1038/s41593-019-0350-2

Henken, D. B., and Martin, J. R. (1992a). Herpes simplex virus infection induces a selective increase in the proportion of galanin-positive neurons in mouse sensory ganglia. *Exp. Neurol.* 118, 195–203. doi: 10.1016/0014-4886(92)90036-P

Henken, D. B., and Martin, J. R. (1992b). The proportion of galanin-immunoreactive neurons in mouse trigeminal ganglia is transiently increased following corneal inoculation of herpes simplex virus type-1. *Neurosci. Lett.* 140, 177–180.

Hibaoui, Y., and Feki, A. (2012). Human pluripotent stem cells: applications and challenges in neurological diseases. *Front. Physiol.* 3:267. doi: 10.3389/fphys.2012.00267

Ida-Hosonuma, M., Iwasaki, T., Yoshikawa, T., Nagata, N., Sato, Y., Sata, T., et al. (2005). The alpha/beta interferon response controls tissue tropism and pathogenicity of poliovirus. *J. Virol.* 79, 4460–4469. doi: 10.1128/JVI.79.7.4460-4469.2005

John, T. J., Nambiar, A., Samuel, B. U., and Rajasingh, J. (1992). Ulnar nerve inoculation of poliovirus in bonnet monkey: a new primate model to investigate neurovirulence. *Vaccine* 10, 529–532. doi: 10.1016/0264-410X(92)90352-K

Jubelt, B., Narayan, O., and Johnson, R. T. (1980). Pathogenesis of human poliovirus infection in mice. II. Age-dependency of paralysis. *J. Neuropathol. Exp. Neurol.* 39, 149–159. doi: 10.1097/00005072-198003000-00004

Karber, G. (1931). 50% end-point calculation. *Arch. Exp. Pathol. Pharmak.* 162, 480–484.

Kennedy, J., McKee, M., and King, L. (2015). Islamist insurgency and the war against polio: a cross-national analysis of the political determinants of polio. *Global. Health* 11:40. doi: 10.1186/s12992-015-0123-y

Kew, O. M., Sutter, R. W., de Gourville, E. M., Dowdle, W. R., and Pallansch, M. A. (2005). Vaccine-derived polioviruses and the endgame strategy for global polio eradication. *Annu. Rev. Microbiol.* 59, 587–635. doi: 10.1146/annurev.micro.58.030603.123625

Kriks, S., Shim, J. W., Piao, J., Ganat, Y. M., Wakeman, D. R., Xie, Z., et al. (2011). Dopamine neurons derived from human ES cells efficiently engraft in animal models of Parkinson's disease. *Nature* 480, 547–551. doi: 10.1038/nature10648

Lancaster, M. A., Renner, M., Martin, C. A., Wenzel, D., Bicknell, L. S., Hurles, M. E., et al. (2013). Cerebral organoids model human brain development and microcephaly. *Nature* 501, 373–379. doi: 10.1038/nature12517

Lang, R., Gundlach, A. L., and Kofler, B. (2007). The galanin peptide family: receptor pharmacology, pleiotropic biological actions, and implications in health and disease. *Pharmacol. Ther.* 115, 177–207. doi: 10.1016/j.pharmthera.2007.05.009

Molla, A., Hellen, C. U., and Wimmer, E. (1993). Inhibition of proteolytic activity of poliovirus and rhinovirus 2A proteinases by elastase-specific inhibitors. *J. Virol.* 67, 4688–4695. doi: 10.1128/JVI.67.8.4688-4695.1993

Mueller, S., Wimmer, E., and Cello, J. (2005). Poliovirus and poliomyelitis: a tale of guts, brains, and an accidental event. *Virus Res.* 111, 175–193. doi: 10.1016/j.virusres.2005.04.008

Qian, X., Nguyen, H. N., Song, M. M., Hadiono, C., Ogden, S. C., Hammack, C., et al. (2016). Brain-region-specific organoids using mini-bioreactors for Modeling ZIKV exposure. *Cell* 165, 1238–1254. doi: 10.1016/j.cell.2016.04.032

Racaniello, V. R. (2006). One hundred years of poliovirus pathogenesis. *Virology* 344, 9–16. doi: 10.1016/j.virol.2005.09.015

Raudvere, U., Kolberg, L., Kuzmin, I., Arak, T., Adler, P., Peterson, H., et al. (2019). g:Profiler: a web server for functional enrichment analysis and

conversions of gene lists (2019 update). *Nucleic Acids Res.* 47, W191–W198. doi: 10.1093/nar/gkz369

Sadler, A. J., and Williams, B. R. (2008). Interferon-inducible antiviral effectors. *Nat. Rev. Immunol.* 8, 559–568. doi: 10.1038/nri2314

Shimizu, H., Agoh, M., Agoh, Y., Yoshida, H., Yoshii, K., Yoneyama, T., et al. (2000). Mutations in the 2C region of poliovirus responsible for altered sensitivity to benzimidazole derivatives. *J. Virol.* 74, 4146–4154. doi: 10.1128/JVI.74.9.4146-4154.2000

Tseligka, E. D., Sobo, K., Stoppini, L., Cagno, V., Abdul, F., Piuz, I., et al. (2018). A VP1 mutation acquired during an enterovirus 71 disseminated infection confers heparan sulfate binding ability and modulates *ex vivo* tropism. *PLoS Pathog.* 14:e1007190. doi: 10.1371/journal.ppat.1007190

van der Sanden, S. M., Wu, W., Dybdahl-Sissoko, N., Weldon, W. C., Brooks, P., O'Donnell, J., et al. (2016). Engineering enhanced vaccine cell lines to eradicate vaccine-preventable diseases: the polio end game. *J. Virol.* 90, 1694–1704. doi: 10.1128/JVI.01464-15

Yalamanchili, P., Datta, U., and Dasgupta, A. (1997). Inhibition of host cell transcription by poliovirus: cleavage of transcription factor CREB by poliovirus-encoded protease 3Cpro. *J. Virol.* 71, 1220–1226. doi: 10.1128/JVI.71.2.1220-1226.1997

Conflict of Interest: The authors declare that the research was conducted in the absence of any commercial or financial relationships that could be construed as a potential conflict of interest.

frontiers in Cell and Developmental Biology

REVIEW
published: 10 May 2021
doi: 10.3389/fcell.2021.640212

Modeling Neurological Disorders in 3D Organoids Using Human-Derived Pluripotent Stem Cells

Raj Bose[1,2,3,4]*, *Soumyabrata Banerjee*[1,2,3] and *Gary L. Dunbar*[1,2,3,5]*

[1] Field Neurosciences Institute Laboratory for Restorative Neurology, Central Michigan University, Mount Pleasant, MI, United States, [2] Department of Psychology, Central Michigan University, Mount Pleasant, MI, United States, [3] Program in Neuroscience, Central Michigan University, Mount Pleasant, MI, United States, [4] Department of Neuroscience, Karolinska Institute, Stockholm, Sweden, [5] Field Neurosciences Institute, Ascension St. Mary's, Saginaw, MI, United States

Modeling neurological disorders is challenging because they often have both endogenous and exogenous causes. Brain organoids consist of three-dimensional (3D) self-organizing brain tissue which increasingly is being used to model various aspects of brain development and disorders, such as the generation of neurons, neuronal migration, and functional networks. These organoids have been recognized as important *in vitro* tools to model developmental features of the brain, including neurological disorders, which can provide insights into the molecular mechanisms involved in those disorders. In this review, we describe recent advances in the generation of two-dimensional (2D), 3D, and blood-brain barrier models that were derived from induced pluripotent stem cells (iPSCs) and we discuss their advantages and limitations in modeling diseases, as well as explore the development of a vascularized and functional 3D model of brain processes. This review also examines the applications of brain organoids for modeling major neurodegenerative diseases and neurodevelopmental disorders.

Keywords: neurological disorders, hiPSCs, neural organoids, vascularization, blood-brain barrier

OPEN ACCESS

Edited by:
Eumorphia Remboutsika, National and Kapodistrian University of Athens, Greece

Reviewed by:
Panagiotis Politis, Biomedical Research Foundation of the Academy of Athens (BRFAA), Greece
George I. Lambrou, National and Kapodistrian University of Athens, Greece
Dimitra Thomaidou, Pasteur Hellenic Institute, Greece

***Correspondence:**
Gary L. Dunbar
dunba1g@cmich.edu
Raj Bose
bose1rk@cmich.edu

Specialty section:
This article was submitted to Stem Cell Research, a section of the journal Frontiers in Cell and Developmental Biology

Received: *10 December 2020*
Accepted: *15 March 2021*
Published: *10 May 2021*

Citation:
Bose R, Banerjee S and Dunbar GL (2021) Modeling Neurological Disorders in 3D Organoids Using Human-Derived Pluripotent Stem Cells. Front. Cell Dev. Biol. 9:640212. doi: 10.3389/fcell.2021.640212

INTRODUCTION

Neurons and glial cells (astrocytes, oligodendrocytes, and microglia) are major cellular types of the central nervous system, which are essential for normal brain function and are implicated in most neurological disorders. During brain development, neurons, astrocytes, and oligodendrocytes are derived from neuroepithelial cells, called neural stem cells (NSCs). Both neurons and glia are found to be affected in various neurodegenerative disorders, including Huntington's disease (HD), Alzheimer's disease (AD), and Parkinson's disease (PD) (Phatnani and Maniatis, 2015; Tao and Zhang, 2016; Blanco-Suárez et al., 2017; Fu et al., 2018). Although more abundant than neurons, astrocytes and oligodendrocytes develop from NSCs after neurogenesis. While microglia are present throughout the CNS and play important roles in the development and functions of CNS, they are not generated from NSCs (Schwartz, 1997). Microglia play an important role in normal brain function. They are involved in a wide variety of neurological and psychiatric disorders, such as multiple sclerosis (MS), amyotrophic lateral sclerosis (ALS), spinocerebellar ataxia, PD, HD, AD, brain ischemia, autism spectrum disorder, obsessive-compulsive disorder, and schizophrenia (Schwartz, 1997; Menassa and Gomez-Nicola, 2018; Zhao et al., 2018).

While the etiology and pathophysiology of many neurological disorders are largely unknown, it is generally acknowledged that these conditions are caused or affected by interactions of genetic and

environmental factors (Kwon et al., 2016; Berson et al., 2018; De Boni and Wüllner, 2019; Li et al., 2019). While the human brain is the ideal model to study such disorders, there are obvious ethical and technical limitations preventing this, not the least of which include unavailability of healthy and diseased brain tissue, as well as the difficulties with *in vitro* culture or genetic manipulation of adult brain tissue (Lee et al., 2017). Although animal models are commonly used to mimic human diseases, the high failure rate of translating most animal-based research into successful treatments in the clinic underscores their inadequacy to accurately model all critical features that characterize most human neurological disorders (Wang, 2018). For example, microcephaly, a neurodevelopmental disorder which is characterized by reduced brain size, has been modeled in transgenic mice, which contain microcephaly-related gene mutations, but does not adequately simulate this disorder, even in terms of brain size (Barrera et al., 2010; Pulvers et al., 2010; Lancaster et al., 2013). Likewise, many pharmacological interventions that proved successful in animal models of human neurological disorders do not translate into effective treatments in clinical trials (Burke, 2007; Pulvers et al., 2010; Takao and Miyakawa, 2015). As a further example, none of the ∼25 transgenic rodent models of HD can reproduce all neurodegenerative features and recapitulate the progression of this disease as presented clinically in HD patients (Pouladi et al., 2013; Bhalerao et al., 2020).

Fortunately, newly developed, human-derived *in vitro* models provide promising tools to overcome several of these limitations. For example, neurons and other cells, along with their transcriptional profiles, which are generated from human-derived induced pluripotent stem cells (hiPSCs) can be used to simulate a fetal brain. Human embryonic stem cells (hESCs) and hiPSCs are similar in their cell morphology, proliferation, and differentiation capacity, although some DNA methylation profiles are changed in iPSCs because of the reprogramming process (Deng, 2010; Kim et al., 2010; Liang and Zhang, 2013). Moreover, hiPSCs are scalable, reproducible models, which are capable of recapitulating complex neurodevelopmental events during early embryogenesis and disease pathogenesis. Thus, the generation of patient-specific hiPSCs through cellular reprogramming can closely recapitulate disease manifestations of the clinical phenotypes observed in patients (Wu et al., 2019). The main advantages of using hiPSCs, compared to hESCs, are that they are patient-specific, which eliminates the risk of immunological rejection when they are obtained from the patient who will receive the transplant (Ho et al., 2018).

Currently, organoids are most often used to model the development and pathological alterations in various human organs, including the brain (Völkner et al., 2016; Czerniecki et al., 2018; Kim et al., 2019). Neural organoids that have been derived from differentiating iPSCs have been developed by using different methods (Lancaster et al., 2013; Jo et al., 2016; Qian et al., 2018). The 3D brain organoid consists of various cell types that can recapitulate cortical neuronal layers, cellular compartmentalization, and brain-like functions. In addition, such organoids can recapitulate the development of embryonic tissue more accurately than that of the 2D culture of hiPSCs. Thus, 3D organoids have more promise for the investigation of human brain development and complex human diseases, including neurodevelopmental and neurodegenerative disorders. In this review, we first present different 2D culture methods that are used to generate various neuronal and non-neuronal cells derived from hiPSCs. Next, we discuss the organoid technologies that use iPSCs as *in vitro* models of neurological disorders. Finally, we examine recent advances in 3D neural organoid technologies, as well as their applications and limitations as model systems.

RECAPITULATION OF NSCS AND NEURONAL SUBTYPES FROM iPSCs

Neurons are generated first during brain development, although the exact number of neural subtypes in the immature brain is unknown (Phatnani and Maniatis, 2015). Most neurological diseases are associated with damage to specific neural subtypes, such as midbrain dopamine neurons in PD (Luk et al., 2012), medium spiny GABA neurons in the striatum in HD (Reinius et al., 2015), and motor neurons in ALS (Kanning et al., 2010). Therefore, modeling neurological diseases using hiPSCs has enhanced our understanding of how those neural subtypes alter their function in each of these disease processes. Following multiple protocols in 2D cultures, NSCs, and then neurons and glial cells, are generated from hiPSCs (Chambers et al., 2009; Zheng et al., 2018b; Soubannier et al., 2020) as can be seen in **Tables 1**, **2**. When hiPSCs are grown without medium components that promote self-renewal, embryoid bodies (EBs) are formed, and when fibroblast growth factor (FGF) or bone morphogenetic protein (BMP) inhibitors are absent, most hiPSCs form neuroepithelia (NE) or neural stem cells (NSCs) (Reubinoff et al., 2001). However, a single BMP or dual-SMAD inhibition method can be more useful than the EB method, due to culture variability. While the single BMP or dual-SMAD inhibition methods are equally effective in inducing neural differentiation, the dual-SMAD inhibition method with hiPSCs is more efficient in terms of forming neural rosettes (Zhang et al., 2018).

The dual-SMAD inhibition method is a procedure that inhibits SMAD-dependent transforming growth factor-beta (TGFβ) and BMP signaling pathways with SB431542 and noggin. This efficiently converts hiPSCs to NSCs, which are characterized by specific markers (**Table 1**). In this method, human iPSCs are cultured with EB medium for 5 days and the medium is replaced with a neural induction medium for the next 4–14 days (Zhang et al., 2018). To produce mature neurons, EB-derived rosettes can then be re-plated on poly-ornithine/laminin-coated plates and cultured using a neural differentiation medium for several weeks (Zhang et al., 2018). Specific neuronal subtypes from iPSCs have been generated by using a neural differentiation medium that contains various inducing factors, as can be seen in **Table 1**. Because the ability to induce several types of neurons in culture is critically important for receiving, processing, and transmitting the information through their self-created networks and because neurodegenerative diseases may affect many of these neuronal connections, the production of different subtypes of neurons

TABLE 1 | Differentiation of NSCs and neuronal subtypes from human iPSCs.

Generation of cell type	Origin	Factors inducing hiPSCs into NSCs	Factors inducing NSCs into neuronal subtypes	Characterization	References
NSC	hiPSC	Dual-SMAD inhibition together with bFGF, N2, B27, ascorbic acid, and PMA		NSC expresses Nestin and Sox2, expression of Pax6, OCT4, and SSEA4 in hiPSC, and NSC forms neural rosettes and differentiates into neural lineages	Chambers et al., 2009; Wattanapanitch et al., 2014; Palm et al., 2015
Neurons					
GABAergic neurons	hiPSC-derived NSCs		BMPRIA, Dkk1, and PM	Neurons express GABA and VGAT	Nicholas et al., 2013
Cortical neurons			FGF-2 or PD0325901, SU5402, and DAPT	Expression of FOXP2 and SATB2 in cortical neurons	Shi et al., 2012; Qi et al., 2017
Motor neurons			SAG, FGF-2, and RA	ChAT positive neurons	Maury et al., 2015
DA neurons			FGF-8, RA, and N2 together with BDNF, GDNF, and dCAMP	TH and FoxA2 positive neurons	Hartfield et al., 2014
Serotonin neurons			SHH and FGF-4	Neurons express TPH-2	Liu et al., 2018a,b

NSC, neural stem cells; DA, dopaminergic; bFGF, basicfibroblast growth factor; FGF-8, fibroblast growth factor-8; RA, retinoic acid; N2 supplement; BDNF, brain-derived neurotrophic factor; GDNF, glial-derived neurotrophic factor; dCAMP, dibutyryl cyclic adenosine monophosphate; SHH, sonic hedgehog; FGF-4,fibroblast growth factor-4; BMPRIA, bone morphogenetic protein receptor; Dkk1,Dickkopf-related protein 1; PM, purmorphamine; TPH-2, tryptophan hydroxylase-2; TH, tyrosine hydroxylase.

TABLE 2 | Differentiation of glial subtypes from human hiPSC-derived NSCs.

Generation of cell type	Origin	Factors inducing NSCs into astrocytes	Factors inducing NSCs into OPCs	Factors inducing OPCs into Oligos	Characterization	References
Astrocyte	hiPSC- derived NSCs	Astrocytic differentiating medium with 1-2 % FBS			Expression of GFAP, S100β, and AQ4.	Palm et al., 2015; Tcw et al., 2017; Soubannier et al., 2020
Oligodendrocyte	hiPSC- derived NSCs		RA and SAG or Sox10, olig2 and NKX6.2	PDGF-AA, NT3, and IGF-1	Expression of SOX10, PDGFRα, OLIG2, and NKX2.2	Douvaras et al., 2014; Ehrlich et al., 2017

OPC, oligodendrocyte progenitor cell; Oligo, oligodendrocyte; FBS, fetal bovine serum;PDGF-AA, platelet-derived growth factor-AA; IGF-1, insulin growth factor-1; NT3, neurotrophin-3.

from patient-derived iPSCs has been crucial to characterize disease phenotypes (Wu et al., 2019; Tran et al., 2020).

Recapitulation of Glial Subtypes From hiPSCs

Glial cells include oligodendrocytes, astrocytes, and microglia, which constitute almost half of the brain size (Azevedo and Feldman, 2010). Glia play important roles in many aspects of CNS, including brain development, homeostasis, and protection of neurons from brain injury and diseases (Reemst et al., 2016). Several neurological disorders, such as MS and Guillain–Barre syndrome, have been linked to glial cell dysfunction (Notturno et al., 2008). Here we describe current protocols for deriving various glial cells from hiPSCs and indicate how these glial cells can be used for future disease-modeling applications.

Astrocytes

Generating astrocytes in a 2D culture of hiPSCs takes longer than 3 months because the process involves the induction of cell-fate decisions. The EB or dual-SMAD inhibition method is usually used to differentiate hiPSCs into NSCs and then for differentiating neuronal and glial subtypes (Chambers et al., 2009). Currently, there is no effective method that can circumvent neurogenesis and/or promote direct generation of glia. Therefore, NSCs need to be expanded until the onset of glial development, which is characterized by expression of NF1A, S100β, CD44, and downregulation of PAX6 expression, which usually occurs during the third month of hiPSC differentiation (Krencik and Zhang, 2011). Thereafter, the glial progenitors are differentiated into astrocytes under specific differentiating conditions, such as BMPs and CNTF (ciliary neurotrophic factor), which induce astrocyte differentiation by activating the STAT3 pathway (Rajan and McKay, 1998). While glial progenitors are generated by the end of the 3rd month, another 3 months are required to generate functional astrocytes (Krencik and Zhang, 2011).

Recently, some researchers recommend using protocols that differentiate astrocytes from hiPSCs with the expression of GFAP and S100β more quickly (Palm et al., 2015; Ben-Reuven and Reiner, 2020; Soubannier et al., 2020) (**Table 2**). Like neurons, astrocytes are also classified into many subtypes because of their location, morphology, and molecular /physiological functions.

For example, fibrous astrocytes and protoplasmic astrocytes are found in white matter and gray matter, respectively (Wang, 2018). However, the current protocols need further improvement to produce regional-specific astrocytes from hiPSCs, which can be obtained by the modulation of RA, BMPs, and sonic hedgehog (SHH) in differentiating astrocytes, which, in turn, were derived from NSCs. Astrocyte dysfunction may be crucial in the malfunction of neurons (Phatnani and Maniatis, 2015; Garwood et al., 2017) and display disease-related phenotypes in AD and HD patients (Khakh et al., 2017). Thus, a further improved protocol may lead to the differentiation of mature and regionally-specific astrocytes, which would be a critical improvement for future applications in disease-modeling.

Oligodendrocytes

During development, oligodendrocytes start to appear from NSCs later than neurons and astrocytes and provide support through the formation of myelin sheath that wraps around and insulates the axons in the CNS. While the origin of oligodendrocytes includes the ventral neural tube, the dorsal neural tube, and the subventricular zone (SVZ) during development (Wang et al., 2012), most studies have focused on the area, such as the ventral part of the telencephalon and spinal cord, where the oligodendrocyte progenitor cells (OPCs) are differentiated from NE in response to SHH-induced expression of the Olig1/2 gene (Tao and Zhang, 2016). To produce oligodendrocytes, iPSC-derived NSCs are moved to a glial-induction media, containing platelet-derived growth factor-AA (PDGF-AA), insulin growth factor-1 (IGF-1), and Neurotrophin-3 (NT3) (Wang et al., 2012). Gliospheres can be derived from these NSCs in presence of these factors, which can be re-plated in smaller sizes to differentiate into oligodendrocytes. To date, these essential steps have been followed to differentiate oligodendrocytes from hiPSCs (Ehrlich et al., 2017). Similar to what is observed in brain development, neural specification is the first step of oligodendrocyte differentiation from hiPSCs, which is the same as that for differentiation of neurons and astrocytes (**Table 2**). The duration of differentiation of iPSCs into oligodendrocytes varies from 110 to 150 days.

Recently, Ehrlich et al. (2017) demonstrated a rapid and efficient protocol for generating oligodendrocytes from hiPSC-derived NSCs by inducing three transcription factors (SOX10, OLIG2, and NKX6.2). This method yields up to 70% O4+ expressing oligodendrocytes within 28 days of differentiation and 30% of these cells differentiate into mature myelin basic protein positive (MBP+) cells within 35 days. However, induction of specific transcription factors may interrupt the production of disease phenotypes of patient-derived iPSC models. Therefore, the simplest solution would be finding a mitogen that is neutral to the fate of the differentiation process undergone by the progenitor cell, which would be a crucial feature for a stable organoid model.

Microglia

Microglia are known as macrophages of the CNS, which account for 5–10% of total neural cells in parenchyma (Zhao et al., 2018). They are uniformly distributed throughout the brain. While the identity of microglial progenitors remains controversial, it is hypothesized that microglial differentiation has occurred in the CNS from embryonic and perinatal hematopoietic cells. Immune defense and maintenance of homeostasis are two key functions of microglia in the CNS. They are required for inflammatory responses of the CNS, and they are dysregulated in several different diseases, including AD and PD (Zheng et al., 2018b; Song et al., 2019a,b). In recent years, different protocols have been proposed to generate microglial cells from iPSCs (McQuade et al., 2018; Menassa and Gomez-Nicola, 2018). Colony-stimulating-factor-1 (CSF1) receptor ligands are available in all these protocols, which are required for the proliferation, differentiation, and survival of normal macrophages. However, batch-to-batch variability and cellular heterogeneity are the limiting factors for the use of these methods (Quadrato et al., 2017; Pollen et al., 2019).

To bypass the formation of EBs, Abud et al. (2017) proposed a different protocol for the differentiation of hematopoietic progenitors directly from iPSCs, which were further differentiated into functional microglial-like cells. Recently, the earlier methods have been improved by adding IL-34 and granulocyte-macrophage colony-stimulating factor (GM-CSF), instead of CSF1 (Song et al., 2019b). This method provides higher cell proliferation (higher BrdU+ cells) and reduced ROS expression and produces a more accurate simulation of the tissue-specific microenvironment. The co-culture of the microglia-like cells (MG) with different neural organoids produces different migration patterns and functional activities, including variation in response to exogenous factors. In addition, transcriptome analysis revealed that microglia-related genes are expressed differently in MG when they are co-cultured with neural organoids (Song et al., 2019b). These findings indicate that generating microglial from iPSCs is a significant advance in iPSC technology, whereby non-neuronal cells can be readily derived from iPSCs, providing an avenue for more efficient designs of organoid models in the future.

THE BLOOD-BRAIN BARRIER (BBB), BRAIN MICROVASCULAR ENDOTHELIAL CELLS (BMECS), AND PERICYTE PRODUCTION OF iPSCs

The precise organized activity among different cell types within the neurovascular unit (NVU) is required to maintain CNS functions (Zhao et al., 2015). The interaction of NVU components, such as pericytes, endothelial cells, smooth muscle cells, astrocytes, oligodendroglia, microglia, and neurons is critical for the energy demands of the brain. The blood-brain barrier (BBB) is an important part of NVU, which consists of unique microvascular endothelial cells (BMECs), neurons, astrocytes, microglial cells, and pericytes. These multiple cell types are interconnected by tight and adherent junctions and express specific molecular transporters (Benson and Joseph, 1961). Furthermore, these dynamic cellular complexes are essential for brain homeostasis and regulate active interaction between the bloodstream and CNS. The transport of essential

molecules and nutrients into brain is regulated by the BBB, which is required to maintain an optimal CNS function (Fernández-López et al., 2012) by responding to many physiological and pathological cues (Erickson et al., 2020). Thus, the complex vascular network of the BBB protects the CNS from not only systemic fluctuations but also various harmful substances, including pathogens and toxins (Bhalerao et al., 2020).

BMECs form the innermost layer of the vasculature, which is characterized as a physiological barrier, and active metabolic system. Therefore, these unique cell types can regulate tissue microenvironment by synthesizing various materials. Structural and functional alterations of the BMECs have been reported in several neurological disorders, such as stroke, traumatic brain injury, and neurodegenerative diseases (Liu et al., 2018a,b; Jarazo et al., 2019). BMECs malfunction when they are removed from the brain microenvironment and cultured for extended periods of time. Fortunately, new iPSC technologies are opening up unique opportunities to generate BMECs that can be used in the modeling of various diseases with different components of the BBB.

The first iPSC-derived BMEC population was detected by co-differentiating neural-like and endothelial cells (Lippmann et al., 2012). Thereafter, several protocols have been published with modification of cell culture conditions, with more efficient differentiation processes, and with the integration of the specific disease pathology (Canfield et al., 2017; Erickson et al., 2020). Canfield et al. (2017) first demonstrated that iPSCs can generate functional BMECs, in conjunction with neurons and astrocytes. When BMECs are co-cultured with neurons and astrocytes, the barrier tightens, and tight junction localization is significantly improved. Furthermore, the iPSC-derived BBB can be used as a model by improving functional properties, such as improved transporter activity, barrier tightening, tight-junction localization, and paracellular permeability (Appelt-Menzel et al., 2017; Hollmann et al., 2017). However, the generation of BBB components from hiPSC and precisely coordinated activity among these dynamic cellular complexes in real-time is needed for the reproducibility and application of iPSC-derived multicellular BBB models.

Pericytes are part of the NVU, with stem cell-like properties, and consist of multi-functional cells located inside capillaries throughout the body, including the brain. They are critical for the regulation of cerebral blood flow, BBB, neuroinflammation, vascular development, and angiogenesis. Pericyte dysfunction may induce vascular diseases, such as stroke and neurodegenerative diseases. These cells may also cause transcytosis across the interior of BMECs (Armulik et al., 2010). As multi-faceted mural cells, pericytes are found in smaller vascular structures, including capillaries, and are characterized by specific markers, such as platelet-derived growth factor receptor-beta, smooth muscle protein 22 alpha, and calponin-1 (Armulik et al., 2011). During development, neural crest stem cells give rise to CNS mural cells, while peripheral mural cells are generated from a mesodermal lineage (Etchevers et al., 2001). CNS mural cells can also be produced from iPSCs, but their functionality as part of the BBB is still unknown.

A recent study demonstrated an updated protocol to produce brain pericyte–like attributes from hiPSC-derived neural crest stem cells (NCSCs) (Stebbins et al., 2019), which can integrate with endothelial cells to form vascular networks. Moreover, these cells have been characterized as scalable and reproducible, with BBB properties. Thus, the generation of pericytes from patient-derived iPSCs delivers a unique tool for the investigation of CNS disorders, including stroke, epilepsy, demyelinating disease, and AD (Stebbins et al., 2019).

The generation of patient-specific iPSCs can recapitulate disease phenotypes that are reported in patients. The iPSC-based 2D protocols have been used to investigate the pathophysiology of specific cell types that are involved in neurological diseases. However, these methods are still unable to provide the complex organization that mimics such complicated processes as embryonic development, cellular networking, and disease development (Dang et al., 2016). Moreover, the diversity of iPSC-derived cells and various types of neuronal and glial precursors are too immature to provide the metabolic, structural integrity, and neuronal activity that is observed in the mature brain. The genomic and epigenomic signatures are also more vulnerable to time-dependent alterations in 2D culture systems.

In this context, hiPSC-derived 3D brain organoids are more attractive tools for *in vitro* disease modeling because they can undergo multi-lineage differentiation and self-organization to form heterogeneous cell populations and tissue-like architecture (Lee et al., 2017). This 3D environment is more conducive to the differentiation of specific cell types that can mimic the early stages of human CNS maturation. Gene regulatory mechanisms observed during neurogenesis in the primary cortex are more accurately recapitulated in organoid models, which further support their utility. In addition, 3D brain organoids are appropriate tools for drug screening and tissue replacement therapy, especially in the context of neurodevelopmental and neurodegenerative disorders.

CURRENT PROTOCOLS FOR THE GENERATION OF 3D ORGANOIDS AND SELF-PATTERNING OF hiPSCs

During brain development, the patterning of anterior-posterior (A-P) and dorsal-ventral (D-V) axes are regulated by specific signaling molecules. For example, FGFs, retinoic acid (RA), and WNT signaling regulate the A-P patterning, whereas Wntss, BMPs, and SHH influence D-V patterning. The most common method of simulating brain development processes involves the generation of neurons from hiPSCs by producing NE or NSCs as a preliminary step toward differentiating neural subtypes as a function of activating specific types of growth factors or signaling pathways. Either the single BMP or the dual-SMAD inhibition approach can produce NE from hiPSCs, allowing certain region-specific markers, such as paired box 6 (PAX6) and orthodenticle homeobox 2 (OTX2), to be expressed in an anterior part of the brain (Zhang et al., 2018). Later, this NE gives rise to a specific brain region within 2 weeks in presence of morphogens. For example, CHIR99021 (CHIR), which activates

the Wnt pathway, can establish an incrementally increased concentration gradient that can differentiate the NE into different brain regions (forebrain, midbrain, and hindbrain) as a function of its increased concentration along the A-P axis (Kirkeby et al., 2012). A specific concentration of CHIR can generate specific neuronal populations, such as midbrain DA neurons and hindbrain serotonin neuronal populations. Following these principles, the combination of Wnt, RA, and FGFs on NE can also generate spinal cord cells (Maury et al., 2015).

The SHH, the WNT canonical pathway, and the BMP pathway regulate D-V patterning. These signaling molecules are secreted from the notochord and/or the floor plate. In absence of SHH signaling, the anterior NE give rise to the cerebral cortical identity (Le Dréau and Martí, 2012). The NE give rise to the lateral ganglionic eminence (LGE) when the expression of SHH is low. The specific markers, GS Homeobox 2 (GSX2), B-cell CLL/lymphoma 11B (CTIP2), and Meis homeobox 2 (MEIS2) are expressed in this region. Primarily, the medium spiny GABA neurons are produced from these progenitors (Arber et al., 2015). In the presence of a high concentration of SHH, the NE become progenitors for the medial ganglionic eminence (MGE), which is identified by the expression of NK2 homeobox 1 (NKX2.1). These progenitors differentiate into GABAergic interneurons and forebrain cholinergic neurons (Liu et al., 2013; Kim et al., 2014). Thus, the production of different cell types that forward the D-V axis is regulated by the level of SHH and /or a balance between SHH and Wnt pathways.

As an example of this D-V patterning, radial glia progenitor cells first generate neurons in cortical layer VI and I during the development of the cerebral cortex. Then these progenitors gradually differentiate into neurons in layers V, IV, III, and II (Gaspard et al., 2008). Based on morphogen availability along D-V axes during brain development, the most common approach for simulating neuronal induction from hiPSC involves the dual-SMAD inhibition factors, noggin and SB431542, and the Wnt pathway activator, CHIR. Later, SHH along with either RA or FGF8, is added to the culture medium to produce cerebral or midbrain patterned organoids, respectively. Brain-derived neurotrophic factor (BDNF), and glial cell-derived neurotrophic factor (GDNF) are important for the maturation, function, and survival of different types of neurons, including cholinergic, dopaminergic, serotonergic, and gamma-aminobutyric acid (GABA)-ergic neurons. Along with these specific factors, other complementary molecules are included in the medium to facilitate organoid development, including rho-associated protein kinase (ROCK) inhibitors for the survival of iPSCs, heparin for enhancing the activity of Wnt signaling, 2-mercaptoethanol for the reduction of oxidative stress and cell death, laminin and insulin for the tissue growth, and ascorbic acid and DB-cAMP for enhancing neuronal differentiation.

Based on the protocol developed by Lancaster et al. (2013), iPSCs can be differentiated into organoids between 1–2 months and maintained for up to a year, although the rate of growth is reduced gradually after 2 months due to necrosis inside the organoids (Lancaster et al., 2013). Later, Lancaster et al. found that agitation of the organoids using a spinning bioreactor decreased necrosis and increased the rate of organoid growth. Such improvement of their growth could be due to the availability of sufficient oxygen and nutrients during the differentiation process (Lancaster and Knoblich, 2014). Although comparing neurodevelopmental sequelae of organoids with those that occur in humans is somewhat speculative, given our current knowledge, it does appear that a 2-month-old organoid brain parallels the neuronal development occurring during the first trimester in humans (Lancaster et al., 2013). Cerebral organoids at 2 months contain NSCs, astrocytes, neurons, and synaptic structures, suggesting increased cellular diversity and neuronal organization.

The field of neural organoids has been advanced and made more sophisticated by the modification of current protocols and applying advanced technologies in recent years (Kelava and Lancaster, 2016). For example, the methylome and transcriptome profiles of cerebral organoids possess significant similarities to human fetal brains (Luo et al., 2016), although further studies are required to ensure stable reproducibility (Luo et al., 2016). More recently, the development and characterization of vascularized organoids have been one of the most significant advances in this field (Mansour et al., 2018).

While chemical signals can be used to manipulate most of the changes in the self-organization of organoids, there still remain several shortcomings to overcome. It is difficult to predict how these current methods regulate spatiotemporal patterning and differentiation in neural organoids, given that critical morphogens can be secreted endogenously, including BMPs and Wnts, as well as SHH and RA. Recently, Lancaster et al. (2017) showed that poly (lactide-co-glycolide) copolymer (PLGA) fiber microfilaments can be used to produce enlarged EBs. Moreover, organoids produced in these conditions not only lengthen the NE production, but also improve the formation of neuroectoderm, cortical layers, and even increase reproducibility (Lancaster et al., 2017). One new development involves fusing organoids. For example, organoids with dorsal identity are fused with those with a ventral identity to form a D-V axis (Xiang et al., 2017). However, a D-V axis can also be formed in a single organoid and display a self-organized cortical plate as Lancaster et al. (2017) demonstrated earlier.

While current 3D organoid protocols have taken precedence over 2D methods in the context of cellular diversity, neuronal connection, and tissue-like functions, these models are still unable to respond appropriately to infection, toxic substances, and age-associated inflammation, due to their lack of vascularization and immune cells, such as endothelial cells, monocytes, macrophages, or leukocytes (Ho et al., 2018). The currently used organoids do not recapitulate the later stages of the human embryonic brain (Monzel et al., 2017; Pham et al., 2018) and to do this would require further improvement in culture methods that are more physiologically and biologically relevant in order to accurately model the human brain. The lack of cellular diversity, the establishment of circuits, cell viability, and maturation are the major concerns for current organoid development.

Crucially, the formation of a vascular system, which is essential for oxygen penetration, nutrient supply, and NSC migration and differentiation is needed. The deficiency of vascular dissemination can induce hypoxia in organoid cultures

and may enhance necrosis in the center of the organoid, which can hinder the neurogenesis, their migration routes, and networking. In addition, current organoids are limited in their ability to exhibit cell–tissue interactions, patterns of neuronal networking, and integration of the brain immune system with organoids. Clearly, a more extensive method for establishing better vascularized neural organoids to model human neurodevelopment and neurological diseases is needed.

Generation of Patient-Derived Organoids With Vasculature and Microglia Components

A vascularized organoid could recapitulate the *in vivo* vascularization process that occurs during brain development and may reveal new features that have not yet been observed. A critical component for recapitulating vascularized organoids is the BBB, which, as indicated above, is a highly selective border consisting of BMECs, basement membrane, along with pericytes, astrocytes, and microglia. Brain homeostasis is regulated by BBB, which is essential for neuronal activities. The murine CNS starts to form vascularization at embryonic day 7.5–9.5, whereas human brain vascular components are detected within a gestational week 7 (Cakir et al., 2020). ECs play a critical role for neuronal maturation of cortex (Cakir et al., 2020) as it provides a protective layer of tightly joined cells that prevent diffusing toxins and infectious agents into the surrounding brain tissue. Disruption of the BBB has been associated with numerous neurological disorders, including HD, in which the breakdown of the BBB is thought to accelerate the progression of the neuropathological processes in the R6/2 mouse model of HD (Di Pardo et al., 2017), and post-mortem tissue from HD patients (Di Pardo et al., 2017; Bhalerao et al., 2020).

The recruitment of vascular networks, immune cells, and the BBB within organoids would make them a more physiologically relevant model of the human brain. Therefore, the generation of vascularized organoids has been recognized as a more relevant model to human diseases, which would allow for diffusing oxygen and nutrients throughout the mass that would support differentiation of multiple cell types into complex organization-like structures (**Figure 1**; **Table 3**). From a therapeutic perspective, a vascularized organoid could mimic normal physiological and pharmacological events that occur in the body, such as drug uptake, circulation, and metabolism. Although transplantation of human-derived nonvascular brain organoids into the rodent brain can produce integration, viability, long-term survival, increased angiogenesis, functional neuronal activity, and synaptic connectivity of the grafted organoid (Daviaud et al., 2018; Mansour et al., 2018), these beneficial effects are likely to be enhanced with transplants of vascularized organoids. In addition, a vascularized organoid developed from patient-specific hiPSCs might be grafted more successfully into patients, as it may integrate more readily with the vascular network of the patient (Ho et al., 2018).

ECs can be generated from hiPSCs, which support the feasibility of producing and integrating a vasculature using current organoid models (Pham et al., 2018). Briefly, to produce these vascularized organoids, iPSCs were first cultured and differentiated to ECs using the Stem Diff APEL medium, supplemented with morphogenetic protein 4 (BMP4), FGF-2, and vascular endothelial growth factor (VEGF). Thereafter, ECs derived from iPSCs were co-cultured with the cerebral organoid for 3–5 weeks before transplantation, which resulted in robust vascularization of organoids within 5 weeks. However, the limitation of the transplanted vascularized organoids is that capillaries were found in the center of rosettes, as well as in between rosettes, although the presence of rodent blood in these capillaries was not verified, as the brains were perfused with saline and formalin (Pham et al., 2018). Moreover, proof of any connectivity between the human brain organoid capillaries and the rodent host brain is lacking (Pham et al., 2018), which is a hurdle in the combination of *in vitro* and *in vivo* models, as disease modeling should be maintained under physiological conditions. Human umbilical vein endothelial cells (HUVECs) are derived from the endothelium of veins of the umbilical cord, which form a tube, and have been widely used to characterize angiogenesis and other biological processes (Shi et al., 2020). More recently, another study reported that co-cultures of hESCs or hiPSCs with HUVECs generate human brain microvascular endothelial cells (HBMECs), which were characterized by P-glycoprotein (P-gp), and are the main ECs in the human brain, playing important roles in the BBB formation (Shi et al., 2020). However, evidence of ECs clustering and forming a functional BBB in the organoids is lacking (Shi et al., 2020).

ETS variant 2 (hETV2) is a transcription factor that is essential for the development of vascular endothelial cells. Based on this idea, Cakir et al. (2020), demonstrated a robust vascularization in cortical organoids, *in vitro*, with the induction of ETS variant 2 (hETV2). This vascularized organoid acquired several BBB characteristics, including an elevated expression of tight junctions, nutrient transporters, and trans-endothelial electrical resistance. Furthermore, the transcriptome profiles of neurons generated in non-vascularized and vascularized organoids were compared with human embryonic brains at gestational weeks 8–23. The transcriptome analysis of these neurons revealed that vascularized organoid-derived neurons resemble more mature neurons of a developing brain than that of non-vascularized organoids (Cakir et al., 2020). These results suggest that vascularization accelerates the maturation of neurons.

Recently, amyloid (Aβ1–42) oligos have been found to damage endothelial cells, tight junctions, and the BBB in AD (Wan et al., 2015). The biological function of BBB was further evaluated in this study by the deposition of Aβ peptide species (Aβ1–42-oligos or Aβ1–42-fibrils) in these vascularized organoids (Cakir et al., 2020). The results of this study indicated that Aβ1–42-fibrils do not damage tight junctions as effectively as Aβ1–42-oligos. Altogether, these results indicate that overexpression of hETV2 gene induces functional endothelial tight junctions and BBB-like characteristics. Nonetheless, several unresolved limitations remain, such as the lack of functional blood vessels, absence of the six distinct cortical layers, and the limited formation of microglia (**Table 3**), which play important roles in the formation of subventricular vascular plexus (SVP). Most notably, the absence of a vascular system can be detrimental to long-term organoid

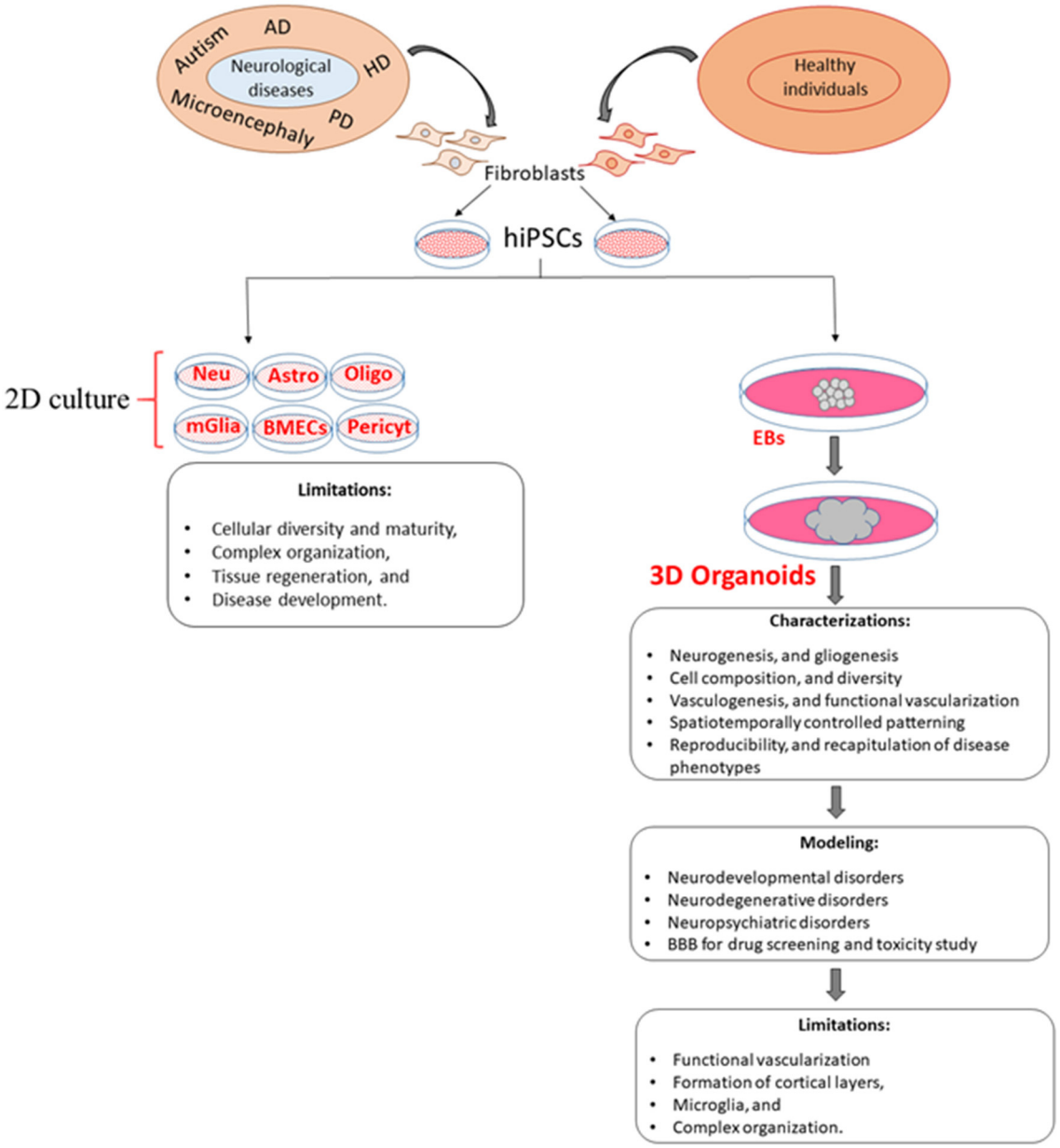

FIGURE 1 | Comparison of 2D and 3D cell culture models and their limitations. Although 3D models overcome some of the limitations of 2D models, the generation of new 3D models is needed to increase vascularization, cellular diversity, viability, and reproducibility as well as a more accurate recapitulation of disease phenotypes. EBs, embryoid bodies; Neu, Neuron; Astro, astrocytes; Oligo, oligodendrocyte; mGlia, microglia; BMECs, brain microvascular endothelial cells; Pericyt, pericyte.

survival, as long-term culture of organoids demonstrates a continuous apoptotic cell death at the inner-most regions (Cakir et al., 2020). Moreover, neuron progenitor differentiation is impaired without a functional vasculature (Cakir et al., 2020).

Microglia and the neurovasculature display physical interactions, although they do not appear in the developing CNS at the same time. During brain development, microglia originate from the embryonic yolk sac, then migrate and colonize the neuroepithelium (Reemst et al., 2016). While several protocols have been developed to produce microglia-like cells or precursors derived from hiPSCs (Muffat et al., 2016; Abud et al., 2017; Song et al., 2019b), most microglia derivations lack a microenvironment that promotes region-specific microglia function. For example, forebrain microglia, but not cerebellar microglia, depend on IL-34 for maintenance. Microglial cells are found in the conjunction with the vasculature in the developing rodent brain and are sometimes referred to as "pericytic macrophages" (Thomas, 1999), which play critical roles in angiogenesis and the maintenance of the BBB integrity.

TABLE 3 | Current protocols for hiPSC-derived 3D vascularized organoids.

Cell types	Organoid types	Characterization	Recapitulation of disease phenotypes	Limitations	References
HiPSCs with HUVECs-derived ECs	Cortical	Lack of connection between human brain organoid capillaries with the rodent host brain	Not addressed	Limited regulation in Vasculature, and formation of microglia	Pham et al., 2018
HiPSCs with HUVECs-derived ECs	Cortical	Lack of ECs cluster and the functional BBB	Not addressed	Limited regulation in Vasculature, and formation of microglia	Shi et al., 2020
HESCs with the induction of ETS variant 2 (hETV2)	Cortical	Functional BBB, and maturation of neurons	Not addressed	Lack of functional blood vessels, the six distinct cortical layers, and the limited formation of microglia	Cakir et al., 2019

HiPSCs, human induced pluripotent stem cells; HUVECs, human umbilical vein endothelial cell; HESCs, human embryonic stem cells.

We mentioned earlier that different cell signaling molecules, such as Wnt, BMP, and SHH control the regional identity of the developing brain. While organoid technologies have been promising models to study *in vivo* brain development and disease phenotypes, the major limitation is to achieve truly *in vivo*-like functionality due to the lack of reasonable size and structural organization of tissues, such as the shape of the D-V, mediolateral, and A-P axes. Organoids are most often grown as floating in the culture medium, and morphogens are added to the medium uniformly for self-organizing and cell fate-patterning. However, compared to what occurs *in vivo*, organoids exposed to this conditional media lack concentration gradients of morphogens, which results in a stochastic organization of the developing organoids, rather than asymmetric brain development, such as the establishment of the D-V, mediolateral, and A-P axes.

While different protocols (Bagley et al., 2017; Wang et al., 2018) were established to develop the D-V and A-P axis in human brain organoids, morphogen-loaded beads were found to be more effective in establishing spatial identities in human brain organoids (Ben-Reuven and Reiner, 2020). In this method, organoids with morphogen-soaked beads were co-cultured to diffuse morphogens from the beads to the tissue, which create a concentration gradient of morphogen secretions in the developing organoids. For example, organoids embedded on Wnt and BMP4-soaked agarose beads may increase the local concentration of morphogens, which is decreased within the tissues. Making such gradient of morphogen availability allows for high and low concentration of morphogens to induce dorsal and ventral patterning of the developing brain organoids, respectively. However, providing vasculature and microglial integration would further improve the current status of organ-on-chip technology. In embryonic brain development, developing tissues can interpenetrate and interact with the complex vasculature system, which facilitates diffusion of oxygen, nutrient, and exchanging waste, as well as a structural template for growth. However, a perfect protocol for *in vitro* organoid development with the integration of vasculature has remained largely missing, which may be a crucial requirement for large-scale and more reproducible tissue organization, including D-V and A-P identity in the organoids. Meanwhile, microglial integration with organoids may enhance migration ability and immune response, which may facilitate maturation and neural circuit development. Different cutting-edge technologies, including 3D microelectrode arrays (MEAs) and optogenetics, have been used to characterize neural circuits. However, an advanced method for the development and characterization of vascularized organoids is needed.

Organoids that integrate microglial cells with ECs to develop vascularization should provide new insights into how microglia can interact with neurovascular systems to form a functional BBB, as well as how microglia-neuron and microglia-astrocyte communication function in both normal and pathological conditions (Zhao et al., 2018) (see **Figure 1**). Such newly developed systems could also facilitate replicating organoids of the same size and shape, as well as similar cellular composition, phenotypic and molecular characteristics (Lee et al., 2017), along with greater integration of vascular endothelial cells, immune cells, microglia, and BBB within organoids.

Organoid on ChiP

Recently, organ-on-a-chip technology has captured the attention of researchers and inspired the development of a new complement to current organoid models. This technology is a promising tool for disease modeling, drug screening, and toxicity testing. Organ-on-chip systems have become more advanced because of using microfluidic technology. Therefore, different microfluidic organ-on-chip systems have been developed to model various organs, including the liver, kidney, intestine, lung, heart, and brain. Recently, Zhang et al. (2017) built a device that has physical, biochemical, and optical sensing capabilities to regulate the cellular microenvironment for recapitulating complex organization and functions. Subsequently, Wang et al. (2018) developed a perfusion-based organoid culture on a microfluidic chip where the EB is matured into self-organized organoids under a controlled microenvironment, such as diffusion of oxygen and nutrient to the growing cells and removing of waste from these cells. Such a microenvironment is essential for self-organized organoids to mimic the *in vivo* organ structure and function, which currently is lacking unconventional organoid models.

Recent advances of these devices provide more transparent *in situ* real-time imaging of the neurodevelopmental process and

the brain organoid responses to exogenous factors, including nicotine, valproic acid, and cannabis (Wang et al., 2018; Ao et al., 2020; Cui et al., 2020), suggesting an alternative approach for characterizing 3D organoids in the human neurodevelopmental disorders. The new edition of these devices can integrate multiple organs for simulation, and pharmacokinetic assays for new drugs (Skardal et al., 2017). In addition, multi-organ chips are important systems for studying the efficacy and toxicity of new drugs, interaction among different organs, and developing drugs that are tailored to specific individuals (Skardal et al., 2017; Schimek et al., 2020).

While these microfluidic platforms can improve brain organoid uniformity by minimizing size variation, as well as hypoxia and cell death inside of the organ due to the availability of a controlled microenvironment as mentioned above, the system still cannot recapitulate fully the physiological and disease features that occur *in vivo*. Difficulties in standardizing and scaling up these types of organoids remain formidable challenges. In addition, a means fo producing microglia and a functional vasculature are lacking in those devices, which impede the development of mature and functional organoids, which are important for simulating the later stages of *in vivo* neurodevelopment and disease features.

Characterization of 3D Organoids With Cutting-Edge Technologies

Characterization of many developmental and disease-specific features of these organoids has been challenging due to lack of proper technologies, while several cutting-edge technologies have been used to characterize the organoids such as MEA, patch-seq, and optogenetics. The potential application and limitations of these methods in 3D organoids are briefly discussed below.

Microelectrode arrays (MEA) Non-invasiveMEA recordings are often used to investigate the effects on neuronal impulse activity and to analyze the underlying ion currents in isolated individual neurons. The design of MEAs for 2D cultures of neurons is different from 3D cultures of neurons, while recordings of neuronal action potentials are common between these two arrays. The design of such 3D MEAs is challenging because the materials used need to be sufficiently pliable to avoid damaging the tissue. Polyimide is a good choice because of its favorable thermal and chemical tolerance and it can be integrated without causing 3D tissue damage. While *in vitro* culture of 3D organoids has been advanced, lack of appropriate 3D MEA methods for precisely monitoring and modulating neuronal activities in organoids remains a challenge. Recently, Soscia et al. (2020) designed 3D MEAs which can provide multi-channel recordings as well as record precise signals that are appropriate to the cellular morphology, neural network dynamics, and drug responses. Recent advances of 3D MEAs have demonstrated integrated capabilities to stimulate surrounding neurons to form a neural network in real-time in such 3D neural organoid models (Shin et al., 2021). However, further refinements of these 3D MEAs, with appropriate size and density of electrodes to accommodate 3D organoids is needed.

Optogenetics is based on genes coding for light-sensitive proteins (opsins) and the expression of these genes requires a specific color of light. For example, channelrhodopsin-2 (ChR2) expression is turned on by blue light and halorhodopsins are active in dark conditions. In this method, a combined (optical and genetic) tool is used to regulate individual neuronal activity. This technique has been successfully applied to embryonic stem cells (ESCs) to study motor deficits (Baker et al., 2016). Quadrato et al. (2017) performed single-cell sequencing and analyzed the data to demonstrate that light stimulation of photosensitive cells could regulate neuronal activity within organoids. This tool has also been used in grafted cerebral organoids (Mansour et al., 2018) and cortical spheroids (Yoon et al., 2019) to study host-graft functional connectivity, and express opsin by blue light. Thus, this technique could be a very useful tool to elucidate light-sensitive tissue organization and functional human neuronal circuits in the developing human brain. Finally, a combination of both the organoid system and optogenetic technology may allow neuroscientists to study morphological and functional diversity of neural circuits precisely in the healthy and diseased brain tissue.

Patch-seq can be considered as a different approach from high-throughput droplet-based single-cell RNA sequencing (scRNAseq), which has revolutionized neuroscience. In this technique, first functional properties of a specific neuron are measured by patch-clamp electrophysiology before studying the molecular basis of morphologic and functional diversity using transcriptional profiling of the cell. Currently, the technique has potential application in a variety of models, including hiPSC-derived neurons (Yoon et al., 2019). While Patch-seq has been used for *in vivo* recordings (Cadwell et al., 2016; Liu et al., 2020), the cell culture-based approaches make it easier for identifying live cells by high-resolution imaging and increases the capability of collecting RNA from the entire neuron. However, the significant challenges of this technique are that it is laborious and has a relatively low throughput compared to droplet-based scRNAseq. An advanced improvement of patch-clamp recordings and sequencing methodologies will certainly extend the application of Patch-seq methods in organoid technology.

Recapitulation of Neurodegenerative and Neurodevelopmental Disorders Associated With the Genetic Signature in Patient-Derived Organoids

Organoids that have been derived from hiPSCs from patients with neurodegenerative disorders, such as HD, AD, and PD, or neurodevelopmental disorders, such as microencephaly and autism spectrum disorder, can be useful tools for understanding the pathophysiological mechanisms of these disorders.

Huntington's disease is a devastating neurodegenerative disease, which is characterized by motor dysfunction, cognitive impairment, and psychiatric symptoms (Walker, 2007; Zheng et al., 2018a). The major cause of HD is a mutation in exon 1 of the *HTT* gene, while other factors, such as environmental factors, may be involved in the progression of this destructive disorder. The mutation of the *HTT* gene results in an expansion

of cytosine-adenine-guanine (CAG) trinucleotide repeats (TNR) (MacDonald et al., 1993). These CAG repeats form abnormal aggregates, which become toxic to both the neuronal population and their neural networks by interfering with the cellular machinery, including axonal transport, mitochondrial, and synaptic function. These toxic aggregates initially damage the medium spiny neurons (MSNs) of the striatum. To date, various 2D culture methods have been used to generate MSNs from hESCs and human iPSCs as MSNs are the major susceptible cell type in HD (Adil et al., 2018; Wu et al., 2018, 2019). Although 2D culture methods provide highly enriched MSNs from HD patient-derived iPSCs with higher than 50 CAG repeats for disease modeling, the recapitulation of HD-relevant phenotypes, including neuronal degeneration, often requires the addition of other cellular stressors. For example, mitochondrial dysfunction and oxidative stress occur when HD-iPSC-derived neurons are exposed to oxidative stress-inducing molecules. Recently, Conforti et al. (2018) produced a 3D cortical organoid using hiPSCs derived from HD patients, which was characterized by developmental defects in ventral-telencephalic and striatal formation during maturation. However, this model failed to show HTT protein aggregation and cell viability as the main pathogenesis of HD, suggesting that more work is needed to ensure that patient-derived organoids accurately recapitulate the disease phenotype (**Table 4**).

Alzheimer's disease is a complex, multifactorial disorder with genetic, and environmental factors that ultimately lead to premature neuronal death. Early-onset familial AD (EOAD) is a rare autosomal dominant form of AD with predictive gene mutations, but genetic and environmental factors that affect susceptible genes are the major risk factors for late-onset AD (LOAD), which is also called sporadic AD. Furthermore, genetic variations by susceptibility genes play a crucial role in determining the risk of LOAD (Papaspyropoulos et al., 2020). Raja et al. (2016) demonstrated disease phenotypes (amyloid and tau pathology) in organoids (**Table 4**), which were derived from multiple familial AD (FAD) patients whose genotype consisted of amyloid precursor protein (APP) duplication or presenilin1 (*PSEN1*) mutations. Moreover, the treatment of patient-derived organoids with β- and γ-secretase inhibitors significantly reduced amyloid and tau pathology. Recently, Gonzalez et al. (2018) generated cerebral organoids from patient iPSCs affected by familial AD or Down syndrome (DS). These organoids manifested pathological properties of AD, such as Aβ and p-tau protein aggregates, as well as the elevated degree of cellular apoptosis (**Table 4**). These studies demonstrate that AD pathology can be at least partially recapitulated in patient-derived organoids and, compared to current methods, these organoids offer a new platform for the investigation of drug screening for therapeutic intervention.

Parkinson's disease is a major neurodegenerative disorder that is characterized by the loss of DA neurons within the substantia nigra pars compacta and the presence of numerous Lewy bodies in surviving neurons (Jellinger, 2009). The degeneration of these neurons causes a variety of motor dysfunctions, including tremors, rigidity, and bradykinesia, which gradually increase over time. Only 10% of PD is described as familial and involves several mutated genes, including *SNCA, PRKN, PINK1, DJ-1, LRRK2*, and *VSP35*. While the mechanisms of the neurodegenerative process in PD are still unknown, most PD patients suffer from idiopathic or sporadic forms of PD, emerging from unknown causes.

Focusing on familial forms of PD, the mutation of the α-synuclein (SNCA) gene leads to protein aggregation and is thought to be a major cause of the pathophysiology of PD (Jellinger, 2009). Over 385 iPSC lines have been developed to

TABLE 4 | Modeling neurodegenerative diseases in hiPSC-derived organoids.

Cell types	Organoid types	Characterizations	Recaptitulation of disease phenotypes	Limitations	References
HD-hiPSCs with more than 50 CAG repeats	Cortical	Abnormal neural cell positional identity, self-organizing, and maturation	Not addressed	Lack of Vasculature and microglia formation	Conforti et al., 2018
FAD-hiPSC with PSEN1 mutation FAD or DS-hiPSCs	Cortical Cerebral	Amyloid aggregation, hyperphosphorylated tau protein, and endosome abnormalities Aβ and p-tau protein aggregates, the elevated degree of cellular apoptosis	Partial AD-like pathologies	Lack of Vasculature and microglia formation	Gonzalez et al., 2018 Raja et al., 2016
hiPSCs derived NESCs PD-hiPSCs with PINK1 mutation PD-hiPSCs derived from idiopathic PD PD-hiPSC with LRRK2-G2019S mutation	Midbrain Midbrain Midbrain Midbrain	Synaptic connection and electrophysiological activity Abnormal cell proliferation, differentiation, and apoptosis. Normal cell morphology but altered gene expression A decrease in the number and complexity of mDANs	Not addressed PD-like phenotypes Not addressed PD-relevant phenotypes.	Lack of Vasculature and microglia formation	Monzel et al., 2017 Jarazo et al., 2019 Chlebanowska et al., 2020 Smits et al., 2019

HD-hiPSCs, human induced pluripotent stem cells from patients with Huntington's disease; FAD-hiPSCs, human induced pluripotent stem cells from patients with familial Alzheimer's disease; DS-hiPSCs, human induced pluripotent stem cells from individuals with Down's syndrome; PD-hiPSCs, human induced pluripotent stem cells from individuals with Parkinson's disease.

TABLE 5 | Modeling neurodevelopmental disorders in hiPSC-derived organoids.

Cell types	Organoid types	Characterizations	Recapitulation of disease phenotypes	Limitations	References
hiPSCs derived from MCPH patients with Aspm mutation	Cerebral	A decreased size of EBs. Anormal cell aggregates, self-organizing, and defective layer lamination. Fewer mature neurons and defective neuronal activities	MCPH like phenotypes	Lack of Vasculature and microglia formation	Lancaster et al., 2013; Li et al., 2017
hiPSCs derived from severe idiopathic ASD	Cerebral	Accelerated cell cycle and overproduction of GABAergic inhibitory neurons.	ASD-relevant phenotypes		Mariani et al., 2015
hiPSCs derived from ASD patients	Cerebral	Abnormal neurogenesis and reduced synaptogenesis leading to functional defects in neuronal networks.	ASD-relevant phenotypes		Marchetto et al., 2017
hiPSCs with CHD8 mutation	Cerebral	Alteration ASD and SZ candidate genes expression	Not addressed		Wang et al., 2017

hiPSCs, human induced pluripotent stem cells; MCPH, microencephaly; ASD, autism spectrum disorder; EBs, embryoid bodies; GABAergic, relating to gama aminobutyric acid; SZ, schizophrenia.

investigate disease-like phenotypes of PD since 2011. Among these lines, most of them are familial PD with a single-gene mutation (Tran et al., 2020). For example, patient-derived iPSCs were prepared with *PINK1* mutations and differentiated into neuroepithelial stem cells (NESCs), and later into neurons (Jarazo et al., 2019). This finding demonstrates that patient-derived NESCs can recapitulate PD-like phenotypes, such as reduction of differentiation efficiency, impaired mitophagy capacity, and increased cell death of dopaminergic neurons. However, patient-derived iPSCs demonstrate only partial disease phenotypes, such as the reduction of cell viability or neuronal differentiation defects (**Table 4**).

The limitations of 2D iPSCs cultures suggest that the generation of patient-derived 3D organoids are needed to provide more relevant models that more accurately recapitulate the pathophysiology of PD, as organoids can also provide more accurate models of the genetic- and epigenetic-mediated disease phenotypes. Recently, 3D ventral midbrain-like organoids have been developed that consist of dopaminergic neurons and neuromelanin granules, similar to what is observed in human substantia nigra tissue (Jo et al., 2016; Monzel et al., 2017; Qian et al., 2018). These 3D organoids faithfully mimic the early developmental and functional patterning of brain regions, providing highly accurate simulations of degenerative neuropathology (Shi et al., 2012). A very recent study indicated that treatment with 2-hydroxypropyl-β-cyclodextrin (HP-β-CD) restores differentiation of patient-specific neurons in midbrain organoids by increasing neuronal mitophagy capacity (Jarazo et al., 2019).

Primary microcephaly and autism spectrum disorder are neurodevelopmental disorders whose neuronal pathologies may be modeled by 3D organoids. Primary microcephaly (MCPH) is a neurodevelopmental disorder, which causes a reduction of brain size due to autosomal recessive mutations in several genes. Mutations for several of the known genes in mice have failed to recapitulate MCPH pathogenesis, but recent evidence shows that recapitulation of such pathogenesis of MCPH can be achieved using patient-derived iPSCs and cerebral-organoid cultures (Lancaster et al., 2013; Li et al., 2017). For example, patient-derived organoids exhibit premature neural differentiation at the expense of early neural progenitors, disrupted radial glia spindle orientation, reduced total neural tissue, and increased neuronal outgrowth (**Table 5**).

Autism spectrum disorders (ASDs) consist of a spectrum of neurodevelopmental disorders and are characterized by impaired social interaction, repetitive or restrictive behaviors, and problems with speech. The genetic and environmental risk factors have been shown to contribute to ASD prevalence. Recently, 2D- and 3D- cultures of hiPSCs, which were derived from patients with idiopathic autism (with an increased head/brain size), recapitulated the phenotypic signature of the autistic brain, such as abnormal cell proliferation and an over-production of inhibitory neurons due to dysregulation of the transcriptional cascade (Mariani et al., 2015; Marchetto et al., 2017). The development of 3D organoids for ASD promises to elucidate some of the neuronal mechanisms of this disorder, as well as providing useful insights for therapeutic interventions.

Recapitulation of Disease Phenotypes Associated With the Epigenetic Signatures in Patient-Derived Organoids

Epigenetic alterations can regulate the expression of genes through chromatin remodeling without changing its DNA sequence. Our DNA code remains fixed for life and all parts of our body, such as cell types and organs, are characterized by one genome, but the epigenome can be organ-, or even, cell-specific. DNA methylation, modifications of core histones, and non-coding RNA (ncRNA) are major epigenetic mechanisms that act jointly in chromatin remodeling for suppression or induction of gene expression. These epigenetic mechanisms are dynamic and cell-specific; they display inter-individual variability and can also

occur in non-dividing cells, such as neurons (Fraga et al., 2005). Nutrients, pollutants, chemicals, physical and mental stress are major environmental factors, which can alter epigenetic markers in the developing and adult organism.

Epigenetic alterations are also associated with aging. For example, global DNA methylation levels are decreased with aging (Fraga et al., 2005). In addition, gene mutation can cause secondary epigenetic modifications (Cakir et al., 2020). Thus, the epigenetic alterations have been implicated in a diverse range of cellular functions and pathologies, which are generally associated with a repressed chromatin state and inhibition of promoter activity, such as transcriptional repression (Navarro-Sánchez et al., 2018). For example, cell proliferation and differentiation during prenatal development are regulated by epigenetic mechanisms.

The genetic and epigenetic variations in patient-derived iPSCs change their differentiation efficiency and developmental capacity (Liang and Zhang, 2013). A major concern for disease modeling is that the genetic and epigenetic variations detected in iPSCs may cause unexpected phenotypic changes after the iPSCs differentiate into target cells. In addition, such variations in hiPSCs may lead to the acquisition of phenotypes that are unrelated to the disease being modeled or to the disappearance of disease-related phenotypes (Liang and Zhang, 2013). Studies show that cell reprogramming, such as genes that change fibroblasts into iPSCs, removes a significant epigenetic modification (Perrera and Martello, 2019). Therefore, the biggest challenge for using iPSCs from patients is to recapitulate the pathogenesis of the neurodevelopmental and neurodegenerative diseases that are induced by environmental factors, while epigenetic modifications are partially recapitulated following neuronal maturation *in vitro* (Parr et al., 2017).

Genetic predisposition and epigenetic alterations are both considered to contribute to neurodegenerative diseases, including AD and PD. Although iPSC-derived *in vitro* models cannot display the full range of defects that contribute to neurodegenerative diseases, they are useful for modeling cellular and molecular abnormalities of neuronal development and contribute to our understanding of the causes and progression of neurodegenerative diseases (Lewis and Kroll, 2018). However, the successful use of hiPSCs to model neurodegenerative disease requires assuring genetic and epigenetic stability.

Genome-wide studies demonstrated several point mutations in all hiPSC, which raise concerns over their ability to model disease states, as well as their safety for clinical applications (Perrera and Martello, 2019). Moreover, the additional mutations in hiPSCs during the several passages that occur when cells are cultured for long periods of time (Liang and Zhang, 2013) may result in increased susceptibility to diseases or abnormal cell morphology and functions.

Recently, the data from transcriptome profiles and epigenome-wide sequencing of cerebral organoids, when compared with human fetal brain (Luo et al., 2016), revealed a recapitulation of the key characteristics of human brain development, including regional cell specification, the formation of progenitor layers, and the generation of diverse types of functional neurons (Lancaster et al., 2013). Importantly, the transcriptomic dynamics were recapitulated in hiPSC-derived organoids, which were equivalent to fetal brain of gestational week 8–16 (Luo et al., 2016). Luo et al. (2016) also demonstrated a new type of cytosine DNA methylation in non-CG contexts (mCH) that indicate transcriptional repression in later brain development (Luo et al., 2016).

However, the fate of patient-derived organoids is found to be dependent on genetic inheritance and disease phenotype of its constituent hiPSCs, which often require exogenous exposure of disease-inducing factors for the pathogenesis of diseases to develop. This indicates that disease phenotypes are associated with genetic mutations and environmental factors. If cell reprogramming removes the epigenetic code and cell aging is associated with sporadic neurodegenerative diseases, like PD and AD, then the accurate recapitulation of stable disease-like phenotypes in patient-derived organoids is a major challenge that will need to be addressed.

CONCLUSIONS AND PERSPECTIVES

Patient-derived brain organoids have provided new insights into disease modeling and have opened new possibilities for personalized medicine. Even though 3D cultures of patient-derived iPSCs hold great promise for modeling diseases, such as AD, PD, and HD, only a few studies have effectively utilized 3D vascularized organoids. New and advanced methods are required to overcome the current limitations for creating functional vascular systems and for accurately recapitulating pathogenesis and many complex physiological features of the human brain. In addition, batch-to-batch variations are often observed among organoids, due to genetic and epigenetic variations resulting from the origin or reprogramming approaches used to obtain the hiPSCs, which may change the differentiation and function of the organoids from which they were derived. Therefore, a better understanding of cell-ECM and cell-cell interaction, incorporation of microglia and vascularization into the models, and the use of self-patterning, and advanced protocols for iPSC reprogramming are required to recreate reliable 3D organoid models. Such vascularized organoids might have diverse applications as BBB model systems for various diseases, including neurodegenerative and neurodevelopmental disorders, as well as for transplantation to treat brain injury. Moreover, they can also be used as models for drug-screening, brain-infection, and neurotoxicity studies.

Although hiPSC-derived organoid models are promising tools to recapitulate developmental and disease phenotypes, these *in vitro* models are not a substitute for animal models, especially those that model behavior and psychological disorders. In addition, animal models are still needed to investigate long-term drug responses and multi-organ drug toxicity tests. However, because many promising pharmacological findings from animal studies have high failure rates in clinical trials, the parallel use of hiPSC-derived organoids could augment the translatability of animal studies to humans. As hiPSC-derived *in vitro* models more closely resemble complex *in vivo* processes and the current limitations of organoids are addressed, a new

era of translatable therapies will emerge. Although there is still a long way to go before iPSC-based methods can be used directly in clinics, the modification of current organoid technology with genome editing, drug screening, and other technologies, as well as precise characterization of these organoids using cutting edge technologies, will certainly advance the generation of new therapies for human developmental and neurodegenerative diseases.

AUTHOR CONTRIBUTIONS

RB had the main idea of the article, made a substantial contribution in the literature survey, designed and written the original manuscript, designed original figures and tables, corrections, and critical revisions. SB contributed to the revision, modification of the manuscript, and plotting of the figure. GD reviewed and edited the manuscript including figures and tables. All authors contributed to the article and approved the submitted version.

FUNDING

This project was supported by funds from the Field Neurosciences Institute and the John G. Kulhavi Professorship in Neuroscience at Central Michigan University.

REFERENCES

Abud, E. M., Ramirez, R. N., Martinez, E. S., Healy, L. M., Nguyen, C. H. H., Newman, S. A., et al. (2017). iPSC-derived human microglia-like cells to study neurological diseases. *Neuron* 94, 278–293.e9. doi: 10.1016/j.neuron.2017.03.042

Adil, M. M., Gaj, T., Rao, A. T., Kulkarni, R. U., Fuentes, C. M., Ramadoss, G. N., et al. (2018). hPSC-derived striatal cells generated using a scalable 3D hydrogel promote recovery in a huntington disease mouse model. *Stem Cell Rep.* 10, 1481–1491. doi: 10.1016/j.stemcr.2018.03.007

Ao, Z., Cai, H., Havert, D. J., Wu, Z., Gong, Z., Beggs, J. M., et al. (2020). One-stop microfluidic assembly of human brain organoids to model prenatal cannabis exposure. *Anal. Chem.* 92, 4630–4638. doi: 10.1021/acs.analchem.0c00205

Appelt-Menzel, A., Cubukova, A., Günther, K., Edenhofer, F., Piontek, J., Krause, G., et al. (2017). Establishment of a human blood-brain barrier co-culture model mimicking the neurovascular unit using induced pluri- and multipotent stem cells. *Stem Cell Rep.* 8, 894–906. doi: 10.1016/j.stemcr.2017.02.021

Arber, C., Precious, S. V., Cambray, S., Risner-Janiczek, J. R., Kelly, C., Noakes, Z., et al. (2015). Activin A directs striatal projection neuron differentiation of human pluripotent stem cells. *Development* 142, 1375–1386. doi: 10.1242/dev.117093

Armulik, A., Genové, G., and Betsholtz, C. (2011). Pericytes: developmental, physiological, and pathological perspectives, problems, and promises. *Dev. Cell* 21, 193–215. doi: 10.1016/j.devcel.2011.07.001

Armulik, A., Genové, G., Mäe, M., Nisancioglu, M. H., Wallgard, E., Niaudet, C., et al. (2010). Pericytes regulate the blood-brain barrier. *Nature* 468, 557–561. doi: 10.1038/nature09522

Azevedo, J. L., and Feldman, R. A. (2010). Tinkering with transcription factors uncovers plasticity of somatic cells. *Genes Cancer* 1, 1089–1099. doi: 10.1177/1947601911401908

Bagley, J. A., Reumann, D., Bian, S., Lévi-Strauss, J., and Knoblich, J. A. (2017). Fused dorsal-ventral cerebral organoids model complex interactions between diverse brain regions. *Nat. Methods* 14, 743–751. doi: 10.1038/nmeth.4304

Baker, C. A., Elyada, Y. M., Parra, A., and Bolton, M. M. (2016). Cellular resolution circuit mapping with temporal-focused excitation of somatargeted channelrhodopsin. *eLife.* 5:e14193. doi: 10.7554/eLife.14193

Barrera, J. A., Kao, L.-R., Hammer, R. E., Seemann, J., Fuchs, J. L., and Megraw, T. L. (2010). CDK5RAP2 regulates centriole engagement and cohesion in mice. *Dev. Cell* 18, 913–926. doi: 10.1016/j.devcel.2010.05.017

Ben-Reuven, L., and Reiner, O. (2020). Toward spatial identities in human brain organoids-on-chip induced by morphogen-soaked beads. *Bioengineering* 7:164. doi: 10.3390/bioengineering7040164

Benson, P. F., and Joseph, M. C. (1961). The blood-brain barrier. *Dev. Med. Child Neurol.* 3, 510–514. doi: 10.1111/j.1469-8749.1961.tb10410.x

Berson, A., Nativio, R., Berger, S. L., and Bonini, N. M. (2018). Epigenetic regulation in neurodegenerative diseases. *Trends Neurosci.* 41, 587–598. doi: 10.1016/j.tins.2018.05.005

Bhalerao, A., Sivandzade, F., Archie, S. R., Chowdhury, E. A., Noorani, B., and Cucullo, L. (2020). *In vitro* modeling of the neurovascular unit: advances in the field. *Fluids Barriers CNS* 17, 1–20. doi: 10.1186/s12987-020-00183-7

Blanco-Suárez, E., Caldwell, A. L. M., and Allen, N. J. (2017). Role of astrocyte–synapse interactions in CNS disorders. *J. Physiol.* 595, 1903–1916. doi: 10.1113/JP270988

Burke, W. J. (2007). Neuroprotective agents for clinical trials in ALS: systematic assessment. *Neurology* 68, 709–710. doi: 10.1212/01.wnl.0000258815.56062.43

Cadwell, C. R., Palasantza, A., Jiang, X., Berens, P., Deng, Q., Yilmaz, M., et al. (2016). Electrophysiological, transcriptomic and morphologic profiling of single neurons using Patch-seq. *Nat. Biotechnol.* 34, 199–203. doi: 10.1038/nbt.3445

Cakir, B., Xiang, Y., Tanaka, Y., Kural, M. H., Parent, M., Kang, Y., et al. (2020). Development of human brain organoids with functional vascular- like system. *Development* 16, 1169–1175. doi: 10.1038/s41592-019-0586-5

Cakir, B., Xiang, Y., Tanaka, Y., Kural, M. H., Parent, M., Kang, Y. J., et al. (2019). Engineering of human brain organoids with a functional vascular-like system. *Nat. Methods.* 16, 1169–1175.

Canfield, S. G., Stebbins, M. J., Morales, B. S., Asai, S. W., Vatine, G. D., Svendsen, C. N., et al. (2017). An isogenic blood-brain barrier model comprising brain endothelial cells, astrocytes, and neurons derived from human induced pluripotent stem cells. *J. Neurochem.* 140, 874–888. doi: 10.1111/jnc.13923

Chambers, S. M., Fasano, C. A., Papapetrou, E. P., Tomishima, M., Sadelain, M., and Studer, L. (2009). Erratum: highly efficient neural conversion of human ES and iPS cells by dual inhibition of SMAD signaling. *Nat. Biotechnol.* 27, 275–280. doi: 10.1038/nbt.1529

Chlebanowska, P., Tejchman, A., Sułkowski, M., Skrzypek, K., and Majka, M. (2020). Use of 3D organoids as a model to study idiopathic form of parkinson's disease. *Int. J. Mol. Sci.* 21:30694. doi: 10.3390/ijms21030694

Conforti, P., Besusso, D., Bocchi, V. D., Faedo, A., Cesana, E., Rossetti, G., et al. (2018). Faulty neuronal determination and cell polarization are reverted by modulating HD early phenotypes. *Proc. Natl. Acad. Sci. U. S. A.* 115, E762–E771. doi: 10.1073/pnas.1715865115

Cui, K., Wang, Y., Zhu, Y., Tao, T., Yin, F., Guo, Y., et al. (2020). Neurodevelopmental impairment induced by prenatal valproic acid exposure shown with the human cortical organoid-on-a-chip model. *Microsyst. Nanoeng.* 6:49. doi: 10.1038/s41378-020-0165-z

Czerniecki, S. M., Cruz, N. M., Harder, J. L., Menon, R., Annis, J., Otto, E. A., et al. (2018). High-throughput screening enhances kidney organoid differentiation from human pluripotent stem cells and enables automated multidimensional phenotyping. *Cell Stem Cell* 22, 929–940.e4. doi: 10.1016/j.stem.2018.04.022

Dang, J., Tiwari, S. K., Lichinchi, G., Qin, Y., Patil, V. S., Eroshkin, A. M., et al. (2016). Zika virus depletes neural progenitors in human cerebral organoids through activation of the innate immune receptor TLR3. *Cell Stem Cell* 19, 258–265. doi: 10.1016/j.stem.2016.04.014

Daviaud, N., Friedel, R. H., and Zou, H. (2018). Vascularization and engraftment of transplanted human cerebral organoids in mouse cortex. *eNeuro* 5, 1–18. doi: 10.1523/ENEURO.0219-18.2018

De Boni, L., and Wüllner, U. (2019). Epigenetic analysis in human neurons: considerations for disease modeling in PD. *Front. Neurosci.* 13, 1–12. doi: 10.3389/fnins.2019.00276

Deng, W. (2010). Induced pluripotent stem cells: paths to new medicines. *EMBO Rep*. 11, 161–165. doi: 10.1038/embor.2010.15

Di Pardo, A., Amico, E., Scalabrì, F., Pepe, G., Castaldo, S., Elifani, F., et al. (2017). Impairment of blood-brain barrier is an early event in R6/2 mouse model of Huntington Disease. *Sci. Rep.* 7, 1–8. doi: 10.1038/srep41316

Douvaras, P., Wang, J., Zimmer, M., Hanchuk, S., O'Bara, M. A., Sadiq, S., et al. (2014). Efficient generation of myelinating oligodendrocytes from primary progressive multiple sclerosis patients by induced pluripotent stem cells. *Stem Cell Rep.* 3, 250–259. doi: 10.1016/j.stemcr.2014.06.012

Ehrlich, M., Mozafari, S., Glatza, M., Starost, L., Velychko, S., Hallmann, A. L., et al. (2017). Rapid and efficient generation of oligodendrocytes from human induced pluripotent stem cells using transcription factors. *Proc. Natl. Acad. Sci. U. S. A.* 114, E2243–E2252. doi: 10.1073/pnas.1614412114

Erickson, M. A., Wilson, M. L., and Banks, W. A. (2020). *In vitro* modeling of blood-brain barrier and interface functions in neuroimmune communication. *Fluids Barriers CNS* 17, 1–16. doi: 10.1186/s12987-020-00187-3

Etchevers, H. C., Vincent, C., Le Douarin, N. M., and Couly, G. F. (2001). The cephalic neural crest provides pericytes and smooth muscle cells to all blood vessels of the face and forebrain. *Development* 128, 1059–1068.

Fernández-López, D., Faustino, J., Daneman, R., Zhou, L., Lee, S. Y., Derugin, N., et al. (2012). Blood-brain barrier permeability is increased after acute adult stroke but not neonatal stroke in the rat. *J. Neurosci.* 32, 9588–9600. doi: 10.1523/JNEUROSCI.5977-11.2012

Fraga, M. F., Ballestar, E., Paz, M. F., Ropero, S., Setien, F., Ballestar, M. L., et al. (2005). Epigenetic differences arise during the lifetime of monozygotic twins. *Proc. Natl. Acad. Sci. U. S. A.* 102, 10604–10609. doi: 10.1073/pnas.0500398102

Fu, H., Hardy, J., and Duff, K. E. (2018). Selective vulnerability in neurodegenerative diseases. *Nat. Neurosci.* 21, 1350–1358. doi: 10.1038/s41593-018-0221-2

Garwood, C. J., Ratcliffe, L. E., Simpson, J. E., Heath, P. R., Ince, P. G., and Wharton, S. B. (2017). Review: astrocytes in Alzheimer's disease and other age-associated dementias: a supporting player with a central role. *Neuropathol. Appl. Neurobiol.* 43, 281–298. doi: 10.1111/nan.12338

Gaspard, N., Bouschet, T., Hourez, R., Dimidschstein, J., Naeije, G., van den Ameele, J., et al. (2008). An intrinsic mechanism of corticogenesis from embryonic stem cells. *Nature* 455, 351–357. doi: 10.1038/nature07287

Gonzalez, C., Armijo, E., Bravo-Alegria, J., Becerra-Calixto, A., Mays, C. E., and Soto, C. (2018). Modeling amyloid beta and tau pathology in human cerebral organoids. *Mol. Psychiatry* 23, 2363–2374. doi: 10.1038/s41380-018-0229-8

Hartfield, E. M., Yamasaki-Mann, M., Ribeiro Fernandes, H. J., Vowles, J., James, W. S., Cowley, S. A., et al. (2014). Physiological characterisation of human iPS-derived dopaminergic neurons. *PLoS ONE* 9:e87388. doi: 10.1371/journal.pone.0087388

Ho, B. X., Pek, N. M. Q., and Soh, B. S. (2018). Disease modeling using 3D organoids derived from human induced pluripotent stem cells. *Int. J. Mol. Sci.* 19:40936. doi: 10.3390/ijms19040936

Hollmann, E. K., Bailey, A. K., Potharazu, A. V., Neely, M. D., Bowman, A. B., and Lippmann, E. S. (2017). Accelerated differentiation of human induced pluripotent stem cells to blood-brain barrier endothelial cells. *Fluids Barriers CNS* 14:9. doi: 10.1186/s12987-017-0059-0

Jarazo, J., Barmpa, K., Rosety, I., Smits, L., Arias-Fuenzalida, J., Walter, J., et al. (2019). Parkinson's disease phenotypes in patient specific brain organoids are improved by HP-β-CD treatment. *Biorxiv.* doi: 10.1101/813089

Jellinger, K. A. (2009). Formation and development of Lewy pathology: a critical update. *J. Neurol.* 256(Suppl.), 270–279. doi: 10.1007/s00415-009-5243-y

Jo, J., Xiao, Y., Sun, A. X., Cukuroglu, E., Tran, H.-D., Göke, J., et al. (2016). Midbrain-like organoids from human pluripotent stem cells contain functional dopaminergic and neuromelanin-producing neurons. *Cell Stem Cell* 19, 248–257. doi: 10.1016/j.stem.2016.07.005

Kanning, K. C., Kaplan, A., and Henderson, C. E. (2010). Motor neuron diversity in development and disease. *Annu. Rev. Neurosci.* 33, 409–440. doi: 10.1146/annurev.neuro.051508.135722

Kelava, I., and Lancaster, M. A. (2016). Dishing out mini-brains: current progress and future prospects in brain organoid research. *Dev. Biol.* 420, 199–209. doi: 10.1016/j.ydbio.2016.06.037

Khakh, B. S., Beaumont, V., Cachope, R., Munoz-Sanjuan, I., Goldman, S. A., and Grantyn, R. (2017). Unravelling and exploiting astrocyte dysfunction in Huntington's disease. *Trends Neurosci.* 40, 422–437. doi: 10.1016/j.tins.2017.05.002

Kim, H., Park, H. J., Choi, H., Chang, Y., Park, H., Shin, J., et al. (2019). Modeling G2019S-LRRK2 sporadic Parkinson's disease in 3D midbrain organoids. *Stem Cell Rep.* 12, 518–531. doi: 10.1016/j.stemcr.2019.01.020

Kim, K., Doi, A., Wen, B., Ng, K., Zhao, R., Cahan, P., et al. (2010). Epigenetic memory in induced pluripotent stem cells. *Nature* 467, 285–290. doi: 10.1038/nature09342

Kim, T.-G., Yao, R., Monnell, T., Cho, J.-H., Vasudevan, A., Koh, A., et al. (2014). Efficient specification of interneurons from human pluripotent stem cells by dorsoventral and rostrocaudal modulation. *Stem Cells* 32, 1789–1804. doi: 10.1002/stem.1704

Kirkeby, A., Grealish, S., Wolf, D. A., Nelander, J., Wood, J., Lundblad, M., et al. (2012). Generation of regionally specified neural progenitors and functional neurons from human embryonic stem cells under defined conditions. *Cell Rep.* 1, 703–714. doi: 10.1016/j.celrep.2012.04.009

Krencik, R., and Zhang, S.-C. (2011). Directed differentiation of functional astroglial subtypes from human pluripotent stem cells. *Nat. Protoc.* 6, 1710–1717. doi: 10.1038/nprot.2011.405

Kwon, M. J., Kim, S., Han, M. H., and Lee, S. B. (2016). Epigenetic changes in neurodegenerative diseases. *Mol. Cells* 39, 783–789. doi: 10.14348/molcells.2016.0233

Lancaster, M., and Knoblich, J. (2014). Generation of cerebral organoids from human pluripotent stem cells. *Nat. Protoc.* 9, 2329–2340. doi: 10.1038/nprot.2014.158

Lancaster, M. A., Corsini, N. S., Wolfinger, S., Gustafson, E. H., Phillips, A. W., Burkard, T. R., et al. (2017). Guided self-organization and cortical plate formation in human brain organoids. *Nat. Biotechnol.* 35, 659–666. doi: 10.1038/nbt.3906

Lancaster, M. A., Renner, M., Martin, C.-A., Wenzel, D., Bicknell, L. S., Hurles, M. E., et al. (2013). Cerebral organoids model human brain development and microcephaly. *Nature* 501, 373–379. doi: 10.1038/nature12517

Le Dréau, G., and Martí, E. (2012). Dorsal-ventral patterning of the neural tube: a tale of three signals. *Dev Neurobiol.* 72, 1471–1481. doi: 10.1002/dneu.22015

Lee, C. T., Bendriem, R. M., Wu, W. W., and Shen, R. F. (2017). 3D brain Organoids derived from pluripotent stem cells: promising experimental models for brain development and neurodegenerative disorders. *J. Biomed. Sci.* 24, 1–12. doi: 10.1186/s12929-017-0362-8

Lewis, E. M. A., and Kroll, K. L. (2018). Development and disease in a dish: the epigenetics of neurodevelopmental disorders. *Epigenomics* 10, 219–231. doi: 10.2217/epi-2017-0113

Li, P., Marshall, L., Oh, G., Jakubowski, J. L., Groot, D., He, Y., et al. (2019). Epigenetic dysregulation of enhancers in neurons is associated with Alzheimer's disease pathology and cognitive symptoms. *Nat. Commun.* 10, 1–14. doi: 10.1038/s41467-019-10101-7

Li, R., Sun, L., Fang, A., Li, P., Wu, Q., and Wang, X. (2017). Recapitulating cortical development with organoid culture *in vitro* and modeling abnormal spindle-like (ASPM related primary) microcephaly disease. *Protein Cell* 8, 823–833. doi: 10.1007/s13238-017-0479-2

Liang, G., and Zhang, Y. (2013). Genetic and epigenetic variations in iPSCs: potential causes and implications for application. *Cell Stem Cell.* 13, 149–159. doi: 10.1016/j.stem.2013.07.001

Lippmann, E. S., Azarin, S. M., Kay, J. E., Nessler, R. A., Wilson, H. K., Al-Ahmad, A., et al. (2012). Derivation of blood-brain barrier endothelial cells from human pluripotent stem cells. *Nat. Biotechnol.* 30, 783–791. doi: 10.1038/nbt.2247

Liu, C., Oikonomopoulos, A., Sayed, N., and Wu, J. C. (2018a). Modeling human diseases with induced pluripotent stem cells: from 2D to 3D and beyond. *Development* 145:156166. doi: 10.1242/dev.156166

Liu, J., Wang, M., Sun, L., Pan, N. C., Zhang, C., Zhang, J., et al. (2020). Integrative analysis of in vivo recording with single-cell RNA-seq data reveals molecular properties of light-sensitive neurons in mouse V1. *Protein Cell* 11, 417–432. doi: 10.1007/s13238-020-00720-y

Liu, X., Jiao, B., and Shen, L. (2018b). The epigenetics of Alzheimer's disease: factors and therapeutic implications. *Front. Genet.* 9, 1–10. doi: 10.3389/fgene.2018.00579

Liu, Y., Weick, J. P., Liu, H., Krencik, R., Zhang, X., Ma, L., et al. (2013). Medial ganglionic eminence-like cells derived from human embryonic stem cells correct learning and memory deficits. *Nat. Biotechnol.* 31, 440–447. doi: 10.1038/nbt.2565

Luk, K. C., Kehm, V., Carroll, J., Zhang, B., O'Brien, P., Trojanowski, J. Q., et al. (2012). Pathological α-synuclein transmission initiates Parkinson-like neurodegeneration in nontransgenic mice. *Science* 338, 949–953. doi: 10.1126/science.1227157

Luo, C., Lancaster, M. A., Castanon, R., Nery, J. R., Knoblich, J. A., and Ecker, J. R. (2016). Cerebral organoids recapitulate epigenomic signatures of the human fetal brain. *Cell Rep.* 17, 3369–3384. doi: 10.1016/j.celrep.2016.12.001

MacDonald, M. E., Ambrose, C. M., Duyao, M. P., Myers, R. H., Lin, C., Srinidhi, L., et al. (1993). A novel gene containing a trinucleotide repeat that is expanded and unstable on Huntington's disease chromosomes. *Cell* 72, 971–983. doi: 10.1016/0092-8674(93)90585-E

Mansour, A. A., Gonçalves, J. T., Bloyd, C. W., Li, H., Fernandes, S., Quang, D., et al. (2018). An *in vivo* model of functional and vascularized human brain organoids. *Nat. Biotechnol.* 36, 432–441. doi: 10.1038/nbt.4127

Marchetto, M. C., Belinson, H., Tian, Y., Freitas, B. C., Fu, C., Beltrao-braga, P., et al. (2017). Altered proliferation and networks in neural cells derived from idiopathic autistic individuals. *Mol. Psychiatry* 22, 820–835. doi: 10.1038/mp.2016.95

Mariani, J., Coppola, G., Zhang, P., Abyzov, A., Provini, L., Tomasini, L., et al. (2015). FOXG1-dependent dysregulation of GABA/glutamate neuron differentiation in autism spectrum disorders. *Cell* 162, 375–390. doi: 10.1016/j.cell.2015.06.034

Maury, Y., Côme, J., Piskorowski, R. A., Salah-Mohellibi, N., Chevaleyre, V., Peschanski, M., et al. (2015). Combinatorial analysis of developmental cues efficiently converts human pluripotent stem cells into multiple neuronal subtypes. *Nat. Biotechnol.* 33, 89–96. doi: 10.1038/nbt.3049

McQuade, A., Coburn, M., Tu, C. H., Hasselmann, J., Davtyan, H., and Blurton-Jones, M. (2018). Development and validation of a simplified method to generate human microglia from pluripotent stem cells. *Mol. Neurodegener.* 13, 1–13. doi: 10.1186/s13024-018-0297-x

Menassa, D. A., and Gomez-Nicola, D. (2018). Microglial dynamics during human brain development. *Front. Immunol.* 9:14. doi: 10.3389/fimmu.2018.01014

Monzel, A. S., Smits, L. M., Hemmer, K., Hachi, S., Moreno, E. L., van Wuellen, T., et al. (2017). Derivation of human midbrain-specific organoids from neuroepithelial stem cells. *Stem Cell Rep.* 8, 1144–1154. doi: 10.1016/j.stemcr.2017.03.010

Muffat, J., Li, Y., Yuan, B., Mitalipova, M., Omer, A., Corcoran, S., et al. (2016). Efficient derivation of microglia-like cells from human pluripotent stem cells. *Nat. Med.* 22, 1358–1367. doi: 10.1038/nm.4189

Navarro-Sánchez, L., Águeda-Gómez, B., Aparicio, S., and Pérez-Tur, J. (2018). Epigenetic study in Parkinson's disease: a pilot analysis of DNA methylation in candidate genes in brain. *Cells* 7:150. doi: 10.3390/cells7100150

Nicholas, C. R., Chen, J., Tang, Y., Southwell, D. G., Chalmers, N., Vogt, D., et al. (2013). Functional maturation of hPSC-derived forebrain interneurons requires an extended timeline and mimics human neural development. *Cell Stem Cell* 12, 573–586. doi: 10.1016/j.stem.2013.04.005

Notturno, F., Caporale, C., De Lauretis, A., and Uncini, A. (2008). Glial fibrillary acidic protein: a marker of axonal Guillain-Barre syndrome and outcome. *Muscle Nerve* 38, 899–903. doi: 10.1002/mus.20983

Palm, T., Bolognin, S., Meiser, J., Nickels, S., Träger, C., Meilenbrock, R. L., et al. (2015). Rapid and robust generation of long-term self-renewing human neural stem cells with the ability to generate mature astroglia. *Sci. Rep.* 5, 1–16. doi: 10.1038/srep16321

Papaspyropoulos, A., Tsolaki, M., Foroglou, N., and Pantazaki, A. A. (2020). Modeling and targeting Alzheimer's disease with organoids. *Front. Pharmacol.* 11, 1–8. doi: 10.3389/fphar.2020.00396

Parr, C. J. C., Yamanaka, S., and Saito, H. (2017). An update on stem cell biology and engineering for brain development. *Mol. Psychiatry* 22, 808–819. doi: 10.1038/mp.2017.66

Perrera, V., and Martello, G. (2019). How does reprogramming to pluripotency affect genomic imprinting? *Front. Cell Dev. Biol.* 7, 1–16. doi: 10.3389/fcell.2019.00076

Pham, M. T., Pollock, K. M., Rose, M. D., Cary, W. A., Stewart, H. R., Zhou, P., et al. (2018). Generation of human vascularized brain organoids. *Neuroreport* 36, 588–593. doi: 10.1097/WNR.0000000000001014

Phatnani, H., and Maniatis, T. (2015). Astrocytes in neurodegenerative disease. *Cold Spring Harb. Perspect. Biol.* 7, 1–18. doi: 10.1101/cshperspect.a020628

Pollen, A. A., Bhaduri, A., Andrews, M. G., Nowakowski, T. J., Meyerson, O. S., Mostajo-Radji, M. A., et al. (2019). Establishing cerebral organoids as models of human-specific brain evolution. *Cell* 176, 743–756.e17. doi: 10.1016/j.cell.2019.01.017

Pouladi, M. A., Morton, A. J., and Hayden, M. R. (2013). Choosing an animal model for the study of Huntington's disease. *Nat. Rev. Neurosci.* 14, 708–721. doi: 10.1038/nrn3570

Pulvers, J. N., Bryk, J., Fish, J. L., Wilsch-Bräuninger, M., Arai, Y., Schreier, D., et al. (2010). Mutations in mouse Aspm (abnormal spindle-like microcephaly associated) cause not only microcephaly but also major defects in the germline. *Proc. Natl. Acad. Sci. U. S. A.* 107, 16595–16600. doi: 10.1073/pnas.1010494107

Qi, Y., Zhang, X.-J., Renier, N., Wu, Z., Atkin, T., Sun, Z., et al. (2017). Combined small-molecule inhibition accelerates the derivation of functional cortical neurons from human pluripotent stem cells. *Nat. Biotechnol.* 35, 154–163. doi: 10.1038/nbt.3777

Qian, X., Jacob, F., Song, M. M., Nguyen, H. N., Song, H., and Ming, G. L. (2018). Generation of human brain region–specific organoids using a miniaturized spinning bioreactor. *Nat. Protoc.* 13, 565–580. doi: 10.1038/nprot.2017.152

Quadrato, G., Nguyen, T., Macosko, E. Z., Sherwood, J. L., Yang, S. M., Berger, D., et al. (2017). Cell diversity and network dynamics in photosensitive human brain organoids. *Nature* 545, 48–53. doi: 10.1038/nature22047

Raja, W. K., Mungenast, A. E., Lin, Y. T., Ko, T., Abdurrob, F., Seo, J., et al. (2016). Self-organizing 3D human neural tissue derived from induced pluripotent stem cells recapitulate Alzheimer's disease phenotypes. *PLoS ONE* 11, 1–18. doi: 10.1371/journal.pone.0161969

Rajan, P., and McKay, R. D. (1998). Multiple routes to astrocytic differentiation in the CNS. *J. Neurosci.* 18, 3620–3629. doi: 10.1523/JNEUROSCI.18-10-03620.1998

Reemst, K., Noctor, S. C., Lucassen, P. J., and Hol, E. M. (2016). The indispensable roles of microglia and astrocytes during brain development. *Front. Hum. Neurosci.* 10, 1–28. doi: 10.3389/fnhum.2016.00566

Reinius, B., Blunder, M., Brett, F. M., Eriksson, A., Patra, K., Jonsson, J., et al. (2015). Conditional targeting of medium spiny neurons in the striatal matrix. *Front Behav Neurosci.* 9:71. doi: 10.3389/fnbeh.2015.00071

Reubinoff, B. E., Itsykson, P., Turetsky, T., Pera, M. F., Reinhartz, E., Itzik, A., et al. (2001). Neural progenitors from human embryonic stem cells. *Nat. Biotechnol.* 19, 1134–1140. doi: 10.1038/nbt1201-1134

Schimek, K., Frentzel, S., Luettich, K., Bovard, D., Rütschle, I., Boden, L., et al. (2020). Human multi-organ chip co-culture of bronchial lung culture and liver spheroids for substance exposure studies. *Sci. Rep.* 10:7865. doi: 10.1038/s41598-020-64219-6

Schwartz, J. P. (1997). Development and plasticity. Overview. *Adv. Pharmacol.* 42, 877–882. doi: 10.1016/S1054-3589(08)60887-X

Shi, Y., Kirwan, P., Smith, J., Robinson, H. P. C., and Livesey, F. J. (2012). Human cerebral cortex development from pluripotent stem cells to functional excitatory synapses. *Nat. Neurosci.* 15, 477–486, S1. doi: 10.1038/nn.3041

Shi, Y., Sun, L., Wang, M., Liu, J., Zhong, S., Li, R., et al. (2020). Vascularized human cortical organoids (vOrganoids) model cortical development *in vivo*. *PLoS Biol.* 18, 1–29. doi: 10.1371/journal.pbio.3000705

Shin, H., Jeong, S., Lee, J. H., Sun, W., Choi, N., and Cho, I. J. (2021). 3D high-density microelectrode array with optical stimulation and drug delivery for investigating neural circuit dynamics. *Nat. Commun.* 12, 1–18. doi: 10.1038/s41467-020-20763-3

Skardal, A., Murphy, S. V., Devarasetty, M., Mead, I., Kang, H. W., Seol, Y. J., et al. (2017). Multi-tissue interactions in an integrated three-tissue organ-on-a-chip platform. *Sci. Rep.* 7, 1–16. doi: 10.1038/s41598-017-08879-x

Smits, L. M., Reinhardt, L., Reinhardt, P., Glatza, M., Monzel, A. S., Stanslowsky, N., et al. (2019). Modeling Parkinson's disease in midbrain-like organoids. *NPJ Park. Dis.* 5:4. doi: 10.1038/s41531-019-0078-4

Song, L., Yan, Y., Marzano, M., and Li, Y. (2019a). Studying Heterotypic Cell–cell interactions in the human brain using pluripotent stem cell models for neurodegeneration. *Cells* 8:299. doi: 10.3390/cells8040299

Song, L., Yuan, X., Jones, Z., Vied, C., Miao, Y., Marzano, M., et al. (2019b). Functionalization of brain region-specific spheroids with isogenic microglia-like cells. *Sci. Rep.* 9, 1–18. doi: 10.1038/s41598-019-47444-6

Soscia, D. A., Lam, D., Tooker, A. C., Enright, H. A., Triplett, M., Karande, P., et al. (2020). A flexible 3-dimensional microelectrode array for: *in vitro* brain models. *Lab Chip*. 20, 901–911. doi: 10.1039/C9LC01148J

Soubannier, V., Maussion, G., Chaineau, M., Sigutova, V., Rouleau, G., Durcan, T. M., et al. (2020). Characterization of human iPSC-derived astrocytes with potential for disease modeling and drug discovery. *Neurosci. Lett.* 731:135028. doi: 10.1016/j.neulet.2020.135028

Stebbins, M. J., Gastfriend, B. D., Canfield, S. G., Lee, M. S., Richards, D., Faubion, M. G., et al. (2019). Human pluripotent stem cell–derived brain pericyte–like cells induce blood-brain barrier properties. *Sci. Adv.* 5:aau7375. doi: 10.1126/sciadv.aau7375

Takao, K., and Miyakawa, T. (2015). Genomic responses in mouse models greatly mimic human inflammatory diseases. *Proc. Natl. Acad. Sci. U.S.A.* 112, 1167–1172. doi: 10.1073/pnas.1401965111

Tao, Y., and Zhang, S. C. (2016). Neural subtype specification from human pluripotent stem cells. *Cell Stem Cell* 19, 573–586. doi: 10.1016/j.stem.2016.10.015

Tcw, J., Wang, M., Pimenova, A. A., Bowles, K. R., Hartley, B. J., Lacin, E., et al. (2017). An efficient platform for astrocyte differentiation from human induced pluripotent stem cells. *Stem Cell Rep.* 9, 600–614. doi: 10.1016/j.stemcr.2017.06.018

Thomas, W. E. (1999). Brain macrophages: on the role of pericytes and perivascular cells. *Brain Res. Brain Res. Rev.* 31, 42–57. doi: 10.1016/S0165-0173(99)00024-7

Tran, J., Anastacio, H., and Bardy, C. (2020). Genetic predispositions of Parkinson's disease revealed in patient-derived brain cells. *NPJ Park. Dis.* 6:8. doi: 10.1038/s41531-020-0110-8

Völkner, M., Zschätzsch, M., Rostovskaya, M., Overall, R. W., Busskamp, V., Anastassiadis, K., et al. (2016). Retinal organoids from pluripotent stem cells efficiently recapitulate retinogenesis. *Stem Cell Rep.* 6, 525–538. doi: 10.1016/j.stemcr.2016.03.001

Walker, F. O. (2007). Huntington's disease. *Lancet* 369, 218–228. doi: 10.1016/S0140-6736(07)60111-1

Wan, W., Cao, L., Liu, L., Zhang, C., Kalionis, B., Tai, X., et al. (2015). Aβ(1-42) oligomer-induced leakage in an *in vitro* blood-brain barrier model is associated with up-regulation of RAGE and metalloproteinases, and down-regulation of tight junction scaffold proteins. *J. Neurochem.* 134, 382–393. doi: 10.1111/jnc.13122

Wang, H. (2018). Modeling neurological diseases with human brain organoids. *Front. Synaptic Neurosci.* 10, 1–14. doi: 10.3389/fnsyn.2018.00001

Wang, P., Mokhtari, R., Pedrosa, E., Kirschenbaum, M., Bayrak, C., Zheng, D., et al. (2017). CRISPR/Cas9-mediated heterozygous knockout of the autism gene CHD8 and characterization of its transcriptional networks in cerebral organoids derived from iPS cells. *Mol. Autism* 8, 1–17. doi: 10.1186/s13229-017-0124-1

Wang, S., Bates, J., Li, X., Schanz, S., Chandler-Militello, D., Levine, C., et al. (2012). Human iPSC-derived oligodendrocyte progenitor cells can myelinate and rescuea mouse model of congenital hypomyelination. *Cell Stem Cell* 12, 252–264. doi: 10.1016/j.stem.2012.12.002

Wang, Y., Wang, L., Guo, Y., Zhu, Y., and Qin, J. (2018). Engineering stem cell-derived 3D brain organoids in a perfusable organ-on-a-chip system. *RSC Adv.* 8:1677. doi: 10.1039/C7RA11714K

Wattanapanitch, M., Klincumhom, N., Potirat, P., Amornpisutt, R., Lorthongpanich, C., Pratya, U-Y., et al. (2014). Dual small-molecule targeting of SMAD signaling stimulates human induced pluripotent stem cells toward neural lineages. *PLoS ONE* 9, 1–8. doi: 10.1371/journal.pone.0106952

Wu, M., Zhang, D., Bi, C., Mi, T., Zhu, W., Xia, L., et al. (2018). A chemical recipe for generation of clinical-grade striatal neurons from hESCs. *Stem Cell Rep.* 11, 635–650. doi: 10.1016/j.stemcr.2018.08.005

Wu, Y. Y., Chiu, F. L., Yeh, C. S., and Kuo, H. C. (2019). Opportunities and challenges for the use of induced pluripotent stem cells in modelling neurodegenerative disease. *Open Biol.* 9:180177. doi: 10.1098/rsob.80177

Xiang, Y.,Tanaka, Y., Patterson, B., Kang, Y.-J., Govindaiah, G., Roselaar, N., et al. (2017). Fusion of regionally-specified hPSC-derived organoids models human brain development and interneuron migration. *Cell Stem Cell.* 21:7. doi: 10.1016/j.stem.2017.07.007

Yoon, S., Elahi, L. S., Paşca, A. M., Marton, R. M., Gordon, A., Revah, O., et al. (2019). Reliability of human 3D cortical organoid generation. *Nat. Methods* 16, 75–78. doi: 10.1038/s41592-018-0255-0

Zhang, M., Ngo, J., Pirozzi, F., Sun, Y. P., and Wynshaw-Boris, A. (2018). Highly efficient methods to obtain homogeneous dorsal neural progenitor cells from human and mouse embryonic stem cells and induced pluripotent stem cells. *Stem Cell Res. Ther.* 9, 1–13. doi: 10.1186/s13287-018-0812-6

Zhang, Y. S., Aleman, J., Shin, S. R., Kilic, T., Kim, D., Shaegh, S. A. M., et al. (2017). Multisensor-integrated organs-on-chips platform for automated and continual in situ monitoring of organoid behaviors. *Proc. Natl. Acad. Sci. U. S. A.* 2017, E2293–E2302. doi: 10.1073/pnas.1612906114

Zhao, X., Eyo, U. B., Murguan, M., and Wu, L.-J. (2018). Microglial interaction with the neurovascular system in physiology and pathology. *Dev. Neurobiol.* 78, 604–617. doi: 10.1002/dneu.22576

Zhao, Z., Nelson, A. R., Betsholtz, C., and Zlokovic, B. V. (2015). Establishment and dysfunction of the blood-brain barrier. *Cell* 163, 1064–1078. doi: 10.1016/j.cell.2015.10.067

Zheng, J., Winderickx, J., Franssens, V., and Liu, B. (2018a). A mitochondria-associated oxidative stress perspective on Huntington's disease. *Front. Mol. Neurosci.* 11, 1–10. doi: 10.3389/fnmol.2018.00329

Zheng, W., Li, Q., Zhao, C., Da, Y., Zhang, H. L., and Chen, Z. (2018b). Differentiation of glial cells from hiPSCs: potential applications in neurological diseases and cell replacement therapy. *Front. Cell. Neurosci.* 12:239. doi: 10.3389/fncel.2018.00239

Conflict of Interest: The authors declare that the research was conducted in the absence of any commercial or financial relationships that could be construed as a potential conflict of interest.

frontiers in Physiology

REVIEW
published: 10 June 2021
doi: 10.3389/fphys.2021.621970

From Brain Organoids to Networking Assembloids: Implications for Neuroendocrinology and Stress Medicine

Evanthia A. Makrygianni[1]* *and George P. Chrousos*[1,2]

[1] University Research Institute of Maternal and Child Health and Precision Medicine, National and Kapodistrian University of Athens, Athens, Greece, [2] Center for Adolescent Medicine and UNESCO Chair on Adolescent Health Care, First Department of Pediatrics, School of Medicine, National and Kapodistrian University of Athens, Aghia Sophia Children's Hospital, Athens, Greece

OPEN ACCESS

Edited by:
Eumorphia Remboutsika, National and Kapodistrian University of Athens, Greece

Reviewed by:
Konstantinos Zarbalis, University of California, Davis, United States
Guya Diletta Marconi, Università degli Studi "G. d'Annunzio" Chieti - Pescara, Italy

***Correspondence:**
Evanthia A. Makrygianni
evanthia.makrygianni@hotmail.com

Specialty section:
This article was submitted to Craniofacial Biology and Dental Research, a section of the journal Frontiers in Physiology

Received: *27 October 2020*
Accepted: *19 April 2021*
Published: *10 June 2021*

Citation:
Makrygianni EA and Chrousos GP (2021) From Brain Organoids to Networking Assembloids: Implications for Neuroendocrinology and Stress Medicine. Front. Physiol. 12:621970. doi: 10.3389/fphys.2021.621970

Brain organoids are three-dimensional cultures that contain multiple types of cells and cytoarchitectures, and resemble fetal human brain structurally and functionally. These organoids are being used increasingly to model brain development and disorders, however, they only partially recapitulate such processes, because of several limitations, including inability to mimic the distinct cortical layers, lack of functional neuronal circuitry as well as non-neural cells and gyrification, and increased cellular stress. Efforts to create improved brain organoid culture systems have led to region-specific organoids, vascularized organoids, glia-containing organoids, assembloids, sliced organoids and polarized organoids. Assembloids are fused region-specific organoids, which attempt to recapitulate inter-regional and inter-cellular interactions as well as neural circuitry development by combining multiple brain regions and/or cell lineages. As a result, assembloids can be used to model subtle functional aberrations that reflect complex neurodevelopmental, neuropsychiatric and neurodegenerative disorders. Mammalian organisms possess a highly complex neuroendocrine system, the stress system, whose main task is the preservation of systemic homeostasis, when the latter is threatened by adverse forces, the stressors. The main central parts of the stress system are the paraventricular nucleus of the hypothalamus and the locus caeruleus/norepinephrine-autonomic nervous system nuclei in the brainstem; these centers innervate each other and interact reciprocally as well as with various other CNS structures. Chronic dysregulation of the stress system has been implicated in major pathologies, the so-called chronic non-communicable diseases, including neuropsychiatric, neurodegenerative, cardiometabolic and autoimmune disorders, which lead to significant population morbidity and mortality. We speculate that brain organoids and/or assembloids could be used to model the development, regulation and

dysregulation of the stress system and to better understand stress-related disorders. Novel brain organoid technologies, combined with high-throughput single-cell omics and gene editing, could, thus, have major implications for precision medicine.

Keywords: brain organoids, assembloids, neuroendocrinology, stress response system, stress-related disorders, hypothalamus, locus caeruleus

INTRODUCTION

Scientists have been seeking to understand mechanisms of human disease since the time of Hippocrates. However, the traditional use of animal models has been somewhat problematic, because of evolutionary divergence. On the other hand, immortalized human cell lines (e.g., HeLa cells) are characterized by chromosomal instability and restricted tissue specificity (Adey et al., 2013). Stem cell-derived *in vitro* life model systems have been the focus of recent efforts. Stem cells are defined as cells that have the ability to divide indefinitely and produce different cellular types as their progeny (Tajbakhsh, 2009; Zakrzewski et al., 2019). Human embryonic (hESCs) and induced pluripotent (hiPSCs) stem cells, collectively called human pluripotent stem cells (hPSCs), can be induced to spontaneously undergo differentiation and morphogenesis, mimicking the formation of embryonic tissues. This process can be achieved by aggregating in 3D structures, called embryoid bodies (EBs). Within EBs, morphogenesis can be directed toward specific germ layers, when specific growth factors are applied (Lancaster and Huch, 2019).

Organoids are spatially organized 3D tissues that consist of multiple cell types which self-organize through similar processes as these observed *in vivo* (i.e., cell-sorting and spatially restricted lineage commitment) and, thus, their progressive organization is highly reminiscent of the actual organ morphogenesis (Lancaster and Knoblich, 2014). Brain organoids are hPSC-derived organoids which are representative of tissue architecture (i.e., they contain progenitor, neuronal and glial cells) and developmental trajectory of the fetal human brain (Qian et al., 2019). These organoids are of great interest, as the living human brain is technically and ethically inaccessible for *in vivo* studies (Benito-Kwiecinski and Lancaster, 2019).

This review will focus on brain organoids and their potential use in studying and understanding the stress system, a highly conserved neuroendocrine system, which is essential for systemic homeostasis. We first introduce briefly the history of brain organoid generation, then we discuss recent advances in brain organoid technologies and, finally, we speculate on their potential applications as model systems of neurodevelopment and neurological or psychiatric disease. In this context, we introduce neuroendocrinology and the neuroendocrine stress system and stress-related disorders and discuss the potential applications of brain organoid technologies in these fields.

CNS EMBRYOLOGY

The central nervous system (CNS) originates from the neural ectoderm, which gives rise to the neural plate, which further differentiates into the neural tube. The latter is organized around a fluid-filled lumen, representative of the brain ventricles (**Figure 1C**). Morphogens are secreted by multiple organizing centers and their gradient defines the axes, i.e., the ventral-dorsal axis is influenced by Sonic Hedgehog (SHH)-Wnt-bone morphogenetic proteins (BMPs), whereas the rostral-caudal axis is defined by retinoic acid (RA) and fibroblast growth factors (FGFs) (**Figure 1B**). Initially, the neural tube is divided into prosencephalon (forebrain), mesencephalon (midbrain), and rhombencephalon (hindbrain) (**Figure 1A**). As embryogenesis proceeds, the prosencephalon further differentiates into telencephalic and diencephalic structures, while the rhombencephalon differentiates to form metencephalon and myelencephalon, which give rise to the pons, the cerebellum, the medulla oblongata and the spinal cord. Neurons are generated from neural stem cells (NSCs) which are situated next to ventricular walls. During neurogenesis, NSCs give rise to neural progenitors as well as more differentiated neural cells, such as intermediate progenitors and neurons. According to differentiation stage, neural cells migrate further outwards, and thus multilayered, stratified structures are formed. These structures have different number of layers, dependent on CNS topology and specialization e.g., the medulla, the cerebral cortex and the optic tectum (superior colliculus) have three, six and seven layers, respectively (Stiles and Jernigan, 2010; Lancaster and Knoblich, 2014; Clevers, 2016; Agirman et al., 2017). Neural induction to rostral identities (forebrain) represents the default pathway of differentiation and is achieved *in vivo* via inhibition of BMP/Nodal signaling (Suzuki and Vanderhaeghen, 2015).

Abbreviations: ACTH, adrenocorticotropin; AD, Alzheimer disease; ANS, autonomic nervous system; ASD, autism spectrum disorder; AVP, arginine vasopressin; BBB, blood–brain barrier; BMECs, brain microvascular endothelial cells; BMP, bone morphogenetic protein; BNST, bed nucleus of the stria terminalis; CeA, central nucleus of the amygdala; CNS, central nervous system; CRH, corticotropin-releasing hormone; DA, dopamine; DMH, dorsomedial hypothalamic nucleus; DR, dorsal raphe nucleus; EB, embryoid body; ECM, extracellular matrix; EC, endothelial cell; ETV2, ETS variant transcription factor; FGF, fibroblast growth factor; GE, ganglionic eminence; GH, growth hormone; hESCs, human embryonic stem cells; hiPSCs, human induced pluripotent stem cells; hPSCs, human pluripotent stem cells; HPA, hypothalamic-pituitary axis; HRCT, hypocretin; LC, locus caeruleus; LH, luteinizing hormone; MD, major depression; mESCs, mouse embryonic stem cells; ME, median eminence; mPFC, medial prefrontal cortex; NAcc, nucleus accumbens; NCCs, neural crest cells; NE, norepinephrine; NSCs, neural stem cells; OPCs, oligodendrocyte progenitor cells; Pa, paraventricular nucleus of the thalamus; PAG, periaqueductal gray; PD, Parkinson's disease; PFC, prefrontal cortex; PNS, peripheral nervous system; PRL, prolactin; PVN, paraventricular nucleus of the hypothalamus; RA, retinoic acid; scRNA-seq, single cell RNA sequencing; SHH, sonic hedgehog; SNS, sympathetic nervous system; sgPFC, subgenual prefrontal cortex; TF, transcription factor; VTA, ventral tegmental area.

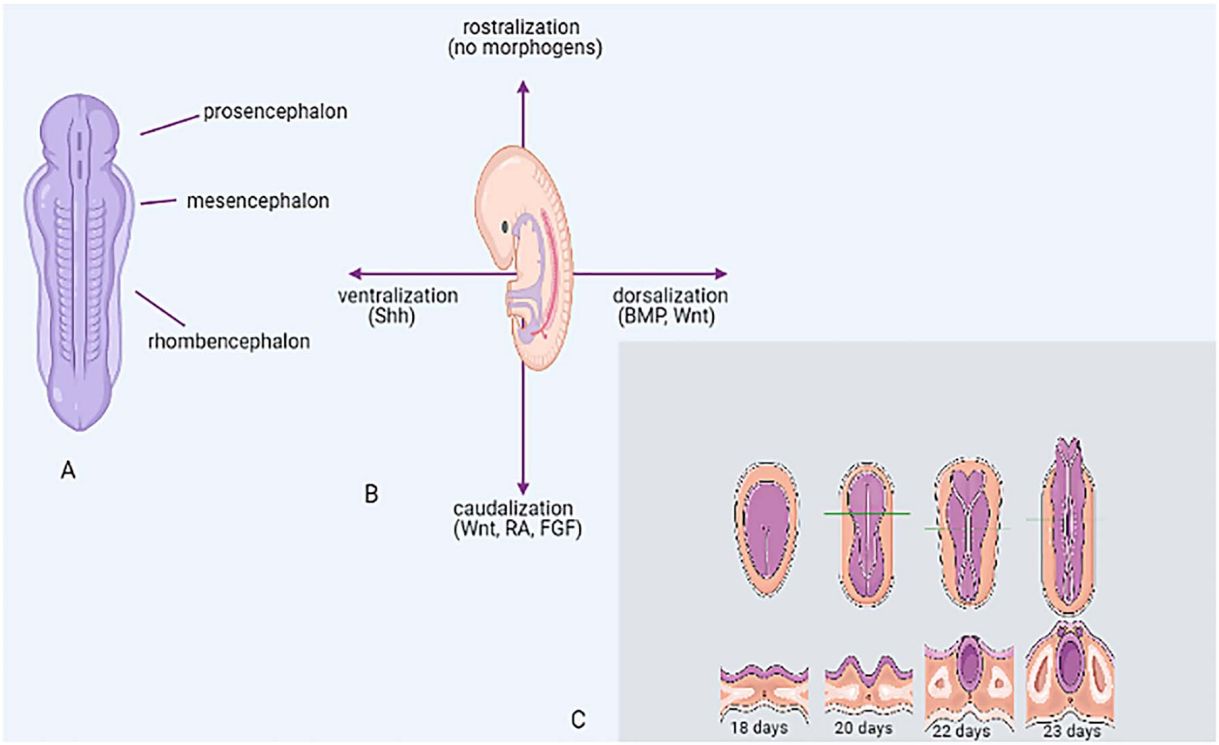

FIGURE 1 | CNS embryology. **(A)** Brain vesicles giving rise to prosencephalon, mesencephalon, rhombencephalon (axial view). **(B)** Establishment of axes through morphogen gradient, *in vivo* (lateral view). **(C)** Embryogenesis of the neural tube around a fluid-filled lumen and development of brain vesicles at 18, 20, 22, and 23 days. BMP, bone morphogenetic protein; FGF, fibroblast growth factor; RA, retinoic acid; SHH, sonic hedgehog.

FROM PSCs TO BRAIN ORGANOIDS

The brain has an intrinsic self-organizing capacity, i.e., if neuroepithelial cells are derived from PSCs, they will subsequently self-organize spontaneously into laminar structures. Zhang et al. (2001) discovered that hESCs could form neural rosettes (2D neural tube-like structures), revealing the self-organization potential of neural progenitors. Neural rosettes recapitulated apical-basal polarity and exhibited spontaneous radial organization, but they could not mimic the overall organization of the developing brain due to their 2D nature (Lancaster and Knoblich, 2014). Subsequently, efforts were made to recapitulate brain tissue organization with 3D cultures. Eiraku et al. (2008) used a 3D aggregation culture (serum-free culture of embryoid body-like aggregates with quick reaggregation, SFEBq) to generate ESC-derived, self-organized cortical tissues with apicobasal polarity. Kadoshima et al. (2013) further improved this method, obtaining telencephalic structures with multiple laminar and separated cortical zones as observed in the embryonic cortex during the second trimester. Initial cultures used dual SMAD and Wnt inhibition for neural induction as well as for direct differentiation toward a telencephalic fate (Lancaster and Huch, 2019). Lancaster et al. (2013) showed that a broader brain regional identity could be generated by simply providing an extracellular matrix (ECM, Matrigel) to EBs without any signaling molecules. The resultant cerebral organoids (heterogeneous neural organoids) contained several different brain regions within individual organoids (Lancaster et al., 2013). After that, several studies generated region-specific organoids by using patterning factors. These organoids included cortical spheroids (Pasca et al., 2015), hippocampal (Sakaguchi et al., 2015), hypothalamic and pituitary (Suga et al., 2011; Ozone et al., 2016), cerebellar (Muguruma et al., 2015), and midbrain organoids (Jo et al., 2016). Subsequently, the assembly of region-specific (ventral and dorsal forebrain) organoids showed that ventral forebrain organoid interneurons have the ability to migrate to dorsal forebrain, resembling *in vivo* brain development (Bagley et al., 2017; Birey et al., 2017; Xiang et al., 2017).

BRAIN ORGANOID METHODOLOGIES

Methods for generating brain organoids can be classified into unguided and guided. Unguided methods are based on spontaneous morphogenesis, intrinsic differentiation capacities and developmental programs within hPSCs; hPSC-derived EBs are grown in ECM and self-organize into distinct brain regions via endogenous signaling (Qian et al., 2019). The resultant

cerebral organoids contain heterogeneous tissues, resembling brain regions (Lancaster and Knoblich, 2014). During this self-organizing process, extensive neuroepithelial conformations may arise with a wide range of cell lineage identities such as forebrain, midbrain, hindbrain, choroid plexus and retina (Lancaster et al., 2013; Quadrato et al., 2017). Interestingly, neuroepithelial tissue within cerebral organoids was capable of developing signaling centers and local tissue patterning (Benito-Kwiecinski and Lancaster, 2019). Nevertheless, the described spontaneous differentiation is characterized by stochasticity. As a result, each lineage and cell type can be represented by unpredictable proportions and a heterogeneous arrangement across organoid batches as well as across hPSC lines. Similarly, proportion and spatial organization of various interacting brain regions can be heterogeneous and unpredictable (Qian et al., 2019). On the other hand, during guided methods, excessive regional heterogeneity is overcome and regional identity is limited to a specific brain region. By using external patterning factors at an early stage (which may be removed at later stages), hPSCs are induced to differentiate toward desired lineages, mimicking *in vivo* development. Different *region-specific organoids* can be fused into *assembloids*. However, the addition of excessive patterning signals, during guided approaches, may reduce organoid complexity and mask important aspects of development and subtle phenotypes. The choice between unguided and guided methodologies will depend on the specific focus of research and weighing between diversity and consistency. Unguided organoids may facilitate the study of cellular diversity during brain development. Among guided methods, brain region-specific organoids may be suitable for the exploration of less heterogeneous brain cytoarchitectures, whereas assembloids may allow the study of molecular and functional interactions and the cross-talk between specific brain regions (Benito-Kwiecinski and Lancaster, 2019; Qian et al., 2019).

BRAIN ASSEMBLOIDS

Assembloids are the next generation of brain organoids that can combine multiple brain regions and/or cell lineages in 3D culture. They can be used to model interactions between different brain regions, to capture cell–cell interactions, and to study the assembly of neural circuits. To model interactions between cortical glutamatergic neurons and GABAergic interneurons, several groups developed separate organoids resembling the dorsal and ventral forebrain and then fused them together into a *multi-region assembloid* (Bagley et al., 2017; Birey et al., 2017; Xiang et al., 2017; Sloan et al., 2018) (**Figure 2**). Similarly, Xiang et al. (2019) generated thalamocortical assembloids that recapitulate thalamic development and may model cortico-thalamic interactions, which shape cortical circuits. During brain development, extensive reciprocal projections between the thalamus and the cortex are formed and are involved in sensory-motor processing, attention and arousal, as the thalamus is an information relay hub. Thalamic dysfunction has been implicated in neurodevelopmental disorders, including autism, schizophrenia and epilepsy (Xiang et al., 2019). Assembloids can also be used to assemble other region-specific organoids, such as the cortex to the striatum or midbrain, e.g., to study corticostriatal interactions, as there is evidence that several neurodevelopmental, neuropsychiatric and movement disorders might be attributed to disordered corticostriatal connectivity (Shepherd, 2013). Nevertheless, further work is needed to reliably assess connectivity *in vitro* and to learn to what extent assembloids can capture more subtle inter-regional changes, associated with the so-called connectopathies. Besides input from other brain regions, neural development and function is shaped by interactions with other cell types, including microglia, astrocytes, oligodendrocytes, or mesoderm-derived blood vessels. It is increasingly recognized that neuroimmune and neurovascular interactions are important for brain development. Neural/non-neural interactions can be modeled *in vitro* by adding non-neural cells in brain region–specific organoids, at various stages of differentiation, to form *multilineage assembloids* (Paşca, 2019; Qian et al., 2019) (**Figure 2**).

CELLULAR INTERACTIONS WITHIN BRAIN ORGANOIDS

Neuronal Interactions

The cerebral cortex comprises neurons (glutamatergic pyramidal neurons and GABAergic interneurons) as well as glial cells (astrocytes, oligodendrocytes and microglia). The maturing forebrain can be subdivided into dorsal forebrain (glutamatergic neurons) and ventral forebrain (GABAergic interneurons); the former gives rise to the cortex, while the latter comprises the various divisions of the ganglionic eminence (GE), from which cortical interneurons derive. Most interneurons originate from medial and caudal GE, in which they acquire specific identities (e.g., parvalbumin, somatostatin, and calbindin). Then, they start a migratory journey to populate the developing dorsal forebrain, via tangential migration. This process starts in humans around gestational age 15 weeks and continues throughout the second year of life (Sloan et al., 2018). After having undergone activity-dependent maturation, interneurons are then integrated into neural circuits, characterized by an excitation/inhibition balance, which plays a central role in the development of the CNS. Aberrations in this fine balance may contribute to neurodevelopmental/neuropsychiatric disorders (Sloan et al., 2018; Marton and Pasca, 2019). Studies in forebrain organoids have reproducibly demonstrated that dorsal organoid glutamatergic neurons form synapses with the migrating ventral organoid interneurons and integrate into a microcircuit with increased morphological complexity, in a similar way as in the cerebral cortex (Pasca et al., 2015; Birey et al., 2017; Yoon et al., 2019). Interestingly, the 3D nature of forebrain assembloids is essential for migration (Birey et al., 2017). Additionally, organoid neurons have been shown to interact with host neurons and develop functional connectivity after transplantation into adult mouse brain (neurological chimeras). This implies that host neurons may influence the function, maturation and

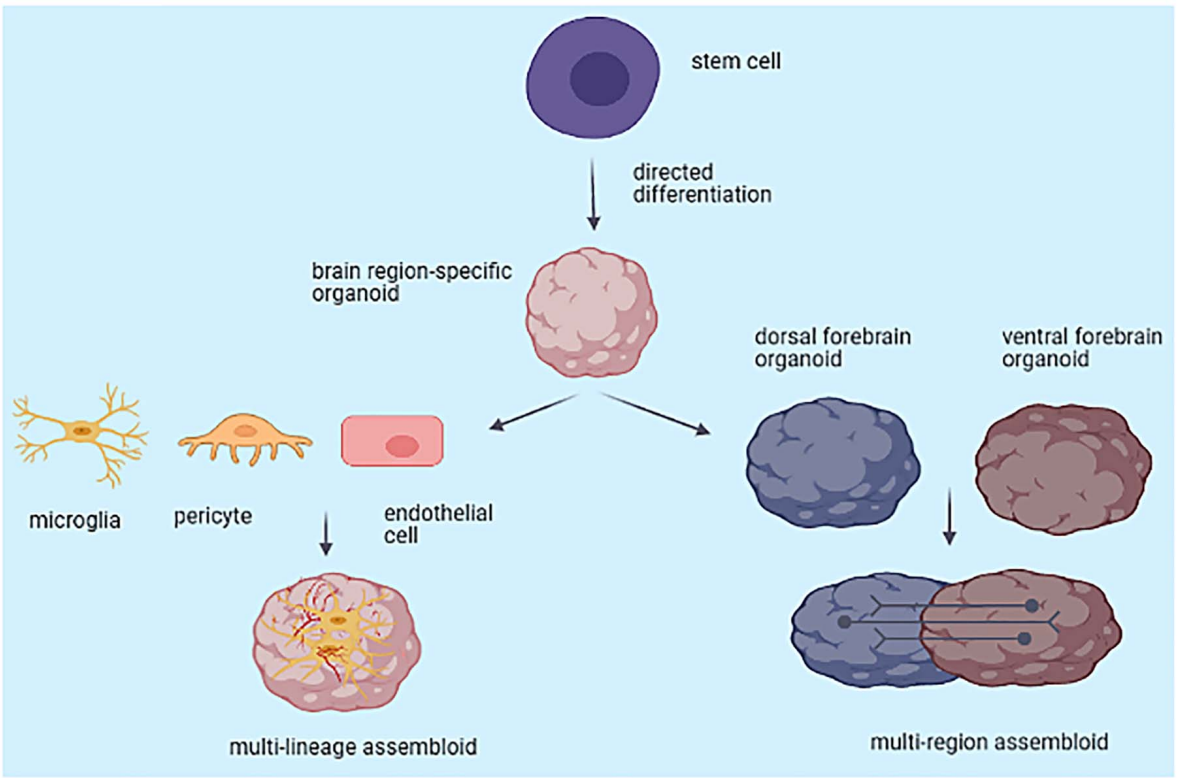

FIGURE 2 | Generation of multi-region and multi-lineage brain assembloids from stem cells.

differentiation of the transplanted neurons (Daviaud et al., 2018; Mansour et al., 2018).

Astrocyte Interactions

It has been increasingly recognized that glial cells are important for neuronal development. Astrocytes play a central role in brain homeostasis and synaptic plasticity, and have been characterized as the housekeeper of the CNS (Logan et al., 2019). They affect neurons pleiotropically through extensive interactions, which influence neuronal development, maturation and survival as well as formation of synapses (Marton and Pasca, 2019). The exact nature of this influence (i.e., direct intercellular or indirect via secreted molecules) is unknown. Abnormal astrocyte function has been mechanistically implicated in the etiology of neuropsychiatric disorders (Sloan et al., 2018). Temporally, astrogenesis takes place after neurogenesis in *in vitro* 3D cultures, and astrocytes increase in number and become more mature over time as observed *in vivo*. Long-term organoid cultures allow for advanced astrocytic maturation, simulating *in vivo* developmental stages; this maturation would be difficult to obtain in a 2D culture (Sloan et al., 2017). Currently, mature organoid astrocytes can only be studied by isolation and placing into tissue culture plates. Exploring how astrocytes behave within organoids (e.g., by imaging methods) would elucidate the mechanisms through which astrocytes modulate neuronal development (Marton and Pasca, 2019).

Oligodendrocyte Interactions

Initially, brain organoids lacked oligodendrocytes. Although several attempts have been made to produce oligodendrocytes from hiPSCs in 2D cultures, various functional aspects of oligodendrocytes – including myelination – are difficult to study in 2D (Marton and Pasca, 2019). Alternatively, oligodendrocytes have been generated in addition to astrocytes and neurons in organoids; this allows the formation of compact myelin through interactions with neuronal processes. These cultures can be used to model white matter formation and its disorders as well as interactions between oligodendrocytes and other types of cells (Madhavan et al., 2018; Marton et al., 2019).

CNS and Non-CNS Lineage Cell Interactions in Brain Organoids

Microglial Interactions

Microglia are the main immune cells of the CNS. Microglial precursors arise from the yolk sac, migrate to the brain and quickly diverge from macrophages, which reside in other tissues; this process takes place under the influence of unknown brain-derived signals (Li and Barres, 2018). The presence of microglia in organoids would allow the study of the roles of microglia in phagocytosis of damaged cells, release of cytokines as well as synaptogenesis and elimination of synapses (Marton and Pasca, 2019). Because it is difficult to reproduce the development

of microglia in culture, attempts to study microglial-neural interactions have converged into two methods. According to the first one, microglial cells are produced from hiPSCs, outside organoids, and then are integrated into the latter to form multi-lineage assembloids; this allows the study of morphological and functional aspects of microglia in 3D, including response to injury (Abud et al., 2017; Paşca, 2019; Song et al., 2019a). In the second method, minimally patterned organoids – which contain multiple germ layer progenitor cells – are used to derive microglial cells (Ormel et al., 2018). Microglia generation *in vitro* is essential for modeling neuroimmunological disorders, including multiple sclerosis (MS) and autoimmune encephalitis (Marton and Pasca, 2019). Assembloids that contain microglia and neurons could be valuable for the study of immune-mediated pathways during synaptic elimination. Additionally, mutations in genes that are expressed in myeloid cells, including monocytes and microglia, have been associated with neuropsychiatric diseases, but the mechanism is unknown (Paşca, 2019).

Vascular Cell Interactions/Brain Organoids With a Functional Vascular-Like System and BBB Characteristics

The wall of brain blood vessels consists of the mesoderm-derived endothelial cells (ECs), whereas pericytes are also found in capillaries (Alberts et al., 2002; Marton and Pasca, 2019). The presence of blood vessels within brain organoids is essential for reducing the levels of cellular stress and death and for generating mature organoids. Additionally, the blood–brain barrier (BBB) as well the influence of neural activity on blood flow could be studied in brain organoids that contain blood vessels (Marton and Pasca, 2019). Several attempts have been made to generate blood vessels within organoids. Mansour et al. (2018) used a mouse host to transplant human-derived brain organoids; organoids were invaded with host blood vessels. Pham et al. (2018) vascularized brain organoids with patient-derived ECs. Song et al. (2019b) fused cortical spheroids and isogenic endothelial spheroids from hiPSCs alongside mesenchymal stem cells (MSCs). Cakir et al. (2019) generated human cortical organoids with ETS variant transcription factor 2 (ETV2) induction. In accordance with their hypothesis that ETV2 expression induces ECs and structures similar to blood vessels in organoids, they engineered hESCs to ectopically express ETV2. The resultant vascularized organoids formed functional vasculature, when implanted in mice (Cakir et al., 2019). Bergmann et al. (2018) created BBB organoids by co-culturing primary brain ECs, pericytes and astrocytes. The main components of BBB are brain microvascular endothelial cells (BMECs), pericytes, neurons and astrocytes. Unique features of the BBB, including the high transendothelial electrical resistance (TEER), have been attributed to tight junctions formed by BMECs (Marton and Pasca, 2019). The production of BMECs *in vitro* can be challenging. Hence, further research is needed to generate these cells *in vitro* (Lu et al., 2021).

BRAIN ORGANOIDS AND CELLULAR STRESS

By using single-cell transcriptomics, Bhaduri et al. (2020) concluded that cortical organoids contain a smaller number of cell subtypes, compared to the human cortex and this may be attributed to ectopic activation of cellular stress pathways, which leads to disordered cell-type specification. Immature, broader cell classes, not representative of cellular subtypes can be contained within brain organoids. Consequently, brain organoids may not be reliable models for the study of developmental processes, disease phenotypes that depend on specific cell types, and inter-cellular connectivity. Of note, cellular stress and impaired cellular specificity are reduced when organoids are transplanted into mouse cortex (Bhaduri et al., 2020).

SLICED CORTICAL ORGANOIDS

Because cortical organoids lack functional blood vessels, organoid cells show impaired viability, due to inadequate supply of oxygen and nutrients via surface diffusion; this prevents organoids from reaching the cytoarchitecture of late developmental stages. Qian et al. (2020) used a slicing method to develop a sliced neocortical organoid model with well-separated upper and deep cortical layers. This model prevented cell death within organoids and allowed growth over long-term culture, thus recapitulating late stage human cortical developmental features. This method may be used to improve cell viability in 3D culture systems and may also be applied to other brain regions or other organs. Interestingly, slicing could be combined with hyperoxia, which has already been employed in organoid protocols. This combination would further reduce cellular hypoxia and improve cell viability, while distinct cortical layers would be achieved at the same time (Qian et al., 2020).

POLARIZED BRAIN ORGANOIDS

Brain organoids lack topographical organization along dorsoventral and anteroposterior axes. During CNS development, combinations of morphogens (e.g., SHH, Wnt, and BMPs) are secreted by organizing centers, in complex spatiotemporal patterns; this allows cells to acquire discrete regional identities as a function of their position. This process could be mimicked in brain organoids/assembloids by precise positioning of signaling centers via engineering methods (Cederquist et al., 2019; Miura and Pasca, 2019). Cederquist et al. (2019) generated a signaling center within forebrain organoids by assembling them with a group of SHH-secreting cells. Organoids became polarized into several forebrain regions. Further studies are needed to test whether differentiating organizer-like cells from hPSCs and then combining them with brain organoids could be used as a general approach to establish topographies across all regions of the CNS. Polarized organoids provide the opportunity to study a wide range of phenotypes in a single organoid system. They could be used

to model complex neurodevelopmental disorders, in which altered regional specification during forebrain patterning has been hypothesized or to study the effects of hypothalamic peptidergic system on the cerebral cortex (Cederquist et al., 2019; Miura and Pasca, 2019).

CORTICAL ORGANOIDS FOR MODELING THE DEVELOPMENT OF CEREBRAL CORTEX AND THEIR LIMITATIONS

The human cortex is profoundly different from those of other species and is the most uniquely evolutionary expanded region of the human brain. Hence, hPSC-derived cortical organoids are advantageous, compared to animal models. Nevertheless, these organoids are far from identical to *in vivo* and *in situ* cerebral cortex. Firstly, conventional cortical organoids are much smaller than human cerebral cortex. Their size can reach up to ∼5–6 mm in diameter, whereas the human cortex is about 15 cm in diameter, with gray matter being 2–4 mm thick (Qian et al., 2019) and cortical surface area being around 2,000 cm^2 (Hofman, 2014). Secondly, they lack vascularization and contain a necrotic core, which further limits their viable thickness. Thirdly, although cortical organoids recapitulate the organization of neural progenitor zones in a spatiotemporal manner (i.e., deep layer neurons are formed first, followed by upper layer neurons), there is extensive mixing and co-localization; this leads to restricted neuronal spatial layering and incomplete cortical lamination (Benito-Kwiecinski and Lancaster, 2019; Qian et al., 2019).

Distinct cortical layers are established around the second trimester of pregnancy and thus conventional organoids are suitable models of this embryonic period; this is congruent with the finding that organoids have similar transcriptomic and epigenetic profiles to those of early human fetal cortex up to the second trimester (Camp et al., 2015; Luo et al., 2016; Qian et al., 2016; Quadrato et al., 2017). Recent advances in organoid technologies have led to organoids with well-separated layers, which is a feature of human cortical development at late stages (Qian et al., 2020).

Organoid neurons are able to form synapses, with a synaptic density similar to that observed in fetal brain. These neurons show spontaneous and coordinated firing activity, resulting in neuronal networks with self-organized firing patterns (Quadrato et al., 2017; Benito-Kwiecinski and Lancaster, 2019). Accordingly, forebrain assembloids generate functional, interacting, excitatory and inhibitory neurons and provide the opportunity to study cell migration, neuronal circuit formation and interregional interactions, which shape brain development. However, these networks are less mature compared to adult neuronal networks (Sloan et al., 2018). Interestingly, assembloids show improved firing frequency compared to non-fused organoids, indicating that fusion confers additional neuronal properties, not obtainable in a single organoid (Seto and Eiraku, 2019). Nevertheless, further studies are needed to examine the genesis and regulatory mechanisms of functional circuits in the fusion system (Xiang et al., 2019).

Brain organoids lack sensory input (Amin and Pașca, 2018; Velasco et al., 2020). During early embryonic development, there are patterns of spontaneous neuronal activity that synchronize local and large-scale cortical networks; these later guide the establishment of global thalamocortical and intracortical networks. The earliest neuronal networks are autonomous and transient. After sensory input from the periphery has reached the cortex, circuits are reshaped and matured by integration of sensory input with spontaneous neuronal activity (Molnár et al., 2020).

Brain organoids lack gyrification, possibly because they do not have the ability to reach the developmental stage where this takes place. Alternatively, this may be due to the small size of brain organoids, as cortical folding is associated with the surface area and the thickness of CP (cortical plate) (Qian et al., 2019). Synthetic biomaterial-based methods have been used to model the physics of the folding brain (Karzbrun et al., 2018) and control the geometrical and biomechanical properties of brain organoids (Oksdath et al., 2018). Additionally, it has been increasingly recognized that the biochemical composition of the ECM may influence the biomechanical properties of the brain and may have a central role in the cellular differentiation and brain architecture. Matrigel, currently used as ECM in brain 3D culture technologies, partly reflects the complex composition of brain ECM. New biosynthetic matrices may provide control over the physicochemical and mechanical characteristics of the microenvironment of brain organoids (Oksdath et al., 2018).

One of the most significant limitations of brain organoids is organoid-to-organoid and batch-to-batch variability, especially when unguided methods are used (Velasco et al., 2020). Recent efforts have focused on generating reproducible brain organoids (Velasco et al., 2019; Yoon et al., 2019). By using scRNA-seq (single cell RNA sequencing), Velasco et al. (2019) characterized cells of different mature cortical organoids at 3 and 6 months. Cortical organoids derived from different stem cells yielded similar ratios of different cellular types, and were highly reproducible across cell lines and batches. Similarly, Yoon et al. (2019) generated highly reliable and replicable cortical spheroids (region-specific organoids), regardless of initial cell line and experiment. However, generating reproducible organoids of other brain regions remains challenging. This may be explained by the fact that the default differentiation state of neural progenitors is to become cortex and this can be fulfilled even outside the embryonic brain (Velasco et al., 2020).

DISEASE MODELING

Due to their versatility, brain organoids are suitable for modeling diseases of either genetic or environmental etiology (Adams et al., 2019). They have been extensively used to model structural neurodevelopmental brain disorders, attributed to disordered progenitor cell migration, including microcephaly, macrocephaly and lissencephaly (Lancaster et al., 2013; Gabriel and Gopalakrishnan, 2017; Li et al., 2017a,b). However, due

to their inability to form cortical folds, modeling diseases such as Miller–Dieker syndrome (characterized by prominent lissencephaly) is difficult (Bershteyn et al., 2017; Iefremova et al., 2017). Additionally, effects of neurotrophic pathogens on brain development can be modeled. Interestingly, when brain organoids are exposed to Zika virus, neural progenitor cells (NPCs) are preferentially infected, leading to cell death and reduced organoid size (Cugola et al., 2016; Dang et al., 2016; Garcez et al., 2016; Qian et al., 2016).

Modeling neurodevelopmental disorders which are characterized by less prominent or no structural malformations is more difficult. However, the use of organoids, in this case, can provide insights into disease-related cellular and molecular mechanisms. For example, an imbalance between excitatory/inhibitory neurons (associated with overexpression of FOXG1) has been shown in forebrain organoids from autism spectrum disorder (ASD)-derived PSCs (Mariani et al., 2015; Choi et al., 2017). On the other hand, in ihPSCs-derived dorsal-ventral forebrain assembloids from individuals with Timothy syndrome (a genetic, multisystem disorder characterized by ASD features), defects in interneuron migration have been observed (Birey et al., 2017). Brain organoids have also been generated to model Rett syndrome (Mellios et al., 2018), tuberous sclerosis (TS) (Blair et al., 2018) and schizophrenia (Stachowiak et al., 2017; Kathuria et al., 2020). The modeling of diseases associated with abnormalities in network-level activity among distant brain regions remains a challenge (Seto and Eiraku, 2019).

Brain organoids have been utilized to model neurodegenerative diseases. However, the majority of neurodegenerative diseases present later in life, are age-related, and are usually progressive. Hence, brain organoids may not be accurate neurodegeneration models. Additionally, neurovascular interactions are indispensable for the modeling of neurodegenerative disorders, as they recapitulate the neurodegenerative microenvironment (Paşca, 2019; Grenier et al., 2020). Several groups have generated cortical organoids to model Alzheimer disease (AD) and recapitulated the molecular phenomena that are observed in AD, such as aggregation of β-amyloid, hyperphosphorylation of tau protein, and endosomal abnormalities (Lee et al., 2016; Raja et al., 2016; Lin et al., 2018; Gonzalez et al., 2018).

Midbrain organoids containing functional dopaminergic neurons have been generated, mainly for modeling Parkinson's disease (PD). These organoids, especially when disease-specific mutations are introduced or pharmacological treatment is applied to induce neurodegeneration, may be used as disease models. Midbrain organoids could also be valuable in the context of cell-replacement therapies (Kim et al., 2019; Smits et al., 2019; Kwak et al., 2020). Additionally, brain organoids capable of modeling both early development and features of neurodegeneration could be revolutionary in the study of chronic neuropsychiatric disorders, which are often characterized by alterations in both neurodevelopmental and neurodegenerative processes (Grenier et al., 2020). Moreover, hypothalamic organoids containing nuclei-like clusters of neuropeptidergic neurons could be promising models for studying metabolic disorders and obesity (Qian et al., 2016; Qian et al., 2018; Rajamani et al., 2018).

Brain Organoids and Aging

Brain organoids are derived from either ESCs or iPSCs. Apart from aging-induced somatic mutations, many features of aging including epigenetic changes, DNA/oxidative damage and reduced telomere length are reverted during iPSC reprogramming (Cornacchia and Studer, 2017). However, there is evidence that several epigenetic characteristics of aging are conserved after reprogramming of iPSCs that are derived from patients with syndromes associated with premature aging (Agarwal et al., 2010; Batista et al., 2011; Andrade et al., 2012; Grenier et al., 2020). As a result, accelerated aging could be studied in brain organoids that are derived from these iPSCs. Additionally, aging could be induced by introducing disease (including neurodegeneration and progeria)-associated mutations into PSCs via genome editing. Alternatively, it has been proposed that aging could be induced by exposing cells to aging-associated stress such as ROS (reactive oxygen species), pro-inflammatory molecules and radiation (Hu et al., 2018; Grenier et al., 2020). However, it remains unclear which of these factors would optimally induce cellular aging-related changes (Hu et al., 2018). Interestingly, age-related changes of neurons are retained after direct neuronal reprogramming (i.e., the direct conversion of cells from one lineage to another without going through the pluripotent stage) and, thus, induced neuron models may allow the modeling of age-associated diseases (Mertens et al., 2015; Mertens et al., 2018).

Of note, 3D cultures allow long culture periods (e.g., 60 weeks), which can be used to study chronological aging *in vitro* (Grenier et al., 2020). Additionally, there is increasing evidence that there may be an interaction between ECM and senescent cells (Levi et al., 2020). Age-related changes in the components of the ECM may disrupt cellular homeostasis and cellular aging may change the composition of ECM. As a result, organoids are more suitable to model *in vitro* the microenvironment of aging, compared to cell lines (Birch, 2018; Hu et al., 2018).

In summary, although brain organoids provide a window into understanding complex neurological diseases, at this time, they are simplistic and at an early stage, while they may be biased models because of their *in vitro* nature. Further improvements, including generation of organoids with well-defined connectivity between several brain regions, acceleration of functional maturation, efficient incorporation of other cell and tissue types (e.g., glia and vasculature), and effective modeling of aging could lead to more comprehensive and realistic models. **Supplementary Table 1** shows advances in brain organoid methodologies to date.

SINGLE-CELL OMICS AND BRAIN ORGANOIDS

Sequencing of bulk tissues has been increasingly replaced by single cell genomics, which is moving rapidly from scRNA-seq to single-cell multi-omics. This is because scRNA-seq snapshots

may provide insight into cellular diversity, but cannot explain why and how a cell adopts a certain state (Packer and Trapnell, 2018; Schier, 2020).

On the other hand, combined multi-modal analysis of genome, transcriptome, epigenome, chromatin organization and proteome as well as information about spatial localization of cells can shed light on multiple aspects of cellular identity (Burgess, 2019; Efremova and Teichmann, 2020). Genome sequencing combined with scRNA-seq may elucidate genotype-phenotype correlations and the phenotypic impact of genetic variants. Because other genes and molecules can affect gene transcription, scRNA-seq may provide evidence about potential gene-regulatory networks. Joint transcriptomics and chromatin accessibility analysis could reveal novel cell states and investigate the activity of TFs and enhancer elements (Efremova and Teichmann, 2020). Additionally, by using single cell proteomics, ligands, receptors as well as downstream signaling molecules and lineage-specific TFs could be quantified and inter- and intra-cellular signaling network maps could be constructed. Simultaneous measurement of proteins and RNAs could associate cell-signaling with gene expression; poor association between gene and protein expression is indicative of post-transcriptional modifications (Efremova and Teichmann, 2020).

Organoids consist of various cellular types and states and are characterized by high organoid to organoid variability. Applying single-cell omics to brain organoids could improve our mechanistic understanding of human brain development and disease-related phenomena, through the study of lineage relationships and regulatory networks (Camp and Treutlein, 2017; Atamian et al., 2021).

GENE EDITING IN BRAIN ORGANOIDS

Brain organoids can be genetically modified either transiently or permanently. Stable modifications (by lentivirus, transposon and CRISPR/Cas9 systems) are typically performed at early developmental stages (hPSCs, or EBs), whereas transient modifications [by adeno-associated virus (AAV) and electroporation-based techniques] are performed at later stages (mature organoids) (Fischer et al., 2019).

Among stable methods, older nuclease-based methods have been replaced by CRISPR/Cas9. Currently, the major application of CRISPR-Cas9 is to model monogenic neurodevelopmental and neurodegenerative diseases as well as oncogenesis, by either introducing pathogenic mutations into control hiPSCs, or utilizing patient hiPSCs to generate isogenic controls (Fischer et al., 2019). However, the modeling of complex disorders remains a challenge. In the future, a combination of transient and stable gene editing methods may allow modeling complex diseases and developmental processes, as transient methods can be more versatile and efficient in mature brain organoids (Camp and Treutlein, 2017; Fischer et al., 2019).

Another future application of genetically modified brain organoids could be cell-lineage tracing to explore the developmental history of individual cells. This could be accomplished by single-cell sequencing and labeling via lineage-specific expression of fluorescent proteins (Fischer et al., 2019). Additionally, introduction of DNA mutations with CRISPR/Cas9 could create genetic scars, which could be used as cell-specific markers (Camp and Treutlein, 2017).

NEUROENDOCRINOLOGY

The hypothalamus is highly conserved anatomically and functionally throughout vertebrates, due to its essential role in regulating homeostasis and behavior. It regulates pituitary gland secretion (**Figures 3A,C**), but also regulates sleep, body temperature, feeding and aging through connections via the autonomic nervous system (ANS) and other pathways. Pituitary hormones and their targets regulate multiple functions, including fluid balance, stress response, reproduction, growth, metabolism and pain. The hypothalamus and the hypophysis are developmentally and functionally connected (Rizzoti et al., 2016; Xie and Dorsky, 2017) (**Figure 3A**).

The morphogenesis of the hypothalamus is complex, compared to other regions of the brain, because its structural organization lacks clear landmarks (Bedont et al., 2015; Rizzoti et al., 2016). In contrast to the columnar organization of other brain regions, the hypothalamus consists of various nuclei, organized in a 3D network (**Figure 3B**).

Secretion of gradients of morphogens is essential for patterning of the hypothalamus during development. Wnt, SHH, BMP, FGF, Nodal and Notch signaling determine the hypothalamic identity. During this process, variable gradients of multiple TFs are secreted to fine-tune the patterning and define the various hypothalamic nuclei (Bedont et al., 2015; Xie and Dorsky, 2017).

The posterior lobe of the pituitary arises from the neuroectoderm, whereas the anterior pituitary derives from non-neural ectoderm. Pituitary morphogenesis is regulated by interactions between the presumable posterior lobe, the infundibulum (an early diencephalic structure) and the Rathke's pouch (derived from oral ectoderm). Additionally, the anterior pituitary placode and the hypothalamic anlage interact with each other; SHH, Wnt, BMP, and FGF signaling seem to determine this interaction and the hypophyseal patterning (Takuma et al., 1998; Brinkmeier et al., 2007; Zhu et al., 2007).

Rathke's pouch expresses the TFs LHX3 and LHX4 (Rizzoti and Lovell-Badge, 2005). Additionally, TFs including TBX19, POU1F1, GATA2 are essential for subsequent lineage commitment and differentiation to adrenocorticotropin (ACTH)-, growth hormone (GH)-, prolactin (PRL)-, thyroid-stimulating hormone (TSH)-, luteinizing hormone (LH)- and follicle-stimulating hormone (FSH)-producing cells (Rizzoti and Lovell-Badge, 2005; Kelberman et al., 2009; Suga, 2019).

The neuroendocrine system comprises many functionally diverse cell types. Mature endocrine cells can be difficult to obtain, thus, the *in vitro* study of specific subtypes of human neuroendocrine cells has not been feasible; this could be overcome by the use of hPSCs. There have been several efforts to generate neuroendocrine tissues and organoids from PSCs

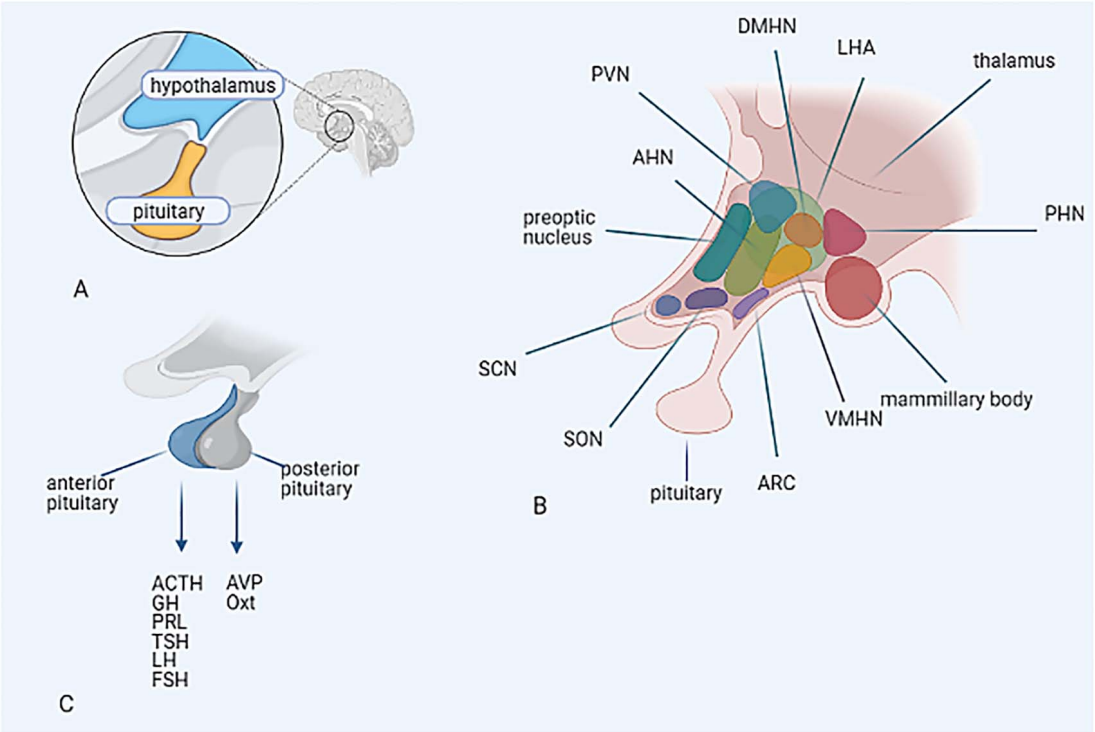

FIGURE 3 | (A) Anatomical characterization of the hypothalamus and the pituitary. **(B)** Structural organization of the hypothalamic nuclei. **(C)** Hypothalamic control of hormonal output of the pituitary. Hypothalamic nuclei: AHN, anterior hypothalamic nucleus; ARC, arcuate nucleus; DMHN, dorsomedial hypothalamic nucleus; LHA, lateral hypothalamic area; PHN, posterior hypothalamic nucleus; PVN, paraventricular nucleus; SCN, suprachiasmatic nucleus; SON, supraoptic nucleus; VMHN, ventromedial hypothalamic nucleus. Pituitary hormones: ACTH, adrenocorticotropic hormone; AVP, arginine vasopressin; FSH, follicle-stimulating hormone; GH, growth hormone; LH, luteinizing hormone; Oxt, oxytocin; PRL, prolactin; TSH, thyroid-stimulating hormone.

(Suga et al., 2011; Ozone et al., 2016; Ogawa et al., 2018; Kasai et al., 2020). Ogawa et al. (2018) induced arginine vasopressin (AVP)-secreting neurons from hESCs. Suga et al. (2011) and Ozone et al. (2016) recapitulated pituitary development in 3D. Kasai et al. (2020) generated a functional hypothalamus-pituitary unit. The culture methods used in the above studies have been shown to recapitulate effectively the hypothalamic and hypophyseal embryogenesis, and therefore could have applications in developmental neuroendocrinology. Adhya et al. (2018) suggested that brain organoids could be used to study the impact of neurosteroids on brain development. This study could lead to a better understanding of developmental phenomena, such as the sexual dimorphism of the brain as well as the relation of neurosteroids to neurodevelopmental and neurodegenerative diseases (Adhya et al., 2018).

Another potential use of hPSC-derived hypothalamic-pituitary cells could be in regenerative medicine, although, at this time, generated tissues are not as functional as normal tissues (Kasai et al., 2020). PSC-derived ACTH-producing cells have been shown to function efficiently, if they are extrinsically controlled by releasing factors or small molecules, even after ectopic transplantation. However, in ectopic transplantation, hypothalamic corticotropin-releasing hormone (CRH) release does not affect the grafts. Orthotopic transplantation of hormone-producing cells could be advantageous in the future (Rizzoti et al., 2016; Suga, 2019).

PITUITARY ORGANOIDS

Several studies have reported methods to differentiate hPSCs into anterior pituitary, *in vitro*. Suga et al. (2011) produced functional 3D pituitary tissues from mouse embryonic cells (mESCs). After that, Ozone et al. (2016) produced regulator hormone-responsive pituitary tissue from hESCs. In addition to corticotrophs, they generated somatotrophs with appropriate GH secretion in response to growth hormone-releasing hormone (GHRH) and somatostatin, which had not been achieved by Suga et al. (2011) (**Supplementary Table 1**).

HYPOTHALAMIC-PITUITARY UNITS

Kasai et al. (2020) generated a functional hypothalamic-pituitary unit from 3D-cultured hiPSCs. During embryonic development, the hypothalamus interacts with the anterior pituitary and this interaction is considered to be essential for pituitary development (Takuma et al., 1998; Scully and Rosenfeld, 2002;

Rizzoti and Lovell-Badge, 2005; Zhu et al., 2007). In that context, Kasai et al. (2020) juxtaposed anterior pituitary and hypothalamic neurons and observed that their proximity increased the ACTH secretion capacity of the pituitary, but also resulted in regulation of ACTH by hypothalamic CRH. The authors concluded that the hypothalamus plays a crucial role in the development and maturation of the anterior pituitary. *In vivo*, anterior pituitary secretion is regulated by the hypothalamus, depending on the micro-environment, so that homeostasis is maintained; ACTH cells are stimulated by hypothalamic CRH, whereas they are inhibited by glucocorticoids. The aggregates generated by Kasai et al. (2020) responded appropriately to both CRH and glucocorticoids. The results of this study suggest that $ACTH^+$ cells function under the control of CRH^+ cells in this 3D, *in vitro* model (Kasai et al., 2020).

THE NEUROENDOCRINE STRESS RESPONSE SYSTEM

Stress is a state of disrupted organismal homeostasis, due to physical or emotional forces, called stressors. When these forces exceed a certain threshold, adaptive compensatory physiologic responses are activated, which constitute the neuroendocrine stress or adaptation response (Chrousos, 2007, 2009). This response is essential for survival and is remarkably consistent, so that it has been postulated that a discrete, dedicated neuroendocrine system has evolved for its coordination (Chrousos and Gold, 1992). The stress response allows an organism to make the necessary physiological and metabolic changes that are needed to cope with homeostatic demands (Miller and O'Callaghan, 2002).

The stress response system has two major arms: (a) the CRH system and (b) the locus caeruleus*-norepinephrine (LC-NE) system. The major central components of these arms are the *paraventricular nucleus (PVN)* of the hypothalamus and the pontine *locus caeruleus (LC)* alongside their projections to the *brainstem autonomic nuclei*. The peripheral components are the pituitary-adrenal axis and sympathetic nervous (SNS)/sympathoadrenal system as well as components of the parasympathetic nervous system (PSNS).

The CRH system is widespread throughout the brain (hypothalamic and extra-hypothalamic CRH system), but it is best characterized in the PVN and amygdala (central nucleus of the amygdala, CeA) (Chrousos and Gold, 1992; Chrousos, 2007; Gold et al., 2015b). The amygdala CRH system induces anxiety, but also activates the hypothalamic CRH system and the LC-NE system. The hypothalamic CRH system regulates the HPA axis and activates the LC-NE system (Gold et al., 2015b) (**Figure 4**, Inset).

The PVN plays a central role as an initiator of endocrine and autonomic responses, which are essential for maintaining homeostasis and adapting to stressors. It has a magnocellular, parvocellular and an autonomic subdivision. The first two control the hormonal output of the posterior and anterior pituitary, respectively (**Figure 3C**). Neurons of the autonomic subdivision project to the brainstem autonomic nuclei and the spinal cord. The PVN receives both excitatory and inhibitory input, mediated by glutamate and GABA, respectively. Limbic inputs from the prefrontal cortex (PFC) and amygdala, involved in the stress response, are relayed to the PVN, primarily via the bed nucleus of the stria terminalis (BNST) and the dorsomedial hypothalamic nucleus (DMH). Interestingly, direct projections from the CeA to the PVN are limited. Stress causes rapid activation of neural pathways afferent to the PVN, resulting in rapid CRH and AVP release to the pituitary portal circulation. Induction of AVP expression enhances stress-induced activation of HPA axis and the effect of CRH on ACTH (Chrousos and Gold, 1992; Benarroch, 2005).

Activation of the CRH system promotes arousal, fear-related behaviors and inhibits sleep, feeding and reproductive activity, which could be distractive during threatening conditions. Additionally, during the stress response, activation of CRH neurons leads to activation of pro-opiomelanocortin (POMC) neurons of the hypothalamic arcuate nucleus, which inhibit both the CRH neurons and the LC-NE system and mediate opioid receptor-induced analgesia (Chrousos and Gold, 1992; Chrousos, 2007).

The LC is the principal noradrenergic nucleus of the CNS, regulating arousal and autonomic activity by extensive projections to numerous structures of the CNS and peripheral nervous system (PNS). These projections can be either excitatory, through activation of α_1-adrenoreceptors, or inhibitory via activation of α_2-adrenoreceptors (Samuels and Szabadi, 2008b). The LC projects to the entire cortex to increase cortical activity, and is reciprocally connected with the PFC, regulating cognition, attention and vigilance. Also, it is reciprocally connected with the amygdala to process the emotional valence of the stimuli and promote fear/anxiety as well as increase sympathetic activity in the presence of threatening stimuli. It is reciprocally connected to the serotoninergic dorsal raphe nucleus (DR) and also projects to the thalamus to further promote wakefulness. It receives input from the midbrain periaqueductal gray (PAG), which is involved in sleep-wakefulness and REM sleep regulation. It projects to the pendunculopontine (PPT) and laterodorsal tegmental nuclei (LDT) of the brainstem to regulate wakefulness and inhibit REM sleep. Additionally, it inhibits the GABAergic neurons of the hypothalamic ventrolateral preoptic area (VLPO) to maintain arousal, thus simultaneously disinhibiting the hypothalamic histaminergic projections to the cortex. It inhibits the hypocretin (HRCT) neurons of lateral hypothalamus to suppress feeding. It projects to the hippocampus, which is mostly inhibitory on both the amygdala and the PVN CRH system (Chrousos, 2007; Samuels and Szabadi, 2008a,b). Also, it projects to the cerebellum to enhance motor performance and planning. It inhibits the preganglionic parasympathetic nuclei and the rostral ventrolateral medulla (RVLM) to control cardiovascular function and projects to sympathetic and parasympathetic neurons of the spinal cord (Samuels and Szabadi, 2008a,b).

Additionally, the LC is connected to the *mesocortical* and *mesolimbic dopaminergic pathways,* which are involved in motivation, reward and drug addiction. The former connects

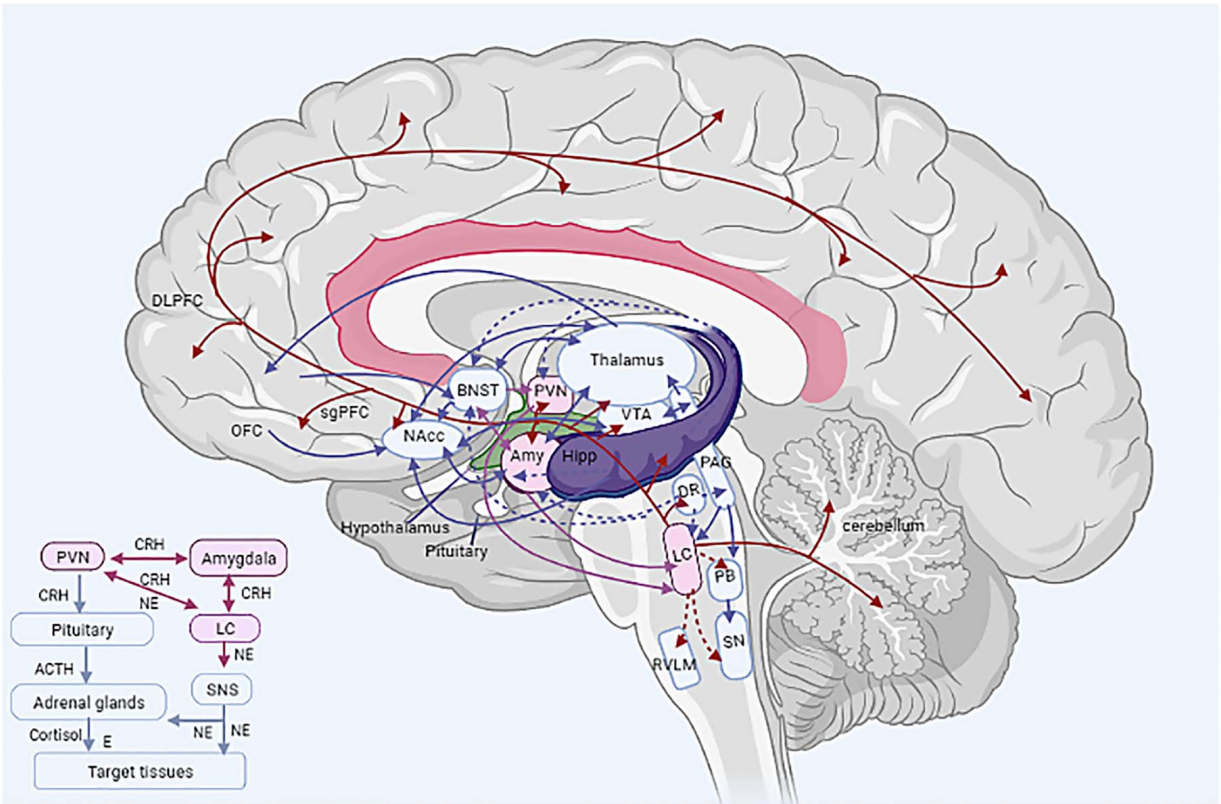

FIGURE 4 | The stress system. Main figure: central components of the stress system. Inset (bottom left corner): Simplified overview of the stress system (central and peripheral). ACTH, adrenocorticotropic-releasing hormone; Amy, amygdala; BNST, bed nucleus of the stria terminalis; CRH, corticotropin-releasing hormone; DLPFC, dorsolateral prefrontal cortex; DR, dorsal raphe nucleus; E, epinephrine; Hipp, hippocampus; LC, locus caeruleus; NE, norepinephrine; NAcc, nucleus accumbens; OFC, orbitofrontal cortex; PAG, periaqueductal gray matter; PB, parabrachial nucleus; PFC, prefrontal cortex; PVN, paraventricular nucleus of the hypothalamus; RVLM, rostral ventrolateral medulla; sgPFC, subgenual prefrontal cortex; SN, solitary nucleus; SNS, sympathetic nervous system; VTA, ventral tegmental area. Solid line arrows represent excitatory projections, whereas dashed line arrows represent inhibitory ones. Double-headed arrows represent reciprocal connections. Efferent LC pathways are depicted in red.

the midbrain ventral tegmental area (VTA) to the PFC and the latter connects the VTA to the ventral striatum in the basal ganglia (including the nucleus accumbens, NAcc) (Chrousos and Gold, 1992; Chrousos, 2007). Afferent excitatory fibers from the VTA project to the LC via the mesocaeruleal pathway which contributes to the maintenance of arousal, whereas efferent fibers project from the LC to both the VTA and the NAcc. The VTA has reciprocal connections with the PFC (Samuels and Szabadi, 2008a,b; Haber, 2011; Ferrucci et al., 2013; Gold, 2015a). The NAcc seems to be the main input nucleus of the basal ganglia, and receives input from the amygdala, hippocampus, thalamus and PFC, participating in a cortico-pallido-thalamo-cortical loop (Salgado and Kaplitt, 2015).

The LC-NE system has many similar effects to those of the CRH system, e.g., arousal, inhibition of neuro-vegetative functions, loss of affective and cognitive flexibility and reciprocally activates the amygdala and the CRH system (Gold et al., 2015b). The CRH and the LC-NE systems seem to be part of a positive feedback loop, where activation of one system tends to also activate the other. These interactions could be explained by projections from the PVN CRH neurons to the LC-NE system and vice versa by noradrenergic projections of the LC-NE system to the PVN (**Figure 4**, Inset). Furthermore, the CRH and the LC-NE systems seem to respond in a similar way to several neurochemical modulators, i.e., both serotonin and acetylcholine (Ach) are excitatory to CRH neurons and the LC-NE system, whereas GABA, opioids and glucocorticoids are inhibitory to both systems (Chrousos and Gold, 1992; Chrousos, 2007).

The PFC participates in the stress system. The function of sgPFC (subgenual PFC) – a term used interchangeably with subgenual anterior cingulate cortex (sgACC) (Drevets et al., 2008; Price and Drevets, 2012) – is moderately diminished during normal stress to disinhibit the CRH and the LC-NE systems and consequently to promote anxiety and arousal, while diminishing appetite and sleep. Additionally, the dorsolateral prefrontal cortex (DLPFC) and the orbitofrontal cortex (OFC) are moderately inhibited, thus decreasing cognitive regulation of anxiety and information processing concerning reward/pleasure (Gold, 2015a; Gold et al., 2015b).

The BNST, located in the basal forebrain, is the center of a network that connects the amygdala and the PVN. It is important for the regulation of the HPA response to stress, and is considered to be a component of the "extended amygdala", but also a node which connects stress-related loci with the reward system. The BNST is interconnected with the amygdala, DR, hippocampus, hypothalamus, NAcc, VTA, thalamus, PFC. It also receives input from brainstem noradrenergic neurons, by which the BNST exerts inhibition on the HPA response to stress (Crestani et al., 2013; Stamatakis et al., 2014; Lebow and Chen, 2016; Goode and Maren, 2017). The HPA axis may be activated when inhibitory BNST neurons – which project to the PVN – are disinhibited. Responsiveness to stress stimuli depends on the duration of exposure (acute versus chronic stress activates different cells).

The PAG is a complex structure that coordinates the antinociceptive, behavioral and autonomic reactions to stress and injury. It connects the forebrain to the brainstem by receiving input from the cortex, the amygdala and hypothalamus and projects to the brainstem LC and autonomic nuclei. Stimulation of the dorsolateral PAG by escapable stress causes hypertension, tachycardia and aggressive behavior consistent with the fight-or-flight response, whereas stimulation of the ventrolateral PAG by non-escapable stress causes the opposite response, including bradycardia, hypotension and passive behavior. The PAG is reciprocally connected with the CeA and also projects to both the NAcc and the VTA as well as the thalamus (Benarroch, 2012).

The DR and the median raphe nucleus (MR) contain the majority of the forebrain–projecting serotoninergic neurons. The DR has reciprocal projections to anxiety-related structures including the CeA, BNST, PAG, mPFC (medial prefrontal cortex), and also receives input from the DMH and PVN. Serotoninergic activity depends on a fine balance between excitatory and inhibitory inputs to serotoninergic neurons, which is constantly changing (Hornung, 2003; Hale et al., 2012; Pollak Dorocic et al., 2014).

The paraventricular nucleus of the thalamus (Pa) seems to be a component of the stress system. There is evidence that the Pa is connected to the amygdala, BNST, NAcc, and sgPFC. Interestingly, hypothalamic HRCT projections to the Pa, via the amygdala and BNST, may facilitate HPA axis response to novel stress (after repeated and chronic stress) and regulate the facilitation/habituation balance. Because the Pa has a few direct projections to the PVN, regulation of the HPA axis by the Pa may be accomplished through the BNST to the PVN (Hsu et al., 2014).

New CNS loci are implicated increasingly in the stress response; for instance, the lateral habenula, an anti-reward diencephalic structure, seems to be involved in the stress system. The lateral habenula has been found to be connected reciprocally with the PVN, but the precise nature of these interactions remains unknown. This structure also interacts with dopaminergic and serotoninergic neurotransmission (Gold and Kadriu, 2019).

Figure 4 only partially depicts the complexity of the stress system.

DISORDERS OF THE STRESS SYSTEM

The stress system is characterized by circadian rhythmicity and also responds to stressors on demand. During brief, controllable stress, the stress response is characterized by several short-term, temporarily beneficial, adaptive mechanisms, which activate this response only when it is needed (Chrousos, 2007, 2009). On the other hand, chronic, uncontrollable stress might affect development, growth and metabolism and may have a detrimental impact on many physiological systems, leading to neurobehavioral, metabolic, cardiovascular or autoimmune disorders. Genetic and epigenetic factors that determine the susceptibility or resilience of individuals to stress, environmental factors as well as exposure during critical developmental periods, but also the intensity and duration of stress may influence the development and severity of stress-related disorders (Chrousos, 2007, 2009). Stress induces altered neurogenesis and structural remodeling of the brain, including replacement of neurons and remodeling of dendrites and synapses (McEwen, 2007). Additionally, the stress itself causes transient or permanent epigenetic changes, which may alter gene expression and may determine resilience or susceptibility to stress (e.g., genes regulating the HPA axis, including genes for CRH, AVP, and the glucocorticoid receptor) (Nestler, 2012, 2014; Gold, 2015a).

DEPRESSION AS A MODEL OF DYSREGULATION OF THE STRESS RESPONSE

The stress response and major depression (MD) share major brain circuitries and mediators, including the PFC, amygdala, the LC-NE and CRH system, which participate in multiple inter-relating feedback loops. Hence, many of the features of MD reflect dysregulation of the stress response (Gold and Chrousos, 2002; Gold, 2015a). In melancholic depression, hypothalamic CRH hypersecretion leads to hypercortisolism and activation of the LC-NE system, whereas the gonadal, GH and thyroid axes are inhibited. Activation of the amygdala CRH system promotes anxiety and fear and activates the PVN CRH and the LC-NE systems. CRH activates the secretion of NE and vice versa, due to the interconnection of the CRH and LC-NE systems (Chrousos, 2007; Gold, 2015a). Inhibition of the sgPFC leads to disinhibition of the amygdala and vice versa (Gold et al., 2015b). The NAcc is suppressed by profound hypercortisolemia, leading to inability to adaptively alter reward-seeking behavior, to anhedonia and loss of motivation. On the other hand, mild cortisol elevation during normal stress increases the activity of the NAcc. Dopaminergic and serotonin neurotransmission are reduced. Premature aging and death may be attributed to a general dyshomeostatic state, which is characterized by activation of the CRH system, increased sympathetic activity, increased secretion of pro-inflammatory cytokines in both the brain and the periphery, insulin resistance and a prothrombotic state (Gold and Chrousos, 2002; Gold, 2015a; Gold et al., 2015b). Furthermore, chronic, uncontrollable stress and depression are both characterized by

decreased neuroplasticity and neurogenesis, in which brain-derived neurotrophic factor (BDNF) signaling is disordered (Autry and Monteggia, 2012).

DISORDERS OF THE LC-NE SYSTEM

Stress alters LC neurons, and changes are dependent on its intensity and duration. A mild stress of short duration causes axonal sprouting, whereas prolonged, severe stress leads to axonal retraction or degeneration, possibly attributed to increased secretion of glucocorticoids (Nakamura and Sakaguchi, 1990; Nakamura et al., 1991).

Dysfunction of the LC-NE system is strongly correlated with several neurodegenerative disorders, including AD and PD, in which LC noradrenergic neurons undergo selective and early degeneration. Similar pathological changes are described in both AD and PD, indicating that AD and PD may be the two poles of a spectrum of neurodegenerative disorders, associated with LC-NE neuronal loss (Samuels and Szabadi, 2008b). Because the LC-NE system regulates attention, arousal and mood, degeneration of the LC may account for several neurobehavioral symptoms observed in both AD and PD, such as anxiety, depression and sleep disorders (Weinshenker, 2018). Additionally, LC-NE neurons have neuromodulatory and neuroprotective effects on the dopaminergic neurons of the substantia nigra and, thus, when the LC is compromised, it further contributes to neurodegeneration and the development of PD. Of note, patients with a history of depression show more profound neuronal loss within the LC (Samuels and Szabadi, 2008b).

Interestingly, the cognitive symptoms of schizophrenia may be attributed to the interaction between genetic susceptibility and dysfunction of the LC-NE system, which is triggered by stress (Mäki-Marttunen et al., 2020). Besides NE, disrupted neuromodulator signaling may contribute to alterations in LC-NE system activity in AD and PD, but also in chronic stress (Weinshenker, 2018).

SPECIFICATION OF NORADRENERGIC NEURONS

The generation and specification of noradrenergic neurons in the CNS and PNS, though poorly characterized, seems to be mediated by very similar transcriptional control mechanisms. In particular, the bHLH gene TFs Mash1 and Phox2b have been shown to be essential and sufficient for the generation of the LC and sympathetic ganglia. Previous studies have demonstrated *in vivo* that BMPs are essential for sympathetic neuron development and that the TFs Mash1, Phox2a, Phox2b, and dHAND are downstream regulators of BMPs in the sympathetic lineage.

In LC noradrenergic neurons, expression of Phox2a precedes and is essential for the later induction of Phox2b, which is followed by expression of dopamine beta-hydroxylase (DBH) and tyrosine hydroxylase (TH). BMP5 and BMP7 are expressed in the dorsal neuroepithelium, in proximity to Phox2-expressing cells, and they have been identified as likely candidates in LC generation. FGF8 is also essential for specification of noradrenergic neuron progenitors, early in neural tube development (Vogel-Höpker and Rohrer, 2002).

GENERATION OF NORADRENERGIC NEURONS *IN VITRO*

Mong et al. (2014) generated noradrenergic neurons from mESCs by forced expression of Phox2b, under the signaling influence of FGF8 and BMP7. Nevertheless, when they repeated their experiment in hESCs, there was lower expression of noradrenergic markers; BMP7 did not promote noradrenergic marker expression in hESCs. However, forced expression of Phox2b in hESCs, which were cultured with FGF8, promoted generation of noradrenergic cells (Mong et al., 2014). Kirino et al. (2018) generated sympathetic neurons from hPSCs. *In vivo*, sympathetic neurons originate from trunk neural crest cells (NCCs) cells, which in turn derive from neuromesodermal progenitor cells (NMPs). The authors concluded that BMPs and RA are essential for induction of Phox2b-expressing NCCs (Kirino et al., 2018). Eura et al. (2020) produced brainstem organoids that contained NCCs, midbrain and hindbrain progenitors as well as noradrenergic, dopaminergic and cholinergic neurons.

CHALLENGES AND OPPORTUNITIES: USING BRAIN ORGANOIDS TO MODEL THE STRESS SYSTEM AND STRESS-RELATED DISORDERS, TOWARD A UNIFIED THEORY OF STRESS

The stress response is orchestrated by a sophisticated system that consists of various interacting CNS structures, groups of neurons and circuits, which extend from the neocortex to primitive structures of the limbic system and participate in multiple regulatory loops (Chrousos and Gold, 1992; Gold and Chrousos, 2002; Chrousos, 2007, 2009; Gold, 2015a) (**Figure 4**). Among them, the hypothalamus is remarkably anatomically and functionally conserved among vertebrates (Xie and Dorsky, 2017). The LC is the major noradrenergic nucleus with numerous projections to almost all brain regions (Samuels and Szabadi, 2008a,b; Schwarz and Luo, 2015). Dysregulation of the stress system and the associated epigenetic changes may account for numerous complex diseases.

Despite the complexity of the stress system, brain organoids could be invaluable in the modeling of the stress response and stress-related disorders. Advances in brain organoid technologies include functional hypothalamic-pituitary organoids (Kasai et al., 2020), human brainstem organoids containing noradrenergic neurons (Eura et al., 2020), fused forebrain and thalamocortical assembloids (Birey et al., 2017; Bagley et al., 2017; Xiang et al., 2017, 2019), midbrain organoids (Jo et al., 2016; Monzel et al., 2017; Kim et al., 2019; Kwak

et al., 2020), oligocortical spheroids with oligodendrocytes (Madhavan et al., 2018), hippocampal organoids (Sakaguchi et al., 2015), assembloids integrated with isogenic microglia (Song et al., 2019a), vascularized organoids with BBB properties (Cakir et al., 2019), polarized forebrain organoids (Cederquist et al., 2019), sliced forebrain organoids (Qian et al., 2020) (**Supplementary Table 1**). Central noradrenergic neurons and peripheral sympathetic neurons have been generated from hESCs (Mong et al., 2014; Kirino et al., 2018). On the other hand, LC-NE system or amygdala organoids have not been generated to date.

Modeling inter-cellular and inter-regional interactions within the stress system would necessitate the co-culture/assembly of multiple components of the stress system into *multi-region assembloids*. More subtle interactions and the developmental spatial topography of specific regions could be recapitulated by *polarized organoids/assembloids*. Initially, fused assembloids of the PVN, the LC, amygdala and PFC could be generated. However, the optimal goal would be the assembly of functional *whole brain polarized assembloids,* which would enable the elucidation of new stress-associated CNS loci. Additionally, non-neural cells, e.g., microglia to study neural/non-neural cellular interactions, and vascular cells to provide vascularization (which is essential for mature organoids) would be needed (*multi-region/multilineage assembloid*s).

However, it should be kept in mind that current organoid technologies are not able to accurately recapitulate *in vivo* functional connectivity between various distant brain regions. Furthermore, comprehensive understanding of the programs that drive the differentiation of various cells and regional morphogenesis in the CNS is lacking. Hence, identifying the minimal signals that are necessary for specification and self-organization would be essential for the development of other region-specific organoids (e.g., LC-NE system and amygdala organoids) as well as *polarized multi-region brain structures in vitro*.

Interestingly, the assembly of organoids from different tissue types could recapitulate the interaction between the brain and other organs toward *multi-organ assembloids* (e.g., hypothalamic-pituitary-adrenal or LC-NE system/adrenal assembloids). Of note, no hPSC-derived adrenal organoids have been generated to date. Poli et al. (2019) developed an *in vitro* human fetal cell model, representative of the adrenal gland components.

The generation of "*stress system organoids*" could provide a window of opportunity for basic and translational research. What are the molecular mechanisms that delineate the molecular stress response within individual region-specific organoids? How are these molecular signals integrated among the various region-specific organoids within the "*stress assembloids*" to establish a physiological stress response? How do the interactions of neural and non-neural cells within region-specific organoids, but also among different region-specific organoids within the "*stress system assembloids*", delineate the development of the stress system and how does the early environment (prenatal, perinatal, and postnatal) affect this process? What are the genetic marks that confer vulnerability or resilience to stress? What are the associated epigenetic changes? Are they inherited? Are there differences between acute and chronic, mild and severe stress? How are the various components of the stress system engaged differently in different contexts?

The combination of brain organoids with multi-modal single-cell omics and lineage tracing could provide information about different cell types, their developmental trajectories and cell lineage as well as gene regulatory and signaling networks and could identify new cell types (Camp and Treutlein, 2017; Efremova and Teichmann, 2020). Insertion of fluorescent tags and reporter systems in PSCs (before the generation of organoids) could be used to study inter-cellular connectivity and cellular migration (Camp and Treutlein, 2017; Fischer et al., 2019).

Profiles of control *vs*. disease organoids could be compared. Initially, a representative stress-related disorder, such as depression, could be chosen to compare with controls. After that, other candidate disease groups could be studied to define whether dysregulation of the stress system is mechanistically implicated in the specific phenotype. Lineage-coupled single cell omics combined with CRISPR/Cas9 mutagenesis could make possible the localization of network perturbations, determine dysregulated genes and elucidate mechanisms of cell communication, regulation of cell specification as well as how environmental factors affect these processes during development (Camp and Treutlein, 2017; Fischer et al., 2019). Computational methods, including multi-modal deep learning and network-based fusion could further clarify causal relations between different omics layers and could be used to study genotype-phenotype correlations and to associate transcriptional with epigenetic phenomena that determine cellular phenotypes (Efremova and Teichmann, 2020; Schier, 2020).

We speculate that dysregulation of the stress system is involved in the pathophysiology of numerous complex systemic disorders, including neurodegeneration. We also speculate that the stress system is a ubiquitous, interspersed, conserved system which affects pleiotropically multiple CNS and peripheral targets, as a major regulator of systemic homeostasis and as a protagonist in dyshomeostasis (cacostasis), in the context of a unified theory of stress. The integration of the above methods into a model of the stress system would have a profound impact on precision medicine, in the near future.

CONCLUSION

Despite recent advances in brain organoid technologies, existing cultures are far from perfect; thus, there is still a need for organoids that accurately reflect the characteristics of the human brain regarding regional and cellular diversity, connectivity, myelination, polarization, vascularization and, generally, reproducibility. Additionally, more mature organoids mimicking later developmental stages as well as the aging brain are needed. The generation of 3D, *in vitro* models of the stress system could have a considerable impact on the mechanistic explanation of the pathophysiology of a great number of stress-related disorders, which cause significant morbidity and mortality, as well as on developmental neuroendocrinology and beyond.

*Locus caeruleus means the blue spot/place in Latin. *Caeruleus* means *blue* in classical Latin[1]. It probably derives from the classical Latin word *caelum* which means *sky*[2]. Locus caeruleus is dictated in the list of Latin expressions and English equivalents in Terminologia Anatomica[3], which is the current edition of Nomina Anatomica[4].

AUTHOR CONTRIBUTIONS

EM conceived and designed the work, collected data, analyzed and interpreted data, drafted the article, critically revised the article, and finally approved of the version to be published. GC conceived and designed the work, collected data, analyzed and interpreted data, critically revised the article, and finally approved of the version to be published. Both authors contributed to the article and approved the submitted version.

ACKNOWLEDGMENTS

The authors would like to thank Alexios-Fotios Mentis for his valuable remarks.

SUPPLEMENTARY MATERIAL

The Supplementary Material for this article can be found online at: https://www.frontiersin.org/articles/10.3389/fphys.2021.621970/full#supplementary-material

[1] http://www.perseus.tufts.edu/hopper/resolveform?type=exact&lookup=caeruleus&lang=la

[2] https://en.wiktionary.org/wiki/caeruleus

[3] http://terminologia-anatomica.org/en/Search?query=locus%20caeruleus

[4] https://en.wikipedia.org/wiki/Locus_coeruleus#Etymology

REFERENCES

Abud, E. M., Ramirez, R. N., Martinez, E. S., Healy, L. M., Nguyen, C., Newman, S. A., et al. (2017). iPSC-derived human microglia-like cells to study neurological diseases. *Neuron* 94, 278–293.e9. doi: 10.1016/j.neuron.2017.03.042

Adams, J. W., Cugola, F. R., and Muotri, A. R. (2019). Brain organoids as tools for modeling human neurodevelopmental disorders. *Physiology (Bethesda, Md.)* 34, 365–375. doi: 10.1152/physiol.00005.2019

Adey, A., Burton, J. N., Kitzman, J. O., Hiatt, J. B., Lewis, A. P., Martin, P. K., et al. (2013). The haplotype-resolved genome and epigenome of the aneuploid HeLa cancer cell line. *Nature* 500, 207–211. doi: 10.1038/nature12064

Adhya, D., Annuario, E., Lancaster, M. A., Price, J., Baron-Cohen, S., and Srivastava, D. P. (2018). Understanding the role of steroids in typical and atypical brain development: advantages of using a "brain in a dish" approach. *J. Neuroendocrinol.* 30:e12547. doi: 10.1111/jne.12547

Agirman, G., Broix, L., and Nguyen, L. (2017). Cerebral cortex development: an outside-in perspective. *FEBS Lett.* 591, 3978–3992. doi: 10.1002/1873-3468.12924

Agarwal, S., Loh, Y. H., McLoughlin, E. M., Huang, J., Park, I. H., Miller, J. D., et al. (2010). Telomere elongation in induced pluripotent stem cells from dyskeratosis congenita patients. *Nature* 464, 292–296. doi: 10.1038/nature08792

Alberts, B., Johnson, A., Lewis, J., Raff, M., Roberts, K., and Walter, P. (2002). *Molecular Biology of the Cell. Blood Vessels and Endothelial Cells*, 4th Edn. New York, NY: Garland Science.

Amin, N. D., and Paşca, S. P. (2018). Building models of brain disorders with three-dimensional organoids. *Neuron* 100, 389–405. doi: 10.1016/j.neuron.2018.10.007

Andrade, L. N., Nathanson, J. L., Yeo, G. W., Menck, C. F., and Muotri, A. R. (2012). Evidence for premature aging due to oxidative stress in iPSCs from Cockayne syndrome. *Hum. Mol. Genet.* 21, 3825–3834. doi: 10.1093/hmg/dds211

Atamian, A., Cordón-Barris, L., and Quadrato, G. (2021). Taming human brain organoids one cell at a time. *Semin. Cell Dev. Biol.* 111, 23–31. doi: 10.1016/j.semcdb.2020.05.022

Autry, A. E., and Monteggia, L. M. (2012). Brain-derived neurotrophic factor and neuropsychiatric disorders. *Pharmacol. Rev.* 64, 238–258. doi: 10.1124/pr.111.005108

Bagley, J. A., Reumann, D., Bian, S., Leìvi-Strauss, J., and Knoblich, J. A. (2017). Fused cerebral organoids model interactions between brain regions. *Nat.Methods* 14, 743–751. doi: 10.1038/nmeth.4304

Batista, L. F., Pech, M. F., Zhong, F. L., Nguyen, H. N., Xie, K. T., Zaug, A. J., et al. (2011). Telomere shortening and loss of self-renewal in dyskeratosis congenita induced pluripotent stem cells. *Nature* 474, 399–402. doi: 10.1038/nature10084

Bhaduri, A., Andrews, M. G., Mancia Leon, W., Jung, D., Shin, D., Allen, D., et al. (2020). Cell stress in cortical organoids impairs molecular subtype specification. *Nature* 578, 142–148. doi: 10.1038/s41586-020-1962-0

Benarroch, E. E. (2005). Paraventricular nucleus, stress response, and cardiovascular disease. *Clin. Autonomic Res. Official J. Clin. Auto. Res. Soc.* 15, 254–263. doi: 10.1007/s10286-005-0290-7

Benarroch, E. E. (2012). Periaqueductal gray: an interface for behavioral control. *Neurology* 78, 210–217. doi: 10.1212/WNL.0b013e31823fcdee

Bedont, J. L., Newman, E. A., and Blackshaw, S. (2015). Patterning, specification, and differentiation in the developing hypothalamus. *Wiley Interdisciplinary Rev. Dev. Biol.* 4, 445–468. doi: 10.1002/wdev.187

Benito-Kwiecinski, S., and Lancaster, M. A. (2019). Brain Organoids: Human Neurodevelopment in a Dish. *Cold Spring Harb. Perspect. Biol.* 12:a035709. doi: 10.1101/cshperspect.a035709

Bergmann, S., Lawler, S. E., Qu, Y., Fadzen, C. M., Wolfe, J. M., Regan, M., et al. (2018). Blood-brain-barrier organoids for investigating the permeability of CNS therapeutics. *Nat. Protoc.* 13, 2827–2843. doi: 10.1038/s41596-018-0066-x

Bershteyn, M., Nowakowski, T. J., Pollen, A. A., Di Lullo, E., Nene, A., Wynshaw-Boris, A., et al. (2017). Human iPSC-derived cerebral organoids model cellular features of lissencephaly and reveal prolonged mitosis of outer radial glia. *Cell Stem Cell* 20, 435–449.e4. doi: 10.1016/j.stem.2016.12.007

Birey, F., Andersen, J., Makinson, C. D., Islam, S., Wei, W., Huber, N., et al. (2017). Assembly offunctionally integrated human forebrain spheroids. *Nature* 545, 54–59. doi: 10.1038/nature22330

Birch, H. L. (2018). Extracellular Matrix and Ageing. *Sub Cell. Biochem.* 90, 169–190. doi: 10.1007/978-981-13-2835-0_7

Blair, J. D., Hockemeyer, D., and Bateup, H. S. (2018). Genetically engineered human cortical spheroid models of tuberous sclerosis. *Nat. Med.* 24, 1568–1578. doi: 10.1038/s41591-018-0139-y

Brinkmeier, M. L., Potok, M. A., Davis, S. W., and Camper, S. A. (2007). TCF4 deficiency expands ventral diencephalon signaling and increases induction of pituitary progenitors. *Dev. Biol.* 311, 396–407. doi: 10.1016/j.ydbio.2007.08.046

Burgess, D. J. (2019). Spatial transcriptomics coming of age. *Nat. Rev. Genet.* 2: 317. doi: 10.1038/s41576-019-0129-z

Cakir, B., Xiang, Y., Tanaka, Y., Kural, M. H., Parent, M., Kang, Y. J., et al. (2019). Engineering of human brain organoids with a functional vascular-like system. *Nat. Methods* 16, 1169–1175. doi: 10.1038/s41592-019-0586-5

Camp, J. G., Badsha, F., Florio, M., Kanton, S., Gerber, T., Wilsch-Bräuninger, M., et al. (2015). Human cerebral organoids recapitulate gene expression programs of fetal neocortex development. *Proc. Natl. Acad. Sci. U.S.A.* 112, 15672–15677. doi: 10.1073/pnas.1520760112

Camp, J. G., and Treutlein, B. (2017). Human organomics: a fresh approach to understanding human development using single-cell transcriptomics. *Development (Cambridge, England)* 144, 1584–1587. doi: 10.1242/dev.150458

Cederquist, G. Y., Asciolla, J. J., Tchieu, J., Walsh, R. M., Cornacchia, D., Resh, M. D., et al. (2019). Specification of positional identity in forebrain organoids. *Nat. Biotechnol.* 37, 436–444. doi: 10.1038/s41587-019-0085-3

Choi, H., Song, J., Park, G., and Kim, J. (2017). Modeling of Autism using organoid technology. *Mol. Neurobiol.* 54, 7789–7795. doi: 10.1007/s12035-016-0274-8

Cornacchia, D., and Studer, L. (2017). Back and forth in time: directing age in iPSC-derived lineages. *Brain Res.* 1656, 14–26. doi: 10.1016/j.brainres.2015.11.013

Chrousos, G. P., and Gold, P. W. (1992). The concepts of stress and stress system disorders. *Overv. Phys. Behav. Homeostasis. JAMA* 267, 1244–1252. doi: 10.1001/jama.1992.03480090092034

Chrousos, G. P. (2009). Stress and disorders of the stress system. *Nat. Rev. Endocrinol.* 5, 374–381. doi: 10.1038/nrendo.2009.106

Chrousos, G. P. (2007). Organization and integration of the endocrine system. *Sleep Med. Clin.* 2, 125–145. doi: 10.1016/j.jsmc.2007.04.004

Clevers, H. (2016). Modeling development and disease with organoids. *Cell* 165, 1586–1597. doi: 10.1016/j.cell.2016.05.082

Crestani, C. C., Alves, F. H., Gomes, F. V., Resstel, L. B., Correa, F. M., and Herman, J. P. (2013). Mechanisms in the bed nucleus of the stria terminalis involved in control of autonomic and neuroendocrine functions: a review. *Curr. Neuropharmacol.* 11, 141–159. doi: 10.2174/1570159X11311020002

Cugola, F. R., Fernandes, I. R., Russo, F. B., Freitas, B. C., Dias, J. L., Guimarães, K. P., et al. (2016). The Brazilian Zika virus strain causes birth defects in experimental models. *Nature* 534, 267–271. doi: 10.1038/nature18296

Dang, J., Tiwari, S. K., Lichinchi, G., Qin, Y., Patil, V. S., Eroshkin, A. M., et al. (2016). Zika virus depletes neural progenitors in human cerebral organoids through activation of the innate immune receptor TLR3. *Cell Stem Cell* 19, 258–265. doi: 10.1016/j.stem.2016.04.014

Daviaud, N., Friedel, R. H., and Zou, H. (2018). Vascularization and engraftment of transplanted human cerebral organoids in mouse cortex. *eNeuro* 5, ENEURO.0219–18.2018. doi: 10.1523/ENEURO.0219-18.2018

Drevets, W. C., Savitz, J., and Trimble, M. (2008). The subgenual anterior cingulate cortex in mood disorders. *CNS Spectrums* 13, 663–681. doi: 10.1017/s1092852900013754

Efremova, M., and Teichmann, S. A. (2020). Computational methods for single-cell omics across modalities. *Nat. Methods* 17, 14–17. doi: 10.1038/s41592-019-0692-4

Eiraku, M., Watanabe, K., Matsuo-Takasaki, M., Kawada, M., Yonemura, S., Matsumura, M., et al. (2008). Self-organized formation of polarized cortical tissues from ESCs and its active manipulation by extrinsic signals. *Cell Stem Cell* 3, 519–532. doi: 10.1016/j.stem.2008.09.002

Eura, N., Matsui, T. K., Luginbühl, J., Matsubayashi, M., Nanaura, H., Shiota, T., et al. (2020). Brainstem organoids from human pluripotent stem cells. *Front. Neurosci.* 14:538. doi: 10.3389/fnins.2020.00538

Ferrucci, M., Giorgi, F. S., Bartalucci, A., Busceti, C. L., and Fornai, F. (2013). The effects of locus coeruleus and norepinephrine in methamphetamine toxicity. *Curr. Neuropharmacol.* 11, 80–94. doi: 10.2174/157015913804999522

Fischer, J., Heide, M., and Huttner, W. B. (2019). Genetic modification of brain organoids. *Front. Cell. Neurosci.* 13:558. doi: 10.3389/fncel.2019.00558

Gabriel, E., and Gopalakrishnan, J. (2017). Generation of iPSC-derived human brain organoids to model early neurodevelopmental disorders. *J. Visualized Exp. JoVE* 14:55372. doi: 10.3791/55372

Garcez, P. P., Loiola, E. C., Madeiro da Costa, R., Higa, L. M., Trindade, P., et al. (2016). Zika virus impairs growth in human neurospheres and brain organoids. *Science (New York, N.Y.)* 352, 816–818. doi: 10.1126/science.aaf6116

Gold, P. W., and Chrousos, G. P. (2002). Organization of the stress system and its dysregulation in melancholic and atypical depression: high vs low CRH/NE states. *Mol. Psychiatry* 7, 254–275. doi: 10.1038/sj.mp.4001032

Gold, P. W. (2015a). The organization of the stress system and its dysregulation in depressive illness. *Mol. Psychiatry* 20, 32–47. doi: 10.1038/mp.2014.163

Gold, P. W., Machado-Vieira, R., and Pavlatou, M. G. (2015b). Clinical and biochemical manifestations of depression: relation to the neurobiology of stress. *Neural Plasticity* 2015:581976. doi: 10.1155/2015/581976

Gold, P. W., and Kadriu, B. (2019). A major role for the lateral habenula in depressive illness: physiologic and molecular mechanisms. *Front. Psychiatry* 10:320. doi: 10.3389/fpsyt.2019.00320

Gonzalez, C., Armijo, E., Bravo-Alegria, J., Becerra-Calixto, A., Mays, C. E., and Soto, C. (2018). Modeling amyloid beta and tau pathology in human cerebral organoids. *Mol. Psychiatry* 23, 2363–2374. doi: 10.1038/s41380-018-0229-8

Goode, T. D., and Maren, S. (2017). Role of the bed nucleus of the stria terminalis in aversive learning and memory. *Learn. Memory (Cold Spring Harbor, N.Y.)* 24, 480–491. doi: 10.1101/lm.044206.116

Grenier, K., Kao, J., and Diamandis, P. (2020). Three-dimensional modeling of human neurodegeneration: brain organoids coming of age. *Mol. Psychiatry* 25, 254–274. doi: 10.1038/s41380-019-0500-7

Haber, S. N. (2011). "Neuroanatomy of reward: a view from the ventral striatum," in *Neurobiology of Sensation and Reward*, Chap. 11, ed. J. A. Gottfried (Boca Raton, FL: CRC Press/Taylor & Francis).

Hale, M. W., Shekhar, A., and Lowry, C. A. (2012). Stress-related serotonergic systems: implications for symptomatology of anxiety and affective disorders. *Cell. Mol. Neurobiol.* 32, 695–708. doi: 10.1007/s10571-012-9827-1

Hofman, M. A. (2014). Evolution of the human brain: when bigger is better. *Front. Neuroanatomy* 8:15. doi: 10.3389/fnana.2014.00015

Hornung, J. P. (2003). The human raphe nuclei and the serotonergic system. *J. Chem. Neuroanat.* 26, 331–343. doi: 10.1016/j.jchemneu.2003.10.002

Hsu, D. T., Kirouac, G. J., Zubieta, J. K., and Bhatnagar, S. (2014). Contributions of the paraventricular thalamic nucleus in the regulation of stress, motivation, and mood. *Front. Behav. Neurosci.* 8:73. doi: 10.3389/fnbeh.2014.00073

Hu, J. L., Todhunter, M. E., LaBarge, M. A., and Gartner, Z. J. (2018). Opportunities for organoids as new models of aging. *J. Cell Biol.* 217, 39–50. doi: 10.1083/jcb.201709054

Iefremova, V., Manikakis, G., Krefft, O., Jabali, A., Weynans, K., Wilkens, R., et al. (2017). An organoid-based model of cortical development identifies non-cell-autonomous defects in wnt signaling contributing to miller-dieker syndrome. *Cell Rep.* 19, 50–59. doi: 10.1016/j.celrep.2017.03.047

Jo, J., Xiao, Y., Sun, A. X., Cukuroglu, E., Tran, H. D., Göke, J., et al. (2016). Midbrain-like organoids from human pluripotent stem cells contain functional dopaminergic and neuromelanin-producing neurons. *Cell Stem Cell* 19, 248–257. doi: 10.1016/j.stem.2016.07.005

Kadoshima, T., Sakaguchi, H., Nakano, T., Soen, M., Ando, S., Eiraku, M., et al. (2013). Self-organization of axial polarity, inside-out layer pattern, and species-specific progenitor dynamics in human ES cell-derived neocortex. *Proc. Natl. Acad. Sci. U.S.A.* 110, 20284–20289. doi: 10.1073/pnas.1315710110

Karzbrun, E., Kshirsagar, A., Cohen, S. R., Hanna, J. H., and Reiner, O. (2018). Human brain organoids on a chip reveal the physics of folding. *Nat. Phys.* 14, 515–522. doi: 10.1038/s41567-018-0046-7

Kasai, T., Suga, H., Sakakibara, M., Ozone, C., Matsumoto, R., Kano, M., et al. (2020). Hypothalamic contribution to pituitary functions is recapitulated *In Vitro* Using 3D-cultured human iPS cells. *Cell Rep.* 30, 18–24.e5. doi: 10.1016/j.celrep.2019.12.009

Kathuria, A., Lopez-Lengowski, K., Jagtap, S. S., McPhie, D., Perlis, R. H., Cohen, B. M., et al. (2020). Transcriptomic landscape and functional characterization of induced pluripotent stem cell-derived cerebral organoids in schizophrenia. *JAMA Psychiatry* 77, 745–754. doi: 10.1001/jamapsychiatry.2020.0196

Kelberman, D., Rizzoti, K., Lovell-Badge, R., Iain, C., Robinson, A. F., and Dattani, M. T. (2009). Genetic regulation of pituitary gland development in human and mouse. *Endocrine Rev.* 30, 790–829. doi: 10.1210/er.2009-0008

Kim, H., Park, H. J., Choi, H., Chang, Y., Park, H., Shin, J., et al. (2019). Modeling G2019S-LRRK2 sporadic parkinson's disease in 3D midbrain organoids. *Stem Cell Rep.* 12, 518–531. doi: 10.1016/j.stemcr.2019.01.020

Kirino, K., Nakahata, T., Taguchi, T., and Saito, M. K. (2018). Efficient derivation of sympathetic neurons from human pluripotent stem cells with a defined condition. *Sci. Rep.* 8:12865. doi: 10.1038/s41598-018-31256-1

Kwak, T. H., Kang, J. H., Hali, S., Kim, J., Kim, K. P., Park, C., et al. (2020). Generation of homogeneous midbrain organoids with in vivo-like cellular composition facilitates neurotoxin-based Parkinson's disease modeling. *Stem Cells (Dayton, Ohio)* 38, 727–740. doi: 10.1002/stem.3163

Lancaster, M. A., and Huch, M. (2019). Disease modelling in human organoids. *Dis. Models Mech.* 12:dmm039347. doi: 10.1242/dmm.039347

Lancaster, M. A., and Knoblich, J. A. (2014). Organogenesis in a dish: modeling development and disease using organoid technologies. *Science* 345:1247125. doi: 10.1126/science.1247125

Lancaster, M. A., Renner, M., Martin, C.-A., Wenzel, D., Bicknell, L. S., Hurles, M. E., et al. (2013). Cerebral organoids model human brain development and microcephaly. *Nature* 501, 373–379. doi: 10.1038/nature12517

Lebow, M. A., and Chen, A. (2016). Overshadowed by the amygdala: the bed nucleus of the stria terminalis emerges as key to psychiatric disorders. *Mol. Psychiatry* 21, 450–463. doi: 10.1038/mp.2016.1

Lee, H. K., Velazquez Sanchez, C., Chen, M., Morin, P. J., Wells, J. M., Hanlon, E. B., et al. (2016). Three dimensional human neuro-spheroidmodel of Alzheimer's disease based on differentiated inducedpluripotent stem cells. *PLoS ONE* 11:e0163072. doi: 10.1371/journal.pone.0163072

Levi, N., Papismadov, N., Solomonov, I., Sagi, I., and Krizhanovsky, V. (2020). The ECM path of senescence in aging: components and modifiers. *FEBS J.* 287, 2636–2646. doi: 10.1111/febs.15282

Li, Y., Muffat, J., Omer, A., Bosch, I., Lancaster, M. A., Sur, M., et al. (2017a). Induction of expansion and folding in human cerebral organoids. *Cell Stem Cell* 20, 385–396.e3. doi: 10.1016/j.stem.2016.11.017

Li, R., Sun, L., Fang, A., Li, P., Wu, Q., and Wang, X. (2017b). Recapitulating cortical development with organoid culture in vitro and modeling abnormal spindlelike (ASPM related primary) microcephaly disease. *Protein Cell* 8, 823–833. doi: 10.1007/s13238-017-0479-2

Li, Q., and Barres, B. (2018). Microglia and macrophages in brain homeostasis and disease. *Nat. Rev. Immunol.* 18, 225–242. doi: 10.1038/nri.2017.125

Lin, Y. T., Seo, J., Gao, F., Feldman, H. M., Wen, H. L., Penney, J., et al. (2018). APOE4 causes widespread molecular and cellular alterations associated with Alzheimer's disease phenotypes in humaniPSCderived brain cell types. *Neuron.* 98:1294. doi: 10.1016/j.neuron.2018.06.011

Logan, S., Arzua, T., Canfield, S. G., Seminary, E. R., Sison, S. L., Ebert, A. D., et al. (2019). Studying human neurological disorders using induced pluripotent stem cells: from 2D Monolayer to 3D Organoid and Blood Brain Barrier Models. *Comp. Physiol.* 9, 565–611. doi: 10.1002/cphy.c180025

Luo, C., Lancaster, M. A., Castanon, R., Nery, J. R., Knoblich, J. A., and Ecker, J. R. (2016). Cerebral organoids recapitulate epigenomic signatures of the human fetal brain. *Cell Rep.* 17, 3369–3384. doi: 10.1016/j.celrep.2016.12.001

Lu, T. M., Houghton, S., Magdeldin, T., Durán, J., Minotti, A. P., Snead, A., et al. (2021). Pluripotent stem cell-derived epithelium misidentified as brain microvascular endothelium requires ETS factors to acquire vascular fate. *Proc. Natl. Acad. Sci. U.S.A.* 118:e2016950118. doi: 10.1073/pnas.2016950118

Madhavan, M., Nevin, Z. S., Shick, H. E., Garrison, E., Clarkson-Paredes, C., Karl, M., et al. (2018). Induction of myelinating oligodendrocytes in human cortical spheroids. *Nat. Methods* 15, 700–706. doi: 10.1038/s41592-018-0081-4

Mäki-Marttunen, V., Andreassen, O. A., and Espeseth, T. (2020). The role of norepinephrine in the pathophysiology of schizophrenia. *Neurosci. Biobehav. Rev.* 118, 298–314. doi: 10.1016/j.neubiorev.2020.07.038

Mansour, A. A., Gonçalves, J. T., Bloyd, C. W., Li, H., Fernandes, S., Quang, D., et al. (2018). An in vivo model of functional and vascularized human brain organoids. *Nat. Biotechnol.* 36, 432–441. doi: 10.1038/nbt.4127

Mariani, J., Coppola, G., Zhang, P., Abyzov, A., Provini, L., Tomasini, L., et al. (2015). FOXG1-dependent dysregulation of GABA/Glutamate neuron differentiation in autism spectrum disorders. *Cell* 162, 375–390. doi: 10.1016/j.cell.2015.06.034

Marton, R., and Pasca, S. (2019). Organoid and assembloid technologies for investigating cellular crosstalk in human brain development and disease. *Trends Cell Biol.* 30, 133–143. doi: 10.1016/j.tcb.2019.11.004

Marton, R. M., Miura, Y., Sloan, S. A., Li, Q., Revah, O., Levy, R. J., et al. (2019). Differentiation and maturation of oligodendrocytes in human three-dimensional neural cultures. *Nat. Neurosci.* 22, 484–491. doi: 10.1038/s41593-018-0316-9

McEwen, B. S. (2007). Physiology and neurobiology of stress and adaptation: central role of the brain. *Physiol. Rev.* 87, 873–904. doi: 10.1152/physrev.00041.2006

Mellios, N., Feldman, D. A., Sheridan, S. D., Ip, J., Kwok, S., Amoah, S., et al. (2018). MeCP2-regulated miRNAs control early human neurogenesis through differential effects on ERK and AKT signaling. *Mol. Psychiatry* 23, 1051–1065. doi: 10.1038/mp.2017.86

Mertens, J., Paquola, A., Ku, M., Hatch, E., Böhnke, L., Ladjevardi, S., et al. (2015). Directly reprogrammed human neurons retain aging-associated transcriptomic signatures and reveal age-related nucleocytoplasmic defects. *Cell Stem Cell* 17, 705–718. doi: 10.1016/j.stem.2015.09.001

Mertens, J., Reid, D., Lau, S., Kim, Y., and Gage, F. H. (2018). Aging in a Dish: iPSC-derived and directly induced neurons for studying brain aging and age-related neurodegenerative diseases. *Annu. Rev. Genet.* 52, 271–293. doi: 10.1146/annurev-genet-120417-031534

Miller, D. B., and O'Callaghan, J. P. (2002). Neuroendocrine aspects of the response to stress. *Metab. Clin. Exp.* 51(6 Suppl. 1), 5–10. doi: 10.1053/meta.2002.33184

Miura, Y., and Pasca, S. P. (2019). Polarizing brain organoids. *Nat. Biotechnol.* 37, 377–378. doi: 10.1038/s41587-019-0084-4

Molnár, Z., Luhmann, H. J., and Kanold, P. O. (2020). Transient cortical circuits match spontaneous and sensory-driven activity during development. *Science (New York, N.Y.)* 370, eabb2153. doi: 10.1126/science.abb2153

Mong, J., Panman, L., Alekseenko, Z., Kee, N., Stanton, L. W., Ericson, J., et al. (2014). Transcription factor-induced lineage programming of noradrenaline and motor neurons from embryonic stem cells. *Stem Cells (Dayton, Ohio)* 32, 609–622. doi: 10.1002/stem.1585

Monzel, A. S., Smits, L. M., Hemmer, K., Hachi, S., Moreno, E. L., van Wuellen, T., et al. (2017). Derivation of human midbrain-specific organoids from neuroepithelial stem cells. *Stem Cell Rep.* 8, 1144–1154. doi: 10.1016/j.stemcr.2017.03.010

Muguruma, K., Nishiyama, A., Kawakami, H., Hashimoto, K., and Sasai, Y. (2015). Self-organization of polarized cerebellar tissue in 3D culture of human pluripotent stem cells. *Cell Rep.* 10, 537–550. doi: 10.1016/j.celrep.2014.12.051

Nakamura, S., and Sakaguchi, T. (1990). Development and plasticity of the locus coeruleus: a review of recent physiological and pharmacological experimentation. *Prog. Neurobiol.* 34, 505–526. doi: 10.1016/0301-0082(90)90018-c

Nakamura, S., Kitayama, I., and Murase, S. (1991). Electrophysiological evidence for axonal degeneration of locus coeruleus neurons following long-term forced running stress. *Brain Res. Bull.* 26, 759–763. doi: 10.1016/0361-9230(91)90172-g

Nestler, E. J. (2012). Epigenetics: stress makes its molecular mark. *Nature* 490, 171–172. doi: 10.1038/490171a

Nestler, E. J. (2014). Epigenetic mechanisms of depression. *JAMA Psychiatry* 71, 454–456. doi: 10.1001/jamapsychiatry.2013.4291

Nzou, G., Wicks, R. T., Wicks, E. E., Seale, S. A., Sane, C. H., Chen, A., et al. (2018). Human cortex spheroid with a functional blood brain barrier for high-throughput neurotoxicity screening and disease modeling. *Sci. Rep.* 8:7413. doi: 10.1038/s41598-018-25603-5

Ogawa, K., Suga, H., Ozone, C., Sakakibara, M., Yamada, T., Kano, M., et al. (2018). Vasopressin-secreting neurons derived from human embryonic stem cells through specific induction of dorsal hypothalamic progenitors. *Sci. Rep.* 8:3615. doi: 10.1038/s41598-018-22053-x

Oksdath, M., Perrin, S. L., Bardy, C., Hilder, E. F., DeForest, C. A., Arrua, R. D., et al. (2018). Review: synthetic scaffolds to control the biochemical, mechanical, and geometrical environment of stem cell-derived brain organoids. *APL Bioeng.* 2:041501. doi: 10.1063/1.5045124

Ozone, C., Suga, H., Eiraku, M., Kadoshima, T., Yonemura, S., Takata, N., et al. (2016). Functional anterior pituitary generated in selforganizing culture of human embryonic stem cells. *Nat. Commun.* 7:10351. doi: 10.1038/ncomms10351

Ormel, P. R., Vieira, de Sá, R., van Bodegraven, E. J., Karst, H., Harschnitz, O., et al. (2018). Microglia innately develop within cerebral organoids. *Nat. Commun.* 9:4167. doi: 10.1038/s41467-018-06684-2

Packer, J., and Trapnell, C. (2018). Single-Cell Multi-omics: an engine for new quantitative models of gene regulation. *Trends Genet. TIG* 34, 653–665. doi: 10.1016/j.tig.2018.06.001

Pasca, A. M., Sloan, S. A., Clarke, L. E., Tian, Y., Makinson, C. D., Huber, N., et al. (2015). Functional cortical neurons and astrocytes from human pluripotent stem cells in 3D culture. *Nat. Methods* 12, 671–678. doi: 10.1038/nmeth.3415

Paşca, S. (2019). Assembling human brain organoids. *Science* 363, 126–127. doi: 10.1126/science.aau5729

Pollak Dorocic, I., Fürth, D., Xuan, Y., Johansson, Y., Pozzi, L., and Silberberg, G. (2014). A whole-brain atlas of inputs to serotonergic neurons of the dorsal

and median raphe nuclei. *Neuron* 83, 663–678. doi: 10.1016/j.neuron.2014.07.002

Pham, M. T., Pollock, K. M., Rose, M. D., Cary, W. A., Stewart, H. R., Zhou, P., et al. (2018). Generation of human vascularized brain organoids. *Neuroreport* 29, 588–593. doi: 10.1097/WNR.0000000000001014

Poli, G., Sarchielli, E., Guasti, D., Benvenuti, S., Ballerini, L., Mazzanti, B., et al. (2019). Human fetal adrenal cells retain age-related stem- and endocrine-differentiation potential in culture. *FASEB J. Official Publication Federation Am. Soc. Exp. Biol.* 33, 2263–2277. doi: 10.1096/fj.201801028RR

Price, J. L., and Drevets, W. C. (2012). Neural circuits underlying the pathophysiology of mood disorders. *Trends Cogn. Sci.* 16, 61–71. doi: 10.1016/j.tics.2011.12.011

Qian, X., Nguyen, H. N., Song, M. M., Hadiono, C., Ogden, S. C., Hammack, C., et al. (2016). Brain-region-specific organoids using mini-bioreactors for modeling zikv exposure. *Cell* 165, 1238–1254. doi: 10.1016/j.cell.2016.04.032

Qian, X., Jacob, F., Song, M. M., Nguyen, H. N., Song, H., and Ming, G. L. (2018). Generation of human brain region-specific organoids using a miniaturized spinning bioreactor. *Nat. Protoc.* 13, 565–580. doi: 10.1038/nprot.2017.152

Qian, X., Song, H., and Ming, G. L. (2019). Brain organoids: advances, applications and challenges. *Development (Cambridge, England)* 146:dev166074. doi: 10.1242/dev.166074

Qian, X., Su, Y., Adam, C. D., Deutschmann, A. U., Pather, S. R., Goldberg, E. M., et al. (2020). Sliced human cortical organoids for modeling distinct cortical layer formation. *Cell Stem Cell* 26, 766–781.e9. doi: 10.1016/j.stem.2020.02.002

Quadrato, G., Nguyen, T., Macosko, E. Z., Sherwood, J. L., Min Yang, S., Berger, D. R., et al. (2017). Cell diversity and network dynamics in photosensitive human brain organoids. *Nature* 545, 48–53. doi: 10.1038/nature22047

Raja, W. K., Mungenast, A. E., Lin, Y. T., Ko, T., Abdurrob, F., Seo, J., et al. (2016). Self-organizing 3D human neural tissue derived from induced pluripotent stem cells recapitulate Alzheimer's diseasephenotypes. *PLoS One* 11:e0161969. doi: 10.1371/journal.pone.0161969

Rajamani, U., Gross, A. R., Hjelm, B. E., Sequeira, A., Vawter, M. P., Tang, J., et al. (2018). Superobese patient-derived iPSC hypothalamic neurons exhibit obesogenic signatures and hormone responses. *Cell Stem Cell* 22, 698.e–712.e.

Rizzoti, K., and Lovell-Badge, R. (2005). Early development of the pituitary gland: induction and shaping of Rathke's pouch. *Rev. Endocr. Metab. Disord.* 6, 161–172. doi: 10.1007/s11154-005-3047-7

Rizzoti, K., Pires, C., and Lovell-Badge, R. (2016). "Perspective on Stem Cells in Developmental Biology, with Special Reference to Neuroendocrine Systems," in *Stem Cells in Neuroendocrinology*, eds D. Pfaff and Y. Christen (Berlin: Springer), 135–156. doi: 10.1007/978-3-319-41603-8_11

Sakaguchi, H., Kadoshima, T., Soen, M., Narii, N., Ishida, Y., Ohgushi, M., et al. (2015). Generation of functional hippocampal neurons from self-organizing human embryonic stem cell-derived dorsomedial telencephalic tissue. *Nat. Commun.* 6:8896. doi: 10.1038/ncomms9896

Salgado, S., and Kaplitt, M. G. (2015). The nucleus accumbens: a comprehensive review. *Stereotact. Funct. Neurosurg.* 93, 75–93. doi: 10.1159/000368279

Samuels, E. R., and Szabadi, E. (2008a). Functional neuroanatomy of the noradrenergic locus coeruleus: its roles in the regulation of arousal and autonomic function part I: principles of functional organisation. *Curr. Neuropharmacol.* 6, 235–253. doi: 10.2174/157015908785777229

Samuels, E. R., and Szabadi, E. (2008b). Functional neuroanatomy of the noradrenergic locus coeruleus: its roles in the regulation of arousal and autonomic function part II: physiological and pharmacological manipulations and pathological alterations of locus coeruleus activity in humans. *Curr. Neuropharmacol.* 6, 254–285. doi: 10.2174/157015908785777193

Schwarz, L. A., and Luo, L. (2015). Organization of the locus coeruleus-norepinephrine system. *Curr. Biol. CB* 25, R1051–R1056. doi: 10.1016/j.cub.2015.09.039

Scully, K. M., and Rosenfeld, M. G. (2002). Pituitary development: regulatory codes in mammalian organogenesis. *Science* 295, 2231–2235. doi: 10.1126/science.1062736

Seto, Y., and Eiraku, M. (2019). Toward the formation of neural circuits in human brain organoids. *Curr. Opin. Cell Biol.* 61, 86–91. doi: 10.1016/j.ceb.2019.07.010

Schier, A. F. (2020). Single-cell biology: beyond the sum of its parts. *Nat. Methods* 17, 17–20. doi: 10.1038/s41592-019-0693-3

Shepherd, G. M. (2013). Corticostriatal connectivity and its role in disease. *Nat. Rev. Neurosci.* 14, 278–291. doi: 10.1038/nrn3469

Sloan, S. A., Darmanis, S., Huber, N., Khan, T. A., Birey, F., Caneda, C., et al. (2017). Human astrocyte maturation captured in 3D cerebral corticalspheroids derived from pluripotent stem cells. *Neuron* 95, 779.e–790.e. doi: 10.1016/j.neuron.2017.07.035

Sloan, S. A., Andersen, J., Pasca, A., Birey, F., and Pasca, S. (2018). Generation and assembly of human brain region-specific three-dimensional cultures. *Nat. Protoc.* 13, 2062–2085. doi: 10.1038/s41596-018-0032-7

Smits, L. M., Reinhardt, L., Reinhardt, P., Glatza, M., Monzel, A. S., Stanslowsky, N., et al. (2019). Modeling Parkinson's disease in midbrain-like organoids. *NPJ Parkinson's Dis.* 5:5. doi: 10.1038/s41531-019-0078-4

Song, L., Yuan, X., Jones, Z., Vied, C., Miao, Y., Marzano, M., et al. (2019a). Functionalization of brain region-specific spheroids with isogenic microglia-like cells. *Sci. Rep.* 9:11055. doi: 10.1038/s41598-019-47444-6

Song, L., Yuan, X., Jones, Z., Griffin, K., Zhou, Y., Ma, T., et al. (2019b). Assembly of human stem cell-derived cortical spheroids and vascular spheroids to model 3-D Brain-like Tissues. *Sci. Rep.* 9:5977. doi: 10.1038/s41598-019-42439-9

Stachowiak, E. K., Benson, C. A., Narla, S. T., Dimitri, A., Chuye, L. E. B., Dhiman, S., et al. (2017). Cerebral organoids reveal early cortical maldevelopment in schizophrenia—computational anatomy and genomics, role of FGFR1. *Transl. Psychiatry* 7:6. doi: 10.1038/s41398-017-0054-x

Stamatakis, A. M., Sparta, D. R., Jennings, J. H., McElligott, Z. A., Decot, H., and Stuber, G. D. (2014). Amygdala and bed nucleus of the stria terminalis circuitry: Implications for addiction-related behaviors. *Neuropharmacology* 76, 320–328. doi: 10.1016/j.neuropharm.2013.05.046

Stiles, J., and Jernigan, T. L. (2010). The basics of brain development. *Neuropsychol. Rev.* 20, 327–348. doi: 10.1007/s11065-010-9148-4

Suga, H., Kadoshima, T., Minaguchi, M., Ohgushi, M., Soen, M., Nakano, T., et al. (2011). Self-formation of functional adenohypophysis in three-dimensional culture. *Nature* 480, 57–62. doi: 10.1038/nature10637

Suga, H. (2019). Application of pluripotent stem cells for treatment of human neuroendocrine disorders. *Cell Tissue Res.* 375, 267–278. doi: 10.1007/s00441-018-2880-4

Suzuki, I. K., and Vanderhaeghen, P. (2015). Is this a brain which I see before me? Modeling human neural development with pluripotent stem cells. *Development (Cambridge, England)* 142, 3138–3150. doi: 10.1242/dev.120568

Takuma, N., Sheng, H. Z., Furuta, Y., Ward, J. M., Sharma, K., Hogan, B. L., et al. (1998). Formation of Rathke's pouch requires dual induction from the diencephalon. *Development* 125, 4835–4840.

Tajbakhsh, S. (2009). Stem cell: what's in a name? *Nat. Rep. Stem Cells* doi: 10.1038/stemcells.2009.90

Velasco, S., Kedaigle, A. J., Simmons, S. K., Nash, A., Rocha, M., Quadrato, G., et al. (2019). Individual brain organoids reproducibly form cell diversity of the human cerebral cortex. *Nature* 570, 523–527. doi: 10.1038/s41586-019-1289-x

Velasco, S., Paulsen, B., and Arlotta, P. (2020). 3D Brain Organoids: Studying Brain Development and Disease outside the Embryo. *Annual review of neuroscience* 43, 375–389. doi: 10.1146/annurev-neuro-070918-050154

Vogel-Höpker, A., and Rohrer, H. (2002). The specification of noradrenergic locus coeruleus (LC) neurons depends on bone morphogenetic proteins (BMPs). *Development (Cambridge, England)* 129, 983–991.

Weinshenker, D. (2018). Long road to ruin: noradrenergic dysfunction in neurodegenerative disease. *Trends Neurosci.* 41, 211–223. doi: 10.1016/j.tins.2018.01.010

Xiang, Y., Tanaka, Y., Patterson, B., Kang, Y.-J., Govindaiah, G., Roselaar, N., et al. (2017). Fusion of regionally specified HPSC-derived organoids models human brain developmentand interneuron migration. *Cell Stem Cell* 21, 383–398.e7. doi: 10.1016/j.stem.2017.07.007

Xiang, Y., Tanaka, Y., Cakir, B., Patterson, B., Kim, K. Y., Sun, P., et al. (2019). hESC derived thalamic organoids form reciprocal projections when fused with cortical organoids. *Cell Stem Cell* 24, 487–497.e7. doi: 10.1016/j.stem.2018.12.015

Xie, Y., and Dorsky, R. I. (2017). Development of the hypothalamus: conservation, modification and innovation. *Development* 144, 1588–1599. doi: 10.1242/dev.139055

Yoon, S. J., Elahi, L. S., Pasca, A. M., Marton, R. M., Gordon, A., Revah, O., et al. (2019). Reliability of human cortical organoid generation. *Nat. Methods* 16, 75–78. doi: 10.1038/s41592-018-0255-0

Zakrzewski, W., Dobrzyñski, M., Szymonowicz, M., and Rybak, Z. (2019). Stem cells: past, present, and future. *Stem Cell Res. Ther.* 10:68. doi: 10.1186/s13287-019-1165-5

Zhang, S. C., Wernig, M., Duncan, I. D., Brüstle, O., and Thomson, J. A. (2001). In vitro differentiation of transplantable neural precursors from human embryonic stem cells. *Nat. Biotechnol.* 19, 1129–1133. doi: 10.1038/nbt1201-1129

Zhu, X., Gleiberman, A. S., and Rosenfeld, M. G. (2007). Molecular physiology of pituitary development: signalling and transcriptional networks. *Physiol. Rev.* 87, 933–963. doi: 10.1152/physrev.00006.2006

Conflict of Interest: The authors declare that the research was conducted in the absence of any commercial or financial relationships that could be construed as a potential conflict of interest.

Advantages of publishing in Frontiers

OPEN ACCESS
Articles are free to read for greatest visibility and readership

FAST PUBLICATION
Around 90 days from submission to decision

HIGH QUALITY PEER-REVIEW
Rigorous, collaborative, and constructive peer-review

TRANSPARENT PEER-REVIEW
Editors and reviewers acknowledged by name on published articles

Frontiers
Avenue du Tribunal-Fédéral 34
1005 Lausanne | Switzerland

Visit us: www.frontiersin.org
Contact us: frontiersin.org/about/contact

REPRODUCIBILITY OF RESEARCH
Support open data and methods to enhance research reproducibility

DIGITAL PUBLISHING
Articles designed for optimal readership across devices

FOLLOW US
@frontiersin

IMPACT METRICS
Advanced article metrics track visibility across digital media

EXTENSIVE PROMOTION
Marketing and promotion of impactful research

LOOP RESEARCH NETWORK
Our network increases your article's readership